MILENE LOPES DA SILVA

XANTENODIONAS: SÍNTESE, ASPECTOS TEÓRICOS E ESTRUTURAIS E AVALIAÇÃO DAS ATIVIDADES FUNGICIDA E LEISHMANICIDA

Tese apresentada à Universidade Federal de Viçosa, como parte das exigências do Programa de Pós-Graduação em Agroquímica, para obtenção do título de *Doctor Scientiae*.

VIÇOSA
MINAS GERAIS-BRASIL
2017

Ficha catalográfica preparada pela Biblioteca Central da Universidade Federal de Viçosa - Câmpus Viçosa

T
S586
2017

Silva, Milene Lopes da, 1988-
Xantenodionas: Síntese, aspectos teóricos, estruturais e avaliação das atividades fungicida e leishmanicida / Milene Lopes da Silva. – Viçosa, MG, 2017.
365 : il. (algumas color.) ; 29 cm.

Inclui anexo.
Orientador: Róbson Ricardo Teixeira.
Tese (doutorado) - Universidade Federal de Viçosa.
Inclui bibliografia.

1. Xantenodionas. 2. Derivados xantenos. 3. Raio X. I. Universidade Federal de Viçosa. Departamento de Química. Doutorado em Agroquímica. II. Título.

CDD 22. ed. 632

MILENE LOPES DA SILVA

XANTENODIONAS: SÍNTESE, ASPECTOS TEÓRICOS, ESTRUTURAIS E AVALIAÇÃO DAS ATIVIDADES FUNGICIDA E LEISHMANICIDA

Tese apresentada à Universidade Federal de Viçosa, como parte das exigências do Programa de Pós-Graduação em Agroquímica, para obtenção do título de *Doctor Scientiae*.

APROVADA: 24 de abril de 2017.

Antônio Jacinto Demuner

Marcelo Henrique dos Santos

Cleiton Moreira da Silva

Eduardo Seiti Gomide Mizubuti
(Coorientador)

Róbson Ricardo Teixeira
(Orientador)

AGRADECIMENTOS

Primeiramente, agradeço a Deus pelo dom da vida e por todas as oportunidades que Ele me possibilitou vivenciar durante todos estes anos. Sem a Tua graça e misericórdia eu não teria chegado até aqui.

Aos meus pais Sebastião e Terezinha, pelos anos de dedicação, pelo apoio irrestrito e pelas lições de vida, e também a todos os meus irmãos, que sempre estiverem ao meu lado, me dando apoio, carinho e motivação.

Ao meu marido Jander, fiel companheiro, amigo de todas as horas, amor verdadeiro, que desde o primeiro momento tem me ajudado e incentivado, diuturnamente, a alcançar os meus objetivos.

Agradeço ao professor Róbson, que, além de ser meu professor e orientador, demonstrou ser um amigo, colaborador e motivador durante todo o desenvolvimento deste trabalho. Obrigada pelos ensinamentos e pelo profissionalismo demonstrado desde o início, algo raro nos dias de hoje.

Ao professor Eduardo Mizubuti, meu co-orientador, que me incentivou a fazer o doutorado, acreditando no meu trabalho e confiando a mim a responsabilidade de auxiliá-lo na condução das pesquisas realizadas no laboratório.

Ao professor Felipe Passero (Unesp), por colaborar com os ensaios leishmanicida, que foram peças importantes para a construção de um capítulo desta tese.

Aos professores Antônio Jacinto Demuner, Marcelo Henrique dos Santos e Cleiton Moreira da Silva, por aceitarem participar da banca.

Agradeço aos meus amigos e colegas de laboratório Wagner, José Luís, Fernanda, Simone, Daniel, Jaqueline, Raphael, Thaís, Elisângela, Miller e João, que contribuíram de alguma forma para o desenvolvimento do trabalho.

Ao Departamento de Fitopatologia e à Universidade Federal de Viçosa, por permitir a conclusão da Pós-Graduação em Agroquímica.

SUMÁRIO

LISTA DE FIGURAS

CAPÍTULO I

CAPÍTULO II

CAPÍTULO V

CAPÍTULO VI

ANEXOS

LISTA DE ESQUEMAS

CAPÍTULO II

LISTA DE TABELA

CAPÍTULO II

CAPÍTULO VI

RESUMO

SILVA, Milene Lopes da, D.Sc., Universidade Federal de Viçosa, abril de 2017. **Xantenodionas: síntese, aspectos teóricos, estruturais e avaliação das atividades fungicida e leishmanicida**. Orientador: Róbson Ricardo Teixeira. Coorientador: Eduardo Seiti Gomide Mizubuti.

As xantenodionas (1,8-dioxooctaidroxantenos) são uma classe de compostos que apresentam importantes atividades biológicas tais como atividade leishmanicida, antibacteriana, antifúngica e antiproliferativa, além de serem potencialmente úteis em aplicações tecnológicas. Estes compostos são caracterizados pela presença de um anel pirânico fundido a dois anéis cicloex-2-enona. Diferentes metodologias catalíticas, utilizando ácidos de Lewis, ácidos de Brønsted, ácido de Lewis e Brønsted, líquidos iônicos, nanocatalisadores e organocatalisadores, são descritas na literatura para a síntese desta classe de compostos. Cinquenta e três xantenodionas foram preparadas por meio de reações entre 1,3-dicetonas e diferentes aldeídos. As reações foram catalisadas pelo ácido de Lewis $ZrOCl_2 \cdot 8H_2O$ e realizadas na ausência de solvente. Os rendimentos de reação variaram de 34% a 99% e tempo máximo de reação de 120 minutos. Dentre as xantenodionas sintetizadas, as derivadas da 5-isopropilcicloexan-1,3-diona e da 5-metilcicloexan-1,3-diona, bem como aquelas derivadas dos aldeídos 5-(4-clorofenil)furanilbenzaldeído, 5-(4-bromofenil)furanilbenzaldeído e 5-fenil-tiofen-2-ilbenzaldeído ainda não foram descritas na literatura. Para algumas reações entre 1,3-dicetonas e aldeídos, intermediários foram obtidos no lugar das xantenodionas. Neste sentido, quatro tetracetonas e um derivado arilideno contendo um grupo 2,6-diclorobenzaldeído foram isolados com rendimentos variando de 33% a 73%. Todos os compostos foram caracterizados empregando-se técnicas espectroscópicas e espectrométricas. Para alguns dos compostos, monocristais foram obtidos o que permitiu um estudo de suas estruturas cristalinas via difração de raios-X de monocristal. Dentre os cinquenta compostos que tiveram sua atividade antifúngica avaliada, oito apresentaram inibição da atividade metabólica superior a 50% para *Fusarium oxysporum* f. sp. *cubense* e *Alternaria grandis*, sendo que o intermediário 2-(2,6-diclorobenzilideno)-5,5-dimetilcicloexan-1,3-diona (88%) foi o mais ativo para a primeira espécie de fungo e o intermediário tetracetônico 2,2'-((5-(4-bromofenil)furan-2-il)metileno)*bis*(3-hidroxi-5,5-dimetilcicloex-2-enona) (85%) mais ativo para a segunda. Estes dois compostos também estão entre os três mais promissores nos ensaios de avaliação de atividade leishmanicida. Neste caso, porém, o mais ativo foi o intermediário tetracetônico 2,2'-((5-(4-clorofenil)furan-2-il)metileno)*bis*(3-hidroxi-5,5-dimetilcicloex-2-enona).

ABSTRACT

SILVA, Milene Lopes da, D.Sc., Universidade Federal de Viçosa, April, 2017. **Xanthenodiones: synthesis, theoretical, strutural aspects and evaluation of antifungal and leishmanicide activities**. Adviser: Róbson Ricardo Teixeira. Co-adviser: Eduardo Seiti Gomide Mizubuti.

The xanthenodiones (1,8-dihidro-octahidroxanthenes) are a class of synthetic compounds presenting important biological activities, such as leishmanicidal, antibacterial, fungicide, and antiproliferative. In addition, they are considered interesting compounds for technological applications. In the literature, there are a variety of catalytic methodologies described for the preparation of this class of compounds. The methods utilize as catalysts Lewis acids, Brønsted acids, Lewis and Brønsted acids, ionic liquids, nanocatalysts, and organocatalysts. In the present investigation, it is described the synthesis of fifty three xanthenodiones. The compounds were prepared via $ZrOCl_2 \cdot 8H_2O$ catalyzed reactions between 1,3-diketones and different aldehydes. The synthesized compounds were obtained with yields ranging from 34% to 99% and within 15 to 120 minutes. Among the xanthenodiones, the compounds obtained from 5-methyl-cyclohexane-1,3-dione and 5-isopropyl-cyclohexane-1,3-dione, as well as the xanthenodiones derived from 5-(4-chlorophenyl)furan-2-carbaldehyde and 5-(4-bromophenyl)furan-2-carbaldehyde have not been described in the literature. For some reactions, intermediates instead of xanthenodiones were obtained. In this case, four tetraketones and one arylidene derivative containing a 2,6-dichlorobenzaldehyde moiety was obtained in 33% to 73%. All synthesized compounds were fully characterized by spectroscopic and spectrometric means. In addition, it was possible to obtain good crystals of some compounds which allowed the in investigation by X-ray diffraction. Fifty compounds had their fungicide activity evaluated against *Alternaria grandis* e *Fusarium oxysporum* f. sp. *cubense*. Among the evaluated compounds, eight were capable of inhibiting the metabolic activity by more than 50%. For *F. oxysporum f.* sp *cubense*, the most active compound corresponded to intermediary 2-(2,6-dichlorobenzylidene)-5,5-dimethylcyclohexan-1,3-dione, while for *A. grandis* the tetraketone 2,2'-((5-(4-bromophenyl) furan-2-yl)methylene)bis(3-hydroxy-5,5-dimethylcyclohex-2-enone) had the highest inhibitory effect. Additionally, these compounds are among the most active ones concerning leishmanicide activity which and the tetraketone 2,2'-((5-(4-chlorophenyl) furan-2-yl)methylene)bis(3-hydroxy-5,5-dimethylcyclohex-2-enone) was the most potent.

CAPÍTULO I

XANTENODIONAS: IMPORTÂNCIA E MÉTODOS DE OBTENÇÃO

1. INTRODUÇÃO

As xantenodionas (1,8-dioxo-octaidroxantenos) caracterizam-se, do ponto de vista estrutural, pela presença de um anel pirânico fundido a dois anéis cicloexen-2-ona (Figura I-1).

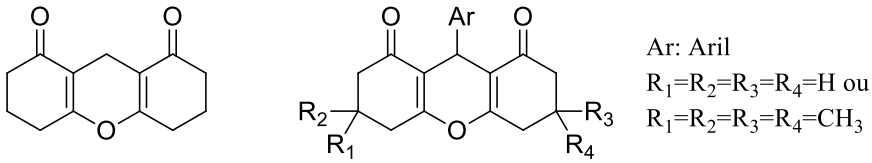

Figura I- 1. Estrutura básica das xantenodionas e padrão típico de substituição.

Estes compostos ainda não foram isolados de fontes naturais e apresentam importantes atividades biológicas, além de possuirem aplicações tecnológicas. Como consequência disso, as xantenodionas vêm atraindo a atenção dos químicos orgânicos e diferentes metodologias para a obtenção destas substâncias, empregando diferentes classes de catalisadores, têm sido reportadas em literatura. Os diferentes tipos de metodologias catalíticas disponíveis para a síntese de xantenodionas são descritas neste capítulo. Os aspectos relacionados a estes métodos foram organizados e resultaram na redação de um capítulo de livro submetido para avaliação e publicação como parte do e-book "*Advances in Organic Synthesis*" a ser publicado pela Bentham Science Publishers.

CHAPTER XXX

Different concepts of catalysis in the synthesis of xanthenediones: A brief overview

Milene Lopes da Silva[a], Róbson Ricardo Teixeira[a] and Giovanni Wilson Amarante[b]

[a]*Universidade Federal de Viçosa, Av. P. H. Rolfs, s/n, Viçosa, Minas Gerais State, Brazil*
[b]*Universidade Federal de Juiz de fora, Rua José Lourenço Kelmer, s/n, Cidade Universitária, São Pedro, Juiz de Fora, Minas Gerais State, Brazil*

Abstract – Xanthenediones, also known as 1,8-dioxo-octahydroxanthenes, are synthetic compounds characterized by the presence of a pyran nucleus fused to two cyclohexen-2-one rings. They present important biological activities as well as possible technological applications. This class of organic compounds has attracted the attention of organic chemists, who have developed several methods to synthesize them. It is herein described an overview of catalytic methodologies that have been reported to achieve the preparation of xanthenediones.

Keywords: xanthenediones; xanthenes; 1,8-dioxo-octahydroxanthenes

XANTHENEDIONES: IMPORTANCE AND SYNTHESIS

Xanthenes (*9H*-xanthene, Figure 1) and their derivatives have raised great interest among a number of research groups because of their several properties and biological activities. They have coloring properties [1], which make them useful as photosensitizers in photodynamic therapy for the destruction of tumors [2]. Xanthenes can be applied in laser therapy technology [3] and they are fluorescent materials for visualization of biomolecules [4]. Some pharmacological activities described for xanthenes include antiviral [5], antibacterial [6], anti-inflammatory [7], cytotoxicity, and antimalarial [8].

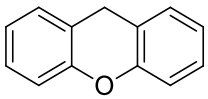

xanthene (*9H*-xanthene)

Figure 1. Xanthene structure.

Several xanthenes have been isolated from natural sources. In this regard, a well-known example is the xanthones (*9H*-xanthen-9-one) which contain in their structures two aromatic rings fused to a γ-piranone (**1**, Figure 2). The first natural occurring xanthone, α-mangostin, was isolated in 1855 by the German chemist Dr. W. Schmid, from the bark of mangosteen (*Garcinia mangostana*), a native tree of tropical regions of Thailand and Malaysia that belongs to family *Guttiferae* [9]. This fruit has bright yellow color, the reason why this researcher coined the name xanthene (derived from the Greek word "xanthos", which means yellow) for the new class of discovered compounds. Currently, there are reports on the isolation of these compounds from other families of higher plants such as *Gentianaceae*, *Guttiferae*, *Polygalaceae*, *Leguminosae*, *Lythraceae*, *Moraceae*, *Loganiaceae*, and *Rhamnaceae*, besides fungi, lichens, and bacteria [10].

Xanthones are classified as dihydroxanthone (**3** and **4**), tetrahydroxanthone (**5** and **6**) and hexahydroxanthone (**2**) according to the number of double bonds in their structures (Figure 2). The two formers are rarely found in nature. So far, only six compounds have been isolated: garcinianones A (**5a**) and B (**5b**), isolated from *Garcinia multiflora*; allanxanthone C (**5c**), isolated from *Allanblackia gabonensis* (used as a synonymous *Allanblackia monticola*); 1,2-dihydro-3,6,8-trihydroxy-1,1-isopropyl-5-(1,1-dimethylprop-2-enyl) xanthen-2,9-dione (**5d**), isolated from *Hypericum erectum* [11]; zeyloxanthonone (**3a**), isolated from *Calophyllum lankaensis* and wightianone (**3b**) isolated from *Calophyllum wightianum* [12] (Figure 2).

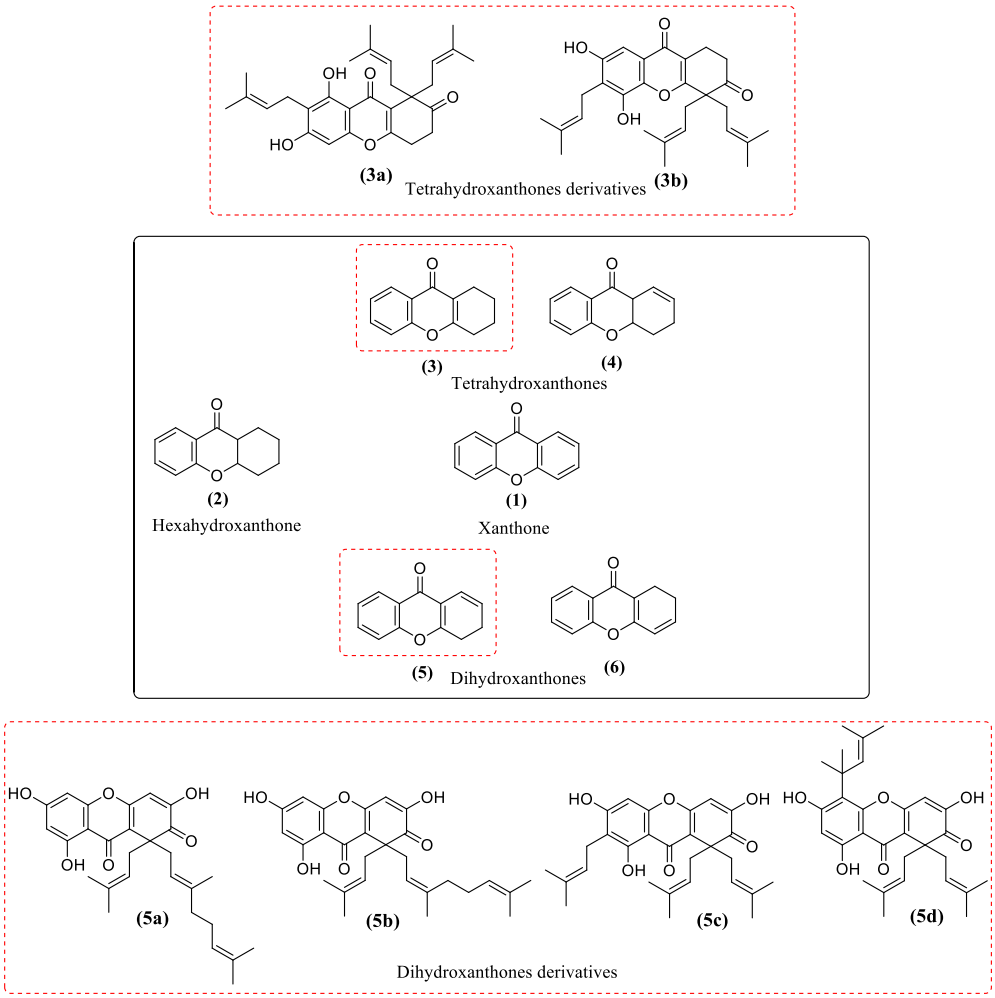

Figure 2. Xanthones subclasses and natural derivatives dihydro-xanthone (3) and tetrahydro-xanthone (5) [10,11,12].

Recently, Negi and collaborators published a review in which they have gathered all the several biological activities of natural occurring xanthones: hepatoprotective, anticarcinogenic, antihansenic, antimalarial, antioxidant, anticholinergics, mutagenicity, radioprotective, immunomodulatory, anti-bone resorption, antiparasitic, inhibition of neuraminidase, anti-addition, antibacterial, antifungal, algicidal, anti-HIV, cardioprotective, anti-tumor, anti-diabetes, antihyperlipidemic, antiatherogenic, antiinflammatory, anti-ulcer, anti-diabetic, hypolipidemic, analgesic, antiasthmatic, antihistaminic, antiamoebic, diuretic, antidiarrheal, larvicidal and ovicidal [13].

Xanthenediones, also known as 1,8-dioxo-octahydro-xanthenes, are xanthene derivatives characterized by the presence of a pyran nucleus fused to two cyclohexen-2-one rings (Figure 3). These synthetic derivatives are known to have antiproliferative [14], leishmanicidal [15], antibacterial [16,17] and fungicidal [17] activities. For these compounds, the most common substitution pattern is depicted in Figure 3 [10].

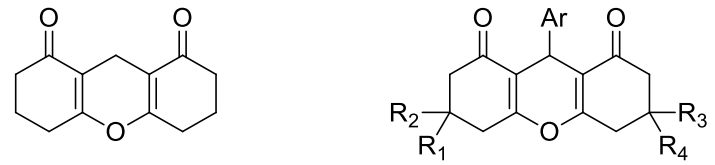

Figure 3. The structure of xanthenedione core and substitution pattern typically described in the literature.

Due to their properties, xanthenediones have drawn the attention of synthetic organic chemists, resulting in the development of several methods for the preparation of these compounds. In general, xanthenediones are derived from the following reaction sequence: Knoevenagel condensation, Michael addition and dehydration [18]. From the mechanistic point of view, these steps are shown in Scheme 1. Thus, condensation of an aromatic aldehyde (**II**) with two molecules of a cyclic diketone with an activated methylene (**I**) in the presence of a basic or acid catalyst results in the formation of the intermediate (**III**). The formation of (**III**) may occur in the absence of a catalyst. However, during the cyclization step, which leads to the final product (**IV**), the use of a catalyst is required (Scheme 1) [19]. In this context, a variety of catalysts has been employed for the synthesis of xanthenediones.

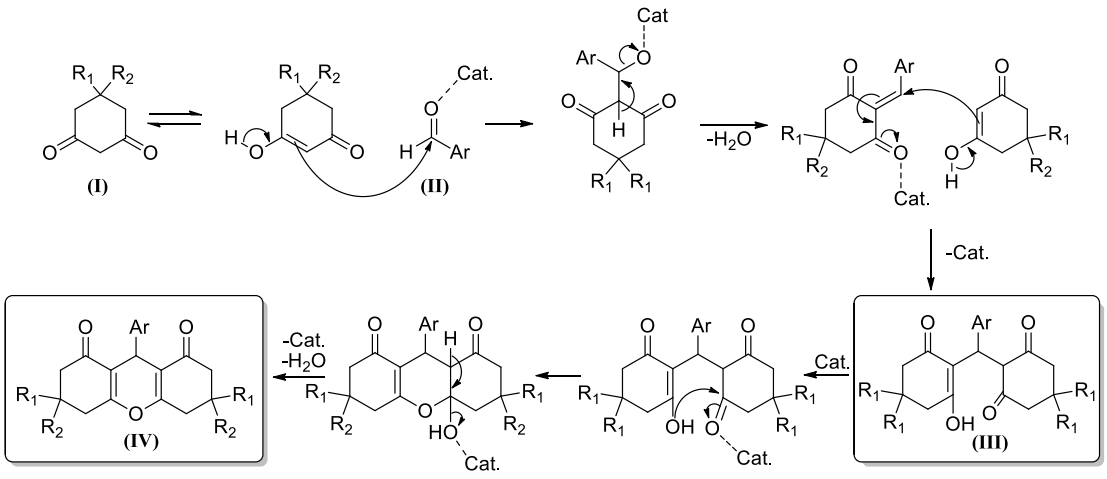

Scheme 1. Xanthenedione formation mechanism.

CATALYSTS USED IN XANTHENEDIONE SYNTHESIS

As described earlier, the catalysts play a crucial role in the synthesis of xanthenediones. Moreover, the success of the reaction, in terms of rate and yield, depends on this variable. On the other hand, there is a growing environmental concern with the reactants, catalysts, and solvents used in chemical reactions, which must be environmentally harmless, desirable that they are placed in the context of Green Chemistry.

In organic chemistry, the concept of "ideal synthesis", defined by Wender, means to obtain the target in a single step with quantitative yield from readily available and inexpensive reagents [20]. Many research groups have tried to meet this demand. Within this context, the multicomponent condensation, as the reaction that results in the formation of xanthenediones (Figure 1), appears as a good strategy. Several methodologies for xanthenedione synthesis have been developed, which can be divided according to the catalyst used: Lewis acid, Brønsted acid, organocatalysts, ionic liquids, and nanocatalysts.

In the following sections, it will be discussed different groups of catalysts that have been employed in the preparation of xanthenediones. As someone will realize, each method has its merit and limitations [21].

Lewis acids

Xanthenedione synthesis using Lewis acids as catalysts, in the absence of solvents, has received particular attention (Table 1). Most of the solvent- free catalytic processes are heterogeneous in nature, as in the case of iron(III) sulfate heptahydrate ($Fe(SO_4)_3 \cdot 7H_2O$) [22], tin chloride dihydrate ($SnCl_2 \cdot 2H_2O$) [23], silica-supported antimony trichloride ($SbCl_3/SiO_2$) [24], zirconyl chloride octahydrate ($ZrOCl_2 \cdot 8H_2O$) [25], zinc nitrate ($Zn(NO_3)_2$) [26], silica-supported diphosphorus pentoxide (P_2O_5/SiO_2), Silphos ($[PCl_{3-n}(SiO)_2]_n$) [27], ceric ammonium nitrate supported on zeolite (CAN/HY-zeolite) [28], and triethylammonium acetate/gallium trichloride (TEAA/$GaCl_3$) [29]. Although the described methods are heterogeneous, the reuse of the catalyst, an important parameter regarding heterogeneous catalysis, is mentioned only in the cases of $SnCl_2 \cdot 2H_2O$, $SbCl_3/SiO_2$ and $ZrOCl_2 \cdot 8H_2O$. No significant loss of catalytic activity occurred for these materials.

In addition to the investigation of Lu and co-workers in 2008, which describes the use of $ZrOCl_2 \cdot 8H_2O$, Mosaddegh and co-authors also had success with the use of this catalyst in the synthesis of xanthenediones [30]. In the Mosaddegh´s investigation, the employed reaction conditions were a little milder (85 °C), and the amount of the catalyst was reduced to 2 mol%. Besides, yields higher than 90% were achieved, and reaction times ranging from 10 to 35 minutes.

The synthesis of 1,8-dioxo-octahydroxanthene derivatives employing indium(III) chloride ($InCl_3$) and diphosphorus pentoxide (P_2O_5) by Verma and collaborators [31] is homogeneous in nature, being highly regio and chemoselective.

In all cases mentioned so far, xanthenediones were obtained with high yields, in short reaction times and simple preparation procedures. All of these advantages are in agreement with the Green Chemistry principles.

Table 1. Methodologies for the preparation of xanthenediones using Lewis acids as catalysts

Entry	Catalyst	Reactions conditions	Reaction time/Yield (%)
1	$Ba(ClO_4)_2$	CH_3CH_2OH, reflux, 15 mol%	3 h/91
2	$CeCl_3 \cdot 7H_2O$	CH_3CH_2OH/H_2O, reflux, 10 mol%	3-7 h/82-92
3	I_2	$(CH_3)_2CH(OH)$, 70-80 °C, 20 mol%	16-20 min/90-96
4	CAN	$(CH_3)_2CH(OH)$, 50 °C, 5 mol%	35-60 min/89-98
5	I_2/Zn	CH_3OH, 70 °C, 1-15 mol%	89-95
6	$MgSO_4$	CH_3OH, reflux, 1 mmol	1-2 h/65-80
7	$SiCl_4$	$ClCH_2CH_2Cl$, 60-70 °C, 20 mol%	2-3 h/85-95
8	ZnO/CH_3COCl	CH_3CN, reflux, 30 mol%	6-15 h/85-92
9	$In(OTf)_3$	Toluene, reflux, 30 mol%	4-6 h/71-98
10	$KAl(SO_4)_2 \cdot 12H_2O$	H_2O, 80 °C, 10 mol%	25-60 min/90-96
11	$SmCl_3$	H_2O, 100 °C, 20 mol%	8-24 h/20-98
12	$ZnCl_2$	H_2O, 120 °C, 25 mol%	45-180 min/75-97
13	$Y(NO_3)_3 \cdot 6H_2O$	H_2O, reflux, 10 mol%	20-75 min/86-96
	$SnCl_2 \cdot 2H_2O$	Solvent-free, 100 °C, 10 mol%	30-110 min/84-96
14	$Fe(SO_4)_3 \cdot 7H_2O$	Solvent-free, 120 °C, 10 mol%	1-4.5 h/71-94
15	CAN/HY-zeolite	Solvent-free, 80 °C, 0.1 g	45-160 min/74-93
16	$InCl_3$	Solvent-free, 100 °C, 15 mol%	15-70 min/58-98
	P_2O_5	Solvent-free, 100 °C, 20 mol%	20-74 min/56-96
17	P_2O_5/SiO_2	Solvent-free, 80 °C, 0.12 g	1-4 h/76-97
	$[PCl_{3-n}(SiO)_2]_n$	Solvent-free, 80 °C, 1.0 g	1-3.5 h/83-97
18	$SbCl_3/SiO_2$	Solvent-free, 120 °C, 10 mol%	45-80 min/85-95
19	$Zn(NO_3)_2$	Solvent-free, 110 °C, 6 mol%	10 min/90
20	$ZrOCl_2 \cdot 8H_2O$	Solvent-free, 120 °C, 10 mol%	40-80 min/75-96
21	$TEAA/GaCl_3$	Solvent-free, 65 °C, 2 mL	30-45 min/86-96
22	[Fe(III)(Salen)Cl]	IL, 110 °C, 10 mol%	10-60 min/52-98
23	$BiCl_3$	IL, 60 °C, 0.1 mmol	5-7 h/85-95
24	$FeCl_3 \cdot 6H_2O$	IL, 80 °C, 10 mol%	5-7 h/85-95
25	$InCl_3 \cdot 4H_2O$	IL, 80 °C, 10 mol%	4-10 h/76-95

Ceric ammonium nitrate (CAN) has been extensively explored by researchers in the synthesis of xanthenediones. The most recent work was reported by Sivaguru and Lalitha [28], in which the authors supported CAN in zeolite and described a method under solvent-free conditions. In this methodology, the products were obtained in high yields and in short reaction times. Related work reported the use of CAN as the catalyst, under homogeneous reaction conditions, and in the presence of water. This method also resulted in the formation of xanthenediones with high yields. Inspired by the methodologies cited above, the research group of Mulakayala and colleagues [33] (Table 1, entry 4), has described an ultrasound assisted method.

As can be observed in Table 1, other methods are in line with the principles of Green Chemistry, as in the case of dodecahydrate alumen potassium ($KAl(SO_4)_2 \cdot 12H_2O$) [34], samarium chloride ($SmCl_3$) [35], zinc chloride ($ZnCl_2$) [36] and hexahydrate yttrium nitrate ($Y(NO_3)_3 \cdot 6H_2O$) [15], since these catalysts were used in processes in which water was the solvent. Another important feature to be highlighted is regarding the availability, cost, and toxicity of these catalysts, which, in general, are commercially available, cheap and non-toxic. In addition to these advantages, the methodologies reported by Ilangovan

and co-authors [35] and Ganesan and colleagues [36] demonstrated the possibility of reusing the catalysts $SmCl_3$ and $ZnCl_2$. Despite of this advantage, the reaction times were longer and the yields were lower when compared to the methods that used alumen and yttrium nitrate.

One class of solvents which has been used in the synthesis of xanthenediones is the ionic liquids (IL), also known as fused salts. These are known as "green solvents". Motivated by this premise, researchers have developed xanthenedione synthesis methods that employ IL and the following Lewis acids as catalysts: *N*,*N'*-bis (salicylidene) ethylenediamine iron(III) ([Fe (III) (Salen) Cl]) [37], bismuth(IIII) chloride ($BiCl_3$) [38], iron(III) chloride hexahydrate ($FeCl_3 \cdot 6H_2O$) [39] and indium(III) tetrahydrate chloride ($InCl_3 \cdot 4H_2O$) [40]. There are advantages of using these fused salts, such as they can be easily filtered off and/or removed from the crude reaction mixture, in most of the cases, by simple decantation. Furthermore, the ionic phase in which the catalyst is found can be reused in new batch processes without loss of activity. Despite the high yields obtained (Table 1, entries 22-25) and the mentioned benefits, the ionic liquids have an inherent disadvantage, which is related to their high costs.

Besides the use of solvents regarded as green, there are methodologies that use organic solvents (Table 1, entries 1-9) in combination with Lewis acids. For these methods, the catalysts barium perchlorate ($Ba(ClO_4)$) [41] and cerium chloride hexahydrate ($CeCl_3 \cdot 7H_2O$) [42], molecular iodine (I_2) [43], molecular iodine and zinc (I_2/Zn) [44], magnesium sulfate ($MgSO_4$) [45], silicon tetrachloride ($SiCl_4$) [46], zinc oxide/acetyl chloride (ZnO/CH_3COCl) [47] and indium(III) triflate ($In(OTf)_3$) [48], have been described. In particular, the methodology described by Rong and colleagues [44] reports the synthesis of xanthenediones from a multicomponent reaction mixture containing I_2/Zn, methanol, dimedone and imines. It is important to mention that most articles involving the preparation of xanthenediones use aromatic aldehydes instead of imines. Moreover, unlike other studies, zinc powder behaves as a co-catalyst. Despite these relevant aspects, this methodology uses methanol, a solvent with recognized toxicity, and it does not describe the reaction time for each synthesized compound. Subsequently, Mulakayala and co-workers [43] improved the method discussed above, replacing the imine by aromatic aldehydes, changing the solvent for propan-2-ol and removing zinc powder. Thus, they obtained xanthenediones with high yields and in short reaction times.

In general, the methods carried out in organic solvents (Table 1) use inexpensive catalysts; one exception to this statement is $In(OTf)_3$. The method which utilizes this catalyst results in the preparation of 1,8-dioxo-octahydro-xanthenes in two stages, unlike the other methods described which correspond to multicomponent reactions. Recently, Karami and colleagues [49] published a study employing $InCl_3$, similar to that reported by Verma and co-authors. These authors employed milder reaction conditions (80 °C) and 10 mol% catalyst loading. Under these reaction conditions, xanthenediones were obtained in high yields and in short periods of time (88-96%/40-70 min). The most common reasons for using this metal include its low toxicity, compatibility with air and water, the operational simplicity of the reactions in which it is used, and outstanding capacity to suppress side reactions as in the case of the presence of sensitive groups to acidic reaction conditions.

Brønsted acid

Mineral acids are Brønsted acids, which are well known and widely used in organic synthesis. The use of hydrochloric acid (HCl) [50], sulfuric acid (H_2SO_4) [51]

and metaphosphoric acid ($(HPO_3)_n$) [49] for the preparation of xanthenediones has been described. However, the use of these acids has some disadvantages such as corrosion of reactors, more laborious work up, and difficulty in the reuse of the catalysts because the processes that they are involved are homogenous in nature [50,51]. Despite these drawbacks, xanthenediones preparation processes employing these acids occur with high yields and in short reaction times, as it can be seen in Table 2, entries 3, 6 and 11.

In order to avoid problems related to the use of mineral acids, many researchers have sought alternatives to convert them into heterogeneous catalysts. In this regard, mineral acids supported on oxides have been considered an attractive alternative. These catalysts have unique properties, such as high efficiency due to the large contact surface, low toxicity and increased stability, reuse capacity, selectivity and they are easy to manipulate [52]. The Seyyedhamzeh group [53] employed supported on silica sulfuric acid (SiO_2-OSO_3H) and obtained excellent conversion for the target products (xanthenediones), in short reaction times and in the absence of a solvent. It is noteworthy that in addition to being inexpensive and easy to be prepared, this catalyst can be recycled and reused. Later, Pramanik and Bhar [54] published a study using alumina-supported sulfuric acid (OSO_3H/Al_2O_3). Unlike the methodology developed by Seyyedhamzeh, in Pramanik and Bhar's study, solvent was used and the reaction times were longer. The silica covalently anchored sulfonic acid (SiO_2-R-SO_3H) [55] was also synthesized and evaluated in the preparation of 1,8-dioxo-octahydroxanthenes. It is a low cost, recyclable catalyst, and compatible with several functional groups. In addition, the method catalyzed by this anchored sulfonic acid does not require a solvent.

Another class of mineral acids, phosphoric acid derivatives were also submitted to adsorption/impregnation processes on oxides to become heterogeneous catalysts. In the method developed by Kantevari and colleagues [56], using polyphosphoric acid adsorbed on silica (PPA-SiO_2) as the catalyst, the formation of xanthenodiones under three different conditions was evaluated. The researchers conducted the reactions in the absence of solvent and in the presence of water and acetonitrile. The results showed that those reactions conducted in water resulted in the formation of the intermediate 2,2'- aryl-methylene-*bis*(3-hydroxy-cyclohex-2-enones) as the main products, while the processes carried out in the absence of solvent resulted in xanthenediones in high yields. For the reactions run in acetonitrile, long periods of time were necessary to get the tricyclic product.

Two other phosphorus-based catalysts are phosphate anchored MnO_2 and phospho-sulfonic acid (PSA) [58]. In both cases, the catalyst was recycled and reused without the loss of activity. The reaction conditions were similar as it can be seen in Table 2, entries 12 and 23. Among the advantages of these methods are the low cost and easy preparation of the catalysts, the high yields achieved in the transformations, short reaction times, and no need for solvents.

Iron(III) hydrogen sulfate ($Fe(HSO_4)_3$) [59], tetrabutylammonium hydrogen sulfate ($(CH_3CH_2CH_2CH_2)_4N(HSO_4)$) [60] and sodium hydrogen sulfate supported on silica ($NaHSO_4 \cdot SiO_2$) [61], have also been utilized in xanthenedione synthesis. In general, excellent yields were obtained with these catalysts (Table 2, entries 5, 7 and 8). Another advantage associated with the use of ($Fe(HSO_4)_3$) and ($NaHSO_4 \cdot SiO_2$) is the fact that they are employed under heterogeneous conditions, allowing easy separation at the end of the reaction and the possibility of recycling and reuse. Although ($(CH_3CH_2CH_2CH_2)_4N(HSO_4)$) does not present the characteristics previously mentioned, it has the benefit of keeping unchanged the compounds containing sensitive groups to acidic conditions (Entry 7). Furthermore, the solvent system employed in the reaction

enables the separation of the product by simple filtration, since there are solubility differences between the starting material and the synthesized compounds.

Table 2. Methodologies for xanthenediones synthesis using Brønsted acids as catalysts

Entry	Catalyst	Reaction conditions	Reaction time/Yield (%)
1	HPWA/MCM-41	CH_3CH_2OH, 90 °C, 20 mol%	5 h/81-94
2	OSO_3H/Al_2O_3	CH_3CH_2OH, reflux, 200 mg	3-8 h/77-89
3	HCl	CH_3CH_2OH 80%, reflux, 10 drops of concentrated HCl	20-30 min/60-95
4	PMA-SiO_2	CH_3CN, reflux, 0,1 mol%	4-5 h/15-96
5	$NaHSO_4$-SiO_2	CH_3CN, reflux, 100 mg	6-6.5 h/90-98
6	H_2SO_4	H_2O, 70-80 °C, 0,1 mL	2 h/84-95
7	TBAHS	H_2O/Dioxan, reflux, 10 mol%	3-3.5 h/88-94
		H_2O, reflux, 0.14 mmol	1.5-3 h/70-94
8	$Fe(HSO_4)_3$	Solvent-free, 120 °C, 0.14 mmol	5-18 min/81-98
		Solvent-free, 450 W, 0.29 mmol	3-11 min/70-93
9	Dowex-50W	Solvent-free, 100 °C, 0.4 g	2-5 h/78-91
10	Nafion-H	Solvent-free, 125 °C, 485 mg	12 h/74-91
11	$(HPO_3)_n$	Solvent-free, 80 °C, 8 mol%	40-100 min/85-95
12	PSA	Solvent-free, 110 °C, 5 mol%	20-55 min/88-98
13	$Mn(H_2PO_4)_2 \cdot 2H_2O$	Solvent-free, 100 °C, 10 mol%	15-45 min/85-98
14	MSA	Solvent-free, 100 °C, 5 mol%	30-110 min/86-96
15	PPA-SiO_2	Solvent-free, 140 °C, 10 mol%	30 min/71-93
16	SiO_2-OSO_3H	Solvent-free, 80 °C, 0.03 g	1-2.5 h/88-97
17	SiO_2-R-SO_3H	Solvent-free, 80 °C, 5-20 mol%	3.5-5 h/35-93

The Shaterian group [59] explored the use of $Fe(HSO_4)_3$ as catalyst, performing reactions under different conditions: without the presence of solvent, using conventional heating (120 °C); without the presence of solvent and employing heating by microwave at a power of 450 W and using H_2O as solvent. Among the mentioned conditions, those with no solvent showed to be more attractive, since they resulted in the desired products in high yields and with shorter reaction times.

Heteropolyacids (HPAs) have a significantly higher Brønsted acidity than mineral acids; their catalytic activity, for example, is 10-1000 fold higher than H_2SO_4. This is one of the reasons of using HPAs as phosphomolybdic acid supported on silica gel (PMA-SiO_2) [62] and phosphotungstic acid supported on molecular sieves (HPWA/MCM-41) [63] for the synthesis of 1,8-dioxo-octahydroxanthenes. As it can be seen in Table 2, entries 1 and 4, high yields were obtained with these catalysts in the preparation of xanthenediones. Another advantage associated with the use of these catalysts is the possibility of recycling and reuse of them at the end of the reaction. As an important drawback, in general, these methods require the presence of organic solvents.

Polymer resins such as Dowex-50W (cation exchange sulphonic acid resin) [64] and Nafion-H (perfluorinated sulfonic acid resin) [65] were also evaluated as catalysts in the synthesis of xanthenediones. These materials are inexpensive, recyclable, their reactions are easy to be carried out and are high-yielding chemical transformations.

Another catalyst of low cost and easy preparation is molybdate sulfonic acid (MSA) described by Karami and colleagues [66]. The condensation processes between aromatic aldehydes and cyclic diketones, catalyzed by this acid, are operationally simple, and the catalyst can be reused after processes are finished. In addition, the reactions are completed in a short period of time.

Lewis and Brønsted acid

The catalysts that have in their structures Lewis and Brønsted acid character were also investigated in the condensation between aromatic aldehydes and cyclic diketones. In addition to presenting that characteristic in their structure, Montmorillonite clays are environmentally harmless, reusable, non-toxic, non-corrosive, inexpensive and readily available. With these characteristics in mind, two groups of researchers evaluated the use of different clays belonging to this class in the synthesis of xanthenediones. The first report by Song and co-authros [67] describes as catalyst Fe^{3+}-montmorillonite, that is, Fe^{3+} was introduced into the matrix of K10 montmorillonite. This procedure raised Lewis acidity of the catalyst thereby providing excellent yields of the condensation products. A year later, the group of Dabiri [68] evaluated K10 montmorillonite in the absence of solvent and the desired products were obtained with synthetically useful yields and shorter reaction times.

Metal oxide sulfates also present this duality with respect to the acid sites. Those materials are easy to prepare, can be reused and are environmentally innocuous. These characteristics encouraged investigators to use tin sulfate (SnO_2/SO_4^{2-}) [69] and titanium sulfate (TiO_2/SO_4^{2-}) [70] in the synthesis of 1,8-dioxo-octahydroxanthenes. High yields were obtained in both cases, but reactions in the presence of TiO_2/SO_4^{2-} were performed under milder conditions (Table 3, entries 4 and 5). Despite this advantage, a longer reaction time was required.

Another catalyst that presents Lewis and Brønsted acid sites is iron (III) chloride supported on silica ($FeCl_3$-SiO_2) [71]. It was employed in two different reaction conditions, both in the absence of solvent: conventional heating (120° C) and heating by microwave radiation at a power of 450 W. Good yields were found in both cases; however, the reactions conducted in microwave led to an even shorter time for the formation of the desired product.

Table 3. Synthetic methods for the preparation of xanthenediones using catalysts having Lewis and Brønsted acid sites

Entry	Catalyst	Reaction conditions	Reaction time/Yield (%)
1	Montmorillonite K10	Solvent-free, 100 °C, 0.3 g	1-2 h/75-86
2	$FeCl_3$-SiO_2	Solvent-free, 120 °C, 0.03 g	6-50 min/76-95
		Solvent-free, 450 W, 0.03 g	4-17 min/60-89
3	Fe^{3+}-montmorillonite	CH_3CH_2OH, 100 °C, 15 mol%	6 h/84-96
4	SnO_2/SO_4^{2-}	CH_3COOH, reflux, 10 mol%	4-5.5 h/75-88
5	TiO_2/SO_4^{2-}	Solvent-free, 25 °C, 100 mg	24 h/87-92

Organocatalysts

The term organocatalyst relates to the connection between the words organic and catalyst. An organocatalyst corresponds to a low molecular weight organic molecule that in under-stoichiometric amounts catalyzes a chemical reaction. The organocatalyst may be composed of C, H, N, S, and P, and it even may be chiral or achiral. In addition, they are classified according to their acidity and basicity, therefore divided into five groups:

Lewis acid, Lewis base, Brønsted acid, Brønsted base, and bifunctional, where the later presents Lewis base and Brønsted acid sites in their structures [72].

Since the 1990s, the use of this class of catalysts has increased significantly, which may be evidenced by the increasing number of publications related to this theme [73]. The use of organocatalysts has important advantages, such as: in general, the substances used as organocatalysts exhibit stability when exposed to the air, they can be stored, they are low cost, easy to be obtained and have low toxicity. In addition, many reactions employing organocatalysts require no special precautions, such as the use of inert atmosphere and anhydrous solvents for their performance. It should also be highlighted the fact that reactions with organocatalysts do not involve transition metals, an important benefit when the objective is metal-free products, such as substances designed to pharmaceutical applications [72].

All these advantages have led several researchers to evaluate the activity of different organocatalysts in xanthenedione synthesis. Organic compounds that have been used for this purpose are, mostly, Brønsted acids, such as *p*-dodecylbenzenesulfonic acid (DBSA) [74], lignin sulfonic acid (LSA) [75], 1,4-diazabicyclo[2.2.2]octane bromide (TDB) [76], *p*-toluenesulfonic acid (*p*-TSA) [77], citric acid [78], melanin trisulfonic acid (MTSA) [79], hydroxylamine-O-sulfonic acid (HOSA) [80], sulphone saccharin acid (SaSA) [81], ascorbic acid [82], trichloroisocyanuric acid (TCCA) [83], trifluoroacetic acid (TFA) [84], amberlyst-15 [85], pentafluorophenyl ammonium triflate (PFPAT) [86] and mesoporous silica grafted on propyl sulphonic acid (LUS-Pr-SO_3H) [87]. Table 4 shows that the reactions conducted in the presence of Brønsted acid character organocatalysts may occur, mostly, in the absence of a solvent or in the presence of H_2O.

The reactions carried out in accordance with the principles of Green Chemistry, regarding the non-use of organic solvents, afforded xanthenediones in high yields and short reaction times, except for the catalysts DBSA and citric acid which their reactions took 6 hours to completion (Table 4, entries 1 and 15). In order to overcome this disadvantage inherent to the use of DBSA, an ultrasound-assisted methodology was developed [88] which reduced the reaction time in 1 hour, the reaction temperature was decreased to 25-30 ^oC and, the yields were similar to previously found ones.

The Lewis bases are another important group of organocatalysts. Among those used in the condensation of aromatic aldehydes and cyclic diketones are 1,4-diazobicycle [2.2.2]octane (DABCO) [89], 2,4,6-trichloro-1,3,5-triazine (TCT) [90], trizme [91], and thiourea (NH_2CSNH_2) [92]. Regarding these organocatalysts, high yields of xanthenediones were obtained in short reaction times. However, the authors did not mention the yield found for the described xanthenodione in the methodology using thiourea; the main purpose of the article was the preparation of pyrimidin-2-thiones derivatives.

An important peculiarity observed with regard to the use of TCT is that in free-solvent conditions, this organocatalyst did not lead to the formation of xanthenediones. To make this possible, the researchers added two drops of H_2O in the system, which resulted in the reaction between TCT and water with the formation of HCl and cyanuric acid *in situ*. As previously described, HCl acts as an effective Brønsted acid in condensation reactions.

Two bifunctional organocatalysts were also studied, namely thiourea dioxide (TUD) [93] and imidazol-1-yl-acetic acid [94]. The existence of these functionalities in

the molecules make them ideal for condensation reactions aiming the preparation of xanthenediones, as it can be seen in Table 4 (entries 3 and 16).

The organic salts polyaniline-*p*-toluenesulfonate (PANI-PTSA) [95], sodium dodecylphosphonate (Na_2DP) [96] and aluminum dodecyl sulfate trihydrate ($[Al(DS)_3]\cdot 3H_2O$) [97] were evaluated in xanthenedione synthesis. Good yields were obtained in the processes involving these catalysts. However, in some cases, [94,95] reaction times were too long. Nevertheless, PANI-PTSA and $[Al(DS)_3]\cdot 3H_2O$ catalysts could be recycled and reused at the end of the reactions.

In addition to the aforementioned organocatalysts, others such as polyethylene glycol (PEG-6000) [98], ß-cyclodextrin (ß-CD) [99], ß-cyclodextrin grafted with sulphonic butyl acid (ß-CD-BSA) [100], hypervalent iodine (DIB) [101], *N*-bromosuccinimide (NBS) [102] and tetramethylsylil chloride (TMSCl) [103] have been described in xanthenediones synthesis and, in general, the desired products were obtained with excellent yields. However, some of these organocatalysts have some particular characteristics regarding the mechanism of action. PEG-6000 and ß-CD activate the aldehyde through hydrogen-bonding thereby contributing to the reaction process. For ß-CD-BSA, there are some BSA-derivative acid groups with Brønsted acid character.

In relation to the role of NBS in the condensation reactions that afford xanthenediones, two hypotheses have been reported. The first suggests that the NBS generates Br^+ ions, therefore, activating the aldehyde. In the second, the NBS forms small amounts of HBr and Br_2 in the reaction medium and HBr may be the effective catalyst for the reaction. The results obtained by these authors are in agreement with reports by Karimi and colleagues, who describe the formation of Br^+ in the presence of *N*, *N*-dimethylacetamide (DMAC) and HBr generation in protic solvent such as ethanol (CH_3CH_3OH).

Two other interesting methodologies, not shown in Table 4, were developed for the xanthenedione syntheses. The first was described by He and colleagues [104] who used glycerol as solvent and catalyst for the reaction. Glycerol activated carbonyl group of the aldehyde via hydrogen-bonding, accelerating the reactions, leading to the formation of xanthenediones in yields ranging from 50% to 99%, and with reaction times ranging from 2.5 to 6.0 hours. The second used different aldehyde derivatives of formyl phenoxy acetic acid [105], which has an acid group in its structure. This enabled this reagent to act as Brønsted acid during the reaction, also providing good yields (80% to 86%) in a short period of time (10 min).

Table 4. Synthetic methodologies for the preparation of xanthenediones that utilizes organocatalysts

Entry	Catalyst	Reaction conditions	Reaction time/Yield (%)
1	DBSA	H_2O, reflux, 10 mol%	6 h/89-96
2	Na_2DP	H_2O, reflux, 3,2 mg	24-48 h/73-98
3	TUD	H_2O, 50-60 ^oC, 2%	30-50 min/82-97
4	LSA/TBAB	H_2O, 450 W, 5/2 mol%	1-5 min/88-96
5	PEG-6000	H_2O, 90 ^oC, 5 mol%	1.3-4 h/88-97
6	TDB	H_2O, reflux, 1 mol%	1-2.5h/80-90
7	PANI-PTSA	H_2O, reflux, 25 mol%	6 h/73-84
8	β-CD	H_2O, 60-65 ^oC, 100 mol%	10-12 h/80-96
9	β-CD-BSA	H_2O, reflux, 1 mol%	15-60 min/88-97
10	DABCO	H_2O, reflux, 10 mol%	30-60 min/76-96

11	DIB	H_2O, reflux, 5 mol%	20-60 min/84-95
12	TCT	Solvent-free, 120 °C, 10 mol%	40-70 min/87-95
13	$[Al(DS)_3]\cdot 3H_2O$	Solvent-free, 80 °C, 20 mol%	10-55 min/75-93
14	*p*-TSA	Solvent-free, 80 °C, 30 mol%	15-30 min/97-99
15	Citric acid	Solvent-free, 90 °C, 1200 mol%	6 h/73-85
16	Imidazol-1-yl acetic acid	Solvent-free, 60 °C, 60 mol%	7-15 min/85-95
17	MTSA	Solvent-free, 80 °C, 5 mol%	5-25 min/87-94
18	HOSA	Solvent-free, 90 °C, 5 mol%	15-40 min/80-95
19	SaSA	Solvent-free, 90 °C, 15 mol%	10-45 min/90-97
20	TFA	Solvent-free, 75 °C, 20 mol%	20-30 min/91-97
21	LUS-Pr-SO_3H	Solvent-free, 140 °C, 0,02 g	5-15 min/80-94
22	NBS	CH_3CH_2OH, reflux, 20 mol%	10-12 h/82-96
		DMAC, 600 W, 20 mol%	4-8 min/75-93
23	Trizma	CH_3CH_2OH, reflux, 100 mmol%	5 h/63-90
24	Ascorbic acid	CH_3CH_2OH, reflux, 5,6 mol%	6 h/80-88
25	TCCA	CH_3CH_2OH, reflux, 0,01 g	0.5 h/80-95
26	Amberlyst-15	CH_3CN, reflux, 200 mg	5 h/90-96
27	TMSCl	CH_3CN, reflux, 10 mmol	8-10 h/72-84
28	NH_2CSNH_2	CH_3OH, 600 W, 100 mol%	2-3 min
29	PFPAT	Toluene, 25-30 °C, 10 mol%	3-5 h/85-97

Ionic liquids

Ionic liquids (ILs) are considered important solvents and catalysts as they have organic and ionic nature in their constitution. This feature enables these liquids to interact with the reacting species and transition states. Interactions allow the reduction of activation energy, either by stabilizing the transition states or by improving reagent reactivities. As a result, the catalytic activity of ILs strongly relies upon their physical and chemical properties, which are directly connected with the cations and anions that constitute them [106]. Furthermore, the reactions using ILs as solvent or catalyst are inserted in the context of Green Chemistry due to their non-volatility, non-flammability and potential recycling and reuse.

All these properties and advantages led several researchers to propose synthetic methodologies for xanthenedione preparation by including ILs in the reaction mixture. As it can be seen in Table 5, excellent yields were obtained in short reaction times for all evaluated ILs. Among the described ILs, there are those known as Brønsted acids, that is, they present useful characteristics of the solids with acid character and mineral acids. The 2-pyrrolidone hydrogen sulfate ([H-NMP]·[HSO_4]) [107], *N*,*N*,*N*-trimethyl-*N*-propane sulfonic acid ammonium hydrogen sulfate ([TMPSA]·[HSO_4]) [108], 1-butyl-3-methyllimidazolium acid hydrogen sulfate ([bmim]·[HSO_4]) [109], triethylamine dihydrogen fosfate ([Et_3 NH]·[H_2PO_4]) [110], triethylamine hydrogensulfate ([Et_3NH]·[HSO_4]) [111] are some examples of ILs that present Brønsted acid characteristics and used as catalysts in condensation reactions of aldehydes and diketones for xanthenedione synthesis. In particular, researchers have studied the effect of [TMPSA]·[HSO_4] and [bmim]·[HSO_4] in xanthenedione synthesis and evaluated other ionic liquids, which showed lower activity than those previously mentioned.

In addition, Salvi group [112] published a study in 2011 which evaluated the catalytic activity of six different ionic liquids, [BMIM]·[BF_4], [CMIM]·[HSO_4], [NMP]·[HSO_4], [BMIM]·[HSO_4], [$(CH_2)_4SO_3$HMIM]·[HSO_4] and [BMIM]·[H_2PO_4] in the xanthenedione synthesis derived from benzaldehyde and dimedone. The catalytic loading range from 10 to 20 mol%. Among these, only [BMIM]·[BF_4] (20 mol%), which has no counter-ion with Brønsted acid character, led to a low yield product (8.9%). The best IL correspodend to [CMIM]·[HSO4], which afforded the xanthenedione product in high yield (90%), in 2.5 h, even when it was utilized in smaller amount (5 mol%).

The mentioned catalysts present Brønsted acid character mainly related to the counter-ion, but in other cases, this acidity is directly connected to the ion itself. This is the case of 1-*n*-butyl imidazolium tetrafluoroborate ([Hbim]·[BF_4]) [113], 1-carboxymethyl-3-methylimidazolium tetrafluoroborate ([cmmim]·[BF_4]) [114], 1-(3,4-dichlorobenzenesulfonyl)-3-methyl-1H-imidazolium chloride ([3,4-dcbsmin]·[Cl]) [115], 1-butyl-3-methylimidazolium perchlorate ([bmim]·[ClO_4]) [116] and triethylamine chloride linked to sulphonic acid ([$Et_3N–SO_3H$]·[Cl]) [117]·

Other ionic liquids such as 1,3-dibromo-5,5-dimethylhydantoin (DBH) and benziltrifenil phosphonium tribromide (BTPTB) [118] and magnesium *bis*-tetrafluoroborate doped in 1-butyl-3-methylimidazolium tetrafluoroborate ([BMIm][BF_4]-$Mg(BF_4)_2$) [106] were also tested. However, the active catalytic species was the Br^+ for the former and Mg^{2+} for the latter, unlike those cited so far involving Brønsted acidity, either from the ion or from the counter-ion.

Table 5. Xanthenedione synthesis catalyzed by ionic liquids

Entry	Catalyst	Reaction conditions	Reaction time/Yield (%)
1	[Hbim]·[BF_4]	CH_3OH, 30 °C, 2 mL	30-90 min/75-95
2	[TMPSA]·[HSO_4]	H_2O, 100 °C, 10 mol%	1-2 h/88-95
3	[cmmim]·[BF_4]	H_2O, 80 °C, 20 mol%	2 h/83-91
4	[3,4-dcbsmin]·[Cl]	H_2O, MW, 10 mol%	3-5 min/85-95
5	[H-NMP]·[HSO_4]	H_2O, Ultrasound, 20 mol%	40-75 min/70-94
6	DBH	Solvent-free, 100 °C, 5 mol%	1-14 min/80-93
	BTPTB		2-29 min/76-94
7	[bmim]·[HSO_4]	Solvent-free, 100 °C, 1 mL	20-40 min/82-95
8	[bmim]·[BF_4]-$Mg(BF_4)_2$	Solvent-free, 80 °C, 1 mL	15-30 min/81-97
9	[bmim]·[ClO_4]	Solvent-free, 100 °C, 4 mmol	40-90 min/85-95
10	[Et_3NH]·[H_2PO_4]	Solvent-free, 100 °C, 0.4 g	5-30 min/84-96
11	[Et_3NH]·[HSO_4]	Solvent-free, 100 °C, 20 mol%	20-70 min/82-97
12	[$Et_3N–SO_3H$]·[Cl]	Solvent-free, 80 °C, 25 mol%	30-60 min/85-97

Nanocatalysts

Nanocatalysts are nanometer scale (10^{-9} m) materials that gather characteristics of homogeneous and heterogeneous catalysts. Therefore, they show some advantages such as high catalytic activity, high selectivity, in addition to being easily removed from the reaction medium due to their insolubility. These properties are directly related to the effects of surface and electronics, which are differentiated when substances/compounds are on this scale. Because of this, several reports have been published on the use of nanocatalysts in the synthesis of 1,8-dioxooctahydroxanthenes.

The metal oxides at nanometric scale have unusual physicochemical properties, due to the several and enhanced reactive sites on the surface that may be formed. As a consequence, most described nanocatalysts are metal oxides, as it can be seen in Table 6.

Table 6. Synthetic methodologies using nanocatalysts for the synthesis of xanthenodiones

Entry	Catalyst	Reaction conditions	Reaction time/Yield (%)
1	$CuO\text{-}CeO_2$	H_2O, reflux, 0.05 g	5-60 min/86-92
2	Fe_3O_4	H_2O, 80 °C, 1 mol%	6-62 min/86-96
3	$MCM\text{-}41\text{-}SO_3H$	H_2O, 25 °C, 0.05 g	15-90 min/86-99
4	$SiO_2/H_{14}[NaP_5W_{30}O_{110}]$	H_2O, reflux, 0.5 mol%	3 h/82-96
5	$BiVO_4$	Solvent-free, 120 °C, 20 mg	3 s-6 min/90-99
6	CeO_2	Solvent-free, 110 °C, 0.15 g	6 h/71-92
7	$CuFe_2O_4$	Solvent-free, 120 °C, 15 mol%	5-30 min/80-95
8	ES/Fe_3O_4	Solvent-free, 80 °C, 100 mg	15 min/82-92
9	$Fe_3O_4\text{-}SiO_2\text{-}SO_3H$	Solvent-free, 110 °C, 0.05 g	4-8 min/88-97
10	$FeCl_3.SiO_2$	Solvent-free, 100 °C, 20 mol%	15-35 min/80-95
11	$P_4VPy–CuI$	Solvent-free, 80 °C, 0.1 g	7-36 min/85-91
12	TiO_2	Solvent-free, 100 °C, 10 mol%	15-90 min/81-96
13	VSA NRs	Solvent-free, 80 °C, 10 mol%	10-60 min/75-93
14	ZnO	Solvent-free, 120 °C, 30 mol%	45-120 min/80-93
15	Ni-Mg-ferrite	CH_3CH_2OH, reflux, 0.2 mg	180-210 min/90-98
16	ZrO_2/SO_4^{2-}	CH_3CH_2OH, reflux, 10 mg	60-70 min/85-94
17	ZnO	CH_3CH_2OH, reflux, 25 mol%	75-120 min/52-88
18	γ-alumina	CH_3CH_2OH, reflux, 10 mg	90-120 min/75-90
19	ZSM-5	CH_3CH_2OH, reflux, 10 mg	70-95 min/80-92

They are nanoparticles of copper oxide and cerium oxide ($CuO\text{-}CeO_2$) [119], ferrite (Fe_3O_4) [120], bismuth vanadate ($BiVO_4$) [121], cerium oxide (IV) (CeO_2) [122], ferrite copper ($CuFe_2O_4$) [123], ferrite coated with eggshell porous ceramic residues (ES/Fe_3O_4) [124], ferrite encapsulated in silica containing sulfonic acid groups ($Fe_3O_4\text{-}SiO_2\text{-}SO_3H$) [125], titanium oxide (TiO_2) [126], zinc oxide (ZnO) [127], Ni-Mg-ferrite (Ni-Mg-Fe_3O_4) [128] and γ-alumina (γ-Al_2O_3) [129]. Among these, ZnO nanoparticles are the most investigated ones. In addition to the methodology presented in Table 6, four other research groups [117,130,131,132] evaluated this nanocatalyst in xanthenediones synthesis. In general, yields and reaction times were similar; however, the methodos are dissimilar in terms of the methods used to prepare the nanoparticles, the amount of catalyst used, and the solvents utilized in the reactions.

Other nanomaterials had their catalytic activity measured, as it is the case of Preyssler acid ($SiO_2/H_{14}[NaP_5W_{30}O_{110}]$) [133], which belongs to the family of heteropolyacids, and iron(III) chloride ($FeCl_3\text{-}SiO_2$) [134], which were supported on silica. In addition, the molecular sieve with anchored sulfonic groups ($MCM\text{-}41\text{-}SO_3H$) [135], copper iodide immobilized in poly(4-vinylpyridine) ($P_4VPy\text{-}CuI$) [136], vanadate sulfuric acid (VSA) [137], zirconium sulfate (ZrO_2/SO_4^{2-}) [129] and zeolite (ZSM-5) [129] were evaluated.

The methodologies using nanocatalysts are in accordance with the concepts set by Green Chemistry in as much as they are recyclable and reusable, provide excellent yields of the produts in short reaction times, employ mild conditions and are conducted, in most cases, in the absence of organic solvents or in the presence of H_2O.

CONCLUDING REMARKS

In this book chapter, it was presented a variety of catalyzed methods that have been developed to prepared xanthenediones (1,8-dioxo-octahydroxanthenes). The preparation of these xanthene derivatives, tipically, involves reactions between aromatic aldehydes and 1,3-cyclohexanediones. Generally, these reactions afford the xanthenediones in good to excelent yields. The type of substituent attached to the aromatic ring of the aldehydes does not have influence on the reaction yields. It was attempted to point out the merits and limitations of the methodologies so far described in the literature. Considering that, from our point of view, it is not possible to establish the best catalytic methodology for the preparation of xanthenediones.

ACKNOWLEDGMENTS

The authors are greatful to Brazilian Agencies CNPq, CAPES, and Fundação de Amparo à Pesquisa de Minas Gerais (FAPEMIG—CEX APQ 01287/14) for financial support.

REFERENCES

[1] BHOWMIK, B. B.; GANGULY, P. Photophysics of xanthene dyes in surfactant solution. *Spectrochim. Acta A*, **2005**, *61*(9), 1997–2003.

[2] ION, R. M.; FRACKOWIAK D.; WIKTOROWICZ, K. The incorporation of various porphyrins into blood cells measured via flow cytometry, absorption and emission spectroscopy. *Acta Biochim. Pol.*, **1988**, *45*(3), 833–845.

[3] AHMAD, M.; KING, T. A.; KO, A. K.; CHA, B. H.; LEE, J. Performance and photostability of xanthene and pyrromethene laser dyes in sol–gel phases. *J. Phys. D Appl. Phys.*, **2002**, *35*(13), 1473–1476.

[4] KNIGHT, C. G.; STEPHENS, T. Xanthene-dye-labelled phosphatidylethanolamines as probes of interfacial pH. Studies in phospholipid vesicles. *Biochem. J.*, **1989**, *258*(3), 683–689.

[5] NAIDU, K. R. M.; KRISHNA, B. S.; KUMAR, M. A.; ARULSELVAN, P.; KHALIVULLA, I.; LASEKAN, O. Design, synthesis and antiviral potential of 14-aryl/heteroaryl-14*H*-dibenzo[a,j]xanthenes using an efficient polymer-supported catalyst. *Molecules*, **2012**, *17*, 7543-7555.

[6] KAYA, M.; DEMIR, E.; BEKCI, H. Synthesis, characterization and antimicrobial activity of novel xanthene sulfonamide and carboxamide derivatives. *J. Enzyme Inhib. Med. Chem.* **2013**, *28*(5), 885-893.

[7] POUPELIN, J. P.; SAINT-RUT, G.; FOUSSARD-BLANPIN, O.; NARCISSE, G.; UCHIDA-ERNOUF, G.; LACROIX, R. Synthesis and anti-inflammatory properties of bis(2-hydroxy-1-naphthyl)methane derivatives. I. Monosubstituted derivatives. *Eur. J. Med. Chem.*, **1978**, *13*(1), 67–71.

[8] ZELEFACK, F.; GUILET, D.; FABRE, N.; BAYET, C.; CHEVALLEY, S.; NGOUELA, S.; LENTA, B. N.; VALENTIN, A.; TSAMO, E.; DIJOUX- FRANCA, M. G. Cytotoxic and antiplasmodial xanthones from *Pentadesma butyracea*. *J. Nat. Prod.*, **2009**, *72*(5), 954–957.

[9] KUAN, L. C. Synthesis and characterisation of 1,3-dihydroxyxanthone derivatives and their antioxidant activities. Degree of Bachelor of Science (Hons.) Chemistry. University Tunku Abdul Rahman, October, **2012**.

[10] MASTERS, K. S.; BRÄSE, S. Xanthones from fungi, lichens, and bacteria: The natural products and their synthesis. *Chem. Rev.*, **2012**, *112*(7), 3717−3776.

[11] PINTO, D. C. G. A.; SECA, A. M. L.; LEAL, S. B.; SILVA, A. M. S.; CAVALEIRO, J. A. S. A novel short-step synthesis of new xanthenedione derivatives from the cyclization of 3-cinnamoyl-2-styrylchromones. *Synlett*, **2011**, 2005-2008.

[12] DEAN, F. M.; HERBSTEIN, F. H.; KAPON; M.; REISNER, G. M. Structure of the channel inclusion complex of 1,2,3,4-tetrahydro-6,8-dihydroxy-1,1,7-tris(3-methylbut-2-enyl)xanthen-2,9-dione (wightianone, zeyloxanthonone) with palmitic acid. *Acta Cryst.*, **1991**, 137-141.

[13] NEGI, J. S.; BISHT, V. K.; SINGH, P.; RAWAT, M. S. M.; JOSHI, G. P. Naturally occurring xanthones: Chemistry and biology. *J. Appl. Chem.*, **2013**, 1-9.

[14] MULAKAYALA, N.; MURTHY, P. V. N. S.; RAMBABU, D.; AELURI, M.; ADEPU, R.; KRISHNA, G. R.; REDDY, C. M.; PRASAD, K. R. S.; CHAITANYA, M.; KUMAR, C. S.; RAO, M. V. B.; PAL, M. Catalysis by molecular iodine: A rapid synthesis of 1,8-dioxo-octahydroxanthenes and their evaluation as potential anticancer agents. *Bioorg. Med. Chem. Lett*, **2012**. *22*(6), 2186–2191.

[15] NISAR, M.; ALI, I.; SHAH, M. R.; BADSHAH, A.; QAYUM, M.; KHAN, H.; KHAND, I.; ALIA, S. Amberlite IR-120H as a recyclable catalyst for the synthesis of 1,8-dioxo-octahydroxanthene analogs and their evaluation as potential leishmanicidal agents. *RSC Adv.*, **2013**, 21753-21758.

[16] MURTHY, Y. L. N.; MAHESH, P.; DEVI, B. R.; DURGESWARAI, L. K.; MANI, P. Synthesis and antibacterial assay of 9-substituted aryl-1,8-dioxo-octahydroxanthenes. *Asian J. Chem.*, **2014**, *26*(15), 4594-4598.

[17] RAHIMIFARD, M.; ZIARANI, G. M.; BADIEI, A.; ASADI, S.; SOORKI, A. A. One-pot solvent-free synthesis of 1,8-dioxooctahydroxanthene derivatives using sulfonic acid functionalized LUS-1 and their antimicrobial activities. *Res. Chem. Intermed.*, **2016**, *42*(4), 3847-3861.

[18] KHOEINIHA, R.; EZABADIA, A.; OLYAEI, A. An efficient solvent-free synthesis of 1,8-dioxooctahydroxanthenes using $Fe_2(SO_4)_3{\cdot}7H_2O$ as catalyst. *Iran. Chem. Commun.*, **2016**, *4*(3), 273-282.

[19] GANESAN, S. S.; KOTHANDAPANI, J.; GANESAN, A. Zinc chloride catalyzed collective synthesis of arylmethylene *bis*(3-hydroxy-2-cyclohexene-1-ones) and 1,8-dioxo-octahydroxanthene/acridine derivatives. *Lett. Org. Chem.*, **2014**, *11*(9), 682-687.

[20] JIN, T. S.; ZHANG, J. S.; XIAO, J. C.; WANG, A. Q.; LI, T. S. Clean synthesis of 1,8-dioxo-octahydroxanthene derivatives catalyzed by *p*-dodecylbenezenesulfonic acid in aqueous media. *Synlett*, **2004**, *5*(5), 866-870.

[21] BORAH, R.; DUTTA, P.; SARMA, P. Investigation of efficient synthesis of 1,8-dioxo-octahydroxanthene derivatives under solvent-free grinding method. *Curr. Chem. Lett.*, **2013**, *2*(4), 159–166.

[22] KHOEINIHA, R.; EZABADIA, A.; OLYAEI, A. An efficient solvent-free synthesis of 1,8-dioxooctahydroxanthenes using $Fe_2(SO_4)_3{\cdot}7H_2O$ as catalyst. *Iran. Chem. Commun.*, **2016**, 273-282.

[23] KARAMI, B.; ESKANDARI, K.; ZARE1, Z.; GHOLIPOUR, S. A new access to 1,8-dioxooctahydroxanthenes using yttrium(III) nitrate hexahydrate and tin(II) chloride dihydrate as effective and reusable catalysts. *Chem. Heterocyc. Compd.*, **2014**, *49*(12), 1715-1722.

[24] ZHANG, Z. H.; LIU, Y. H. Antimony trichloride/SiO_2 promoted synthesis of 9-ary-3,4,5,6,7,9-hexahydroxanthene-1,8-diones. *Catal. Commun.*, **2008**, *9*(8), 1715–1719.

[25] LU, H. Y.; LI, J. J.; ZHANG, Z. H. $ZrOCl_2.8H_2O$: a highly efficient catalyst for the synthesis of 1,8-dioxo-octahydroxanthene derivatives under solvent-free conditions. *Appl. Organomet. Chem.*, **2009**, *23*(4), 165–169.

[26] VAHABI, S. A. H.; HATAMJAFARI, F.; POURSHAMSIAN, K. One-pot synthesis of 1,8-dioxo-octahydroxanthene derivatives using $Zn(NO_3)_2$ under solvent-free conditions. *Orient. J. Chem.* **2014**, *30*(2), 849-851.

[27] HASANINEJAD, A.; DADAR, M.; ZARE, A. Silica-supported phosphorus-containing catalysts efficiently promoted synthesis of 1,8-dioxo-octahydroxanthenes under solvent-free conditions. *Chem. Sci Trans.*, **2012**, *1*(2), 233-238.

[28] SIVAGURU, P.; LALITHA, A. Ceric ammonium nitrate supported HY-zeolite: An efficient catalyst for the synthesis of 1,8-dioxo-octahydroxanthenes. *Chinese Chem. Lett.*, **2014**, *25*(2), 321–323.

[29] SURESH, D. K.; SANDHU, J. S. An efficient green protocol for the production of 1,8-dioxo-octahydroxanthenes in triethylammonium acetate (TEAA) a recyclable inexpensive ionic liquid. Rasayan *J. Chem.*, **2009**, *2*(4), 937-940.

[30] MOSADDEGH, E.; ISLAMI, M. R.; HASSANKHANI, A. $ZrOCl_2{\cdot}8H_2O$ as an efficient and recyclable catalyst for the clean synthesis of xanthenedione derivatives under solvent-free conditions. *Arab. J. Chem.*, **2012**, *5*(1), 77–80.

[31] VERMA, G. K.; RAGHUVANSHI, K.; VERMA, R. K.; DWIVEDI, P.; SINGH, M. S. An efficient one-pot solvent-free synthesis and photophysical properties of 9-aryl/alkyl-octahydroxanthene-1,8-diones. *Tetrahedron*, **2011**, *67*(20), 3698-3704.

[32] SHITOLE, B. V.; SHITOLE, N. V.; KAKDE, G. K. A Simple, proficient and green approach for the synthesis of 1,8-dioxo-octahydroxanthenes catalyzed by cerium(IV) ammonium nitrate in aqueous media. *Orbital: The Electron. J. Chem.*, **2014**, *6*(3), 191-194.

[33] MULAKAYALA, N.; KUMAR, G. P.; RAMBABU, D.; AELURI, M.; RAO, M. V. B.; PAL, M. A greener synthesis of 1,8-dioxo-octahydroxanthene derivatives under ultrasound. *Tetrahedron Lett.*, **2012**, *53*(51), 6923–6926.

[34] MADJE, B. R.; UBALE, M . B.; BHARAD, J. V.; SHINGARE, M. S. Alum-promoted synthesis of 1,8-dioxo-octahydroxanthenes in water. *S. Afr. J. Chem.*, **2010**, *63*(1), 36–39.

[35] ILANGOVAN, A.; MALAYAPPASAMY, S.; MURALIDHARAN, S.; MARUTHAMUTHU, S. A highly efficient green synthesis of 1,8-dioxooctahydroxanthenes. *Chem. Cent. J.*, **2011**, 81.

[36] GANESAN, S. S.; KOTHANDAPANI, J.; GANESAN, A. Zinc chloride catalyzed collective synthesis of arylmethylene *bis*(3-hydroxy-2-cyclohexene-1-ones) and 1,8-Dioxo-octahydroxanthene/acridine derivatives. *Lett. Org. Chem.*, **2014**, *11*(9), 682-687.

[37] KHABAZZADEH, H.; SHEIKHSHOAIE, I.; SOTUDEH, N. [Fe(III)(Salen)Cl] Complex as a catalyst for the synthesis of 1,8-dioxo-octahydroxanthene derivatives. *J. Sci.*, **2013**, *24*(2), 123-127.

[38] THIRUPATHAIAH, A.; PRASANNA, B. RAVINDER, M.; SUDHAKAR, T.; BHASKAR, J.; RAMANNA, S. $BiCl_3$ catalyzed reaction of aromatic aldehydes with 5,5-dimethyl-1,3-cyclohexandione in ionic liquids. *Orient. J. Chem.*, **2010**, *26*(4), 1589-1591.

[39] FAN, X. S.; LI, Y. Z.; ZHANG, X. Y.; HU, H. Y.; WANG, J. J. $FeCl_3{\cdot}6H_2O$ catalyzed condensation of aromatic aldehydes with 5,5-dimethyl-1,3-cyclohexanedione in ionic liquids. *Chinese J. Org. Chem.*, **2005**, *25*(11), 1482-1486.

[40] FAN, X.; HU, X.; ZHANG, X.; WANG, J. $InCl_3.4H_2O$-promoted green preparation of xanthenedione derivatives in ionic liquids. *Can. J. Chemistry*, **2005**, 83 (1), 16–20.

[41] SADAT, S. N.; HATAMJAFARI, H. One-pot synthesis of 1,8-dioxo-octahydroxanthene derivatives. *Orient. J. Chem.*, **2015**, *31*(2), 1191-1193.

[42] PRABHAKAR, G.; RAJU, D.; RAJESH, M.; MADHAVARAO, B. Cerium (III) chloride efficient synthesis of 1,8-dioxo-octahydro xanthene and 12-aryl (or) 12-alkyl-8,9,10,12-tetrahydrobenzo[*a*]xanthene-11-one derivatives. *World J. Pharm. Pharm. Sci.*, **2014**, *3*(9), 1410-1417.

[43] MULAKAYALA, N.; MURTHY, P. V. N. S.; RAMBABU, D.; AELURI, M.; ADEPU, R.; KRISHNA, G. R.; REDDY, C. M.; PRASAD, K. R. S.; CHAITANYA, M.; KUMAR, C. S.; RAO, M. V. B.; PAL, M. Catalysis by molecular iodine: A rapid synthesis of 1,8-dioxo-octahydroxanthenes and their evaluation as potential anticancer agents. *Bioorg. Med. Chem. Lett.*, **2012**, *22*(6), 2186–2191.

[44] RONG, L.; LI, X.; WANG, H.; SHI, D.; TU, S.; ZHUANG, Q. Reaction of imines with 5,5-dimethyl-1,3-cyclohexanedione. *Synth. Commun.*, **2006**, *36*(16), 2345–2353.

[45] DARVICHE, F.; BALALAIE, S.; CHADEGANI, F. Diammonium hydrogen phosphate as a neutral and efficient catalyst for synthesis of 1,8-dioxo-octahydroxanthene derivatives in aqueous media. *Synth. Commun.*, **2007**, *37*(7), 1059–1066.

[46] SOLIMAN, H. A.; SALAMA, T. A. Silicon-mediated highly efficient synthesis of 1,8-dioxo-octahydroxanthenes and their transformation to novel functionalized pyrano-tetrazole [1,5-a] azepine derivatives. *Chinese Chem. Lett.*, **2013**, *24*(5), 404–406.

[47] MAGHSOODLOU, M. T.; KHORASSANI, S. M. H.; SHAHKARAMI, Z.; MALEKI, N.; ROSTAMIZADEH, M. An efficient synthesis of 2,2'-arylmethylene *bis*(3-hydroxy-5,5-dimethyl-2-cyclohexene-1-one) and 1,8-dioxooctahydroxanthenes using ZnO and ZnO–acetyl chloride. *Chinese Chem. Lett.*, **2010**, *21*(6), 686–689.

[48] JUNG, D. H.; LEE, Y. R.; KIM, S. H.; LYOO, W. S. New and general methods for the synthesis of arylmethylene *bis*(3-hydroxy-2-cyclohexene-1-ones) and xanthenediones by EDDA and $In(OTf)_3$-catalyzed one-pot domino Knoevenagel/Michael or Koevenagel/Michael/cyclodehydration reactions. *B. Kor. Chem. Soc.*, **2009**, *30*(9), 1989-1195.

[49] KARAMIA, B.; NEJATIB, S.; ESKANDARI, K. An adapted route to efficient synthesis of 1,8-dioxooctahydro-xanthene derivatives using $InCl_3$ and $(HPO_3)_n$ as recyclable catalysts. *Curr. Chem. Lett.*, **2015**, *4*(4), 169–180.

[50] SULIMAN, R. B. *Synthesis and antimicrobial activities of some octahydroxanthen-1,8- Dione derivatives.* 2003. Master Dissertation (Master in Chemistry). Sudan University of Science and Teconology.

[51] WANG, R. H.; CUI, B.; ZHANG, W. T.; HAN, G. F. Green synthesis of 1,8-dioxo-octahydroxanthene derivatives using catalytic amount of H_2SO_4 in water. *Synth. Commun.*, **2010**, *40*(12), 1867-1872.

[52] ZOLFIGOL, M. A. Silica sulfuric acid/$NaNO_2$ as a novel heterogeneous system for production of thionitrites and disulfides under mild conditions. *Tetrahedron*, **2001**, *57*(46), 9509-9511.

[53] SEYYEDHAMZEH, M.; MIRZAEI, P.; BAZGIR, A. Solvent-free synthesis of aryl-*14H*-dibenzo[a,j]xanthenes and 1,8-dioxo-octahydro-xanthenes using silica sulfuric acid as catalyst. *Dyes Pigments*, **2008**, *76*(3), 836-839.

[54] PRAMANIK, A.; BHAR, S. Alumina-sulfuric acid catalyzed eco-friendly synthesis of xanthenediones. *Catal. Commun.*, **2012**, 17–24.

[55] MAHDAVINIA, G. H.; BIGDELI, M. A.; HAYENIAZ, Y. S. Covalently anchored sulfonic acid on silica gel (SiO_2-R-SO_3H) as an efficient and reusable heterogeneous catalyst for the one-pot synthesis of 1,8-dioxo-octahydroxanthenes under solvent-free conditions. *Chinese Chem. Lett.*, **2009**, *20*(5), 539–541.

[56] KANTEVARI, S.; BANTU, R.; NAGARAPU, L. $HClO_4$–SiO_2 and PPA–SiO_2 catalyzed efficient one-pot Knoevenagel condensation, Michael addition and cyclo-dehydration of dimedone and aldehydes in acetonitrile, aqueous and Solvent-free conditions: Scope and limitations. *J. Mol. Catal. A Chem*, **2007**, *269*(1-2), 53–57.

[57] HARICHANDRAN, G.; AMALRAJ, S. D.; SHANMUGAM, P. Synthesis and characterization of phosphate anchored MnO_2 catalyzed Solvent-free synthesis of xanthene laser dyes. *J. Mol. Catal. A Chem*, **2014**, 31–38.

[58] KIASAT, A. R.; MOURADZADEGUN, A.; SAGHANEZHAD, S. J. Phosphosulfonic acid, an efficient solid acid catalyst for the one-pot preparation of 14-aryl-14*H*-dibenzo[*a*,*j*]xanthenes and 1,8-dioxooctahydroxanthenes under solvent-free conditions. *J. Serb. Chem. Soc.*, **2013**, *78*(9), 1291–1299.

[59] SHATERIAN, H. R.; HOSSEINIAN, A.; GHASHANG, M. Ferric hydrogen sulfate as an efficient heterogeneous catalyst for environmentally friendly greener synthesis of 1,8-dioxo-octahydroxanthenes. *Turk. J. Chem.*, **2009**, *33*(2), 233-240.

[60] KARADE, H. N.; SATHE, M.; KAUSHIK, M. P. An efficient synthesis of 1,8-dioxo-octahydroxanthenes using tetrabutylammonium hydrogen sulfate. *Arkivoc*, **2007**, *2007*(13), 252-258.

[61] DAS, B.; THIRUPATHI, P.; REDDY, K. R.; RAVIKANTH, B.; NAGARAPU, L. An efficient synthesis of 1,8-dioxo-octahydroxanthenes using heterogeneous catalysts. *Catal. Commun.*, **2007**, *8*(3), 535–538.

[62] SRIHARI, P.; MANDAL, S. S.; REDDY, J. S. S.; RAO, R. S.; YADAV, J. S. Synthesis of 1,8-dioxo-octahydroxanthenes utilizing PMA-SiO_2 as an efficient reusable catalyst. *Chinese Chem. Lett.*, **2008**, *19*(7), 771–774.

[63] KARTHIKEYAN, G.; PANDURANGAN, A. Heteropolyacid ($H_3PW_{12}O_{40}$) supported MCM-41: An efficient solid acid catalyst for the green synthesis of xanthenedione derivatives. *J. Mol. Catal. A Chem.*, **2009**, *311*(1-2), 36–45.

[64] SHAKIBAEI, G. I.; MIRZAEI, P.; BAZGIR, A. Dowex-50W promoted synthesis of 14-aryl-*14H*-dibenzo[a,j]xanthenes and 1,8-dioxo-octahydroxanthene derivatives under solvent-free conditions. *Appl. Catal. A Gen.*, **2007**, *325*(1), 188–192.

[65] SAJADI, S. M.; MAHAM, M.; AHMAD, B. O. Perfluorinated resin-sulfonic acid (Nafion-H): an efficient, environment friendly and recyclable heterogeneous catalyst for the one-pot synthesis of 1,8-dioxo-octahydroxanthenes. *Lett. Org. Chem.*, **2014**, *11*(5), 317-320.

[66] KARAMI, B.; ZARE, Z.; ESKANDARI, K. Molybdate sulfonic acid: preparation, characterization, and application as an effective and reusable catalyst for octahydroxanthene-1,8-dione synthesis. *Chem. Pap.*, **2013**, *67*(2), 145–154.

[67] SONG, G.; WANG, B.; LUO, H.; YANG, L. Fe^{3+}-montmorillonite as a cost-effective and recyclable solid acidic catalyst for the synthesis of xanthenediones. *Catal. Commun.*, **2007**, *8*(4), 673–676.

[68] DABIRI, M.; AZIMI, S. C.; BAZGIR, A. One-pot synthesis of xanthene derivatives under solvent-free conditions. *Chem. Pap.*, **2008**, *62*(5), 522–526.

[69] NARAYANA, V. R.; PUDUKULATHAN, Z.; VARALA, R. SO_4^{2-}/SnO_2-catalyzed efficient one-pot synthesis of 7,8-dihydro-2*H*-chromen-5-ones by formal [3+3] cycloaddition and 1,8-dioxo-octahydroxanthenes *via* a Knoevenagel condensation. *Org. Commun.*, **2013**, *6*(3), 110-119.

[70] JIN, T. S.; ZHANG, J. S.; WANG, A. Q.; LI, T. S. Solid-state condensation reactions between aldehydes and 5,5-dimethyl-1,3-cyclohexanedione by grinding at room temperature. *Synth. Commun.*, **2005**, *35*(17), 2339–2345.

[71] SHATERIAN, H. R.; HOSSEINIAN, A.; GHASHANG, M. Reaction in dry Media: Silica gel supported ferric chloride catalyzed synthesis of 1,8-dioxo-octahydroxanthene derivatives. *Phosphorus, Sulfur*, **2008**, *183*(12), 3136–3144.

[72] SHAIKH, I. R. Organocatalysis: Key trends in green synthetic chemistry, challenges, scope towards heterogenization, and importance from research and industrial point of view. *J. Catal.*, **2014**, 1-35.

[73] POLIAKOFF, M.; J. FITZPATRICK, M. J.; FARREN, T. R.; ANASTAS, P. T. Green chemistry: Science and politics of change. *Science*, **2002**, *297*(5582), 807-810.

[74] JIN, T. S.; ZHANG, J. S.; XIAO, J. C.; WANG, A. Q.; LI, T. S. Clean synthesis of 1,8-dioxo-octahydroxanthene derivatives catalyzed by *p*-dodecylbenezenesulfonic acid in aqueous Media. *Synlett*, **2004**, *5*(5), 0866–0870.

[75] SAGAR, A. D.; CHAMLE, S. N.; YADAV, M. V. Microwave assisted rapid synthesis of 1,8-dioxo-octahydroxanthenes using lignin sulphonic acid. *J. Chem. Pharm. Res.*, **2013**, *5*(7), 156-160.

[76] BIGDELI, M. Clean synthesis of 1,8-dioxooctahydroxanthenes promoted by DABCO-bromine in aqueous media. *Chinese Chem. Lett.*, **2010**, *21*(10), 1180–1182.

[77] BAYAT, M.; IMANIEH, H.; HOSSIENI, S. H. An efficient Solvent-free synthesis of 1,8-dioxo-octahydroxanthene using *p*-toluene sulfonic acid. *Chinese J. Chem*., **2009**, *27*(11), 2203-2206.

[78] NAVARRO, C. A.; SIERRA, C. A.; PUENTES, C. O. Aqueous citric acid as "green" reaction media for the synthesis of octahydroxanthenes. *Rev. Colomb. Quim.*, **2013**, *42*(2), 5-11.

[79] ALBADI, J.; SHIRINI, F.; MANSOURNEZHAD, A. Efficient synthesis of 1,8-dioxo-octahydroxanthenes catalyzed by melamine trisulfonic acid as a heterogenous and recyclable organocatalyst. *Curr. Organocatal.*, **2014**, *1*(1), 66-69.

[80] ZOLFIGOL, M. A.; YARIE, M. Hydroxylamine-*O*-sulfonic acid (HOSA): as a task specific catalyst for the synthesis of 1,8-dioxo-octahydroxanthenes under mild, green and solvent-free condition. *Org. Chem. Res.*, **2016**, 1-8.

[81] ZARE, A.; MOKHLESI, M.; HASANINEJAD, A.; ZADEH, T. Solvent-free synthesis of 1,8-dioxo-octahydroxanthenes and 14-aryl-14*H*-dibenzo[*a*,*j*]xanthenes using saccharin sulfonic acid as an efficient and green catalyst. *E-J. Chem.*, **2012**, *9*(4), 1854-1863.

[82] NAPOLEON, A. A.; KHAN, F. R. N.; JEONG, E. D.; CHUNG, E. H. Regioselective synthesis of 3,4,6,7-tetrahydro-3,3-dimethyl-9-phenyl-2*H*-xanthene-1,8(5*H*,9*H*)-diones through ascorbic acid catalyzed three-component domino reaction. *Tetrahedron Lett.*, **2014**, *55*(41), 5656-5659.

[83] BIGDELI, M. A.; NEMATI, F.; MAHDAVINIA, G. H.; DOOSTMOHAMMADI, H. A series of 1,8-dioxooctahydroxanthenes are prepared using trichloroisocyanuric acid. *Chinese Chem. Lett.*, **2009**, *20*(11), 1275–1278.

[84] RAHMATI, A. rapid and efficient method for the synthesis of 14H-dibenzo[a.j] xanthenes, aryl-5H-dibenzo [b.i]xanthene-5,7,12,14-(13*H*)-tetraone and 1,8-dioxo-octahydroxanthenes by acidic ionic liquid. *Chinese Chem. Lett.*, **2010**, *21*(7), 761–764.

[85] DAS, B.; THIRUPATHI, P.; MAHENDER, I.; REDDY, V. S.; RAO, Y. K. Amberlyst-15: An efficient reusable heterogeneous catalyst for the synthesis of 1,8-dioxo-octahydroxanthenes and 1,8-dioxo-decahydroacridines. *J. Mol. Catal. A Chem.*, **2009**, *247*(1-2), 233–239.

[86] KHAKSAR, S.; BEHZADI, N. Mild and highly efficient method for synthesis of 14-aryl(alkyl)-14*H*-dibenzo[a,j]xanthenes and 1,8-dioxo-octahydroxanthene derivatives using pentafluorophenyl ammonium triflate as a novel organocatalyst. *Chinese J. Catal.*, **2012**, *33*(4-6), 982-985.

[87] RAHIMIFARD, M.; ZIARANI, G. M.; BADIEI, A.; ASADI, S.; SOORKI, A. A. One-pot solvent-free synthesis of 1,8-dioxooctahydroxanthene derivatives using sulfonic acid functionalized LUS-1 and their antimicrobial activities. *Res. Chem. Intermediat.*, **2016**, *42*(4), 3847-3861.

[88] JIN, T. S.; ZHANG, J. S.; WANG, A. Q.; LI, T. S. Ultrasound-assisted synthesis of 1,8-dioxo-octahydroxanthene derivatives catalyzed by *p*-dodecylbenzenesulfonic acid in aqueous media. *Ultrason. Sonochem.*, **2006**, *13*(3), 220–224.

[89] PALIWAL, P.; JETTI, S. R.; BHATEWARA, A.; KADRE, T.; JAIN, S. DABCO catalyzed synthesis of xanthene derivatives in aqueous media. *Org. Chem.*, **2013**, 1-6.

[90] ZHANG, Z. H.; TAO, X. Y. 2,4,6-trichloro-1,3,5-triazine-promoted synthesis of 1,8-dioxo-octahydroxanthenes under solvent-free conditions. *Aust. J. Chem.*, **2008**, *61*(2), 77-79.

[91] MOHAMED, S. K.; ABDELHAMID, A. A.; MAHARRAMOV, A.M.; KHALILOV, A. N.; GURBANOV, A. V.; ALLAHVERDIYEV, M. A. Synthesis of hydroacridines and 1,8-dioxo-octahydroxanthenes using primary amino alcohols as reagent or catalysis via three-component condensation reactions. *J. Chem. Pharm. Res.*, **2012**, *4*(2), 955-965.

[92] AL-ALSHAIKH, M. A.; AL-MARHOON, Z. M.; AL-HAZIMI, H. M. Microwave assisted synthesis of some tetrahydropyrimidinethione, thiazolo[3,2-*a*]pyrimidinone and xanthenedione derivatives. *J. Saudi Chem. Soc.*, **2006**, *10*(3), 527-538.

[93] BHALE, P.; DONGARE, S.; MULE, Y. B. An efficient synthesis of 1,8-dioxo-octahydroxanthenes catalysed by thiourea dioxide (TUD) in aqueous media. *Chem. Sci. Trans.*, **2015**, *4*(1), 246-250.

[94] SIMIN NAZARI, S.; KESHAVARZ, M.; KARAMI, B.; IRAVANI, N.; NEZHAD, M. V. Imidazol-1-yl-acetic acid as a novel green bifunctional organocatalyst for the synthesis of 1,8-dioxooctahydroxanthenes under solvent-free condition. *Chinese Chem. Lett.*, **2014**. 25(2), 317–320.

[95] JOHN, A.; YADAV, P. J. P.; PALANIAPPAN, S. Clean synthesis of 1,8-dioxo-dodecahydroxanthene derivatives catalyzed by polyaniline-*p*-toluenesulfonate salt in aqueous media. *J. Mol. Catal. A Chem.*, **2006**, *248*(1-2), 121–125.

[96] GHASHGHAEI, R.; GHASSAMIPOUR, S. A green procedure for synthesis of xanthene derivatives: Micellar solution of sodium dodecylphosphonate catalyzes condensation reaction of aldehydes and *β*-naphthol in aqueous media. *Iran. J. Catal.*, **2014**, *4*(1), 49-53.

[97] HASANINEJAD, A.; YOUSEFY, T.; FIROOZI, S. Aluminium dodecyl sulfate trihydrate $[Al(DS)_3]\cdot 3H_2O$: An efficient Lewis acid-surfactant-combined catalyst for synthesis of 1,8-dioxo-octahydroxanthens and 1,8-dioxo-decahydroacridines. *Iran. J. Sci. Technol.*, **2015**, *39*(2), 129-140.

[98] CHAVAN, A. P. A versatile and practical synthesis of 1,8-dioxo-octahydroxanthene derivatives catalyzed by polyethylene glycol (PEG) in water. *J. Kor. Chem. Soc.*, **2009**, *53*(4), 415-421.

[99] KOKKIRALA, S.; SABBAVARAPU, N. M.; YADAVALLI, V. D. N. *β* - Cyclodextrin mediated synthesis of 1,8 - dioxo-octahydroxanthenes in water. *Eur. J. Chem.*, **2011**, *2*(2), 272-275.

[100] GONG, K.; WANG, H.; WANG, S.; WANG, Y.; CHEN, J. Efficient synthesis of 1,8-dioxo-octahydroxanthenes catalyzed by *β*-cyclodextrin grafted with butyl sulfonic acid in aqueous media. *Chinese J. Catal.*, **2015**, *36*(8), 1249–1255.

[101] WAGHMARE, A. S.; KADAM, K. R.; PANDIT, S. S. Hypervalent iodine catalysed synthesis of 1, 8-dioxooctahydroxanthenes in aqueous media. *Appl. Sci. Res.*, **2011**, *3*(6), 423-427.

[102] MAHDAVINIA, G. H.; BIGDELI, M. A.; NEMATI, N. Synthesis of 1,8-dioxo-octahydroxanthene derivatives using NBS under mild conditions. *J. Sci. Tarbiat Moallem University*, **2010**, *9*(1), 59-68.

[103] KANTEVARI, S.; BANTU, R.; NAGARAPU, L. TMSCl mediated highly efficient one-pot synthesis of octahydroquinazolinone and 1,8-dioxo-octahydroxanthene derivatives. *Arkivoc*, **2006**, *16*(6), 136-148.

[104] HE, F.; LI, P.; GU, Y.; LI, G. Glycerol as a promoting medium for electrophilic activation of aldehydes: catalyst-free synthesis of di(indolyl)methanes, xanthene-1,8(2*H*)-diones and 1-oxo-hexahydroxanthenes. *Green Chem.*, **2011**, (11), 1767–1773.

[105] KUMAR, G. S. S; PRABHU, A. A. M.; SEETHALASHMI, P. G.; BHUVANESH, N.; KUMARESAN, S. Self-catalyzed syntheses, structural characterization, DPPH radical scavenging-, cytotoxicity-, and DFT studies of phenoxyaliphatic acids of 1,8-dioxo-octahydroxanthene derivatives. *J. Mol. Struct.*, **2014**, 51–60.

[106] MOGHADAM, K. R.; AZIMI, S. C. $Mg(BF_4)_2$ doped in [BMIm][BF4]: A homogeneous ionic liquid-catalyst for efficient synthesis of 1,8-dioxo-octahydroxanthenes, decahydroacridines and 14-aryl-14H-dibenzo[a,j]xanthenes. *J. Mol. Catal. A Chem.*, **2012**, 465– 469.

[107] NAEIMI, H.; NAZIFI, Z. S.; A facile one-pot ultrasound assisted synthesis of 1,8-dioxo-octahydroxanthene derivatives catalyzed by Brønsted acidic ionic liquid (BAIL) under green conditions. *J. Ind. Eng. Chem.*, **2014**, *20*(3), 1043–1049.

[108] FANG, D.; GONG, K. LIU, Z. L.; Synthesis of 1,8-dioxo-octahydroxanthenes catalyzed by acidic ionic liquids in aqueous media. *Catal. Lett.*, **2009**, *127*(3), 291-295.

[109] MA, J. J.; WANG, C.; WU, Q. H.; TANG, R. X.; LIU, H. Y.; LI, Q. An efficient green synthesis of xanthenedione derivatives promoted by acidic ionic liquid. *Heteroatom Chem.*, **2008**, *19*(6), 609-611.

[110] KALANTARI, M. Synthesis of 1,8-dioxo-octahydroxanthenes and *bis*(indolyl)methanes catalyzed by $[Et_3NH][H_2PO_4]$ as a cheap and mild acidic ionic liquid. *Arab. J. Chem.*, 2012, *5*(3), 319–323.

[111] ZHOU, Z.; DENG, X. $[Et_3NH][HSO_4]$ catalyzed efficient and green synthesis of 1,8-dioxo-octahydroxanthenes. *J. Mol. Catal. A Chem.*, **2013**, 99–102.

[112] SALVI, P. P.; MANDHARE, A. M.; SARTAPE, A. S.; PAWAR, D. K.; HAN, S. H.; KOLEKAR, S. S. Brønsted acidic ionic liquids promoted cyclocondensation reaction: Synthesis of 1,8-dioxo-octahydroxanthene. *C. R. Chim*, **2011**, *14*(10), 883-886.

[113] VENKATESAN, K.; PUJARI, S. S.; LAHOTI, R. J.; SRINIVASAN, K. V. An efficient synthesis of 1,8-dioxo-octahydro-xanthene derivatives promoted by a room temperature ionic liquid at ambient conditions under ultrasound irradiation. *Ultrason. Sonochem*, **2008**, *15*(4), 548–553.

[114] KUMBHAR, A.; KAMBLE, S.; RASHINKAR, G.; MOTE, K.; SALUNKHE, R. The task specific ionic liquid promoted reaction: An expeditious synthesis of privileged 1,8-dioxo-octahydroxanthene. *Appl. Sci. Res.*, **2010**, *2*(4), 235-239.

[115] JAGANNATH, K. V.; GANTIGAIAH, K. 1-(3,4-dichlorobenzenesulfonyl)-3-methyl-1H-imidazolium chloride: An efficient catalyst for the synthesis of 1,8-dioxo-octahydroxanthenes under microwave irradiation. *Int. J. Chem. Pharm. Sci.*, **2014**, *5*(2), 98-104.

[116] MAKONE, S.; MAHURKAR, S. A Green protocol for efficient synthesis of 1,8-dioxo-octahydroxanthenes using ionic liquid. *GSC.*, **2013**, *3*(4A), 27-32.

[117] ZARE, A.; ZARE, A. R. M.; MERAJODDIN, M.; ZOLFIGOL, M. A.; ZADEH, T. H.; HASANINEJAD, A.; KHAZAEI, A.; MOKHLESI, M.; KHAKYZADEH, V.; PANAH, F. D.; BEYZAVI, M. H.; ROSTAMI, E.; ARGHOON, A.; ROOHANDEH, R. Ionic liquid triethylamine-bonded sulfonic acid $\{[Et_3N–SO_3H]Cl\}$ as a novel, highly efficient and homogeneous catalyst for the synthesis of β-acetamido ketones,1,8-dioxo-octahydroxanthenes and 14-aryl-14H-dibenzo[a,j]xanthenes. *J. Mol. Liq.*, **2012**, 69–77.

[118] SHIRINI, F.; IMANZADEH, G. H.; ABEDINI, M.; GHAZIANI, M. A. D.; GHASEMABADIA, P. G.; LANGROODI, M. S. Introduction of two efficient catalysts for the synthesis of 1,8-dioxo-octahydroxanthene derivatives in the absence of solvent. *Iran. J. Catal.*, **2012**, *2*(3), 115-119.

[119] ALBADI, J.; MANSOURNEZHAD, A.; ABBASZADEH, H. CuO-CeO_2 Nanocomposite: A highly efficient recyclable catalyst for the green synthesis of 1,8-dioxo-octahydroxanthenes in water. *J. Chin. Chem. Soc. TAIP*, **2013**, *60*(10), 1-4.

[120] KARAMI, B.; JAFAR HOSEINI, S.; ESKANDARI, K.; GHASEMI, A.; NASRABADI, H. Synthesis of xanthene derivatives by employing Fe_3O_4 nanoparticles as an effective and magnetically recoverable catalyst in water. *Catal. Sci. Technol.*, **2012**, (2), 331-338.

[121] SHOJA, A.; SHIRINI, F.; ABEDINI, M.; ZANJANCHI, M. A. $BiVO_4$-NPs as a new and efficient nano-catalyst for the synthesis of 1,8-dioxo-octahydro xanthenes. *J. Nanostruct Chem*., **2014**, *4*(110), 1-5.

[122] BABADOUST, S. Efficient and reusable heterogeneous nano sized CeO_2 catalyst for the synthesis of 1, 8-dioxo-octahydroxanthenes. *IJCBS*, **2014**, 72-75.

[123] MURTHY, Y. L. N.; MAHESH, P.; DEVI, B. R.; DURGESWARAI, L. K.; MANI, P. Synthesis and antibacterial Assay of 9-substituted aryl-1,8-dioxo-octahydroxanthenes. *Asian J. Chem.*; **2014**, *26*(15), 4594-4598.

[124] MOSADDEGH, E.; HOSSEININASAB, F. A.; HASSANKHANI, A. Eggshell/Fe_3O_4 nanocomposite: A novel magnetic nanoparticles coated on porous ceramic eggshell waste as an efficient catalyst in the synthesis of 1,8-dioxo-octahydroxanthene. *RSC Adv*., **2015**, *5*(129), 106561-106567.

[125] NAEIMI, H.; NAZIFI, Z. S. A highly efficient nano-Fe_3O_4 encapsulated-silica particles bearing sulfonic acid groups as a solid acid catalyst for synthesis of 1,8-dioxo-octahydroxanthene derivatives. *J. Nanopart. Res*., **2013**, *15*(2026), 1-11.

[126] KHAZAEI, A.; ZARE, A. R. M.; MOHAMMADI, Z.; ZARE, A. KHAKYZADEH, V.; DARVISHI, G. Efficient preparation of 9-aryl-1,8-dioxooctahydroxanthenes catalyzed by nano-TiO_2 with high recyclability. *RSC Adv*., **2013**, (3), 1323-1326.

[127] RAO, G. B. D.; KAUSHIK, M. P.; HALVE, A. K. Zinc oxide nanoparticles: an environmentally benign and reusable catalyst for the synthesis of 1,8-dioxo-octahydroxanthene derivatives under solvent-free conditions. *Heteroletters*, **2012**, *2*(4), 411-418.

[128] KHILLARE, S.; DHOKTE, A.; LANDE, M.; ARBAD, B. One-pot synthesis of 1,8-dioxo-octahydroxanthenes using Ni–Mg Ferrite as novel, magnetically separable and efficient reusable heterogeneous catalyst. *Chem. Sci. Rev. Lett.*, **2014**, *3*(12), 1199-1207.

[129] TEIMOURI, A.; CHERMAHINI, A. N.; GHORBANIAN, L. The green synthesis of xanthenedione and dihydropyrimidone derivatives catalyzed by nanocrystalline solid acid catalysts. *Chemija*, **2013**, *24*(3), 223–233.

[130] GHOMI, J. S.; GHASEMZADEH, M. A. ZAHEDI, S. ZnO Nanoparticles: A Highly Effective and Readily Recyclable Catalyst for the One-Pot Synthesis of 1,8-dioxo-decahydroacridine and 1,8-dioxooctahydro-xanthene Derivatives. *J. Mex. Chem. Soc.*, **2013**, *57*(1), 1-7.

[131] LASEMI, Z.; MEHRASBI, E. ZnO nanoparticles: an efficient and reusable catalyst for one-pot synthesis of 1,8-dioxo-octahydroxanthenes. *Res. Chem. Intermed.*, **2015**, *41*(5), 2855-2866.

[132] GHARIB, A.; FARD, L. V.; PESYAN, N. N.; ROSHANI, M. Novel catalytic synthesis of xanthene and 1,8-dioxo-octahydroxanthene derivatives using ZnO nanoparticles catalyst under green conditions. *Chem. J.*, **2015**, *1*(3), 58-67.

[133] JAVID, A.; HERAVI, M. M.; BAMOHARRAM, F. F. One-pot synthesis of 1,8-dioxo-octahydroxanthenes utilizing silica-supported Preyssler nano particles as novel and efficient reusable heterogeneous acidic catalyst. *E-J. Chem.*, **2011**, *8*(2), 910-916.

[134] GHOMI, J. S.; GHASEMZADEH, M. A.; ZAHEDI, S. $FeCl_3$.nano SiO_2: An efficient heterogeneous nano catalyst for the synthesis of 14-Aryl-14*H*-dibenzo[a,j]xanthenes and 1,8-dioxo-octahydro-xanthenes under solvent-free conditions. *S. Afr. J. Chem*., **2012**, 191-195.

[135] ROSTAMIZADEH, S.; AMANI, A. M.; MAHDAVINIA, G. H.; AMIRI, G.; SEPEHRIAN, H. Ultrasound promoted rapid and green synthesis of 1,8-dioxo-octahydroxanthenes derivatives using nanosized MCM-41-SO_3H as a nanoreactor, nanocatalyst in aqueous media. *Ultrason. Sonochem.*, **2010**, *17*(2), 306–309.

[136] ALBADI, J.; KESHAVARZ, M.; ABEDINI, M.; KHOSHAKHLAGH, M. Copper iodide nanoparticles on poly(4-vinylpyridine): A new and efficient catalyst for the synthesis of 1,8-dioxo-octahydroxanthenes under solvent-free conditions. *J. Chem. Sci.*, **2013**, *125*(2), 295-298.

[137] ESFAHANI, M. N.; ABDIZADEH, T. Vanadatesulfuric acid nanorod particles: A novel and eco-benign catalyst for rapid and green synthesis of 1,8-dioxooctahydroxanthenes under solvent-free conditions. *J. Chem. Sci. Technol.*, **2013**, *2*(1), 14-20.

CAPÍTULO II

SÍNTESE DE XANTENODIONAS CATALISADA POR OXICLORETO DE ZIRCÔNIO(IV)

1 INTRODUÇÃO

No Capítulo 1 foram descritas diversas metodologias para a síntese de xantenodionas. Estas metodologias utilizam catalisadores com características de ácido de Lewis, ácido de Brønsted, ácido de Lewis e Brønsted, organocatalisadores, líquidos iônicos, e nanocatalisadores. Porém, muitas destas metodologias apresentam desvantagens tais como: o uso de solventes tóxicos; o emprego de catalisadores tóxicos e de custo elevado; reações que necessitam de elevadas temperaturas para sua ocorrência; além de processos que requerem procedimentos de elaboração laboriosos.

Algumas destas metodologias, entretanto, mostram-se atrativas, como é o caso daquela desenvolvida por Mosaddegh *et al.*[1]. Neste caso, o preparo de uma série de xantenodionas foi realizado na ausência de solvente e utilizando quantidades catalíticas do oxicloreto de zircônio(IV) octaidratado, $ZrOCl_2 \cdot 8H_2O$, um composto de baixo custo, disponível comercialmente e de fácil manipulação. As xantenodionas preparadas por esta metodologia foram obtidas com elevados rendimentos e seletividade e o catalisador pôde ser reciclado e reutilizado sem perda considerável de atividade catalítica. Com base nestas importantes características mencionadas, descreve-se neste capítulo a síntese e caracterização estrutural de cinquenta e três diferentes xantenodionas, além de um intermediário benzilideno (**32**) e quatro tetracetônicos (**33**, **34**, **35** e **36**).

Monocristais das xantenodionas **8**, **15-17, 20, 38-40** e **49** e dos intermediários tetracetônicos **33** e **34** foram obtidos, o que permitiu a caracterização destes compostos via difração de raios-X de monocristal. Os resultados obtidos pelos estudos de difração de raios-X estão descritos em dois artigos (artigos 1 e 2) apresentados ao final deste capítulo. O artigo 1 foi submetido ao Arabian Journal of Chemistry e o artigo 2 encontra-se em estágio final de escrita. Além de estudos de difração de raios-X são apresentados ainda resultados teóricos relativos aos compostos investigados.

[1]MOSADDEGH, E.; ISLAMI, M. R.; HASSANKHANI, A. $ZrOCl_2 \cdot 8H_2O$ as an efficient and recyclable catalyst for the clean synthesis of xanthenedione derivatives under solvent-free conditions. *Arabian Journal of Chemistry*, v. 5, p. 77–80, 2012.

2 MATERIAL E MÉTODOS

2.1 Generalidades metodológicas

Os reagentes benzaldeído (99%), 4-clorobenzaldeído (97%), 4-fluorobenzaldeído (98%), 4-bromobenzaldeído (99%), 4-nitrobenzaldeído (98%), 4-trifluorometilbenzaldeído (98%), 4-formilbenzonitrila (95%), 4-(dimetilamino)benzaldeído (99%), 4-hidroxibenzaldeído (98%), 4-metoxibenzaldeído (98%), 3,4-dimetoxibenzaldeído (99%), 2,3,4-trimetoxibenzaldeído (99%), 4-hidroxi-3-metoxibenzaldeído (98%), piperonal (99%), 2,6-diclorobenzaldeído (99%), 5-feniltiofeno-2-carbaldeído (98%), 5-(4-bromofenil)furfural (97%), 5-(4-clorofenil)furfural (95%), cicloexano-1,3-diona (97%), 5-metilcloexano-1,3-diona (98%), 5,5-dimetilcloexano-1,3-diona (95%) e 5-isopropilcicloexano-1,3-diona (99%) foram adquiridos da Sigma Aldrih (St. Louis, MO, US) e utilizados sem prévia purificação. O diclorometano (99,5%), o etanol (95%), o hexano (99%), o acetato de etila (99,5%) e o oxicloreto de zircônio(IV) octaidratado ($ZrOCl_2 \cdot 8H_2O$) foram adquiridos da Vetec (Rio de Janeiro, Brasil) e utilizados sem nenhum tratamento prévio.

A aquisição dos espectros de ressonância magnética nuclear (RMN) de ^{1}H e ^{13}C foram realizadas em instrumento Varian Mercury 300 (300 MHz e 75 MHz, respectivamente), utilizando clorofórmio deuterado ou dimetilsulfóxido (DMSO) como solvente. Os espectros no infravermelho (IV) foram obtidos utilizando o equipamento Varian 660-IR com acessório GladiATR ou no espectrofotômetro Perkin Elmer Paragon 1000 FTIR, empregando discos de brometo de potássio. A varredura foi relizada entre 4000 e 600 cm^{-1}. Os espectros de massas de baixa resolução foram adquiridos em instrumento SHIMADZU GCMS-QP5050A sob impacto de elétrons (70 eV). As massas exatas dos compostos foram obtidas em espectrômetro de massas do tipo micrOTOF QII® (Bruker Daltonics, Alemanha), equipado com fonte de ionização microESI (*Electrospray*), operando no modo positivo. A varredura foi realizada apenas no método MS para a faixa de massas entre *m/z* 50 e *m/z* 1000. As amostras foram diluídas em acetonitrila 100% LCMS, acidificada com ácido fórmico 0,1% LCMS (ambos adquiridos da Sigma Aldrich, Alemanha). As temperaturas de fusão foram determinadas utilizando o aparelho MQAPF-301 (Microquimica, Rio de Janeiro, Brasil) e não foram corrigidas. Nas análises por cromatografia em camada delgada (CCD) foram utilizadas placas de alumínio impregnadas com sílica gel (espessura de 250 mm). Após serem eluídas as placas foram

observadas em câmara contendo luz ultravioleta. Não foram empregados agentes reveladores químicos.

2.2 Síntese

2.2.1 Procedimento geral de síntese dos compostos 1-58

A um balão de fundo redondo foram adicionados a dicetona (2 mmol), o aldeído (1 mmol) e o catalisador $ZrOCl_2 \cdot 8H_2O$ (2 mol%, 0,012 g). Para alguns derivados da 5-metilcicloexan-1,3-diona (**18**, **21**, **23** - **25** e **27** - **29**) as quantidades da dicetona, do aldeído e do catalisador foram 1 mmol, 0,5 mmol e 1 mol%, respectivamente. Esta mistura foi mantida sob agitação a 85 °C até o término da reação, o qual foi observado mediante monitoramento da transformação por cromatografia em camada delgada (CCD). A mistura foi arrefecida até 25 °C e cerca de 50 mL de diclorometano frio foi adicionado. Em seguida, a mistura foi agitada por 5 minutos e o catalisador foi separado por filtração simples. Ao filtrado adicionou-se cerca de 50 mL de etanol e manteve-se o sistema em repouso para o processo de recristalização.

Com respeito à preparação dos compostos **33** e **34**, menciona-se que foram adicionados 100 μL de água destilada após 10 minutos de reação.

A seguir encontram-se descritos os dados espectroscópicos e espectrométricos obtidos para a caracterização estrutural de cada um dos compostos, bem como informações à respeito dos rendimentos, aspectos físicos, temperaturas de fusão e fatores de retenção (R_f) das substâncias sintetizadas. Vale ressaltar que a numeração adotada para a caracterização dos compostos não corresponde a adotada pela IUPAC.

9-fenil-3,4,5,6,7,9-hexaidro-1*H*-xanteno-1,8(2*H*)-diona **(1)**

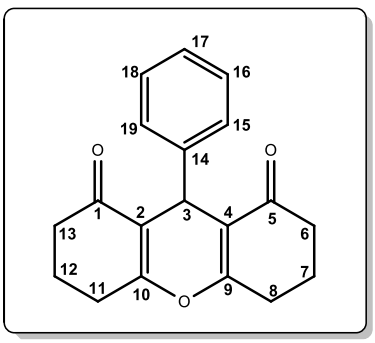

ASPECTO: Sólido amarelo.

MASSA OBTIDA: 153,2 mg (0,52 mmol, 52% de rendimento).

CCD: R_f = 0,42 (hexano-diclorometano-acetato de etila 3:2:1 (v/v).

FAIXA DE FUSÃO: 257 - 258 °C.

IV (ATR) ν (cm^{-1}): 2948, 2888, 1649, 1617, 1451, 1203, 1172. O espectro é apresentado na Figura 1, pg. 175 do anexo.

MS/EI (*m/z*/int. rel.) M+: $C_{19}H_{18}O_3$, 294/52, 276/7, 237/7, 217/100, 55/11. O espectro é apresentado na Figura 2, pg. 175 do anexo.

RMN de ^{1}H (300 MHz, $CDCl_3$) δ (integração, atribuição, constante de acoplamento, multiplicidade): 7,29 (2H, 15-C<u>H</u>, 19-C<u>H</u>, *J* = 7,0 Hz, d), 7,21 (2H, 16-C<u>H</u>, 18-C<u>H</u>, *J* = 7,0 Hz, t), 7,14 (1H, 17-C<u>H</u>, m), 4,81 (1H, 3-C<u>H</u>, s), 2,69 – 2,52 (4H, 8-C<u>H$_2$</u>, 11-C<u>H$_2$</u>, m), 2,38 – 2,27 (4H, 6-C<u>H$_2$</u>, 13-C<u>H$_2$</u>, m), 2,06 – 1,92 (4H, 7-C<u>H$_2$</u>, 12-C<u>H$_2$</u>, m). O espectro é apresentado na Figura 3, pg. 176 do anexo.

RMN de ^{13}C (75 MHz, $CDCl_3$) δ: 196,5 (C1 e C5), 163,9 (C9 e C10), 144,4 (C14), 128,3 (C15 e C19), 128,1 (C16 e C18), 126,4 (C17), 116,9 (C2 e C4), 36,9 (C6 e C13), 31,6 (C3), 27,1 (C8 e C11), 20,3 (C7 e C12). O espectro é apresentado na Figura 4, pg. 177 do anexo.

9-(4-fluorofenil)-3,4,5,6,7,9-hexahidro-1*H*-xanteno-1,8(2*H*)-diona **(2)**

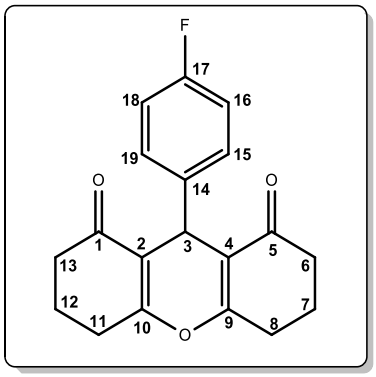

ASPECTO: Sólido branco.

MASSA OBTIDA: 236,8 mg (0,76 mmol, 76% de rendimento).

CCD: R_f = 0,25 (hexano-acetato de etila 2:1 v/v).

FAIXA DE FUSÃO: 266 - 267 °C.

IV (KBr) ν (cm^{-1}): 2949, 2889, 1653, 1618, 1205, 1177. O espectro é apresentado na Figura 5, pg. 178 do anexo.

MS/EI (*m/z*/int. rel.): 312/64, 255/10, 217/100, 55/14. O espectro é apresentado na Figura 6, pg. 178 do anexo.

HRMS *m/z* (M+H$^+$): Calculado para $C_{19}H_{18}FO_3$: 313,1240; encontrado: 313,1271.

RMN de ^{1}H (300 MHz, $CDCl_3$) δ (integração, atribuição, constante de acoplamento, multiplicidade): 7,25 (2H, 15-C<u>H</u>, 19-C<u>H</u>, *J* = 8,3 Hz, t), 6,89 (2H, 16-C<u>H</u>, 18-C<u>H</u>, *J* = 8,3 Hz, t), 4,77 (1H, 3-C<u>H</u>, s), 2,68 – 2,53 (4H, 8-C<u>H$_2$</u>, 11-C<u>H$_2$</u>, m), 2,39 – 2,29 (4H, 6-C<u>H$_2$</u>, 13-C<u>H$_2$</u>, m), 2,07 – 1,92 (4H, 7-C<u>H$_2$</u>, 12-C<u>H$_2$</u>, m). O espectro é apresentado na Figura 7, pg. 179 do anexo.

RMN de ^{13}C (75 MHz, $CDCl_3$) δ: 196,6 (C1 e C5), 164,0 (C9 e C10), 161,4 (d, *J* = 242,7, C17), 140,1 (d, *J* = 3,0 Hz, C14), 129,8 (d, *J* = 8,0 Hz, C15 e C19), 116,7 (C2 e C4), 114,8 (d, *J* = 21,2 Hz, C16 e C18), 36,9 (C6 e C13), 31,0 (C3), 27,1 (C8 e C11), 20,3 (C7 e C12). O espectro é apresentado na Figura 8, pg. 180 do anexo.

9-(4-clorofenil)-3,4,5,6,7,9-hexahidro-1*H*-xanteno-1,8(2*H*)-diona **(3)**

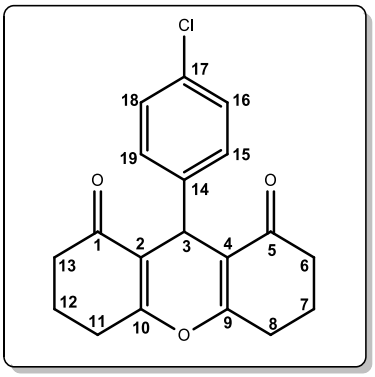

ASPECTO: Sólido branco.

MASSA OBTIDA: 310,3 mg (0,94 mmol, 94% de rendimento).

CCD: R_f = 0,25 (hexano-acetato de etila 2:1 v/v).

FAIXA DE FUSÃO: 271 - 272 °C.

IV (KBr) ν (cm^{-1}): 2957, 2869, 1667, 1616, 1489, 1201, 1172. O espectro é apresentado na Figura 9, pg. 181 do anexo.

MS/EI (*m/z*/int. rel.): 330/8, 328/24, 293/22, 217/100, 165/11, 152/19, 139/19, 75/17, 55/40, 42/16, 41/23. O espectro é apresentado na Figura 10, pg. 181 do anexo.

HRMS *m/z* (M+H$^+$): Calculado para $C_{19}H_{18}ClO_3$: 329,0944; encontrado: 329,0972.

RMN de ^{1}H (300 MHz, $CDCl_3$) δ (integração, atribuição, constante de acoplamento, multiplicidade): 7,22 (2H, 15-C<u>H</u>, 19-C<u>H</u>, *J* = 8.4 Hz, d), 7,12 (2H, 16-C<u>H</u>, 18-C<u>H</u>, *J* = 8,4 Hz, d), 4,76 (1H, 3-C<u>H</u>, s), 2,68 – 2,54 (4H, 8-C<u>H</u>$_2$, 11-C<u>H</u>$_2$, m), 2,37 – 2,28 (4H, 6-C<u>H</u>$_2$, 13-C<u>H</u>$_2$, m), 2,05 – 1,92 (4H, 7-C<u>H</u>$_2$, 12-C<u>H</u>$_2$, m). O espectro é apresentado na Figura 11, pg. 182 do anexo.

RMN de ^{13}C (75 MHz, $CDCl_3$) δ: 196,5 (C1 e C5), 164,1 (C9 e C10), 142,9 (C14), 132,0 (C17), 129,8 (C16 e C18), 128,2 (C15 e C19), 116,5 (C2 e C4), 36,9 (C6 e C13), 31,3 (C3), 27,1 (C8 e C11), 20,2 (C7 e C12). O espectro é apresentado na Figura 12, pg. 183 do anexo.

9-(4-bromofenil)-3,4,5,6,7,9-hexahidro-1*H*-xanteno-1,8(2*H*)-diona **(4)**

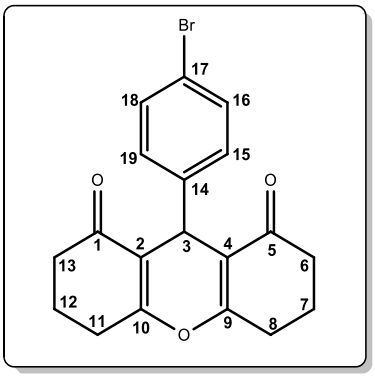

ASPECTO: Sólido branco.

MASSA OBTIDA: 319,1 mg (0,85 mmol, 85% de rendimento).

CCD: R_f = 0,22 (hexano-acetato de etila 2:1 v/v).

FAIXA DE FUSÃO: 270 - 271 °C.

IV (KBr) ν (cm^{-1}): 2957, 2868, 1666, 1619, 1487, 1201, 1171. O espectro é apresentado na Figura 13, pg. 184 do anexo.

MS/EI (*m/z*/ int. rel.): 374/20, 372/20, 293/35, 217/100, 165/16, 155/61, 139/26, 128/15, 115/16, 75/24, 66/17, 55/56, 42/35, 41/44. O espectro é apresentado na Figura 14, pg. 184 do anexo.

HRMS (M+H$^+$): Calculado para $C_{19}H_{18}BrO_3$: 373,0439; encontrado: 373,0466.

RMN de ^{1}H (300 MHz, $CDCl_3$) δ (integração, atribuição, constante de acoplamento, multiplicidade): 7,33 (2H, 16-C<u>H</u>, 18-C<u>H</u>, *J* = 8,2 Hz, d), 7,17 (2H, 15-C<u>H</u>, 19-C<u>H</u>, *J* = 8,2 Hz, d), 4,75 (1H, 3-C<u>H</u>, s), 2,67 – 2,54 (4H, 8-C<u>H</u>$_2$, 11-C<u>H</u>$_2$, m), 2,37 – 2,29 (4H, 6-C<u>H</u>$_2$, 13-C<u>H</u>$_2$, m), 2,13 – 1,86 (4H, 7-C<u>H</u>$_2$, 12-C<u>H</u>$_2$, m). O espectro é apresentado na Figura 15, pg. 185 do anexo.

RMN de ^{13}C (75 MHz, $CDCl_3$) δ: 196,5 (C1 e C5), 164,1 (C9 e C10), 143,4 (C14), 131,0 (C16 e C18), 130,2 (C15 e C19), 120,3 (C17), 116,4 (C2 e C4), 36,9 (C6 e C13), 31,4 (C3), 27,1 (C8 e C11), 20,3 (C7 e C12). O espectro é apresentado na Figura 16, pg. 186 do anexo.

9-(4-(trifluorometil)fenil)-3,4,5,6,7,9-hexahidro-1*H*-xanteno-1,8(2*H*)-diona **(5)**

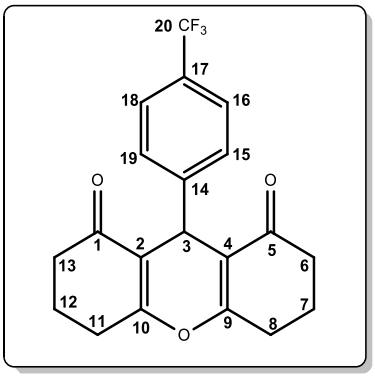

ASPECTO: Sólido branco.

MASSA OBTIDA: 310,3 mg (0,94 mmol, 94% de rendimento).

CCD: R_f = 0,25 (hexano-acetato de etila 2:1 v/v).

FAIXA DE FUSÃO: 242 - 243 °C.

IV (KBr) ν (cm^{-1}): 2959, 2876, 1667, 1617, 1459, 1324, 1201, 1172. O espectro é apresentado na Figura 17, pg. 187 do anexo.

MS/EI (*m/z*/int. rel.): 362/34, 217/100, 145/15, 55/30, 42/11, 41/18. O espectro é apresentado na Figura 18, pg. 187 do anexo.

HRMS *m/z* (M+H$^+$): Calculado para $C_{20}H_{18}F_3O_3$, 363,1208; encontrado: 363, 1226.

RMN de ^{1}H (300 MHz, $CDCl_3$) δ (integração, atribuição, constante de acoplamento, multiplicidade): 7,47 (2H, 16-C<u>H</u>, 18-C<u>H</u>, *J* = 8,4 Hz, d), 7,41 (15-C<u>H</u>, 19-C<u>H</u>, *J*= 8,4 Hz, d), 4,84 (1H, 3-C<u>H</u>, s), 2,68 – 2,55 (4H, 8-C<u>H$_2$</u>, 11-C<u>H$_2$</u>, m), 2,37 – 2,30 (4H, 6-C<u>H$_2$</u>, 13-C<u>H$_2$</u>, m), 2,08 – 1,94 (4H, 7-C<u>H$_2$</u>, 12-C<u>H$_2$</u>, m). O espectro é apresentado na Figura 19, pg. 188 do anexo.

RMN de ^{13}C (75 MHz, $CDCl_3$) δ: 196,4 (C1 e C5), 164,3 (C9 e C10), 148,2 (C14), 128,7 (C15 e C19), 126,2 (q, *J* = 32,2 Hz, C17), 125,1 (q, *J* = 3,9 Hz, C16 e C18), 124,2 (q, *J* = 270,2 Hz, 20-<u>C</u>F$_3$), 116,2 (C2 e C4), 36,8 (C6 e C13), 31,8 (C3), 27,1 (C8 e C11), 20,2 (C7 e C12). O espectro é apresentado na Figura 20, pg. 189 do anexo.

4-(1,8-dioxo-2,3,4,5,6,7,8,9-octaidro-1*H*-xanten-9-il)benzonitrila **(6)**

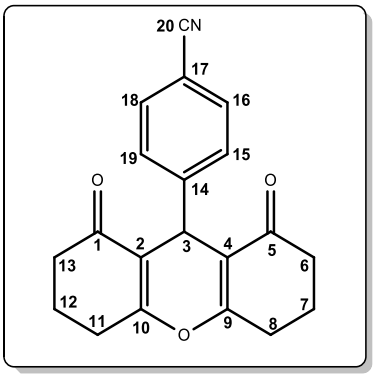

ASPECTO: Sólido branco.

MASSA OBTIDA: 258,2 mg (0,81 mmol, 81% de rendimento).

CCD: R_f = 0,09 (hexano-acetato de etila 2:1 v/v).

FAIXA DE FUSÃO: 260 - 262 °C.

IV (KBr) ν (cm^{-1}): 2951, 2872, 2227, 1661, 1620, 1458, 1201, 1177. O espectro é apresentado na Figura 21, pg. 190 do anexo.

MS/EI (*m/z*/int. rel.): 319/25, 217/100, 102/22, 55/39, 42/21, 41/31. O espectro é apresentado na Figura 22, pg 190 do anexo.

HRMS (M+H$^+$): Calculado para $C_{20}H_{18}NO_3$: 320,1287; encontrado: 320,1275.

RMN de ^{1}H (300 MHz, $CDCl_3$) δ (integração, atribuição, constante de acoplamento, multiplicidade): 7,50 (2H, 16-C<u>H</u>, 18-C<u>H</u>, *J* = 8,2 Hz, d), 7,41 (2H, 15-C<u>H</u>, 19-C<u>H</u>, *J* = 8,2 Hz, d), 4,81 (1H, 3-C<u>H</u>, s), 2,69 – 2,53 (4H, 8-C<u>H$_2$</u>, 11-C<u>H$_2$</u>, m), 2,48 – 2,19 (4H, 6-C<u>H$_2$</u>, 13-C<u>H$_2$</u>, m), 2,07 – 1,94 (4H, 7-C<u>H$_2$</u>, 12-C<u>H$_2$</u>, m). O espectro é apresentado na Figura 23, pg. 191 do anexo.

RMN de ^{13}C (75 MHz, $CDCl_3$) δ: 196,4 (C1 e C5), 164,5 (C9 e C10), 149,6 (C14), 132,0 (C15 e C19), 129,3 (C16 e C18), 119,0 (C20), 115,8 (C2 e C4), 110,1 (C17), 36,8 (C6 e C13), 32,3 (C3), 27,1 (C8 e C11), 20,2 (C7 e C12). O espectro é apresentado na Figura 24, pg. 192 do anexo.

9-(4-nitrofenil)-3,4,5,6,7,9-hexahidro-1*H*-xanteno-1,8(2*H*)-diona **(7)**

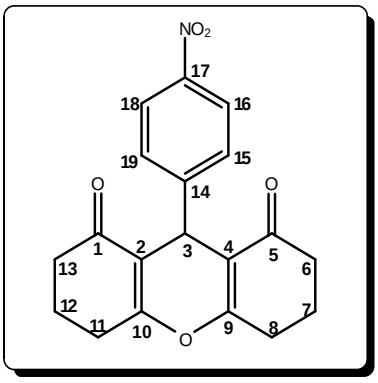

ASPECTO: Sólido amarelo.

MASSA OBTIDA: 237,0 mg (0,70 mmol, 70% de rendimento).

CCD: R_f = 0,09 (hexano-acetato de etila 2:1 v/v).

FAIXA DE FUSÃO: 245 - 246 °C.

IV (KBr) ν (cm^{-1}): 2949, 2873, 1662, 1616, 1517, 1458, 1345, 1202, 1172. O espectro é apresentado na Figura 25, pg. 193 do anexo.

MS/EI (*m/z*/int. rel.): 339/29, 322/37, 292/21, 217/100, 165/16, 152/32, 139/19, 128/16, 115/20, 76/24, 63/16, 55/56, 42/20, 41/39. O espectro é apresentado na Figura 26, pg. 193 do anexo.

HRMS (M^+H^+): Calculado para $C_{19}H_{18}NO_5$: 340,1185; encontrado: 340,1161.

RMN de ^{1}H (300 MHz, $CDCl_3$) δ (integração, atribuição, constante de acoplamento, multiplicidade): 8,01 (2H, 16-C<u>H</u>, 18-C<u>H</u>, *J* = 8,8 Hz, d), 7,47 (2H, 15-C<u>H</u>, 19-C<u>H</u>, *J* = 8,8 Hz, d), 4,86 (1H, 3-C<u>H</u>, s), 2,67 – 2,59 (4H, 8-C<u>H$_2$</u>, 11-C<u>H$_2$</u>, m), 2,37 – 2,31 (4H, 6-C<u>H$_2$</u>, 13-C<u>H$_2$</u>, m), 2,06 – 1,95 (4H, 7-C<u>H$_2$</u>, 12-C<u>H$_2$</u>, m). O espectro é apresentado na Figura 27, pg. 194 do anexo.

RMN de ^{13}C (75 MHz, $CDCl_3$) δ: 196,4 (C1 e C5), 164,6 (C9 e C10), 151,7 (C14), 146,4 (C17), 129,4 (C15 e C19), 123,4 (C16 e C18), 115,7 (C2 e C4), 36,6 (C6 e C13), 32,2 (C3), 27,1 (C8 e C11), 20,2 (C7 e C12). O espectro é apresentado na Figura 28, pg. 195 do anexo.

9-(4-(dimetilamino)fenil)-3,4,5,6,7,9-hexaidro-1*H*-xanteno-1,8(2*H*)-diona **(8)**

Os dados espectroscópicos e detalhes adicionais encontram-se descritos no artigo 1. Os espectros são apresentados nas Figuras 29, 30, 31 e 32, pgs. 196, 197 e 198 do anexo.

9-(4-metoxifenil)-3,4,5,6,7,9-hexaidro-1*H*-xanteno-1,8(2*H*)-diona **(9)**

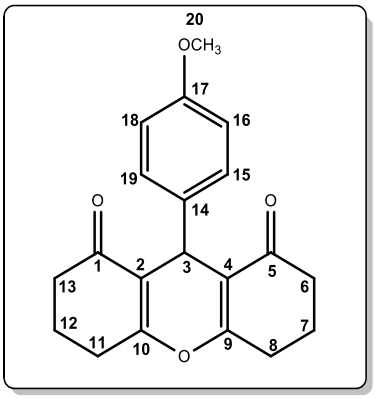

ASPECTO: Sólido amarelo.

MASSA OBTIDA: 159,6 mg (0,49 mmol, 49% de rendimento).

CCD: R_f = 0,25 (hexano-diclorometano-acetato de etila 3:2:1 v/v).

FAIXA DE FUSÃO: 201 - 202 °C.

IV (ATR) ν (cm^{-1}): 2955, 2899, 1652, 1616, 1460, 1233, 1201, 1170. O espectro é apresentado na Figura 33, pg. 199 do anexo.

MS/EI (*m/z*/int. rel.) M+: $C_{20}H_{20}O_4$, 324/100, 307/52, 293/78, 268/18, 217/93, 55/24. O espectro é apresentado na Figura 34, pg. 199 do anexo.

RMN de ^{1}H (300 MHz, $CDCl_3$) δ (integração, atribuição, constante de acoplamento, multiplicidade): 7,20 (2H, 15-C<u>H</u>, 19-C<u>H</u>, *J* = 7,2 Hz, d), 6,75 (2H, 16-C<u>H</u>, 18-C<u>H</u>, *J* = 7,2 Hz, d), 4,75 (1H, 3-C<u>H</u>, s), 3,72 (3H, 20-C<u>H</u>$_3$, s), 2,67 – 2,52 (4H, 8-C<u>H</u>$_2$, 11-C<u>H</u>$_2$, m), 2,38 – 2,27 (4H, 6-C<u>H</u>$_2$, 13-C<u>H</u>$_2$, m), 2,06 – 1,92 (4H, 7-C<u>H</u>$_2$, 12-C<u>H</u>$_2$, m). O espectro é apresentado na Figura 35, pg. 200 do anexo.

RMN de ^{13}C (75 MHz, $CDCl_3$) δ: 196,6 (C1 e C5), 163,7 (C9 e C10), 158,0 (C17), 136,7 (C14), 129,3 (C15 e C19), 117,0 (C2 e C4), 113,5 (C16 e C18), 55,1 (C20), 37,0 (C6 e C13), 30,7 (C3), 27,1 (C8 e C11), 20,3 (C7 e C12). O espectro é apresentado na Figura 36, pg. 201 do anexo.

9-(3,4-dimetoxifenil)-3,4,5,6,7,9-hexaidro-1*H*-xanteno-1,8(2*H*)-diona **(10)**

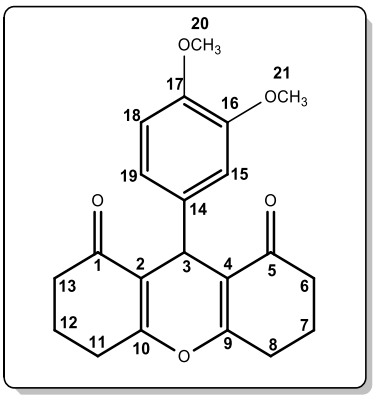

ASPECTO: Sólido branco.

MASSA OBTIDA: 328,7 mg (0,93 mmol, 93% de rendimento).

CCD: R_f = 0,20 (hexano-diclorometano-acetato de etila 3:2:1 v/v).

FAIXA DE FUSÃO: 181 - 182 °C.

IV (ATR) ν (cm^{-1}): 2965, 2862, 1655, 1619, 1461, 1233, 1198, 1020. O espectro é apresentado na Figura 37, pg. 202 do anexo.

MS/EI (*m/z*/int. rel.) M+: $C_{21}H_{22}O_5$, 354/61, 339/12, 323/100, 217/40, 55/14. O espectro é apresentado na Figura 38, pg. 202 do anexo.

RMN de ^{1}H (300 MHz, $CDCl_3$) δ:(integração, atribuição, constante de acoplamento, multiplicidade): 6,98 (1H, 19-C<u>H</u>, s), 6,72 – 6,64 (2H, 15-C<u>H</u> e 18-C<u>H</u>, m), 4,75 (1H, 3-C<u>H</u>, s), 3,86 (3H, 20-C<u>H</u>$_3$, s), 3,77 (3H, 21-C<u>H</u>$_3$, s), 2,69 – 2,52 (4H, 8-C<u>H</u>$_2$ e 11-C<u>H</u>$_2$, m), 2,38 – 2,67 (4H, 6-C<u>H</u>$_2$ e 13-C<u>H</u>$_2$, m), 2,05 – 1,92 (4H, 7-C<u>H</u>$_2$ e 12-C<u>H</u>$_2$, m). O espectro é apresentado na Figura 39, pg. 203 do anexo.

RMN de ^{13}C (75 MHz, $CDCl_3$) δ: 196,6 (C1 e C5), 163,8 (C9 e C10), 148,4 (C17), 147,5 (C16), 137,2 (C14), 119,6 (C19), 116,9 (C2 e C4), 112,7 (C15), 110,9 (C18), 55,9 e 55,8 (C20 e C21), 37,0 (C6 e C13), 30,9 (C3), 27,1 (C8 e C11), 20,3 (C7 e C12). O espectro é apresentado na Figura 40, pg. 204 do anexo.

9-(3,4,5-trimetoxifenil)-3,4,5,6,7,9-hexaidro-1*H*-xanteno-1,8(2*H*)-diona **(11)**

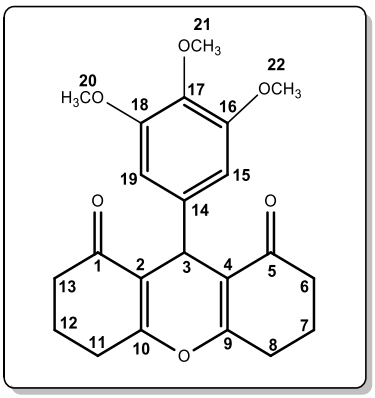

ASPECTO: Sólido amarelo.

MASSA OBTIDA: 358,8 mg (0,93 mmol, 93% de rendimento).

CCD: R_f = 0,16 (hexano-diclorometano-acetato de etila 3:2:1 v/v).

FAIXA DE FUSÃO: 188 - 189 °C

IV (ATR) ν (cm^{-1}): 2963, 2882, 1659, 1619, 1453, 1230, 1170, 1123. O espectro é apresentado na Figura 41, pg. 205 do anexo.

MS/EI (*m/z*/int. rel.) M+: $C_{22}H_{24}O_5$, 384/60, 369/13, 353/100, 217/27, 55/12. O espectro é apresentado na Figura 42, pg. 205 do anexo.

RMN de ^{1}H (300 MHz, $CDCl_3$) δ: (integração, atribuição, constante de acoplamento, multiplicidade): 6,51 (2H, 15-C<u>H</u> e 19-C<u>H</u>, s), 4,77 (1H, 3-C<u>H</u>, s), 3,80 (6H, 20-C<u>H</u>$_3$, 22-C<u>H</u>$_3$, s), 3,75 (3H, 21-C<u>H</u>$_3$, s), 2,70 – 2,53 (4H, 8-C<u>H</u>$_2$ e 11-C<u>H</u>$_2$, m), 2,44 – 2,27 (4H, 6-C<u>H</u>$_2$ e 13-C<u>H</u>$_2$, m), 2,08 – 1,93 (4H, 7-C<u>H</u>$_2$ e 12-C<u>H</u>$_2$, m). O espectro é apresentado na Figura 43, pg. 206 do anexo.

RMN de ^{13}C (75 MHz, $CDCl_3$) δ: 196,6 (C1 e C5), 164,0 (C9 e C10), 152,8 (C16 e C18), 139,9 (C17), 136,7 (C14), 116,7 (C2 e C4), 105,7 (C15 e C19), 60,6 (C21), 56,6 (C20 e C22), 37,0 (C6 e C13), 31,4 (C3), 27,1 (C8 e C11), 20,3 (C7 e C12). O espectro é apresentado na Figura 44, pg. 207 do anexo.

9-(4-hidroxifenil)-3,4,5,6,7,9-hexaidro-1*H*-xanteno-1,8(2*H*)-diona **(12)**

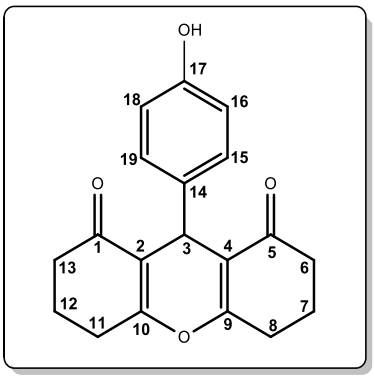

ASPECTO: Sólido marrom.

MASSA OBTIDA: 130,6 mg (0,42 mmol, 42% de rendimento).

CCD: R_f = 0,56 (hexano-acetato de etila 2:1 v/v).

FAIXA DE FUSÃO: 307 - 308 °C

IV (ATR) ν (cm^{-1}): 3370, 2949, 2869, 1657, 1609, 1446, 1206, 1169. O espectro é apresentado na Figura 45, pg. 208 do anexo.

MS/EI (*m/z*/int. rel.) M+: $C_{19}H_{18}O_4$, 310/93, 293/60, 253/17, 217/100, 55/24. O espectro é apresentado na Figura 46, pg. 208 do anexo.

RMN de ^{1}H (300 MHz, $CDCl_3$) δ (integração, atribuição, constante de acoplamento, multiplicidade): 9,16 (1H, OH, s), 6,94 (2H, 16-C<u>H</u> e 18-C<u>H</u>, *J* = 8,4 Hz , d), 6,57 (2H, 15-C<u>H</u> e 19-C<u>H</u>, *J* = 8,4 Hz , d), 4,46 (1H, 3-C<u>H</u>, s), 2,69 – 251 (4H, 8-C<u>H</u>$_2$ e 11-C<u>H</u>$_2$, m), 2,31 – 2,17 (4H, 6-C<u>H</u>$_2$ e 13-C<u>H</u>$_2$, m), 1,99 – 1,76 (4H, 7-C<u>H</u>$_2$ e 12-C<u>H</u>$_2$, m). O espectro é apresentado na Figura 47, pg. 209 do anexo.

RMN de ^{13}C (75 MHz, $CDCl_3$) δ: 196,8 (C1 e C5), 164,9 (C9 e C10), 156,1 (C17), 135,5 (C14), 129,3 (C15 e C19), 116,4 (C2 e C4), 115,1 (C16 e C18), 36,9 (C6 e C13), 30,2 (C3), 26,9 (C8 e C11), 20,3 (C7 e C12). O espectro é apresentado na Figura 48, pg. 210 do anexo.

9-(4-hidroxi-3-metoxifenil)-3,4,5,6,7,9-hexaidro-1*H*-xanteno-1,8(2*H*)-diona **(13)**

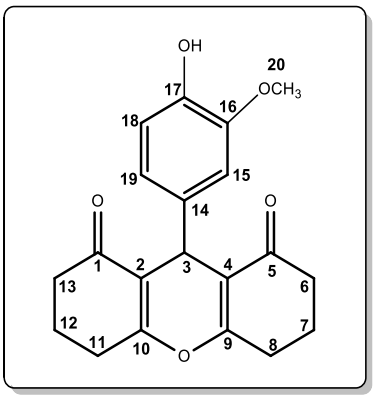

ASPECTO: Sólido amarelo.

MASSA OBTIDA: 319,9 mg (0,94 mmol, 94% de rendimento).

CCD: R_f = 0,09 (hexano-diclorometano-acetato de etila 3:2:1 v/v).

FAIXA DE FUSÃO: 237 - 238 °C

IV (ATR) ν (cm^{-1}): 3316, 2953, 2889, 1663, 1641, 1619, 1467, 1273, 1203, 1170, 1120. O espectro é apresentado na Figura 49, pg. 211 do anexo.

MS/EI (*m/z*/int. rel.) M+: $C_{20}H_{20}O_5$,340/100, 323/52, 309/62, 217/96, 55/31. O espectro é apresentado na Figura 50, pg. 211 do anexo.

RMN de ^{1}H (300 MHz, $CDCl_3$) δ (integração, atribuição, constante de acoplamento, multiplicidade): 7,06 -7,03 (1H, 15-C<u>H</u>, m), 6,74 – 6,69 (1H, 19-C<u>H</u>, m), 6,56 – 6,50(1H, 18-C<u>H</u>, m), 5,82 (1H, O-<u>H</u>, s), 4,72 (1H, 3-CH, s), 3,87 (1H, 20-C<u>H</u>$_3$, s), 2,67 -2,50 (4H, 8-C<u>H</u> e 11-C<u>H</u>, m), 2,40 – 2,26 (4H, 6-C<u>H</u> e 13-C<u>H</u>, m), 2,07 – 1,91 (4H, 7-C<u>H</u> e 12-C<u>H</u>, m). O espectro é apresentado na Figura 51, pg. 212 do anexo.

RMN de ^{13}C (75 MHz, $CDCl_3$) δ: 196,8 (C1 e C5), 163,8 (C9 e C10), 145,9 (C16), 144,1 (C17), 136,6 (C14), 119,8 (C19), 117,0 (C2 e C4), 114,0 (C18), 112,4 (C15), 55,9 (C20), 37,0 (C6 e C13), 31,0 (C3), 27,1 (C8 e C11), 20,3 (C7 e C12). O espectro é apresentado na Figura 52, pg. 213 do anexo.

9-(benzo[d][1,3]dioxol-5-il)-3,4,5,6,7,9-hexaidro-1*H*-xanteno-1,8(2*H*)-diona **(14)**

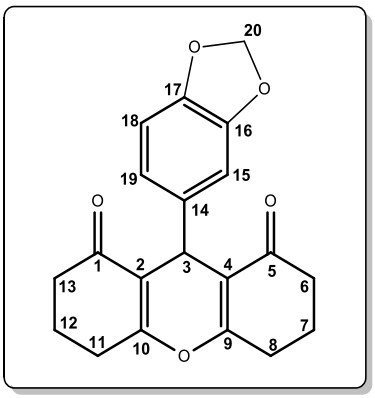

ASPECTO: Sólido amarelo.

MASSA OBTIDA: 149,0 mg (0,44 mmol, 44% de rendimento).

CCD: R_f = 0,25 (hexano-diclorometano-acetato de etila 3:2:1 v/v).

FAIXA DE FUSÃO: 238 - 239 °C

IV (ATR) ν (cm^{-1}): 2953, 2903, 1653, 1618, 1481, 1245, 1199. O espectro é apresentado na Figura 53, pg. 214 do anexo.

MS/EI (*m/z*/int. rel.) M+: $C_{20}H_{18}O_5$, 338/100, 321/23, 308/15, 282/37, 217/79, 55/20. O espectro é apresentado na Figura 54, pg. 214 do anexo.

RMN de ^{1}H (300 MHz, $CDCl_3$) δ (integração, atribuição, constante de acoplamento, multiplicidade): 6,79 -6,74 (2H, 18-C<u>H</u> e 19-C<u>H</u>, m), 6,67 – 6,62 (1H, 15-C<u>H</u>, m), 5,84 (2H, 20-C<u>H</u>$_2$, s), 4,72 (1H, 3-CH, s), 2,67 -2,50 (4H, 8-C<u>H</u> e 11-C<u>H</u>, m), 2,41 – 2,24 (4H, 6-C<u>H</u> e 13-C<u>H</u>, m), 2,07 – 1,97 (4H, 7-C<u>H</u> e 12-C<u>H</u>, m). O espectro é apresentado na Figura 55, pg. 215 do anexo.

RMN de ^{13}C (75 MHz, $CDCl_3$) δ: 196,6 (C1 e C5), 163,8 (C9 e C10), 147,3 (C16), 146,0 (C17), 138,5 (C14), 121,6 (C19), 116,9 (C2 e C4), 109,0 (C15), 107,9 (C18), 100,8 (C20), 37,0 (C6 e C13), 31,2 (C3), 27,1 (C8 e C11), 20,3 (C7 e C12). O espectro é apresentado na Figura 56, pg. 216 do anexo.

9-(5-(4-clorofenil)furan-2-il)-3,4,5,6,7,9-hexahidro-1*H*-xanteno-1,8(2*H*)-diona **(15)**

Os dados espectroscópicos e detalhes adicionais encontram-se no artigo 1 ao final do capítulo. Os espectros são apresentados nas Figuras 57, 58, 59 e 60, pgs. 217, 218 e 219 do anexo.

9-(5-(4-bromofenil)furan-2-il)-3,4,5,6,7,9-hexaidro-1*H*-xanteno-1,8(2*H*)-diona **(16)**

Os dados espectroscópicos e detalhes adicionais encontram-se no artigo 1 ao final do capítulo. Os espectros são apresentados nas Figuras 61, 62, 63 e 64, pgs. 220, 221 e 222 do anexo.

9-(5-feniltiofen-2-il)-3,4,5,6,7,9-hexaidro-1*H*-xanteno-1,8(2*H*)-diona **(17)**

Os dados espectroscópicos e detalhes adicionais encontram-se no artigo 1 ao final do capítulo. Os espectros são apresentados nas Figuras 65, 66, 67 e 68, pgs. 223, 224 e 225 do anexo.

3,6-dimetil-9-fenil-3,4,5,6,7,9-hexaidro-1*H*-xanteno-1,8(2*H*)-diona **(18)**

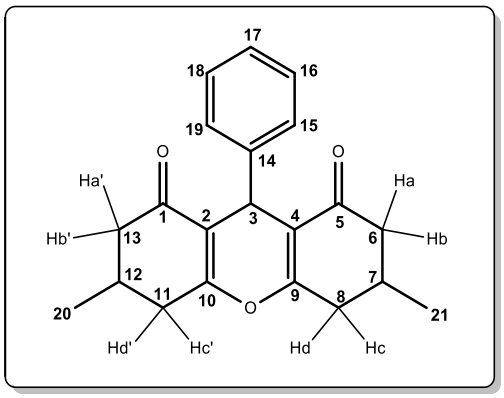

ASPECTO: Sólido amarelo.

MASSA OBTIDA: 54,8 mg (0,17 mmol, 34% de rendimento).

CCD: R_f = 0,47 (hexano-diclorometano-acetato de etila 3:2:1 v/v).

FAIXA DE FUSÃO: 182 - 183 °C.

IV (ATR) ν (cm^{-1}): 2959, 2848, 1657, 1617, 1189. O espectro é apresentado na Figura 69, pg. 226 do anexo.

MS/EI (*m/z*/int. rel.) M+: $C_{21}H_{22}O_3$, 322/47, 305/7, 251/6, 245/100, 203/12. O espectro é apresentado na Figura 70, pg. 226 do anexo.

RMN de ^{1}H (300 MHz, $CDCl_3$) δ (integração, atribuição, constante de acoplamento, multiplicidade): 7,28 (2H, 15-C<u>H</u> e 19-C<u>H</u>, *J* = 7,2 Hz, d), 7,20 (2H, 16-CH e 18-CH, *J* = 7,5 Hz, t), 7,15 (1H, 17-C<u>H</u>, m), 4,79 (1H, 3-C<u>H</u>, s), 2,72 -2,54 (2H, 6Ha e 13Ha', m), 2,45 – 2,17 (6H, 6Hb, 13Hb', 8Hc, 11Hc', 7-C<u>H</u> e 12-C<u>H</u>, m), 2,08 – 1,96 (2H, 8Hd, 13Hd', m), 1,08 (6H, 20-C<u>H</u>$_3$ e 21-C<u>H</u>$_3$, *J* = 6,0 Hz, d). O espectro é apresentado na Figura 71, pg. 227 do anexo.

RMN de ^{13}C (75 MHz, $CDCl_3$) δ: 196,5 (C1 e C5), 163,7 (C9 e C10), 144,4 (C14), 128,3 (C16 e C18), 128,1 e 128,0 (C15 e C19), 126,4 (C17), 116,5 (C2 e C4), 45,2 e 45,1 (C6 e C13), 35,3 e 34,9 (C8 e C11), 31,8 e 31,6 (C3), 28,4 e 27,8 (C7 e C12), 20,8 e 20,7 (C20 e C21). O espectro é apresentado na Figura 72, pg. 228 do anexo.

9-(4-fluorofenil)-3,6-dimetil-3,4,5,6,7,9-hexahidro-1*H*-xanteno-1,8(2*H*)-diona **(19)**

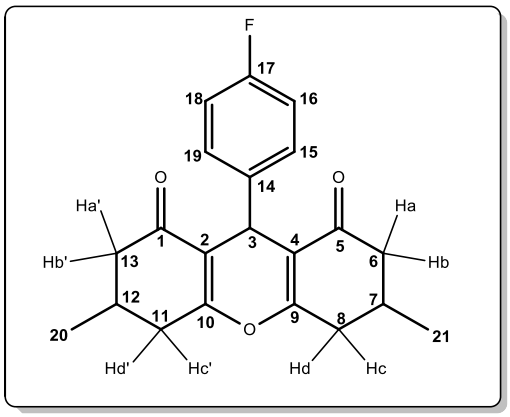

ASPECTO: Sólido branco.

MASSA OBTIDA: 264,6 mg (0,78 mmol, 78% de rendimento).

CCD: R_f = 0,85 (hexano-acetato de etila 2:1 v/v).

FAIXA DE FUSÃO: 177 - 178 ^{o}C.

IV (ATR) ν (**cm^{-1}**): 2953, 2875, 1655, 1622, 1219, 1189. O espectro é apresentado na Figura 73, pg. 229 do anexo.

MS/EI (*m/z*/int. rel.) M+: $C_{21}H_{21}FO_3$, 340/52, 244/100, 203/10. O espectro é apresentado na Figura 74, pg. 229 do anexo.

RMN de ^{1}H (300 MHz, $CDCl_3$) δ (integração, atribuição, constante de acoplamento, multiplicidade): 7,27 – 7,20 (2H, 15-C<u>H</u> e 19-C<u>H</u>, m), 6,87 (2H, 16-CH e 18-CH, J = 8,4 Hz, t), 4,74 (1H, 3-C<u>H</u>, s), 2,69 - 2,56 (2H, 6Ha e 13Ha', m), 2,47 – 2,19 (6H, 6Hb, 13Hb', 8Hc, 11Hc', 7-C<u>H</u> e 12-C<u>H</u>, m), 2,08 – 1,96 (2H, 8Hd, 13Hd', m), 1,10 – 1,03 (6H, 20-C<u>H</u>$_3$ e 21-C<u>H</u>$_3$, m). O espectro é apresentado na Figura 75, pg. 230 do anexo.

RMN de ^{13}C (75 MHz, $CDCl_3$) δ: 196,6 e 196,5 (C1 e C5), 163,7 (C9 e C10), 161,4 (d, J = 242,6 Hz, C17), 140,2 e 140,0 (d, J = 3,0 Hz, C14), 129,8 e 129,7 (d, J = 7,9 Hz, C15 e C19), 116,4, 116,3 e 116,2 (C2 e C4), 114,9 e 114,7 (d, J = 21,2 Hz, C16 e C18), 45,2 e 45,1 (C6 e C13), 35,2 e 34,9 (C8 e C11), 31,3, 31,2 e 31,0 (C3), 28,4, 27,9 e 27,8 (C7 e C12), 20,8 e 20,7 (C20 e C21). O espectro é apresentado na Figura 76, pg. 231 do anexo.

9-(4-clorofenil)-3,6-dimetil-3,4,5,6,7,9-hexaidro-1*H*-xanteno-1,8(2*H*)-diona **(20)**

Os dados espectroscópicos e detalhes adicionais encontram-se no artigo 1 ao final do capítulo. Os espectros são apresentados nas Figuras 77, 78, 79 e 80, pgs. 232, 233 e 234 do anexo.

9-(4-bromofenil)-3,6-dimetil-3,4,5,6,7,9-hexaidro-1*H*-xanteno-1,8(2*H*)-diona **(21)**

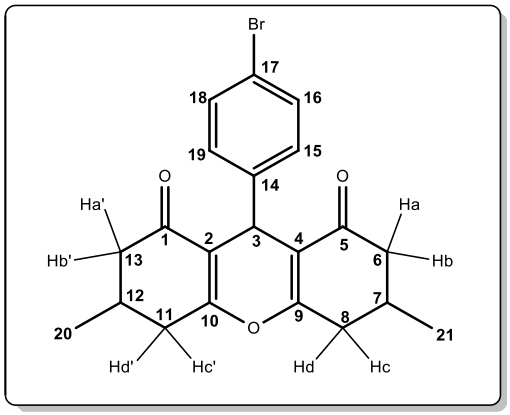

ASPECTO: Sólido branco.

MASSA OBTIDA: 167,6 mg (0,42 mmol, 84% de rendimento).

CCD: R_f = 0,53 (hexano-diclorometano-acetato de etila 3:2:1 v/v).

FAIXA DE FUSÃO: 227 - 229 ºC.

IV (ATR) ν (cm^{-1}): 2947, 2869, 1652, 1619, 1189. O espectro é apresentado na Figura 81, pg. 235 do anexo.

MS/EI (*m/z*/int. rel.) M+: $C_{21}H_{21}BrO_3$, 402/29, 400/29, 321/39, 245/100, 203/12, 69/11. O espectro é apresentado na Figura 82, pg. 235 do anexo.

RMN de ^{1}H (300 MHz, $CDCl_3$) δ (integração, atribuição, constante de acoplamento, multiplicidade): 7,49 (2H, 16-C<u>H</u> e 18-C<u>H</u>, *J* = 8,4 Hz, d), 7,39 (2H, 15-CH e 19-CH, *J* = 8,4 Hz, d), 4,79 (1H, 3-C<u>H</u>, s), 2,70 - 2,57 (2H, 6Ha e 13Ha', m), 2,47 – 2,17 (6H, 6Hb, 13Hb', 8Hc, 11Hc', 7-C<u>H</u> e 12-C<u>H</u>, m), 2,08 – 1,98 (2H, 8Hd, 13Hd', m), 1,11 – 1,03 (6H, 20-C<u>H</u>$_3$ e 21-C<u>H</u>$_3$, m). O espectro é apresentado na Figura 83, pg. 236 do anexo.

RMN de ^{13}C (75 MHz, $CDCl_3$) δ: 196,5 e 196,4 (C1 e C5), 163,8, 163,7 e 163,1 (C9 e C10), 143,5 e 143,3 (C14), 131,2 e 131,1 (C16 e C18),130,2 e 130,1 (C15 e C19), 120,3 e 120,2 (C17), 116,0 e 115,9 (C2 e C4), 45,2 e 45,1 (C6 e C13), 35,2 e 34,9 (C8 e C11), 31,5 e 31,3 (C3), 28,4, 28,3, 27,9 e 27,8 (C7 e C12), 20,8 e 20,7 (C20 e C21). O espectro é apresentado na Figura 84, pg. 237 do anexo.

3,6-dimetil-9-(4-(trifluorometil)fenil)-3,4,5,6,7,9-hexaidro-1*H*-xanteno-1,8(2*H*)-diona **(22)**

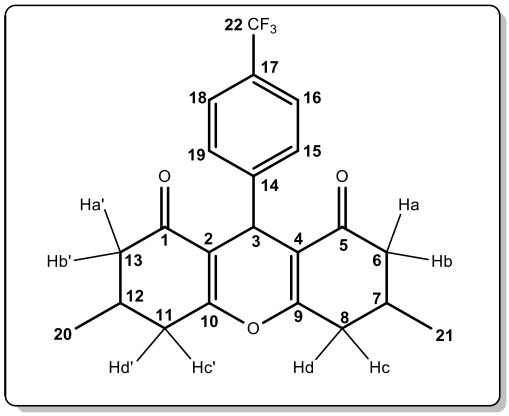

ASPECTO: Sólido branco.

MASSA OBTIDA: 307,0 mg (0,79 mmol, 79% de rendimento).

CCD: R_f = 0,81 (hexano-acetato de etila 2:1 v/v).

FAIXA DE FUSÃO: 212 - 213 °C.

IV (ATR) ν (cm^{-1}): 2951, 2870, 1651, 1619, 1326, 1193. O espectro é apresentado na Figura 85, pg. 238 do anexo.

MS/EI (*m/z*/int. rel.) M+: $C_{22}H_{21}F_3O_3$, 390/38, 320/11, 245/100, 203/10. O espectro é apresentado na Figura 86, pg. 238 do anexo.

RMN de ^{1}H (300 MHz, $CDCl_3$) δ (integração, atribuição, constante de acoplamento, multiplicidade): 7,23 – 7,14 (4H, 15-C<u>H</u>, 16-C<u>H</u>, 18-C<u>H</u> e 19-C<u>H</u>, m), 4,81 (1H, 3-C<u>H</u>, s), 2,70 -2,50 (2H, 6Ha e 13Ha', m), 2,48 – 2,16 (6H, 6Hb, 13Hb', 8Hc, 11Hc', 7-C<u>H</u> e 12-C<u>H</u>, m), 2,09 – 1,97 (2H, 8Hd, 13Hd', m), 1,13 – 0,99 (6H, 20-C<u>H</u>$_3$ e 21-C<u>H</u>$_3$, m). O espectro é apresentado na Figura 87, pg. 239 do anexo.

RMN de ^{13}C (75 MHz, $CDCl_3$) δ: 196,5 e 196,4 (C1 e C5), 164,1, 164,0 e 163,3 (C9 e C10), 148,3 e 148,1 (C14), 128,7 (C15 e C19), 128,5 (q, J = 30,0 Hz, C17), 125,0 (q, J = 4,0 Hz, C16 e C18), 124,2 (q, J = 270,1 Hz, CF_3), 115, 8 e 115,7 (C2 e C4), 45,1 e 45,0 (C6 e C13), 35,2 e 34,9 (C8 e C11), 32,0 e 31,8 (C3), 28,4 e 27,8 (C7 e C12), 20,8 e 20,7 (C20 e C21). O espectro é apresentado na Figura 88, pg. 240 do anexo.

4-(3,6-dimetil-1,8-dioxo-2,3,4,5,6,7,8,9-octaidro-1*H*-xanten-9-il)benzonitrila **(23)**

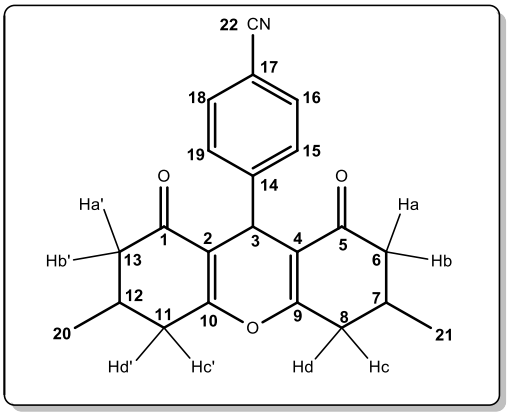

ASPECTO: Sólido branco.

MASSA OBTIDA: 140,2 mg (0,40 mmol, 81% de rendimento).

CCD: R_f = 0,41 (hexano-diclorometano-acetato de etila 3:2:1 v/v).

FAIXA DE FUSÃO: 223 - 224 °C.

IV (ATR) ν (cm^{-1}): 2964, 2876, 2228, 1625, 1616, 1191. O espectro é apresentado na Figura 89, pg. 241 do anexo.

MS/EI (*m/z*/int. rel.) M+: $C_{22}H_{21}NO_3$, 347/36, 245/100, 203/10, 69/7. O espectro é apresentado na Figura 90, pg. 241 do anexo.

RMN de ^{1}H (300 MHz, $CDCl_3$) δ (integração, atribuição, constante de acoplamento, multiplicidade): 7,49 (2H, 15-C<u>H</u> e 19-C<u>H</u>, *J* = 8,4 Hz, d), 7,39 (2H, 16-CH e 18-CH, *J* = 8,4 Hz, d), 4,79 (1H, 3-C<u>H</u>, s), 2,70 -2,58 (2H, 6Ha e 13Ha', m), 2,46 – 2,17 (6H, 6Hb, 13Hb', 8Hc, 11Hc', 7-C<u>H</u> e 12-C<u>H</u>, m), 2,09 – 1,98 (2H, 8Hd, 13Hd', m), 1,11 – 1,03 (6H, 20-C<u>H</u>$_3$ e 21-C<u>H</u>$_3$, m). O espectro é apresentado na Figura 91, pg. 242 do anexo.

RMN de ^{13}C (75 MHz, $CDCl_3$) δ: 196,4 e 196,3 (C1 e C5), 164,2 e 163,5 (C9 e C10), 149,7 e 149,5 (C14), 132,0 e 131,9 (C16 e C18),129,3 e 129,2 (C15 e C19), 119,0 (C22), 115,4 e 115,3 (C2 e C4), 110,1 e 110,0 (C17), 45,1 e 44,9 (C6 e C13), 35,2 e 34,9 (C8 e C11), 32,5 e 32,2 (C3), 28,3, 27,9 e 27,8 (C7 e C12), 20,8 e 20,7 (C20 e C21). O espectro é apresentado na Figura 92, pg. 243 do anexo.

3,6-dimetil-9-(4-nitrofenil)-3,4,5,6,7,9-hexaidro-1*H*-xanteno-1,8(2*H*)-diona **(24)**

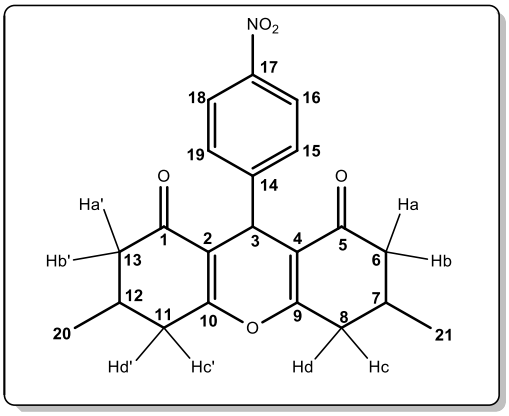

ASPECTO: Sólido branco.

MASSA OBTIDA: 155,1 mg (0,42 mmol, 84% de rendimento).

CCD: R_f = 0,48 (hexano-diclorometano-acetato de etila 3:2:1 v/v).

FAIXA DE FUSÃO: 201 - 202 °C.

IV (ATR) ν (cm^{-1}): 2961, 2876, 1653, 1615, 1513, 1342, 1191. O espectro é apresentado na Figura 93, pg. 244 do anexo.

MS/EI (*m/z*/int. rel.) M+: $C_{21}H_{21}NO_5$, 367/33, 350/62, 320/35, 245/100, 203/17, 69/12. O espectro é apresentado na Figura 94, pg. 244 do anexo.

RMN de ^{1}H (300 MHz, $CDCl_3$) δ (integração, atribuição, constante de acoplamento, multiplicidade): 8,05 (2H, 16-C<u>H</u> e 18-C<u>H</u>, *J* = 8,5 Hz, d), 7,45 (2H, 15-CH e 19-CH, *J* = 8,5 Hz, d), 4,83 (1H, 3-C<u>H</u>, s), 2,72 - 2,58 (2H, 6Ha e 13Ha', m), 2,48 – 2,16 (6H, 6Hb, 13Hb', 8Hc, 11Hc', 7-C<u>H</u> e 12-C<u>H</u>, m), 2,10 – 1,99 (2H, 8Hd, 13Hd', m), 1,13 – 1,03 (6H, 20-C<u>H</u>$_3$ e 21-C<u>H</u>$_3$, m). O espectro é apresentado na Figura 95, pg. 245 do anexo.

RMN de ^{13}C (75 MHz, $CDCl_3$) δ: 196,4 e 196,3 (C1 e C5), 164,3, 164,2, 163,6 e 163,5 (C9 e C10), 151,7 e 151,6 (C17), 146,4 (C14), 129,4 e 129,3 (C15 e C19), 123,4 e 123,3 (C16 e C18), 115,4 e 115,3 (C2 e C4), 45,1 e 44,9 (C6 e C13), 35,2 e 34,9 (C8 e C11), 32,4 e 32,2 (C3), 28,3, 28,2, 27,9 e 27,8 (C7 e C12), 20,8 e 20,6 (C20 e C21). O espectro é apresentado na Figura 96, pg. 246 do anexo.

9-(4-metoxifenil)-3,6-dimetil-3,4,5,6,7,9-hexaidro-1*H*-xanteno-1,8(2*H*)-diona **(25)**

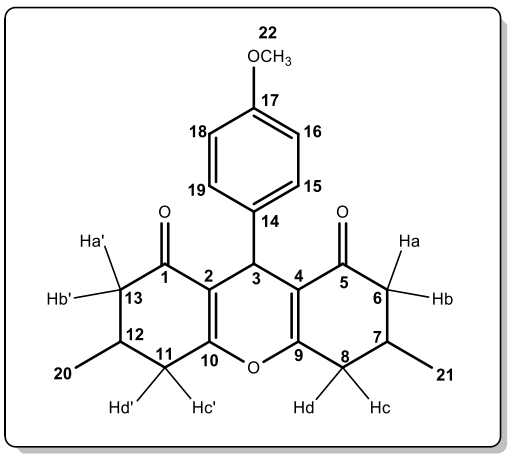

ASPECTO: Sólido branco.

MASSA OBTIDA: 133,7 mg (0,38 mmol, 76% de rendimento).

CCD: R_f = 0,50 (hexano-diclorometano-acetato de etila 3:2:1 v/v).

FAIXA DE FUSÃO: 192 - 193 ºC.

IV (ATR) ν (cm^{-1}): 2964, 2886, 1662, 1620, 1233, 1182, 1031. O espectro é apresentado na Figura 97, pg. 247 do anexo.

MS/EI (*m/z*/int. rel.) M+: $C_{22}H_{24}O_4$, 352/100, 335/53, 321/72, 282/23, 245/100, 203/18, 69/21. O espectro é apresentado na Figura 98, pg. 247 do anexo.

RMN de ^{1}H (300 MHz, $CDCl_3$) δ (integração, atribuição, constante de acoplamento, multiplicidade): 7,19 (2H, 15-C<u>H</u> e 19-C<u>H</u>, *J* = 8,5 Hz, d), 6,74 (2H, 16-CH e 18-CH, *J* = 8,5 Hz, d), 4,73 e 4,71 (1H, 3-C<u>H</u>, s), 3,72 (3H, 22-C<u>H</u>$_3$, s), 2,68 -2,54 (2H, 6Ha e 13Ha', m), 2,44 – 2,17 (6H, 6Hb, 13Hb', 8Hc, 11Hc', 7-C<u>H</u> e 12-C<u>H</u>, m), 2,08 – 1,96 (2H, 8Hd, 13Hd', m), 1,10 – 1,02 (6H, 20-C<u>H</u>$_3$ e 21-C<u>H</u>$_3$, m). O espectro é apresentado na Figura 99, pg. 248 do anexo.

RMN de ^{13}C (75 MHz, $CDCl_3$) δ: 196,6 (C1 e C5), 163,5, 163,4, 162,7 e 162,6 (C9 e C10), 158,0 (C17), 136,8 (C14), 129,3 e 129,2 (C15 e C19), 116,7 e 116,6 e 116,5 (C2 e C4), 113,5 (C16 e C18), 55,1 (C22), 45,2 (C6 e C13), 35,3 e 34,9 (C8 e C11), 30,9 e 30,7 (C3), 28,4, 27,9 e 27,8 (C7 e C12), 20,8 e 20,7 (C20 e C21). O espectro é apresentado na Figura 100, pg. 249 do anexo.

3,6-dimetil-9-(3,4,5-trimetoxifenil)-3,4,5,6,7,9-hexaidro-1*H*-xanteno-1,8(2*H*)-diona **(26)**

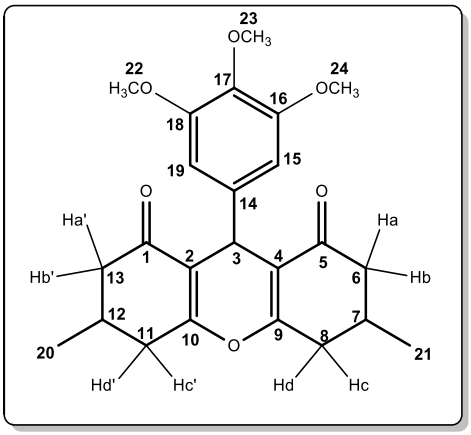

ASPECTO: Sólido branco.

MASSA OBTIDA: 290,0 mg (0,71 mmol, 71% de rendimento).

CCD: R_f = 0,25 (hexano-diclorometano-acetato de etila 3:2:1 v/v).

FAIXA DE FUSÃO: 147 – 148 °C

IV (ATR) ν (cm^{-1}): 2954, 2873, 1659, 1621, 1230, 1184, 1121. O espectro é apresentado na Figura 101, pg. 250 do anexo.

MS/EI (*m/z*/int. rel.) M+: $C_{24}H_{28}O_6$, 412/53, 396/11, 381/100, 245/21, 69/13. O espectro é apresentado na Figura 102, pg. 250 do anexo.

RMN de ^{1}H (300 MHz, $CDCl_3$) δ (integração, atribuição, constante de acoplamento, multiplicidade): 6,49 (2H, 15-C<u>H</u> e 19-C<u>H</u>, *J* = 3,9 Hz, d), 4,74 e 4,72 (1H, 3-C<u>H</u>, s), 3,80 (6H, 22-C<u>H</u>$_3$ e 24-C<u>H</u>$_3$, s), 3,74 (3H, 23-C<u>H</u>$_3$, s), 2,67 – 2,56 (2H, 6Ha e 13Ha', m), 2,47 – 2,11 (6H, 6Hb, 13Hb', 8Hc, 11Hc', 7-C<u>H</u> e 12-C<u>H</u>, m), 2,10 – 1,96 (2H, 8Hd, 13Hd', m), 1,10 – 1,05 (6H, 20-C<u>H</u>$_3$ e 21-C<u>H</u>$_3$, m). O espectro é apresentado na Figura 103, pg. 251 do anexo.

RMN de ^{13}C (75 MHz, $CDCl_3$) δ: 196,7 e 196,6 (C1 e C5), 163,9, 163,7 e 163,0 (C9 e C10), 152,8 e 152,7 (C16 e C18), 139,9, 139,8 e 139,5 (C17), 136,5 (C14), 116,3 e 116,2 (C2 e C4), 105,6 e 105,5 (C15 e C19), 60,6 (C23), 56,1 (C22 e C24), 45,3 e 45,0 (C6 e C13), 35,3 (C8 e C11), 31,4 (C3), 28,3 e 27,9 (C7 e C12), 20,8 e 20,7 (C20 e C21). O espectro é apresentado na Figura 104, pg. 252 do anexo.

9-(4-hidroxifenil)-3,6-dimetil-3,4,5,6,7,9-hexaidro-1*H*-xanteno-1,8(2*H*)-diona **(27)**

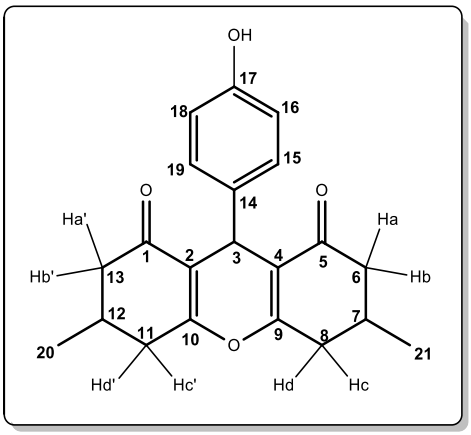

ASPECTO: Sólido amarelo.

MASSA OBTIDA: 87,4 mg (0,26 mmol, 52% de rendimento).

CCD: R_f = 0,20 (hexano-diclorometano-acetato de etila 3:2:1 v/v).

FAIXA DE FUSÃO: 215 - 216 °C

IV (ATR) ν (cm^{-1}): 3600, 3274, 2998, 2964, 2876, 1658, 1638, 1609, 1188. O espectro é apresentado na Figura 105, pg. 253 do anexo.

MS/EI (*m/z*/int. rel.) M+: $C_{21}H_{22}O_4$, 338/87, 321/54, 268/18, 245/100, 203/18, 69/19. O espectro é apresentado na Figura 106, pg. 253 do anexo.

RMN de ^{1}H (300 MHz, DMSO) δ (integração, atribuição, constante de acoplamento, multiplicidade): 9,16 (1H, O-H, s), 6,92 (2H, 15-C<u>H</u> e 19-C<u>H</u>, *J* = 8,3 Hz, d), 6,56 (2H, 16-C<u>H</u> e 18-C<u>H</u>, *J* = 8,3 Hz, d), 4,45 e 4,43 (1H, 3-C<u>H</u>, s), 2,66 - 2,55 (2H, 6Ha e 13Ha', m), 2,50 – 2,21 (6H, 6Hb, 13Hb', 8Hc, 11Hc', 7-C<u>H</u> e 12-C<u>H</u>, m), 2,08 – 2,02 (2H, 8Hd, 13Hd', m), 1,01 – 0,911 (6H, 20-C<u>H</u>$_3$ e 21-C<u>H</u>$_3$, m). O espectro é apresentado na Figura 107, pg. 254 do anexo.

RMN de ^{13}C (75 MHz, DMSO) δ: 196,8, 196,7 e 196,6 (C1 e C5), 164,6, 164,5, 163,7 e 163,6 (C9 e C10), 156,1 e 156,0 (C17), 135,5. 135,4 e 135,2 (C14), 129,4, 129,3 e 129,2 (C15 e C19), 116,1, 115,9 e 115,7 (C2 e C4), 115,1 e 115,0 (C16 e C18), 45,0 e 44,9 (C6 e C13), 34,8 e 34,3 (C8 e C11), 30,4 e 30,2 (C3), 28,2, 28,1 e 27,9 (C7 e C12), 20,8 e 20,7 (C20 e C21). O espectro é apresentado na Figura 108, pg. 255 do anexo.

9-(4-hidroxi-3-metoxifenil)-3,6-dimetil-3,4,5,6,7,9-hexaidro-1*H*-xanteno-1,8(2*H*)-diona **(28)**

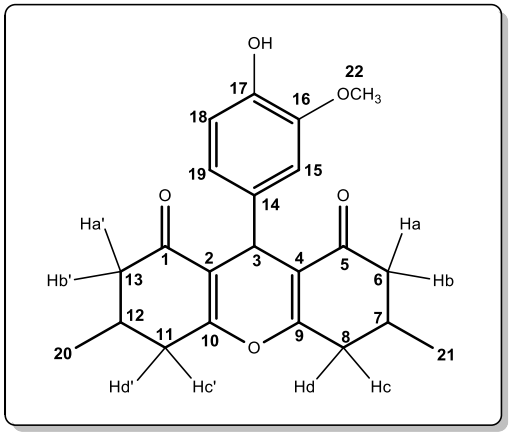

ASPECTO: Sólido amarelo.

MASSA OBTIDA: 147,8 mg (0,40 mmol, 80% de rendimento).

CCD: R_f = 0,28 (hexano-diclorometano-acetato de etila 3:2:1 v/v).

FAIXA DE FUSÃO: 180 - 181 ºC

IV (ATR) ν (cm^{-1}): 3320, 2959, 2871, 1664, 1647, 1616, 1272, 1185, 1127. O espectro é apresentado na Figura 109, pg. 256 do anexo.

MS/EI (*m/z*/int. rel.) M+: $C_{22}H_{24}O_5$, 368/100, 351/52, 337/64, 245/98, 203/20, 69/26. O espectro é apresentado na Figura 110, pg. 256 do anexo.

RMN de ^{1}H (300 MHz, $CDCl_3$) δ (integração, atribuição, constante de acoplamento, multiplicidade): 7,05 -7,01 (1H, 15-C<u>H</u>, m), 6,73 – 6,69 (1H, 19-C<u>H</u>, m), 6,54 – 6,50 (1H, 18-C<u>H</u>, m), 5,58 (1H, O-<u>H</u>, s), 4,71 e 4,68 (1H, 3-CH, s), 3,87 (1H, 22-C<u>H</u>$_3$, s), 2,69 -2,55 (2H, 6Ha e 13Ha', m), 4,45 – 2,20 (6H, 6Hb, 13Hb', 8H, 11Hc', 7-C<u>H</u> e 12-C<u>H</u>, m), 2,08 – 1,97 (2H, 8Hd e 11Hd', m), 1,09 – 1,04 (6H, 20-C<u>H</u>$_3$ e 21-C<u>H</u>$_3$, m). O espectro é apresentado na Figura 111, pg. 257 do anexo.

RMN de ^{13}C (75 MHz, $CDCl_3$) δ: 196,7 (C1 e C5), 163,7, 163,5 e 162,7 (C9 e C10), 145,9 (C16), 144,1 (C17), 136,7 e 136,5 (C14), 119,8 e 119,7 (C19), 116,7, 116,6 e 116,5 (C2 e C4), 114,0 e 113,9 (C18), 112,4 e 112,2 (C15), 55,9 (C22), 45,2 (C6 e C13), 35,3

e 34,9 (C8 e C11), 31,2 e 31,0 (C3), 28,4, 27,9 e 27,8 (C7 e C12), 20,8 e 20,7 (C20 e C21). O espectro é apresentado na Figura 112, pg. 258 do anexo.

9-(benzo[*d*][1,3]dioxol-5-il)-3,6-diimetil-3,4,5,6,7,9-hexaidro-1*H*-xanteno-1,8(2*H*)-diona **(29)**

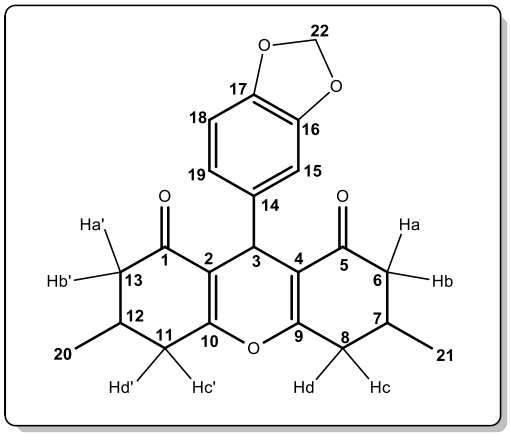

ASPECTO: Sólido branco.

MASSA OBTIDA: 151,5 mg (0,41 mmol, 83% de rendimento).

CCD: R_f = 0,41 (hexano-diclorometano-acetato de etila 3:2:1 v/v).

FAIXA DE FUSÃO: 201 - 202 ^oC

IV (ATR) ν **(cm^{-1})**: 2947, 2924, 2861, 1651, 1617, 1366, 1257, 1186. O espectro é apresentado na Figura 113, pg. 259 do anexo.

MS/EI (*m/z*/int. rel.) M+: $C_{22}H_{22}O_5$, 366/100, 296/56, 245/86, 203/18, 69/21. O espectro é apresentado na Figura 114, pg. 259 do anexo.

RMN de ^{1}H (300 MHz, $CDCl_3$) δ (integração, atribuição, constante de acoplamento, multiplicidade): 6,78 -6,72 (2H, 18-C<u>H</u> e 19-C<u>H</u>, m), 6,66 – 6,61 (1H, 15-C<u>H</u>, m), 5,84 (2H, 22-C<u>H</u>$_2$, s), 4,70 e 4,68 (1H, 3-CH, s), 2,69 -2,54 (2H, 6Ha e 13Ha', m), 4,45 – 2,15 (6H, 6Hb, 13Hb', 8H, 11Hc', 7-C<u>H</u> e 12-C<u>H</u>, m), 2,10 – 1,95 (2H, 8Hd e 11Hd', m), 1,10 – 1,03 (6H, 20-C<u>H</u>$_3$ e 21-C<u>H</u>$_3$, m). O espectro é apresentado na Figura 115, pg. 260 do anexo.

RMN de ^{13}C (75 MHz, $CDCl_3$) δ: 196,6 (C1 e C5), 163,6, 163,5 e 162,8 (C9 e C10), 147,3 (C16), 146,0 e 145,9 (C17), 138,5 e 138,4 (C14), 121,6 e 121,5 (C19), 116,5 e 116,3 (C2 e C4), 109,0 e 108,9 (C15), 107,9 e 107,8 (C18), 100,7 (C22), 45,2 (C6 e C13), 35,3 e 34,9 (C8 e C11), 31,4 e 31,2 (C3), 28,4 e 27,8 (C7 e C12), 20,8 (C20 e C21). O espectro é apresentado na Figura 116, pg. 261 do anexo.

9-(5-(4-clorofenil)furan-2-il)-3,6-dimetil-3,4,5,6,7,9-hexaidro-1*H*-xanteno-1,8(2*H*)-diona **(30)**

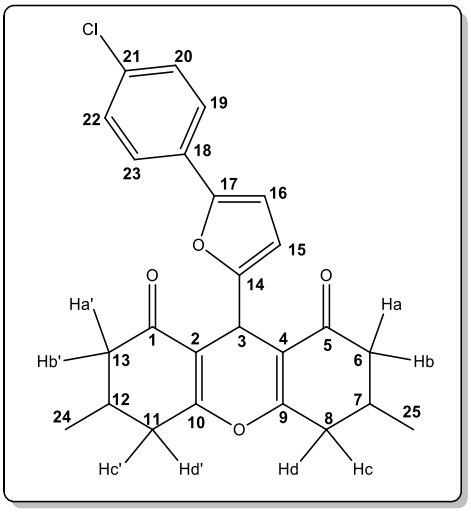

ASPECTO: Sólido amarelo.

MASSA OBTIDA: 188,7 mg (0,45 mmol, 45% de rendimento).

CCD: R_f = 0,37 (hexano-diclorometano-acetato de etila 3:2:1 v/v).

FAIXA DE FUSÃO: 137 - 138 ^{o}C.

IV (ATR) ν **(cm^{-1})**: 2964, 2874, 1659, 1619, 1532, 1483, 1182. O espectro é apresentado na Figura 117, pg. 262 do anexo.

MS/EI (*m/z*/int. rel.) M+: $C_{25}H_{23}ClO_4$, 424/8, 422/25, 376/18, 282/70, 244/100, 140/15, 69/29. O espectro é apresentado na Figura 118, pg. 262 do anexo.

RMN de ^{1}H (300 MHz, $CDCl_3$) δ (integração, atribuição, constante de acoplamento, multiplicidade): 7,42 (2H, 20-C<u>H</u> e 22-C<u>H</u>, *J* = 8,2 Hz, d), 7,27 (2H, 19-C<u>H</u> e 23-C<u>H</u>, *J* = 8,2 Hz, d), 6,47 (1H, 16-C<u>H</u>, s), 6,23 (1H, 15-C<u>H</u>, s), 5,00 (1H, 3-C<u>H</u>, s), 2,72 – 2,58

(2H, 6Ha e 13Ha', m), 2,57 – 2,33 (4H, 6Hb, 13Hb', 8Hc e 11Hc', m), 2,31 – 2,24 (2H, 8Hd e 1Hd', m) 2,16 – 2,01 (2H, 7-C<u>H</u> e 12-C<u>H</u>, m), 1,13 – 1,07 (6H, 24-C<u>H</u>$_3$ e 25-C<u>H</u>$_3$, m). O espectro é apresentado na Figura 119, pg. 263 do anexo.

RMN de ^{13}C (75 MHz, $CDCl_3$) δ: 196,4 (C1 e C5), 164,8 e 164,1 (C9 e C10), 155,2 e 155,1 (C14), 151,1 e 151,0 (C17), 132,2 (C18), 129,6 (C21), 128,7 (C20 e C22), 124,5 (C19 e C23), 113,4 e 113,3 (C2 e C4), 108,8 e 108,6 (C15), 106,8 e 106,7 (C16), 45,2 e 44,9 (C6 e C13), 35,3 e 35,0 (C8 e C11), 28,3 e 27,9 (C3), 25,6 e 25,5 (C7 e C12), 20,8 e 20,6 (C24 e C25). O espectro é apresentado na Figura 120, pg. 264 do anexo.

9-(5-(4-bromofenil)furan-2-il)-3,6-dimetil-3,4,5,6,7,9-hexaidro-1*H*-xanteno-1,8(2*H*)-diona **(31)**

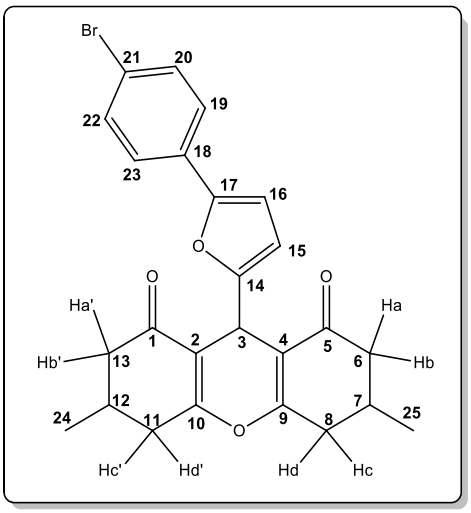

ASPECTO: Sólido amarelo.

MASSA OBTIDA: 197,7 mg (0,44 mmol, 44% de rendimento).

CCD: R_f = 0,39 (hexano-diclorometano-acetato de etila 3:2:1 v/v).

FAIXA DE FUSÃO: 129 - 130 ^{o}C.

IV (ATR) ν **(cm^{-1})**: 2962, 2874, 1660, 1619, 1532, 1479, 1187. O espectro é apresentado na Figura 121, pg. 265 do anexo.

MS/EI (*m/z*/int. rel.) M+: $C_{25}H_{23}BrO_4$, 468/16, 466/20, 282/67, 244/100, 182/20, 69/29. O espectro é apresentado na Figura 122, pg. 265 do anexo.

RMN de ^{1}H (300 MHz, $CDCl_3$) δ (integração, atribuição, constante de acoplamento, multiplicidade): 7,42 (2H, 20-C<u>H</u> e 22-C<u>H</u>, *J* = 8,1 Hz, d), 7,38 (2H, 19-C<u>H</u> e 23-C<u>H</u>, *J* = 8,1 Hz, d), 6,48 (1H, 16-C<u>H</u>, s), 6,23 (1H, 15-C<u>H</u>, s), 5,00 (1H, 3-C<u>H</u>, s), 2,73 – 2,58 (2H, 6Ha e 13Ha', m), 2,56 – 2,35 (4H, 6Hb, 13Hb', 8Hc e 11Hc', m), 2,29 – 2,22 (2H, 8Hd e 1Hd', m) 2,14 – 2,00 (2H, 7-C<u>H</u> e 12-C<u>H</u>, m), 1,12 – 1,07 (6H, 24-C<u>H</u>$_3$ e 25-C<u>H</u>$_3$, m). O espectro é apresentado na Figura 123, pg. 266 do anexo.

RMN de ^{13}C (75 MHz, $CDCl_3$) δ: 196,4 (C1 e C5), 164,8 e 164,1 (C9 e C10), 155,2 e 155,1 (C14), 151,1 e 151,0 (C17), 132,2 e 131,6 (C20 e C22), 126,7 (C18), 124,8 (C19 e C23), 120,3 (C21), 113,3 e 113,1 (C2 e C4), 108,8 e 108,6 (C15), 106,9 e 106,8 (C16), 45,2 e 44,9 (C6 e C13), 35,4 e 35,0 (C8 e C11), 28,3 e 27,9 (C3), 25,6 e 25,5 (C7 e C12), 20,8 e 20,6 (C24 e C25). O espectro é apresentado na Figura 124, pg. 267 do anexo.

2-(2,6-diclorobenzilideno)-5,5-dimetilcicloexan-1,3-diona **(32)**

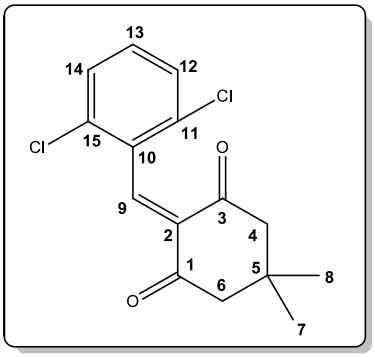

ASPECTO: Sólido amarelo.

MASSA OBTIDA: 140,0 mg (0,47 mmol, 47% de rendimento).

CCD: R_f = 0,87 (hexano-diclorometano-acetato de etila 3:2:1 v/v).

FAIXA DE FUSÃO: 101 - 102 °C

IV (ATR) ν **(cm^{-1})**: 2954, 2870, 1714, 1677, 1608, 1187, 776. O espectro é apresentado na Figura 125, pg. 268 do anexo.

MS/EI (*m/z*/int. rel.) M+: $C_{15}H_{14}Cl_2O_2$, 262/4, 260/12, 247/32, 246/16, 245/100, 91/8, 76/18, 63/11 (O pico do íon molecular (297) não aparece no espectro). O espectro é apresentado na Figura 126, pg. 268 do anexo.

RMN de ^{1}H (300 MHz, $CDCl_3$) δ (integração, atribuição, constante de acoplamento, multiplicidade): 7,83 (1H, 9-C<u>H</u>, s), 7,33 – 7,22 (3H, 12-C<u>H</u>, 13-C<u>H</u> e 14-C<u>H</u>, m), 2,64 (2H, 4-C<u>H</u>$_2$, s), 2,56 (2H, 6-C<u>H</u>$_2$, s), 1,12 (6H, 7-C<u>H</u>$_3$ e 8-C<u>H</u>$_3$, s). O espectro é apresentado na Figura 127, pg. 269 do anexo.

RMN de ^{13}C (75 MHz, $CDCl_3$) δ: 196,6 (C1 e C3), 143,3 (C9), 136,5 (C2), 133,8 (C11 e C15), 132,8 (C13), 129,6 (C12 e C14), 127,8 (C10), 55,1 (C4), 52,7 (C6), 29,9 (C5), 28,6 (C7 e C8). O espectro é apresentado na Figura 128, pg. 270 do anexo.

2,2'-((5-(4-clorofenil)furan-2-il)metileno)*bis*(3-hidroxi-5,5-dimetilcicloex-2-enona) **(33)**

Os dados espectroscópicos e detalhes adicionais encontram-se no artigo 2 ao final do capítulo. Os espectros são apresentados nas Figuras 129, 130 e 131, pgs. 271, 272 e 273 do anexo.

2,2'-((5-(4-bromofenil)furan-2-il)metileno)*bis*(3-hidroxi-5,5-dimetilcicloex-2-enona) **(34)**

Os dados espectroscópicos e detalhes adicionais encontram-se no artigo 2 ao final do capítulo. Os espectros são apresentados nas Figuras 132, 133 e 134, pgs. 274, 275 e 276 do anexo.

2,2'-((4-(dimetilamino)fenil)metileno)bis(5,5-dimetilcicloexan-1,3-diona) **(35)**

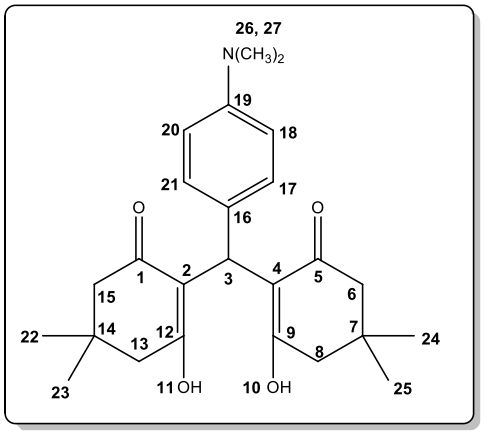

ASPECTO: Sólido amarelo.

MASSA OBTIDA: 252,4 mg (0,61 mmol, 61% de rendimento).

CCD: R_f = 0,71 (hexano-diclorometano-acetato de etila 3:2:1 v/v).

FAIXA DE FUSÃO: 175 – 176 °C

IV (ATR) ν (**cm^{-1}**): 3216 – 1940, 2959, 2872, 1580, 1366, 1160, 1150. O espectro é apresentado na Figura 135, pg. 277 do anexo.

RMN de ^{1}H (300 MHz, $CDCl_3$) δ (integração, atribuição, constante de acoplamento, multiplicidade): 11,94 (1H, 10-O-H e 11-O-H, s), 6,95 (2H, 17-CH e 21-CH, *J* = 7,8 Hz, d), 6,66 (2H, 18-CH e 20-CH, *J* = 7,8 Hz, d), 5,48 (1H, 3-CH, s), 2,90 (6H, 26-CH_3 e 27-CH_3, s), 2,47 – 2,30 (8H, 6-CH_2, 8-CH_2, 13-CH_2 e 15-CH_2, m), 1,23 (6H, 22-CH_3 e 24-CH_3, s), 1,10 (6H, 23-CH_3 e 25-CH_3, s). O espectro é apresentado na Figura 136, pg. 278 do anexo.

RMN de ^{13}C (75 MHz, $CDCl_3$) δ: 190,2 e 189,3 (C1 e C5), 148,7 (C9 e C12), 127,5 (C17 e C21), 125,6 (C16 e C19), 115,9 (C2 e C4), 112,6 (C18 e C20), 47,1 (C6 e C15), 46,4 (C8 e C13), 40,7 (C26 e C27), 31,9 e 31,8 (C3), 31,4 (C7 e C14), 29,7 (C22 e C24), 27,3 (C23 e C25). O espectro é apresentado na Figura 137, pg. 279 do anexo.

2,2'-((3,4,5-trimetoxifenil)metileno)bis(5,5-dimetilcicloexan-1,3-diona) **(36)**

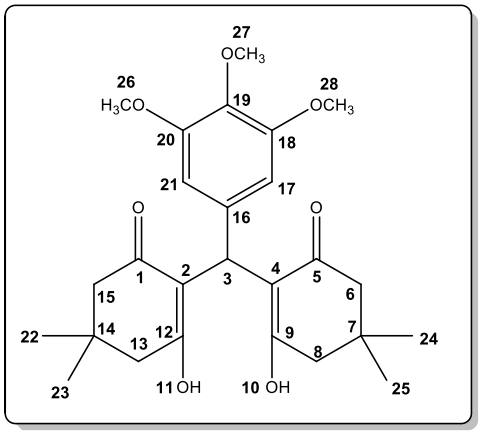

ASPECTO: Sólido branco.

MASSA OBTIDA: 335,9 mg (0,73 mmol, 73% de rendimento).

CCD: R_f = 0,41 (hexano-diclorometano-acetato de etila 3:2:1 v/v).

FAIXA DE FUSÃO: 180 – 181 °C.

IV (ATR) ν (cm^{-1}): 3200 – 1924, 2952, 2867, 1578, 1370, 1231, 1168, 1153. O espectro é apresentado na Figura 138, pg. 280 do anexo.

RMN de ^{1}H (300 MHz, $CDCl_3$) δ (integração, atribuição, constante de acoplamento, multiplicidade): 12,03 (1H, 10-O-H e 11-O-H, s), 6,34 (2H, 17-CH e 21-CH, s), 5,49 (1H, 3-CH, s), 3,80 (3H, 27-CH_3, s), 3, 74 (6H, 26-CH_3 e 28-CH_3, s), 2,40 (4H, 6-CH_2 e 15-CH_2, s), 2,35 (4H, 8-CH_2 e 13-CH_2, s), 1,23 (6H, 22-CH_3 e 24-CH_3, s), 1,11 (6H, 23-CH_3 e 25-CH_3, s). O espectro é apresentado na Figura 139, pg. 281 do anexo.

RMN de ^{13}C (75 MHz, $CDCl_3$) δ: 194,4 (C1 e C5), 189,4 (C9 e C12), 152,8 (C18 e C20), 135,8 (C16), 133,7 (C19), 115,5 (C2 e C4), 104,0 (C17 e C21), 60,8 (C27), 55,8 (C26 e C28), 47,0 (C6 e C15), 46,3 (C8 e C13), 32,7 (C3), 31,1 (C7 e C14), 30,1 (C22 e C24), 26,7 (C23 e C25). O espectro é apresentado na Figura 140, pg. 282 do anexo.

3,3,6,6-tetrametil-9-fenil-3,4,5,6,7,9-hexaidro-1*H*-xanteno-1,8(2*H*)-diona **(37)**

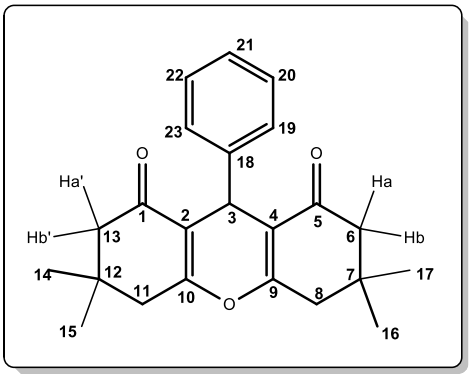

ASPECTO: Sólido amarelo.

MASSA OBTIDA: 275,7 mg (0,79 mmol, 79% de rendimento).

CCD: R_f = 0,53 (hexano-diclorometano-acetato de etila 3:2:1 v/v).

FAIXA DE FUSÃO: 203 - 204 ^{o}C.

IV (ATR) ν (cm^{-1}): 2957, 2871, 1659, 1624, 1359, 1197, 1164, 1139. O espectro é apresentado na Figura 141, pg. 283 do anexo.

MS/EI (*m/z*/int. rel.) M+: $C_{23}H_{26}O_3$, 350/49, 273/100, 217/23, 161/8. O espectro é apresentado na Figura 142, pg. 283 do anexo.

RMN de ^{1}H (300 MHz, $CDCl_3$) δ (integração, atribuição, constante de acoplamento, multiplicidade): 7,28 (2H, 19-C<u>H</u> e 23-C<u>H</u>, *J* = 7,5 Hz, d), 7,20 (2H, 20-C<u>H</u> e 22-C<u>H</u>, *J* = 7,5 Hz, t), 7,09 (1H, 21-C<u>H</u>, *J* = 7,5 Hz, t), 4,74 (1H, 3-C<u>H</u>, s), 2,46 (4H, 8-C<u>H</u>$_2$ e 11-C<u>H</u>$_2$, s), 2,23 (2H, 6 Ha, 13 Ha', *J* = 16,3 Hz, d), 2,15 23 (2H, 6 Hb, 13 Hb', *J* = 16,3 Hz, d), 1,09 (6H, 14-C<u>H</u>$_3$ e 17-C<u>H</u>$_3$, s), 0,98 (6H, 14-C<u>H</u>$_3$ e 16-C<u>H</u>$_3$, s). O espectro é apresentado na Figura 143, pg. 284 do anexo.

RMN de ^{13}C (75 MHz, $CDCl_3$) δ: 196,4 (C1 e C5), 162,3 (C9 e C10), 144,1 (C18), 128,4 (C19 e C23), 128,0 (C20 e C22), 126,3 (C21), 115,6 (C2 e C4), 50,7 (C6 e C13), 40,9 (C8 e C11), 32,2 (C3), 31,8 (C7 e C12), 29,2 (C15 e C16), 27,3 (C14 e C17). O espectro é apresentado na Figura 144, pg. 285 do anexo.

9-(4-fluorofenil)-3,3,6,6-tetrametil-3,4,5,6,7,9-hexahidro-1*H*-xanteno-1,8(2*H*)-diona **(38)**

Os dados espectroscópicos e detalhes adicionais encontram-se no artigo 1 ao final do capítulo. Os espectros são apresentados nas Figuras 145, 146, 147 e 148, pgs. 286, 287 e 288 do anexo.

9-(4-clorofenil)-3,3,6,6-tetrametil-3,4,5,6,7,9-hexaidro-1*H*-xanteno-1,8(2*H*)-diona **(39)**

Os dados espectroscópicos e detalhes adicionais encontram-se no artigo 1 ao final do capítulo. Os espectros são apresentados nas Figuras 149, 150, 151 e 152, pgs. 289, 290 e 291 do anexo.

9-(4-bromofenil)-3,3,6,6-tetrametil-3,4,5,6,7,9-hexaidro-1*H*-xanteno-1,8(2*H*)-diona **(40)**

Os dados espectroscópicos e detalhes adicionais encontram-se no artigo 1 ao final do capítulo. Os espectros são apresentados nas Figuras 153, 154, 155 e 156, pgs. 292, 293 e 294 do anexo.

3,3,6,6-tetrametil-9-(4-(trifluorometil)fenil)-3,4,5,6,7,9-hexahidro-1*H*-xanteno-1,8(2*H*)-diona **(41)**

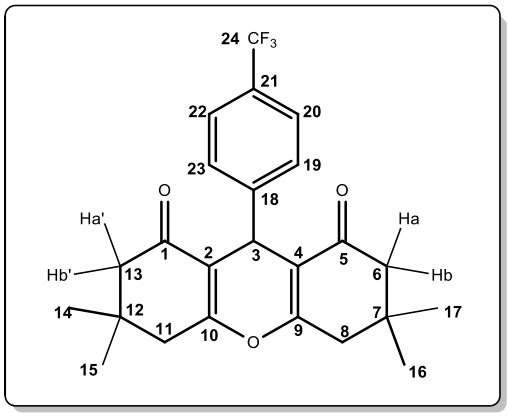

ASPECTO: Sólido branco.

MASSA OBTIDA: 253,6 mg (0,61 mmol, 61% de rendimento).

CCD: R_f = 0,78 (hexano-acetato de etila 2:1 v/v).

FAIXA DE FUSÃO: 242 - 243 °C.

IV (ATR) ν (cm^{-1}): 2961, 2871, 1660, 1617, 1360, 1322, 1198, 1159, 1136. O espectro é apresentado na Figura 157, pg. 295 do anexo.

MS/EI (*m/z*/int. rel.): 418/37, 273/100, 217/22, 161/15, 55/25, 43/21, 41/32. O espectro é apresentado na Figura 158, pg. 295 do anexo.

HRMS (M+H$^+$): Calculado para $C_{24}H_{26}F_3O_3$: 419,1834; encontrado: 419,1839.

RMN de ^{1}H (300 MHz, $CDCl_3$) δ (integração, atribuição, constante de acoplamento, multiplicidade): 7,47 (2H, 20-C<u>H</u> e 22-C<u>H</u>, *J* = 7,8 Hz, d), 7,40 (2H, 19-C<u>H</u> e 23-C<u>H</u>, *J* = 7,8 Hz, d), 4,79 (1H, 3-C<u>H</u>, s), 2,48 (4H, 8-C<u>H</u>$_2$ e 11-C<u>H</u>$_2$, s), 2,24 (2H, 6 Ha e 13 Ha', *J* = 16,3 Hz, d), 2,15 (2H, 6 Hb e 13 Hb', *J* = 16,3 Hz, d), 1,10 (6H, 14-C<u>H</u>$_3$ e 17-C<u>H</u>$_3$, s), 0,98 (6H, 14-C<u>H</u>$_3$ e 16-C<u>H</u>$_3$, s). O espectro é apresentado na Figura 159, pg. 296 do anexo.

RMN de ^{13}C (75 MHz, $CDCl_3$) δ: 196,4 (C1 e C5), 162,7 (C9 e C10), 148,0 (C18), 128,7 (C19 e C23), 128,0 (q, *J* = 31,9 Hz, C21), 124,2 (q, *J* = 270,1 Hz, 24-CF_3), 125,0 (q, *J* =

3,7 Hz, C20 e C22), 115,0 (C2 e C4), 50,6 (C6 e C13), 40,8 (C8 e C11), 32,2 (C3), 32,0 (C7 e C12), 29,2 (C15 e C16), 27,3 (C14 e C17). O espectro é apresentado na Figura 160, pg. 297 do anexo.

4-(3,3,6,6-tetrametil-1,8-dioxo-2,3,4,5,6,7,8,9-octaidro-1*H*-xanten-9-il)benzonitrila **(42)**

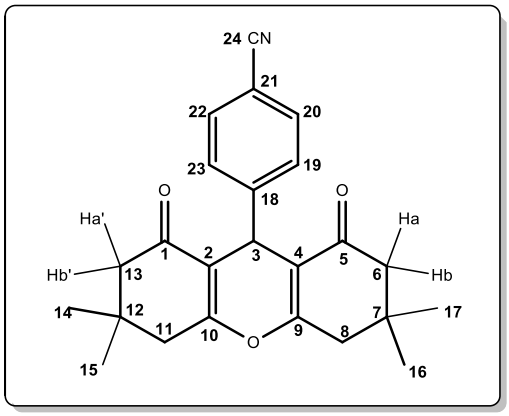

ASPECTO: Sólido branco.

MASSA OBTIDA: 327,7 mg (0,87 mmol, 87% de rendimento).

CCD: R_f = 0,79 (hexano-acetato de etila 2:1 v/v).

FAIXA DE FUSÃO: 198 - 199 °C.

IV (ATR) ν (cm^{-1}): 2961, 2872, 2225, 1659, 1620, 1360, 1197, 1164, 1138. O espectro é apresentado na Figura 161, pg. 298 do anexo.

MS/EI (*m/z*/int. rel.): 375/41, 273/100, 217/21, 161/14, 55/22, 43/17, 41/33. O espectro é apresentado na Figura 162, pg. 298 do anexo.

HRMS (M+H$^+$): Calculado para $C_{24}H_{26}NO_3$: 376,1913; encontrado: 376,1936.

RMN de ^{1}H (300 MHz, $CDCl_3$) δ (integração, atribuição, constante de acoplamento, multiplicidade): 7,50 (2H, 20-C<u>H</u> e 22-C<u>H</u>, *J* = 7,6 Hz, d), 7,40 (2H, 19-C<u>H</u> e 23-C<u>H</u>, *J* = 7,6 Hz, d), 4,75 (1H, 3-C<u>H</u>, s), 2,47 (4H, 8-C<u>H</u>$_2$ e 11-C<u>H</u>$_2$, s), 2,23 (2H, 6 Ha e 13 Ha', *J* = 16,3 Hz, d), 2,14 (2H, 6 Hb e 13 Hb', *J* = 16,3 Hz, d), 1,10 (6H, 14-C<u>H</u>$_3$ e 17-C<u>H</u>$_3$, s), 0,97 (6H, 14-C<u>H</u>$_3$ e 16-C<u>H</u>$_3$, s). O espectro é apresentado na Figura 163, pg. 299 do anexo.

RMN de ^{13}C (75 MHz, $CDCl_3$) δ: 196,3 (C1 e C5), 162,9 (C9 e C10), 149,5 (C18), 131,9 (C19 e C23), 129,3 (C20 e C22), 119,0 (C24), 114,5 (C2 e C4), 110,1 (C21), 50,6 (C6 e C13), 40,8 (C8 e C11), 32,5 (C3), 32,2 (C7 e C12), 29,2 (C15 e C16), 27,2 (C14 e C17). O espectro é apresentado na Figura 164, pg. 300 do anexo.

3,3,6,6-tetrametil-9-(4-nitrofenil)-3,4,5,6,7,9-hexahidro-1*H*-xanteno-1,8(2*H*)-diona **(43)**

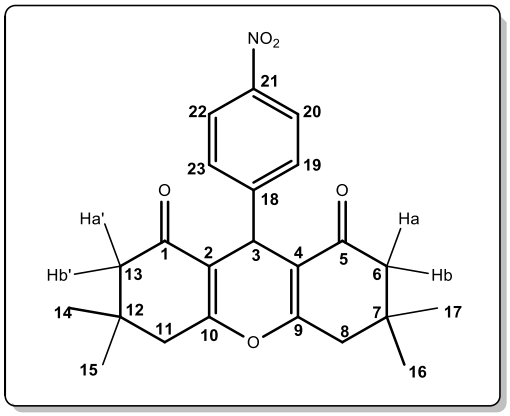

ASPECTO: Sólido branco.

MASSA OBTIDA: 343,9 mg (0,87 mmol, 87% de rendimento).

CCD: R_f = 0,79 (hexano-acetato de etila 2:1 v/v).

FAIXA DE FUSÃO: 221 - 222 °C.

IV (ATR) ν **(cm^{-1})**: 2959, 2871, 1654, 1620, 1515, 1359, 1342, 1199, 1164, 1138. O espectro é apresentado na Figura 165, pg. 301 do anexo.

MS/EI (*m/z*/int. rel.): 395/48, 378/68, 348/25, 273/100, 217/32, 161/24, 152/15, 77/16, 55/33, 43/24, 41/42. O espectro é apresentado na Figura 166, pg. 301 do anexo.

HRMS (M+H$^+$): Calculado para $C_{23}H_{26}NO_5$: 396,1811; encontrado: 396,1841.

RMN de ^{1}H (300 MHz, $CDCl_3$) δ (integração, atribuição, constante de acoplamento, multiplicidade): 8,08 (2H, 20-C<u>H</u> e 22-C<u>H</u>, *J* = 7,9 Hz, d), 7,46 (2H, 19-C<u>H</u> e 23-C<u>H</u>, *J* = 7,9 Hz, d), 4,81 (1H, 3-C<u>H</u>, s), 2,49 (4H, 8-C<u>H</u>$_2$ e 11-C<u>H</u>$_2$, s), 2,24 (2H, 6 Ha e 13 Ha', *J* = 16,3 Hz, d), 2,15 (2H, 6 Hb e 13 Hb', *J* = 16,3 Hz, d), 1,10 (6H, 14-C<u>H</u>$_3$ e 17-C<u>H</u>$_3$,

s), 0,98 (6H, 14-C<u>H</u>$_3$ e 16-C<u>H</u>$_3$, s). O espectro é apresentado na Figura 167, pg. 302 do anexo.

RMN de ^{13}C (75 MHz, $CDCl_3$) δ: 196,3 (C1 e C5), 163,0 (C9 e C10), 151,5 (C18), 146,4 (C21), 129,3 (C19 e C23), 123,4 (C20 e C22), 114,5 (C2 e C4), 50,6 (C6 e C13), 40,8 (C8 e C11), 32,4 (C3), 32,2 (C7 e C12), 29,2 (C15 e C16), 27,2 (C14 e C17). O espectro é apresentado na Figura 168, pg. 303 do anexo.

9-(4-metoxifenil)-3,3,6,6-tetrametil-3,4,5,6,7,9-hexaidro-1*H*-xanteno-1,8(2*H*)-diona **(44)**

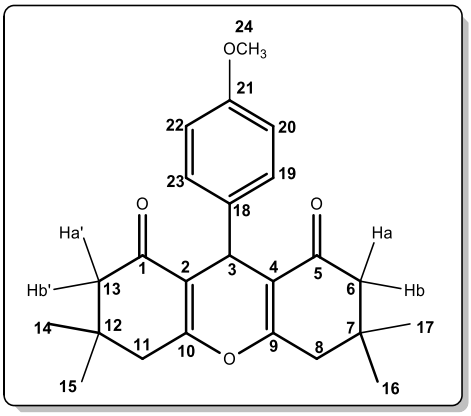

ASPECTO: Sólido branco.

MASSA OBTIDA: 292,3 mg (0,77 mmol, 77% de rendimento).

CCD: R_f = 0,90 (hexano-acetato de etila 2:1 v/v).

FAIXA DE FUSÃO: 252 – 253 ^{o}C.

IV (ATR) ν **(cm^{-1})**: 2957, 2873, 1678, 1662, 1625, 1357, 1234, 1193, 1163, 1136, 1033. O espectro é apresentado na Figura 169, pg. 304 do anexo.

MS/EI (*m/z*/int. rel.) M+: $C_{24}H_{28}O_4$, 380/100, 363/43, 348/43, 296/33, 273/93, 217/31, 161/16, 83/19. O espectro é apresentado na Figura 170, pg. 304 do anexo.

RMN de ^{1}H (300 MHz, $CDCl_3$) δ (integração, atribuição, constante de acoplamento, multiplicidade): 7,20 (2H, 19-C<u>H</u> e 23-C<u>H</u>, *J* = 8,6 Hz, d), 6,75 (2H, 20-C<u>H</u> e 22-C<u>H</u>, *J* = 8,6 Hz, d), 4,69 (1H, 3-C<u>H</u>, s), 3,73 e 3,72 (3H, 24-C<u>H</u>$_3$, s), 2,45 (4H, 8-C<u>H</u>$_2$ e 11-C<u>H</u>$_2$,

s), 2,23 (2H, 6 Ha e 13 Ha', *J* = 15,7 Hz, d), 2,15 (2H, 6 Hb e 13 Hb', *J* = 15,7 Hz, d), 1,09 (6H, 14-C<u>H</u>$_3$ e 17-C<u>H</u>$_3$, s), 0,98 (6H, 15-C<u>H</u>$_3$ e 16-C<u>H</u>$_3$, s). O espectro é apresentado na Figura 171, pg. 305 do anexo.

RMN de ^{13}C (75 MHz, $CDCl_3$) δ: 196,5 (C1 e C5), 162,0 (C9 e C10), 157,9 (C21), 136,5 (C18), 129,3 (C19 e C23), 115,8 (C2 e C4), 113 4 (C20 e C22), 55,1 (C24), 50,8 (C6 e C13), 40,8 (C8 e C11), 32,2 (C3), 30,9 (C7 e C12), 29,2 (C15 e C16), 27,3 (C14 e C17). O espectro é apresentado na Figura 172, pg. 306 do anexo.

9-(3,4-dimetoxifenil)-3,3,6,6-tetrametil-3,4,5,6,7,9-hexaidro-1*H*-xanteno-1,8(2*H*)-diona **(45)**

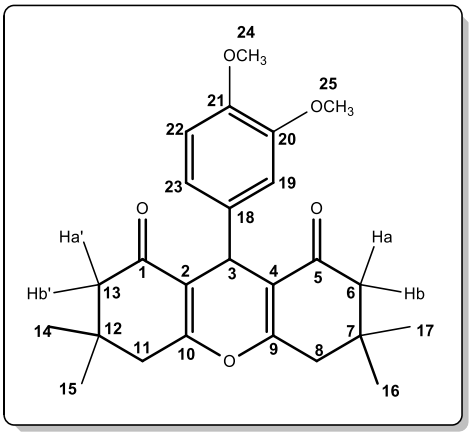

ASPECTO: Sólido amarelo.

MASSA OBTIDA: 406,1 mg (0,99 mmol, 99% de rendimento).

CCD: R_f = 0,58 (hexano-diclorometano-acetato de etila 3:2:1 v/v).

FAIXA DE FUSÃO: 181 – 182 ^{o}C.

IV (ATR) ν **(cm^{-1})**: 2959, 2873, 1656, 1621, 1361, 1260, 1198, 1167, 1136. O espectro é apresentado na Figura 173, pg. 307 do anexo.

MS/EI (*m/z*/int. rel.) M+: $C_{25}H_{30}O_5$, 410/69, 379/100, 273/35, 217/16, 83/18. O espectro é apresentado na Figura 174, pg. 307 do anexo.

RMN de ^{1}H (300 MHz, $CDCl_3$) δ (integração, atribuição, constante de acoplamento, multiplicidade): 6,89 (1H, 19-C<u>H</u>, s), 6,76 - 6,68 (2H, 22-C<u>H</u> e 23-C<u>H</u>, m), 4,68 (1H, 3-C<u>H</u>, s), 3,84 (3H, 25-C<u>H</u>$_3$, s), 3,78 (3H, 24-C<u>H</u>$_3$, s), 2,45 (4H, 8-C<u>H</u>$_2$ e 11-C<u>H</u>$_2$, s), 2,23 (2H, 6 Ha e 13 Ha', *J* = 16,3 Hz, d), 2,16 (2H, 6 Hb e 13 Hb', *J* = 16,3 Hz, d), 1,09 (6H, 14-C<u>H</u>$_3$ e 17-C<u>H</u>$_3$, s), 0,99 (6H, 14-C<u>H</u>$_3$ e 16-C<u>H</u>$_3$, s). O espectro é apresentado na Figura 175, pg. 308 do anexo.

RMN de ^{13}C (75 MHz, $CDCl_3$) δ: 196,5 (C1 e C5), 162,1 (C9 e C10), 148,4 (C20), 147,4 (C21), 136,9 (C18), 120,1 (C23), 115,7 (C2 e C4), 112,2 (C19), 110,8 e 110,4 (C22), 55,8 (C24), 55,7 (C25), 50,7 (C6 e C13), 40,8 (C8 e C11), 32,2 (C7 e C12), 31,1 (C3), 29,3 (C15 e C16), 27,2 (C14 e C17). O espectro é apresentado na Figura 176, pg. 309 do anexo.

9-(4-hidroxifenil)-3,3,6,6-tetrametil-3,4,5,6,7,9-hexaidro-1*H*-xanteno-1,8(2*H*)-diona **(46)**

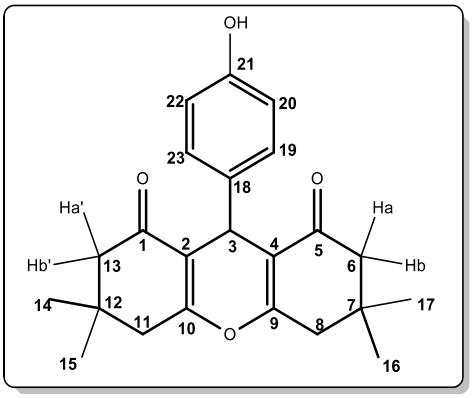

ASPECTO: Sólido branco.

MASSA OBTIDA: 335,55 mg (0,91 mmol, 91% de rendimento).

CCD: R_f = 0,25 (hexano-diclorometano-acetato de etila 3:2:1 v/v).

FAIXA DE FUSÃO: 250 - 251 ^{o}C.

IV (ATR) ν **(cm^{-1})**: 3401, 2961, 2872, 1660, 1613, 1358, 1199, 1165, 1133. O espectro é apresentado na Figura 177, pg. 310 do anexo.

MS/EI (*m/z*/int. rel.) M+: $C_{23}H_{26}O_4$, 366/92, 349/39, 282/25, 273/100, 217/32, 161/15, 83/17. O espectro é apresentado na Figura 178, pg. 310 do anexo.

RMN de ^{1}H (300 MHz, $CDCl_3$) δ (integração, atribuição, constante de acoplamento, multiplicidade): 7,05 (2H, 19-C<u>H</u> e 23-C<u>H</u>, *J* = 8,1 Hz, d), 6,54 (2H, 20-C<u>H</u> e 22-C<u>H</u>, *J* = 8,1 Hz, s), 4,65 (1H, 3-C<u>H</u>, s), 2,45 (4H, 8-C<u>H_2</u> e 11-C<u>H_2</u>, s), 2,24 (2H, 6 Ha e 13 Ha', *J* = 16,5 Hz, d), 2,15 (2H, 6 Hb e 13 Hb', *J* = 16,5 Hz, d), 1,08 (6H, 14-C<u>H_3</u> e 17-C<u>H_3</u>, s), 0,99 (6H, 14-C<u>H_3</u> e 16-C<u>H_3</u>, s). O espectro é apresentado na Figura 179, pg. 311 do anexo.

RMN de ^{13}C (75 MHz, $CDCl_3$) δ: 197,3 (C1 e C5), 162,5 (C9 e C10), 154,7 (C21), 135,5 (C18), 129,3 (C19 e C23), 115,8 (C2 e C4), 115,2 (C20 e C22), 50,7 (C6 e C13), 40,8 (C8 e C11), 32,3 (C7 e C14), 30,9 (C3), 29,3 (C15 e C16), 27,2 (C14 e C17). O espectro é apresentado na Figura 180, pg. 312 do anexo.

9-(4-hidroxi-3-metoxifenil)-3,3,6,6-tetrametil-3,4,5,6,7,9-hexaidro-1*H*-xanteno-1,8(2*H*)-diona **(47)**

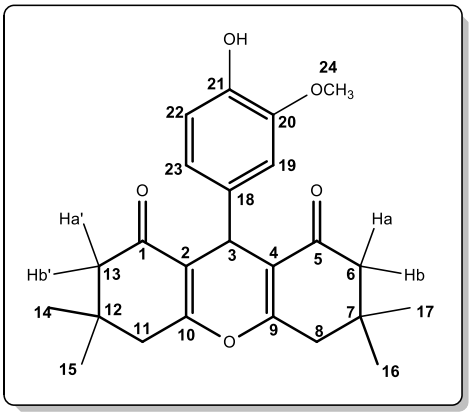

ASPECTO: Sólido amarelo.

MASSA OBTIDA: 359,2 mg (0,91 mmol, 91% de rendimento).

CCD: R_f = 0,26 (hexano-diclorometano-acetato de etila 3:2:1 v/v).

FAIXA DE FUSÃO: 227 -228 ^{o}C.

IV (ATR) ν **(cm^{-1})**: 3398, 2953, 2870, 1657, 1623, 1356, 1277, 1194, 1163, 1133, 1028. O espectro é apresentado na Figura 181, pg. 313 do anexo.

MS/EI (*m/z*/int. rel.) M+: $C_{24}H_{28}O_5$, 396/100, 379/38, 365/60, 273/90, 217/35, 161/20, 83/28. O espectro é apresentado na Figura 182, pg. 313 do anexo.

RMN de ^{1}H (300 MHz, $CDCl_3$) δ (integração, atribuição, constante de acoplamento, multiplicidade): 6,98 (1H, 19-C<u>H</u>, s), 6,72 (1H, 23-C<u>H</u>, *J* = 8,1 Hz, d), 6,57 (1H, 22-CH, *J* = 8,1 Hz, d), 5,56 (1H, O-<u>H</u>, s), 4,65 (1H, 3-CH, s), 3,87 (3H, 24-C<u>H</u>, s), 2,44 (4H, 8-C<u>H</u>$_2$ e 11-C<u>H</u>$_2$, s), 2,23 (2H, 6 Ha e 13 Ha', *J* = 16,3 Hz, d), 2,16 (2H, 6 Hb e 13 Hb', *J* = 16,3 Hz, d),1,09 (6H, 14-C<u>H</u>$_3$ e 17-C<u>H</u>$_3$, s), 0,99 (6H, 15-C<u>H</u>$_3$ e 16-C<u>H</u>$_3$, s). O espectro é apresentado na Figura 183, pg. 314 do anexo.

RMN de ^{13}C (75 MHz, $CDCl_3$) δ: 196,6 (C1 e C5), 162,1 (C9 e C10), 145,9 (C20), 144,0 (C21), 136,4 (C18), 120,0 (C23), 115,8 (C2 e C4), 113,9 (C22), 112,3 (C19), 55,9 (C24), 50,8 (C6 e C13), 40,8 (C8 e C11), 32,2 (C3), 31,3 (C7 e C12), 29,3 (C14 e C14), 27,3 (C15 e C16). O espectro é apresentado na Figura 184, pg. 315 do anexo.

9-(benzo[d][1,3]dioxol-5-il)-3,3,6,6-tetrametil-3,4,5,6,7,9-hexaidro-1*H*-xanteno-1,8(2*H*)-diona **(48)**

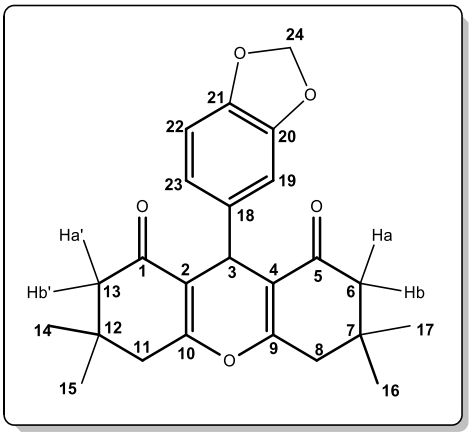

ASPECTO: Sólido amarelo.

MASSA OBTIDA: 349,3 mg (0,89 mmol, 89% de rendimento).

CCD: R_f = 0,50 (hexano-diclorometano-acetato de etila 3:2:1 v/v).

FAIXA DE FUSÃO: 219 - 220 ^{o}C.

IV (ATR) ν **(cm^{-1})**: 2957, 2885, 2870, 1660, 1623, 1257, 1196. O espectro é apresentado na Figura 185, pg. 316 do anexo.

MS/EI (*m/z*/int. rel.) M+: $C_{24}H_{26}O_5$, 394/100, 377/16, 310/78, 273/78, 217/29, 161/15, 83/19. O espectro é apresentado na Figura 186, pg. 316 do anexo.

RMN de ^{1}H (300 MHz, $CDCl_3$) δ (integração, atribuição, constante de acoplamento, multiplicidade): 6,79 (2H, 19-C<u>H</u>, s), 6,73 (1H, 23-C<u>H</u>, *J* = 8,1 Hz, d), 6,64 (1H, 22-C<u>H</u>, *J* = 8,1 Hz, d), 5,85 (2H, 24-C<u>H</u>$_2$, s), 4,66 (1H, 3-CH, s), 2,45 (4H, 8-C<u>H</u>$_2$ e 11-C<u>H</u>$_2$, s), 2,23 (2H, 6 Ha e 13 Ha', *J* = 16,3 Hz, d), 2,16 (2H, 6 Hb e 13 Hb', *J* = 16,3 Hz, d),1,09 (6H, 14-C<u>H</u>$_3$ e 17-C<u>H</u>$_3$, s), 1,00 (6H, 15-C<u>H</u>$_3$ e 16-C<u>H</u>$_3$, s). O espectro é apresentado na Figura 187, pg. 317 do anexo.

RMN de ^{13}C (75 MHz, $CDCl_3$) δ: 196,4 (C1 e C5), 162,1 (C9 e C10), 147,3 (C20), 145,9 (C21), 138,3 (C18), 121,5 (C23), 115,6 (C2 e C4), 109,1 (C19), 107,8 (C22), 100,7 (C24), 50,8 (C6 e C13), 40,8 (C8 e C11), 32,2 (C3), 31,4 (C7 e C12), 29,2 (C15 e C16), 27,4 (C14 e C17). O espectro é apresentado na Figura 188, pg. 318 do anexo.

3,3,6,6-tetrametil-9-(5-feniltiofen-2-il)-3,4,5,6,7,9-hexaidro-1*H*-xanteno-1,8(2*H*)-diona **(49)**

Os dados espectroscópicos e detalhes adicionais encontram-se no artigo 1 ao final do capítulo. Os espectros são apresentados nas Figuras 189, 190, 191 e 192, pgs. 319, 320 e 321 do anexo.

3,6-diisopropil-9-fenil-3,4,5,6,7,9-hexaidro-1*H*-xanteno-1,8(2*H*)-diona **(50)**

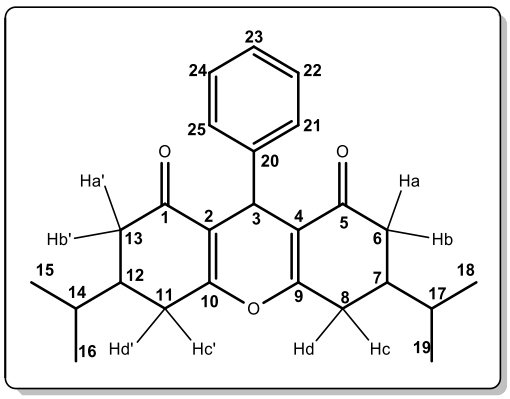

ASPECTO: Sólido amarelo.

MASSA OBTIDA: 177,1 mg (0,47 mmol, 47% de rendimento).

CCD: R_f = 0,62 (hexano-diclorometano-acetato de etila 3:2:1 v/v).

FAIXA DE FUSÃO: 182 - 183 ºC.

IV (ATR) ν (cm^{-1}): 2962, 2866, 1656, 1624, 1366, 1181. O espectro é apresentado na Figura 193, pg. 322 do anexo.

MS/EI (*m/z*/int. rel.) M+: $C_{25}H_{30}O_3$, 378/49, 335/8, 301/100, 231/8, 41/9. O espectro é apresentado na Figura 194, pg. 322 do anexo.

RMN de ^{1}H (300 MHz, $CDCl_3$) δ (integração, atribuição, constante de acoplamento, multiplicidade): 7,32 - 7,19 (4H, 21-C<u>H</u>, 22-C<u>H</u>, 24-C<u>H</u>, 25-C<u>H</u>, m), 7,14 – 7,09 (1H, 23-C<u>H</u>, m), 4,78 (1H, 3-C<u>H</u>, s), 2,68 – 2,28 (6H, 6 Ha, 13 Ha', 8 Hc, 11 Hc', 6 Hb, 13 Hb', m), 2,11 – 1,98 (2H 8 Hd, 11 Hd', m), 1,93 – 1,79 (2H, 7-C<u>H</u>, 12-C<u>H</u>, m), 1,66 – 1,53 (2H, 14-C<u>H</u>, 17-C<u>H</u>, m), 0,98 - 0,89 (12H, 15-C<u>H</u>$_3$, 16-C<u>H</u>$_3$, 18-C<u>H</u>$_3$, 19-C<u>H</u>$_3$, m). O espectro é apresentado na Figura 195, pg. 323 do anexo.

RMN de ^{13}C (75 MHz, $CDCl_3$) δ: 196,8 (C1 e C5), 164,3 (C9 e C10), 144,4 (C20), 128,3 e 128,2 (C21 e C25), 128,1 e 128,1 (C22 e C24), 126,4 (C23), 116,5 (C2 e C4), 41,0 e 40,1 (C7 e C12), 38,8 e 38,7 (C6 e C13), 31,9 e 31,8 (C8 e C13), 31,6 (C3), 31,1 e 30,8 (C14 e C17), 19,6, 19,5 e 19,4 (C15, C16, C18 e C19). O espectro é apresentado na Figura 196, pg. 324 do anexo.

9-(4-fluorofenil)-3,6-diisopropil--3,4,5,6,7,9-hexahidro-1*H*-xanteno-1,8(2*H*)-diona **(51)**

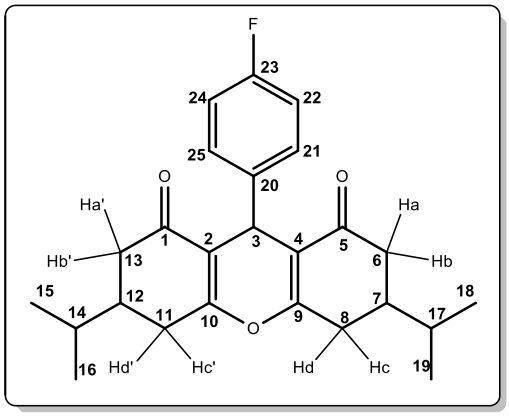

ASPECTO: Sólido branco.

MASSA OBTIDA: 294, 9 mg (0,74 mmol, 74 % de rendimento).

CCD: R_f = 0,62 (hexano-acetato de etila 2:1 v/v).

FAIXA DE FUSÃO: 179 – 181 ºC.

IV (KBr) ν (cm^{-1}): 2959, 2885, 1656, 1623, 1369, 1225, 1188, 1156, 1143. O espectro é apresentado na Figura 197, pg. 325 do anexo.

MS/EI (*m/z*/int. rel.): 396/85, 301/100, 133/19, 95/14, 69/16, 43/71, 41/88. O espectro é apresentado na Figura 198, pg. 325 do anexo.

HRMS (M+H$^+$): Calculado para $C_{25}H_{30}ClO_3$: 397,2179; encontrado: 397,2154.

RMN de ^{1}H (300 MHz, $CDCl_3$) δ (integração, atribuição, constante de acoplamento, multiplicidade): 7,28 - 7,20 (2H, 21-C<u>H</u>, 25-C<u>H</u>, m), 6,93 – 6,85 (2H, 22-C<u>H</u>, 24-C<u>H</u>, m), 4,74 (1H, 3-C<u>H</u>, s), 2,67 – 2,28 (6H, 6 Ha, 13 Ha', 8 Hc, 11 Hc', 6 Hb, 13 Hb', m), 2,11 – 1,99 (2H 8 Hd, 11 Hd', m), 1,98 – 1,78 (2H, 7-C<u>H</u>, 12-C<u>H</u>, m), 1,64 – 1,55 (2H, 14-C<u>H</u>, 17-C<u>H</u>, m), 0,96 -0,89 (12H, 15-C<u>H$_3$</u>, 16-C<u>H$_3$</u>, 18-C<u>H$_3$</u>, 19-C<u>H$_3$</u>, m). O espectro é apresentado na Figura 199, pg. 326 do anexo.

RMN de ^{13}C (75 MHz, $CDCl_3$) δ: 197,0 e 196,8 (C1 e C5), 164,3, 164,2 e 163,7 (C9 e C10), 161,4 (d, J = 243,0 Hz, C23), 140,1 e 140,0 (d, J = 3,1 Hz, C20), 129,9, 129,8 e 129,7 (d, J = 8,0 Hz, C21 e C25), 116,3, 116,4 e 116,0 (C2 e C4), 114,9 e 114,8 (d, J = 21,2 Hz, C22 e C24) 41,4 e 40,9 (C6 e C13), 40,0 (C14 e C17), 38,8 (C7 e C12), 31,8 (C14 e C17), 31,3 (C3), 31,0 e 30,8 (C8 e C11), 19,5 e 19,4 (C15, C16, C18 e C19). O espectro é apresentado na Figura 200, pg. 327 do anexo.

9-(4-clorofenil)-3,6-diisopropil-3,4,5,6,7,9-hexahidro-1*H*-xanteno-1,8(2*H*)-diona **(52)**

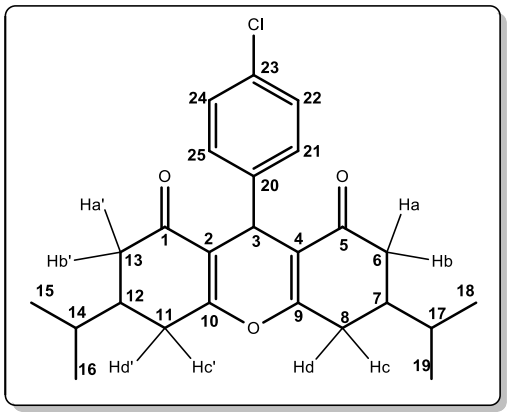

ASPECTO: Sólido branco.

MASSA OBTIDA: 230,0 mg (0,56 mmol, 56 % de rendimento).

CCD: R_f = 0,62 (hexano-acetato de etila 2:1 v/v).

FAIXA DE FUSÃO: 205 – 207 °C.

IV (KBr) ν (cm^{-1}): 2959, 2872, 1665, 1624, 1369, 1186. O espectro é apresentado na Figura 201, pg. 328 do anexo.

MS/EI (*m/z*/int. rel.): 414/21, 412/50, 377/17, 301/93, 231/12, 165/15, 111/19, 55/34, 43/83, 41/100. O espectro é apresentado na Figura 202, pg. 328 do anexo.

HRMS (M+H$^+$): Calculado para $C_{25}H_{30}ClO_3$: 413,1883; encontrado: 413,1854.

RMN de ^{1}H (300 MHz, $CDCl_3$) δ (integração, atribuição, constante de acoplamento, multiplicidade): 7,27 - 7,14 (4H, 21-C<u>H</u>, 22-C<u>H</u>, 24-C<u>H</u>, 25-C<u>H</u>, m), 4,72 (1H, 3-C<u>H</u>, s), 2,68 – 2,27 (6H, 6 Ha, 13 Ha', 8 Hc, 11 Hc', 6 Hb, 13 Hb', m), 2,12 – 1,99 (2H 8 Hd, 11 Hd', m), 1,98 – 1,75 (2H, 7-C<u>H</u>, 12-C<u>H</u>, m), 1,67 – 1,54 (2H, 14-C<u>H</u>, 17-C<u>H</u>, m), 0,98 - 0,86 (12H, 15-C<u>H</u>$_3$, 16-C<u>H</u>$_3$, 18-C<u>H</u>$_3$, 19-C<u>H</u>$_3$, m). O espectro é apresentado na Figura 203, pg. 329 do anexo.

RMN de ^{13}C (75 MHz, $CDCl_3$) δ: 196,9 e 196,8 (C1 e C5), 164,4, 164,3 e 163,8 (C9 e C10), 142,9 e 142,7 (C20), 132,1 e 132,0 (C23), 129,8 e 129,7 (C22 e C24), 128,2 e 128,2 (C21 e C25), 116,2, 116,1 e 115,8 (C2 e C4), 41,3 e 40,9 (C6 e C13), 40,0 (C14 e C17), 38,9 e 38,8 (C7 e C12), 31,5 e 31,3 (C3), 31,0 e 30,8 (C8 e C11), 19,6, 19,5 e 19,4 (C15, C16, C18 e C19). O espectro é apresentado na Figura 204, pg. 330 do anexo.

9-(4-bromofenil)-3,6-diisopropil-3,4,5,6,7,9-hexahidro-1*H*-xanteno-1,8(2*H*)-diona **(53)**

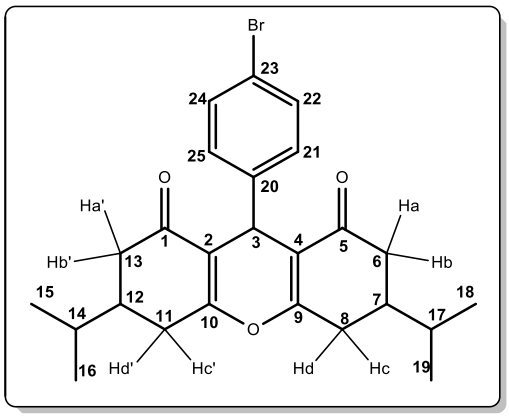

ASPECTO: Sólido branco.

MASSA OBTIDA: 312,4 mg (0,68 mmol, 68% de rendimento).

CCD: R_f = 0,59 (hexano-acetato de etila 2:1 v/v).

FAIXA DE FUSÃO: 167 – 169 ºC.

IV (KBr) ν (cm^{-1}): 2956, 2871, 1666, 1624, 1369, 1183. O espectro é apresentado na Figura 205, pg. 331 do anexo.

MS/EI (*m/z*/int. rel.): 459/8, 457/10, 377/35, 301/77, 231/17, 165/16, 157/20, 152/20, 139/15, 69/16, 55/34, 43/80, 41/100. O espectro é apresentado na Figura 206, pg. 331 do anexo.

HRMS (M+H$^+$): Calculado para $C_{25}H_{30}BrO_3$: 457,1378; encontrado: 457,1356.

RMN de ^{1}H (300 MHz, $CDCl_3$) δ (integração, atribuição, constante de acoplamento, multiplicidade): 7,36 - 7,29 (2H, 21-C<u>H</u>, 25-C<u>H</u>, m), 7,20 – 7,13 (2H, 22-C<u>H</u>, 24-C<u>H</u>, m), 4,71 (1H, 3-C<u>H</u>, s), 2,67 – 2,27 (6H, 6 Ha, 13 Ha', 8 Hc, 11 Hc', 6 Hb, 13 Hb', m), 2,10 – 1,98 (2H 8 Hd, 11 Hd', m), 1,97 – 1,73 (2H, 7-C<u>H</u>, 12-C<u>H</u>, m), 1,64 – 1,53 (2H, 14-C<u>H</u>, 17-C<u>H</u>, m), 0,96 -0,88 (12H, 15-C<u>H</u>$_3$, 16-C<u>H</u>$_3$, 18-C<u>H</u>$_3$, 19-C<u>H</u>$_3$, m). O espectro é apresentado na Figura 207, pg. 332 do anexo.

RMN de ^{13}C (75 MHz, $CDCl_3$) δ: 196,9 e 196,8 (C1 e C5), 164,4, 164,3 e 163,8 (C9 e C10), 143,4 e 143,2 (C20), 131,2 e 131,1 (C22 e C24), 130,2 e 130,1 (C21 e C25), 120,3

(C23), 116,1, 116,0 e 115,7 (C2 e C4), 41,3 e 40,9 (C6 e C13), 40,0 (C14 e C17), 38,8 (C7 e C12), 31,8 (C14 e C17), 31,6 e 31,4 (C3), 31,0 e 30,8 (C8 e C11), 19,6, 19,5 e 19,4 (C15, C16, C18 e C19). O espectro é apresentado na Figura 208, pg. 333 do anexo.

3,6-diisopropil-9-(4-(trifluormeltil)fenil)-3,4,5,6,7,9-hexahidro-1*H*-xanteno-1,8(2*H*)-diona **(54)**

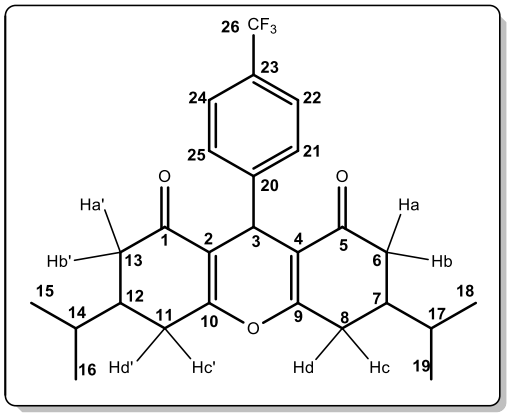

ASPECTO: Sólido branco.

MASSA OBTIDA: 291,6 mg (0,65 mmol, 65 % de rendimento).

CCD: R_f = 0,62 (hexano-acetato de etila 2:1 v/v).

FAIXA DE FUSÃO: 183 – 185 ºC.

IV (KBr) ν (cm^{-1}): 2961, 2873, 1665, 1624, 1370, 1323, 1185, 1158, 1141. O espectro é apresentado na Figura 209, pg. 334 do anexo.

MS/EI (*m/z*/int. rel.): 446/70, 301/100, 231/10, 145/19, 69/16, 55/33, 43/79. O espectro é apresentado na Figura 210, pg. 334 do anexo.

HRMS (M+H$^+$): Calculado para $C_{26}H_{30}F_3O_3$: 447,2147; encontrado: 447,2135.

RMN de ^{1}H (300 MHz, $CDCl_3$) δ (integração, atribuição, constante de acoplamento, multiplicidade): 7,48 - 7,34 (4H, 21-C<u>H</u>, 22-C<u>H</u>, 24-C<u>H</u>, 25-C<u>H</u>, m), 4,81 (1H, 3-C<u>H</u>, s), 2,70 – 2,30 (6H, 6 Ha, 13 Ha', 8 Hc, 11 Hc', 6 Hb, 13 Hb', m), 2,12 – 2,00 (2H 8 Hd, 11 Hd', m), 1,99 – 1,79 (2H, 7-C<u>H</u>, 12-C<u>H</u>, m), 1,65 – 1,56 (2H, 14-C<u>H</u>, 17-C<u>H</u>, m), 0,96 -

0,89 (12H, 15-C<u>H</u>$_3$, 16-C<u>H</u>$_3$, 18-C<u>H</u>$_3$, 19-C<u>H</u>$_3$, m). O espectro é apresentado na Figura 211, pg. 335 do anexo.

RMN de ^{13}C (75 MHz, $CDCl_3$) δ: 196,9 e 196,8 (C1 e C5), 164,6, 164,1 e 164,0 (C9 e C10), 148,2 e 148,1 (C20), 128,7 (C21 e C25), 128,5 (q, J = 2,1 Hz, C23), 125,1 e 124,9 (d, J = 3,7 Hz, C22 e C24), 124,2 (q, J = 270,3 Hz, 26-<u>C</u>F$_3$) 115,9 e 115,5 (C2 e C4), 41,3 e 40,9 (C6 e C13), 40,0 (C14 e C17), 38,8 (C7 e C12), 32,1 (C3), 31,9 e 31,8 (C14 e C17), 31,0 e 30,8 (C8 e C11), 19,6, 19,5 e 19,4 (C15, C16, C18 e C19). O espectro é apresentado na Figura 212, pg. 336 do anexo.

4-(3,6-diisopropil-1,8-dioxo-2,3,4,5,6,7,8,9-octaidro-1*H*-xanten-9-il)benzonitrila **(55)**

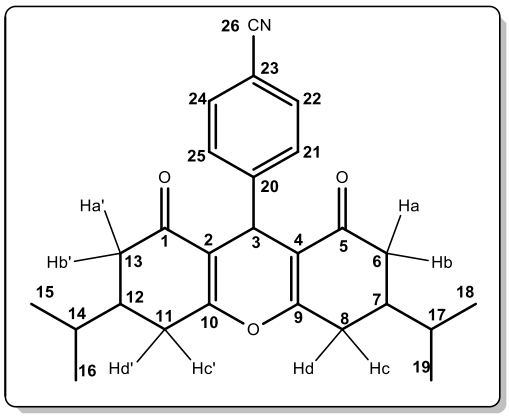

ASPECTO: Sólido branco.

MASSA OBTIDA: 251,5 mg (0,62 mmol, 62 % de rendimento).

CCD: R_f = 0,47 (hexano-acetato de etila 2:1 v/v).

FAIXA DE FUSÃO: 234 - 236 ^{o}C.

IV (KBr) ν **(cm^{-1})**: 2955, 2883, 2225, 1654, 1623, 1370, 1192. O espectro é apresentado na Figura 213, pg. 337 do anexo.

MS/EI (*m/z*/int. rel.): 403/61, 301/85, 231/11, 69/14, 55/32, 43/73, 41/100. O espectro é apresentado na Figura 214, pg. 337 do anexo.

HRMS (M+H$^+$): Calculado para $C_{26}H_{30}NO_3$: 404,2226; encontrado: 404,2214.

RMN de ^{1}H (300 MHz, $CDCl_3$) δ (integração, atribuição, constante de acoplamento, multiplicidade): 7,51 (2H, 22-C<u>H</u>, 24-C<u>H</u>, d, *J* = 8,1 Hz), 7,41 (2H, 21-C<u>H</u>, 25-C<u>H</u>, d, *J* = 8,1 Hz), 4,78 (1H, 3-C<u>H</u>, s), 2,68 – 2,31 (6H, 6 Ha, 13 Ha', 8 Hc, 11 Hc', 6 Hb, 13 Hb', m), 2,12 – 2,00 (2H, 8 Hd, 11 Hd', m),1,98 – 1,76 (2H, 7-C<u>H</u>, 14 C<u>H</u>, m) 1,67 – 1,54 (2H, 14-C<u>H</u>, 17-C<u>H</u>, m), 0,98 -0,88 (12H, 15-C<u>H</u>$_3$, 16-C<u>H</u>$_3$, 18-C<u>H</u>$_3$, 19-C<u>H</u>$_3$, m). O espectro é apresentado na Figura 215, pg. 338 do anexo.

RMN de ^{13}C (75 MHz, $CDCl_3$) δ: 196,8 e 196,7 (C1 e C5), 164,8, 164,7 e 164,3 (C9 e C10), 149,6 e 149,4 (C20), 132,0 e 131,9 (C21 e C25), 129,3 e 129,2 (C22 e C24), 119,0 (C26), 115,5, 115,4 e 115,1 (C2 e C4), 110,2 (C23), 41,2 e 40,8 (C6 e C13), 39,9 (C14 e C17), 38,8 (C7 e C12), 32,5 e 32,3 (C3), 31,8 (C14 e C17), 31,0 e 30,8 (C8 e C11), 19,6 e 19,4 (C15, C16, C18 e C19). O espectro é apresentado na Figura 216, pg. 339 do anexo.

3,6-diisopropil-9-(4-nitrofenil)-3,4,5,6,7,9-hexahidro-1*H*-xanteno-1,8(2*H*)-diona **(56)**

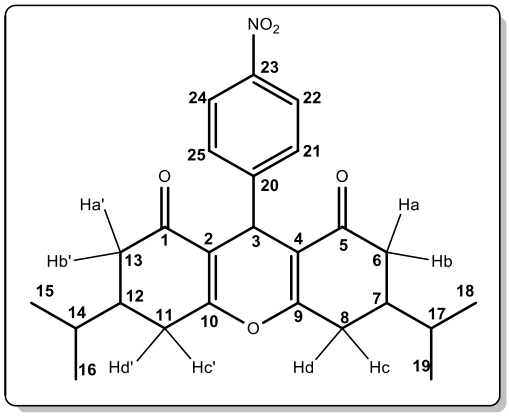

ASPECTO: Sólido branco.

MASSA OBTIDA: 307,5 mg (0,73 mmol, 73 % de rendimento).

CCD: R_f = 0,50 (hexano-acetato de etila 2:1 v/v).

FAIXA DE FUSÃO: 204 - 208 ^{o}C.

IV (KBr) ν **(cm^{-1})**: 2961, 2869, 1664, 1623, 1517, 1370, 1345, 1185. O espectro é apresentado na Figura 217, pg. 340 do anexo.

MS/EI (*m/z*/int. rel.): 423/70, 406/87, 376/22, 301/100, 231/13, 152/12, 69/16, 55/31, 43/65, 41/90. O espectro é apresentado na Figura 218, pg. 340 do anexo.

HRMS (M+H$^+$): Calculado para $C_{25}H_{30}NO_5$: 424,2124; encontrado: 424,2104.

RMN de ^{1}H (300 MHz, $CDCl_3$) δ (integração, atribuição, constante de acoplamento, multiplicidade): 8,01 (2H, 22-C<u>H</u>, 24-C<u>H</u>, d, *J* = 8,7 Hz), 7,45 (2H, 21-C<u>H</u>, 25-C<u>H</u>, d, *J* = 8,7 Hz), 4,83 (1H, 3-C<u>H</u>, s), 2,70 – 2,31 (6H, 6 Ha, 13 Ha', 8 Hc, 11 Hc', 6 Hb, 13 Hb', m), 2,12 – 2,00 (2H, 8 Hd, 11 Hd', m),1,98 – 1,76 (2H, 7-C<u>H</u>, 14 C<u>H</u>, m) 1,67 – 1,54 (2H, 14-C<u>H</u>, 17-C<u>H</u>, *J* = 6,1 Hz, sept), 0,98 -0,89 (12H, 15-C<u>H</u>$_3$, 16-C<u>H</u>$_3$, 18-C<u>H</u>$_3$, 19-C<u>H</u>$_3$, m). O espectro é apresentado na Figura 219, pg. 341 do anexo.

RMN de ^{13}C (75 MHz, $CDCl_3$) δ: 196,8 e 196,7 (C1 e C5), 164,9 e 163,3 (C9 e C10), 151,7, 151,5 e 151,4 (C20), 146,4 (C23), 129,4 e 129,3 (C21 e C25), 123,4 e 123,3 (C22 e C24), 115,4 e 115,0 (C2 e C4), 41,2 e 40,8 (C6 e C13), 39,9 (C14 e C17), 38,9 e 38,9 (C7 e C12), 32,4 e 32,2 (C3), 31,8 (C14 e C17), 31,0 e 30,8 (C8 e C11), 19,6 e 19,4 (C15, C16, C18 e C19). O espectro é apresentado na Figura 220, pg. 342 do anexo.

9-(4-hidroxifenil)-3,6-diisopropil-3,4,5,6,7,9-hexaidro-1*H*-xanteno-1,8(2*H*)-diona **(57)**

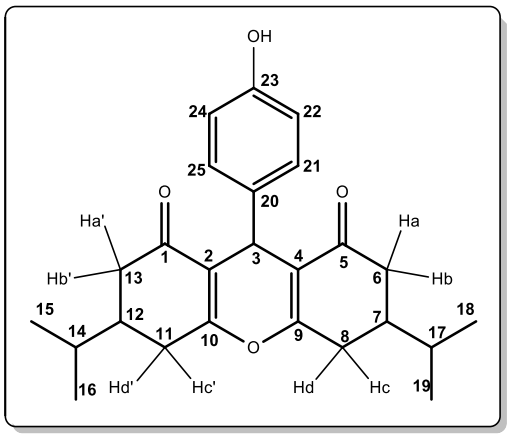

ASPECTO: Sólido amarelo.

MASSA OBTIDA: 227,7 mg (0,58 mmol, 58% de rendimento).

CCD: R_f = 0,28 (hexano-diclorometano-acetato de etila 3:2:1 v/v).

FAIXA DE FUSÃO: 176 - 177 ^{o}C.

IV (ATR) ν **(cm^{-1})**: 3405, 3172, 2959, 2873, 1671, 1645, 1612, 1463, 1372, 1181. O espectro é apresentado na Figura 221, pg. 343 do anexo.

MS/EI (*m/z*/int. rel.) M+: $C_{25}H_{30}O_4$, 394/88, 377/52, 351/15, 301/100, 296/22, 41/19. O espectro é apresentado na Figura 222, pg. 343 do anexo.

RMN de ^{1}H (300 MHz, DMSO) δ (integração, atribuição, constante de acoplamento, multiplicidade): 7,09 – 7,03 (2H, 21-C<u>H</u> e 25-C<u>H</u>, m), 6,61 – 6,55 (2H, 22-C<u>H</u> e 24-C<u>H</u>, m), 4,68 (1H, 3-C<u>H</u>, s), 2,66 – 2,32 (6H, 6 Ha, 13 Ha', 8 Hc, 11 Hc', 6 Hb, 13 Hb', m), 2,13 – 1,99 (2H 8 Hd, 11 Hd', m), 1,96 – 1,79 (2H, 7-C<u>H</u>, 12-C<u>H</u>, m), 1,64 – 1,52 (2H, 14-C<u>H</u>, 17-C<u>H</u>, m), 0,94 -0,89 (12H, 15-C<u>H</u>$_3$, 16-C<u>H</u>$_3$, 18-C<u>H</u>$_3$, 19-C<u>H</u>$_3$, m). O espectro é apresentado na Figura 223, pg. 344 do anexo.

RMN de ^{13}C (75 MHz, DMSO) δ: 198,0 e 197,7 (C1 e C5), 164,5, 164,4 e 163,9 (C9 e C10), 154,8 (C23), 135,8 e 135,6 (C20), 129,3 (C21 e C25), 116,8, 116,7 e 116,4 (C2 e C4), 115,4 (C22 e C24), 41,4 e 41,0 (C6 e C13), 40,1 (C3), 38,7 (C7 e C12), 31,8 (C14 e C17), 31,0 e 30,8 (C8 e C11), 19,6, 19,5 e 19,4 (C15, C16, C18 e C19). O espectro é apresentado na Figura 224, pg. 345 do anexo.

3,6-diisopropil-9-(5-feniltiopen-2-il)-3,4,5,6,7,9-hexaidro-1*H*-xanteno-1,8(2*H*)-diona **(58)**

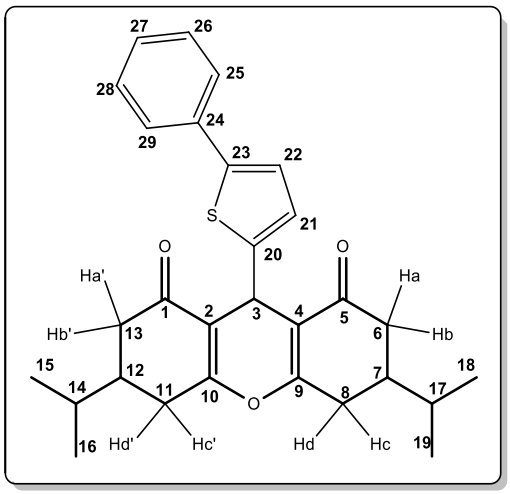

ASPECTO: Sólido amarelo.

MASSA OBTIDA: 335,3 mg (0,73 mmol, 73% de rendimento).

CCD: R_f = 0,50 (hexano-diclorometano-acetato de etila 3:2:1 v/v).

FAIXA DE FUSÃO: 151 - 152 ^{o}C.

IV (ATR) ν **(cm^{-1})**: 2962, 2871, 1668, 1653, 1622, 1370, 1184, 759. O espectro é apresentado na Figura 225, pg. 346 do anexo.

MS/EI (*m/z*/int. rel.) M+: $C_{29}H_{32}O_3S$, 460/100, 443/14, 362/22, 301/20, 121/10. O espectro é apresentado na Figura 226, pg. 346 do anexo.

RMN de ^{1}H (300 MHz, $CDCl_3$) δ (integração, atribuição, constante de acoplamento, multiplicidade): 7,50 (2H, 25-C<u>H</u>, 29-C<u>H</u>, *J* = 7,5 Hz, d), 7,30 (2H, 26-C<u>H</u>, 28-C<u>H</u>, *J* = 9,1 Hz, t), 7,23 – 7,16 (1H, 27-C<u>H</u>, m), 7,05 (1H, 22-C<u>H</u>, *J* = 3,4 Hz, d), 6,90 (1H, 21-C<u>H</u>, *J* = 3,4 Hz, d), 5,13 (1H, 3-C<u>H</u>, s), 2,70 – 2,58 (2H, 6 Ha e 13 Ha'), 2,57 – 2,27 (4H, 6 Hb, 13 Hb', 8 Hc e 11 Hc', m), 2,21 -1,91 (4H, 8 Hd, 11 Hd', 7-C<u>H</u> e 12-C<u>H</u>, m), 1,61 (2H, 14-C<u>H</u> e 17-C<u>H</u>, *J* = 6,6 Hz, sept), 0,98 – 0,91 (12H, 15-C<u>H</u>$_3$, 16-C<u>H</u>$_3$, 18-C<u>H</u>$_3$ e 19-C<u>H</u>$_3$, m). O espectro é apresentado na Figura 227, pg. 347 do anexo.

RMN de ^{13}C (75 MHz, $CDCl_3$) δ: 196,9 e 196,7 (C1 e C5), 164,7 e 164,0 (C9 e C10), 148,1 e 147,9 (C20), 142,4 e 142,3 (C23), 134,7 (C24), 128,6 (C26 e C28), 127,0 (C21), 126,2 e 125,9 (C27), 125,5 (C25 e C29), 122,8 (C22), 116,0 e 115,8 (C2 e C4), 41,3 e 41,0 (C6 e C13), 40,1 (C14 e C17), 38,8 e 38,7 (C7 e C12), 31,9 e 31,8 (C14 e C17), 31,1 e 30,9 (C3), 26,8 e 26,6 (C8 e C11), 19,6, 19,5 e 19,4 (C15, C16, C18 e C19). O espectro é apresentado na Figura 228, pg. 348 do anexo.

3 RESULTADOS E DISCUSSÃO

Os compostos investigados neste trabalho foram sintetizados via reações isentas de solvente e catalisadas por $ZrOCl_2 \cdot 8H_2O$, conforme descrito por Mosaddegh *et al.*[1] Esta metodologia foi empregada sem nenhuma otimização e levou a formação de cinquenta e três xantenodionas, as quais foram preparadas a partir de reações de condensação de Knoevenagel (i) entre diferentes aldeídos aromáticos e quatro β-dicetonas, seguidas de processos de adição de Michael (ii) e reações de desidratação (iii). No Esquema II-1 esta sequência de reações é mostrada para a formação das xantenodionas **37-49** que foram preparadas a partir da dimedona.

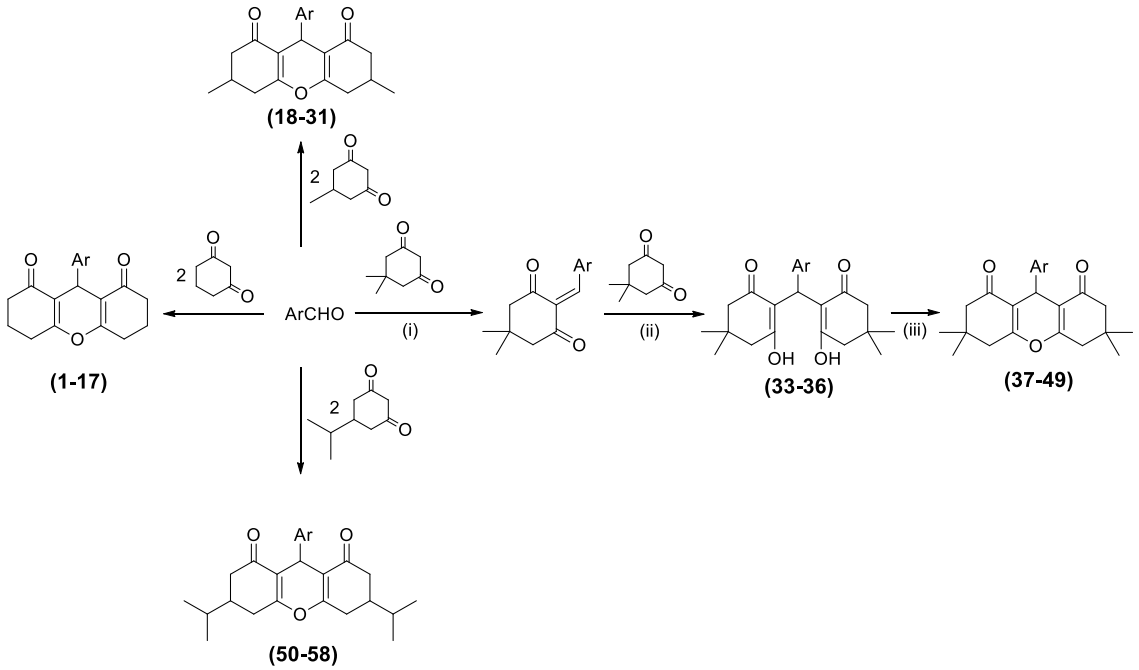

Esquema II-1. Síntese de xantenodionas catalisada por $ZrOCl_2 \cdot 8H_2O$. (i) Condensação de Knoevenagel. (ii) Adição de Michael. (iii) Desidratação.

As estruturas dos compostos obtidos, os tempos de reação e os rendimentos são apresentados na Tabela II-1 (pg. 77). As xantenodionas foram obtidas com rendimentos variando de 33% – 99% e as reações tiveram tempo máximo de duração 135 minutos. Além disso, não foi observada uma correlação entre os substituintes doadores e retiradores de elétrons dos aldeídos com o rendimento e o tempo de reação, tampouco quando modificou-se a β-dicetona empregada. Entretanto, os maiores tempos de reação foram obtidos quando utilizaram-se aldeídos com maior demanda estérica como o 5-(4-

clorofenil)furanilbenzaldeído, 5-(4-bromofenil)furanilbenzaldeído e o 5-fenil-tiofen-2-ilbenzaldeído.

Tabela II-1. Resultados experimentais da reação de síntese de derivados 1,8-dioxo-octaidroxantenos (xantenodionas)

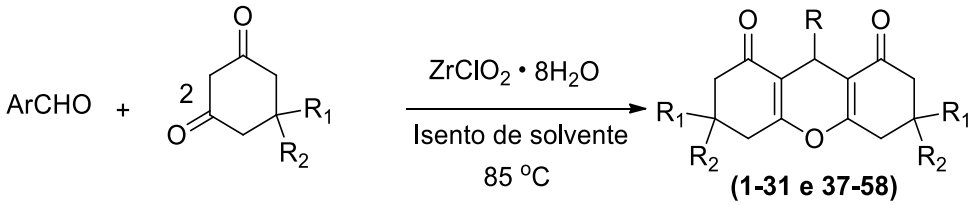

Composto	R	R_1/R_2	Tempo de reação (min)	Rendimento (%)
1[a]	Fenila	$R_1=R_2=H$	40	52
2[a]	4-fluorofenila	$R_1=R_2=H$	25	76
3[a]	4-clorofenila	$R_1=R_2=H$	15	94
4 [a]	4-bromofenila	$R_1=R_2=H$	15	85
5	4-trifluorometilfenila	$R_1=R_2=H$	15	86
6[a]	4-cianofenila	$R_1=R_2=H$	15	81
7[a]	4-nitrofenila	$R_1=R_2=H$	20	70
8[a]	4-dimetilaminofenila	$R_1=R_2=H$	60	70
9[a]	4-metoxifenila	$R_1=R_2=H$	30	49
10[a]	3,4-dimetoxifenila	$R_1=R_2=H$	20	93
11	3,4,5-trimetoxifenila	$R_1=R_2=H$	40	93
12[a]	4-hidroxifenila	$R_1=R_2=H$	65	42
13[a]	4-hidroxi-3-metoxifenila	$R_1=R_2=H$	20	94
14	Benzo[d][1,3]dioxol-5-ila	$R_1=R_2=H$	20	44
15	5-(4-clorofenil)furan-2-ila	$R_1=R_2=H$	120	78
16	5-(4-bromofenil)furan-2-ila	$R_1=R_2=H$	120	75
17	5-feniltiofen-2-ila	$R_1=R_2=H$	50	92
18	Fenila	$R_1=H$, $R_2=Me$	40	34
19	4-fluorofenila	$R_1=H$, $R_2=Me$	45	78
20	4-clorofenila	$R_1=H$, $R_2=Me$	20	80
21	4-bromofenila	$R_1=H$, $R_2=Me$	40	84
22	4-trifluorometilfenila	$R_1=H$, $R_2=Me$	60	79

23	4-cianofenila	R_1=H, R_2=Me	30	81
24	4-nitrofenila	R_1=H, R_2=Me	30	84
25	4-metoxifenila	R_1=H, R_2=Me	40	76
26	3,4,5-trimetoxifenila	R_1=H, R_2=Me	40	71
27	4-hidroxifenila	R_1=H, R_2=Me	40	52
28	4-hidroxi-3-metoxifenila	R_1=H, R_2=Me	20	80
29	Benzo[d][1,3]dioxol-5-ila	R_1=H, R_2=Me	40	83
30	5-(4-clorofenil)furan-2-ila	R_1=H, R_2=Me	120	45
31	5-(4-bromofenil)furan-2-ila	R_1=H, R_2=Me	120	47
37[a]	Fenila	R_1=R_2=Me	60	79
38[a]	4-fluorofenila	R_1=R_2=Me	60	80
39[a]	4-clorofenila	R_1=R_2=Me	30	84
40[a]	4-bromofenila	R_1=R_2=Me	60	80
41[a]	4-trifluorometilfenila	R_1=R_2=Me	60	61
42[a]	4-cianofenila	R_1=R_2=Me	30	87
43[a]	4-nitrofenila	R_1=R_2=Me	60	87
44[a]	4-metoxifenila	R_1=R_2=Me	15	77
45[a]	3,4-dimetoxifenila	R_1=R_2=Me	60	99
46[a]	4-hidroxifenila	R_1=R_2=Me	30	91
47[a]	4-hidroxi-3-metoxifenila	R_1=R_2=Me	40	91
48[a]	Benzo[d][1,3]dioxol-5-ila	R_1=R_2=Me	30	89
49	5-feniltiofen-2-ila	R_1=R_2=Me	50	94
50	Fenila	R_1=H, R_2=^{i}Pr	30	47
51	4-fluorofenila	R_1=H, R_2=^{i}Pr	60	74
52	4-clorofenila	R_1=H, R_2=^{i}Pr	30	56
53	4-bromofenila	R_1=H, R_2=^{i}Pr	25	68
54	4-trifluorometilfenila	R_1=H, R_2=^{i}Pr	45	65
55	4-cianofenila	R_1=H, R_2=^{i}Pr	20	62
56	4-nitrofenila	R_1=H, R_2=^{i}Pr	25	73
57	4-hidroxifenila	R_1=H, R_2=^{i}Pr	80	58
58	5-feniltiofen-2-ila	R_1=H, R_2=^{i}Pr	75	73

[a]Compostos descritos na literatura.

Os processos envolvendo a síntese de xantenodionas descritos na literatura englobam, principalmente, derivados da 5,5-dimetilcicloexan-1,3-diona[2,3] e da cicloexan-1,3-diona[4,5]. Estudos abrangendo a 5-metilcicloexan-1,3-diona e a 5-isopropilcicloexan-1,3-diona bem como os aldeídos 5-(4-clorofenil)furanilbenzaldeído, 5-(4-bromofenil)furanilbenzaldeído e o 5-feniltiofen-2-ilbenzaldeído ainda não foram documentados.

Outras xantenodionas derivadas da 5,5-dimetilcicloexan-1,3-diona e da cicloexan-1,3-diona e diferentes aldeídos tiveram sua síntese documentada[2,3,4,5,6,7,8], como é o caso dos compostos **1-4, 6-10, 12, 13** e **37-48** (Tabela II-1). Os dados espectroscópicos encontrados estão de acordo com os descritos na literatura. No que diz respeito aos rendimentos obtidos e aos tempos de reação, não se observou variação considerável quando comparados aos trabalhos já relatados, exceto para os compostos **1**, **9** e **41**.

Durante o desenvolvimento deste trabalho, verificou-se que em alguns casos a reação entre alguns aldeídos aromáticos e dicetonas não resultaram na formação das xantenodionas desejadas. Por exemplo, a tentativa de obtenção da xantenodiona 9-(2,6-diclorofenil)-3,3,6,6-tetrametil-3,4,5,6,7,9-hexaidro-1*H*-xanteno-1,8(2*H*)-diona a partir da reação entre a 5,5-dimetilcloexan-1,3-diona (dimedona) e o 2,6-diclorobenzaldeído levou a formação do composto **32** (Esquema II-2).

[2] JAGANNATH, K. V.; GANTIGAIAH, K. 1-(3, 4-dichlorobenzenesulfonyl)-3-methyl-1H-imidazolium chloride: An eficiente catalyst for the synthesis of 1, 8-dioxo-octahydroxanthenes under microwave irradiation. *International Journal of Chemical and Pharmaceutical Sciences*, v. 5, p. 98-104, 2014.

[3] DARVICHE, F.; BALALAIE, S.; CHADEGANI, F. Diammonium Hydrogen Phosphate as a Neutral and Efficient Catalyst for Synthesis of 1,8-Dioxo-octahydroxanthene Derivatives in Aqueous Media. *Synthetic Communications*, v. 37, p. 1059–1066, 2007

[4] SHIRINI, F.; IMANZADEH, G. H.; ABEDINI, M.; GHAZIANI, M. A. D.; GHASEMABADIA, P. G.; LANGROODI, M. S. Introduction of two efficient catalysts for the synthesis of 1,8-dioxo-octahydroxanthene derivatives in the absence of solvent. *Iranian Journal of Catalysis*, v. 2, p. 115-119, 2012.

[5] PRAMANIK, A.; BHAR, S. Alumina-sulfuric acid catalyzed eco-friendly synthesis of xanthenediones. *Catalysis Communications*, v. 20, p. 17–24, 2012.

[6] SAJADI, S. M.; MAHAM, M.; AHMAD, B. O. Perfluorinated resin-sulfonic acid (Nafion-H): an efficient, environment friendly and recyclable heterogeneous catalyst for the one-pot synthesis of 1,8-dioxo-octahydroxanthenes. *Letters in Organic Chemistry*, v. 11, p. 317-320, 2014.

[7] ALBADI, J.; MANSOURNEZHAD, A.; ABBASZADEH, H. CuO-CeO_2 Nanocomposite: A highly efficient recyclable catalyst for the green synthesis of 1,8-dioxo-octahydroxanthenes in water. *Journal of the Chinese Chemical Society*, v. 60, p. 1-4, 2013.

[8] SHOJA, A.; SHIRINI, F.; ABEDINI, M.; ZANJANCHI, M. A. $BiVO_4$-NPs as a new and efficient nano-catalyst for the synthesis of 1,8-dioxo-octahydro xanthenes. *Journal Nanostructure Chemistry*, v. 4, p. 1-5, 2014.

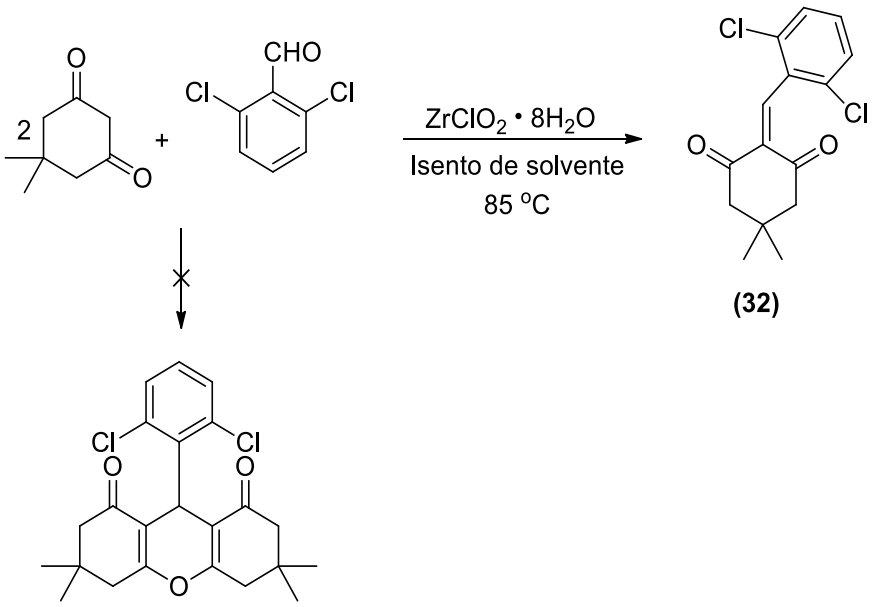

Esquema II- 2. Síntese do composto **32**.

Este fato pode ser atribuído ao impedimento estérico intrínseco ao aldeído empregado, o qual dificultou a aproximação de uma segunda molécula da *β*-dicetona, o que levaria à formação do intermediário tetracetônico e subsequente formação da xantenodiona.

A formação do intermediário de reação (**32**) diverge dos resultados encontrados por Esfahani e Abdizadeh[9], que descreveram o preparo da xantenodiona derivada do aldeído e da β-dicetona anteriormente citados (9-(2,6-diclorofenil)-3,3,6,6-tetrametil-3,4,5,6,7,9-hexaidro-1*H*-xanteno-1,8(2*H*)-diona), empregando um nanocatalisador de vanádio, à 80 °C e em condições livres de solvente. Outro trabalho que relatou a síntese de 9-(2,6-diclorofenil)-3,3,6,6-tetrametil-3,4,5,6,7,9-hexaidro-1*H*-xanteno-1,8(2*H*)-diona foi o desenvolvido por Lu e colaboradores[10], que utilizou $ZrOCl_2 \cdot 8H_2O$ como catalisador a 120 °C e na ausência de solvente, condição esta próxima àquela que levou a obtenção do composto **32**. As diferenças entre estas duas últimas metodologias residem na quantidade de catalisador e na temperatura de reação, ou seja, no presente trabalho utilizou-se 2 mol % de catalisador a 85 °C, enquanto que o grupo de Lu[10] empregou 5 vezes mais de catalisador (10 mol %) a 120 °C.

Outros intermediários obtidos durante a síntese de xantenodionas foram os tetracetônicos (compostos **33**, **34**, **35** e **36**), formados após a condensação de Knoevenagel

[9] ESFAHANI, M. N.; ABDIZADEH, T. Vanadatesulfuric acid nanorod particles: A novel and eco-benign catalyst for rapid and green synthesis of 1,8-dioxooctahydroxanthenes under solvent-free conditions. *Journal of Chemical. Science Technology*, v. 2, p. 14-20, 2013.

[10] LU, H. Y.; LI, J. J.; ZHANG, Z. H. $ZrOCl_2.8H_2O$: a highly efficient catalyst for the synthesis of 1,8-dioxo-octahydroxanthene derivatives under solvent-free conditions. *Applied Organometallic Chemistry*, v. 23, p. 165–169, 2009.

(i) e adição de Michael (ii) (Esquema II-1, pg. 76). Vale ressaltar que o procedimento utilizado na síntese de **33** e **34** foi levemente alterado mediante a adição de água no início da reação. Maiores detalhes com relação à preparação e caracterização destes intermediários encontram-se descritos no artigo 2. Na Tabela II-2 estão os rendimentos e os tempos de reação para os compostos **32** – **36**.

As estruturas de todos os compostos foram confirmadas por meio das espectroscopias de RMN e no IV bem como pela espectrometria de massas. Como aspectos gerais, observou-se nos espectros de RMN de ^{13}C das xantenodionas sinais próximos a δ_C 196 ppm referentes aos grupos carbonila, além dos sinais observados nos intervalos δ_C 164 – 162 ppm e δ_C 116 – 113 ppm correspondentes aos carbonos de ligações duplas. Nos espectros de RMN de ^{1}H, o sinal correspondente ao átomo de hidrogênio do anel pirânico foi observado no intervalo δ_H 4,70 – 5,27 ppm. Nos espectros no IV, frequências de estiramento do grupo carbonila foram observadas entre 1651 – 1670 cm^{-1}, os quais são compatíveis com grupos carbonila conjugados com ligações duplas. As fórmulas moleculares das xantenodionas foram confirmadas via espectrometria de massas. Como um exemplo, será descrito a seguir como foi feita a caracterização do composto **9**.

Tabela II- 2. Tempos de reação e rendimentos obtidos no preparo dos compostos **32 – 36**.

Composto	Estrutura	Tempo de reação (min)	Rendimento (%)
32	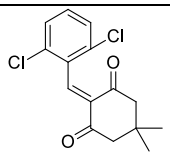	40	33
33	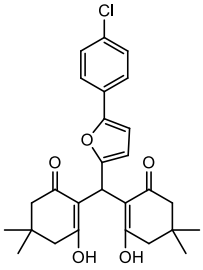	135	59
34	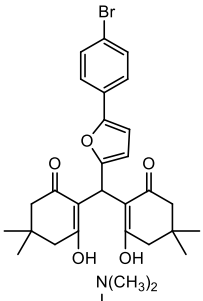	120	63
35	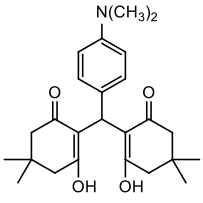	60	61
36	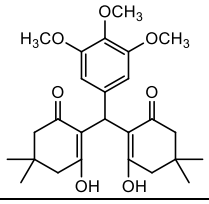	48	73

No espectro no IV do composto **9** (Figura II-1, pg. 84), as bandas em 2955 e 2899 cm^{-1} correspondem aos estiramentos de ligação C-H para carbonos hidrizados sp^3. A banda em 1652 cm^{-1} corresponde ao estiramento do grupo carbonila, enquanto que aquela observada em 1616 cm^{-1} foi atribuída ao estiramento da ligação C=C. Além destas bandas é possível observar também uma em 1460 cm^{-1} referente à deformação angular assimétrica de CH_2, e outras duas em 1201 cm^{-1} e 1170 cm^{-1} atribuídas, respectivamente, ao estiramento simétrico e assimétrico da ligação de carbonos vinílicos. A banda de estiramento assimétrico de =C-O-C de éter aromático apareceu em 1233 cm^{-1}.

No espectro de RMN de ^1H do composto **9** (Figura II-2, pg. 85) pode-se observar dois dupletos, um em δ_H 7,20 ppm e outro em δ_H 6,75 ppm, ambos integrados para dois hidrogênios e apresentando valores de constante de acoplamento igual a 7,2 Hz. Estes

sinais foram atribuídos aos hidrogênios do anel aromático, sendo que o dupleto de maior deslocamento químico corresponde aos hidrogênios ligados aos carbonos 15 e 19 e o de menor relaciona-se aos hidrogênios ligados aos carbonos 16 e 18. O simpleto em δ_H 4,75 ppm (integrado para um átomo de hidrogênio) trata-se do hidrogênio do anel pirânico. Outro simpleto presente em δ_H 3,72 ppm (integrado para três átomos de hidrogênio) relaciona-se aos hidrogênios do grupo metoxila. Além destes sinais, é possível verificar três multipletos (δ_H 2,67 – 2,52 ppm; δ_H 2,38 – 2,27 ppm e δ_H 2,06 – 1,92 ppm) integrados para 4 átomos de hidrogênio, os quais referem-se aos hidrogênios dos grupos metilênicos 8-C$\underline{H_2}$ e 11-C$\underline{H_2}$, 6-C$\underline{H_2}$, e 13-C$\underline{H_2}$ e 7-C$\underline{H_2}$, 12-C$\underline{H_2}$, respectivamente.

No espectro de RMN de ^{13}C deste mesmo composto (Figura II-3, pg. 86) o sinal de maior deslocamento químico (δ_C 196,6 ppm) foi atribuído aos carbonos carbonílicos (C1 e C5). Os sinais em δ_c 163,7 e 117,0 ppm correspondem aos carbonos das duplas ligações, sendo que o sinal de de maior deslocamento químico refere-se aos carbonos C9 e C10 (mais desblindado devido a conjugação com a carbonila) e aquele de menor deslocamento foi associado aos carbonos 2 e 4. Os carbonos C15/C19 e C16/C18 foram observados, respectivamente, em δ_C 129,3 e 113,5 ppm. Os carbonos não hidrogenados do anel aromático foram observados em δ_C 158,0 ppm (C17) e δ_C 136,7 ppm (C14). O carbono da metoxila apareceu em δ_C 55,1 ppm. Os grupos metilênicos apresentaram sinais em δ_C 37,0 ppm (C6 e C13), δ_C 27,1 (C8 e C11), e δ_C 20,3 (C7 e C12). O sinal em δ_c 30,7 foi atribuído ao átomo de carbono C3 do anel pirânico.

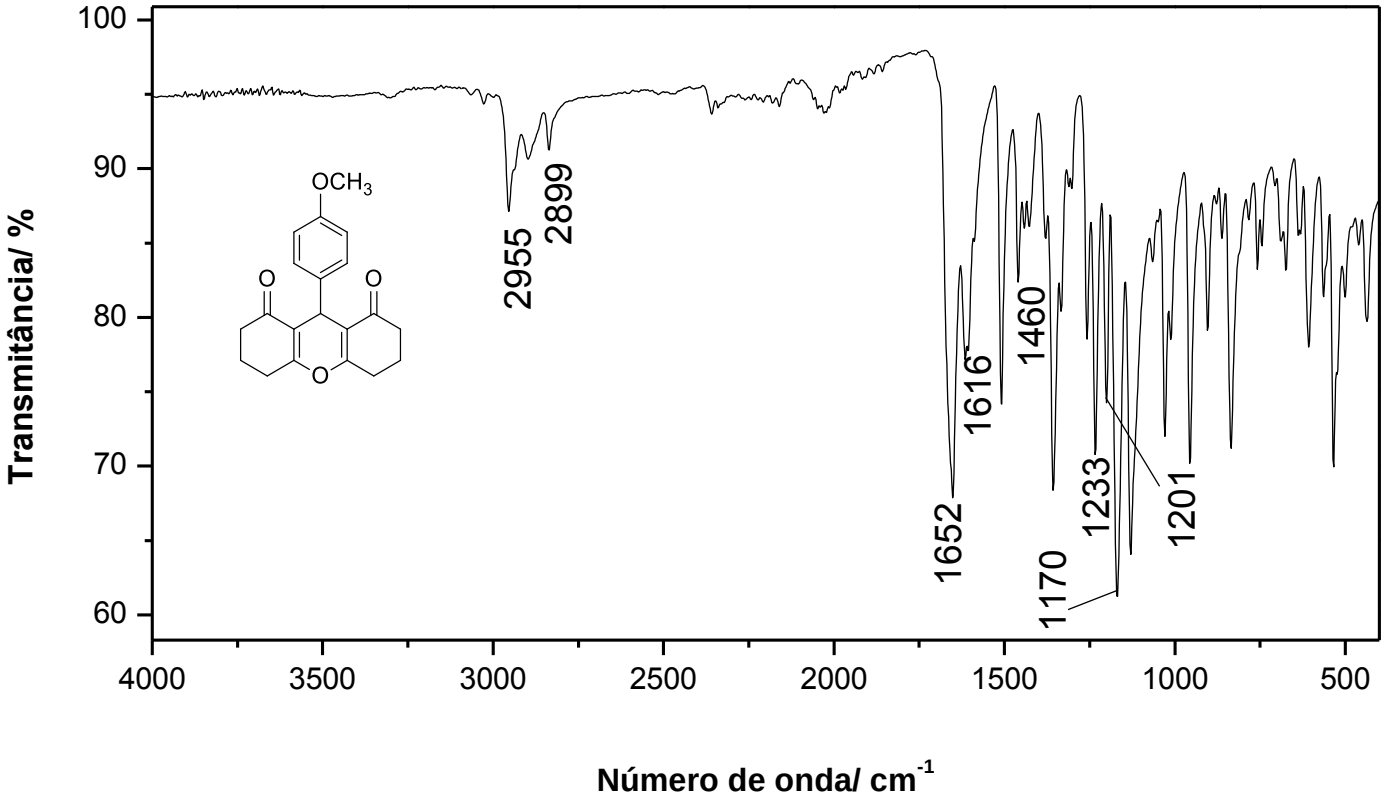

Figura II-1. Espectro no Infravermelho (ATR) do composto **9**.

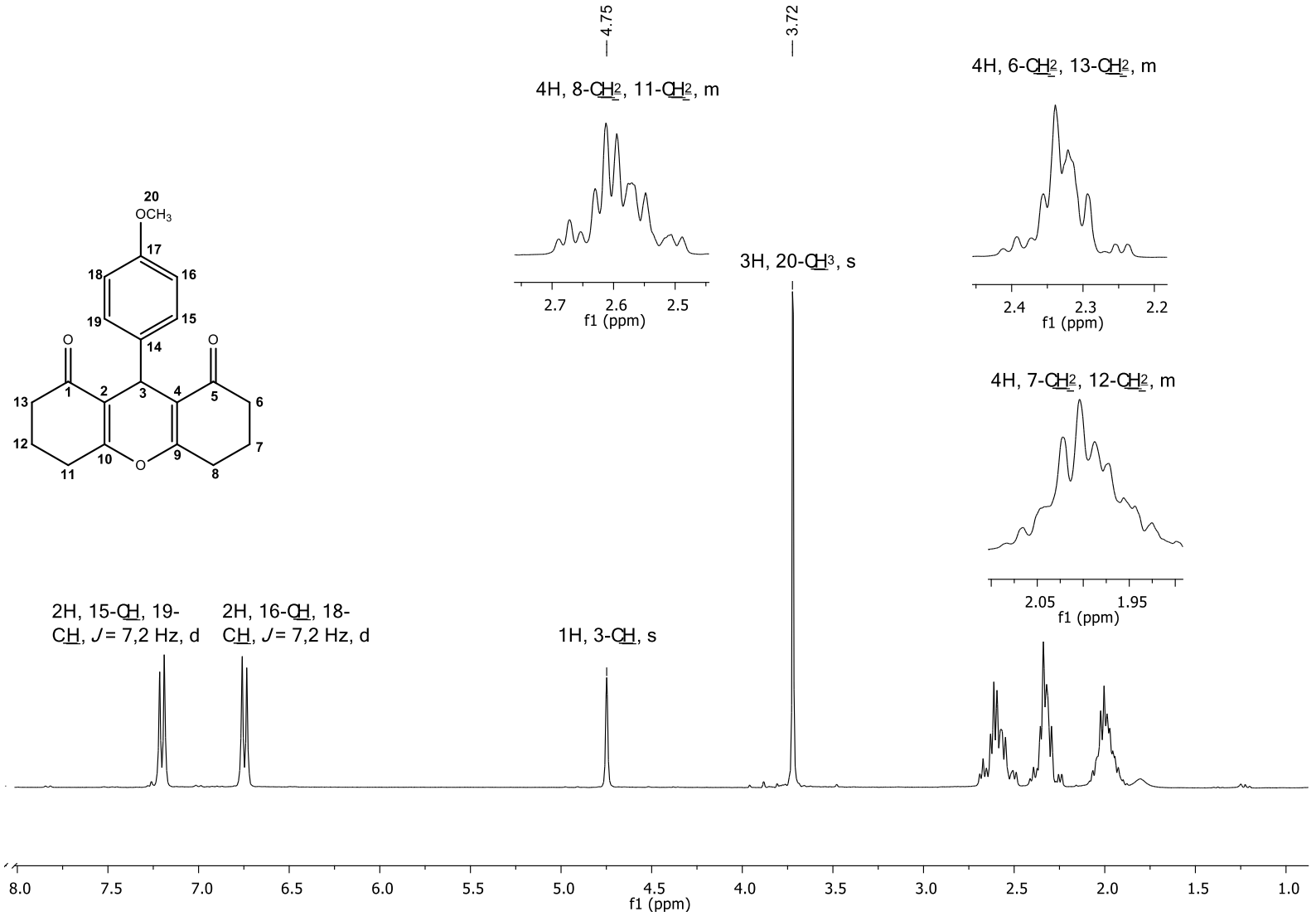

Figura II-2. Espectro de RMN de ^{1}H (300 MHz, $CDCl_3$) do composto **9**.

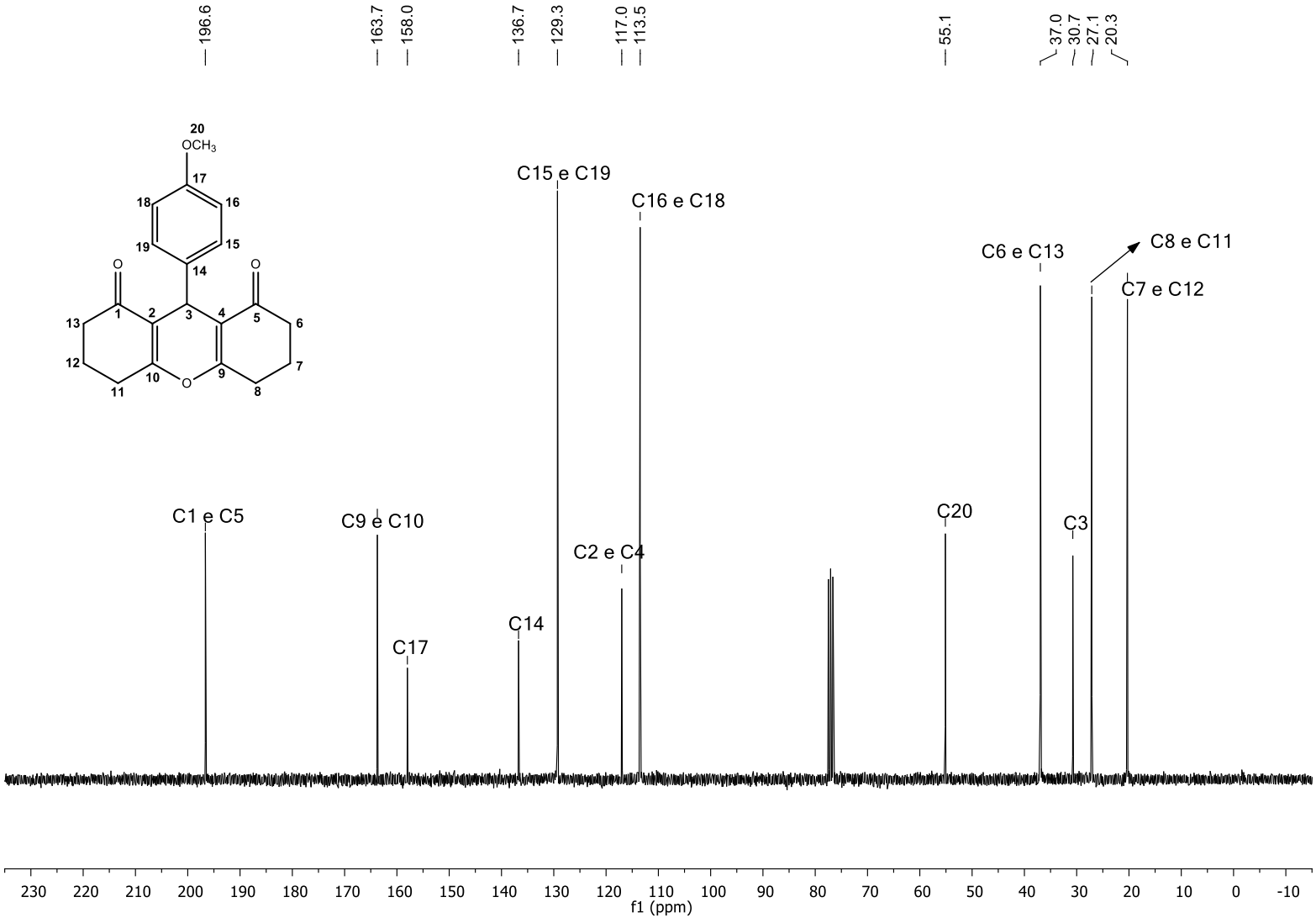

Figura II-3. Espectro de RMN ^{13}C (75 MHz, $CDCl_3$) do composto **9**

CAPÍTULO III

ARTIGO 1

Synthesis, X-ray Analysis and Theoretical Aspects of Xanthenodiones (1,8-dioxooctahydroxanthenes)

Milene Lopes da Silva[a] · Róbson Ricardo Teixeira[a*] · Lucas de Azevedo Santos[b] · Felipe Terra Martins[c] · Teodorico Castro Ramalho[b]

[a]*Chemistry Department, Universidade Federal de Viçosa, CEP 36570-900, Viçosa, MG, Brazil*

[b]*Departament of Chemistry, Federal University of Lavras, CEP 37200-000, Lavras, MG, Brazil*

[c]*Chemical Institute, Federal University of Goiás, CEP 74001-970, Goiânia, GO, Brazil*

[*]Corresponding author. e-mail: robsonr.teixeira@ufv.br

Abstract

Heterocyclic compounds containing a pyran nucleus fused to either side to cyclohex-2-enone rings are collectively called xanthenodiones (1,8-dioxooctahydroxanthenes). These xanthene derivatives display broad biological activities and find applications in laser technologies and photodynamic therapy. It is described herein the preparation of a collection of nine xanthenodiones. The compounds were synthesized *via* Knoevenagel condensation between different aldehydes and *β*-diketones. The reactions were performed free of solvent and the compounds were obtained with yields ranging from 70%-92%. All the compounds were fully characterized by NMR and IR spectroscopy as well mass spectrometry. Among the synthesized compounds, seven of them had their crystal structures elucidated for the first time. In all of the new crystal structures, the three fused rings did form an almost completely planar xanthenodione core, except for the side rings adopting half-chair conformation with both carbons at the flaps oriented towards to the aromatic substituent or with one of the two carbons pointing opposite to the substituent. Another conformational difference among the new compounds investigated by X-ray diffraction resides in the rotation around the bond axis connecting xanthenodione core to its aromatic substituent. It was found different bent levels resulted from weak intermolecular contact patterns. In addition, theoretical calculations for single molecule and dimmers have provided insights into the balance between intra and intermolecular forces driving both conformational features.

Keywords: xanthenodiones, 1,8-dioxooctahydroxanthenes, xanthene derivatives, x-ray analysis, DFT calculations

1. Introduction

The heterocyclic compounds are of great importance in the realm of organic chemistry. They abound in nature and natural heterocycles present a broad range of important biological activities (QUIN and TYRELL, 2010). Several agrochemicals and pharmaceuticals bear in their structures heterocycle functionalities (DUA et al., 2011; LAMBERTH AND DINGES, 2012a, 2012b). Heterocycles are also integrant part of several dyes, luminophores and polymers. Oxygen and nitrogen containing compounds constitute the large and most varied group of heterocycles.

Xanthene (9*H*-xanthene, 10*H*-9-oxaanthracene) is an oxygenated heterocyclic endowed with fungicidal activity. Several xanthene based dyes, such as fluorescein, eosins, and rhodamines are known. These dyes have several uses in textile, paper, food, cosmetics, pharmaceuticals, medicine and biological staining due to superior dyeing and coloring properties. In addition to the dyes, other important xanthene derivatives, for instance xanthones, are well known.

Heterocyclic compounds containing a pyran nucleus fused to either side to cyclohex-2-enone rings are collectively called xanthenodiones (1,8-dioxooctahydroxanthenes). These xanthene derivatives display broad biological activities including antifungal (OMOLO et al., 2011), antibacterial (WANG et al., 2006), anti-inflammatory (POUPELIN et al., 1978), anti leishmanicidal (NISAR et al., 2013) and antitumor (MULAKAYALA et al., 2012). In addition, these compounds are found in cosmetics and pigments (ILANGOVAN et al., 2011), biodegradable agrochemicals (HAFEZ et al., 1987) and fluorescent materials (CALLAN et al. 2005). Xanthenodiones also find applications in laser technologies (BANERJEE and MUKHERJEE, 1981) and photodynamic therapy (ION et al., 1998). All of these biological

activities and applications have attracted the attention of researchers to this class of compounds.

In this paper we describe the synthesis and X-ray analysis of a series of xanthenodiones. Theoretical aspects associated with these compounds are also discussed.

2. Experimental

2.1 Generalities

All reagents were purchased from commercial sources (Sigma Aldrich - St. Louis, MO, US and Vetec - Rio de Janeiro, Brazil) and were employed as received. Solvents were procured from Vetec (Rio de Janeiro, Brazil) and were used as received. The ^{1}H and ^{13}C NMR spectra were recorded on a Varian Mercury 300 instrument (300 MHz and 75 MHz respectively), using deuterated chloroform as solvent. Hydrogen nuclear magnetic resonance (NMR) data are presented as follows: chemical shift (δ) in ppm, number of hydrogen atoms, multiplicity, *J* values in Hertz (Hz). Multiplicities are shown as the following abbreviations: s (singlet), d (doublet), t (triplet), m (multiplet). Infrared spectra (IR) were obtained employing the equipment Varian 660-IR with accessory GladiATR. Mass spectra were recorded on a SHIMADZU GCMS-QP5050A instrument under electron impact (70 eV) conditions. The mass was acquired in positive mode scanning from 50 to 1000 Da. Melting points were determined using MQAPF-301 melting point apparatus (Microquimica, Rio de Janeiro, Brazil). Analytical thin layer chromatography analysis was carried out on TLC plates recovered with 60GF254 silica gel.

2.2 Synthesis

*2.2.1 Synthesis of 9-(4-bromophenyl)-3,3,6,6-tetramethyl-3,4,5,6,7-9-hexahydro-1H-xanthene-1,8(2H)-dione (**3**)*

In a typical procedure, a round-bottomed flask (25 mL) was charged with 5,5-dimethylcyclohexan-1,3-dione (294.9 mg, 2 mmol), 4-bromobenzaldehyde (186.9 mg, 2 mmol) and $ZrOCl_2 \cdot 8H_2O$ (12 mg, 2 mol%). The mixture was stirred at 85 °C and the progress of the reaction was monitored by TLC analysis. After completion of the reaction, the mixture was cooled down to room temperature. Thereafter, it was added to the flask 50 ml of dichloromethane and the mixture was kept under stirring for about 30 minutes. Then, the catalyst, which is insoluble in dichloromethane, was separated by filtration. After that, 50 mL of ethanol was added and the system was kept undisturbed for recrystallization process. This procedure afforded compound **3** as a pale yellow solid in 80% yield (344.0 mg, 0.80 mmol). Crystals suitable for X-ray diffraction studies were obtained from the above mentioned recrystallization method. The obtained crystals were thoroughly washed with cold ethanol and dried. Structure of **3** is supported by the following data.

Mp 239–240 ºC. IR (ATR): 2952, 2876, 1659, 1624, 1360, 1196, 1165, 1139 cm^{-1}. ^1H NMR (300 MHz, $CDCl_3$) δ: 7.32 (2H, d, J = 7.9 Hz), 7.16 (2H, d, J = 7.9 Hz), 4.69 (1H, s), 2.46 (4H, s), 2.23 (d, 2H, J = 16.4 Hz), 2.15 (d, 2H, J = 16.4 Hz), 1.09 (6H, s), 0.98 (6H, s). ^{13}C NMR (75 MHz, $CDCl_3$) δ: 196.3, 162.5, 156.6, 143.2, 131.1, 130.2, 120.2, 115.1, 50.7, 40.8, 32.2, 31.5, 29.3, 27.3. MS, *m/z* (%): 430 (M+2, 30), 428 ($C_{23}H_{25}BrO_3$, M^+, 30), 349 (21), 273 (100), 217 (26), 161 (17), 55 (22), 41 (31).

*2.2.2 Synthesis of **4-11***

A similar procedure to that described for the preparation of **3** was utilized to synthesize compounds **4-11**. The structures of these compounds are supported by the following data.

*9-(4-clorophenyl)-3,3,6,6-tetramethyl-3,4,5,6,7,9-hexahydro-1H-xanthene-1,8 (2H)-dione **(4)***

White solid, Mp 232-233 °C. IR (ATR): 2951, 2875, 1659, 1624, 1360, 1196, 1164, 1139 cm^{-1}. ^{1}H NMR (300 MHz, $CDCl_3$) δ: 7.22 (2H, d, J = 7.9 Hz), 7.17 (2H, d, J = 7.9 Hz), 4.70 (1H, s), 2.46 (4H, s), 2.23 (2H, d, J = 16.4 Hz), 2.15 (2H, d, J = 16.4 Hz), 1.09 (6H, s), 0.98 (6H, s). ^{13}C NMR (75 MHz, $CDCl_3$) δ: 196.4, 162.4, 142.7, 132.0, 129.8, 128.2, 115.2, 50.7, 40.8, 32.2, 31.4, 29.3, 27.3. MS, *m/z* (%): 386 (M+2, 14), 384 ($C_{23}H_{25}ClO_3$, M+, 39), 349 (16), 273 (100), 217 (28), 161 (18) 55 (23), 41 (32).

*9-(4-chlorophenyl)-3,6-dimethyl-3,4,5,6,7,9-hexahydro-1H-xanthene-1,8 (2H)-dione (**5**)*

White solid, Mp 226 - 228 °C. IR (ATR): 2962, 2876, 1665, 1619, 1185. ^{1}H NMR (300 MHz, $CDCl_3$) δ: 7.23 – 7.14 (4H, m), 4.72 (1H, s), 2.70 – 2.50 (2H, m), 2.48 – 2.16 (6H, m), 2.09 – 1.97 (2 H, m), 1.13 - 0.99 (6H, m). ^{13}C NMR (75 MHz, $CDCl_3$) δ: 196.5, 163.8 or 163.7, 163.1 or 163.0, 142.9 or 142.8, 132.1 or 132.0, 129.8 or 129.7, 128.2 or 128.1, 116.1 or 115.9, 45.2 or 45.1, 35.2 or 34.9, 31.4 or 31.2, 28.4 or 28.3, 27.9 or 27.8, 20.8 or 20.7. MS, *m/z* (%): 358 (M+2, 14), 356 ($C_{21}H_{21}ClO_3$, M^+, 42), 321 (33), 245 (100), 203 (11).

*9-(5-(4-bromophenyl)furan-2-yl)-3,4,5,6,7,9-hexahydro-1H-xanthene-1,8 (2H)-dione **(6)***

Yellow solid, Mp 261 - 262 °C. IR (ATR): 2952, 2887, 1653, 1615, 1535, 1479, 1198, 1172. ^{1}H NMR (300 MHz, $CDCl_3$) δ: 7.42 (2H, d, J = 7.9 Hz), 7.36 (2H, d, J = 7.9 Hz), 6.49 (1H, s), 6.23 (1H, s), 5.03 (1H, s), 2.68 – 2.38 (8H, m), 2.05 (4H, m). ^{13}C NMR (75 MHz,

$CDCl_3$) δ: 196.4, 165.1, 155.2, 151.0, 131.6, 130.1, 124.8, 120.3, 113.7, 108.7, 106.9, 36.9, 27.3, 25.5, 20.4. MS, *m/z* (%): 440 (M+2, 66), 438 ($C_{23}H_{19}BrO_4$, M^+, 67), 255 (84), 217 (100), 185 (40), 155 (20), 115 (54), 66 (21), 55 (73), 41 (42).

*9-(5-(4-chlorophenyl)furan-2-yl)-3,4,5,6,7,9-hexahydro-1H-xanthene-1,8 (2H)-dione (**7**)*

Yellow solid, Mp 261 - 262 °C. IR (ATR): 2930, 2888, 1654, 1614, 1484, 1174. ^{1}H NMR (300 MHz, $CDCl_3$) δ: 7.43 (2H, d, *J* = 8.1 Hz), 7.27 (2H, d, *J* = 8.1 Hz), 6.48 (1H, d, *J* = 2.2 Hz), 6.24 (1H, *J* = 2.2 Hz), 5.04 (1H, s), 2.67 – 2.35 (8H, m), 2.09 – 1.99 (4H, m). ^{13}C NMR (75 MHz, $CDCl_3$) δ: 196.4, 165.1, 155.1, 151.0, 132.3, 129.7, 128.7, 124.5, 113.7, 108.7, 106.9, 36.9, 27.2, 25.5, 20.3. MS, *m/z* (%): 396 (M+2, 36), 394 ($C_{23}H_{19}ClO_4$, M^+, 100), 349 (20), 255 (80), 217 (92), 139 (36), 55 (25).

*9-(5-phenylthiophen-2-yl)-3,4,5,6,7,9-hexahydro-1H-xanthene-1,8 (2H)-dione (**8**)*

Yellow solid, Mp 201 - 202 °C. IR (ATR): 2950, 2870, 1659, 1619, 1201, 1171, 756. ^{1}H NMR (300 MHz, $CDCl_3$) δ: 7.49 (2H, d, *J* = 7.5 Hz), 7.29 (2H, t, *J* = 7.3 Hz), 7.23 – 7.16 (1H, m), 7.05 (1H, d, *J* = 3.3 Hz), 6.89 (1H, d, *J* = 3.3 Hz), 5.16 (1H, s), 2.71 – 5.53 (4H, m), 2.50 – 2.33 (4H, m), 2.09 – 2.00 (4H, m). ^{13}C NMR (75 MHz, $CDCl_3$) δ: 196.5, 164.4, 148.1, 142.4, 134.7, 128.7, 127.0, 126.0, 125.5, 122.8, 116.2, 36.9, 27.2, 26.5, 20.3. MS, *m/z* (%): 376 ($C_{23}H_{20}O_3S$, M^+, 100), 359 (30), 320 (38), 217 (50), 160 (21), 121 (24), 115 (65), 77 (37), 55 (60), 41 (41).

*9-(4-(dimethylamino)phenyl)-3,4,5,6,7,9-hexahydro-1H-xanthene-1,8 (2H)-dione (**9**)*

Yellow solid, Mp 231 – 232 °C. IR (ATR): 2944, 2869, 1658, 1610, 1459, 1356, 1199. ^{1}H NMR (300 MHz, $CDCl_3$) δ: 7.15 (2H, d, *J* = 8.5 Hz), 6.62 (2H, d, *J* = 8.5 Hz), 4.76 (1H, s), 2.87 (6H, s), 2.65 – 2.52 (4H, m), 2.37 – 2.28 (4H, m), 2.04 – 1.95 (4H, m).^{13}C NMR (75 MHz, $CDCl_3$) δ: 196.6, 163.5, 149.0, 133.1, 128.9, 117.2, 112.6, 40.8, 37.0, 30.4, 27.1, 20.3. MS, *m/z* (%): 337 ($C_{21}H_{23}NO_3$, M^+, 100), 320 (87), 293 (20), 281 (16), 217 (17).

9-(4-fluorophenyl)-3,3,6,6 tetramethyl-3,4,5,6,7,9-hexahydro-1H-xanthene-1,8(2H)-dione ***(10)***

White solid, Mp 227 - 228 °C. IR (ATR): 2957, 2872, 1657, 1626, 1360, 1222, 1196, 1164, 1139 cm^{-1}. ^{1}H NMR (300 MHz, $CDCl_3$) δ: 7.28 – 7.21 (2H, m), 6.92 – 6.84 (2H, m), 4.72 (1H, s), 2.46 (4H, s), 2.23 (2H, d, J = 16.4 Hz), 2.15 (2H, d, J = 16.4 Hz) 1.09 (6H, s), 0.98 (6H, s). ^{13}C NMR (75 MHz, $CDCl_3$) δ: 196.4, 162.3, 161.3 (d, J = 242.6 Hz), 139.9 (d, J = 3.0 Hz), 129.8 (d, J = 8.0 Hz), 115.5, 114.8 (d, J = 21.2 Hz), 50.7, 40.8, 32.2, 31.2, 29.2, 27.3. MS, *m/z* (%): 368 ($C_{23}H_{25}FO_3$, M^+, 54), 273 (100), 217 (30), 161 (20), 133 (17), 95 (15), 55 (23), 41 (30).

3,3,6,6-tetramethyl-9-(5-phenyl-thiophen-2-yl)-3,4,5,6,7,9-hexahydro-1H-xanthene-1,8 (2H)-dione ***(11)***

White solid, Mp 169 - 170 °C. IR (ATR): 2955, 2867, 1598, 1580, 1359, 1197, 1164, 1145, 755. ^{1}H NMR (300 MHz, $CDCl_3$) δ: 7.63 (2H, d, J = 7.5 Hz), 7.44 (2H, t, J = 7.5 Hz), 7.37 – 7.32 (1H, m), 7.19 (1H, d, J = 3.3 Hz), 7.08 (1H, d, J = 3.3 Hz), 5.27 (1H, s), 2.61 (4H, s), 2.42 (4H, s), 1.26 (6H, s), 1.22 (6H, s). ^{13}C NMR (75 MHz, $CDCl_3$) δ: 196.4, 162.9, 147.9, 142.3, 134.9, 128.8, 127.1, 126.5, 125.6, 123.0, 115.2, 50.9, 41.0, 32.3, 29.4, 27.6, 26.9. MS, *m/z* (%): 432 ($C_{27}H_{28}O_3S$, M^+, 100), 415 (11), 348 (24), 273 (20), 83 (11).

2.3 X-ray diffraction analysis

Well-shaped single crystals of xanthenodione derivatives (Fig. 1) were chosen and mounted on a κ-goniostat and exposed to X-ray beam (Mo Kα, λ = 0.71073 Å) using a Bruker-AXS Kappa Duo diffractometer with an APEX II CCD detector. X-Ray diffraction experiments were carried out at room temperature (see Table 1). Data collection strategy was calculated by setting φ scans and ω scans with κ offsets using the software APEX2 (SADABS

et al., 2009). Other crystallographic softwares were used as follows: SAINT (indexing, integration and scaling of raw data) [15], SHELXL-97 (structure solving) (SHELDRICK, 2008), SHELXL-97 (structure refinement) (SHELDRICK, 2008) and MERCURY (MACRAE et al., 2008) (structure analysis and graphical representations). Direct methods of phase retrieval were used to solve the crystal structures. All non-hydrogen atoms of asymmetric unit were promptly located from the electronic density Fourier map. The early solved model was refined by full-matrix least squares method based on F^2. In the refinements, free anisotropic and fixed isotropic thermal displacement parameters were adopted for non-hydrogen and hydrogen atoms, respectively. The isotropic thermal displacement parameters of hydrogens were 20% greater than the equivalent isotropic parameter of the bonded carbon (except those hydrogens in methyl moieties which were 50%). Concerning the position of all hydrogens, bond distances and angles were stereochemically constrained according to riding model.

2.4 Computational details

The geometries of synthesized compounds (Fig. 1) were optimized at ωb97xD/6-311++** level of theory by Gaussian 09-D01 software (FRISCH et al., 2009). In order to obtain the temperature effect on the electronic energy, the calculations were carried out in gas phase at 25 °C and in water at 85 °C using the PCM solvation model. The conformational preference of cyclohex-2-enone moieties in the synthesized compounds was studied enforcing their respective opposite *syn* or *anti* conformer and calculating their local energy minima and thermodynamics. The conformational preference of aromatic groups was evaluated through potential energy curves scanning the O-C-C-X dihedral angle, where X = O or S, with torsions of 45°.

3. Results and Discussion

*3.1 Preparation of xanthenediones **3-11***

The synthesis of the compounds **3-11** were carried out *via* Knoevenagel condensation between different aromatic aldehydes (**1**) and *β*-diketones (**2**) (MOSADDEGH et al., 2012). The reactions were carried out free of solvent and catalyzed by $ZrOCl_2 \cdot 8H_2O$, a versatile catalyst that has been involved in several synthetically useful transformations (BALTORK et al., 2007; SANGSHETTI et al., 2008; BARDAJEE, 2013) [20-22]. As shown in Fig. 1, the compounds were obtained in good yields within 20 minutes to 2 hours.

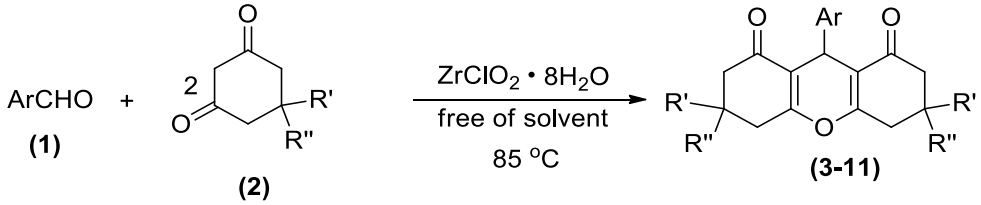

Compound	Ar	R'/R''	Reaction Time (min)	Yield (%)
3	4-bromophenyl	R'=R''=methyl	60	80
4	4-chlorophenyl	R'=R'' =methyl	30	84
5	4-chlorophenyl	R'=H; R"= methyl	20	80
6	5-(4-bromophenyl) furan-2-yl	R'=H; R"=H	120	75
7	5-(4-chlorophenyl) furan-2-yl	R'=H; R"=H	120	78
8	5-phenyl-thiophene-2-yl	R'=H; R"=H	50	92
9	4-dimethylaminophenyl	R'=H; R"=H	60	70
10	4-fluorophenyl	R'=R''=methyl	60	80
11	5-phenyl-thiophen-2-yl	R'=R''=methyl	50	94
12	phenyl [i]	R'=R''=methyl	-	-

Fig. 1. Synthesis of xanthenodiones **3-11**. [i] Compound **12** was not synthetized in this study even though its geometry is key to understand the xanthenodione structures.

The structures of the compounds were confirmed upon NMR (^1H and ^{13}C) and IR spectroscopy as well as mass spectrometry. In the ^1H NMR spectra, the hydrogen atom of

pyran ring was observed within the 4.70-5.27 ppm range. In the ^{13}C, the signals for the carbonyl groups were observed near to 196 ppm. In the IR spectra, carbonyl stretching frequencies were noticed in the range 1653-1670 cm^{-1} which is compatible with a conjugated carbonyl group. The molecular formulas of xanthenodiones were confirmed by mass spectrometry analysis. The structures of compounds **3-11** were also investigated by single-crystal X-ray diffraction.

3.2 Crystal Structures

Crystal structures of compounds **3** and **4** have been previously elucidated (BIGDELI et al., 2007; TU, 2002). Their determined unit cell metrics matched those reported in the literature confirming, therefore, all conformational and intermolecular features already described for these xanthenodiones. Crystal structures of all other compounds have not being described and thus are herein reported for the first time. Crystallographic data of these compounds are presented in Table 1.

Table 1. Crystal data and refinement statistics for the xanthenodiones prepared in this investigation

Compound		**5**	**6**	**7**	**8**	**9**	**10**	**11**
Molecular formula		$C_{21}H_{21}ClO_3$	$C_{23}H_{19}BrO_4$	$C_{23}H_{19}ClO_4$	$C_{23}H_{20}O_3S$	$C_{21}H_{23}NO_3$	$C_{23}H_{25}FO_3$	$C_{27}H_{28}O_3S$
fw (g/mol)		356.83	439.29	394.83	376.45	337.40	368.43	432.55
cryst syst		monoclinic	orthorhombic	orthorhombic	orthorhombic	monoclinic	monoclinic	monoclinic
space group		*C*2/*c*	*Pbca*	*Pbca*	*Pbca*	$P2_1/c$	$P2_1/c$	$P2_1/c$
Z / *Z'*		8 / 1	8 / 1	8 / 1	8/1	4 / 1	4 / 1	4/1
T (K)		296(2)	296(2)	296(2)	296(2)	296(2)	296(2)	296(2)
unit cell dimensions	*a* (Å)	21.3859(6)	13.4419(18)	13.3329(13)	24.2630(14)	9.2929(14)	6.0269(2)	12.2637(5)
	b (Å)	16.0215(6)	13.8418(17)	13.8091(15)	16.2820(10)	11.3538(18)	19.6459(6)	9.6726(4)
	c (Å)	10.7313(4)	20.596(3)	20.4485(18)	9.5470(5)	17.113(3)	16.7818(5)	20.0243(8)
	β (°)	94.126(3)	90	90	90	99.675(6)	99.690(2)	100.546(2)
V (Å^3)		3667.4(2)	3832.1(9)	3764.9(6)	3771.5(4)	1779.9(5)	1958.68(11)	2335.20(16)
calculated density (Mg/m^3)		1.293	1.523	1.393	1.326	1.259	1.249	1.230
absorp. coefficient μ (mm^{-1})		0.225	2.172	0.230	0.192	0.084	0.088	0.164
θ range for data collection (°)		1.59 – 25.64	2.33 – 25.35	2.35 – 25.37	2.09-25.37	2.16-25.86	1.61-25.41	1.69-25.38
index ranges	*h*	-25 to 25	-11 to 16	-16 to 13	-29 to 25	-11 to 10	-7 to 6	-14 to 14
	k	-19 to 19	-16 to 12	-16 to 12	-17 to 18	-10 to 13	-23 to 23	-10 to 11
	l	-12 to 12	-24 to 11	-24 to 13	-11 to 11	-21 to 18	-20 to 20	-24 to 20

Table 1. continued

data collected	14443	9776	10587	12787	15320	39593	23300
unique reflections	3434	3438	3434	3364	3411	3590	4282
observed reflections	2399	2132	2476	2615	2349	2317	3358
symmetry factor (R_{int})	0.0283	0.0567	0.0273	0.0691	0.0531	0.0654	0.0487
completeness to θ_{max} (%)	98.8	97.8	99.2	97.2	99.2	99.3	99.7
F (000)	1504	1792	1648	1584	720	784	920
parameters refined	228	253	254	244	226	244	280
goodness-of-fit on F^2	1.047	1.024	1.047	1.039	1.076	1.053	1.042
final *R1* factor for $I > 2\sigma(I)$	0.0589	0.0479	0.0422	0.0510	0.0615	0.0594	0.0467
wR2 factor for all data	0.1793	0.1184	0.1168	0.1441	0.1909	0.1721	0.1332
largest diff. peak / hole (e/Å^3)	0.441/-0.294	0.574/-0.336	0.246/-0.244	0.589 / -0.317	0.270/-0.213	0.196/-0.209	0.219 / -0.259
CCDC deposit number	1465044	1465043	1465047	1465045	1465042	1465046	1465041

In addition to C1, compound **5** has two stereocenters and it crystallizes in a centrosymmetric space group (*C*2/*c*) as expected from its achiral synthesis. In the chosen asymmetric unit, chiral carbons labeled as C8 and C12 have *S* and *R* configurations; however, the enantiomeric counterpart is also present in the unit cell. Compounds **6** to **11**, each one presenting one stereocenter, have crystallized in centrosymmetric space groups. The crystallographic asymmetric unit of all xanthenodiones is composed by just one molecule, as can be viewed in Fig. 2. In this figure, non-hydrogen atoms are shown with their 50% probability ellipsoids and arbitrary labeling scheme. Labeling of rings is also depicted in Fig. 2.

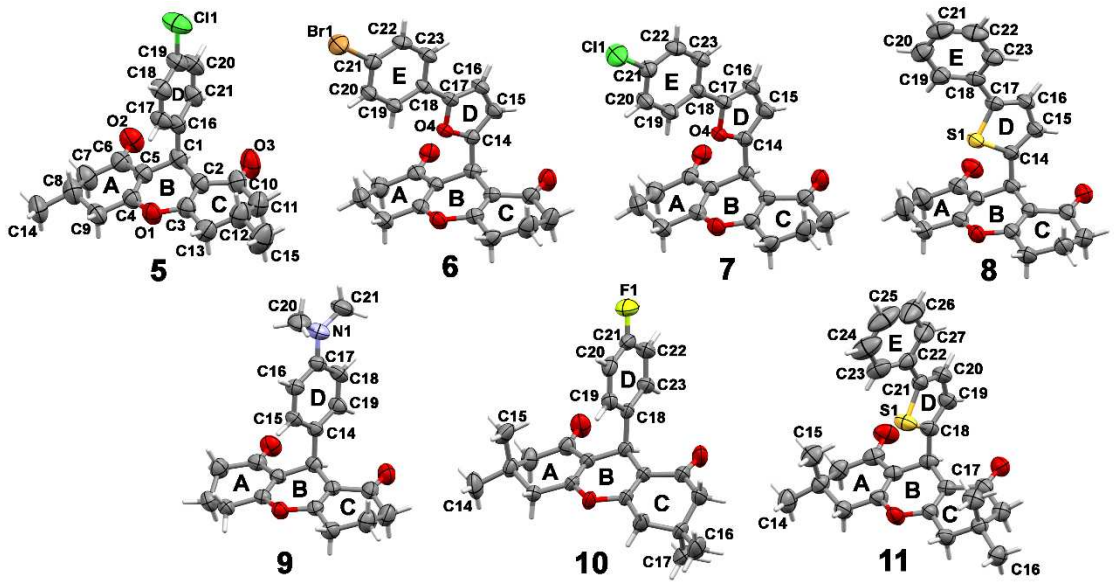

Fig. 2. 50% Ellipsoid plot of the non-hydrogen atoms in the asymmetric unit of compounds **5-11** elucidated by single-crystal X-ray diffraction technique. The labeling scheme of rings as well as non-hydrogen atom numbering follow those shown for compound **5**.

For all compounds reported herein, the three fused rings did form an almost completely planar xanthenodione core, except for side rings A and C adopting a half-chair conformation with C8 and C12 carbons away from the least-squares (l.s.) planes

calculated through the other five coplanar atoms. The distance of these carbons from l.s. planes and the root-mean square deviation of the l.s. fitted atoms are shown in Table 2.

Table 2. Selected torsion angle describing the conformation of the substituent at C1 and descriptors for half-chair conformation of rings A and C and for the planarity of ring B (r.m.s. deviation and carbon deviation in Å) in the xanthenodiones as determined by single-crystal X-ray diffraction

Compound	O1-C1-CX-Y[i]/°	C8 deviation from the l.s. plane A - plane A r.m.s.d.[ii] / Å	C12 deviation from the l.s. plane C - plane C r.m.s.d.[iii] / Å	C1 deviation from the l.s. plane C - plane B r.m.s.d.[iv] / Å
5	-7.0(3)	0.561(4)-0.0301	0.657(4)-0.0398	0.148(2)-0.136
6	-26.1(4)	0.611(5)-0.0435	0.609(5)-0.0513	0.161(4)-0.142
7	-25.3(2)	0.596(3)-0.0432	0.640(3)-0.0537	0.1599(19)-0.145
8	-34.0(2)	0.511(4)-0.0544	0.630(3)-0.0588	0.166(2)-0.146
9	-16.6(3)	-0.525(3)-0.0649	0.601(4)-0.0524	0.160(2)-0.134
10	-5.3(3)	0.610(3)-0.0614	-0.585(3)-0.0670	0.117(2)-0.103
11	-9.3(2)	0.634(2)-0.0475	0.6195(19)-0.0152	-0.1342(19)-0.114

[i] X=14 in 6 to 9; X=16 in 5; X=18 in 10 and 11; Y=S1 in 8 and 11; Y=O4 in 6 and 7; Y=C15, C17 or C19 in 9, 5 and 10. [ii] Plane A was fitted through the C9-C4-C5-C6-C7 atoms. [iii] Plane C was fitted through the C13-C3-C2-C10-C11 atoms. [iv] Plane B was fitted through the C1-C2-C3-O1-C4-C5 atoms.

Taking a xanthenodione mean plane as reference, it is interesting to observe that the flaps C8 and C12 of both half-chairs are oriented towards the aromatic substituent in compounds **5** to **8**, and **11**, which corresponds to a *syn* conformation of cyclohex-2-enone moieties. On the contrary, in xanthenodiones **3, 4**, and **10** C8 points towards to the aromatic substituent while C12 points to the opposite direction, which relates to an *anti* conformation of these two half-chairs. This trend observed for **3**, **4**, and **10** was also noticed for xanthenodione having a *para*-carboxymethoxy phenyl group (CSD ref. code GIWZAP, reference (KUMAR et al., 2014)) as well as in that bearing only one phenyl moiety (hereinafter compound **12**; CSD ref. code VOQSEA, reference (REDDY et al., 2009)). Compound **9** also presents alternated flaps; however, C8 points opposite to the *para*-substituted phenyl ring while C12 points towards it.

Another difference among compounds **5-11**, which is also responsible for the conformational distinction in terms of rings A and C, corresponds to the rotation around the axis of the bond connecting xanthenodione core to its substituent at C1. Such intramolecular feature can be viewed in Fig. 3, a molecular overlay of all asymmetric units (only non-hydrogen atoms) through the xanthenodione core.

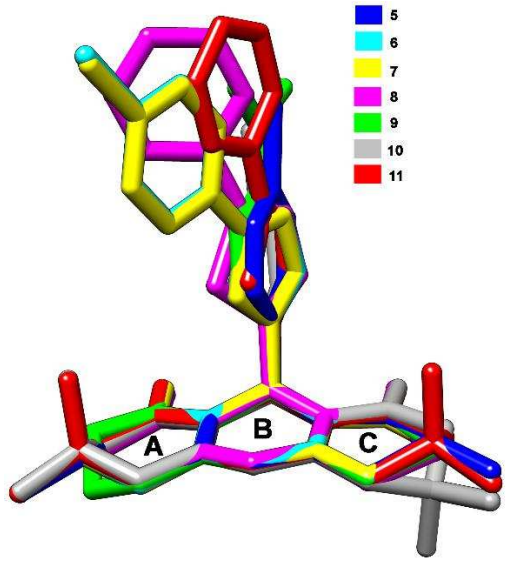

Fig. 3. Molecular overlay of all asymmetric units (only non-hydrogen atoms) through the xanthenodione core and labeling scheme of its rings.

Even so, the plane of the substituent at C1 is pointed towards the ring A in all compounds, but with different bent levels. Such conformational predilection is more prominent in compounds with either furan (**6** and **7**) or thiophene (only **8**) rings as substituents at C1. The dihedral angle among the atoms O1, C1, CX (X=14 in **6** to **9**; X=16 in **5**; X=18 in **10** and **11**) and Y (Y=S1 in **8** and **11**; Y=O4 in **6** and **7**; Y=C15, C17 or C19 in **9**, **5** and **10**) describes this conformational feature (Table 2).

The deviation from 0°, which means the mean plane of the substituent at C1 coinciding with the transverse plane of the xanthenodione core, is more pronounced in compounds **6** to **8** than in the others. In all furan and tiophene based compounds, the heteroatom of the substituent at C1 is positioned on the same side of O1, in a so-called *syn* conformation, relative to xanthenodione core. Also in these compounds, *para*-halogenated phenyl ring is coplanar to furan in **6** and **7**. Their l.s. mean planes form angles of 2.53(11)° and 4.11(7)°. On the other hand, non-substituted phenyl ring and thiophene C are twisted in **8** and **11**, with angles of 33.08(8)° and 16.67(8)° between their l.s. mean planes. In compound **9**, there is an electronic conjugation between the 4-*N*,*N*-dimethylamine group and the phenyl ring bonded to C1, which can be noticed looking at the coplanarity between these moieties. There is an angle of 9.3(2)° between the planes calculated through the atoms C20-N1-C21 and C14-C15-C15-C17-C18-C19 in this compound. At last, ring B is slightly distorted in all structures, with C1 carbon as the most deviated atom from the l.s. mean plane encompassing through the six ring atoms (Table 2).

In all structures, only non classical hydrogen bonds (CH…halogen and CH…O) and other weak contacts involving π-systems ($\pi\ldots\pi$, CH…π) are responsible for keeping the molecules together in the crystals. Compounds **6** and **7**, which are isostructural, are featured by alternation of centrosymmetry-related molecules into one-dimensional (1D)

chains running parallel to the [100] direction through C7-H7A (or B in **7**)…O4, $\pi_{(ring\ D)}\ldots\pi_{(ring\ D)}$, C12-H12A…Br (or Cl in **7**), and C8-H8B…O2 (Fig. 4).

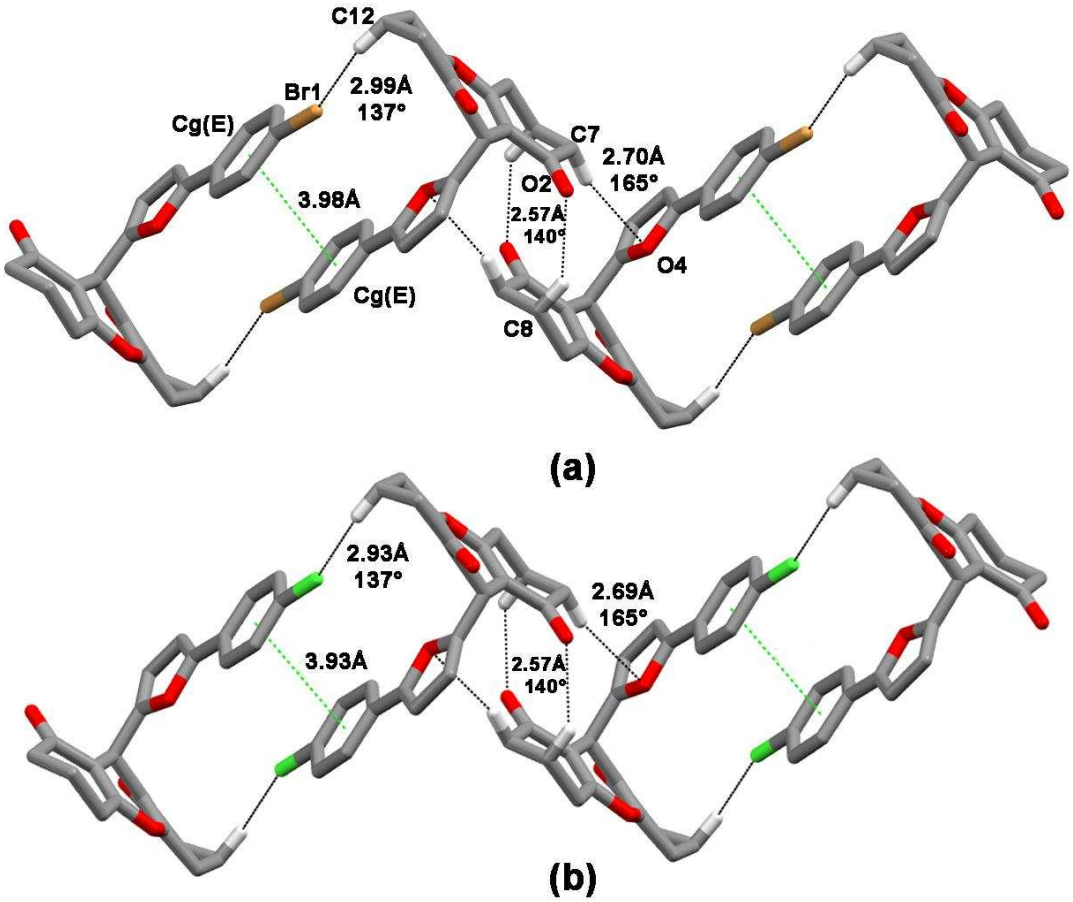

Fig. 4. Isostructural supramolecular chains in (a) **6** and (b) **7** growing parallel to the [100] direction. Cg(E) denotes the centroid calculated through ring E atoms. In this picture and hereinafter, only hydrogen atoms involved in the displayed contacts were not omitted. The shown measurements refer to the hydrogen…acceptor (i. e., oxygen, halogen or Cg) distance and the weak hydrogen bonding angle. When there, Cg…Cg distance is also exhibited.

Both carbons at the half-chair flaps are involved in the last two contacts, which can indicate a conformational adaptability from these moieties in order to favor geometrically the intermolecular interactions around the crystal environment. On contrary, these methylene groups do not participate significantly in the crystal packing of

compound **8**. This structure is marked by formation of a centrosymmetric dimer where the CH moiety at the *para*-position of phenyl ring is a non-classical hydrogen bonding donor to O2 (Fig. 5). This contact explains the phenyl ring twist observed in this structure. Such phenomenon, also found in compound **11**, is a consequence of a geometrical balance to form two CH…π contacts involving the π-system of phenyl ring E (Fig. 5).

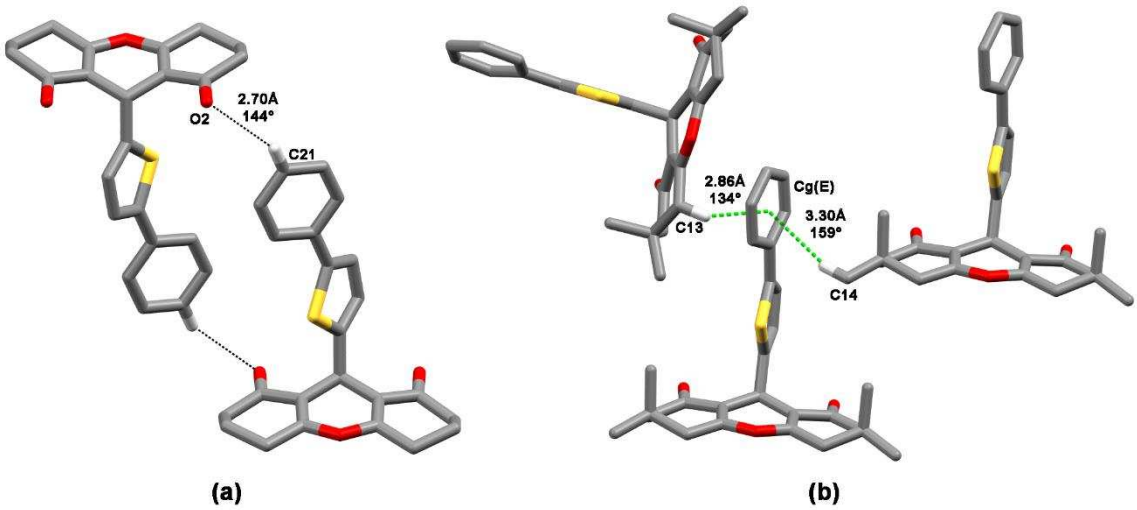

Fig. 5. The pattern of weak intermolecular contacts responsible for phenyl ring E twist in (a) **8** and (b) **11**.

Compounds **3**, **4** and **10** are isostructural as expected from their molecular similarities (differing only for the halogen at *para*-position of phenyl ring bonded to C1) (Fig. 6). Even though there are changes in the nonclassical hydrogen bonding geometry, they keep the same main supramolecular motifs as, for instance, an 1D chain assembled through CH…halogen contact having the methyl moiety at C12 as donor. This chain grows along the [001] direction and is made up of *c*-glide related molecules (Fig. 6).

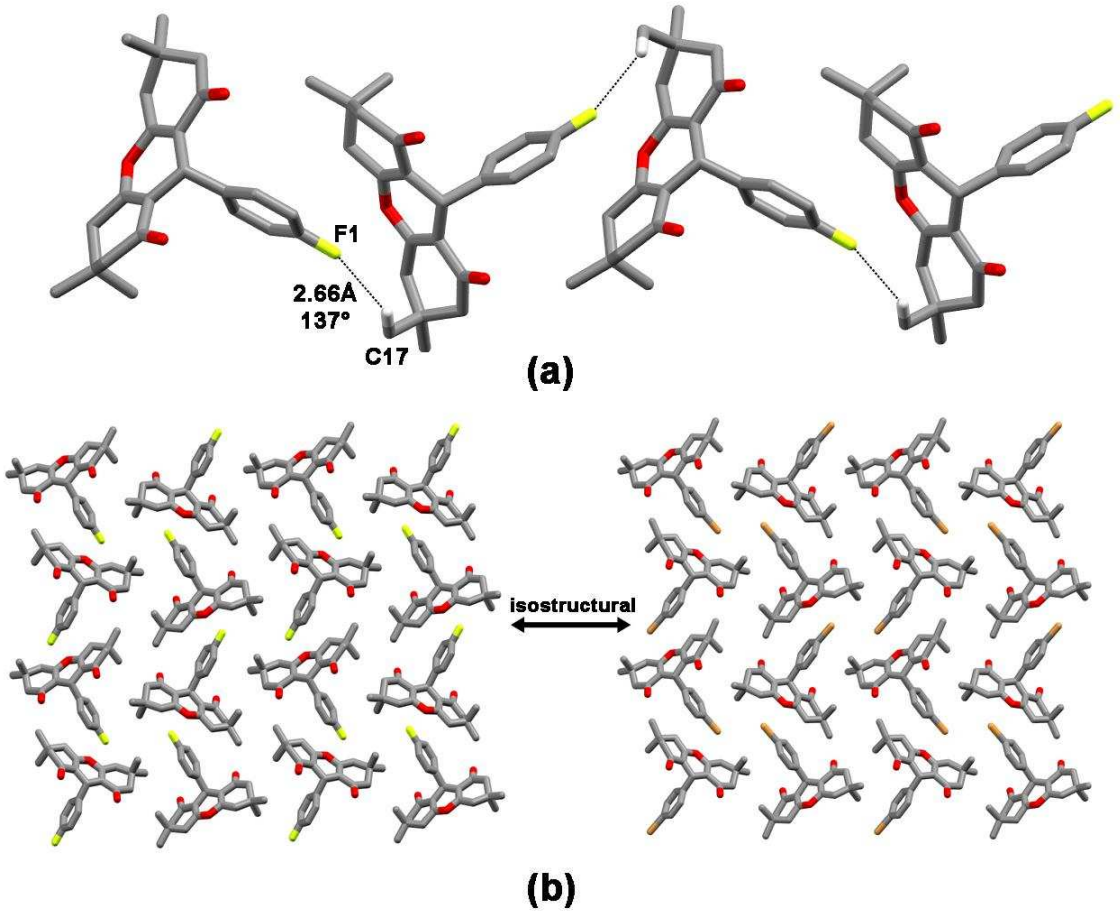

Fig. 6. (a) The supramolecular chain of **10** growing along the [001] direction. (b) Isostructural crystal packing of **10** (left) and of its bromine analog (right).

Crystal packing of **5** is stabilized by mean of CH…O and CH…π interactions, which give rise to chains running parallel to the [101] direction (Fig. 7).

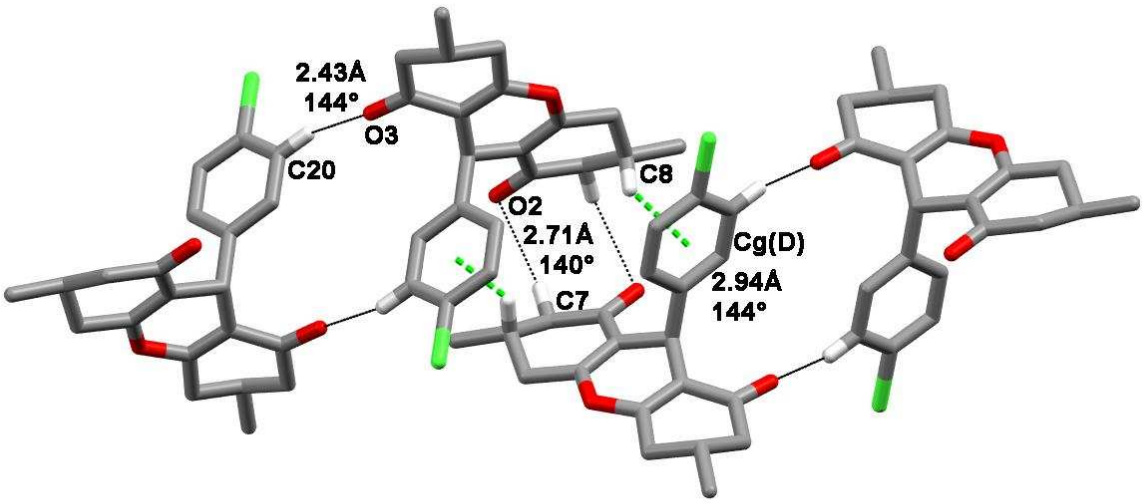

Fig. 7. Supramolecular chain running parallel to the [101] direction in compound **5**. Cg(D) denotes the centroid calculated through ring D atoms.

In the crystal structure of **9**, there is formation of a 1D chain along the [010] direction where both carbonyl oxygens are nonclassical hydrogen bonding acceptors from the methylene groups close to O1 (Fig. 8a). In this structure, there is also the face-to-face stacking of two centrosymmetry-related molecules through π…π interactions. This last interaction occurs between the π-system of phenyl moiety and the π-cloud around the nitrogen in the 4-*N*,*N*-dimethylamine revealing, therefore, a dual intramolecular and intermolecular conjugation phenomenon in this compound (Fig. 8b).

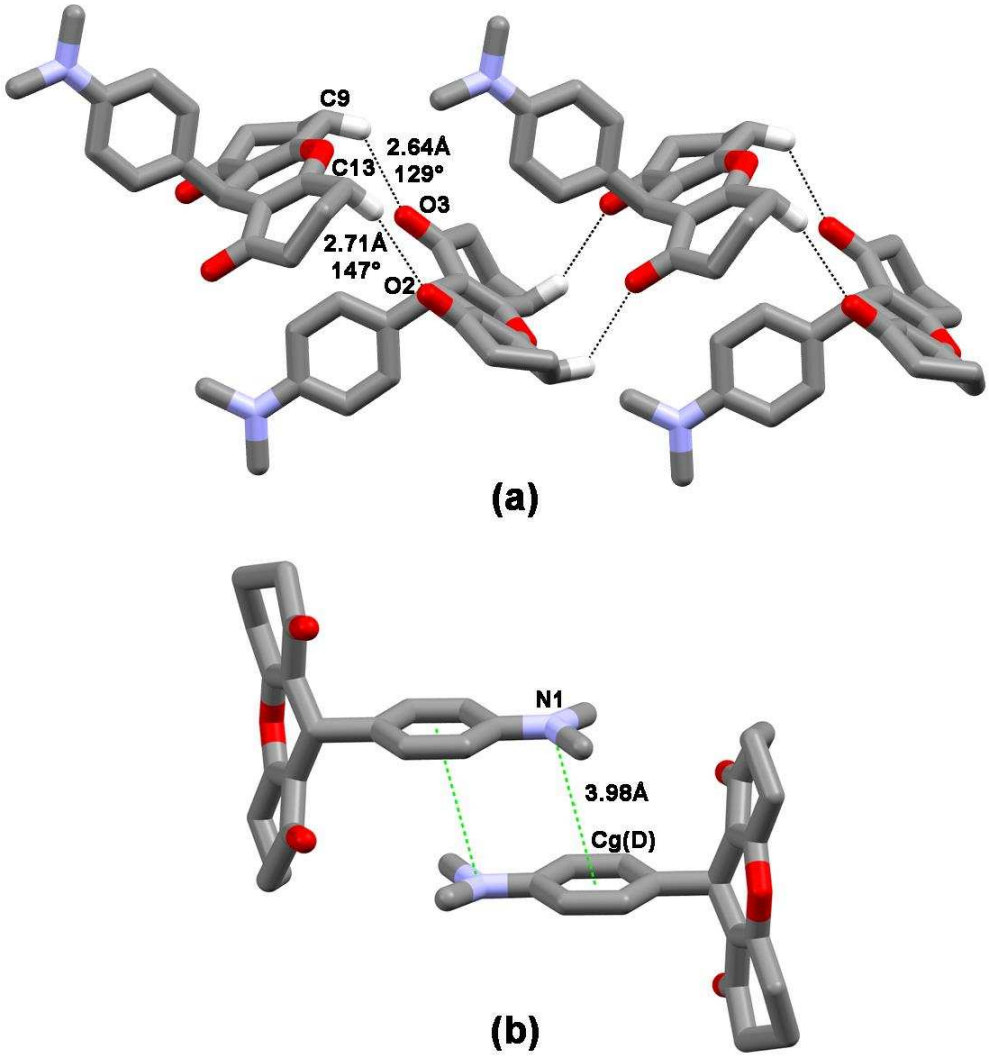

Fig. 8. (a) Supramolecular chain running parallel to the [010] direction in compound **5** and (b) the $\pi_{(N1)}\ldots\pi_{(ring\ D)}$ interactions stabilizing the centrosymmetric dimer in this structure. Cg(D) denotes the centroid calculated through ring D atoms.

3.3 Theoretical Aspects

The theoretical geometries of compounds **3-11** in gas phase and in water are depicted in Figure S1 (see supplementary material). In the crystal phase, molecular backbones have shown a preferential *syn* conformation for compounds **6**, **7**, **8** and **11** regarding to the O1-C1-CX-Y torsion (Y = O4 in **6** and **7** or S1 in **8** and **11**; Fig. 9).

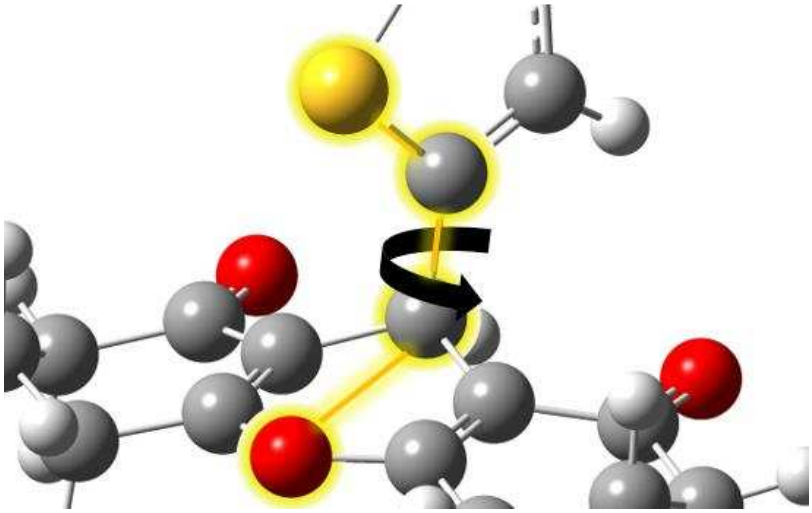

Fig 9. O1-C1-CX-Y dihedral angle in compounds **6**, **7**, **8** and **11** (Y = O4 in **6** and **7** or S1 in **8** and **11)**.

It is important to mention that *anti/syn* conformations, regarding the aforementioned dihedral, occur when the aromatic substituent is a furan or thiophene derivative (compounds **6**, **7**, **8** and **11**). When the aromatic portion is a phenyl group, there is no differentiation considering *anti*/*syn* conformations. With no significant geometry difference between gas phase and water, our calculations converged to similar conformations noticed in the section *3.2*. Applying a conformational screening around this dihedral angle, it was possible to investigate why there is predominance for the *syn* conformations. Thus, from the optimized structure obtained by theoretical calculations, the variation of energy due to torsion of O1-C1-CX-Y dihedral can be seen in Fig. 10. In this case, **D** point is the energy minima and is equivalent to the optimized structure. In addition, compounds **6** and **7** have identical R' and R'' groups (Fig. 1), which result in very similar energy profiles. Because of their similarity, it is possible to discuss them together. Figures S2 and S3 (see supplementary material) illustrate the conformers corresponding to points **A**, **B**, **C** and **D** for compounds **6** and **7** along with some information about important dihedrals and atomic distances. The energy maximum observed in the diagrams of compounds **6** and **7** (Fig. 10) is point **A**. Comparing the structures of conformers associated with points **A** and **B**, it is possible to recognize the

fact that red eclipsed oxygens is not the main feature responsible to the higher energy of point **A** conformer. Considering compound **6,** going from **A** to **B** the dihedral angle decreases from 33.41° to 11.59°. This results in increasing repulsion between these atoms. However, as can be seen in Fig. 10, the energy decreases from **A** to **B**. Moreover, the green-lighted dihedrals also decrease from 93.34° to 48.34° for **6** which results in eclipsing of the oxygen and hydrogen atoms. Furthermore, the decreasing of the aforementioned dihedrals implies in approximation of oxygen and carbon atoms in the conformer related to point **A**. In this conformer, the distance between them is 2.70 Å, whereas in point **B** conformer it grows to 3.05 Å. Points **C** and **D** are the ones where two oxygens are in *anti* and *syn* conformations, respectively. The energy difference between these two points is more than 2.5 kcal.mol^{-1}. The key to understand the higher stability of point **D** conformer is looking at the oxygen atom of the furan ring. In point **C** conformer, this oxygen is eclipsed by a hydrogen in a distance of 2.42 Å whereas in **D** the closest atom to this same oxygen is a carbon in a distance of 2.92 Å. By the same reason, it is also relevant to realize that point **C** conformer is higher in energy than **B**, although the distance between two oxygens being higher in the conformer related to the **C** point. Therefore, it is expected that compounds **6** and **7** adopt the *syn* conformation.

Figures S4 and S5 (see supplementary material) illustrate important aspects for the compounds **8** and **11** (Y = S1) that have differences in terms of R' and R'' groups (Fig. 1). As can be noticed in Fig. 10, the energy maximum for compound **11** (point **A**) is higher than 6 kcal mol^{-1}, while for compound **8** is below 4 kcal mol^{-1}. The superior energy of point **A** conformer of compound **11** in relation to **8** was ascribed to the repulsion among sulfur atom and methyl groups. In point **A** conformer of **8**, there are two carbons which are eclipsed. However, in compound **11** the sulfur atom is eclipsed by the carbon. Therefore, higher repulsion is expected for compound **11** regarding its point **A** conformer. However, the point **C** conformer of compound **8** has also the eclipse of sulfur and carbon

atoms, albeit with almost half of **A** point destabilization energy compared to the same point of **11**. The reason is the existence of methyl groups in **11** which increases the steric repulsion, while for compound **8** R´ and R" are hydrogens (Fig. 1). To be in line with this argumentation, an interesting effect happens considering the **11**-*syn* to **11**-*anti* interconversion (Figure S1). As the O1-C1-CX-S1 dihedrals changes, one methyl group goes down through the plane in order to relieve the repulsion between the other CH_3 and sulfur. This same effect does not occur in the **8**-*syn* to **8**-*anti* interconversion since R' and R'' are hydrogens (Fig. 1). In the *anti* and *syn* conformations (**B** and **D** points, respectively), it is possible to apply the same rationale used for compounds **6** and **7** to justify the preference for the *syn* conformation. In the case of compounds **8** and **11** the reason involves the distance of sulfur to the other atoms. Compounds **8** and **11** are destabilized by more than 2.0 $kcal.mol^{-1}$ considering point **B**. For **8**, the sulfur atom is close to an oxygen and a hydrogen by, respectively, 3.28 Å and 2.60 Å in point **B** conformer. In point **D** conformer, the closest sulfur distances to an oxygen and a carbon atoms are, respectively, 3.82 Å and 3.53 Å. Considering compound **11**, the respective distances are 3.31 Å and 2.79 Å for point **B** conformer and 3.77 Å and 3.55 Å for point **D** conformer. In both cases, in the *anti* conformer the repulsions are more severe than in the *syn* conformation. Thus, the *syn* conformer predominates for both compounds.

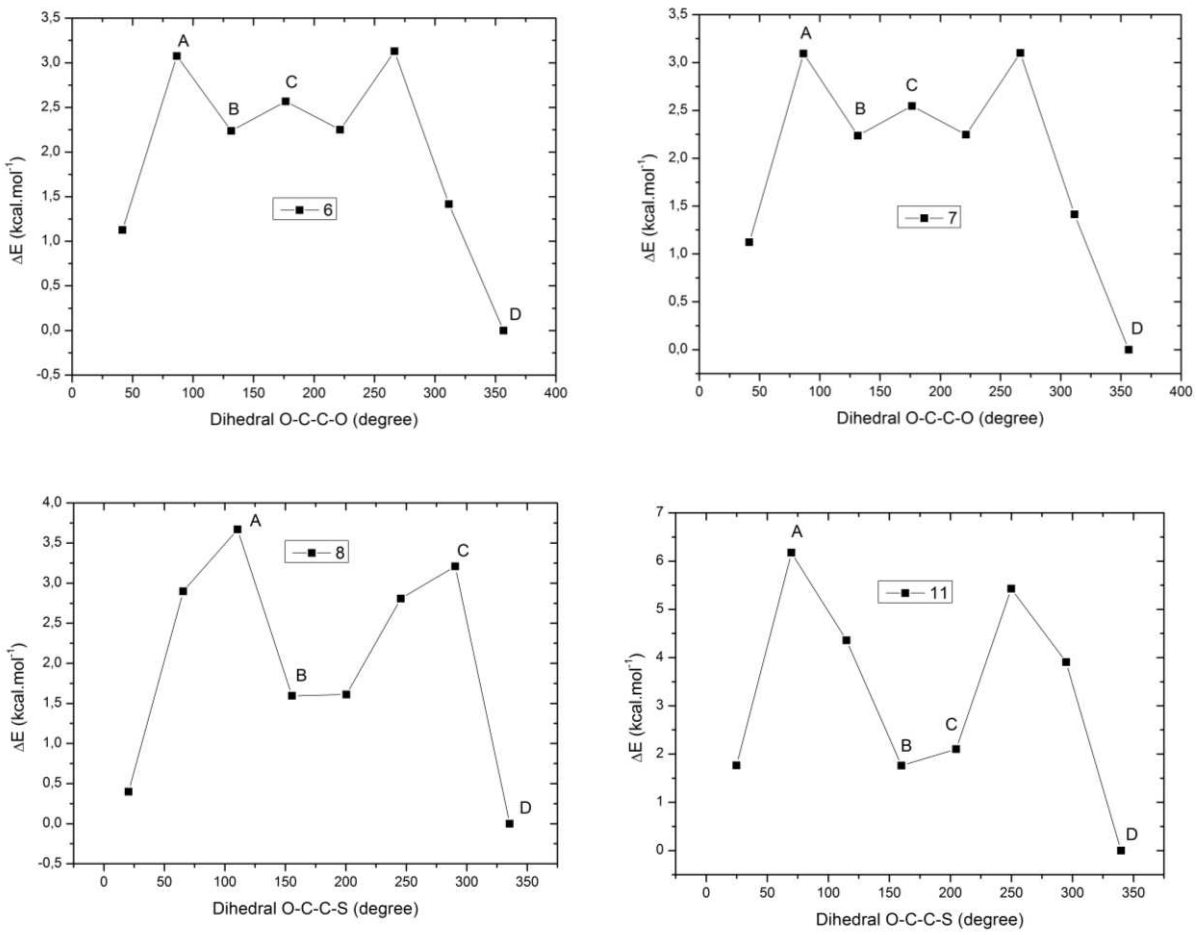

Fig 10. Potential energy curves from the conformational screening of compounds **6**, **7**, **8** and **11**.

Crystal structure analyses have also revealed two distinct conformational preferences for the cyclohex-2-enone moieties of compounds **3-11**. Compounds **3**, **4**, **9**, **10** and **12** have adopted always the *anti* conformation, while compounds **5**, **6**, **7**, **8** and **11** have adopted the *syn* conformation. The geometries of all conformations can be seen in Figure S1 (see supplementary material). Table 3 shows the energy barrier of a possible interconversion between *syn* and *anti* conformations following the equation (1).

$$\Delta E = E_{syn} - E_{anti} \quad (1)$$

Applying the equation (1) for compounds **3-11** energies from crystal geometries, the ΔE values for **3**, **9**, **10** and **12** should be positive due to the higher stability of *anti* conformers. However, our calculations in gas phase and water predicts that *syn* conformers are electronically more stable for all compounds ($\Delta E < 0$). In fact, for an

isolated or solvated molecule, these compounds might exist in a *syn* conformer which is not in agreement with the experimental data. This difference might be due to supramolecular contributions (see Fig. 11).

Table 3. *Syn-anti* interconversion electronic energy barrier (kcal.mol^{-1}) for the cyclohexenone moiety conformation in gas phase at 25 °C (Gp) and water at 85 °C, and in gas phase dimmers (Gp Dim) at 25° (see Fig. 11 for dimmers).

ΔE	**3**[i]	**5**	**6**	**7**	**8**	**9**	**10**	**11**	**12**
Gp	-0.68	-0.91	-0.47	-0.49	-0.44	-0.37	-0.71	-0.48	-0.61
Water	-0.65	-0.96	-0.56	-0.58	-0.53	-0.45	-0.69	-0.57	-0.56
Gp Dim	1.66	-	-	-1.98	-	-	-	-0.82	0.63

[i] Since crystal structure of both related compounds **3** and **4** had been determined previously, in this calculation we have selected only compound **3** to represent these halogenated xanthenodiones.

Fig. 11 shows the built dimmers of compounds **3**, **7**, **11** and **12** that were taken as models to understand the solid state data through the supramolecular model. These dimmers were built following the crystal coordinates. In order to obtain the hypothetic *syn/anti* conformers, the dimmers were optimized using molecular mechanics (UFF) with the aromatic groups frozen. The energy was calculated with a single-point at ωb97xD/6-311++** level. All aromatic groups have aromaticity and conjugated bonds and molecules with *syn*-orientation can potentially perform stacked interactions, such as π-π*-stacking and T-shaped, which have strong dispersive and charge transfer effects that can only be described by suitable quantum mechanics methods (JOSA et al., 2014a; RAMALHO et al., 2013) [27]. The interaction energy of each dimmer was obtained by the equation (2), where A and B are the monomers. Table 3 also shows the interconversion energy barrier between the *syn/anti* dimmers in gas phase (3).

$$\Delta E_{int} = E^{AB} - (E^{A} + E^{B}) \quad (2)$$

$$\Delta E = \Delta E_{int/syn} - \Delta E_{int/anti} \quad (3)$$

Even though it is not exactly identical to the solid state, the supramolecular approach with two monomers have already demonstrated to be in line with the experimental data. The ΔE for **3** and **12** present positive signal indicating that the *anti* conformation is indeed preferred. The calculation results for **7** and **11** have kept the preference for the *syn* conformations as the crystal data have shown, which is the most natural occurrence since the monomers adopt this same conformation. One interesting question is why did the conformational change happen in **3**, **4**, **9**, **10** and **12**?

Looking for the geometries of compound **7** dimmers (Figure 11), it is possible to see that parallel displaced π-π*-stacking are ruling the interaction between the monomers. Even just changing the hydrogens position between its *syn* and *anti* conformations, the energy barrier is -1.98 kcal.mol^{-1}, while ΔE between the monomers was just -0.09 kcal.mol^{-1} in gas phase. In this case, the dispersive interactions between Cl and H could be decisive to stabilize the supramolecule along with stacking interactions.

With a short conjugated chain and a large substituent as bromine, compound **3** cannot perform π-π*-stacking but angular T-shaped $\sigma_{C\text{-}H} \rightarrow \pi^*_{Ar}$ and dispersion interactions (JOSA et al., 2014b; SANTOS et al. 2014). In its *syn* conformation, the methyl group can make these interactions difficult, increasing the system steric repulsion. In addition, the methyl group oriented on the same side of the aromatic group in **3**-*anti* contributes to increasing the dispersion interactions with bromine. This fact can be supported comparing the **3** and **12** dimmers, whose ΔE values are 1.66 kcal.mol^{-1} and 0.63 kcal.mol^{-1}, respectively. The ΔE in gas phase between their monomers were almost the same, -0.68 kcal.mol^{-1} for **3** and -0.61 kcal.mol^{-1} for **12**, which means that somehow **3**-*anti* dimmer is more stabilized than **12**-*anti* dimmer.

The crystal data and the theoretical calculations for compound **11** have also revealed possible T-shaped $\sigma_{C\text{-}H} \rightarrow \pi^*_{Ar}$ interactions in the dimmers of **11**. However, the dispersion can also be important. ΔE for the monomers is -0.48 kcal.mol^{-1} and -0.82

kcal.mol^{-1} for the dimmer. This gain in the stabilization energy can be correlated to the C-H and methyl group dispersive interactions, which are completely erased in **11**-*anti* dimmer. In this prospect, our findings highlight the importance of the intermolecular interactions in this conformational preference. Indeed, intermolecular interactions are crucial for the solid state matter (PEREIRA et al., 2011) and it can show distinct behavior than the solvated molecule if non-classical effects were taken into account, which can be easily understood with the supramolecular approach. It worth emphasizing that all these interactions in the dimmer state can be intensified in solid state by the increasing of monomers present in the supramolecule.

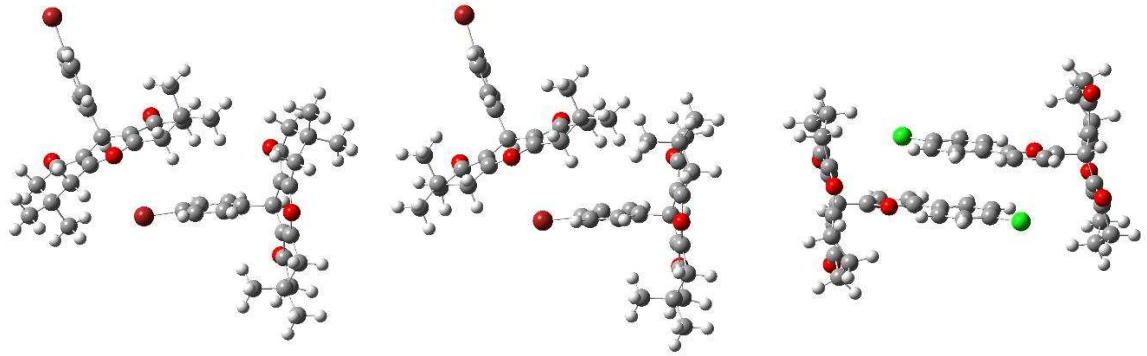

3-*anti* **3-*syn*** **7-*syn***

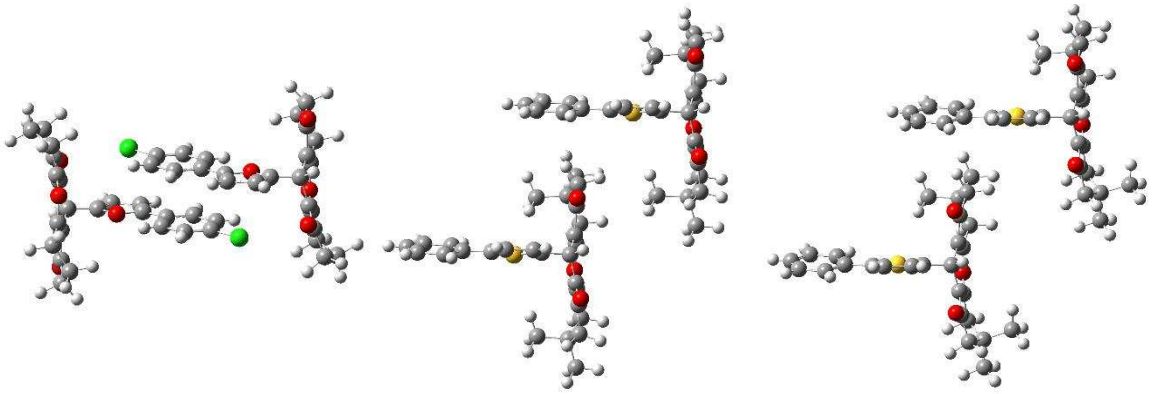

7-*anti* **11-*syn*** **11-*anti***

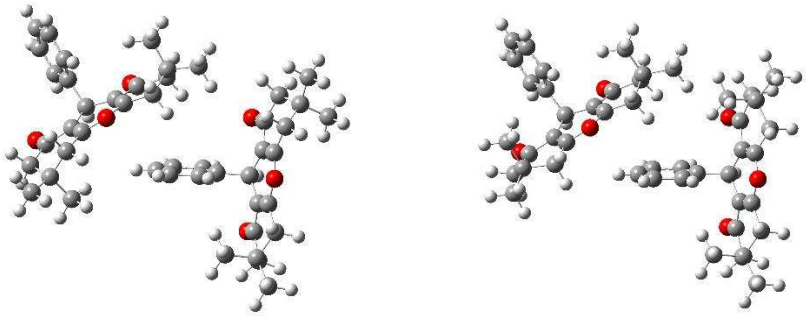

12-*anti* **12-*syn***

Fig 11. Calculated gas phase geometries of the dimmers with either **s***yn* or *anti* cyclohex-2-enone rings conformation.

4. Conclusions

We have here reported the crystal structure of seven related compounds belonging to the xanthenodione class, which have been rarely investigated from a structural point of view. We have interpreted the changes in their conformation based on the energetic profiles of the single molecules and dimers, highlighting the prevalence of intramolecular forces in the *anti* conformation of the C1 substituent, common to all compounds. Likewise, intermolecular forces drive the *anti* conformation of the cyclohex-2-enone half-chair moieties. Based on this study, we hope that similar correlated experimental–theoretical investigations can be performed with other xanthenodione compounds in order to find other examples and exceptions of these supramolecular and conformational features of this class compound, which can impact on their biological and physicochemical properties.

5. Acknowledgments

We are grateful to Fundação de Amparo à Pesquisa do Estado de Minas Gerais (FAPEMIG), Coordenação de Aperfeiçoamento de Pessoal de Nível Superior (CAPES) and Conselho Nacional de Desenvolvimento Científico e Tecnológico (CNPq) for financial support.

References

Baltork, I.M., Khosropur, A.R., Hojati, S.F., 2007. $ZrOCl_2/8H_2O$ as an environmentally friendly and recyclable catalyst for the chemoselective synthesis of 2-aryloxazolines and bis-oxazolines under thermal conditions and microwave irradiation. Catal. Commun. 8, 200-204.

Banerjee, A., Mukherjee, A.K., 1981. Chemical aspects of santalin as a histological stain. Stain Technol. 56, 83-85.

Bardajee, G.R., 2013. C. R. ZrOCl2.8H2O in water: An efficient catalyst for rapid one-pot synthesis of pyridopyrazines, pyrazines and 2,3-disubstituted quinoxalines. Chimie. 16, 872-877.

Bigdeli, M.A., Mahdavinia, G.H., Amani, V., 2007. 9-(4-Bromophenyl)-3,3,6,6-tetramethyl-3,4,6,7-tetrahydro-2H-xanthene-1,8(5H,9H)-dione. Acta. Crystallogr. Sect. E63, o3493.

Callan, J.F., De Silva, P., Magri, D.C., 2005. Luminescent sensors and switches in the early 21st century. Tetrahedron. 61, 8551-8588.

Dua, R., Shrivastava, S., Sonwane, S.K., Shrivastava, S.K., 2011. Pharmacological Significance of Synthetic Heterocycles Scaffold: A Review. Advan. Biol. Res. 5, 120-144.

Frisch, M. J.; Trucks, G. W.; Schlegel, H. B.; Scuseria, G. E.; Robb, M. A.; Cheeseman, J. R.; Scalmani, G.; Barone, V.; Mennucci, B.; Petersson, G. A.; Nakatsuji, H.; Caricato, M.; Li, X.; Hratchian, H. P.; Izmaylov, A. F.; Bloino, J.; Zheng, G.; Sonnenberg, J. L.; Hada, M.; Ehara, M.; Toyota, K.; Fukuda, R.; Hasegawa, J.; Ishida, M.; Nakajima, T.; Honda, Y.; Kitao, O.; Nakai, H.; Vreven, T.; Montgomery, J. A., Jr.; Peralta, J. E.; Ogliaro, F.; Bearpark, M.; Heyd, J. J.; Brothers, E.; Kudin, K. N.; Staroverov, V. N.; Kobayashi, R.; Normand, J.; Raghavachari, K.; Rendell, A.; Burant, J. C.; Iyengar, S. S.; Tomasi, J.; Cossi, M.; Rega, N.; Millam, J. M.; Klene, M.; Knox, J. E.; Cross, J. B.; Bakken, V.; Adamo, C.; Jaramillo, J.; Gomperts, R.; Stratmann, R. E.; Yazyev, O.; Austin, A. J.; Cammi, R.; Pomelli, C.; Ochterski, J. W.; Martin, R. L.; Morokuma, K.; Zakrzewski, V. G.; Voth, G. A.; Salvador, P.; Dannenberg, J. J.; Dapprich, S.; Daniels, A. D.; Farkas, Ö.; Foresman, J. B.; Ortiz, J. V.; Cioslowski, J.; Fox, D. J. Gaussian, Inc., Wallingford CT, 2009.

Hafez, E.A.A., Elnagdi, M.H., Elagamey, A.G.A., El-Taweel, F.M.A.A., 1987. Cycloaddition Reaction of 1,2,4-Trazolium Phenacylides with Cinnamic Esters. Heterocycl. 26: 903-907.

Ilangovan, A., Malayappasamy, S., Muralidharan, S., Maruthamuthu, S., 2011. A highly efficient green synthesis of 1, 8-dioxooctahydroxanthenes. Chem. Cent. J. 5,81.

Ion, R.M., Frackowiak, D., Planner, A., Wiktorowicz, K., 1998. The incorporation of various porphyrins into blood cells measured *via* flow cytometry, absorption and emission spectroscopy. Acta. Biochim. Pol. 45, 833-845.

Josa, D., dos Santos, L.A., Gonzalez-Veloso, I., Rodriguez-Otero, J., Cabaleiro-Lago, E.M., Ramalho, T.C., 2014b. Ring-annelated corannulenes as fullerene receptors. A DFT-D study. RSC Adv. 4, 29826–29833.

Josa, D., Rodriguez-Otero, J., Cabaleiro-lago, E.M., Santos, L.A., Ramalho, T.C., 2014a. Substituted Corannulenes and Sumanenes as Fullerene Receptors: A Dispersion-Corrected Density Funtional Theory Study. J. Phys. Chem. A. 118, 9521–9528.

Kumar, G.S.S., Prabhu, A.A.M., Seethalashmi, P..G, Bhuvanesh, N., Kumaresan, S., 2014. Self-catalyzed syntheses, structural characterization, DPPH radical scavenging-, cytotoxicity-, and DFT studies of phenoxyaliphatic acids of 1,8-dioxo-octahydroxanthene derivatives. J. Mol. Struct. 1059, 51-60.

Lamberth, C., Dinges, J. (Eds.), 2012a. Bioactive heterocyclic compound classes: pharmaceuticals; Wiley-VCH Verlag & Co.: Weinheim, Germany.

Lamberth, C., Dinges, J. (Eds.), 2012b. Bioactive heterocyclic compound classes: agrochemicals; Wiley-VCH Verlag & Co.: Weinheim, Germany.

Macrae, C.F., Bruno, I.J., Chisholm, J.A., Edgington, P.R., Mccabe, P., Pidock, E., Monge, L.R., Taylor, R., van de Streek, J., Wood, P.A., 2008. Mercury CSD 2.0 – new features for the visualization and investigation of crystal structures. J. Appl. Crystallogr. 41, 466-470.

Mosaddegh, E., Islami, M.R., Hassankhani, A., 2012. $ZrOCl_2.8H_2O$ as an efficient and recyclable catalyst for the clean synthesis of xanthenedione derivatives under solvent-free conditions. Arab. J. Chem. 5, 77-80.

Mulakayala, N., Murthy, P.V.N.S., Rambabu, D., Aeluri, M., Adepu, R., Krishna, G.R., Reddy, C.M., Prasad, K.R.S., Chaitanya, M., Kumar, C.S., Rao, M.V.B., Pal, M., 2012. Catalysis by molecular iodine: A rapid synthesis of 1,8-dioxo-octahydroxanthenes and their evaluation as potential anticancer agents. Bioorg. Med. Chem. Lett. 22, 2186-2191.

Nisar, M., Ali, I., Shah, M.R., Badshah, A., Qayum, M., Khan, H., Khan, I., Ali, S., 2013. Amberlite IR-120H as a recyclable catalyst for the synthesis of 1,8-dioxo-octahydroxanthene analogs and their evaluation as potential leishmanicidal agents. RSC. Adv. 3, 21753-21758.

Omolo, J.J., Johnson, M.M., Vuuren, S.F.V., de Koning, C.B., 2011. The synthesis of xanthones, xanthenediones, and spirobenzofurans: Their antibacterial and antifungal activity. Bioorg. Med. Chem. Lett. 21, 7085-7088.

Pereira, M.C., Garcia, E.M., da Silva, A.C., Lorençon, E., Ardisson, J.D., Murad, E., Fabris, J.D., Matencio, T., Ramalho, T.C., Rocha, M.V.J., 2011. Nanostructured d-FeOOH: A novel photocatalyst for water splitting. J. Mater. Chem. 21, 10280–10282.

Poupelin, J.P., Saint-Ruf, G., Foussard-Blanpin, O., Narcisse, G., Uchida-Ernouf, G., Lacroix, R., 1978. Synthesis and ati-inflammatory properties of bis (2-hydroxy-1-naphthyl) methane derivatives. Eur. J. Med. Chem. 13, 67-71.

Quin, L.D., Tyrell JA., 2010. Fundamentals of heterocyclic chemistry: Importance in Nature and in the Synthesis of Pharmaceuticals; John Wiley & Sons: Hoboken, New Jersey.

Ramalho, T.C., Santos, L.A., da Cunha, E.F.J., 2013. Thermodynamic framework of hydrophobic/electrostatic interactions. Biomol. Struct. Dyn. 31, 995–1000.

Reddy, B.P., Vijayakumar, V., Narasimhamurthy, T., Suresh, J., Lakshman, P.L.N., 2009. 3,3,6,6-Tetramethyl-9-phenyl-3,4,5,6- tetrahydro-9H-xanthene-1,8(2H,7H)- dione. Acta. Crystallogr. Sect. E65, o916.

SADABS, APEX2 and SAINT, 2009. Bruker AXS Inc. Madison, Wisconsin, USA.

Sangshetti, J.N., Kokare, N.D., Kotharkar, S.A., Shinde, D.B., 2008. $ZrOCl_2.8H_2O$ catalyzed one-pot synthesis of 2,4,5-triaryl-1H-imidazoles and substituted 1,4-di(4,5-diphenylimidazol-yl)benzene. Chin. Chem. Lett. 19, 762-766.

Santos, L.A., da Cunha, E.F.F., Freitas, M.P., Ramalho, T.C., 2014. Hydrophobic Noncovalent Interactions of Inosine-Phenylalanine: A Theoretical Model for Investigating the Molecular Recognition of Nucleobases. J. Phys. Chem. A 118, 5808–5017.

Sheldrick, G.M., 2008. A short history of SHELX. Acta. Crystallogr. Sect. A. 64, 112-122.

Tu, S., Zhou, J., Lu, Z., Deng, X., Shi, D., Wang, S., 2002. Condensation of aromatic aldehydes with 5,5-dimethyl 1,3-cyclohexanedione without catalyst. Synth. Commun. 32, 3063-3067.

Wang, H., Lu, L., Zhu, S., Li, Y., Cai, W., 2006. The phototoxicity of xanthene derivatives against *Escherichia coli*, *Staphylococcus aureus* and *Saccharomyces cerevisiae*. Curr. Microbiol. 52, 1-5.

CAPÍTULO IV

ARTIGO 2

STRUCTURAL ANALYSIS OF TWO 2,2'-ARYLMETHYLENE *BIS* (3-HYDROXY-5,5-DIMETHYL-2-CYCLOHEXENE-1-ONE) AND THEORETICAL INVESTIGATION OF THE REACTION INVOLVED IN THEIR PREPARATION

Milene Lopes da Silva[a] · Lucas de Azevedo Santos[b] · Róbson Ricardo Teixeira[a*] · Felipe Terra Martins[b] · Teodorico Castro Ramalho[f]

[a]Chemistry Department, Universidade Federal de Viçosa, Viçosa, Brazil

[b]*Departament of Chemistry, Federal University of Lavras, Lavras, Brazil*

[c]*Chemistry Institute, Federal University of Goiás, Goiânia, Brazil*

[*]Corresponding author. e-mail: robsonr.teixeira@ufv.br

Abstract

The 2,2'-((5-(4-bromophenyl)furan-2-yl)methylene) *bis* (5,5-dimethylcyclohexane-1,3-dione) (**3**) and 2,2'-((5-(4-chlorophenyl)furan-2-yl)methylene) *bis* (5,5-dimethylcyclohexane-1,3-dione) (**4**) were prepared in, respectively, 63% and 59% yield, *via* $ZrOCl_2 \cdot 8H_2O$ catalyzed condensation reactions between dimedone and appropriate aldehydes. Their structures were investigated by IR, NMR, and X-ray spectroscopy techniques. The asymmetric unit of tetra ketone **3** is composed of just one molecule, while two almost identical crystallographically independent molecules of compound **4** are present there. Compound **3** is conformationally similar to both molecules of **4**. The diketone rings assume a half-chair conformation with the flaps oriented towards the same side of the substituent at C1. Each diketone ring is featured by an electronic delocalization path encompassed through the keto-enol moiety. All bond lengths inside this conjugated system are intermediate between those of pure double and single bonds. Furthermore, the furan plane of the substituent at C1 is almost parallel to the bond axes bridging the diketone rings as a consequence of steric hindrance effects between the heterocycle moiety and two hydrogen bonded oxygens. The enol forms of compounds **3** and **4** were noticed via IR and NMR spectroscopies. Furthermore, thermodynamics parameters were calculated in order to interpret the experimental results. In this line, theoretical findings reveal that electronic and solvent effects play an important role in the chemical reaction.

Keywords: tetra ketone, 2,2'-aryl methylene *bis* (3-hydroxy-5,5-dimethyl-2-cyclohexene-1-one), X-ray analysis, DFT calculations, zirconium, keto-enol tautomerism.

1. Introduction

The tetra ketones or 2,2'-aryl methylene *bis* (3-hydroxy-5,5-dimethyl-2-cyclohexene-1-one) **(I)** are important intermediates that can be used as versatile precursors in the synthesis of tricyclic heterocycles such as xanthenodiones **(II)**, acridindiones **(III)** [1], benzopyrans **(IV)** and thioxanthenes **(V)** [2] (**Scheme 1**). All of these heterocycles exhibit important biological activities. In addition, tetra ketones are known for their antioxidant properties [3] and the strong potential for repairing inflammation and asthma [4]. These compounds also have significant lipoxygenases [3,5], tyrosinase [6,7] and protein kinases inhibitory activity [8].

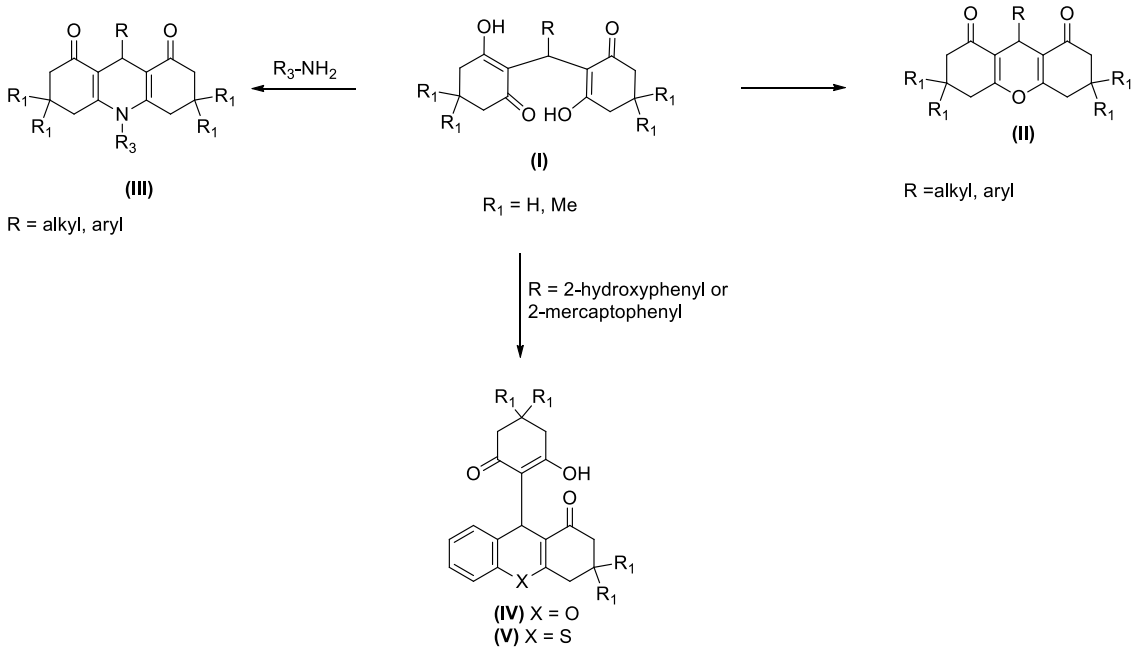

Scheme 1. The general structure of tetra ketones (**I**) and derivatives (**II**)-(**V**).

In general, the tetra ketones can be prepared via Knoevenagel condensation and Michael additions of aldehydes with cyclic 1,3-diketones, with or without the use of catalysts. Because of their synthetic utility and biological activities, various synthetic methodologies have been developed for the preparation of this class of compounds. However, many of these methods utilize toxic solvents and high catalyst loading, present long reaction times, require high temperatures, afford tetra ketones in low yields, and involve laborious workup procedures [9]. In this paper, we describe an alternative

methodology for preparation of tetra ketones via $ZrOCl_2 \cdot 8H_2O$ catalyzed reactions between dimedone and aromatic aldehydes. We also described the results of X-ray, NMR and IR investigations of the synthesized tetra ketones. Theoretical calculations concerning these compounds and the reactions involving them are also presented.

2. Experimental

2.1 Generalities

All reagents were purchased from commercial sources (Sigma-Aldrich - St. Louis, MO, US - and Vetec - Rio de Janeiro, Brazil) and were employed as received. The ^{1}H and ^{13}C NMR spectra were recorded on a Varian Mercury 300 instrument (300 MHz and 75 MHz respectively), using deuterated chloroform as a solvent. Hydrogen nuclear magnetic resonance (NMR) data are presented as follows: chemical shift (δ) in ppm, the number of hydrogen atoms, multiplicity, *J* values in Hertz (Hz). Multiplicities are shown as the following abbreviations: s (singlet), d (doublet), m (multiplet). Infrared spectra (IR) were obtained employing a Varian 660-IR equipment with accessory GladiATR. The exact mass of compounds was determined in micrOTOF QII® (Bruker Daltonis, Germany) equipped with a microESI (Electrospray) ionization source. The compounds were dissolved in acetonitrile (100% LCMS) and acidified with 0.1% formic acid. The mass was acquired in positive mode scanning from 50 to 1000 Da. Melting points were determined using MQAPF-301 melting point apparatus (Microquimica, Rio de Janeiro, Brazil).

2.2. Synthesis

Synthesis of 2,2'-((5-(4-bromophenyl)furan-2-yl)methylene)bis(5,5-dimethylcyclohexane-1,3-dione) ***(3)***

In a typical procedure, a round-bottomed flask (25 mL) was charged with 2 mmol of 5,5-dimethylcyclohexan-1,3-dione (295 mg, 2.00 mmol), 5-(4-bromophenyl)furan-2-carbaldehyde (258 mg, 1.00 mmol) and $ZrOCl_2 \cdot 8H_2O$ (12 mg, 2 mol%). The mixture was stirred at 85 °C and after ten minutes of reaction, 100 μL of distilled water were added. The progress of the reaction was monitored by TLC analysis and it took 2 h for its completion. Then, the mixture was cooled to room temperature. Thereafter, 50 ml of dichloromethane were added to the flask and the mixture was maintained under stirring. The catalyst, which is insoluble in dichloromethane, was separated by filtration. After that, 50 mL of ethanol was added to the filtrate and the system was kept undisturbed for the crystallization process. This procedure afforded compound **3** as yellow solid in 63% yield (321 mg, 0.630 mmol). Crystals suitable for X-ray diffraction studies were obtained from the above-mentioned crystallization procedure. The obtained crystals were thoroughly washed with cold ethanol and dried. The structure of **3** is supported by the following data.

Yellow solid. Mp 159 - 161 ºC. IR (ATR) ν_{max}/cm^{-1}: 2962, 2870, 1588, 1538, 1370, 1165, 1147 cm^{-1}. ^1H NMR (300 MHz, $CDCl_3$) δ: 12.24 (1H, s, O<u>H</u>), 7.42 (2H, d, J = 8.2 Hz), 7.36 (2H, d, J = 8.2 Hz), 6.55 (1H, s), 6.02 (1H, s), 5.46 (1H, s), 2.39 (4H, s), 2.33 (4H, s), 1.22 (6H, s), 1.11 (6H, s). ^{13}C NMR (75 MHz, $CDCl_3$) δ: 189.7, 189.4, 151.9, 151.4, 131.6, 129.9, 124.8, 120.4, 114.0, 108.8, 106.4, 46.9, 46.2, 31.3, 29.9, 29.3, 26.4. HREIMS *m/z* ($M+H^+$): Calculated for $C_{27}H_{30}BrO_5$, 513.1277. Found: 513.1308.

Compound **4** was obtained in 59% yield using a similar procedure to that described for the preparation of **3**. The reaction of **4** took 2h and 15 minutes for its completion. The structure of **4** is supported by the following data.

2,2'-((5-(4-chlorophenyl)furan-2-yl)methylene)bis(5,5-dimethylcyclohexane-1,3-dione) ***(4)***

Yellow solid. Mp = 164 - 166 °C. IR (ATR) ν_{max}/cm^{-1}: 2953, 2871, 1580, 1534, 1372, 1167, 1150 cm^{-1}. ^{1}H NMR (300 MHz, $CDCl_3$) δ: 12.24 (1H, s, O<u>H</u>), 7.42 (2H, d, J = 8.2 Hz), 7.27 (2H, d, J = 8.2 Hz), 6.55 (1H, s), 6.02 (1H, s), 5.46 (1H, s), 2.39 (4H, s), 2.33 (4H, s), 1.22 (6H, s), 1.11 (6H, s). ^{13}C NMR (75 MHz, $CDCl_3$) δ: 189.7, 189.4, 151.9, 151.4, 132.3, 129.5, 128.7, 124.5, 114.0, 108.8, 106.4, 46.9, 46.2, 31.3, 29.9, 29.3, 26.4. HREIMS *m/z* ($M+H^+$): Calculated for $C_{27}H_{30}ClO_5$, 469.1782. Found: 469.1806.

2.3. X-ray diffraction analysis

Prism-shaped single crystals of tetra ketones **3** and **4** were selected and mounted, at room temperature, on a κ-goniostat (Bruker-AXS Kappa Duo diffractometer) and exposed to X-ray beam (Mo Kα, λ = 0.71073 Å). X-Ray diffraction intensity data were recorded using an APEX II CCD detector. Data collection strategy was set with φ scans and ω scans with κ offsets using the APEX2 software [10]. Other crystallographic software were used as follows: SAINT [10] (indexing, integration and scaling of raw data), SHELXL-97 [11] (structure solving using Direct Methods), SHELXL-97 [11] (structure refinement by full-matrix least squares method on F^2) and MERCURY [12] (structure analysis and graphical representations). All non-hydrogen atoms of asymmetric units were directly identified from the electronic density Fourier synthesis. Free anisotropic and fixed isotropic atomic displacement parameters were set for non-hydrogen and hydrogen atoms, respectively (U_{iso}(H) = 1.2U_{iso}(C) or 1.5U_{iso}($C_{\text{-methyl}}$ or O). All hydrogens were positioned at constrained sites according to stereochemical

assumptions for bond lengths and angles and they were not refined. Instead, they followed a riding model. **Table 1** (vide infra) presents a summary of collect data and refinement outputs for tetra ketones **3** and **4**.

2.3. Computational details

The geometries of all reactant (**1** and **2**) and product (**3** and **4**) structures were optimized at ωb97xD/6-311++** level of theory by Gaussian 09 software [13]. The frequency calculations were carried out at the same level in order to obtain the thermodynamic parameters of the reactions. The calculations were performed in the gas phase and at 25 °C as well as in water using the PCM solvation model with a temperature range from 85 °C to 100 °C. From this information, the reaction energies to obtain derivatives **3´** and **4´** were calculated. To quantify the role of the hydrogen bonds to stabilize compounds **3** and **4**, a conformational scan was carried out around the H-O2-C6-C5 and H-O3-C3-C2 dihedrals (see **Fig. 8**). Furthermore, the non-classical interactions were computed via NBO 6.0 software [14].

In order to get further information on the experimental data, theoretical vibrational and NMR spectra were obtained. The NMR analysis was driven by GIAO method with chloroform in the PCM solvation model. Both spectra were obtained at 25 °C by the same previously mentioned theory level.

3. Results and Discussion

The preparation of tetra ketones **3** and **4** was carried out as outlined in **Scheme 2**.

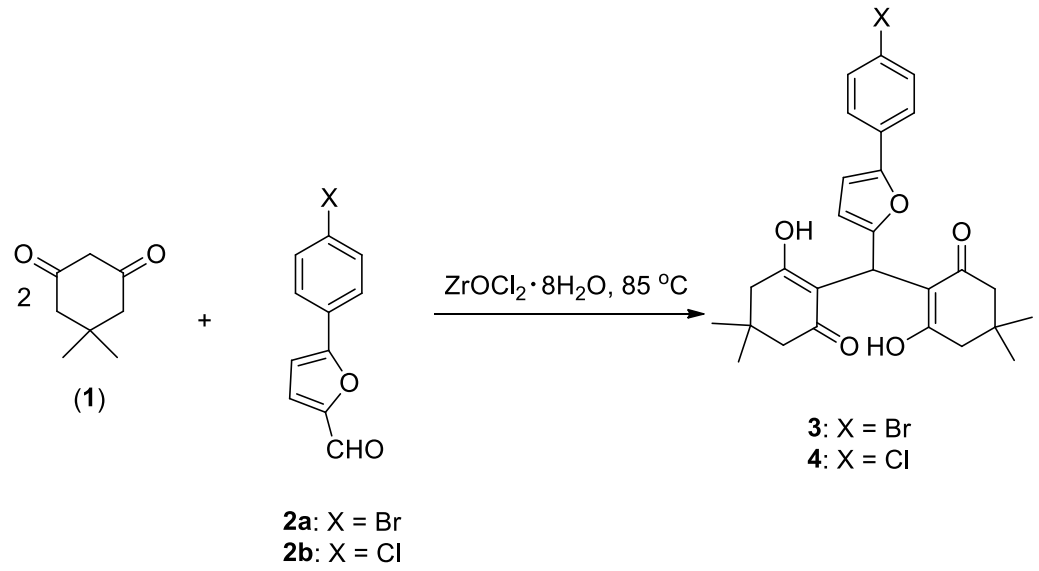

Scheme 2. Preparation of tetra ketones **3** and **4**.

Thus, the reaction of dimedone (**1**) with aromatic aldehydes **2a** and **2b**, catalyzed by $ZrOCl_2 \cdot 8H_2O$, afforded compounds **3** and **4** in, respectively, 63% and 59% yields. This is the first time that the preparation of tetra ketones catalyzed by the aforementioned catalyst is described. Overall, the reactions took about 2h for their completion. It is worth mentioning that the reactions involved in the preparation of **3** and **4** were carried out in the absence of toxic solvents and in an open reaction flask. In addition, the compounds were obtained in high purity after simple work up procedure followed by crystallization. The structures of compounds **3** and **4** were confirmed by IR, NMR and X-ray spectroscopy analyses as well as mass spectrometry.

Crystal structures of compounds **3** and **4** have been solved, respectively, in the centrosymmetric space groups $P2_1/n$ (monoclinic) and P-1 (triclinic). A summary of collected data and refinement outputs for tetra ketones **3** and **4** are presented in **Table 1**.

Table 1.
Crystal data and refinement statistics for tetra ketones elucidated in this study

Compound		**3**	**4**
Molecular formula		$C_{27}H_{29}BrO_5$	$C_{27}H_{29}ClO_5$
fw (g/mol)		513.40	468.95
cryst syst		monoclinic	triclinic
space group		$P2_1/n$	P-1
Z / Z'		4 / 1	4 / 2
T (K)		296(2)	296(2)
unit cell dimensions	a (Å)	12.0552(8)	12.6930(9)
	b (Å)	14.7163(10)	12.7765(7)
	c (Å)	13.9039(10)	15.3915(10)
	α (°)	90	79.537(3)
	β (°)	90.178(2)	87.766(3)
	γ (°)	90	87.994(3)
V (Å^3)		2466.7(3)	2451.7(3)
calculated density (Mg/m^3)		1.383	1.270
absorp. coefficient μ (mm^{-1})		1.701	0.191
θ range for data collection (°)		2.02 – 26.38	1.61 – 25.48
index ranges	h	-13 to 15	-14 to 13
	k	-12 to 18	-15 to 15
	l	-9 to 17	-17 to 18
data collected		7493	18311
unique reflections		4468	8255
observed reflections		2469	4428
symmetry factor (R_{int})		0.0232	0.0414
completeness to $\theta = 25°$ (%)		97.5	98.2
F (000)		1064	992
parameters refined		304	595
goodness-of-fit on F^2		1.032	1.008
final *R1* factor for $I > 2\sigma(I)$		0.0484	0.0648
wR2 factor for all data		0.1359	0.2660
largest diff. peak / hole (e/Å^3)		0.363/-0.622	0.429/-0.488
CCDC deposit number		1476904	1476905

In **Fig. 1**, non-hydrogen atoms are shown with their 50% probability ellipsoids and arbitrary labeling scheme. Labeling of rings is also depicted in this picture. The asymmetric unit of tetra ketone **3** is composed of just one molecule, while two almost identical crystallographically independent molecules are present in the asymmetric unit

of tetra ketone **4**. The conformational similarity between them can be quantitatively described by the low root mean square (RMS) deviation (0.105 Å) of their non-hydrogen atoms. In addition, compound **3** is also conformationally similar to both crystallographic molecules of **4**.

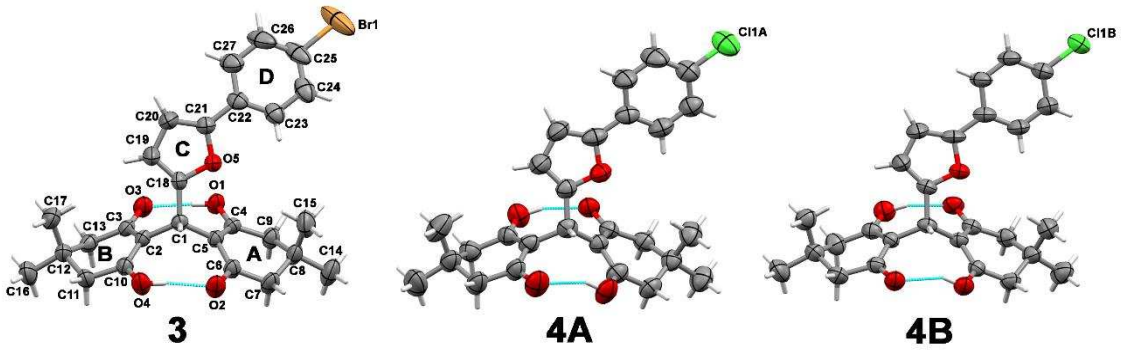

Fig. 1. 50% ellipsoid drawing of the non-hydrogen atoms in the asymmetric unit of the two tetra ketones elucidated in this study. For drawing clarity, molecules **A** and **B** of compound **4** (**4A** and **4B**) were not shown as in their relative orientation in the unit cell. The labeling scheme of rings and non-hydrogen atoms is displayed for compound **3** and is the same for **4A** and **4B**, except for halogens.

Even though the halogen atoms present in the structures of tetra ketones are different, compound **3** is well superimposed on molecules **4A** and **4B**, with RMS deviations of 0.260 Å and 0.186 Å for their non-hydrogen atoms. A superposition of **3** and **4** (both molecules) is illustrated in **Fig. 2**.

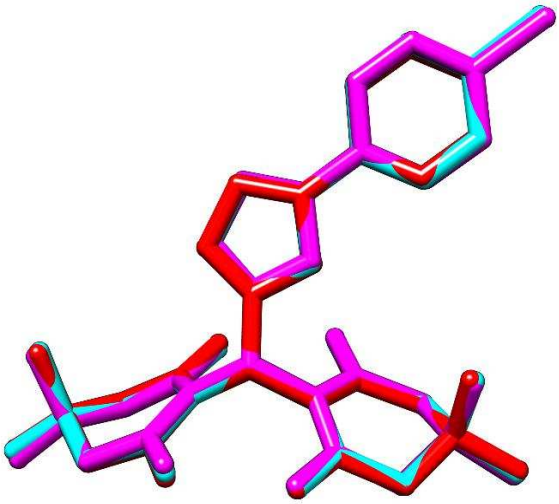

Fig. 2. Molecular overlay through the non-hydrogen atoms of **3** (red), **4A** (pink) and **4B** (cyan).

In the two compounds herein reported, both diketone rings A and B adopt a half-chair conformation with C8 and C12 carbons away from the least-squares (l.s.) planes calculated through the other five coplanar atoms. The distance of these carbons from l.s. planes and the RMS deviation of the l.s. fitted atoms are shown in Table 2.

Table 2
Bond lengths (Å) along the resonant paths, selected dihedral angles (°) describing furan conformation, and descriptors for half-chair conformation of rings A and B (r.m.s. deviation and carbon deviation in Å) in the tetra ketones as determined by single-crystal X-ray diffraction data

	3	**4A**	**4B**
O1-C4	1.284(3)	1.275(4)	1.288(4)
C4-C5	1.400(4)	1.412(5)	1.412(5)
C5-C6	1.394(4)	1.384(5)	1.399(5)
O2-C6	1.288(3)	1.317(5)	1.301(4)
O3-C3	1.282(3)	1.308(5)	1.290(4)
C2-C3	1.398(4)	1.367(5)	1.396(4)
C2-C10	1.399(4)	1.427(6)	1.393(5)
O4-C10	1.292(3)	1.287(5)	1.289(4)
O5-C18-C1-C2	-158.5(2)	-165.7(3)	-168.2(3)
O5-C18-C1-C5	-23.5(3)	-31.4(4)	-35.3(5)
C8 deviation from the l.s. plane A /plane A r.m.s.d.[i]	0.679(3)/0.0611	0.642(4)/0.0648	0.638(4)/0.0612
C12 deviation from the l.s. plane B /plane B r.m.s.d.[ii]	0.693(3)/0.0820	0.630(5)/0.0684	0.639(4)/0.0923

[i] Plane A was fitted through the C7-C6-C5-C4-C9 atoms. [ii] Plane B was fitted through the C11-C10-C2-C3-C13 atoms.

Taking these ring mean planes as references, it is interesting to observe that the flaps C8 and C12 of both half-chairs are oriented towards the same side of the C1 substituent. Another conformational feature resides in the fact that the mean planes crossing through the five coplanar atoms of rings A and B are bent by 54.13(11)°, 58.91(16)°, and 53.20(13)° in **3**, **4A** and **4B**.

Each diketone ring is featured by an electronic delocalization path encompassing the atoms O1-C4-C5-C6-O2 (ring A) and O3-C2-C3-C10-O4 (ring B), which is typical of keto-enol tautomerism. All C-O bond lengths are close 1.30 Å (Table 2), a value between those of a carbonyl (around 1.22 Å) and a hydroxyl (around 1.38 Å) bonds [13]. Similarly, all C-C bond lengths inside this conjugated system are approximately equal to 1.40 Å, which is the most common bond length for phenyl groups [15]. In other words, C4-C5, C5-C6, C2-C3, and C3-C10 exhibit distances typical of a resonant system, without a clear prevalence of either a double bond character or a single. Such keto-enol tautomerism phenomenon has been already reported in crystal structures of related

compounds bearing the same tetra ketone moiety found in **3** and **4 [**16-19]. Furthermore, it is not possible, based on X-ray diffraction data of **3**, to assign where the double and single bonds are in these electronically delocalized pathways, which can be considered as perfectly conjugated two keto-enol moieties. In Molecule **4A**, a subtle difference can be observed between the bond lengths of the bond pairs C4-C5 and C5-C6 [0.028(10) Å]; O1-C4 and O2-C6 [0.042(9) Å] in ring A, and the corresponding ones C2-C3 and C2-C10 [0.060(11) Å]; and O3-C3 and O4-C10 [0.021(10) Å] in ring B (Table 2). Therefore, in **4A**, a slight double bond character can be attributed to O1-C4, C5-C6, O4-C10, and C2-C3, while an almost unnoticeable single bond character can be assigned to O2-C6, C4-C5, O3-C3, and C2-C10. Such mesomerism phenomenon is powered in these compounds by the presence of two intramolecular classical hydrogen bonds between hydroxyl and carbonyl moieties from rings A and B. Since this O-H...O hydrogen atom can be shared between the two oxygens, their carbonyl and hydroxyl characters are indistinguishable. In fact, all residual electronic density peaks in the difference Fourier map referring to the hydroxyl hydrogens were located at practically same distances from the hydrogen bonding donor and acceptor oxygens. Their fixing to a specific oxygen was based only on negligible O-H distance differences that cannot allow for such positioning distinction clearly. However, we choose bind this hydrogen to one oxygen atom instead of leaving it delocalized between two. In Molecule **4A**, the hydrogen hydroxyl assignments were also aided by the slight differences in the C-C and C-O bond lengths as aforementioned.

Another intramolecular characteristic common to the compounds herein described, which is also responsible for the conformational distinction between rings A and B, refers to the rotation on the axis of the bond connecting C1 to its substituent. Such intramolecular feature can be viewed in **Fig. 2**, a molecular overlay of all asymmetric units (only non-hydrogen atoms) through all non-hydrogen atoms. First, the furan plane

of the C1 substituent is almost parallel to the C1-C2 and C1-C5 bond axes. This is a result of steric hindrance effects between the heterocycle and the O1 and O3 oxygens. Second, furan oxygen is pointed towards ring A in both compounds. The O5-C18-C1-C5 and O5-C18-C1-C2 dihedral angles describe well this conformational feature (Table 2), being closer to either 0° or 180°, respectively. The *para*-halogenated phenyl ring is coplanar to the furan one. There are only discrete twists between the rings of the C1 substituent. Their l.s. mean planes form angles of 14.38(11)°, 16.22(17)° and 7.57(13)° in **3**, **4A** and **4B**, respectively.

In both structures, nonclassical CH…O hydrogen bonds are the main contacts responsible for keeping the molecules together in the crystals. Compound **4** is featured by the formation of centrosymmetric dimers made up of either molecules **A** or molecules **B** (**Fig 3a**). Each molecule is bonded to another in the dimer through two C7-$H7_{eq}$...O2 hydrogen bonds, regardless if the crystallographically independent unit is **A** or **B**. These dimers are further held together in one-dimensional chains through two non-classical hydrogen bonds in which molecule **A** is a dual donor to O1B and O3B oxygens from molecule **B** (contacts C26A-H26A...O3B and C27A-H27A...O1B, **Fig. 3a**).

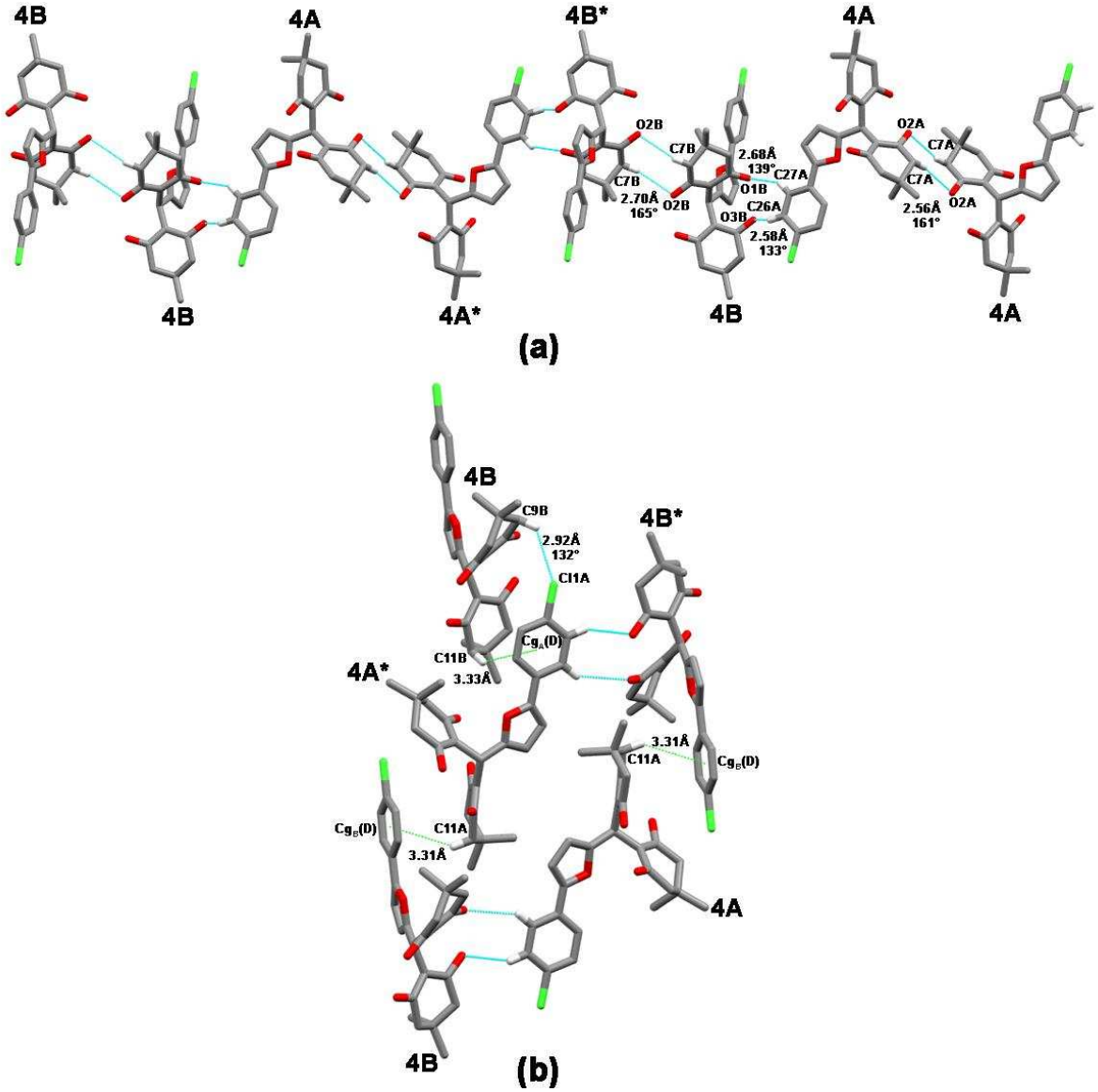

Fig. 3. (a) The one-dimensional chain formed in the crystal structure of **4** and (b) the contacts responsible for sheet assembly therein. Asterisk labeled molecules have almost the same projection in both panels. $Cg_A(D)$ and $Cg_B(D)$ denote the centroid calculated through ring D atoms of molecules **A** and **B**, respectively. In this picture and in the next, only hydrogen atoms involved in the displayed contacts were exhibited. The depicted measurements refer to the hydrogen acceptor (i. e., oxygen, halogen or Cg) distance and the hydrogen bonding angle.

The one-dimensional chain is the main supramolecular motif found in the crystal structure of **3** (**Fig. 4**). In this compound, the chain is formed through the C13-H13$_{eq}$...O2

interaction. The chains are connected by mean of the C11-H11$_{ax}$...π(ring D) contact to assemble a two-dimensional sheet (**Fig. 4**). A similar sheet motif can be also described in **4**, which is constructed through the weaker C9B-H9B$_{ax}$...Cl1A, C11A-H11A$_{ax}$...π(ring D of molecule **B**) and C11B-H11B$_{ax}$...π(ring D of molecule **A**) contacts (**Fig. 3b**).

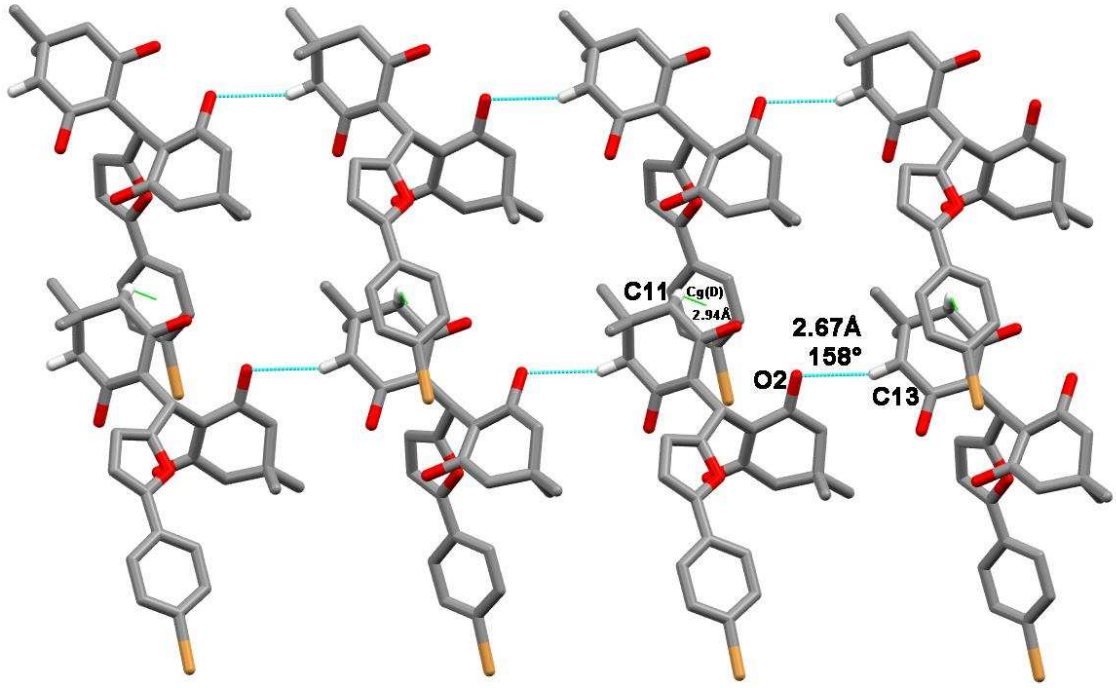

Fig. 4. The two-dimensional sheet formed in the crystal structure of **3.** Cg(D) denotes the centroid calculated through ring D atoms.

The IR spectra of **3** and **4** present a broad band which can be associated with the O-H group of the enol form. In the experimental IR spectrum of compound **3**, the OH band was noticed within the 2000 cm^{-1} - 3200 cm^{-1} range (**Fig. 5**). A similar trend was observed in the IR of enol forms of isobenzofuran-1(*3H*)-one derivatives [20]. The theoretical IR spectrum confirms the OH band range with two vibrational frequencies at 3171.94 cm^{-1} and 3290.78 cm^{-1} related to the O3-H and O2-H stretching respectively (**Fig. 1** labels).

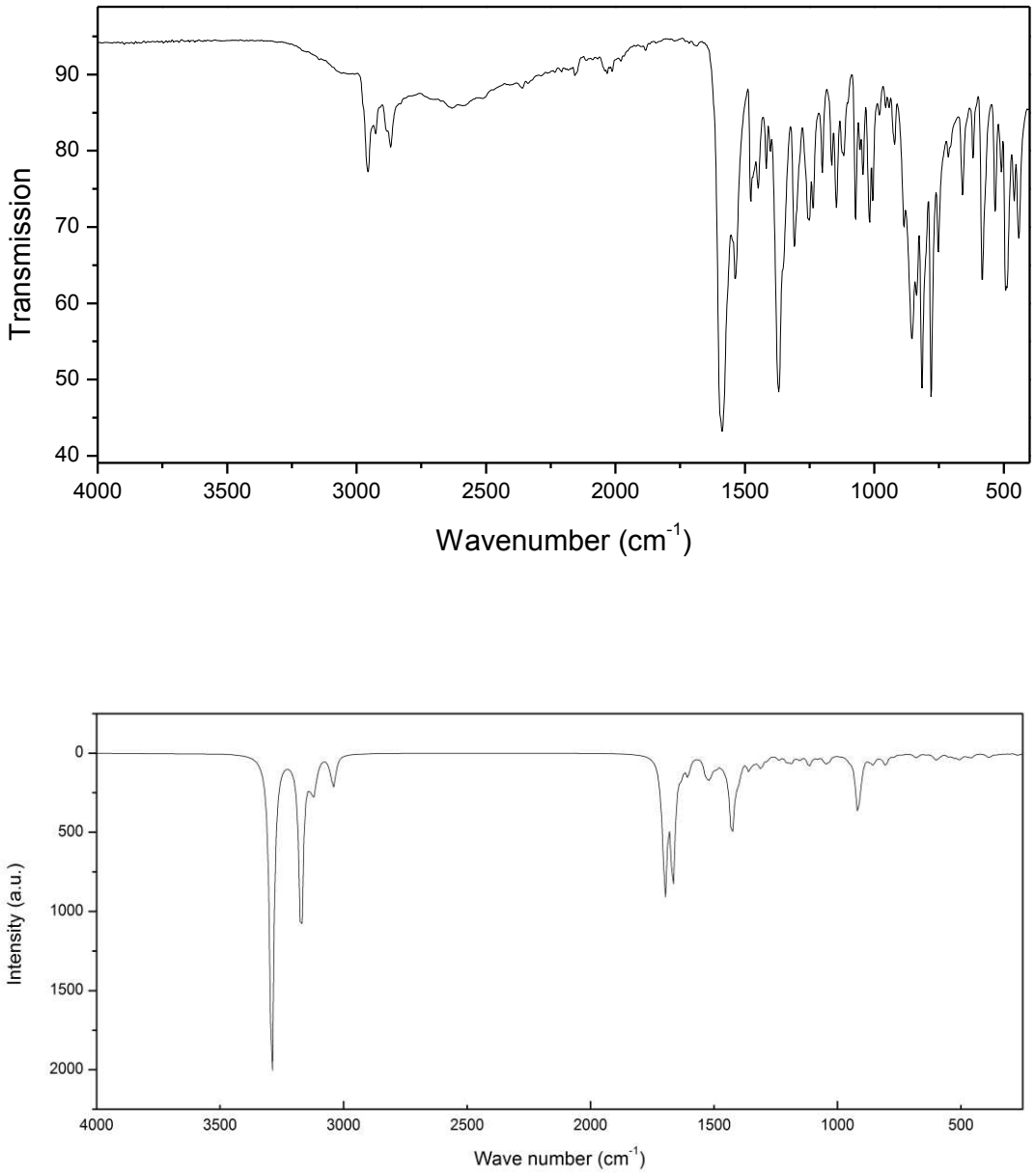

Fig. 5. Experimental (**A**) (ATR) and theoretical (**B**) IR spectra of compound **3**.

In the ^{1}H-NMR spectra of tetra ketones **3** and **4**, the presence of the enol form was also noticed. As can be seen in **Fig. 6**, the OH is observed as a singlet at 12.2 ppm in the spectrum of **4** (**Fig. 6A**). A single deuterium-hydrogen exchange experiment confirmed this signal as corresponding to the OH group (**Fig. 7**). The theoretical spectrum also reinforces the experimental data as one signal for each OH group (**Fig. 6B**). As labeled

in **Fig. 1**, the singlet at 11.61 ppm correspond to O2-H group and the singlet at 12.16 ppm correspond to O3-H group. Regarding the other chemical shifts, the signals at 5.46 ppm in **Fig. 6A** and at 5.22 ppm in **Fig. 6B** correspond to the hydrogen at C1. The singlets at 6.02 ppm and 6.54 ppm in **Fig. 6A** and at 6.29 ppm and 6.94 ppm in **Fig. 6B** correspond to the furan hydrogens. The doublet signals from 7.24 ppm to 7.44 ppm in **Fig. 6A** and from 7.63 ppm to 8.09 ppm in **Fig. 6B** correspond to the benzene hydrogens. Thus, the experimental and theoretical data are in very good agreement.

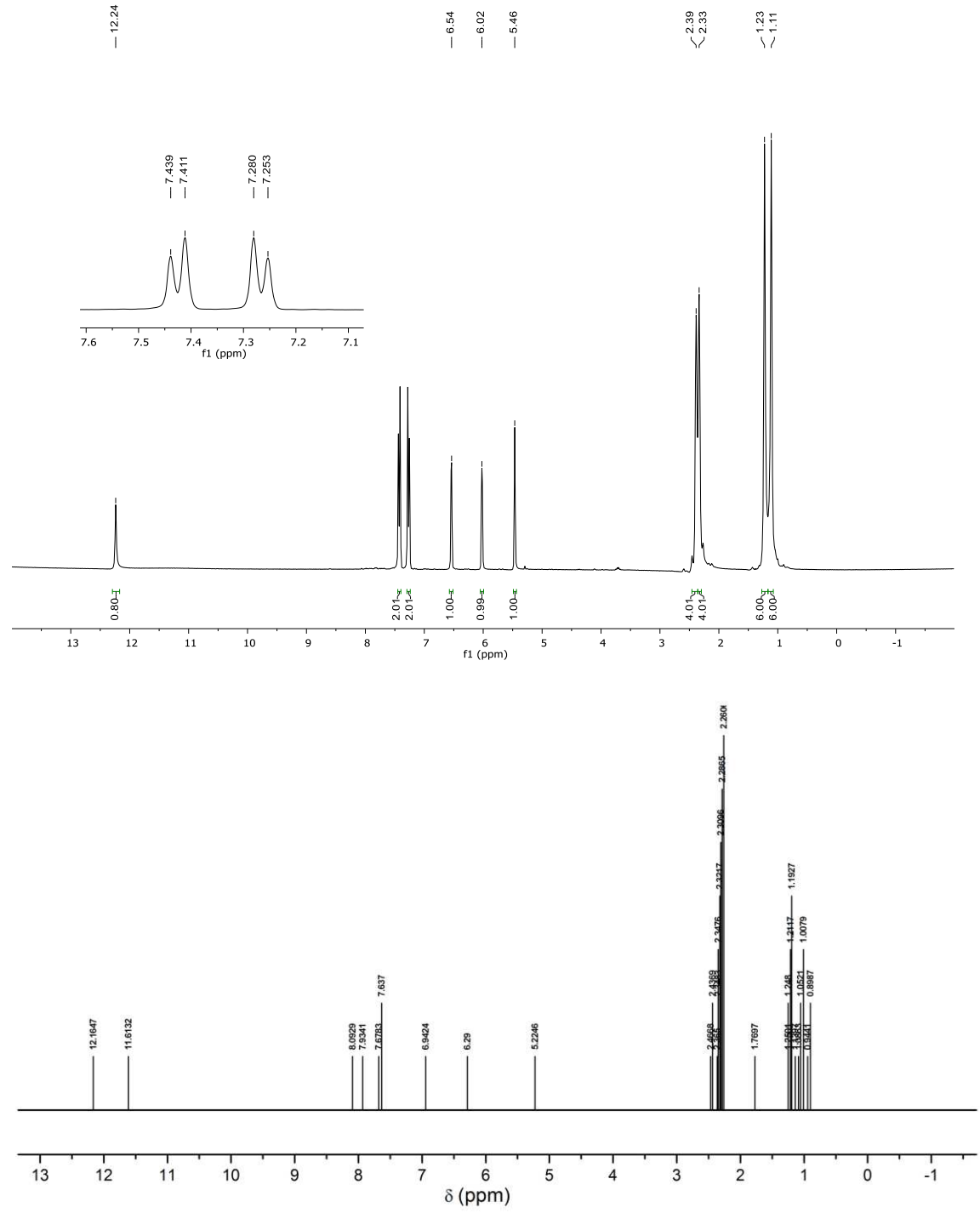

Fig. 6. Experimental (**A**) and theoretical (**B**) ^{1}H NMR (300 MHz, $CDCl_3$) of compound **4**.

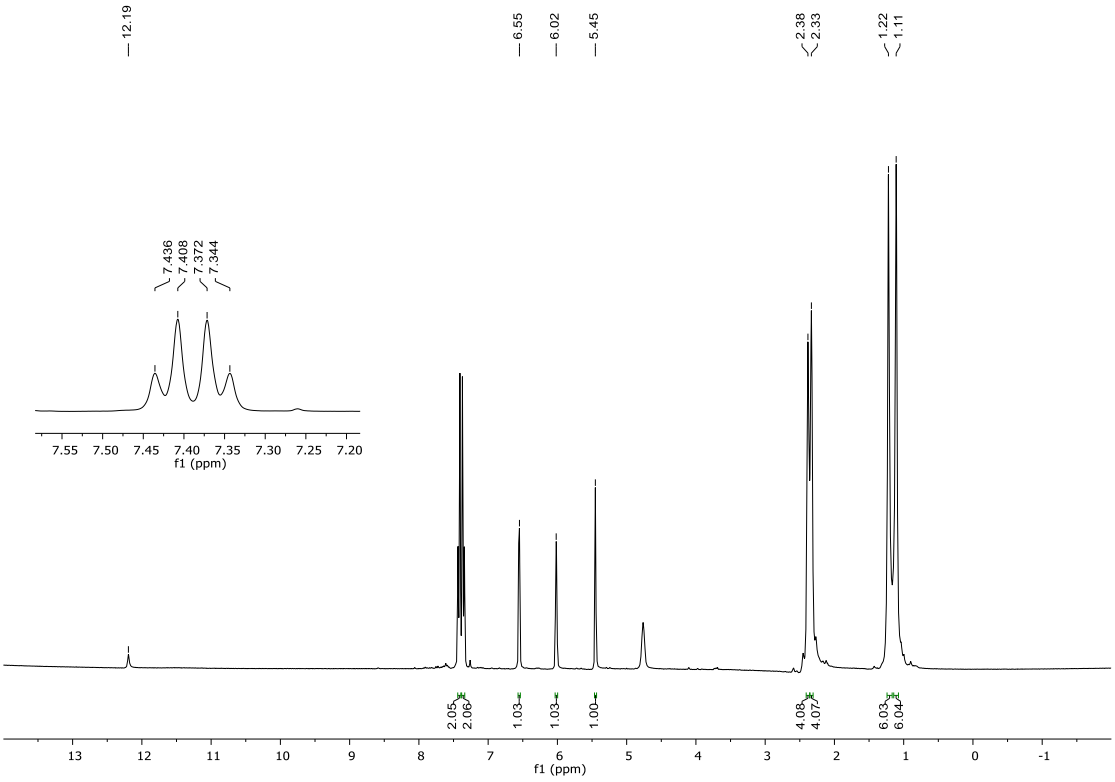

Fig. 7. ^{1}H NMR (300 MHz, $CDCl_3$) associated with deuterium-hydrogen exchange experiment.

In the ^{13}C NMR spectra, the number of signals is in agreement with the structures of **3** and **4**. The theoretical analysis showed signals at 188.7, 187.6, 120.2 and 117.7 correspondent to C6, C3, C5 and C2, respectively (**Fig. 1** labels). In fact, these δ values are very similar to experimental data, which detected signals at 189.7, 189.4, 120.4 and 114.0. High-resolution mass spectrometry confirmed the molecular formulas of the tetra ketones.

The reaction involved in the preparation of compounds **3** and **4** would have resulted in the formation of xanthenodiones **3´** and **4´** as depicted in Scheme 2.

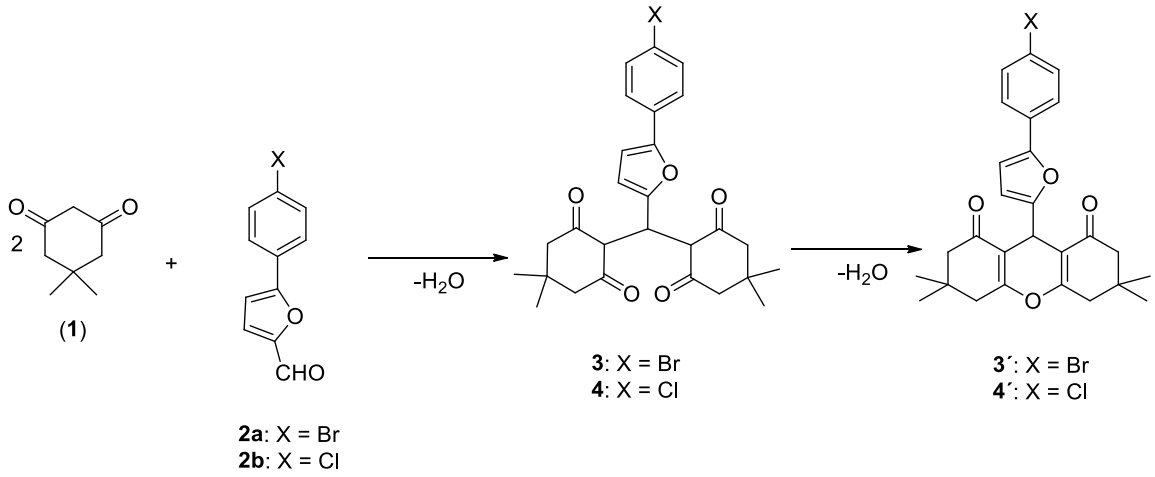

Scheme 2. Reactions involved in the formation of compounds **3/4** and **3´/4´**.

However, as described above, we obtained compounds **3** and **4** by using the conditions described above. Theoretical thermodynamic investigations of the reactions involved in the formation of these compounds were carried out. All energies were obtained by equation (1), where $\Delta_r X$ is the reaction energy, *Xp* is the energy of the compounds **3**, **4**, **3´** and **4´,** X_1 is the energy of compound **1**, X_2 is the energy of compound **2** and *n* is the number of water molecules used to mass balance. For products **3´/4´**, *n* = 2, and for products **3/4**, *n* = 1.

$$\Delta_r \boldsymbol{X} = \left(\boldsymbol{X_p} + \boldsymbol{n X_{H_2O}}\right) - \left(\boldsymbol{X_2} + \boldsymbol{2 X_1}\right) \quad (\mathbf{1})$$

The optimized geometries of compounds **3**, **4**, **3´** and **4´** are shown in **Fig. 8**.

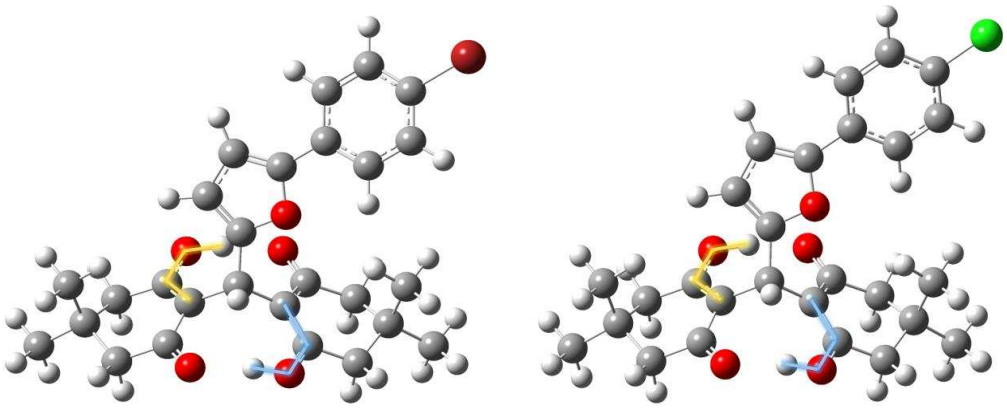

3 **4**

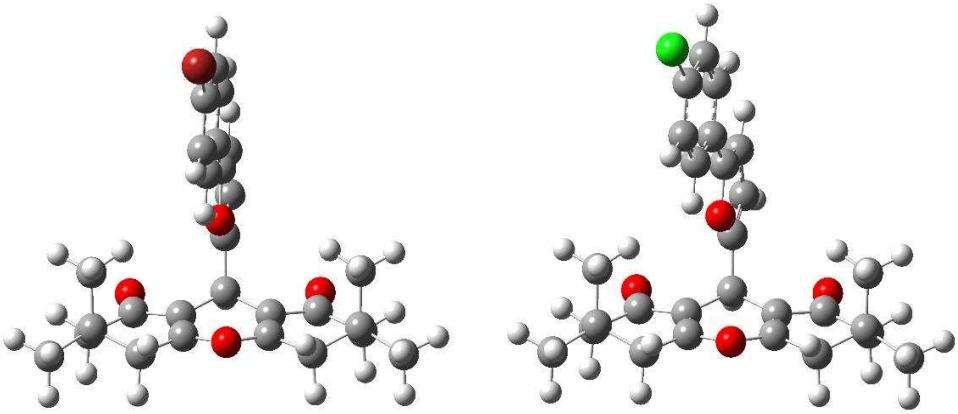

3´ **4´**

.

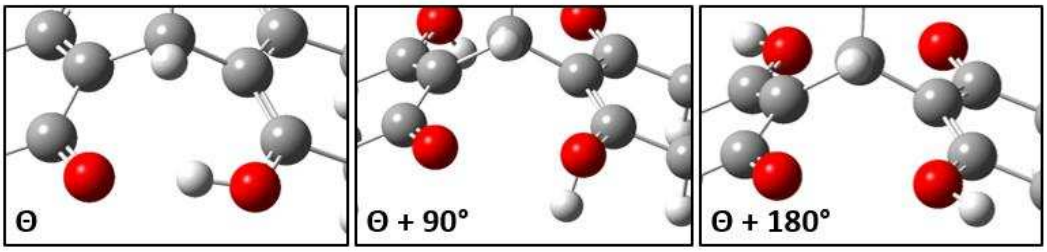

Fig 8. Gas phase optimized structures of compounds **3**, **4**, **3´** and **4´** and highlighted dihedrals (Θ), H-O2-C6-C5 in blue (compound **3**) and H-O3-C3-C2 in yellow (compound **4**).

Table 3 shows the enthalpy (Δ_rH), entropy (Δ_rS) and Gibbs free energy (Δ_rG) associated with the reactions to obtain compounds **3**, **4**, **3´** and **4´**; Boltzmann populations of them are also presented. By analyzing the data, initially at the gas phase, the

populations of **3/4** is slightly higher than **3´/4´** in the equilibria and . The enthalpy differences (**ΔΔ$_r$H**) between **3/3´** and **4/4´** is around -16 kcal.mol^{-1}, while Gibbs free energy differences (**ΔΔ$_r$G**) are -3.50 (**3/3´**) and -4.63 (**4/4´**) kcal.mol^{-1}. The differences in enthalpy and free energy are mainly due to the entropy. Structures of compounds **3/4** have more σ bonds than **3´/4´**, leading to more degrees of freedom. Nevertheless, the reactions that produce **3´/4´** releases two water molecules while the processes that afford **3/4** give just one molecule. Thus, the higher calculated TΔ$_r$S values for the formation of **3/4** can be justified, which is more than 10 kcal.mol^{-1} higher than in the case of **3´/4´**.

Taking into consideration the solvent and the temperature of 85 °C, which corresponds to the temperature used do prepare compounds **3** and **4** (Scheme 2), while the enthalpy and free energy differences between **3**/**3´** and **4/4´** decrease, the populations of **3´/4´** become higher. Under these conditions, ΔΔ$_r$G (**3/3´**) and (**4/4´**) are smaller than 2 kcal.mol^{-1}. By looking at TΔ$_r$S, the difference between **3/3´** is 1.7 kcal.mol^{-1} and 2.27 kcal.mol^{-1} for **4/4´**.

Considering a reaction condition in which the temperature is 100 °C, ΔΔ$_r$G decreases even more in favor of **3**. At this temperature, compound **3** would be thermodynamically more stable, albeit at 85 °C ΔΔ$_r$G is already small enough to indiscriminate such preference to **3/4** or **3´/4´**.

Indeed, if were not for the increase of entropy due to the number of water molecules, certainly compounds **3/4** would be more stable than **3´/4´**, in all aspects, due to the electronic energy, especially when someone pays attention to the gas phase enthalpy. In other words, it means that the entropy cannot explain this phenomenon by itself and it is necessary to better understand the role of the enthalpy contribution. In this case, some hypothesis can be delineated. There should be intramolecular interactions in **3/4** that effectively minimize its electronic structure (vide *infra* for discussion).

Moreover, different reaction conditions are responsible for variations in $\Delta\Delta_rH$(**3/3´**) and $\Delta\Delta_rH$(**4/4´**) as well (**Table 3**). Therefore, the temperature and intermolecular interactions with the solvent could also take place.

Table 3.
Theoretical thermodynamic data, in kcal.mol^{-1}, of the reactions involved in the preparation of compounds **3**, **3´**, **4**, and **4´**

Product	Δ_rG	$\Delta\Delta_rG$	Δ_rH	$\Delta\Delta_rH$	$T\Delta_rS$	Pop(%)
			Gas Phase (25 °C)			
3	-41.41	-3.50	-52.07	-16.19	-10.66	52.44
3´	-37.91		-35.88		2.03	47.56
4	-41.46	-4.63	-51.97	-16.31	-10.51	53.22
4´	-36.83		-35.66		1.18	46.78
			Water (85 °C)			
3	-2.11	1.57	-24.84	-0.15	-22.72	49.09
3´	-3.68		-24.69		-21.02	50.91
4	-2.54	0.77	-24.85	-1.51	-22.30	49.55
4´	-3.31		-23.34		-20.03	50.45
			Water (100 °C)			
3	-0.52	-0.76	-24.74	-2.05	-24.22	50.40
3´	0.24		-22.69		-22.92	49.60
4	-0.98	0.51	-24.75	-1.33	-23.77	49.73
4´	-1.49		-23.42		-21.93	50.27

Besides the temperature, the solvation effect can be determinant in the energy differentiation between **3/3´, 4/4´**. **Table 4** can clarify which factor is relevant for the reaction. Within this context, we also analyzed, in a rough way, the influence of electronic energy (Δ_rE) in the reaction parameters as obtained by equation (1). We can see Δ_rH as the electronic energy with thermodynamic corrections due to the temperature effects. Therefore, we can determine the solvent role in the and equilibria from Δ_rE. For instance, in gas phase and at 25 °C, $\Delta\Delta_rH$ is around -16 kcal.mol^{-1} (**Table 3**). We can see, based on **Table 4**, that in gas phase $\Delta\Delta_rE$ is around -18 kcal.mol^{-1}. Thus, the influence of temperature in the electronic energy to give the enthalpy is just around 2 kcal.mol^{-1}. It is important to emphasize that this is only the temperature effect compared to a zero kelvin situation. **Table 3** also shows that $|\Delta\Delta_rH|$ increases 14~16 kcal.mol^{-1} when the

temperature goes from 25 °C to 85 °C, adding the implicit solvent as well. From this value, we can assume that 6~7 kcal.mol^{-1} comes from the presence of water, leading to $|\Delta\Delta_rE|_{gas\text{-}phase}$ - $|\Delta\Delta_rE|_{water}$ (**Table 4**). These outcomes point to the fact that the solvent has an important contribution to the final $\Delta\Delta_rG$, which will determine the population of **3-4** and **3´-4´**.

Table 4. The solvent influence on **3/4** and **3´/4´** forms equilibrium of compounds **3** and **4**, energies in kcal.mol^{-1}.

Product	**Gas Phase**		**Water**	
	Δ_rE	**$\Delta\Delta_rE$**	**Δ_rE**	**$\Delta\Delta_rE$**
3	-60.56	-18.62	-28.69	-12.70
3´	-41.94		-15.99	
4	-60.47	-18.52	-28.73	-11.75
4´	-41.95		-16.98	

An important difference between compounds **3/4** and **3´/4´** structures is the presence of the hydroxyl groups in compounds **3/4**. The x-ray data (**Fig 1**) have shown the presence of hydrogen bonds between the carbonyl and hydroxyl groups of **3/4**, suggesting the existence of intramolecular hydrogen bonds. The theoretical geometry obtained by quantum calculations has also revealed a similar behavior (**Fig 8**). In this way, a hypothesis of these interactions being heavily responsible for the enolic structures stabilization has to be considered. With a simple scan to the H-O-C-C dihedrals, it is possible to change the hydroxyl groups orientation in such a way as to null the hydrogen bonds and quantify how much the destabilization would be. For Compound **3**, the yellow and blue Θ are 13.9° and 17.4° in gas phase respectively; on the other hand, in water, they are 12.8° and 16.5°, respectively. For Compound **4**, the yellow and blue Θ values are 13.7° and 17° in the gas phase, respectively, while in water they correspond to 13.1° and 16° respectively (**Fig. 8**).

Tables 5 and 6 show how the electronic energy, enthalpy and Gibbs free energy change when the hydrogen bonds are removed, following equation (2). This equation gives the energy difference from the starting dihedral Θ to the point when the compounds

adopt different dihedrals (Θ + y). ΔX is the energy change, X_{Θ} is the energy when the dihedrals are equal to Θ and $X_{\Theta+y}$ is the energy when the dihedrals are equal to Θ + y, with y = 0°, 90° or 180°.

$$\Delta X = X_{\Theta+y} - X_{\Theta} \quad (2)$$

The outcome values for the structures **3/4** are very close suggesting that the halogenated R-groups create a small impact on these intramolecular interactions. Following the ΔG results in the gas phase, it has a maximum in Θ + 90°, an average of 48 kcal.mol^{-1}, which decreases 8 kcal.mol^{-1} in Θ + 180°. The enthalpy has a maximum of 44 kcal.mol^{-1} in Θ + 90° followed by an energy drop of 6 kcal.mol^{-1} in Θ + 180°. Thus, the thermodynamic contribution of TΔS would be near -4 kcal.mol^{-1}. These results suggest that the destabilization can be due to electronic and not thermodynamic effects. In water, the destabilization decreases around 10 kcal.mol^{-1}. It occurs mainly due to the competition between intramolecular and solvent-molecular interactions which weaken electrostatic interactions in the polar environment [21]. This statement is enforced by ΔE data in the gas phase and water. Comparing the Θ and Θ + 90° points, for instance, the difference between $\Delta H_{gas\text{-}phase}$ and ΔH_{water} is around 5.6~5.7 kcal.mol^{-1}. Doing the same operation with ΔE, the difference obtained is 5.5 kcal.mol^{-1} for **3** and **4**. In other words, from the variation of 5.6~5.7 kcal.mol^{-1} in ΔH between the two conditions (gas phase 25 °C and water 85 °C), 5.5 kcal.mol^{-1} can be assigned to the solvent influence. The remaining energy of 0.1~0.2 kcal.mol^{-1} is due to the temperature increase. Indeed, as for entropy, the temperature does not have so much influence in this specific interaction. From these findings, it is possible to understand why ΔE and ΔG are similar. In this line, besides the O-H···O electrostatic intramolecular interactions, a non-classical contribution should take place.

In order to investigate the destabilization energies, we have calculated the sum of electronic delocalization energies through the second-order perturbation theory, ∑E(2),

of all orbital interactions with oxygen lone pairs and a non-bonded O-H orbital. Our calculations have shown that the electronic delocalization stabilizes structures **3/4** around 67 kcal.mol^{-1} in Θ. In Θ + 90° and Θ + 180,° no electronic delocalization between O-H···O have been detected. Thus, our results highlight the importance of the hydrogen bonds to stabilize the **3/4** products *via* non-classical interactions.

Table 5. Relative destabilization energies (kcal.mol^{-1}) of Compound **3** due to the yellow and blue dihedral variations

Dihedral	ΔE	ΔH	ΔG	TΔS	$\sum E(2)_{O(lp)\rightarrow O\text{-}H(\sigma^*)}$
			Gas phase 25 °C		
Θ	0.00	0.00	0.00	0.00	66.64
Θ + 90°	48.19	44.28	48.17	-3.89	0.00
Θ + 180°	40.21	38.78	40.57	-1.79	0.00
			Water 85 °C		
Θ	0.00	0.00	0.00	0.00	67.29
Θ + 90°	42.69	38.62	43.86	-5.24	0.00
Θ + 180°	30.89	29.44	31.69	-2.25	0.00

Table 6. Relative destabilization energies (kcal.mol^{-1}) of compound **4** due to the yellow and blue dihedral variations.

Dihedral	ΔE	ΔH	ΔG	TΔS	$\sum E(2)_{O(lp)\rightarrow O\text{-}H(\sigma^*)}$
			Gas phase 25 °C		
Θ	0.00	0.00	0.00	0.00	66.40
Θ + 90°	48.44	44.53	48.76	-4.23	0.00
Θ + 180°	40.26	38.66	39.99	-1.33	0.00
			Water 85 °C		
Θ	0.00	0.00	0.00	0.00	67.62
Θ + 90°	42.90	38.79	44.35	-5.56	0.00
Θ + 180°	31.07	29.56	32.09	-2.53	0.00

4. Conclusion

A zirconium catalyzed condensation between dimedone and two different aldehydes were used to prepare the compounds 2,2'-((5-(4-bromophenyl)furan-2-yl)methylene) *bis* (5,5-dimethylcyclohexane-1,3-dione) and 2,2'-((5-(4-chlorophenyl)furan-

2-yl)methylene) *bis* (5,5-dimethylcyclohexane-1,3-dione) in synthetically useful yields. Even though the compounds are very similar, X-ray diffraction investigations showed differences in terms of their crystal structures. The reaction involved in the formation of the aforementioned compounds as well as in the preparation of the xanthenodiones derivatives were investigated from the theoretical point of view. It was demonstrated that factors such as temperature and electronic energy influences in the reaction parameters.

References

[1] P. Shanmugasundaram, K. J. Prabahar, V. T. Ramakrishnan, J. Heterocycl. Chem. 30 (1993) 1003-1007.

[2] M.B. -Arias, M.T. -Albarrán, I.P. -Martínez, F.M. -Martínez, G. Espinosa, E. Molins, E. Espinosa, J. Chem. Crystallogr. 29 (1999) 759-763.

[3] G. M. Maharvi, S. Ali, N. Riaz, N. Afza, A. Malik, M. Ashraf, L. Iqbal, M. Lateef, J. Enzyme Inhib. Med. Chem. 23 (2008) 62-69.

[4] Ali S, Maharvi GM, Riaz N, Afza N, Malik A, Rehman AU, Lateef M, Iqbal L., West Indian Med. J. 58 (2009): 92-98.

[5] K. M. Khan, G. M. Maharvi, S. A. Nawaz, S. Perveen, M. I. Choudhary, Lett. Drug Des. Discov. 4 (2007): 272-278.

[6] M. S. Ferreira, D. A. T. Pires,J. D. F. Villar, World J. Pharm. Pharm. Sci. 4 (2015) 1705-1718.

[7] K. M. Khan, G. M. Maharvi, M. T. H. Khan, A. J. Shaikh, S. Perveen, S. Begum, M. I. Choudhary (2005) Bioorg. Med. Chem. 14 (2005) 344-351.

[8] F. Alchab, L. Ettouati, Z. Bouaziz, A. Bollacke, J.G. Delcros, C. G. W. Gertzen, H. Gohlke, N. Pinaud, M. Marchivie, J. Guillon, B. Fenet, J. Jose, M. L. Borgne, Pharmaceuticals 8 (2015) 279-302.

[9] J. K. Rajput, G. Kaur, Catal. Sci. Technol. 4 (2014) 142-151.

[10] SADABS, APEX2 and SAINT. Bruker AXS Inc., Madison, Wisconsin, USA, 2009.

[11] G. M. Sheldrick, Acta Crystallogr. Sect. A 64 (2008) 112-122.

[12] C. F. Macrae, I. J. Bruno, J. A. Chisholm, P. R. Edgington, P. Mccabe, E. Pidcock, L. R. Monge, R. Taylor, J. van de Streek, P. A., J. Appl. Crystallogr. 41 (2008) 466-470.

[13] Frisch, M. J.; Trucks, G. W.; Schlegel, H. B.; Scuseria, G. E.; Robb, M. A.; Cheeseman, J. R.; Scalmani, G.; Barone, V.; Mennucci, B.; Petersson, G. A.; Nakatsuji, H.; Caricato, M.; Li, X.; Hratchian, H. P.; Izmaylov, A. F.; Bloino, J.; Zheng, G.; Sonnenberg, J. L.; Hada, M.; Ehara, M.; Toyota, K.; Fukuda, R.; Hasegawa, J.; Ishida, M.; Nakajima, T.; Honda, Y.; Kitao, O.; Nakai, H.; Vreven, T.; Montgomery, Jr., J. A.; Peralta, J. E.; Ogliaro, F.; Bearpark, M.; Heyd, J. J.; Brothers, E.; Kudin, K. N.; Staroverov, V. N.; Kobayashi, R.; Normand, J.; Raghavachari, K.; Rendell, A.; Burant, J. C.; Iyengar, S. S.; Tomasi, J.; Cossi, M.; Rega, N.; Millam, J. M.; Klene, M.; Knox, J. E.; Cross, J. B.; Bakken, V.; Adamo, C.; Jaramillo, J.; Gomperts, R.; Stratmann, R. E.; Yazyev, O.; Austin, A. J.; Cammi, R.; Pomelli, C.; Ochterski, J. W.; Martin, R. L.; Morokuma, K.; Zakrzewski, V. G.; Voth, G. A.; Salvador, P.; Dannenberg, J. J.; Dapprich, S.; Daniels, A. D.; Farkas, Ö.; Foresman, J. B.; Ortiz, J. V.; Cioslowski, J.; Fox, D. J. Gaussian Inc.: Wallingford CT 2009.

[14] E. D. Glendening, J. K. Badenhoop, A. E. Reed, J. E. Carpenter, J. A. Bohmann, C. M. Morales, C. R. Landis, Weinhold, F. 2013.

[15] F. H. Allen, Acta Crystallogr. Sect. B 58 (2002) 380-388.

[16] C. Bingi, A. Kale, J. B. Nanubolu, K. Atmakur, (2015) RSC Adv. 5 (2015) 106860-106867.

[17] F. Al-Omran, R. M. Mohareb, A. A. El-Khair, (2014) Med. Chem. Res. 23 (2014) 1623-1633.

[18] M. Sigalov , R. Vainer , V. Khodorkovsky, J. Mol. Struct. 977 (2010) 230-236.

[19] A. M. Cagulada, D. E. Lynch, D. G. Hamilton (2009) Cryst. Growth. Des. 9 (2009) 825-832.

[20] D. A. T. Pires, W. L. Pereira, R. R. Teixeira, J. D. F. Villar, C. J. do Nascimento, (2016) J. Mol. Struct. 1113 (2016) 146-152.

[21] C. Wang, F. Ying, W. Wu, Y. Mo, J. Org. Chem. 79 (2014), 1571–1581.

CAPÍTULO V

AVALIAÇÃO DA ATIVIDADE ANTIFÚNGICA DE XANTENODIONAS E TETRACETONAS

1 INTRODUÇÃO

A população mundial tem crescido grandemente nas últimas décadas. Entre os anos de 1950 a 2000, a população passou de 2,5 bilhões para 6,1 bilhões. Estima-se que em 2050 a população mundial chegue a 9,1 bilhões de pessoas. Com isso, aumenta-se também a demanda por alimento e, em última instância uma maior produção agrícola. Os pesticidas têm um papel crucial na agricultura, pois possuem tanto a capacidade de controlar pragas agrícolas, como plantas daninhas, doenças de plantas e seus vetores, quanto aumentar a produtividade (fertilizantes)[1].

Lomborg (2001) ilustram a importância do uso de pesticidas afirmando que: "Se os pesticidas fossem abolidos, as vidas salvas seriam superadas em número por um fator de cerca de 1000 pelas vidas perdidas devido a dietas mais pobres. Penas secundárias seriam o enorme dano ambiental devido à necessidade de terras para a agricultura menos produtiva, e um custo financeiro de cerca de 20 milhões de dólares"[2]. Portanto, o uso de pesticidas permite uma maior produção e disponibilidade de alimentos gerando benefícios econômicos e nutricionais.

Os pesticidas correspondem a uma vasta gama de compostos, que incluem inseticidas, fungicidas, bactericidas, herbicidas, nematicidas, moluscicidas, rodenticidas, reguladores de crescimento de plantas, dentre outros. Em particular, os fungicidas representam cerca de 17% do total de produtos químicos de proteção de culturas utilizados no mundo[3]. Eles são divididos atualmente em mais de 100 grupos químicos[4].

Apesar de apresentarem vantagens, o uso de alguns fungicidas também traz danos à saúde humana e ao ambiente. No que diz respeito a saúde humana, o grupo de maior risco inclui trabalhadores da produção, pulverizadores, batedores, carregadores e trabalhadores rurais. Em processos industriais de formulação e fabricação, os

---

[1] CARVALHO, F. P. Agriculture, pesticides, food security and food safety. *Environmental, science & policy*, v. 9, p. 685–692, 2006.
[2] LOMBORG, B., 2001. The Skeptical Environmentalist. Cambridge University Press, reprint ed. (August 28, 2001). ISBN: 0521010683
[3] COOPER, J.; DOBSON, H. The benefits of pesticides to mankind and the environment. *Crop Protection*, v. 26, p. 1337–1348, 2007.
[4] FRAC Code List 2016, Fungicide Resistance Action Committee.

trabalhadores têm um risco aumentado devido ao manuseio de reagentes químicos e solventes tóxicos que dão origem aos fungicidas. Além destes grupos com exposição elevada, existem os consumidores de produtos agrícolas que podem ter sua saúde comprometida de maneira indireta, devido a ingestão de alimentos com elevados níveis de fungicidas[5].

Os principais impactos ambientais vêm da utilização de fungicidas orgânicos persistentes, também chamados de bioacumulativos, que entram em contato com outros ecossistemas através de lixiviação, volatilização e os fluxos de resíduos provenientes de animais e seres humanos. Os países desenvolvidos têm buscado a utilização de fungicidas menos persistentes no meio ambiente que os clássicos, ou seja, os chamados "produtos verdes". Entretanto, estes novos produtos químicos têm um custo de produção mais elevado[6].

Observa-se, desta maneira, uma necessidade crescente de produção de fungicidas sustentáveis, ou seja, produtos químicos que possam proporcionar alta produtividade e que causem nenhum ou baixos impactos ambientais. A introdução de fungicidas, biodegradáveis, não tóxicos, de fácil preparo e manuseio, pode tornar-se uma alternativa viável e promissora para controle de doenças de plantas. Outro ponto que reforça a busca e prospecção de novos compostos com capacidade fungicida diz respeito desenvolvimento de resistência em patógenos fúngicos de culturas, contra os fungicidas utilizados para controlá-los.

Dentro deste contexto, descreve-se neste capítulo os resultados de uma avaliação preliminar da atividade antifúngica de quarenta e cinco xantenodionas, quatro intermediários tetracetônicos e um derivado da dimedona contendo uma porção arilideno contra os fungos *Fusarium oxysporum* f. sp. *cubense* e a *Alternaria grandis*. O primeiro é o responsável por causar o Mal do Panamá, uma doença de difícil controle, enquanto o segundo causa a pinta preta na batateira, o qual tem um aumentado sua incidência e ressurgência.

[5] AKTAR, M. W.; SENGUPTA, D.; CHOWDHURY, A. Impact of pesticides use in agriculture: their benefits and hazards. *Interdisciplinary Toxicology*, v. 2, p. 1–12, 2009.

[6] TILMAN, D.; CASSMAN, K. G.; MATSON, P. A.;NAYLOR, R. POLASKY, S. Agricultural sustainability and intensive production practices. *Nature*, v. 418, p. 671-677, 2002.

1.1 O Mal do Panamá

A banana possui elevado valor nutricional, sendo rica em vitaminas A e C, fibras e potássio. Estas características, além do seu sabor, representam estímulos ao seu consumo, justificando assim a sua popularidade[7]. Apesar de ser consumida e conhecida mundialmente, a banana é típica de regiões tropicais. A produção de banana no Brasil em 2013 foi de cerca de 6,9 milhões de toneladas, posicionando, desta maneira, o país como quarto maior produtor mundial, ficando atrás somente da Índia, China e Filipinas[8].

Entretanto, a produção mundial de banana é seriamente afetada por uma doença conhecida como o Mal do Panamá ou murcha de *Fusarium*, causada pelo fungo *Fusarium oxysporum* f. sp. *cubense*. Este patógeno se estabelece no sistema radicular e rizoma da bananeira, a infecção ocorre após penetração por ferimentos ocasionados pela emissão das raízes secundárias, alcançando em última instância o xilema, local onde ocorre intensa esporulação[9].

Um dos principais sintomas desta doença é o amarelecimento das folhas, o qual ocorre de maneira progressiva das mais velhas para as mais novas, iniciando pelos bordos do limbo e progredindo em direção a nervura central. Finalmente, as folhas murcham, secam e o pecíolo se quebra junto ao pseudocaule, fazendo com que a bananeira adquira um aspecto de guarda-chuva fechado. Além disso, na parte interna do pseudocaule de plantas, com o estágio avançado da doença, é possível observar pontuações pardo-avermelhadas provocadas pela presença do patógeno, provavelmente resultantes da oxidação de compostos fenólicos[10].

O *Fusarium oxysporum* f. sp. *cubense* é um fungo de solo e produz três tipos de esporos assexuados para sua reprodução e dispersão: os microconídios, os macroconídios e os clamidósporos (Figura V-1). Cada uma destas estruturas reprodutivas possui características peculiares. Os microconídios, por exemplo, são ovais ou reniformes (tamanho entre de 5-16 μm por 2,4-3,5 μm) e sua germinação atinge no máximo 20%. Os macroconídios por sua vez, são fusiformes (tamanho entre de 27-55 μm por 3,3-5,5 μm) e germinam rapidamente sendo, por isso, muito eficientes na propagação da doença. Os

[7] SENA, J. V. C. Aspectos da produção e mercado da banana no Nordeste. Informe Rural Etene, n. 10, 2011.
[8] Food And Agriculture Organization Of The United Nations Statistics Division (FAOSTAT), 2013.
[9] GETHA, K. VIKINESWARY, S. Antagonistic effects of *Streptomyces* violaceusniger strain G10 on *Fusarium oxysporum* f.sp. *cubense* race 4: Indirect evidence for the role of antibiosis in the antagonistic process. *Journal of Industrial Microbiology & Biotechnology*, v. 28, p. 303 – 310, 2002.
[10] PLOETZ, R. C. Fusarium Wilt of Banana Is Caused by Several Pathogens Referred to as *Fusarium oxysporum* f. sp. *cubense*. *Phytopathology*, v. 96, p. 653-656, 2006.

clamidósporos são globosos (com tamanho entre de 5-11 μm) e possuem uma parede celular espessa. Estes correspondem à estrutura de sobrevivência deste patógeno, a qual pode germinar e causar danos mesmo após 20 anos de estabelecimento no solo[11].

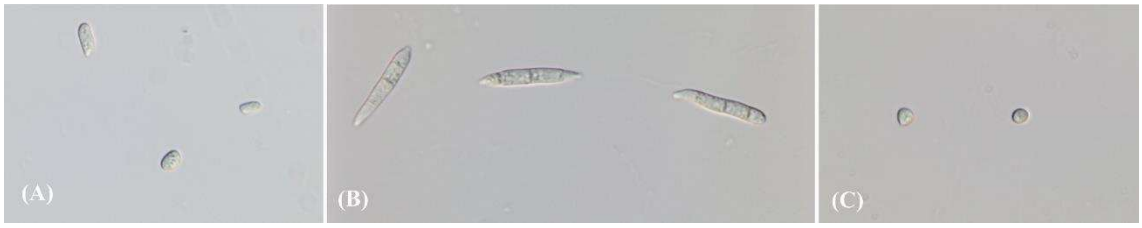

Figura V - 1. Esporos assexuados de *Fusarium oxysporum* f. sp. *cubense*: (A) microconídios, (B) macroconídios e (C) clamidósporos.

O manejo do Mal do Panamá pode ser realizado via controle químico, controle biológico, por meio da supressividade do solo e do emprego de cultivares resistentes ao *F. oxysporum* f. sp. *cubense*. Dentre estes métodos, o único que controla efetivamente o Mal do Panamá é o plantio de clones e cultivares resistentes. Todavia, devido à grande capacidade de adaptação deste patógeno este manejo torna-se temporário. Por isso, tem-se a crescente necessidade de desenvolvimento de métodos eficientes e sustentáveis para o controle desta doença[12].

[11] VICENTE, L. P.; DITA, M. A.; LA PARTE, E. M. Technical manual prevention and diagnostic of *Fusarium* Wilt (Panama disease) of banana caused by *Fusarium oxysporum* f. sp. *cubense* Tropical Race 4 (TR4). Food and Agriculture Organization of the United Nations, 2014.

[12] HECK, D. W. Supressividade A *Fusarium oxysporum* f. sp. *cubense* por produtos orgânicos. 2015. 136 f. Dissertação (Mestrado em Agronomia) - Faculdade de Ciências Agronômicas, Universidade Estadual Paulista, Botucatu. 2015.

1.2 Pinta preta

A batata é um alimento de elevado valor nutricional possuindo em sua composição desde macronutrientes como carboidratos e proteínas até micronutrientes como fósforo, magnésio, potássio e vitaminas do complexo B e C, além de fibras. Esta solanácea é versátil, podendo ser consumida "in natura" ou industrializada. Seu caráter universal aliado à sua rica composição, torna a batata o quarto alimento mais consumido no mundo[13].

No Brasil, em 2013, a produção de batata foi de aproximadamente 3,5 milhões de toneladas, representando cerca de 1% da mundial. Embora a produção não seja tão representativa, a produtividade brasileira é 42% superior[14]. Além disso, este alimento é a hortaliça que apresenta a maior área plantada. Contudo, a produção de batata tem sido comprometida pelo estabelecimento de uma doença conhecida como pinta preta ou pinta miúda, que pode reduzir a produtividade de 5 – 78%[15].

A pinta preta é a segunda doença foliar de maior incidência que acomete a cultura de batata. Ela ocorre em todas as épocas de plantio e caracteriza-se pelo aparecimento de manchas necróticas nas folhas de coloração marrom escuras, com anéis concêntricos em seu interior, os quais podem ter a forma oval, circular ou angular. Com a evolução da doença ocorre um desfolhamento prematuro da planta, reduzindo a taxa fotossintética e aumentando a respiração. Isto causa um desequilíbrio com relação à oferta e demanda de nutrientes. Sintomas similares, porém com lesões alongadas e quase sempre deprimidas, são observados nos caules, hastes, pecíolos. Nos tubérculos as lesões são irregulares, deprimidas e de coloração escura[16].

O agente causal da pinta preta é a *Alternaria solani*. Porém, outras espécies deste mesmo gênero, como *A. grandis*, podem estar associadas a doença. Os esporos assexuados (conídios) da *A. grandis* possuem um bico e são muriformes. Eles apresentam células multinucleadas, septos transversais e longitudinais e são de coloração escura (melanizada) (Figura V-2)[17].

---

[13] LOPES, C. A.; BUSO, J. A. A cultura da batata. Brasília: Embrapa Informação Tecnológia, 184 p, 1999.
[14] Food And Agriculture Organization Of The United Nations Statistics Division (FAOSTAT), 2013.
[15] TSEDALEY, B. Review on early blight (*Alternaria* spp.) of potato disease and its management options. *Journal of Biology, Agriculture and Healthcare*, v. 4, p. 191-198, 2014.
[16] FOOLAD; M. R.; MERK; H. L.; ASHRAFI, H. Genetics, Genomics and Breeding of Late Blight and Early Blight Resistance in Tomato. *Critical Reviews in Plant Sciences*, v. 27, p. 75–107, 2008.
[17] CHAERANI, R.; VOORRIPS, R. E. Tomato early blight (*Alternaria solani*): the pathogen, genetics, and breeding for resistance. *Journal of General Plant Pathology*, v. 72, p. 335-347, 2006.

Figura V - 2. Conídios de *Alternaria* sp.

O manejo desta doença pode ser realizado no contexto de programas de produção integrada com a utilização de sementes certificadas, plantio de cultivares com algum nível de resistência, emprego de fungicidas, dentre outros. A maioria das cultivares plantadas no Brasil é susceptível tornando assim, o uso de agroquímicos extremamente importante na prevenção e redução da doença no campo[18].

[18] TSEDALEY, B. Review on early blight (*Alternaria* spp.) of potato disease and its management options. *Journal of Biology, Agriculture and Healthcare*, v. 4, p. 191-198, 2014.

2 MATERIAIS E MÉTODOS

2.1 Generalidades metodológicas

O dimetil sulfóxido (DMSO) P.A. utilizado no preparo das soluções estoque dos compostos avaliados foi obtido comercialmente (Synth, São Paulo, Brasil) e empregado sem nenhum tratamento prévio. O corante utilizado nos ensaios de colorimetria, resazurina, foi adquirido da Vetec (Rio de Janeiro, Brasil). O fotômetro de microplacas empregado nos testes foi o modelo Multiskan FC e os filtros utilizados foram o de 570 nm e o de 600 nm. A contagem dos esporos dos fungos submetidos aos testes de sensibilidade fungicida foi realizada por meio de uma câmara de Neubauer e um microscópico modelo Olympus CX31.

2.2 Avaliação de atividade antifúngica das xantenodionas, tetracetonas e benzilideno utilizando leitor de ELISA

A sensibilidade de *Fusarium oxysporum* f. sp. *cubense* (*Foc*) (isolado CNPMF0801) e de *Alternaria grandis* (AS588) a 53 diferentes xantenodionas, quatro tetracetonas e um derivado da dimedona contendo uma porção arilideno foi determinada quantitativamente por meio de ensaios empregando placas de 96 poços e o corante resazurina (RZ). Este teste foi realizado em fluxo laminar utilizando técnicas asséptica. O volume de 343 μL do meio de cultura Czapek-Dox (CZ-Dox), com sua concentração dobrada, foi modificado com 2% da solução estoque de cada composto a 20.000 ppm (7 μL), as quais foram preparadas em DMSO. Em seguida, distribuiu-se 50 μL do meio CZ-Dox alterado com os compostos na placa de 96 poços na forma de hexaplicatas.

Posteriormente, preparou-se uma suspensão de microconídios de (*Foc*) a 2 x 10^6 esporos/mL, usando água destilada esterilizada e colocaram-se 50 μL nos poços em três poços de cada tratamento. Aos outros três poços de cada tratamento, adicionaram-se apenas 50 μL de água destilada esterilizada. O meio CZ-Dox, a água e o *Foc* foram empregados como controle negativo, enquanto que os poços contendo apenas o meio CZ-Dox, os fungicidas em potencial e a água foram utilizados para observar se os compostos absorviam no mesmo comprimento de onda em que foi realizada a leitura para a resazurina. A concentração final dos compostos e o número de microconídios nos poços foram, respectivamente, 200 ppm e 1 x 10^6 esporos/mL. Para o *Foc* utilizou-se como controle positivo o tiofanato metílico e para a *A. grandis* a azoxistrobina. Após 18 h de

incubação a 25 ± 2 ºC e agitação a 300 rpm, 10% de RZ (440 μmol L^{-1}) foi acrescentado aos poços da microplaca com auxílio de uma micropipeta multicanal. A microplaca foi mantida no escuro sob agitação por 6 h. A densidade ótica foi medida em leitor de placa de microtitulação a 570 e 600 nm. O experimento foi repetido três vezes. Um procedimento similar foi realizado para a determinação do potencial controle de *A. grandis*, porém a suspensão de conídios utilizada foi calibrada a 1 x 10^5 esporos/mL.

A resazurina possui coloração azul que, na presença de agente redutores (NADPH, FADH, FMNH, NADH e citocromos) provenientes da atividade metabólica muda para a cor rosa[19]. A partir desta mudança de coloração foi possível então mensurar a atividade metabólica dos microorganismos testados e assim o efeito fungicida proporcionado por cada composto envolvido na triagem.

Para os cálculos de porcentagem de inibição foi utilizada a equação a seguir:

$$\%\text{Inibição} = 100 - \left[\left(\frac{\varepsilon_{ox}\lambda_{600}A\lambda_{570} - \varepsilon_{ox}\lambda_{570}A\lambda_{600}}{\varepsilon_{ox}\lambda_{570}A^{0}\lambda_{600} - \varepsilon_{ox}\lambda_{600}A^{0}\lambda_{570}}\right) x\ 100\right]$$

Onde, $\varepsilon_{ox}\lambda_{570}$ corresponde ao valor 117,216 (coeficiente de extinção molar da forma oxidada do corante a 570 nm); $\varepsilon_{ox}\lambda_{600}$ corresponde ao valor 80,586 (coeficiente de extinção molar da forma oxidada do corante a 600 nm); $A\lambda_{570}$ é o valor da absorbância dos poços a 570 nm; $A\lambda_{600}$ é o valor da absorbância dos poços a 600 nm; $A^{o}\lambda_{570}$ é o valor da absorbância do controle positivo a 570 nm e $A^{0}\lambda_{600}$ corresponde à absorbância do controle positivo a 600 nm.

[19] RAMPERSAD, S. N. Multiple Applications of Alamar Blue as an indicator of metabolic function and cellular health in cell viability bioassays. *Sensors*, v. 12, p. 12347-12360, 2012.

3 RESULTADOS E DISCUSSÃO

Os compostos apresentados na Figura V - 3 foram avaliados em uma triagem preliminar para detecção de substâncias com potencial atividade contra os fungos *Fusarium oxysporum* f. sp. *cubense* e *Alternaria grandis*. Para identificar quais compostos apresentaram atividade, empregou-se um ensaio fungicida utilizando-se um sensor colorimétrico de atividade metabólica, a resazurina.

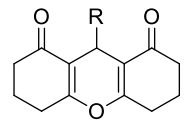

1: R = 4-Fenil
2: R = 4-Fluorofenil
3: R = 4-Clorofenil
4: R = 4-Bromofenil
5: R = 4-Trifluorometilfenil
6: R = 4-Cianofenil
7: R = 4-Nitrofeil
8: R = 4-Dimetiaminofenil
9: R = 4-Metoxifenil
10: R = 3,4-Dimetoxifenil
11: R = 3,4,5-Trimetoxifenil
13: R = 4-Hidroxi-3-metoxifenil
14: R = Benzo[d][1,3]dioxol-5-il
15: R = 5-(4-clorofenil)furan-2-il
16: R = 5-(4-bromofenil)furan-2-il
17: R = 5-Fenil-tiofen-2-il

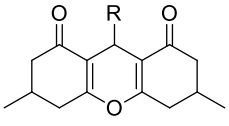

19: R = 4-Fluorofenil
20: R = 4-Clorofenil
21: R = 4-Bromofenil
22: R = 4-Trifluorometilfenil
23: R = 4-Cianofenil
24: R = 4-Nitrofenil
25: R = 4-Metoxifenil
26: R = 3,4,5-Trimetoxifenil
28: R = 4-Hidroxi-3-metoxifenil
29: R = Benzo[d][1,3]dioxol-5-il

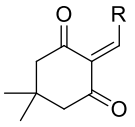

32: R =2,6-Diclorofenil

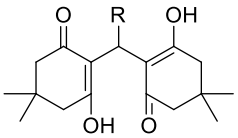

33: R = 5-(4-clorofenil)furan-2-il
34: R = 5-(4-bromofenil)furan-2-il
35: R =4-Dimetilaminofenil
36: R = 3,4,5-Trimetoxifenil

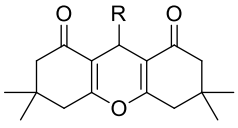

37: R = Fenil
38: R = 4-Fluorofenil
39: R = 4-Clorofenil
40: R = 4-Bromofenil
41: R = 4-Trifluorometilfenil
42: R = 4-Cianofenil
43: R = 4-Nitrofenil
44: R = 4-Metoxifenil
45: R = 3,4-Dimetoxifenil
47: R = 4-Hidroxi-3-metoxifenil
48: R = Benzo[d][1,3]dioxol-5-il
49: R = 5-Fenil-tiofen-2-il

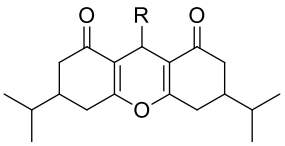

50: Fenil
51: R = 4-Fluorofenil
53: R = 4-Bromofenil
54: R = 4-Trifluorometilfenil
55: R = 4-Cianofenil
56: R = 4-Nitrofenil
58: R = 5-Fenil-tiofen-2-il

Figura V - 3. Xantenodionas, tetracetonas e o derivado da dimedona contendo a porção arilideno avaliados contra *Fusarium oxysporum* f. sp. *cubense* e *Alternaria grandis*.

O resultado da triagem realizada para o *Foc* (Figura V-4) demonstrou que alguns compostos foram mais ativos na inibição da atividade metabólica deste fungo, como é o caso dos compostos **11**, **26**, **32**, **33**, **34**, **36**, **45** e **49** que tiveram a porcentagem de inibição acima de 50% na concentração de 200 ppm. Nestes casos, foi possível observar a sensibilidade do *Foc* sem medição no espectrofotômetro por meio da simples

diferenciação visual. Por outro lado, os compostos **2-4**, **6**, **7**, **10**, **14**, **15**, **19-24**, **38**, **39**, **42**, **43**, **47**, **48**, **51** e **54-58** não apresentaram nenhuma atividade e o restante exibiu uma porcentagem de inibição na faixa de 1 a 43%.

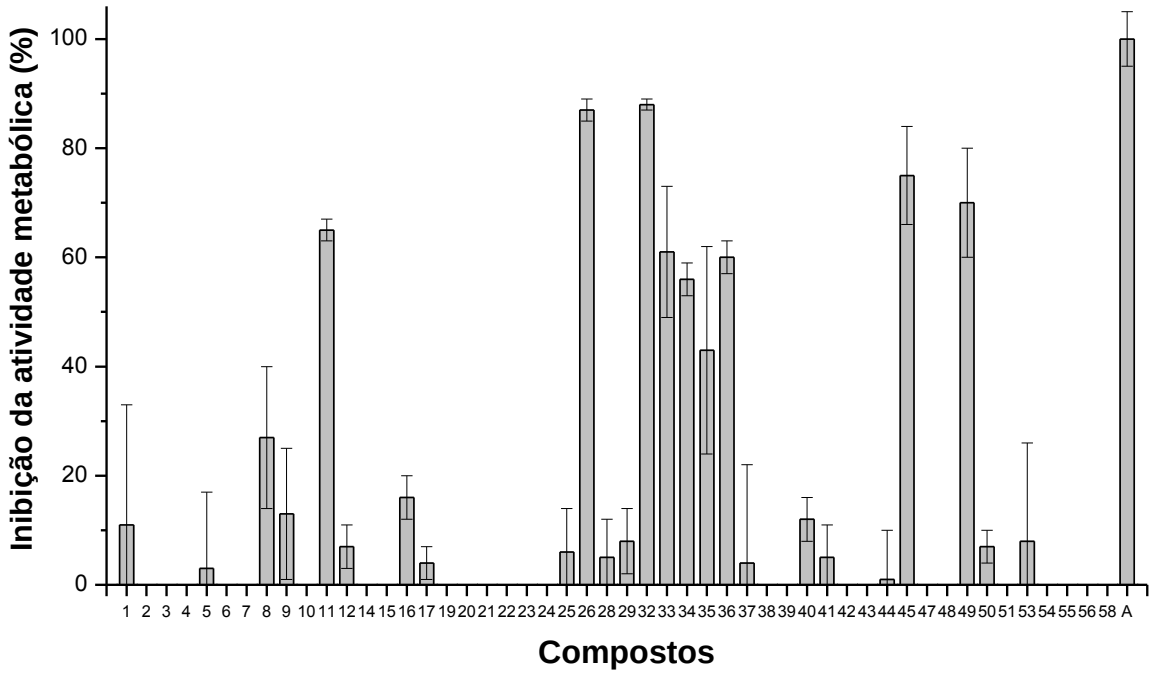

Figura V - 4. Inibição da atividade metabólica do *Fusarium oxysporum* f. sp. *cubense* por diferentes xantenodionas, tetracetonas e o composto **32** na concentração de 200 ppm. A = tiofanato metílico utilizado como controle positivo numa concentração de 500 ppm.

De maneira similar, os compostos que apresentaram maior taxa de inibição de atividade metabólica para o fungo *A. grandis* foram os mesmos obtidos para o *Foc*, exceto para o composto **45**, no qual a taxa foi de apenas 11% (Figura V-5). Apesar desta confluência nos resultados os compostos observados com maior atividade antifúgica para o fungo *A. grandis* foram o **33** e o **34**, enquanto que para o *Foc* foram o **26** e o **32**. Além disso, ao compararmos as Figuras III-4 e III-5, observa-se que o fungo *A. grandis* foi mais sensível à ação dos compostos, visto que o número de tratamentos que não apresentaram atividade foi maior para o *Foc*. Para o fungo *A. grandis* os compostos que não exerceram nenhum controle sobre o metabolismo deste microorganismos foram o **2**, **5**, **6**, **13**, **20**, **25**, **35**, **38**, **39**, **41**, **44**, **47**, **50**, **51** e **53**.

Os substituintes do núcleo xanteno que mostraram ser mais importantes em termos de atividade antifúngica foram o 3,4,5-trimetoxifenila, o 3,4-dimetoxifenila e o 5-fenil-tiofen-2-ila. Entretanto, derivados 5-isopropilcicloexan-1,3-diona contendo estes

substituintes não apresentaram atividade antifúgica consideável (acima de 50%). Já no caso das tetracetonas avaliadas os substituintes mais significativos foram o 3,4,5-trimetoxifenil, o 5-(4-clorofenil)furan-2-ila e o 5-(4-bromofenil)furan-2-ila. Além disso, vale ressaltar que o composto **32**, um derivado da dimedona contendo uma porção arilideno, apresentou a maior taxa de inibição de atividade metabólica para o *Foc* (88%) e foi a quarta maior para o fungo *A. grandis* (64%).

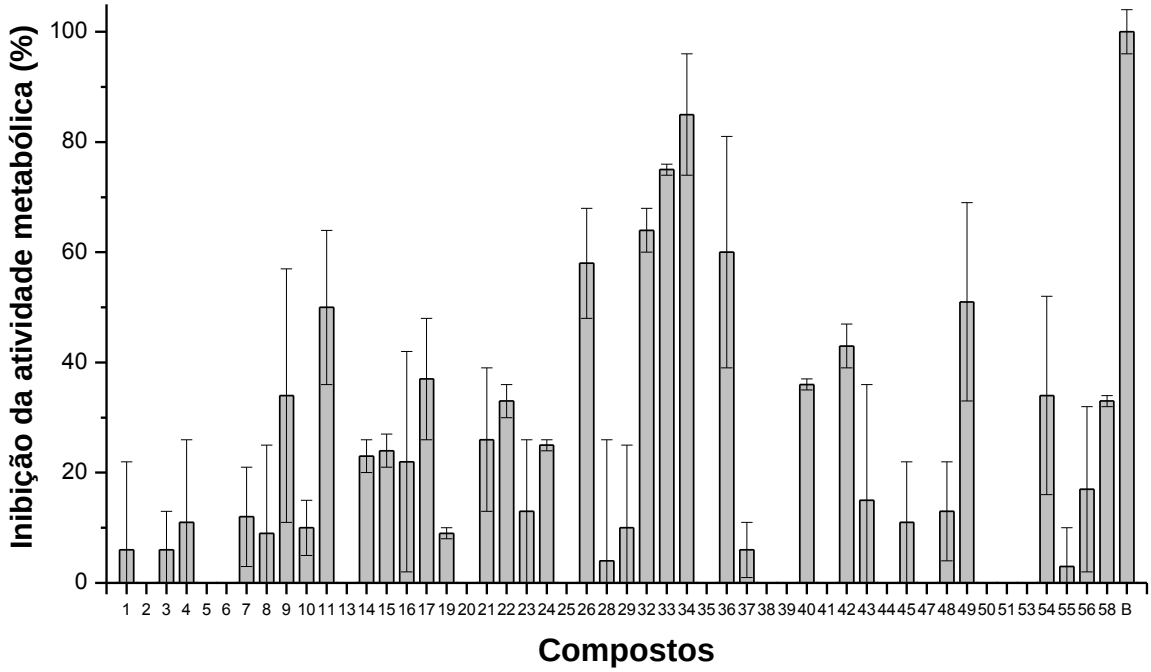

Figura V - 5. Inibição da atividade metabólica da *Alternaria grandis* por diferentes xantenodionas, tetracetonas e o composto **32** na concentração de 200 ppm. B = azoxistrobina utilizado como controle positivo numa concentração de 100 ppm.

Em geral, os ensaios baseados em resazurina foram sensíveis e reprodutíveis, demonstrando ser uma importante ferramenta para a identificação de compostos inibidores de atividade metabólica, independente da estrutura química e do modo de ação. Estes resultados são corroborados por outros relatados na literatura[22,23].

Encorajados por estes resultados todos os compostos que apresentaram uma inibição da atividade metabólica superior a 50%, para ambos os microorganismos avaliados, serão submetidos a novos experimentos para determinação da concentração

[22] HAMID, R.; ROTSHTEYN, Y.; RABADI, L.; PARIKH, R.; BULLOCK, P. Comparison of alamar blue and MTT assays for high through-put screening. *Toxicology in Vitro*, v. 18, p. 703–710, 2004.
[23] Nakayama, G. R.; Caton, M. C.; Nova, M. P.; Parandoosh, Z. Assessment of the Alamar Blue assay for cellular growth and viability in vitro. *Journal of Immunological Methods*, v. 204, p. 205–208, 1997.

mínima inibitória (IC50). A Figura II-6 mostra estes compostos bem como suas estruturas químicas.

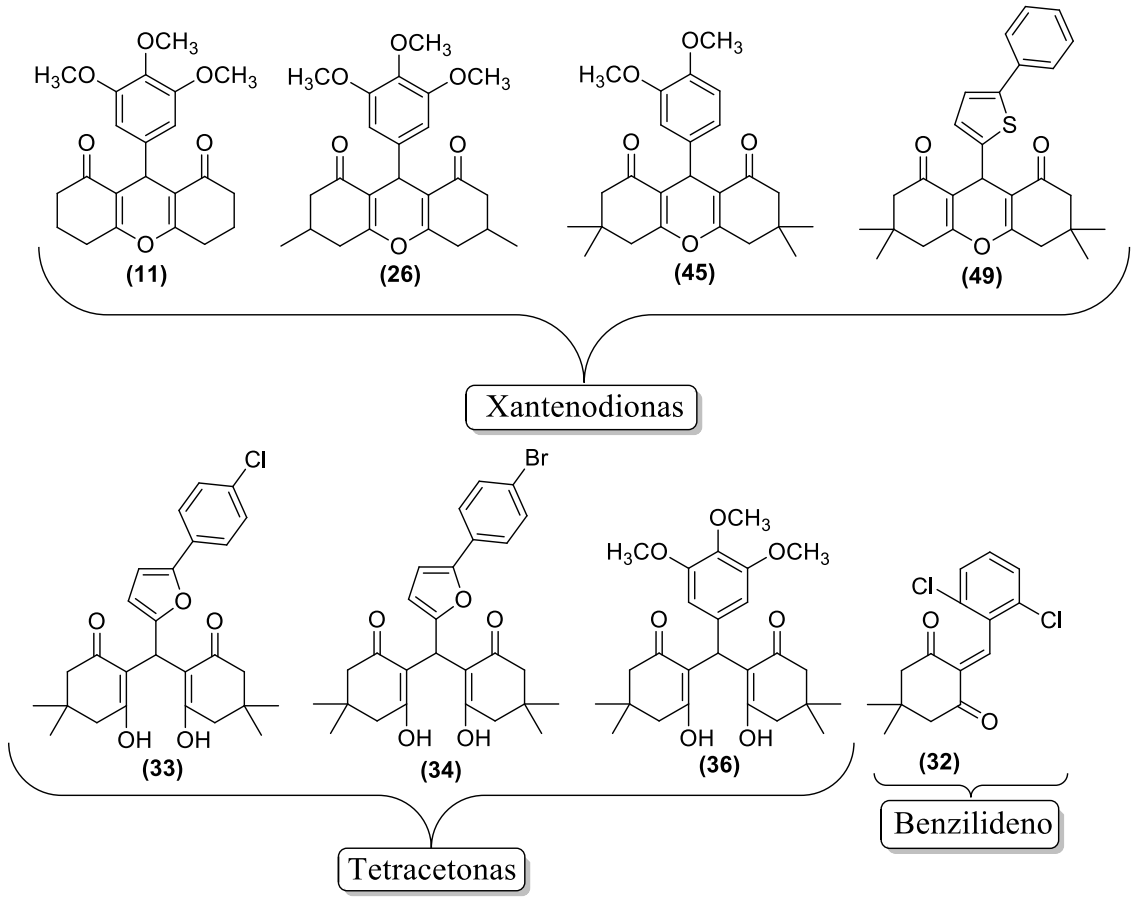

Figura V - 6. Estrutura dos compostos que serão submetidos a novos experimentos para a determinação da concentração mínima inibitória (IC50).

CAPÍTULO VI

AVALIAÇÃO DA ATIVIDADE LEISHMANICIDA DE XANTENODIONAS E TETRACETONAS

1. LEISHMANIOSE

A Leishmaniose é uma zoonose classificada como negligenciada. Ela é causada por agentes infecciosos ou parasitas e também é considerada endêmica por estar circunscrita a áreas com população de baixa renda, principalmente em regiões tropicais e subtropicais da Ásia, Oriente Médio, África e América. A taxa de mortalidade associada a esta doença tem se tornado um caso de saúde pública em pelo menos 98 países ao redor do mundo[1].

Esta doença é causada pelo protozoário do gênero *Leishmania*, que possui um ciclo de vida digenético, ou seja, vive alternadamente em hospedeiros vertebrados (mamíferos) e insetos vetores. Este parasito pode se apresentar sob a forma promastigota (alongada e com flagelo), encontrado no tubo digestivo de vetores invertebrados, ou sob a forma amastigota (arredondada e sem flagelo aparente), presente no interior das células do sistema fagocitário dos hospedeiros mamíferos, tais como macrófagos, neutrófilos, eosinófilos e células de Langerhans[2]. As formas promastigota e amastigota podem ser observados na figura VI-1[3].

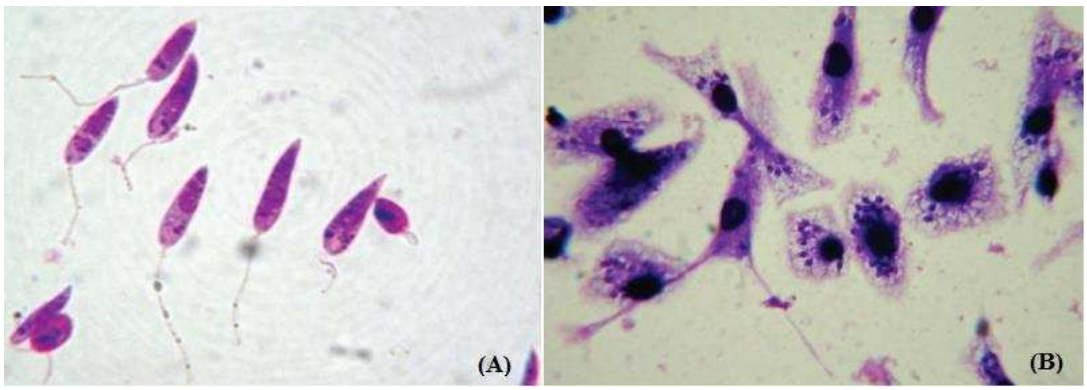

Figura VI - 1. (A) Formas promastigota coradas (aumento de 100 X sob imersão de óleo), **(B)** Macrófagos infectados (corados) com amastigotas (aumento de 100 X sob de imersão de óleo).
Fonte: GUPTA e NISHI, 2011 adaptado.

[1] World Health Organization (WHO), 2016.
[2] DOSTÁLOVÁ, A.; VOLF, P. Leishmania development in sand flies: parasite-vector interactions overview. *Parasites & Vectors*, v. 5, p. 1-12, 2012.
[3] GUPTA, S.; NISHI. Visceral leishmaniasis: Experimental models for drug discovery. *Indian Journal of Medical Research*, v. 133, p. 27-39, 2011.

O modo de transmissão habitual deste protozoário ocorre por meio da picada da fêmea dos mosquitos-palha infectados, pertencentes a subfamília dos flebotomíneos. Estes insetos são normalmente pequenos, possuindo aproximadamente 1,5-2 mm de comprimento corporal. As fêmeas são hematófagas, participam diretamente do processo de infecção e possuem importância epidemiológica. Atualmente, os gêneros *Phlebotomus* (Velho Mundo) e *Lutzomyia* (Novo Mundo) deste inseto são os únicos vetores comprovados da leishmaniose em seres humanos[4].

O ciclo da vida do parasito (Figura VI-2) se inicia quando a fêmea do vetor (flebótomineas) pica o hospedeiro vertebrado infectado. No momento do repasto sanguíneo, células parasitadas com a forma amastigota (macrófagos), contidas no tecido do hospedeiro, são ingeridas. No trato digestivo do vetor, os macrófagos se rompem e as amastigotas são liberadas e se diferenciam na forma promastigota, a qual se multiplica rapidamente. As promastigotas são transformadas em paramastigotas, as quais permanecem aderidas ao epitélio do esôfago e da faringe do vetor através do flagelo. Em seguida, estas formas diferenciam-se em promastigotas metaciclícas infectantes. Durante um novo repasto sanguíneo, a fêmea infectada regurgita as formas promastigotas metacíclicas, juntamente com sua saliva, dentro da pele do hospedeiro vertebrado. Estas formas são rapidamente fagocitadas por células do sistema mononuclear fagocitário e diferenciam-se rapidamente nas amastigotas. Posteriormente, acontece intensa multiplicação desta forma até o rompimento dos macrófagos. As amastigotas liberadas serão fagocitadas por novos macrófagos num processo contínuo. Isto leva à disseminação hematogênica para outros tecidos ricos em células do sistema mononuclear fagocitário, como linfonodos, fígado, baço e medula óssea[5].

[4] BASANO, S. A;. CAMARGO, L. M. A. Leishmaniose tegumentar americana: histórico, epidemiologia e perspectivas de controle. *Revista Brasileira de Epidemiologia*, v. 7, p. 328-337, 2004.
[5] ESCH, K. J.; PETERSEN, C. A. transmission and epidemiology of zoonotic protozoal diseases of companion animal. *Clinical Microbiology. Reviews.* v. 26, p. 58-85, 2013.

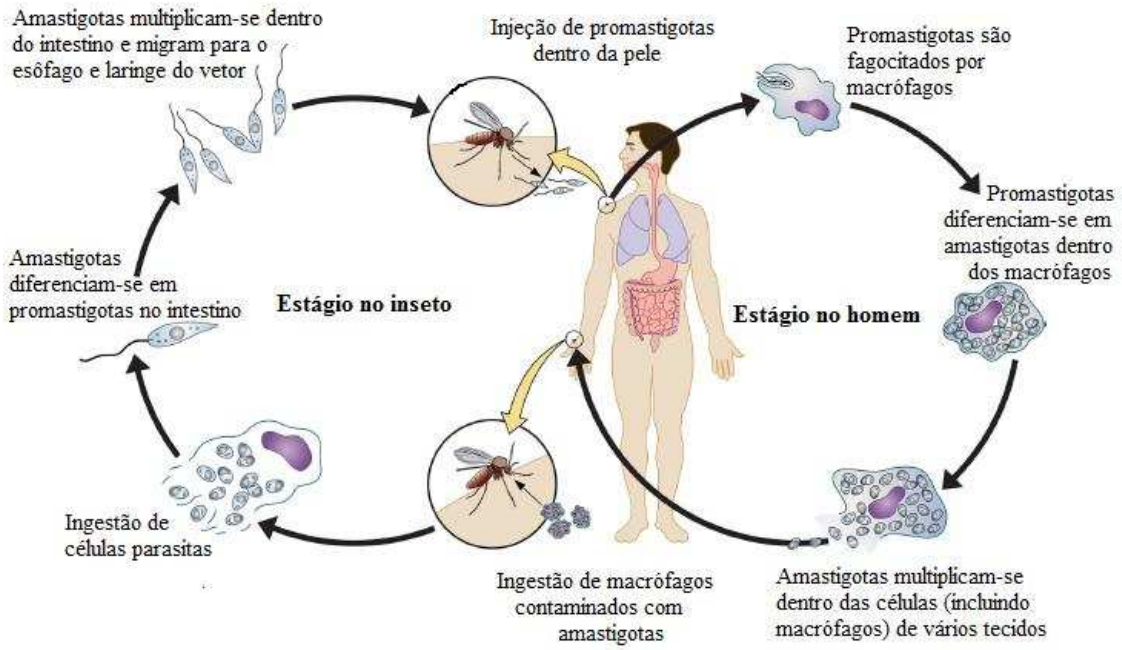

Figura VI - 2. Ciclo de vida de espécies do gênero *Leishmania*.
Fonte: ESCH e PETERSEN, 2013, adaptado.

A leishmaniose pode ser dividida em dois grandes grupos: a visceral (LV) e a tegumentar (LT). A última inclui as formas cutânea, mucocutânea e a cutânea difusa, as quais são caracterizadas por feridas na pele, principalmente em regiões descobertas do corpo, resultantes da multiplicação do parasita em células do sistema fagocitário da pele. Mais tardiamente podem surgir feridas nas mucosas do nariz, boca e garganta. Os protozoários representantes deste grupo são a *Leishmania mexicana* e a *L. brasiliensis* (Novo Mundo). No Brasil existem seis espécies de protozoários causadores da leishmaniose tegumentar, que são divididos em dois subgêneros (*Leishmania* e *Viannia*): *L.* (*Leishmania) amazonensis, L. (Viannia) braziliensis, L. (Viannia) guyanensis, L. (Viannia) lainsoni, L. (Viannia) naiffi* e *L. (Viannia) shawi*[6].

A leishmaniose visceral, popularmente conhecida como "Calazar", é uma doença sistêmica, pois acomete vários órgãos internos, principalmente o baço, o fígado e a medula óssea. Ela possui ampla distribuição e letalidade, principalmente em pacientes portadores do vírus da imunodeficiência humana (HIV), crianças desnutridas, idosos e pacientes não tratados, o que a torna de grande relevância em termos de saúde pública. A leishmaniose visceral é causada por parasitas do complexo *L. donovani* que inclui três espécies de *Leishmania*: *Leishmania (Leishmania) donovani* e *Leishmania (Leishmania)*

[6] GONTIJO, B.; CARVALHO, M. L. R. Leishmaniose tegumentar americana. *Revista da Sociedade Brasileira de Medicina Tropical*, v. 36, p. 71-80, 2003.

infantum (sinônimo *Leishmania (Leishmania) chagasi*). Nas Américas a *Leishmania (Leishmania) chagasi* é a responsável pelas formas clínicas da leishmaniose visceral[7].

No Brasil, a incidência de leishamaniose é considerada alarmante. Entre os anos de 2012 e 2014, 90% dos casos de LV detectados na América Latina foram registrados no país e, no que se refere à LT, 40% das ocorrências que estavam presentes na América como um todo. Dados do último levantamento feito em 2015 pelo Ministério da Saúde registraram 3289 casos de LV no Brasil, sendo que a maior incidência ocorreu na região nordeste, com aproximadamente 55% dos infectados. No que tange à LT, a mesma pesquisa apontou ocorrência de 19395 casos no país, mas desta vez foi a região norte a apresentar mais pessoas infectadas, representando, aproximadamente, 46% dos casos. As regiões Norte e Nordeste concentram cerca 72% do total de casos de leishmaniose (LV e LT) no país[8].

O tratamento da leishmaniose envolve terapia fotodinâmica e fármacos. Para o último observa-se o uso de antimoniais pentavalentes, sendo que no Brasil o medicamento comercializado é o antimoniato *N*-metil glucamina (Glucantime®). Apesar de ser uma droga de primeira escolha, seu uso pode ocasionar efeitos tóxicos no rim, fígado e pâncreas, mas, sobretudo no coração, podendo em alguns casos ser fatal para o paciente. Caso a resposta seja indesejada, medicamentos de segunda escolha como Anfotericina B, Aminosidina, Pentamidina e Imunoterapias com Interferon são prescritos[9]. Além de apresentarem sérios efeitos colaterais, os fármacos utilizados no tratamento da leishmaniose também apresentam custo elevado. Desta maneira, é de potencial interesse a pesquisa e o desenvolvimento de novos quimioterápicos para o tratamento desta patologia[10].

Nisar e colaboradores[11] avaliaram diferentes xantenodionas derivados da 5,5-dimetilcicloexan-1,3-diona (dimedona) contra culturas promastigotas de *Leishmania major*. Os autores observaram baixa citotoxidade e excelentes efeitos leishmanicida para os compostos contendo substituintes como 4-fluorofenila, 4-clorofenila e 4-hidroxifenila. Encorajados por estes resultados, cinquenta e duas xantenodionas, além de duas

---

[7] FOGANHOLI, J. N.; ZAPPA, V. Importância da leishmaniose na saúde pública. *Revista científica eletrônica de medicina veterinária*, 2011.

[8] PORTAL DA SAÚDE – SUS. Casos LV e Casos LT. Disponível em: http://portalsaude.saude.gov.br/

[9] RATH, S.; TRIVELIN, L. A. IMBRUNITO, T. R.; TOMAZELA, D. M.; JESÚS, M. N.; MARZAL, P. C. Antimoniais empregados no tratamento da leishmaniose: estado da arte. *Química Nova*, v.26, p. 550-555, 2003.

[10] MICHELETTI, A. C; BEATRIZ, A. Progressos Recentes na Pesquisa de Compostos Orgânicos com Potencial Atividade Leishmanicida. *Revista Virtual de Química*, v. 4, p. 268 – 286, 2012.

[11] NISAR, M.; ALI, I.; SHAH, M. R.; BADSHAH, A.; QAYUM, M.; KHAN, H.; KHAN, I.; ALI, S. Amberlite IR-120H as a recyclable catalyst for the synthesis of 1,8-dioxo-octahydroxanthene analogs and their evaluation as potential leishmanicidal agentes. *RSC Advances*, v. 3, p.21753-21758, 2013.

tetracetonas e o derivado da dimedona contendo um grupo arilideno foram avaliados contra a forma promastigota da espécie *L. (L.) amazonenses*.

2. MATERIAL E MÉTODOS

2.1 Avaliação do efeito antipromastigota das xantenodionas, das tetracetonas e do derivado da dimedona contendo uma porção arilideno.

As promastigotas de *L. (L.) amazonensis* (concentração de 2 x 10^6 promastigostas/mL) foram dispostas em placas de 96 poços contendo o meio de cultura R10 com os compostos a serem avaliados. As concentrações utilizadas nos ensaios foram 0,78; 1,56; 3,12; 6,25; 12,5; 25; 50 e 100 μg/mL. Como controle positivo utilizou-se a Anfotericina B nas concentrações 0,78; 1,56; 3,12; 6,25; 12,5; 25; 50 e 100 μg/mL. O controle negativo foi cultivado em meio com a solução veículo de DMSO (nunca superior a 1% v/v). Os parasitas foram incubados durante 24 h a 25 °C. Em seguida, adicionou-se o indicador de viabilidade celular, o PrestoBlue (Lifetechnologies). A concentração efetiva (EC_{50}), ou seja, a concentração do composto para qual 50% do efeito leishmanicida foi observado, foi estimada utilizando o software Graph Pad Prism 5.0[12].

2.2 Cultura de macrófagos peritoneais e ensaio de citotoxicidade

Aproximadamente 2 x 10^5 macrófagos peritoneais de camundongos da linhagem J774 foram cultivados em meio R10 com os compostos avaliados ou Anfotericina B nas concentrações 0,78; 1,56; 3,12; 6,25; 12,5; 25; 50 e 100 μg/mL. Como controle negativo, os macrófagos foram cultivados em meio e DMSO como solução veículo (nunca superior a 1% v/v). A placa foi mantida a 37 ºC por 24 h. Após o período de incubação, a viabilidade celular foi avaliada empregando-se o reagente PrestoBlue (Lifetechnologies). A concentração citotóxica (CC_{50}), ou seja, a concentração responsável 50% do efeito citotóxico observado, foi estimada com o software Graph Pad Prism 5.0[10]. O índice de seletividade foi calculado por meio da expressão:

$$IS = \frac{CC_{50}}{EC_{50}}$$

[12] YAMAMOTO, E. S.; CAMPOS, B. L. S.; JESUS, J. A.; LAURENTI, M. D.; RIBEIRO, S. P.; KALLÁS, E. G.; FERNANDES, M. R.; GOMES, G. S.; SILVA, M. S.; SESSA, D. P.; LAGO, J. H. G.; LEVY, D.; PASSERO, L. F. D. The Effect of Ursolic Acid on *Leishmania (Leishmania) amazonensis* is Related to Programed Cell Death and Presents Therapeutic Potential in Experimental Cutaneous Leishmaniasis. *Plos One*, v. 10, p. 1-19, 2015.

3. RESULTADOS E DISCUSSÃO

A forma promastigota de *L. amazonensis* foi exposta a diferentes concentrações dos compostos mostrados na Figura IV-3 e após o período de incubação observou-se atividade leishmanicida para os compostos **18**, **19**, **21**, **23**, **25**, **30**, **31**, **32**, **33**, **34**, **37**, **46**, **47**, **48**, **49**, **50**, **55** e **57** (Tabela VI-I, pg. 173).

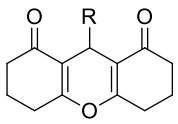

1: R = 4-Fenil
2: R = 4-Fluorofenil
3: R = 4-Clorofenil
4: R = 4-Bromofenil
5: R = 4-Trifluorometilfenil
6: R = 4-Cianofenil
7: R = 4-Nitrofenil
8: R = 4-Dimetiaminofenil
9: R = 4-Metoxifenil
10: R = 3,4-Dimetoxifenil
11: R = 3,4,5-Trimetoxifenil
12: R = 4-hidroxifenil
13: R = 4-Hidroxi-3-metoxifenil
14: R = Benzo[d][1,3]dioxol-5-il
15: R = 5-(4-clorofenil)furan-2-il
16: R = 5-(4-bromofenil)furan-2-il
17: R = 5-Fenil-tiofen-2-il

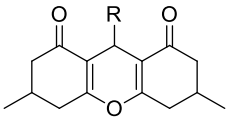

18: R = 4-Fenil
19: R = 4-Fluorofenil
20: R = 4-Clorofenil
21: R = 4-Bromofenil
22: R = 4-Trifluorometilfenil
23: R = 4-Cianofenil
24: R = 4-Nitrofenil
25: R = 4-Metoxifenil
26: R = 3,4,5-Trimetoxifenil
27: R = 4-hidroxifenil
28: R = 4-Hidroxi-3-metoxifenil
29: R = Benzo[d][1,3]dioxol-5-il
30: R = 5-(4-clorofenil)furan-2-il
31: R = 5-(4-bromofenil)furan-2-il

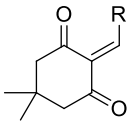

32: R =2,6-Diclorofenil

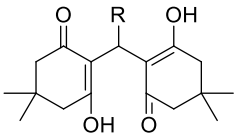

33: R = 5-(4-clorofenil)furan-2-il
34: R = 5-(4-bromofenil)furan-2-il

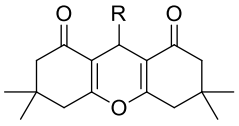

37: R = Fenil
38: R = 4-Fluorofenil
39: R = 4-Clorofenil
40: R = 4-Bromofenil
41: R = 4-Trifluorometilfenil
42: R = 4-Cianofenil
43: R = 4-Nitrofenil
44: R = 4-Metoxifenil
45: R = 3,4-Dimetoxifenil
46: R = 4-hidroxifenil
47: R = 4-Hidroxi-3-metoxifenil
48: R = Benzo[d][1,3]dioxol-5-il
49: R = 5-Fenil-tiofen-2-il

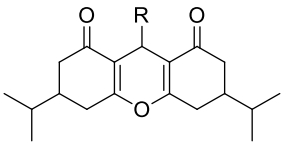

50: Fenil
51: R = 4-Fluorofenil
53: R = 4-Bromofenil
54: R = 4-Trifluorometilfenil
55: R = 4-Cianofenil
56: R = 4-Nitrofenil
57: R = 4-hidroxifenil
58: R = 5-Fenil-tiofen-2-il

Figura VI - 3. Compostos que tiveram sua atividade leishmanicida avaliada.

Para os compostos que apresentaram atividade leishmanicida foram determinados os valores EC_{50}, conforme definido na seção 2.1. Foram realizados ainda ensaios de avaliação de citotoxicidade contra macrófagos para determinação dos valores de CC_{50}, conforme definido na seção 2.2.

De maneira geral, as xantenodionas não apresentaram citotoxidade frente aos macrófagos na concentração avaliada, exceto o composto **49**. Com respeito aos intermediários tetracetônicos , (**33** e **34**) e o derivado da dimedona contendo a porção

arilideno (**32**), todos apresentaram alguma citotoxicidade. Apesar disso, estes intermediários estão entre os cinco compostos que apresentaram atividade leishmanicida mais pronunciada (**31**, **32**, **33**, **34** e **50**), sendo o **33** o composto mais ativo. Estas substâncias apresentaram valores de EC_{50} abaixo de 50 μg/mL.

Do ponto de vista da relação estrutura-atividade, observou-se que aqueles compostos derivados da 5-metilcicloexan-1,3-diona e da 5,5-dimetilcicloexan-1,3-diona (dimedona) foram os mais ativos quando comparados com derivados da 5-isopropilcicloexan-1,3-diona e da cicloexan-1,3-diona. Exceção a esta generalização são os compostos **50**, **55** e **57**.

Conforme destacado na introdução deste capítulo, Nisar e colaboradores avaliaram a atividade leishmanicida de xantenodionas derivadas da dimedona contra culturas promastigotas de *Leishmania major*. No trabalho descrito por estes autores, os compostos contendo os substituintes 4-fluorofenila, 4-clorofenila, e 4-hidroxifenila foram os mais ativos e apresentaram valores de EC_{50} iguais a 3,1, 6,7 e 8,3 μg/mL, respectivamente. Dentre os compostos descritos por Nisar e colaboradores como sendo os mais efetivos em termos de atividade leishmanicida, no presente trabalho de investigação a única xantenodiona que apresentou atividade na dosagem de 0,78 a 100 μg/mL foi aquela contendo o grupo 4-hidroxifenila (**46**); entretanto o valor de EC_{50} foi de 95,52 μg/mL, valor bem mais elevado que o descrito pelo grupo de Nisar para esta mesma substância. Cumpre ressaltar que as espécies de leishmania utilizadas neste trabalho e na investigação descrita pelo grupo de Nisar são diferentes.

De posse dos dados de EC_{50} e CC_{50} foi possível calcular os índices de seletividade (IS) e estes são apresentados na Tabela VI-1. Este permite mensurar a seletividade de um dado composto entre os parasitos (promastigotas) e os macrófagos, indicando seu potencial uso em testes clínicos. Neste estudo, os compostos que apresentaram valores de IS maiores ou iguais a 2,0 foram o **31**, **32** e o **33**. Isto significa que estes compostos são pelo menos duas vezes mais ativos contra a forma promastigota que para os macrófagos.

Tabela VI - 1. Resultados da avaliação da atividade leishmanicida contra promastigotas de *Leishmania amazonensis* e da citotoxicidade contra macrofágos e índice de seletividade.

Compostos	**Promastigotas EC_{50} (μg/mL)**	**Macrófagos CC_{50} (μg/mL)**	**Índice de seletividade (IS)**
18	81,45 ± 3,54	>100	≥1,23
19	68,11 ± 5,22	>100	≥1,47
21	98,51 ± 6,14	>100	≥1,01
23	89,08 ± 3,82	>100	≥1,12
25	79,13 ± 2,86	>100	≥1,26
30	58,80 ± 1,81	>100	≥1,70
31	41,72 ± 3,52	>100	≥2,40
32	38,95 ± 3,83	96,90 ± 10,23	2,49 ± 0,51
33	27,08 ± 8,87	72,25 ± 8,45	2,67 ± 1,19
34	49,31 ± 6,32	57,04 ± 7,23	1,16 ± 0,29
37	64,66 ± 5,21	>100	≥1,55
46	92,52 ± 1,06	>100	≥1,08
47	84,11 ± 2,49	>100	≥1,19
48	72,15 ± 4,14	>100	≥1,39
49	71,97 ± 4,85	68,73 ± 2,34	0,95 ± 0,10
50	44,54 ± 8,04	>100	≥2,24
55	74,78 ± 6,09	>100	≥1,34
57	54,78 ± 0,84	>100	≥1,82
Anfotericina B	0,7 ± 0,2	57,300 ± 9,300	81,85 ± 36,67

Os resultados obtidos na avaliação da atividade leishmanicida demonstraram que as xantenodionas não foram tão ativas para *Leishmania amazonenses* quanto os resultados encontrados para a *Leishmanina major* descrita por Nisar e colaboradores. Em contrapartida o intermediário **32** e o tetracetônico (**33**) foram os mais promissores em termos de atividade. Apesar disso, o EC50 destes dois compostos foi muito maior que fármaco atualmente utilizado no tratamento da leishmaniose (Anfotericina B).

Ensaios de avaliação da atividade leishmanicida destes compostos contra culturas amastigotas de *L. amazonensis* estão em andamento na Unesp em colaboração com o professor Dr. Felipe Passero.

CONSIDERAÇÕES FINAIS

O desenvolvimento deste trabalho resultou na síntese de cinquenta e oito compostos, sendo cinquenta xantenodionas, quatro tetracetonas e um derivado da dimedona contendo uma porção arilideno. Contribuiu-se para a expansão do escopo do processo de preparação de xantenodionas catalisado por zircônio na ausência de solvente. Na maioria das reações, os produtos obtidos a partir da condensação de aldeídos e 1,3-dicetonas foram xantenodionas. Os rendimentos variaram de 34% - 99% e os tempos de reação entre 15 e 120 minutos. Entretanto, em algums casos, derivados tetracetônicos foram obtidos. Deste modo, o processo catalisado por zircônio representa uma alternativa para a síntese destes últimos. Os rendimentos alcançados para a síntese das tetracetonas e do derivado da dimedona contendo uma porção arilideno foram de 33% – 73% e os tempos de reação variaram de 40 a 135 minutos. Além disso, é importante destacar que dentre as xantenodionas sintetizadas, aquelas derivadas da 5-isopropilcicloexan-1,3-diona e da 5-metilcicloexan-1,3-diona, bem como aquelas derivadas dos aldeídos 5-(4-clorofenil)furanilbenzaldeído, 5-(4-bromofenil)furanilbenzaldeído e 5-fenil-tiofen-2-ilbenzaldeído ainda não foram descritas na literatura.

O presente trabalho contribuiu ainda para ampliar o conhecimento a respeito de aspectos estruturas das xantenodionas bem como de derivados tetracetônicos. Tal fato é de relevância uma vez que o entendimento sobre características estruturais de compostos é de utilidade para estudos de correlação estrutura química-atividade biológica.

Os compostos sintetizados foram submetidos a ensaios de avaliação de atividade fungicida e oito deles apresentaram inibição da atividade metabólica superior a 50% para *A. grandis* e *F. oxysporum f.* sp. *cubense,* sendo o 2,2'-((5-(4-bromofenil)furan-2-il)metileno)*bis*(3-hidroxi-5,5-dimetilcicloex-2-enona) (85%) e o 2-(2,6-diclorobenzilideno)-5,5-dimetilcicloexan-1,3-diona (88%) mais ativos respectivamente. No que diz respeito aos testes de avaliação da atividade leshmanicida observou-se baixo efeito citotóxico e o composto mais ativo também é um intermediário de reação, o 2,2'-((5-(4-clorofenil)furan-2-il)metileno)*bis*(3-hidroxi-5,5-dimetilcicloex-2-enona) (EC50 = 27,08 ± 8,87). Outros ensaios visando a complementariedade dos resultados apresentados encontram-se em andamento.

ANEXOS

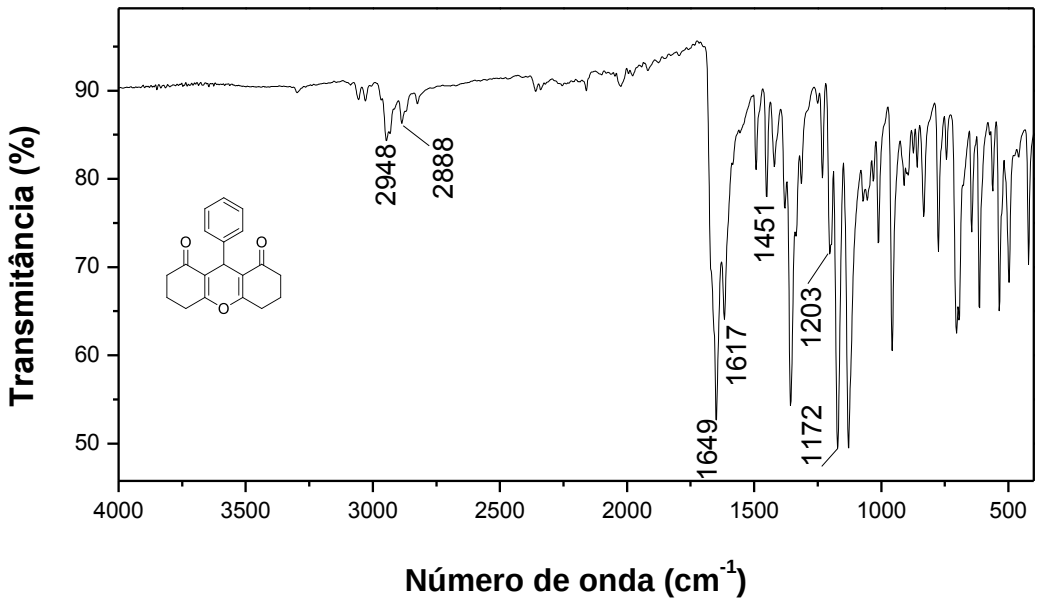

Figura 1. Espectro no infravermelho (ATR) do composto **1**.

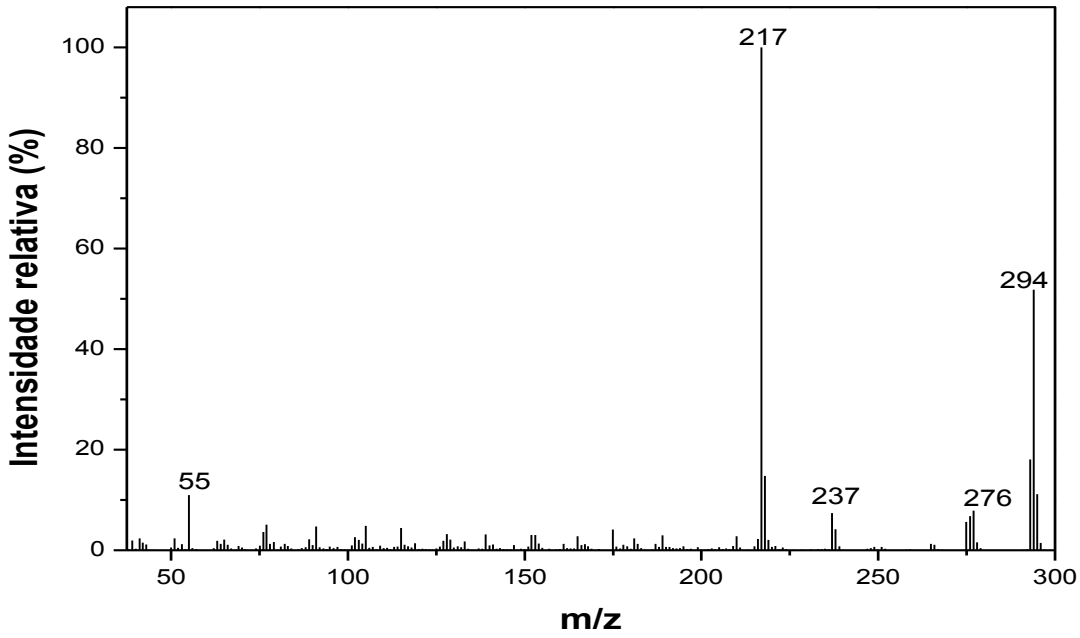

Figura 2. Espectro de massas do composto **1**.

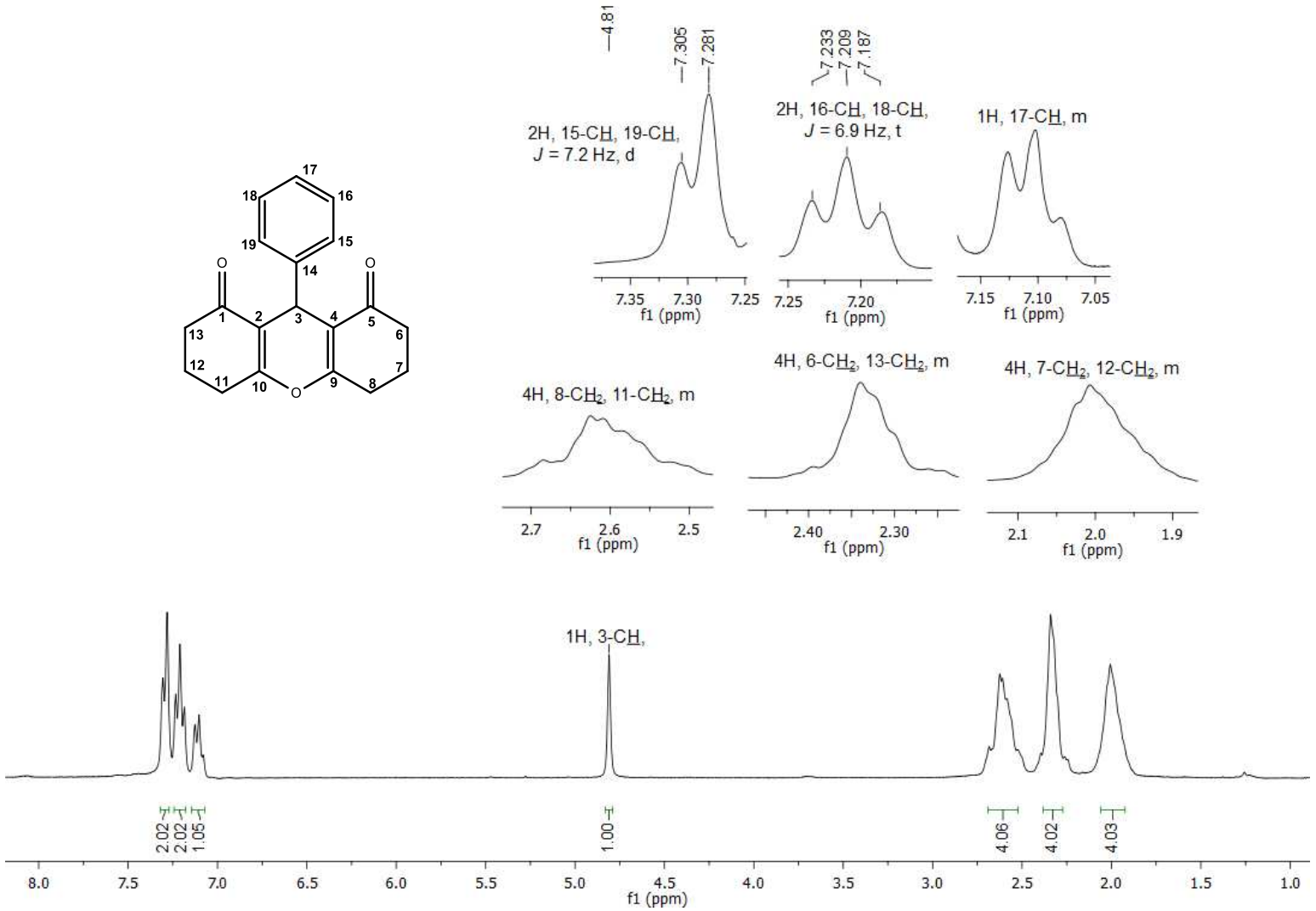

Figura 3. Espectro de RMN de ^{1}H (300 MHz, $CDCl_3$) do composto **1**.

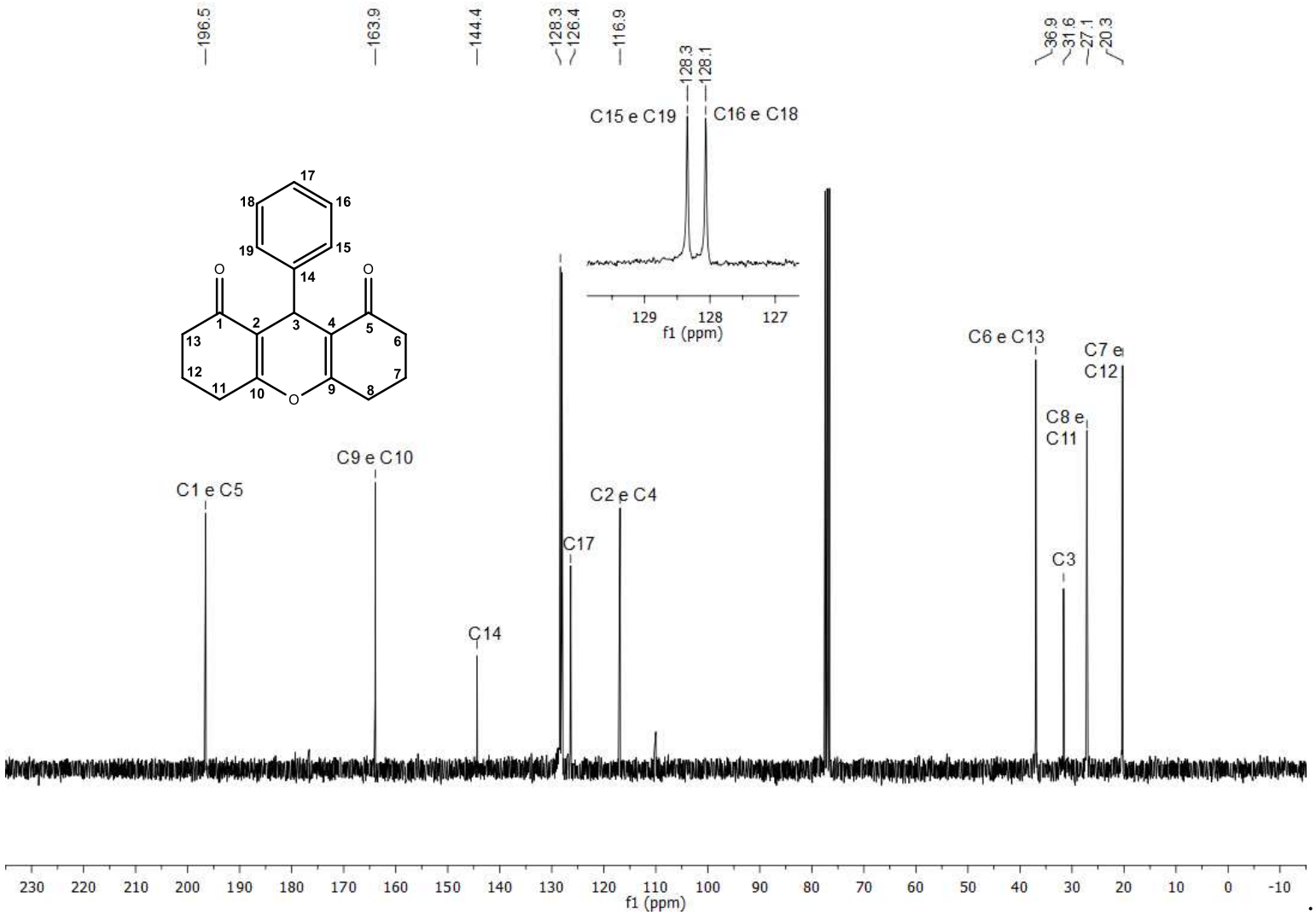

Figura 4. Espectro de RMN de ^{13}C (75 MHz, $CDCl_3$) do composto **1**.

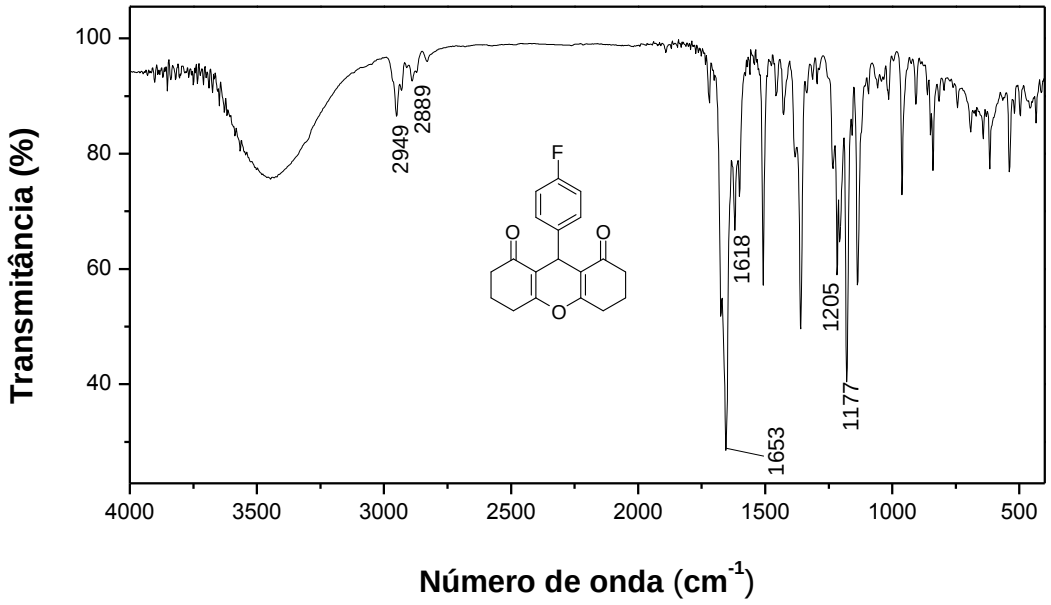

Figura 5. Espectro no infravermelho (KBr) do composto **2**.

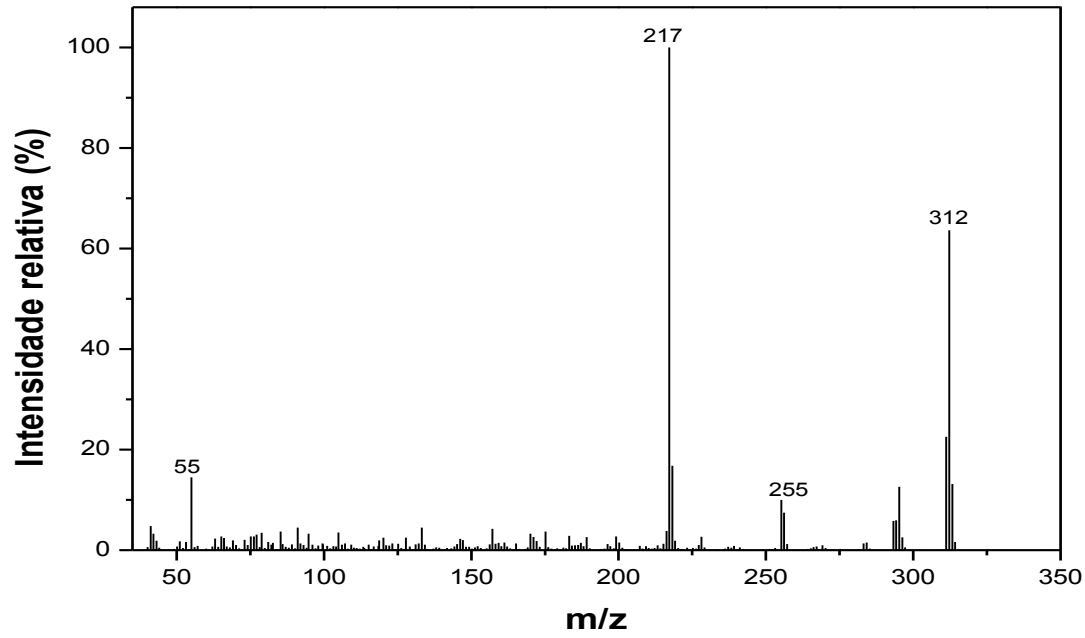

Figura 6. Espectro de massas do composto **2**.

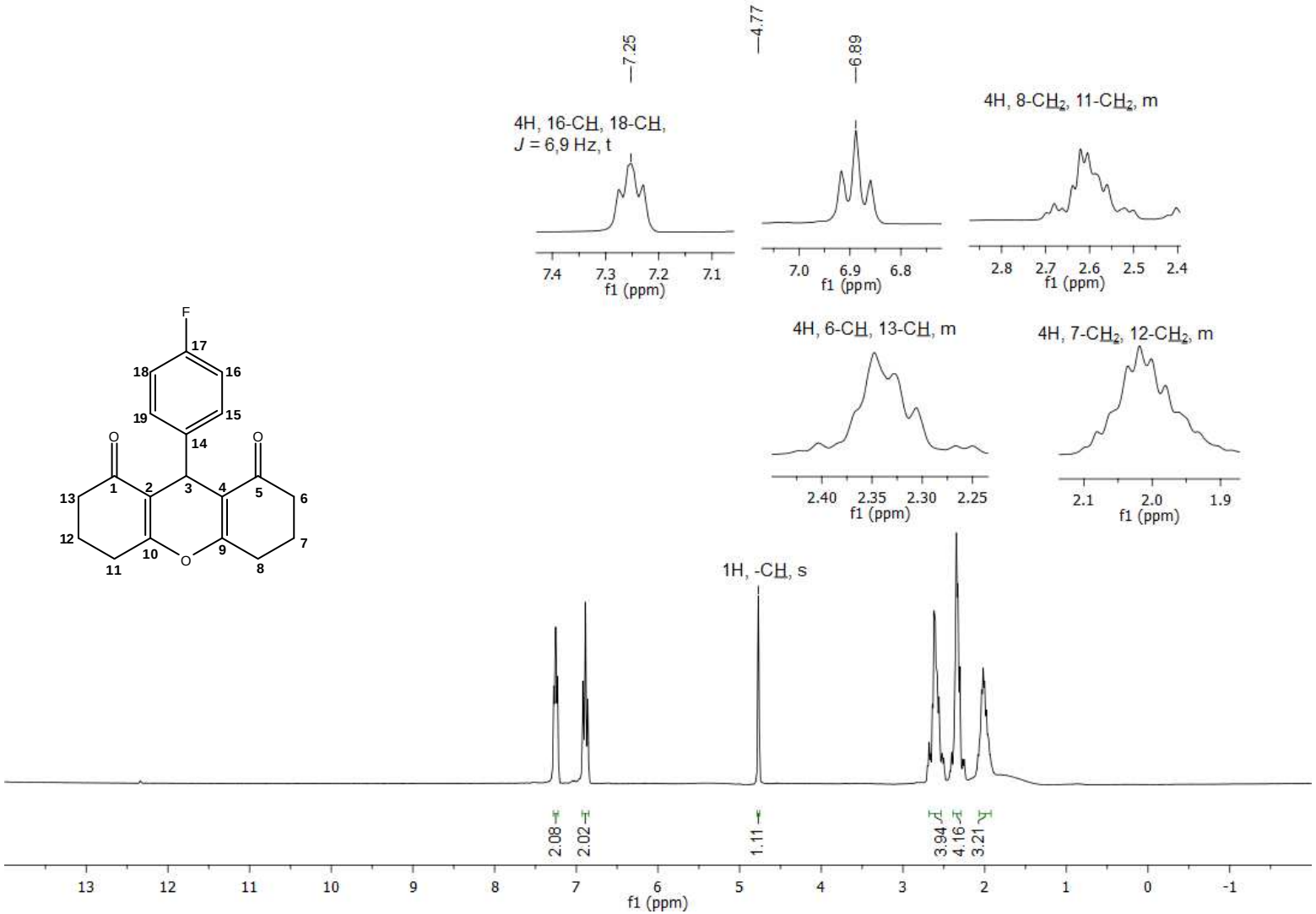

Figura 7. Espectro de RMN de ^{1}H (300 MHz, $CDCl_3$) do composto **2**.

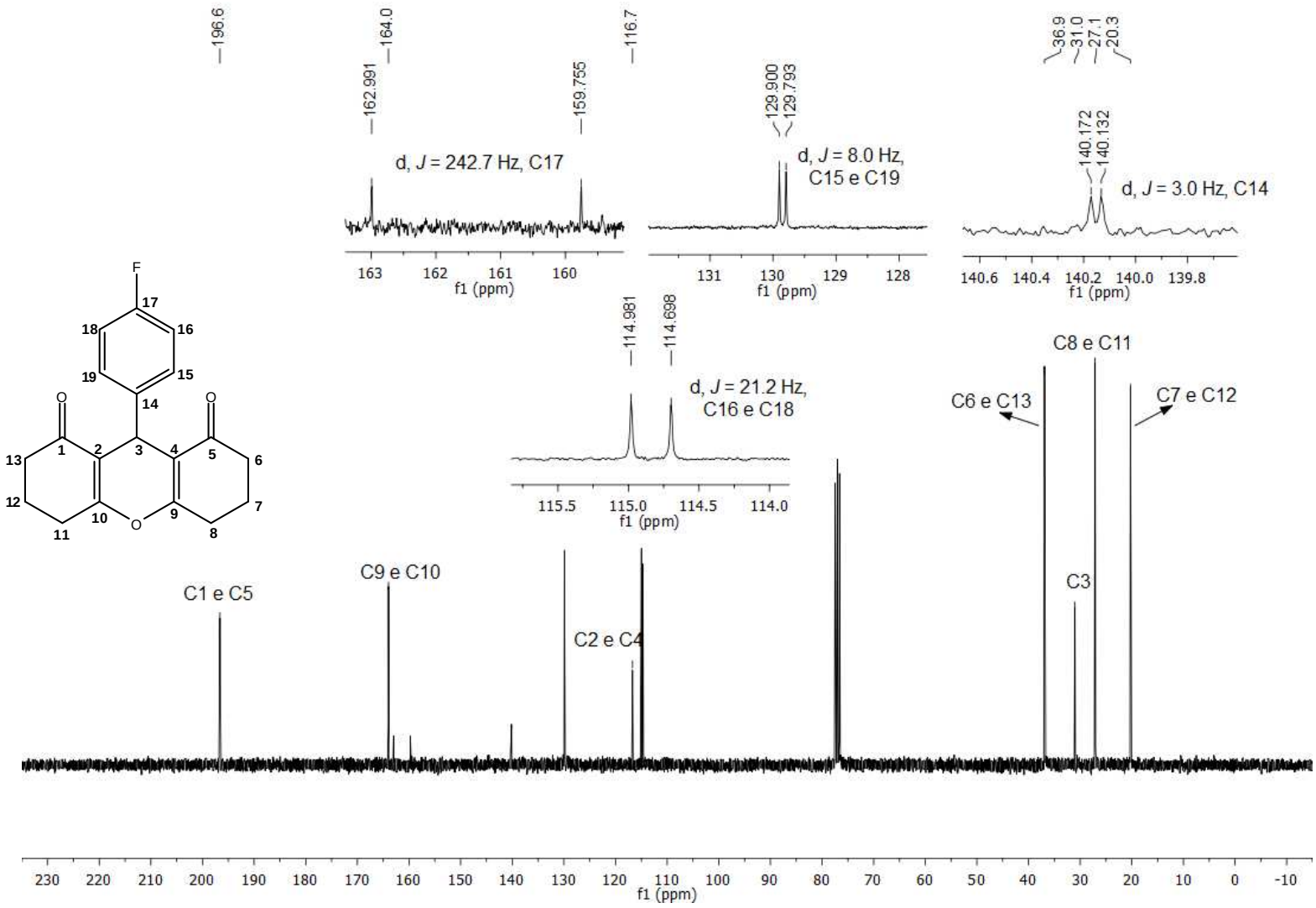

Figura 8. Espectro de RMN de ^{13}C (75 MHz, $CDCl_3$) do composto **2**.

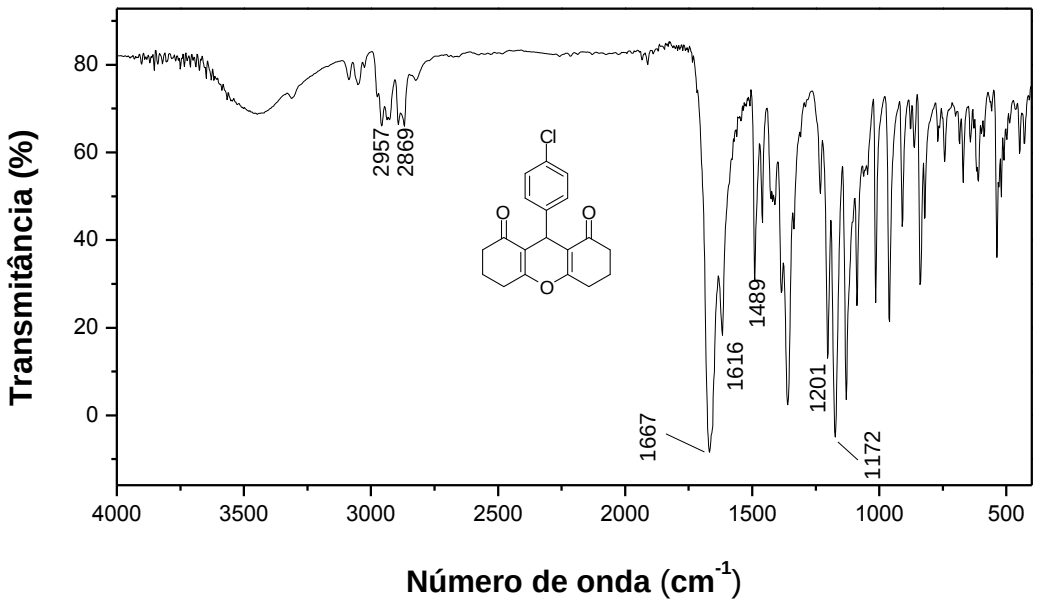

Figura 9. Espectro no infravermelho (KBr) do composto **3**.

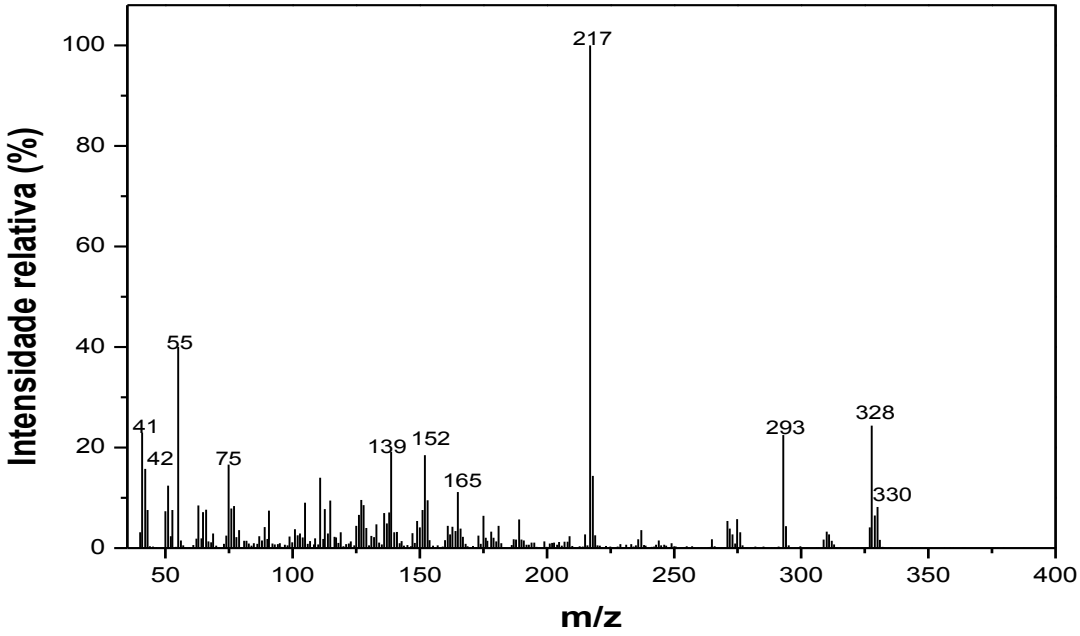

Figura 10. Espectro de massas do composto **3**.

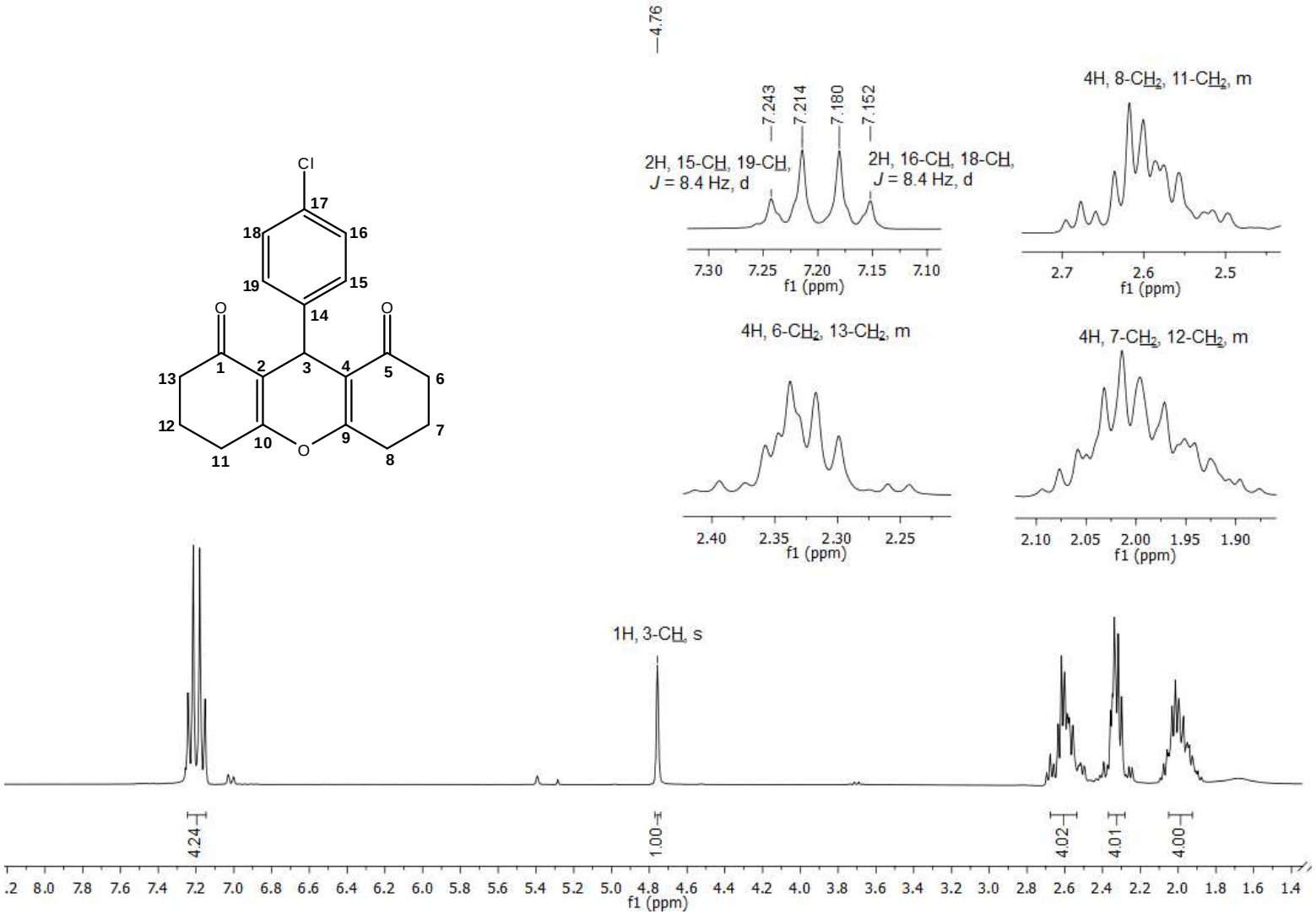

Figura 11. Espectro de RMN de ^{1}H (300 MHz, $CDCl_3$) do composto **3**.

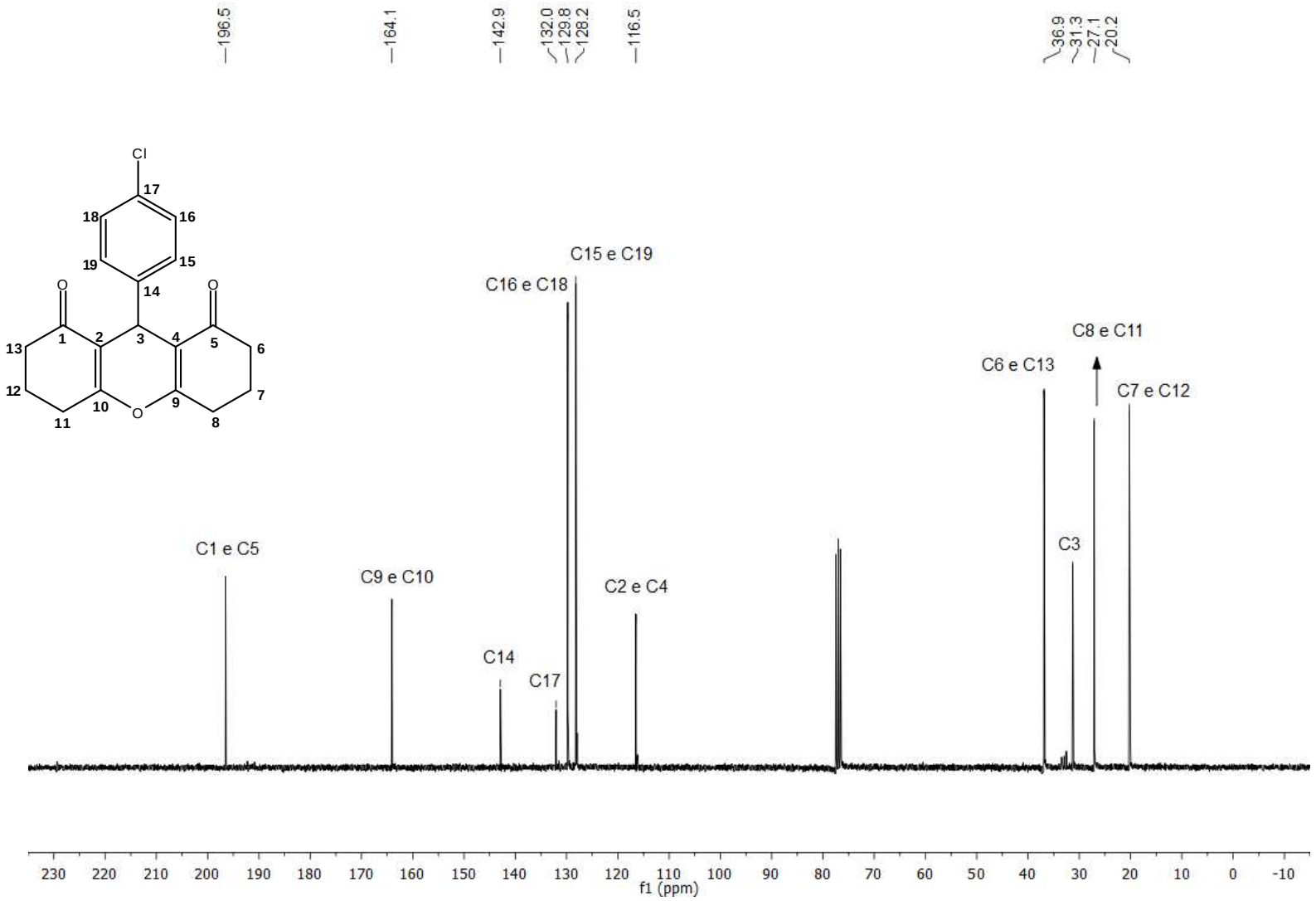

Figura 12. Espectro de RMN de ^{13}C (75 MHz, $CDCl_3$) do composto **3**.

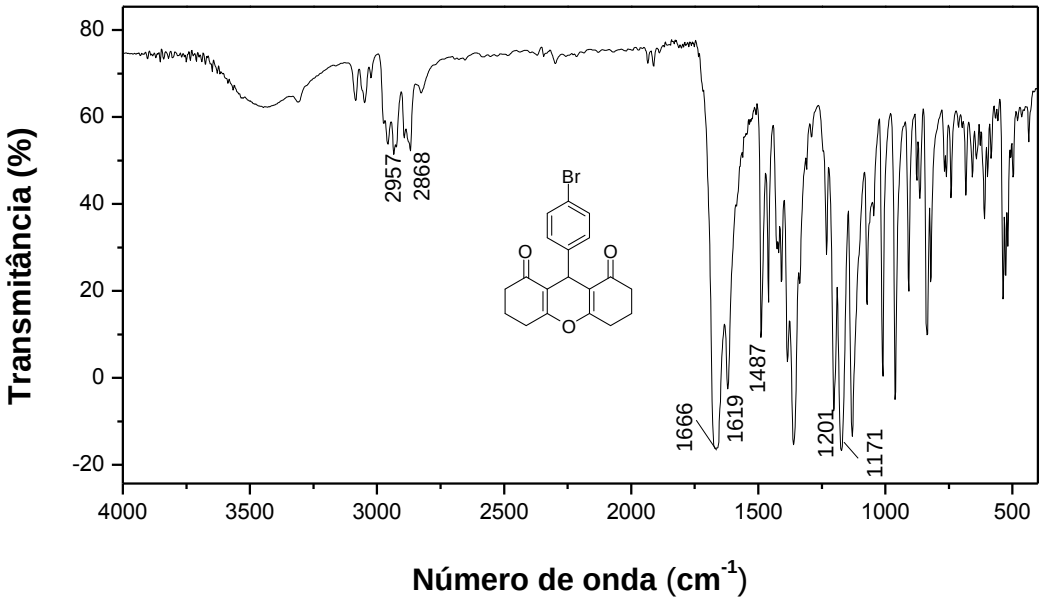

Figura 13. Espectro no infravermelho (KBr) do composto **4**.

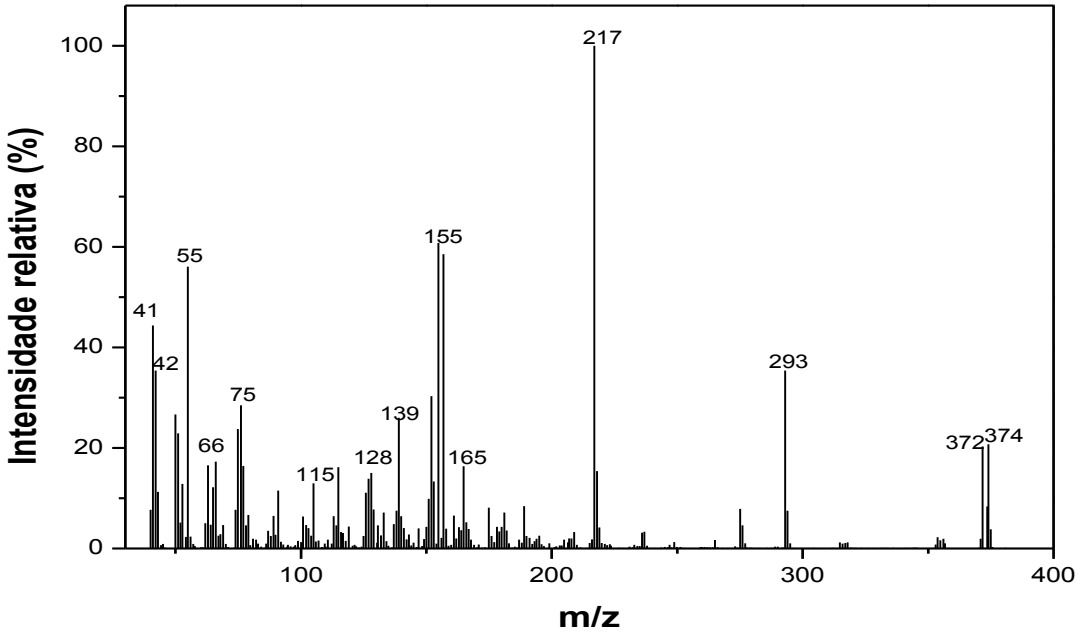

Figura 14. Espectro de massas do composto **4**.

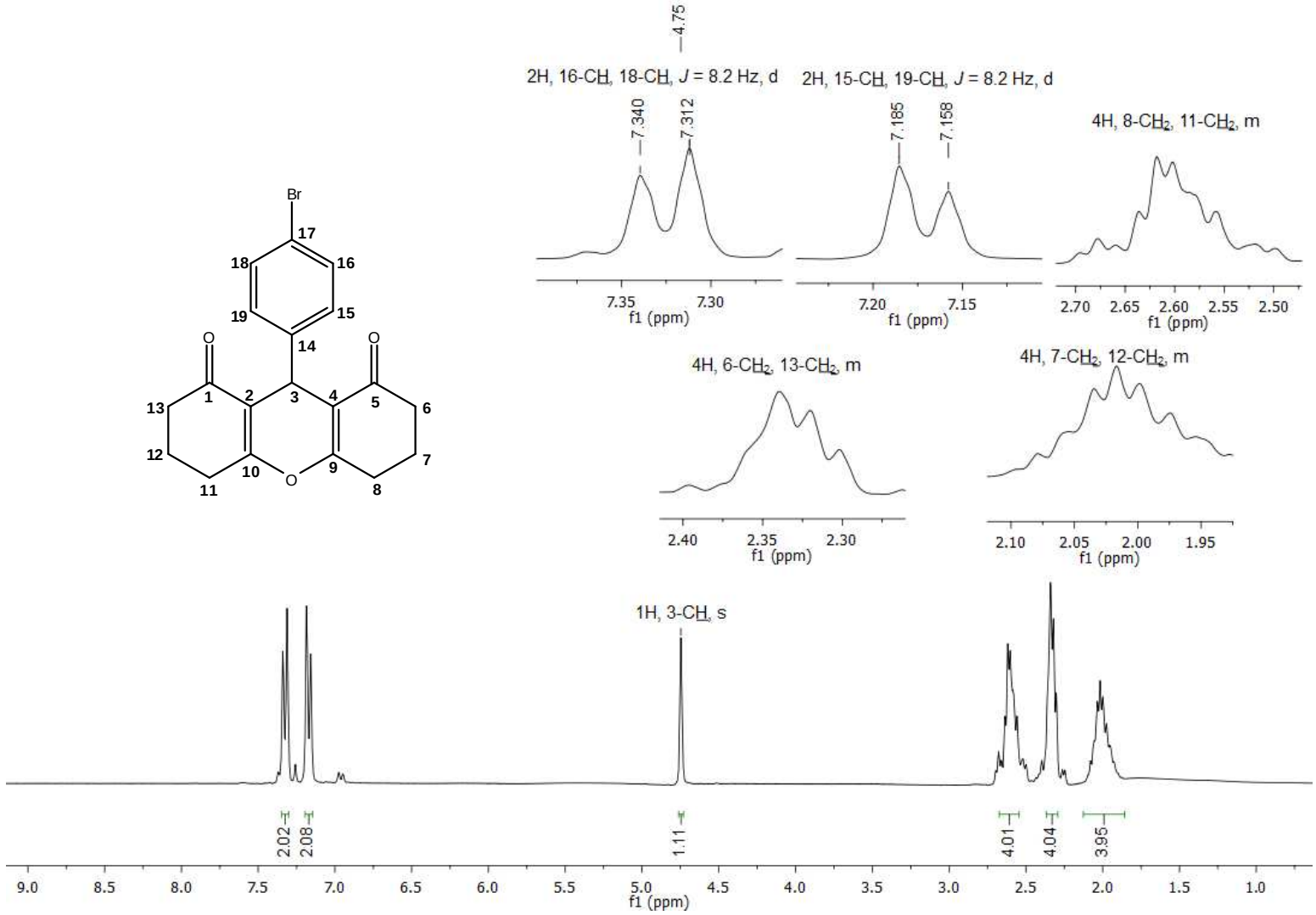

Figura 15. Espectro de RMN de ^{1}H (300 MHz, $CDCl_3$) do composto **4**.

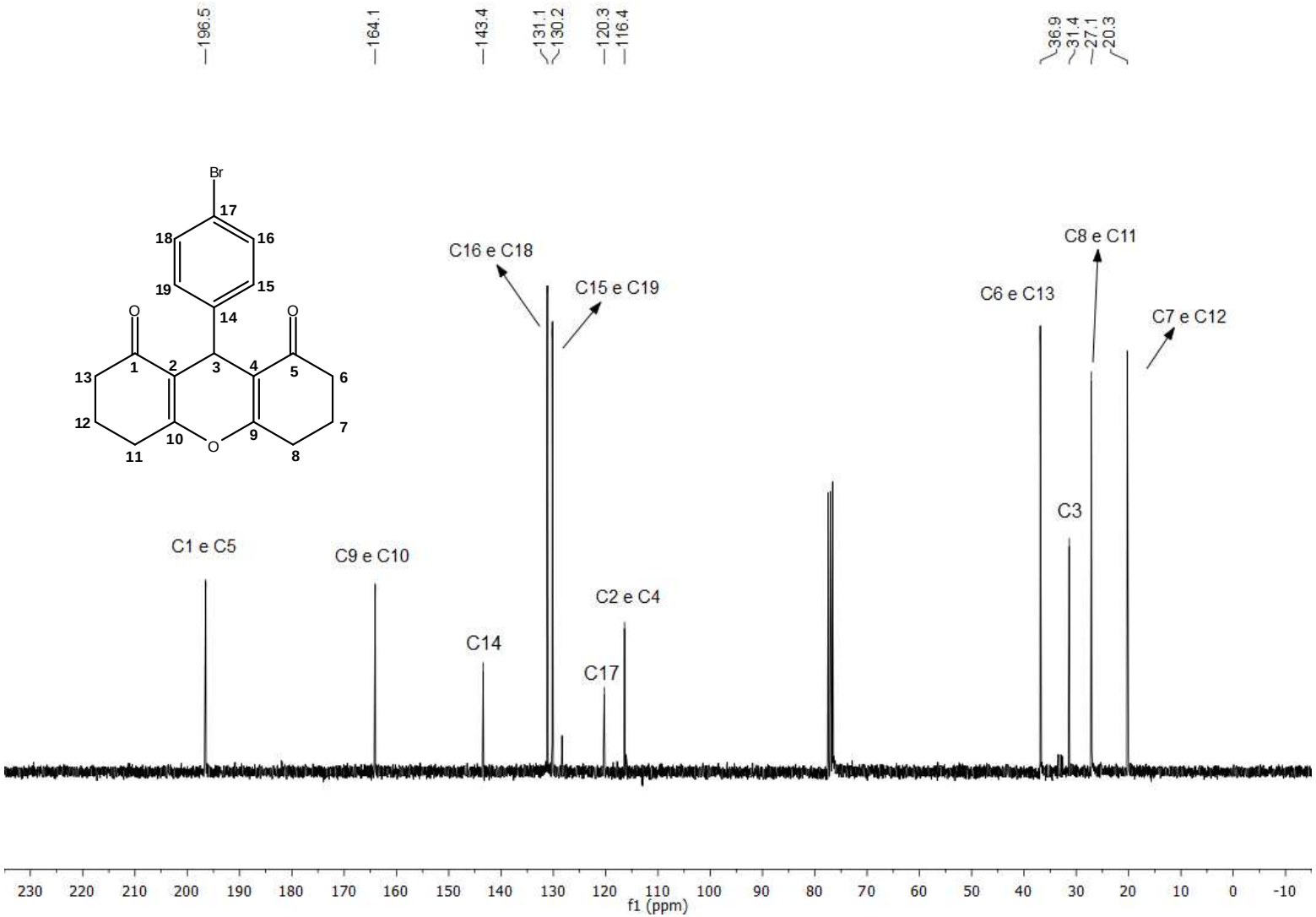

Figura 16. Espectro de RMN de ^{13}C (75 MHz, $CDCl_3$) do composto **4**.

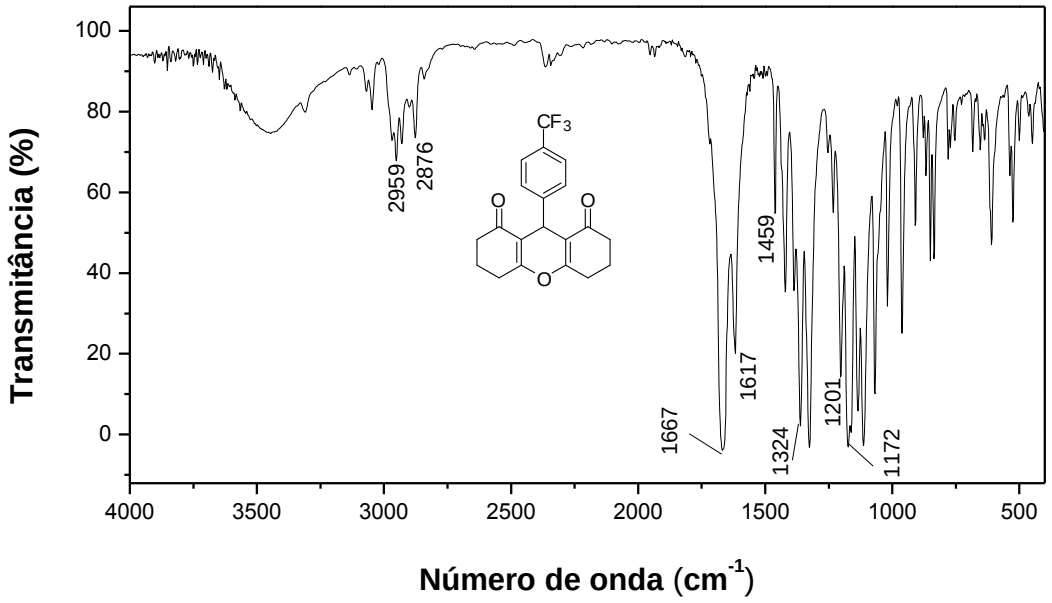

Figura 17. Espectro no infravermelho (KBr) do composto **5**.

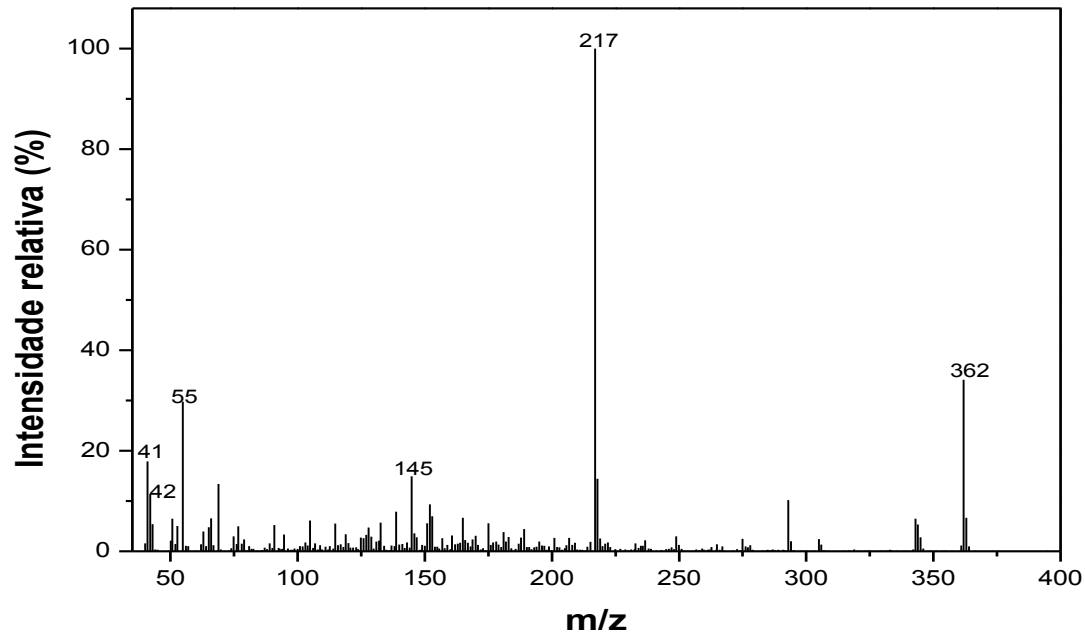

Figura 18. Espectro de massas do composto **5**.

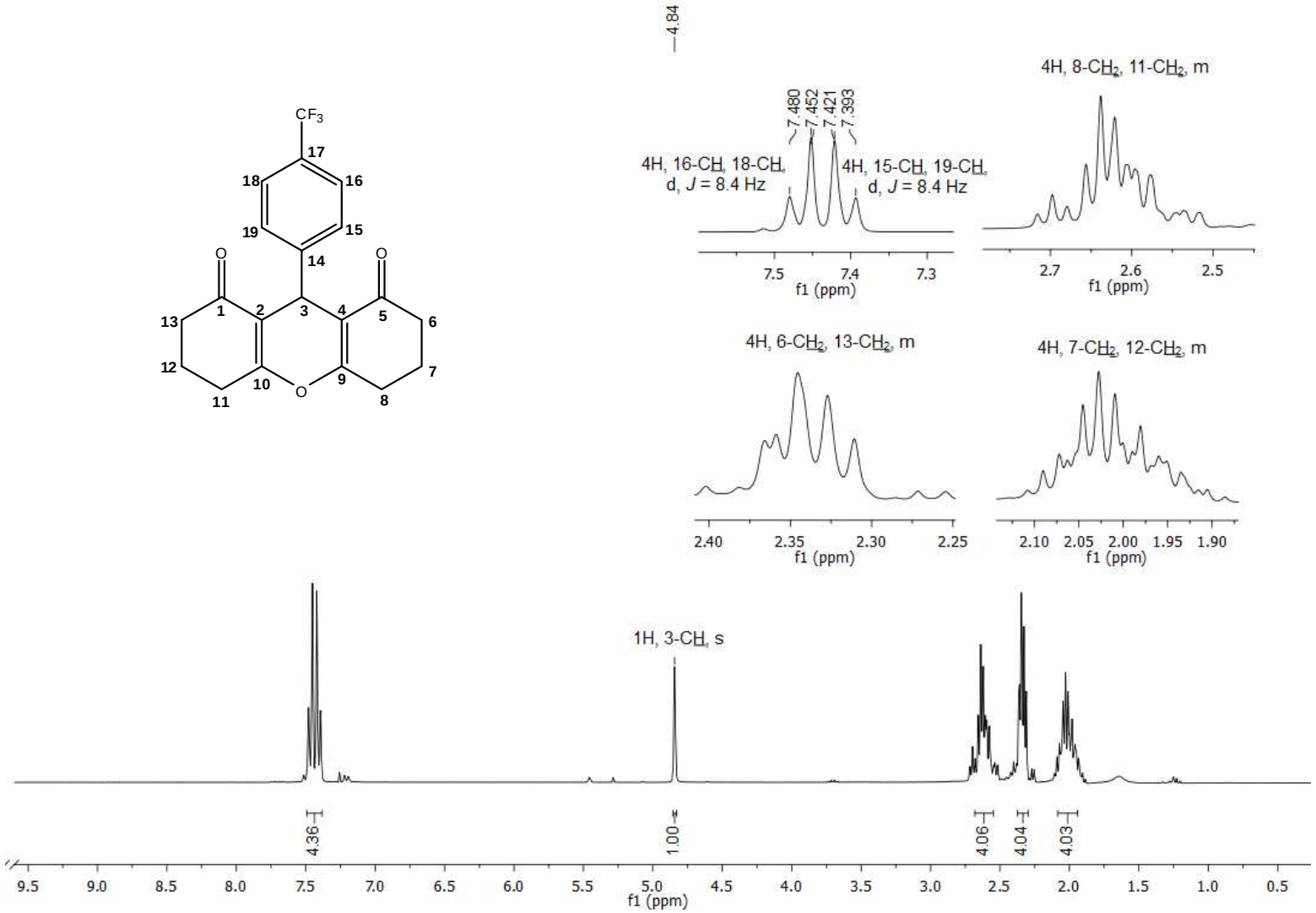

Figura 19. Espectro de RMN de ^{1}H (300 MHz, $CDCl_3$) do composto **5**.

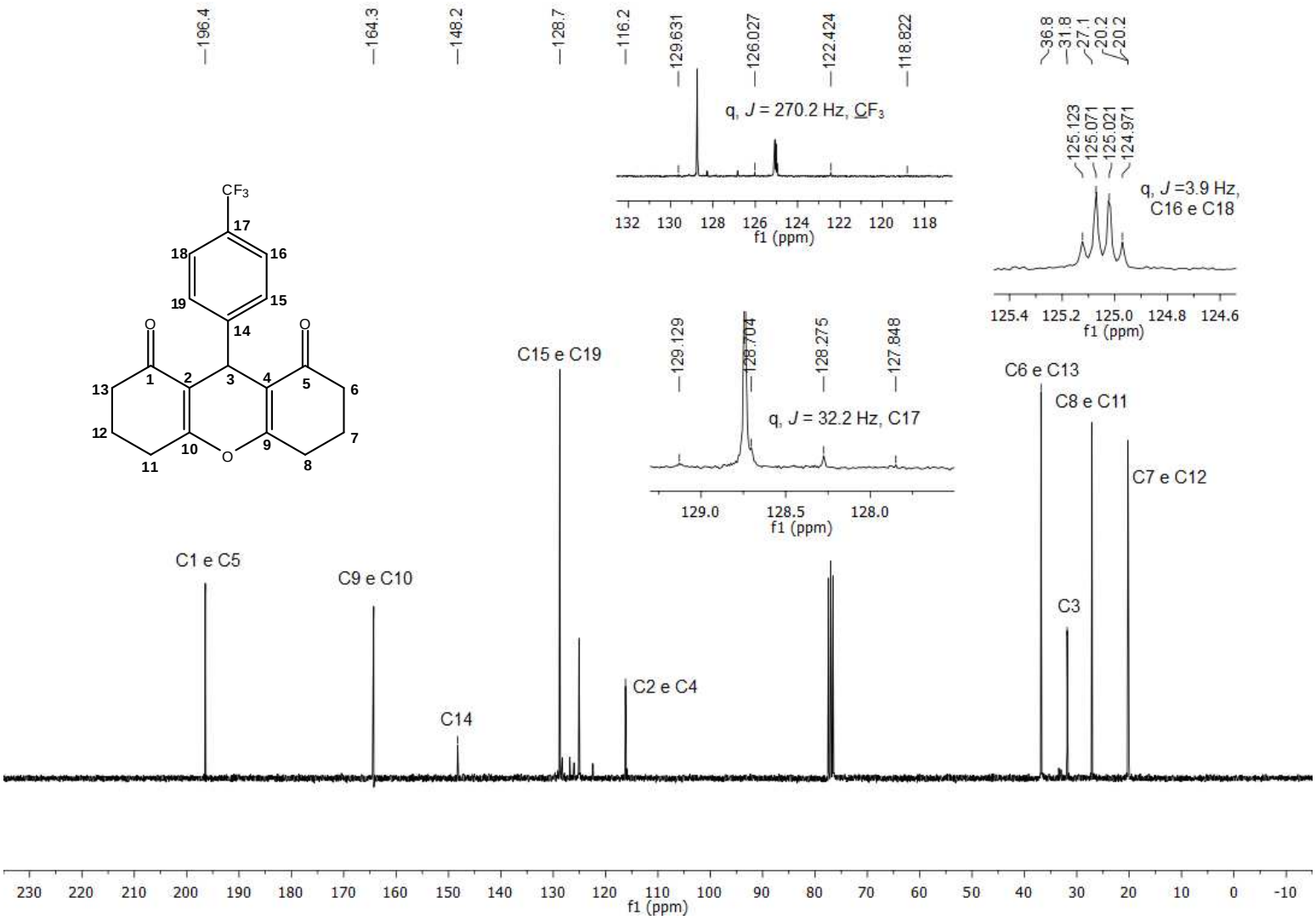

Figura 20. Espectro de RMN de ^{13}C (75 MHz, $CDCl_3$) do composto **5**.

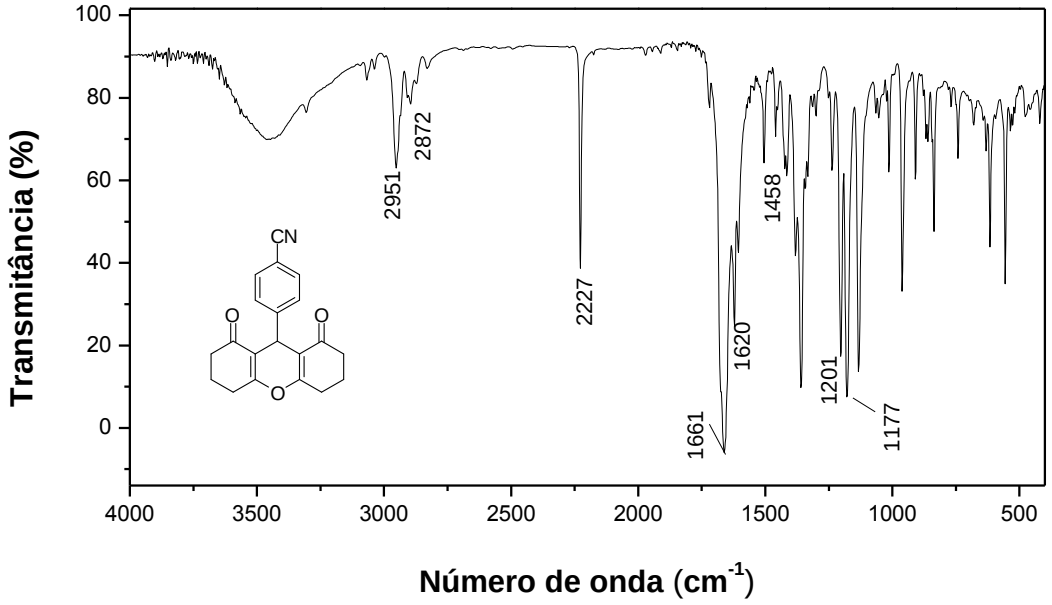

Figura 21. Espectro no infravermelho (KBr) do composto **6**.

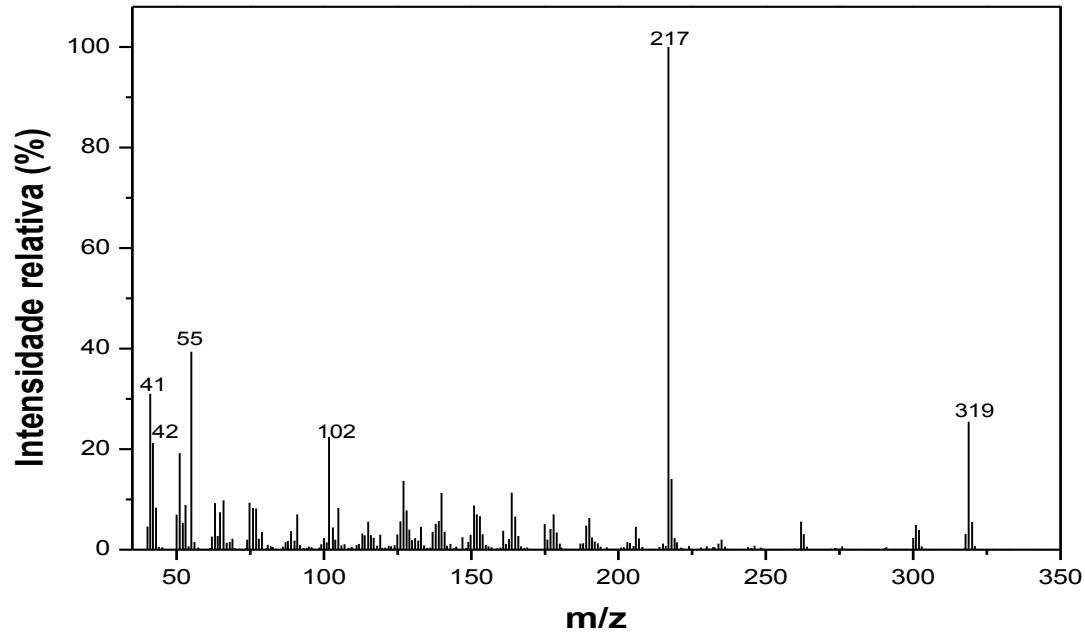

Figura 22. Espectro de massas do composto **6**.

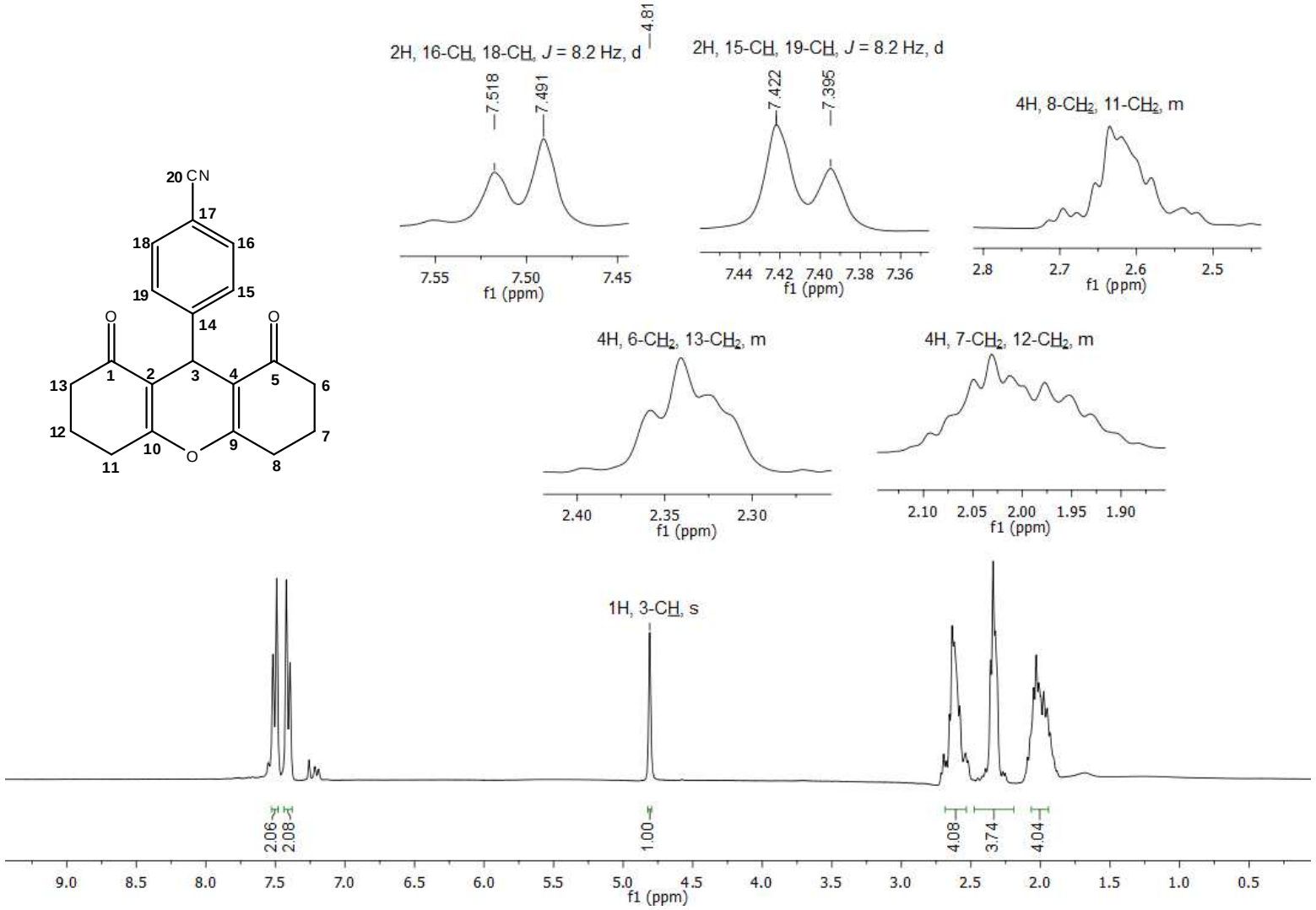

Figura 23. Espectro de RMN de ^{1}H (300 MHz, $CDCl_3$) do composto **6**.

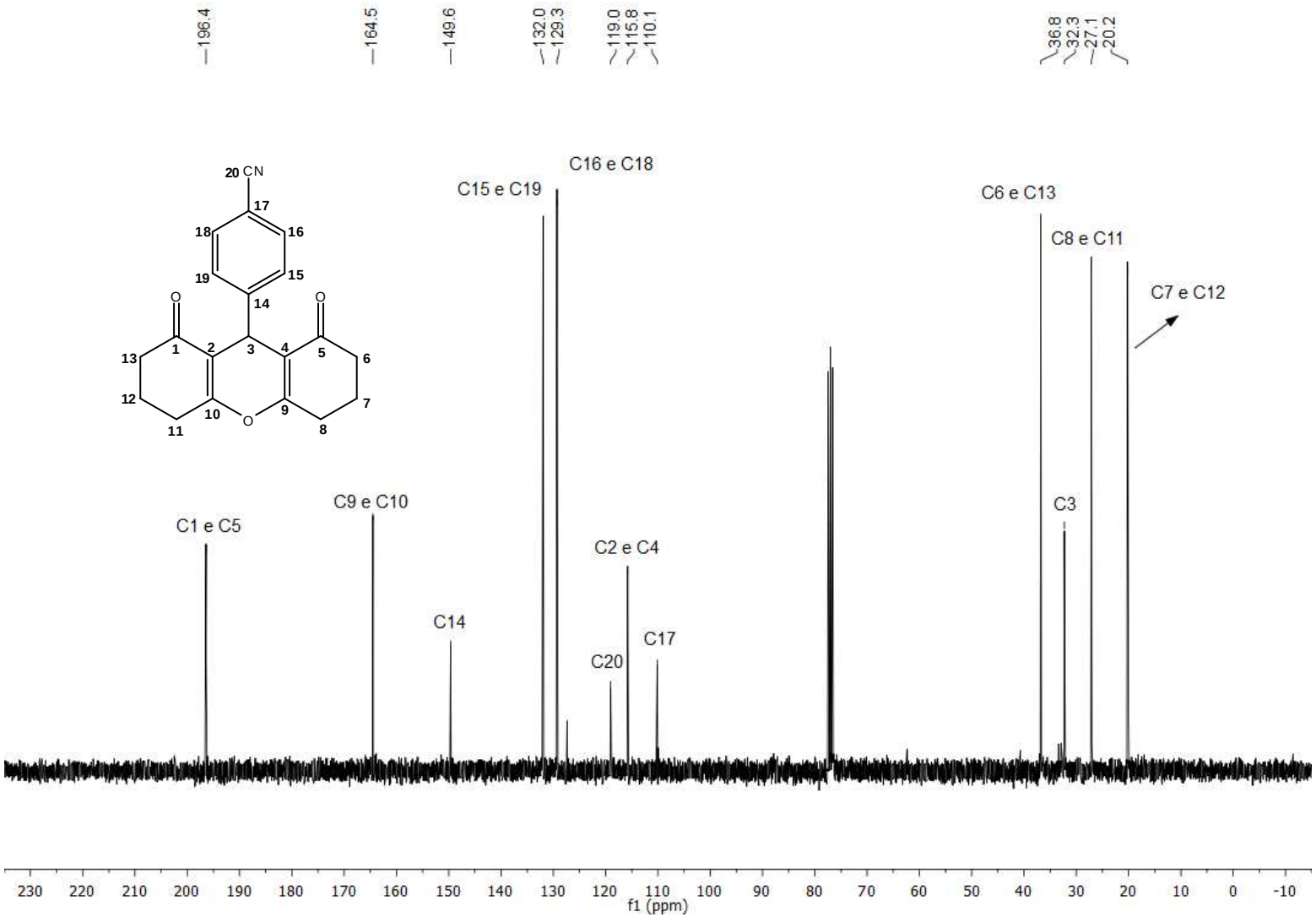

Figura 24. Espectro de RMN de ^{13}C (75 MHz, $CDCl_3$) do composto **6**.

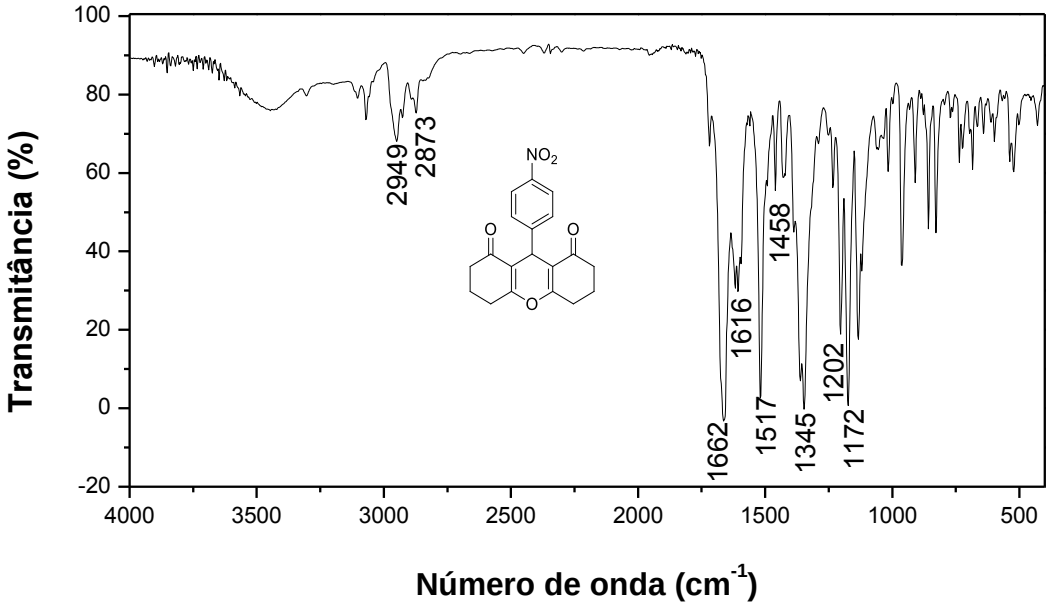

Figura 25. Espectro no infravermelho (KBr) do composto **7**.

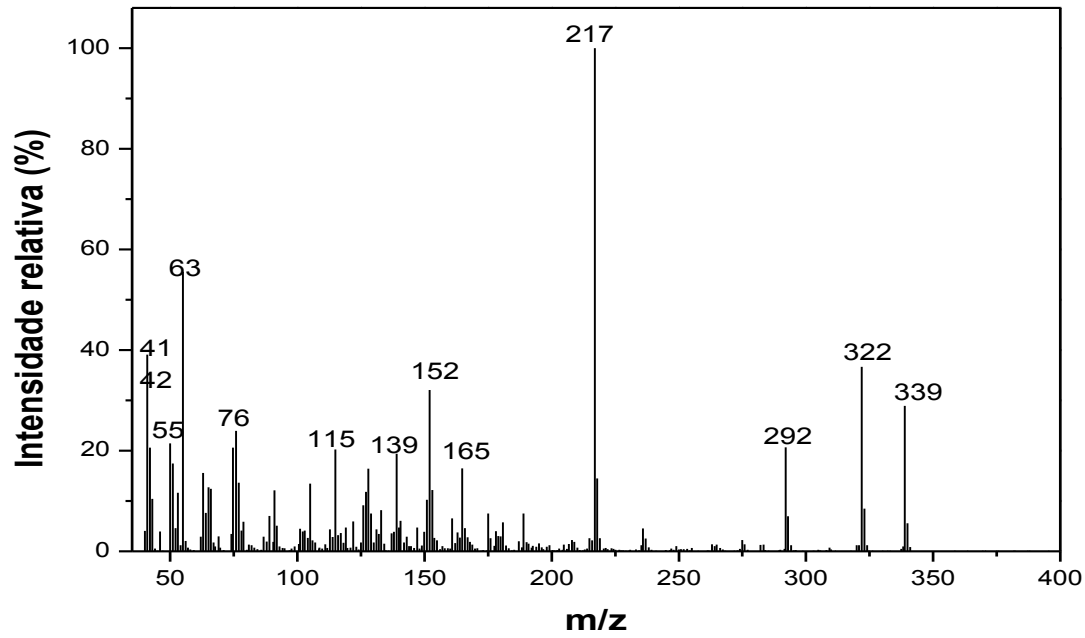

Figura 26. Espectro de massas do composto **7**.

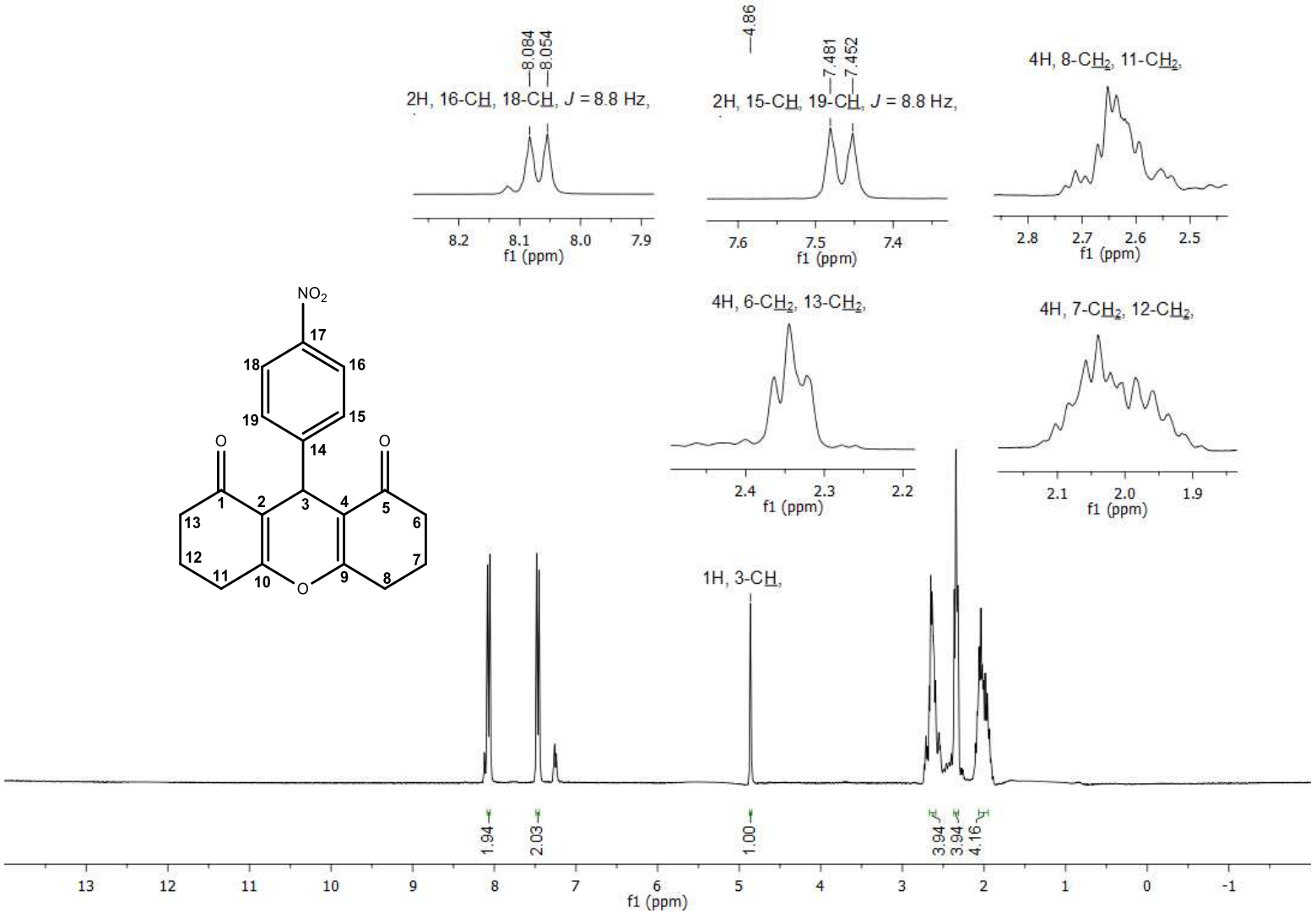

Figura 27. Espectro de RMN de ^{1}H (300 MHz, $CDCl_3$) do composto **7**.

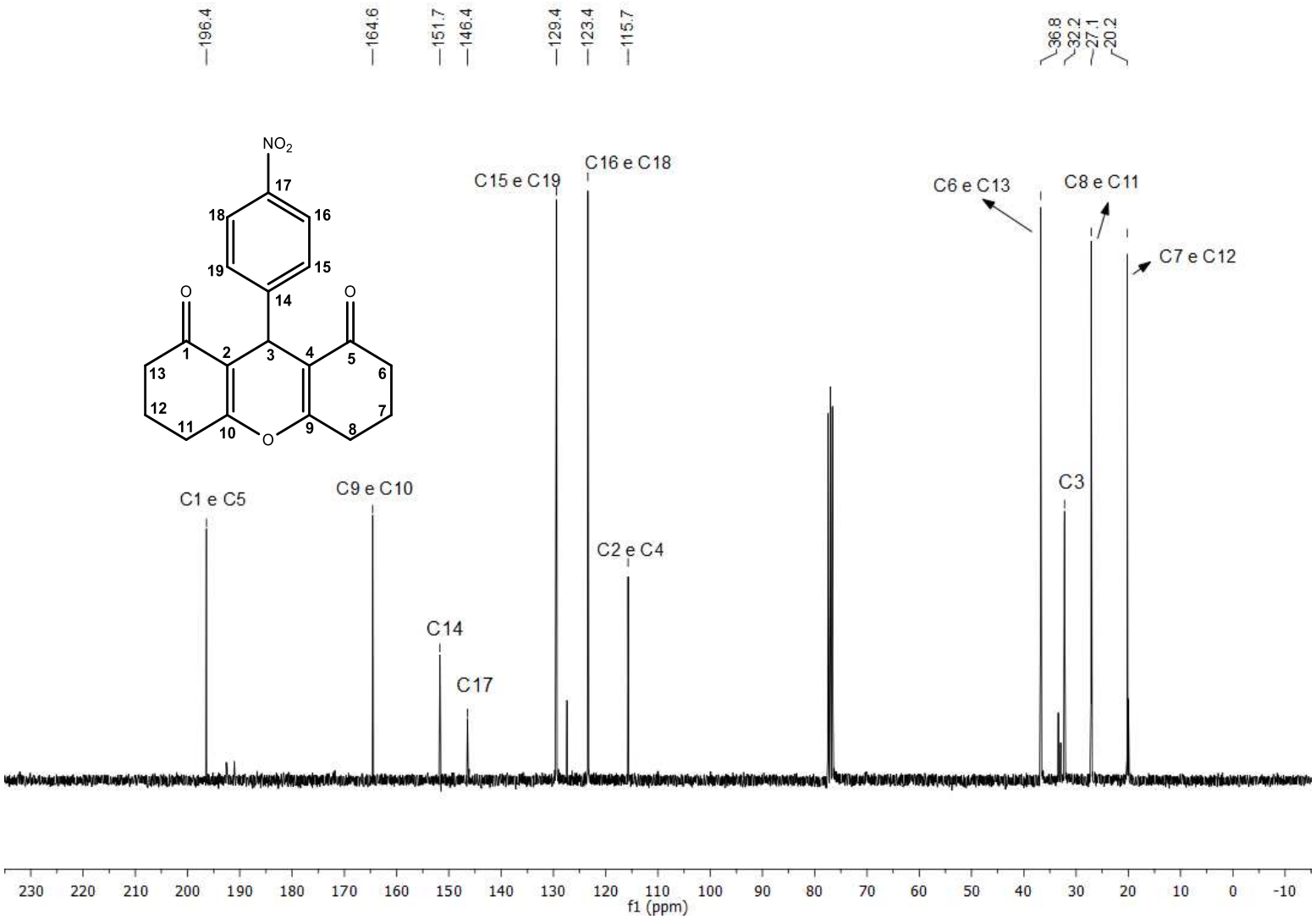

Figura 28. Espectro de RMN de ^{13}C (75 MHz, $CDCl_3$) do composto **7**.

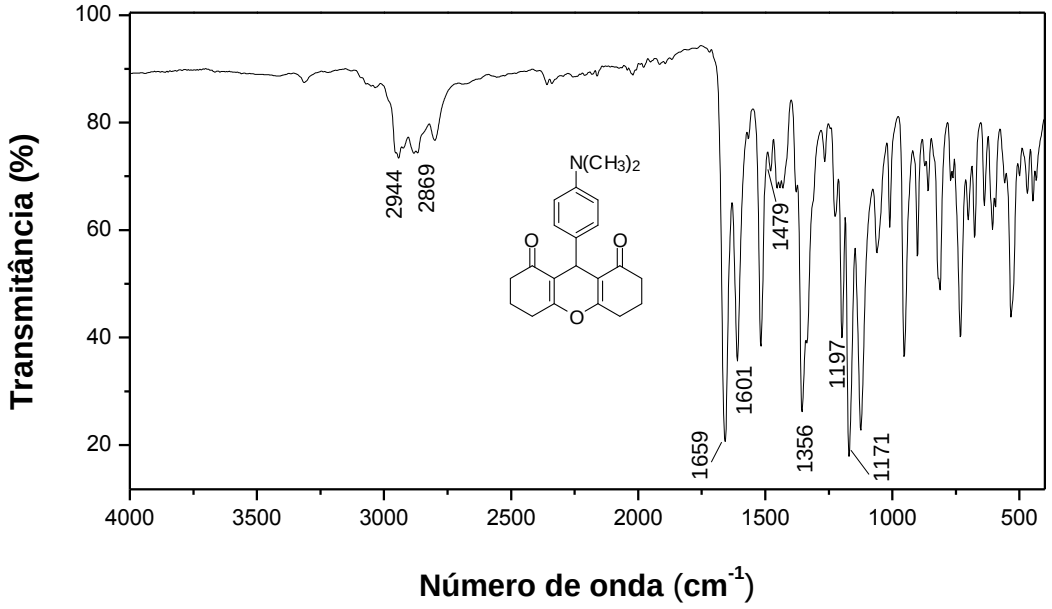

Figura 29. Espectro no infravermelho (ATR) do composto **8**.

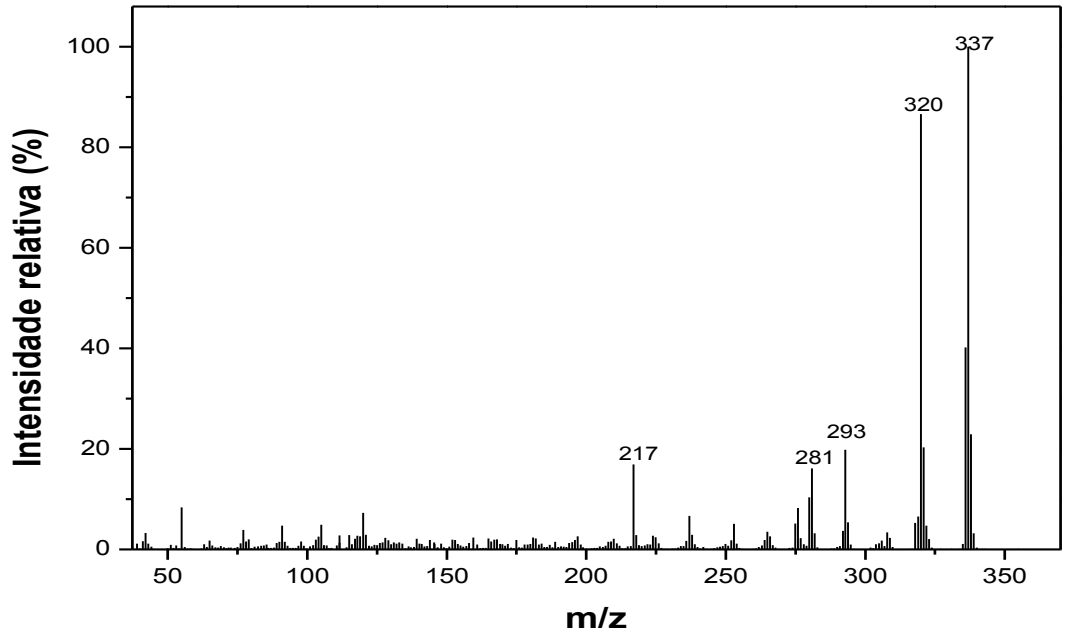

Figura 30. Espectro de massas do composto **8**.

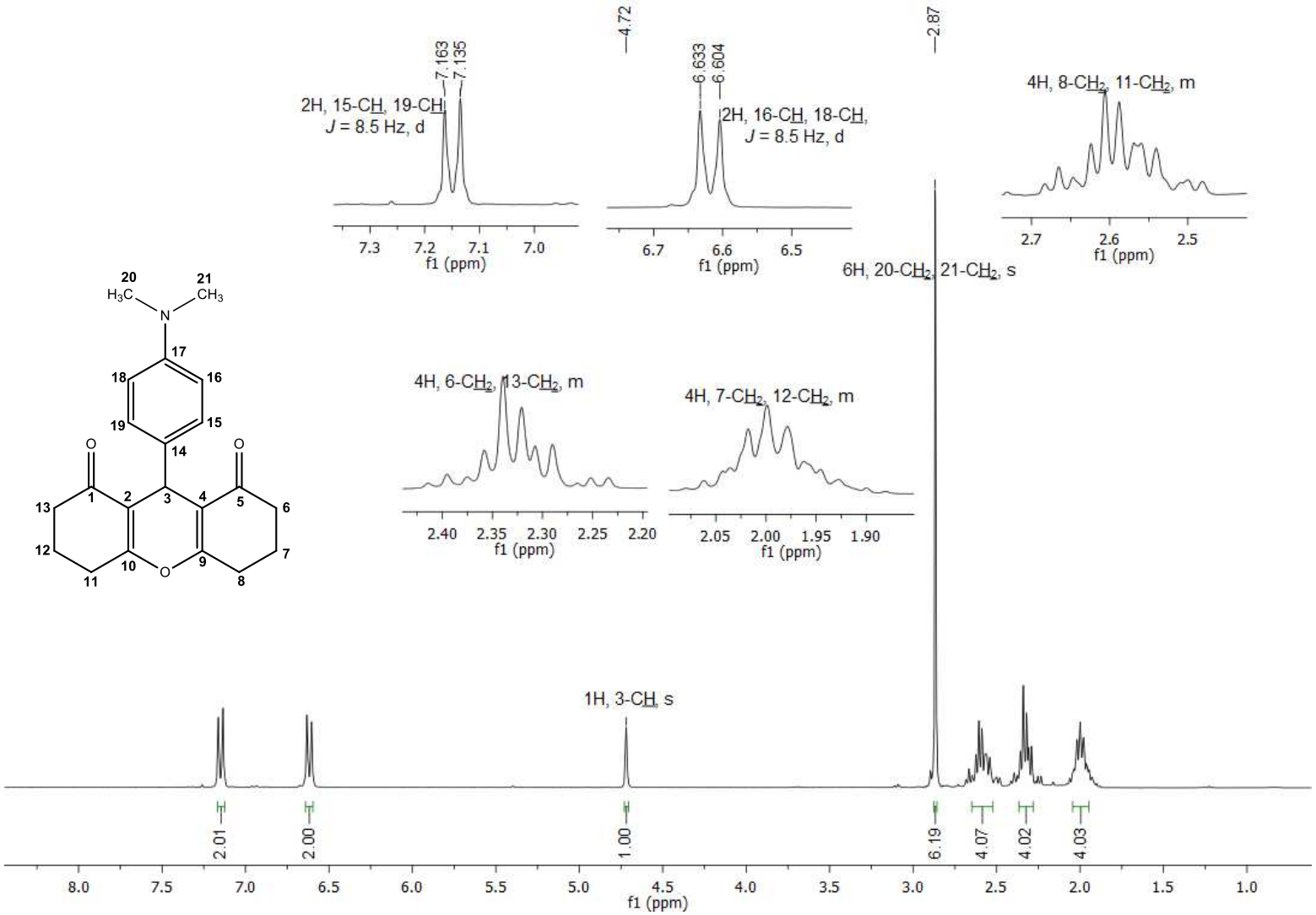

Figura 31. Espectro de RMN de ^{1}H (300 MHz, $CDCl_3$) do composto **8**.

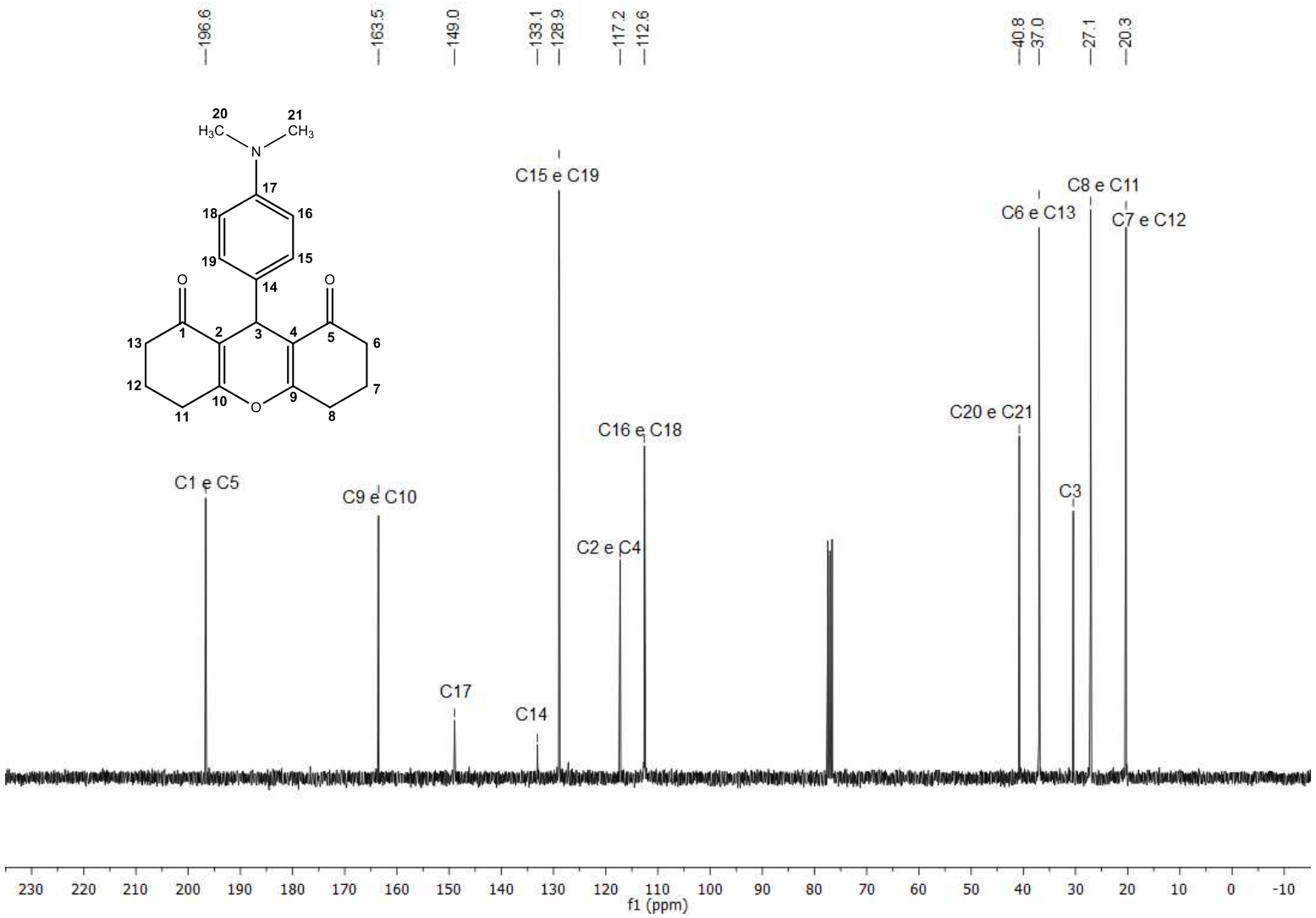

Figura 32. Espectro de RMN de ^{13}C (75 MHz, $CDCl_3$) do composto **8**.

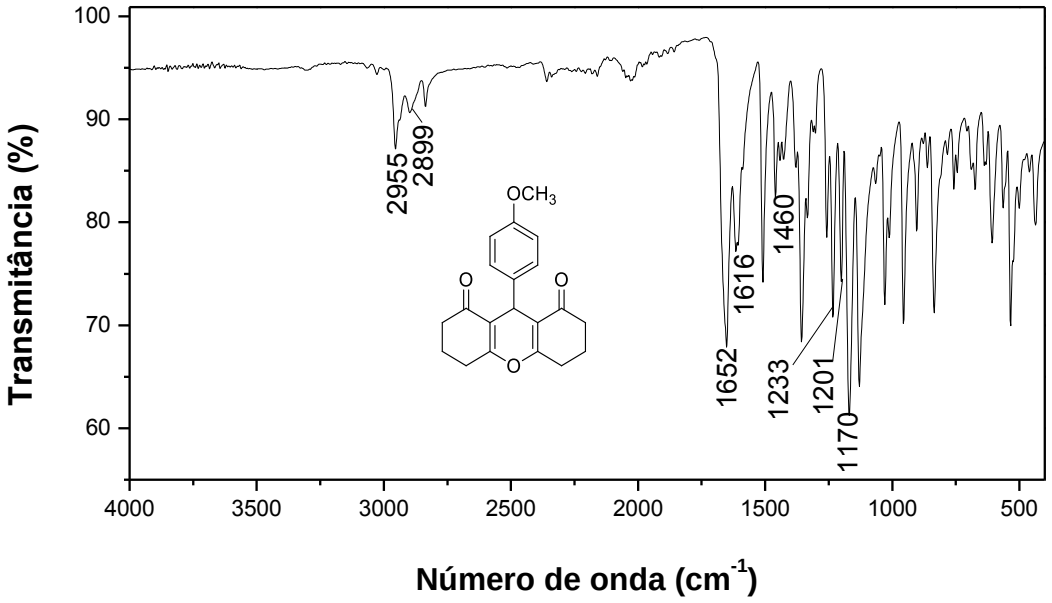

Figura 33. Espectro no infravermelho (ATR) do composto **9**.

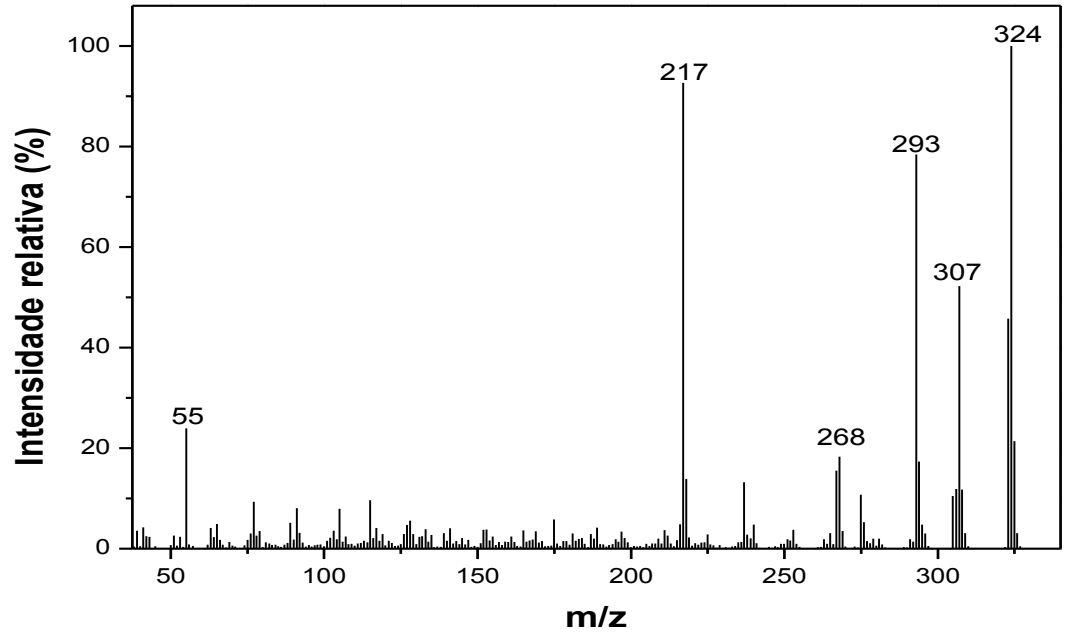

Figura 34. Espectro de massas do composto **9**.

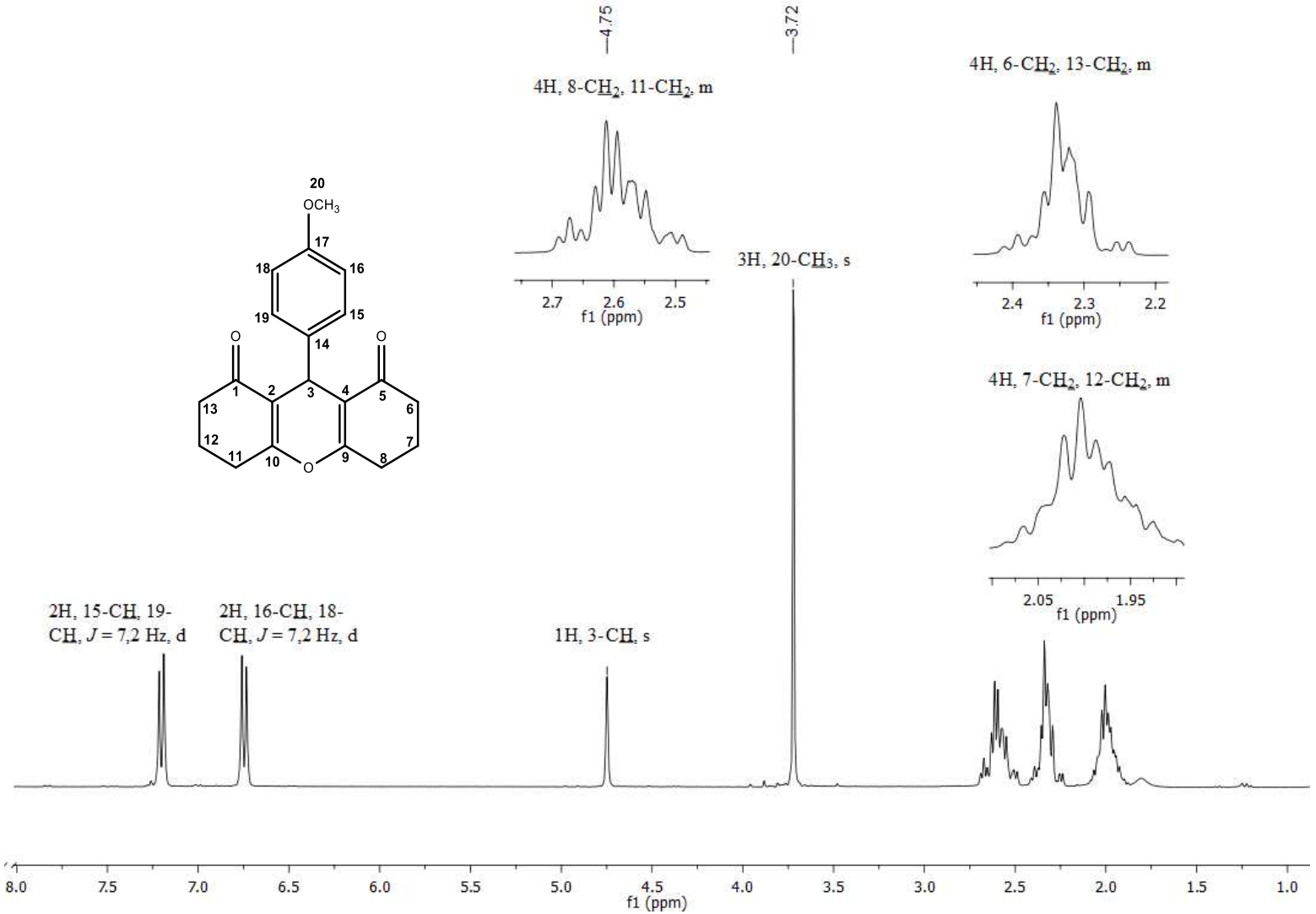

Figura 35. Espectro de RMN de ^{1}H (300 MHz, $CDCl_3$) do composto **9**.

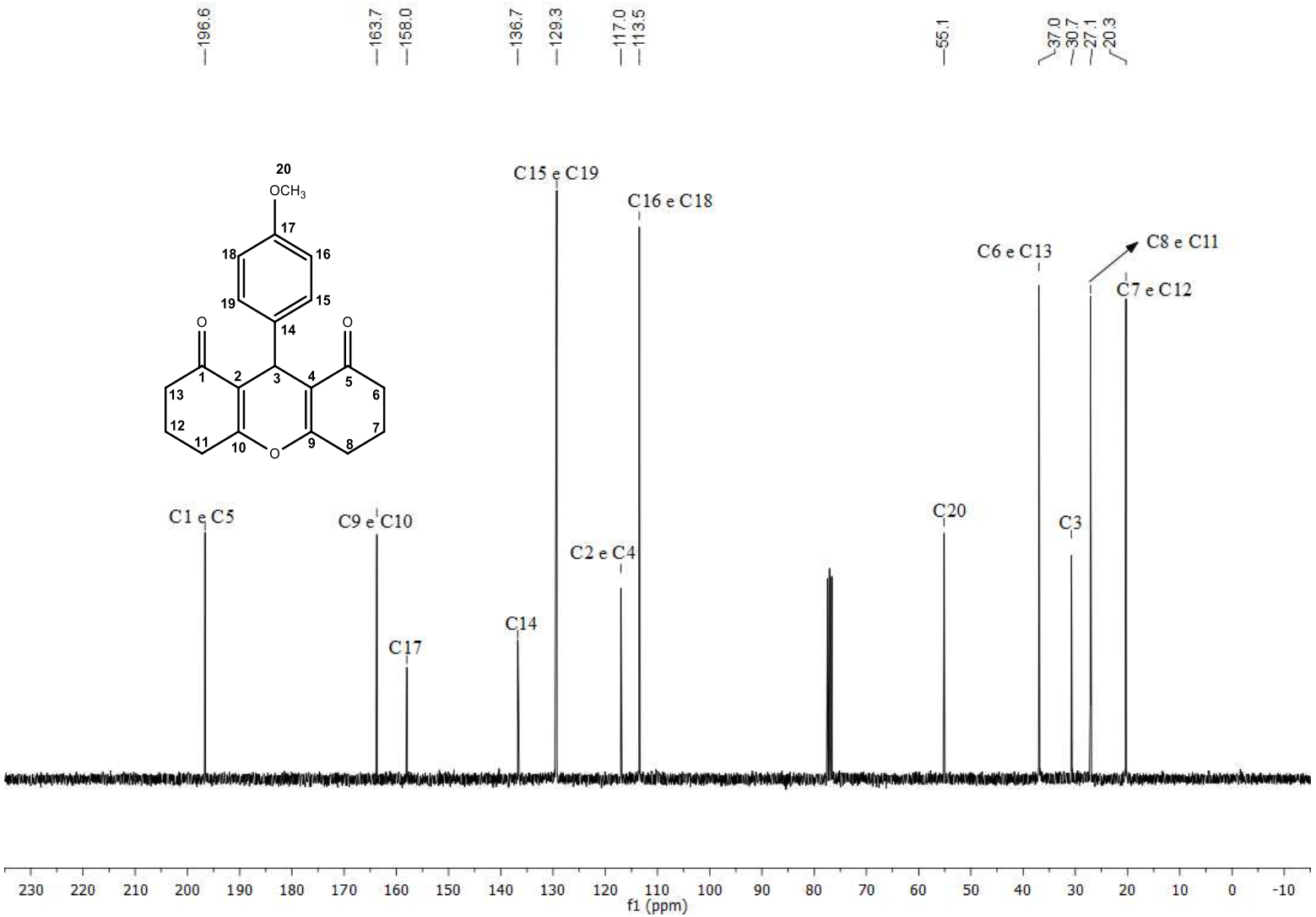

Figura 36. Espectro de RMN de ^{13}C (75 MHz, $CDCl_3$) do composto **9**.

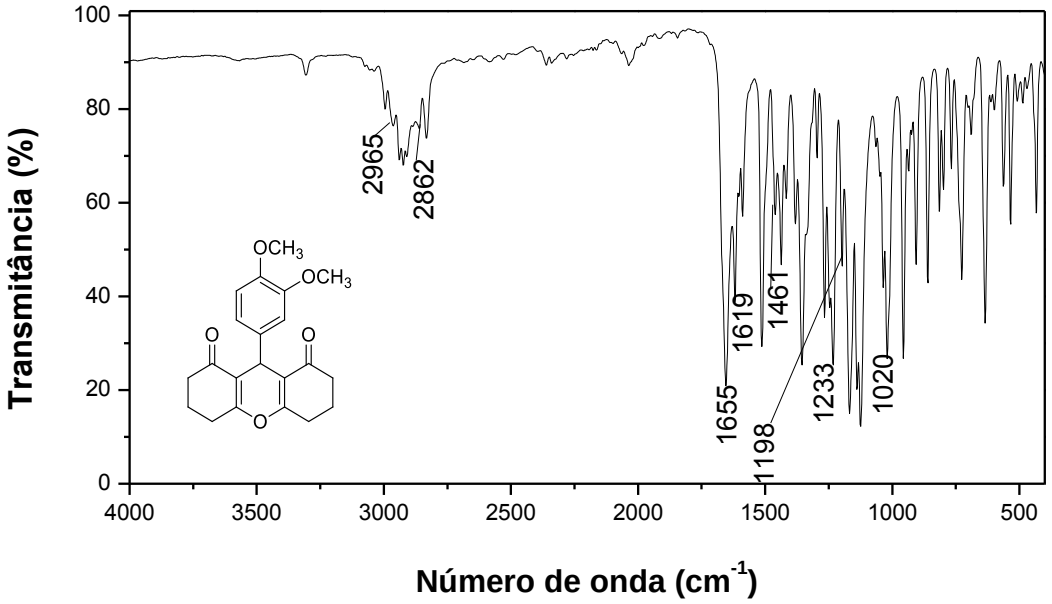

Figura 37. Espectro no infravermelho (ATR) do composto **10**.

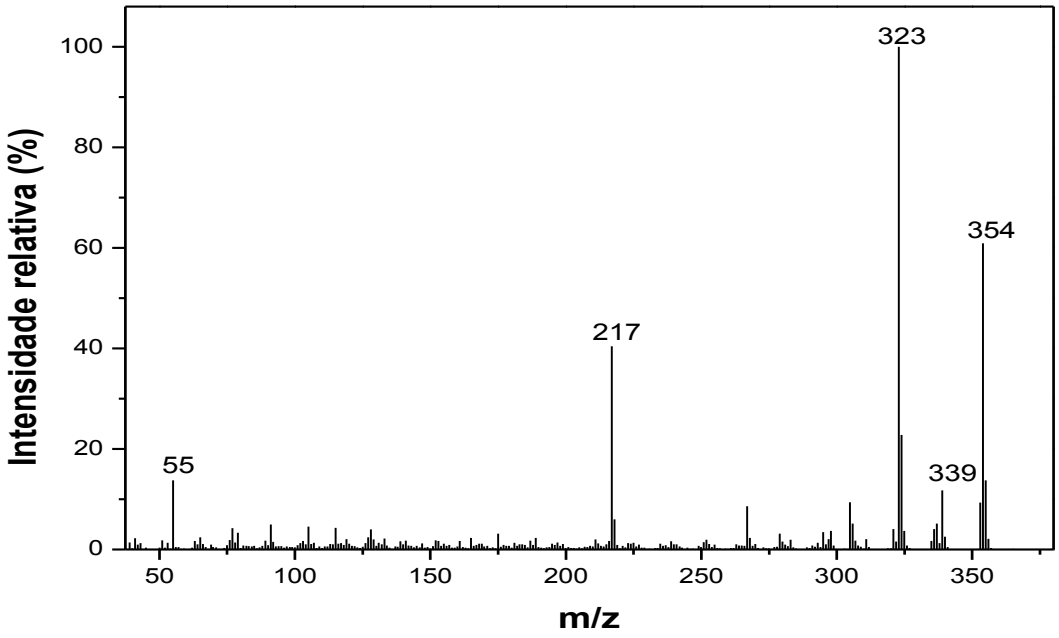

Figura 38. Espectro de massas do composto **10**.

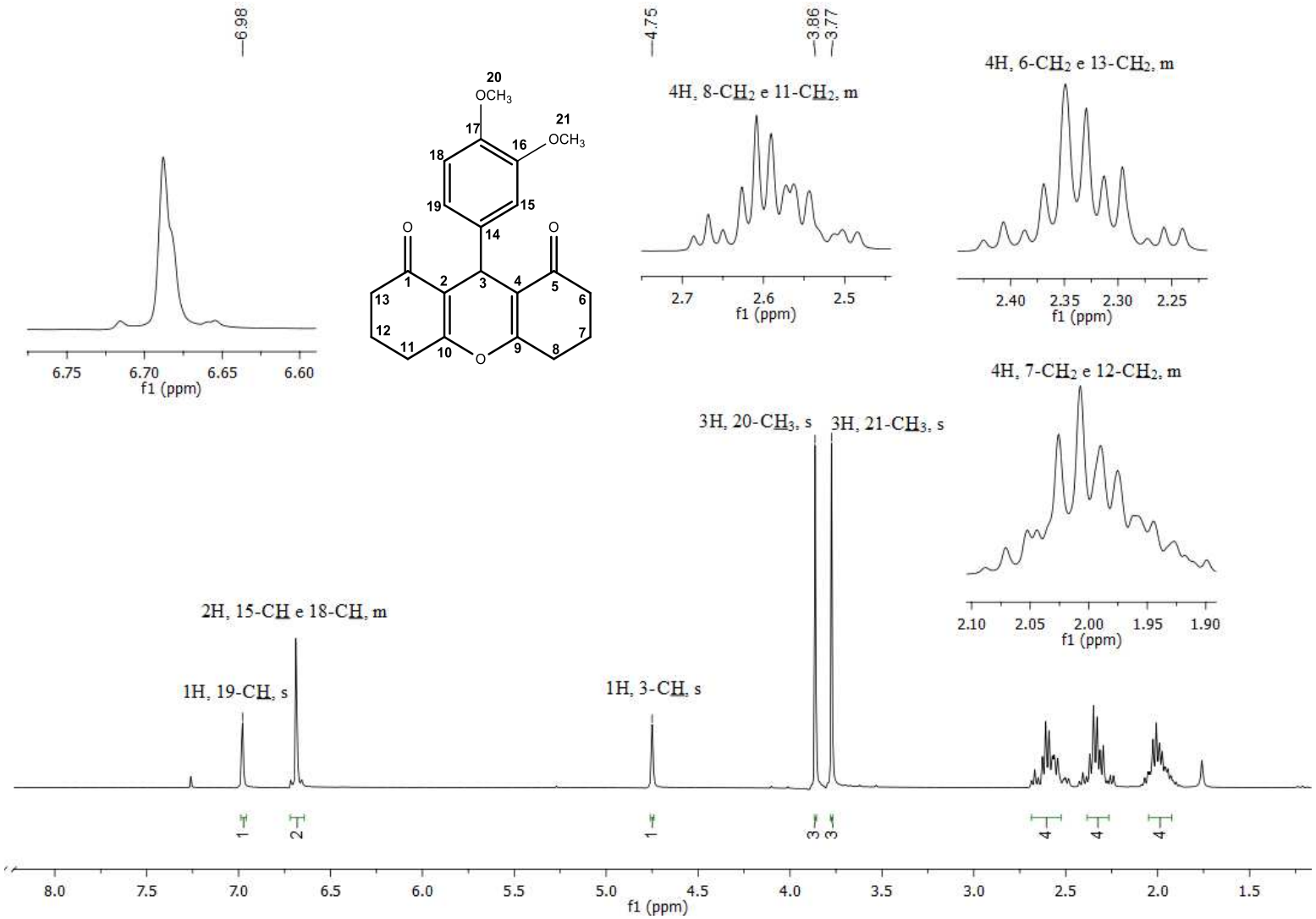

Figura 39. Espectro de RMN de ^{1}H (300 MHz, $CDCl_3$) do composto **10**.

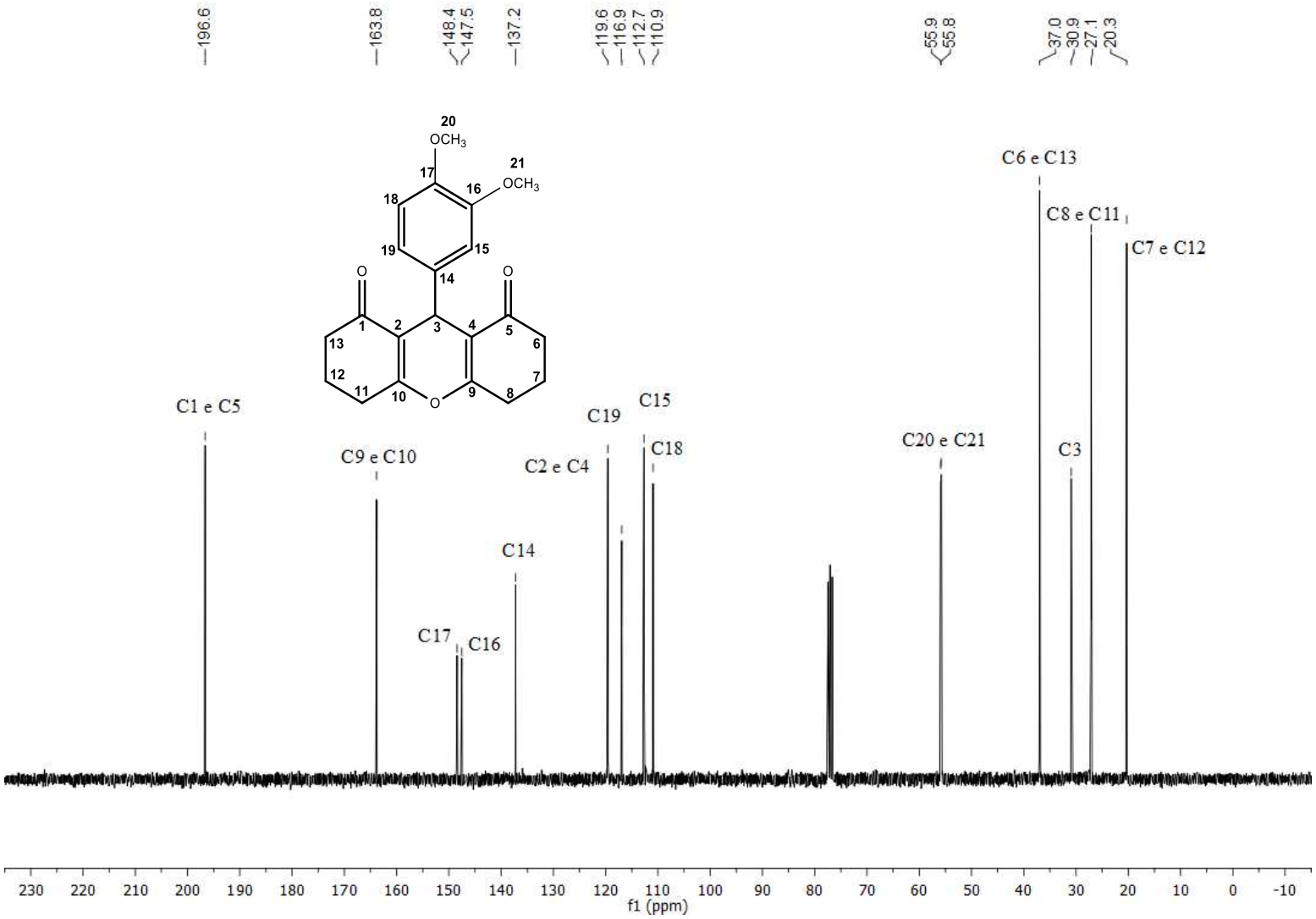

Figura 40. Espectro de RMN de ^{13}C (75 MHz, $CDCl_3$) do composto **10**.

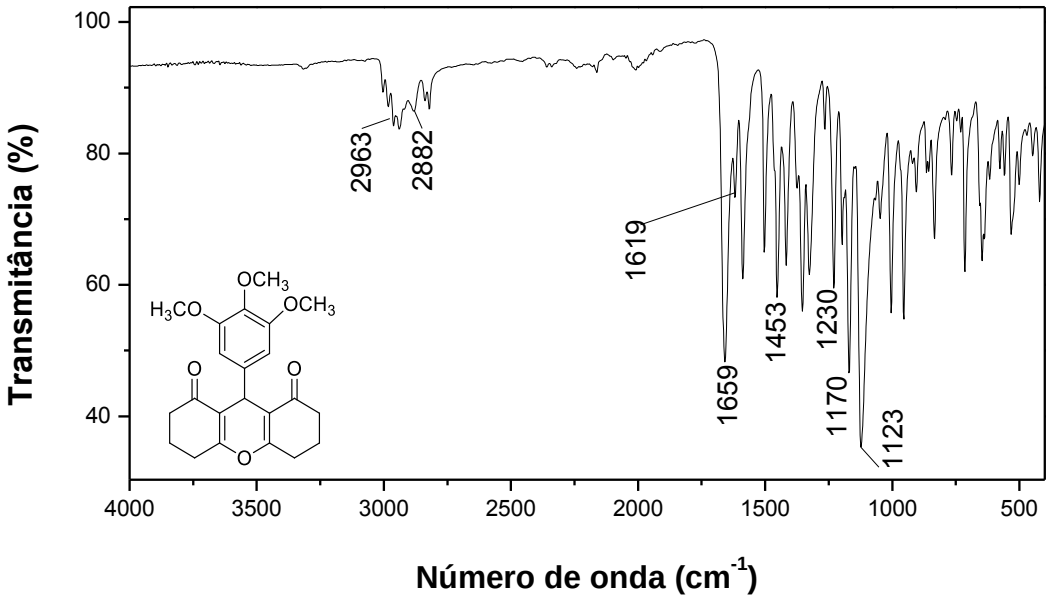

Figura 41. Espectro no infravermelho (ATR) do composto **11**.

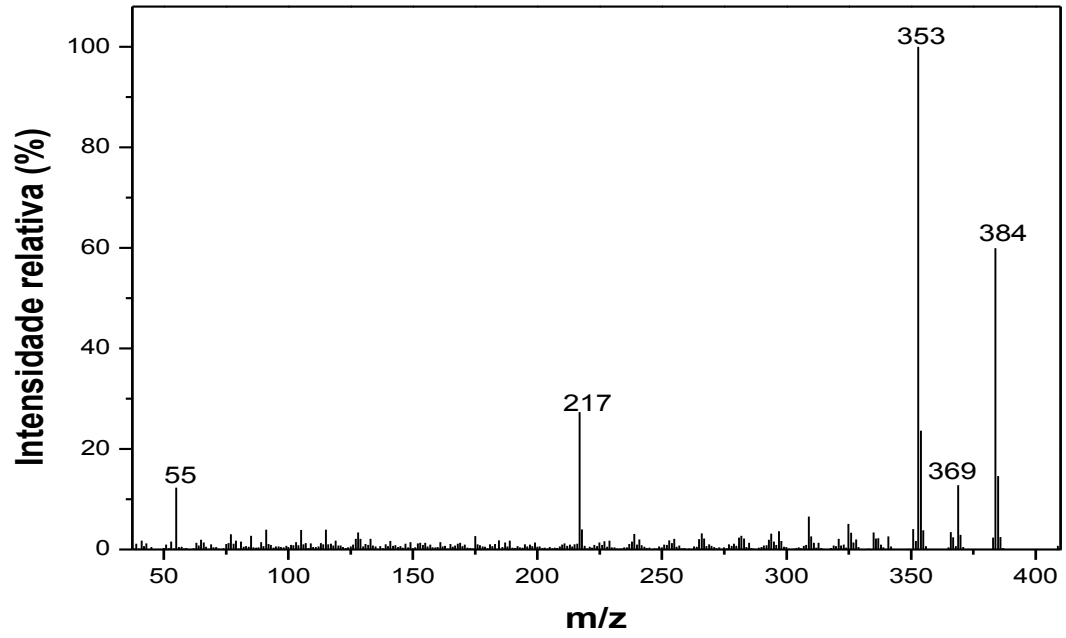

Figura 42. Espectro de massas do composto **11**.

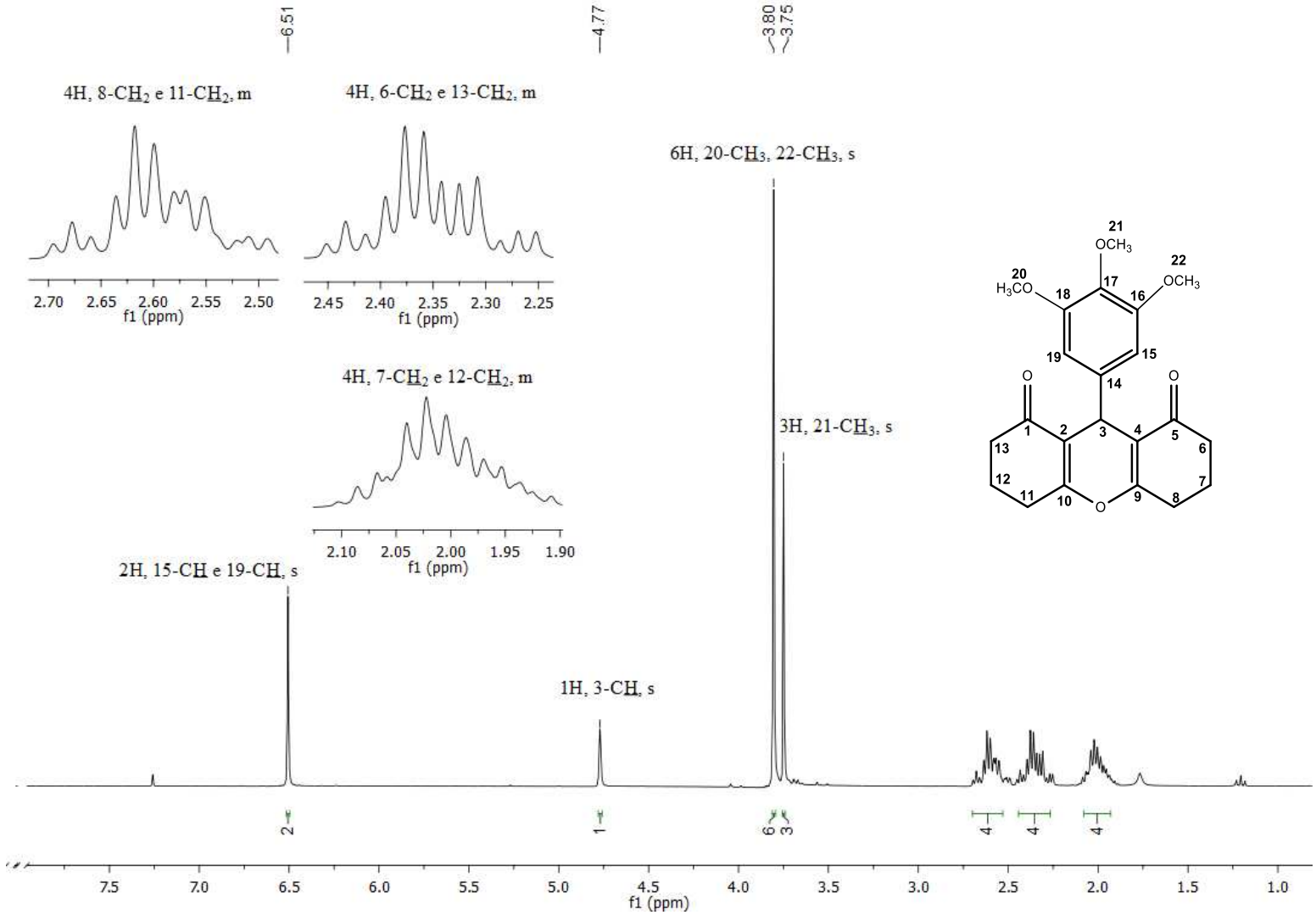

Figura 43. Espectro de RMN de ^{1}H (300 MHz, $CDCl_3$) do composto **11**.

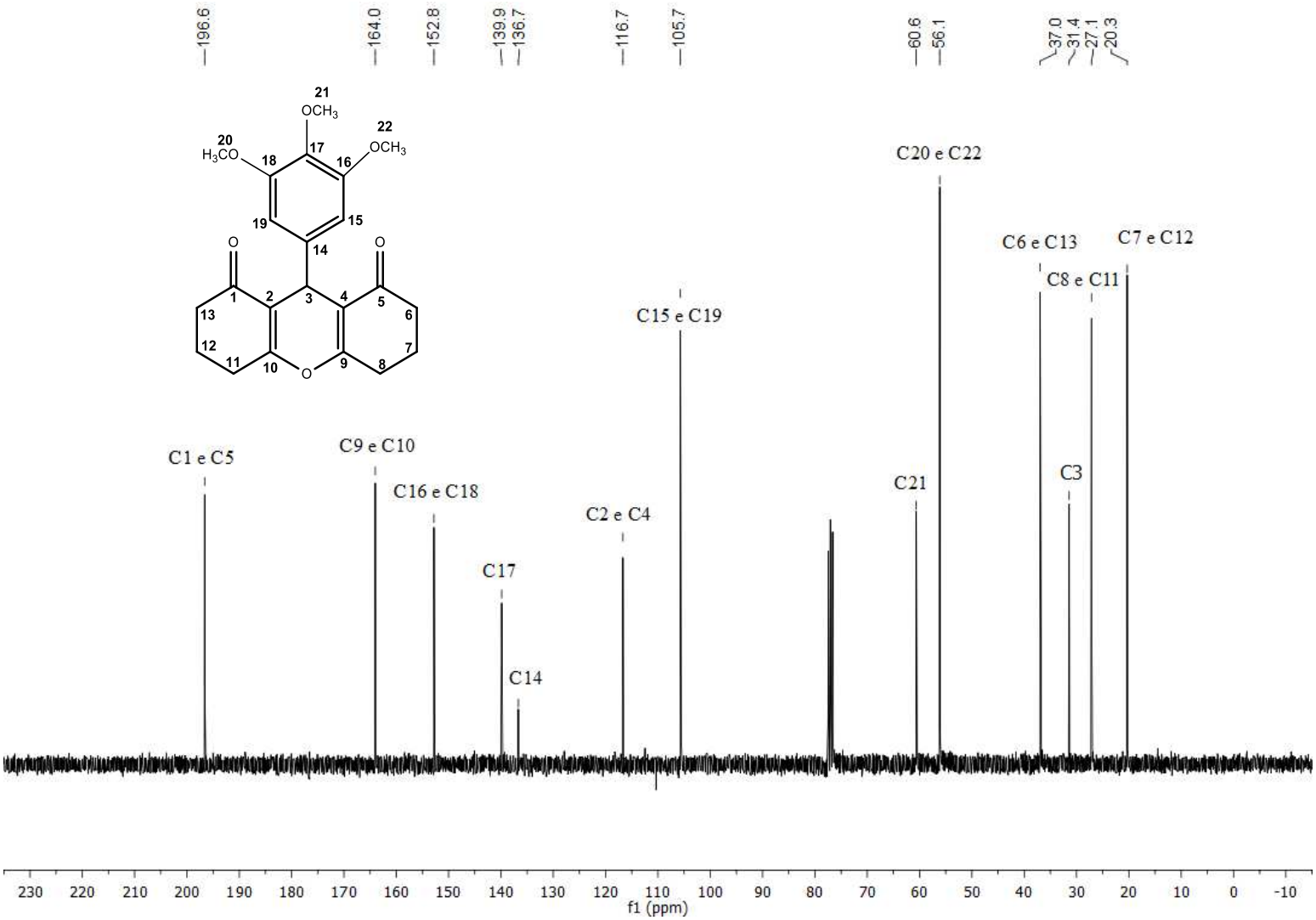

Figura 44. Espectro de RMN de ^{13}C (75 MHz, $CDCl_3$) do composto **11**.

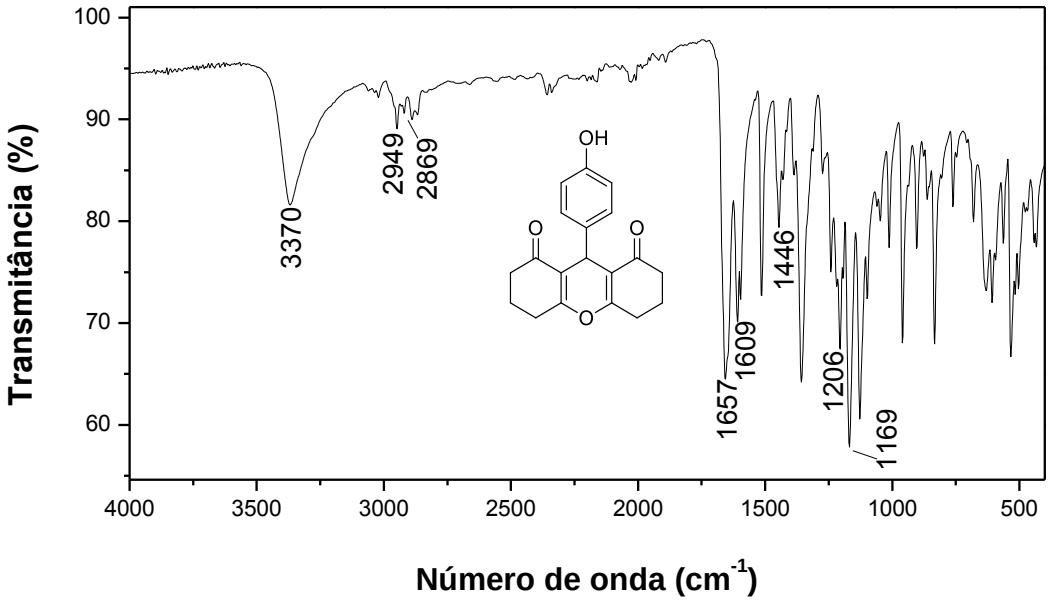

Figura 45. Espectro no infravermelho (ATR) do composto **12**.

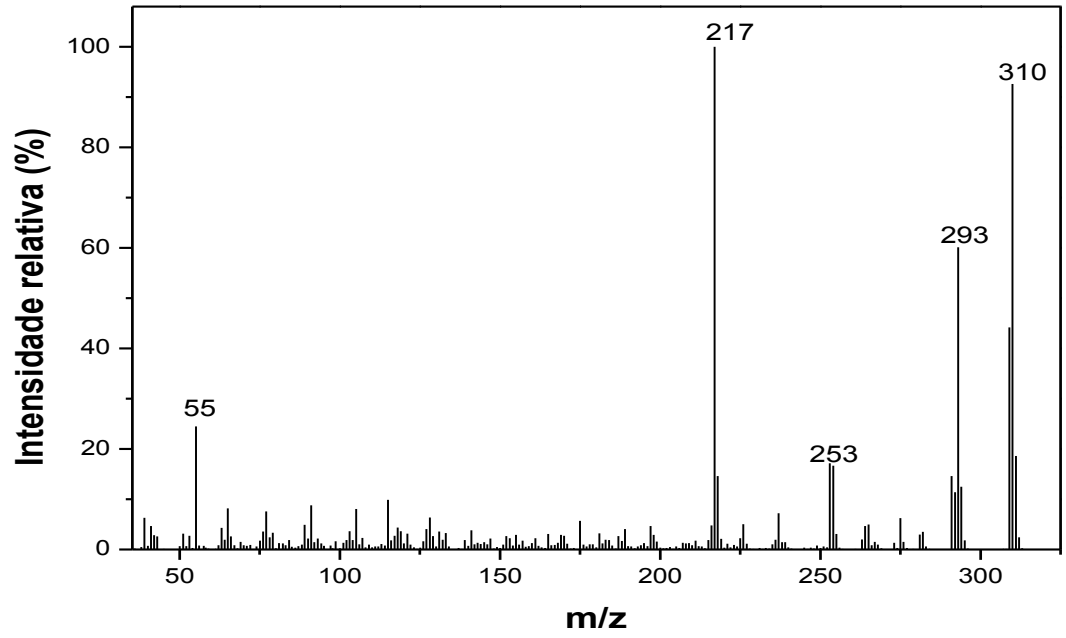

Figura 46. Espectro de massas do composto **12**.

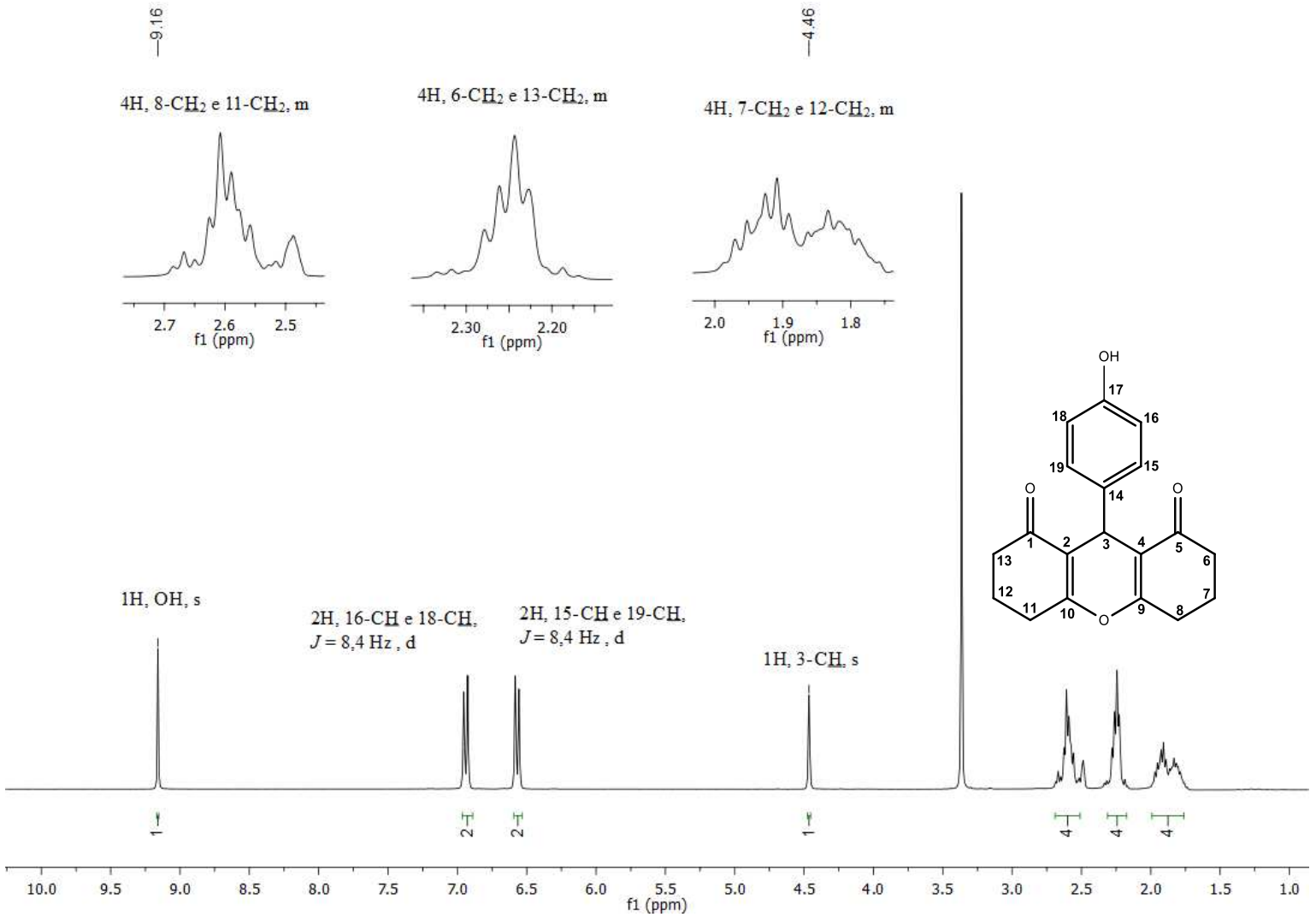

Figura 47. Espectro de RMN de ^{1}H (300 MHz, $CDCl_3$) do composto **12**.

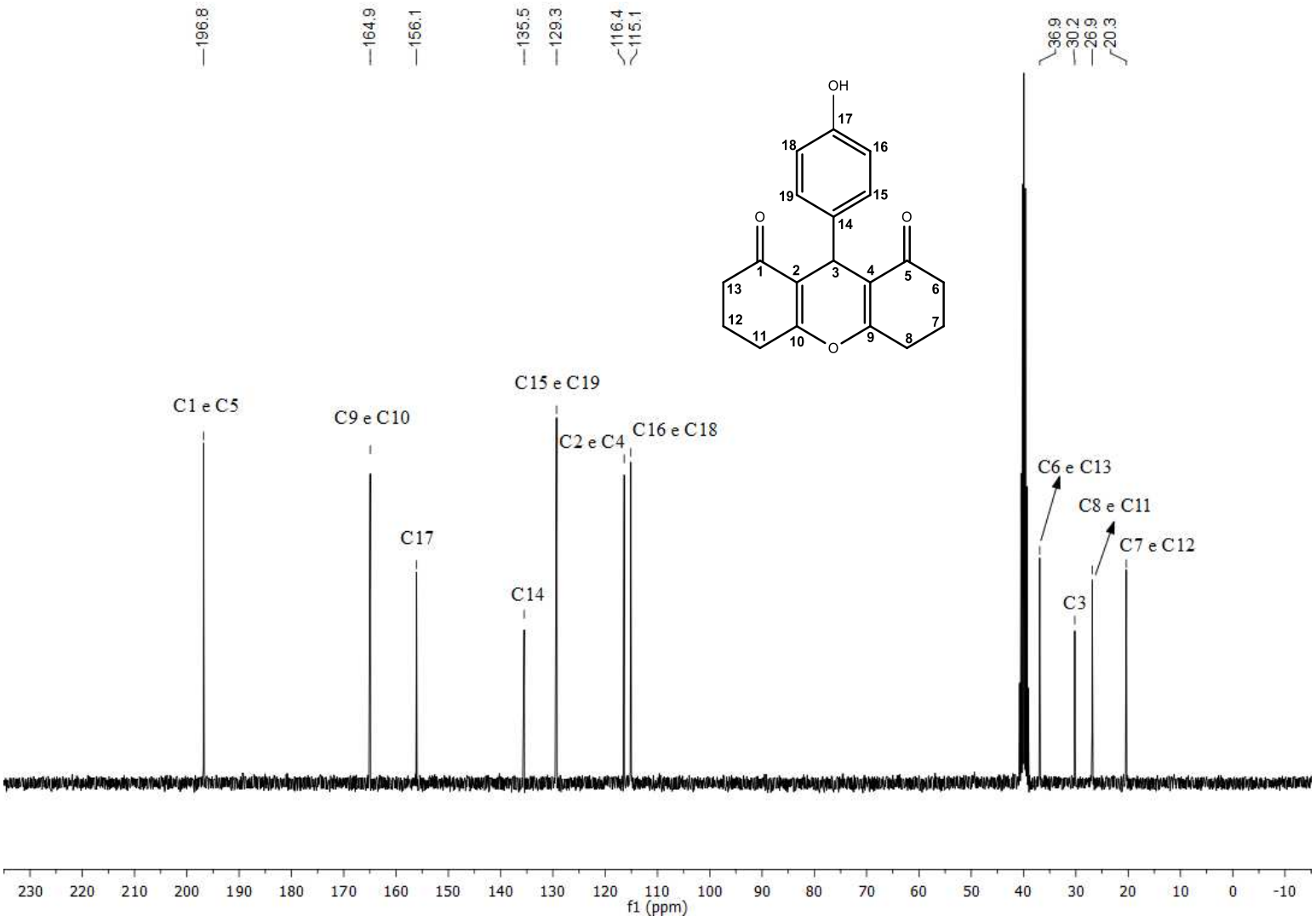

Figura 48. Espectro de RMN de ^{13}C (75 MHz, $CDCl_3$) do composto **12**.

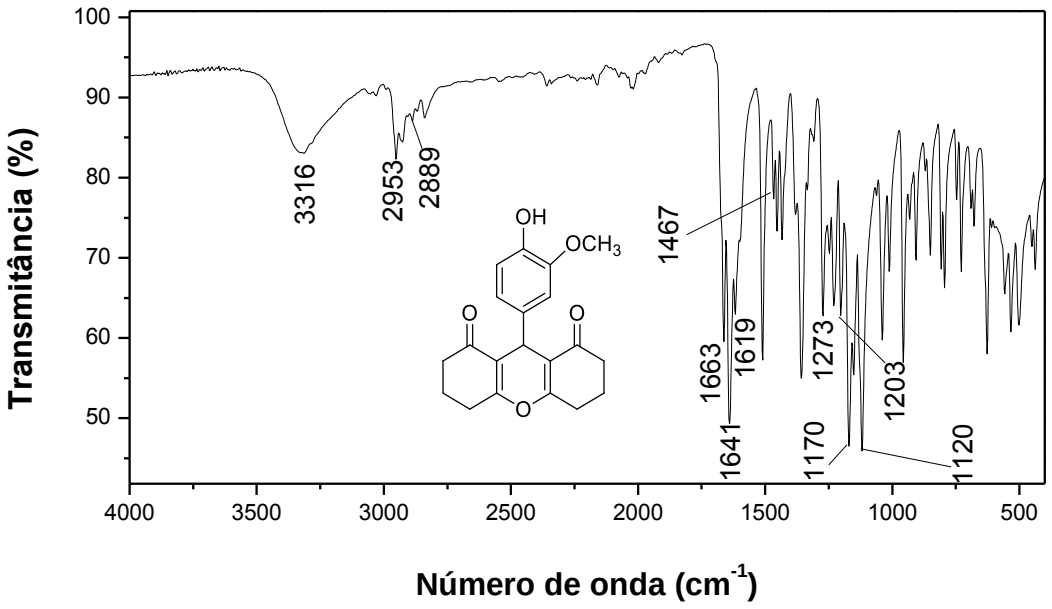

Figura 49. Espectro no infravermelho (ATR) do composto **13**.

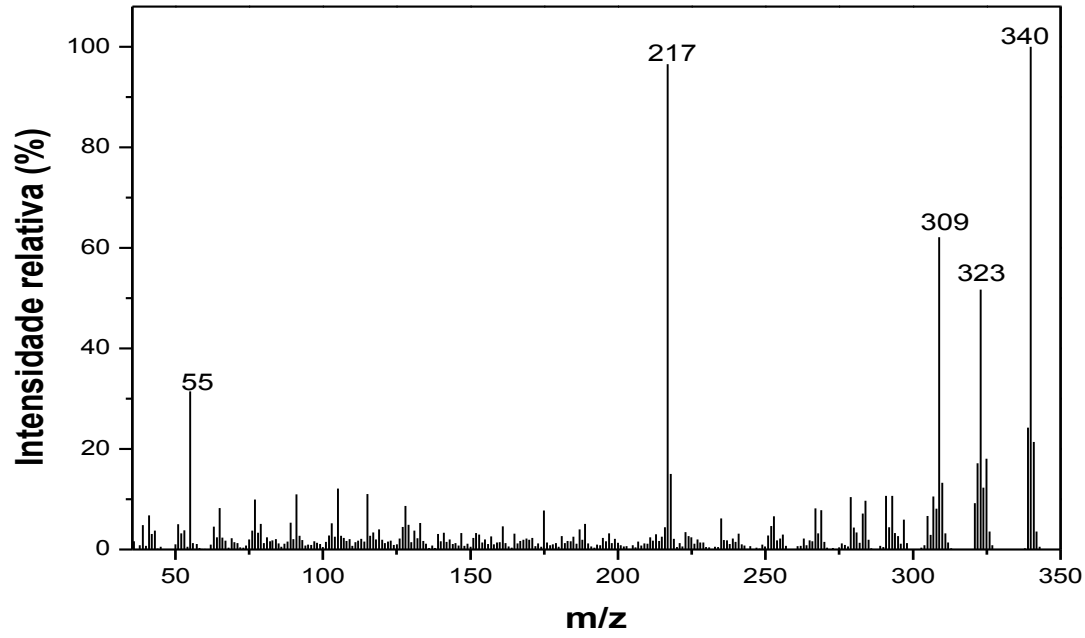

Figura 50. Espectro de massas do composto **13**.

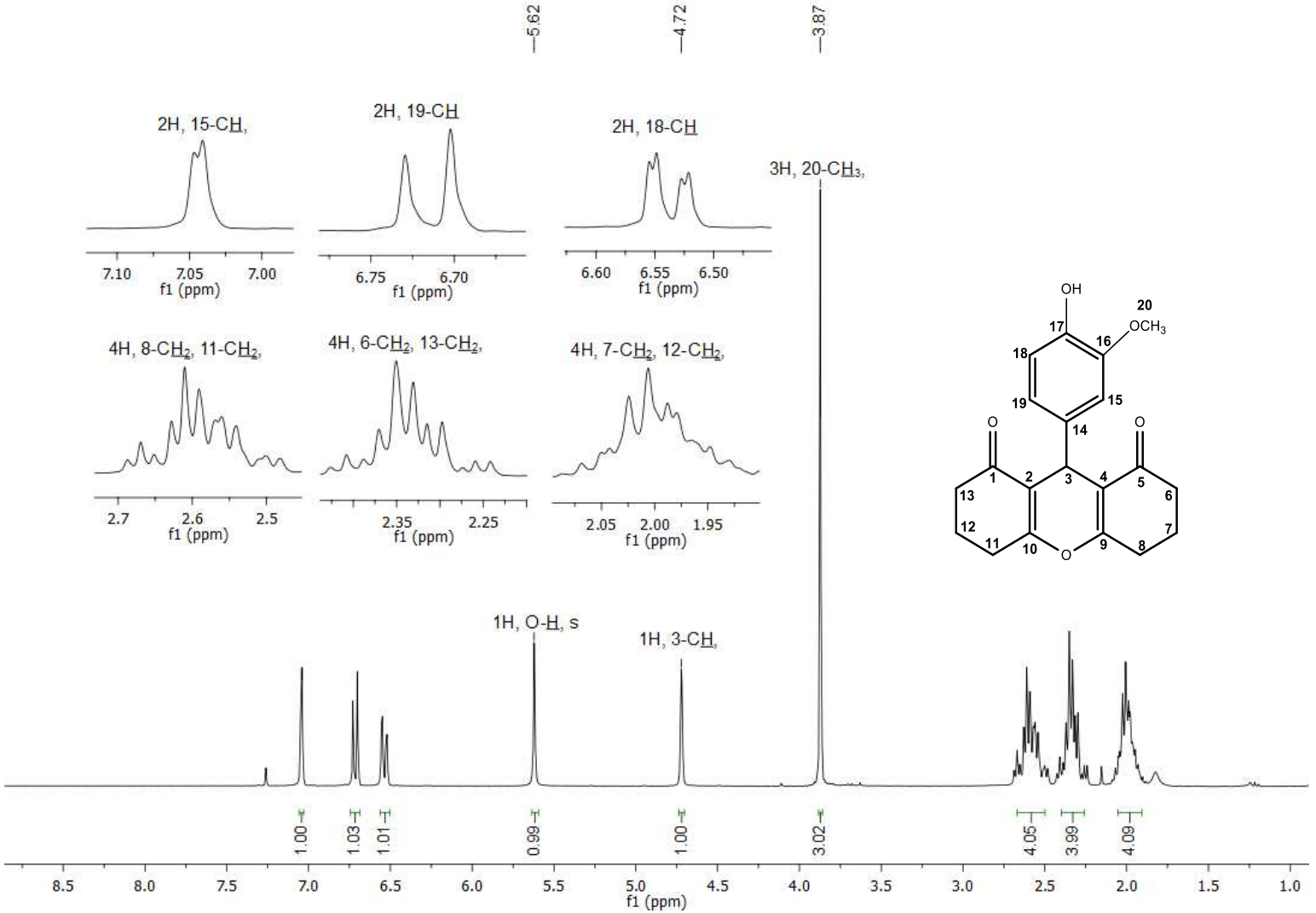

Figura 51. Espectro de RMN de ^{1}H (300 MHz, $CDCl_3$) do composto **13**.

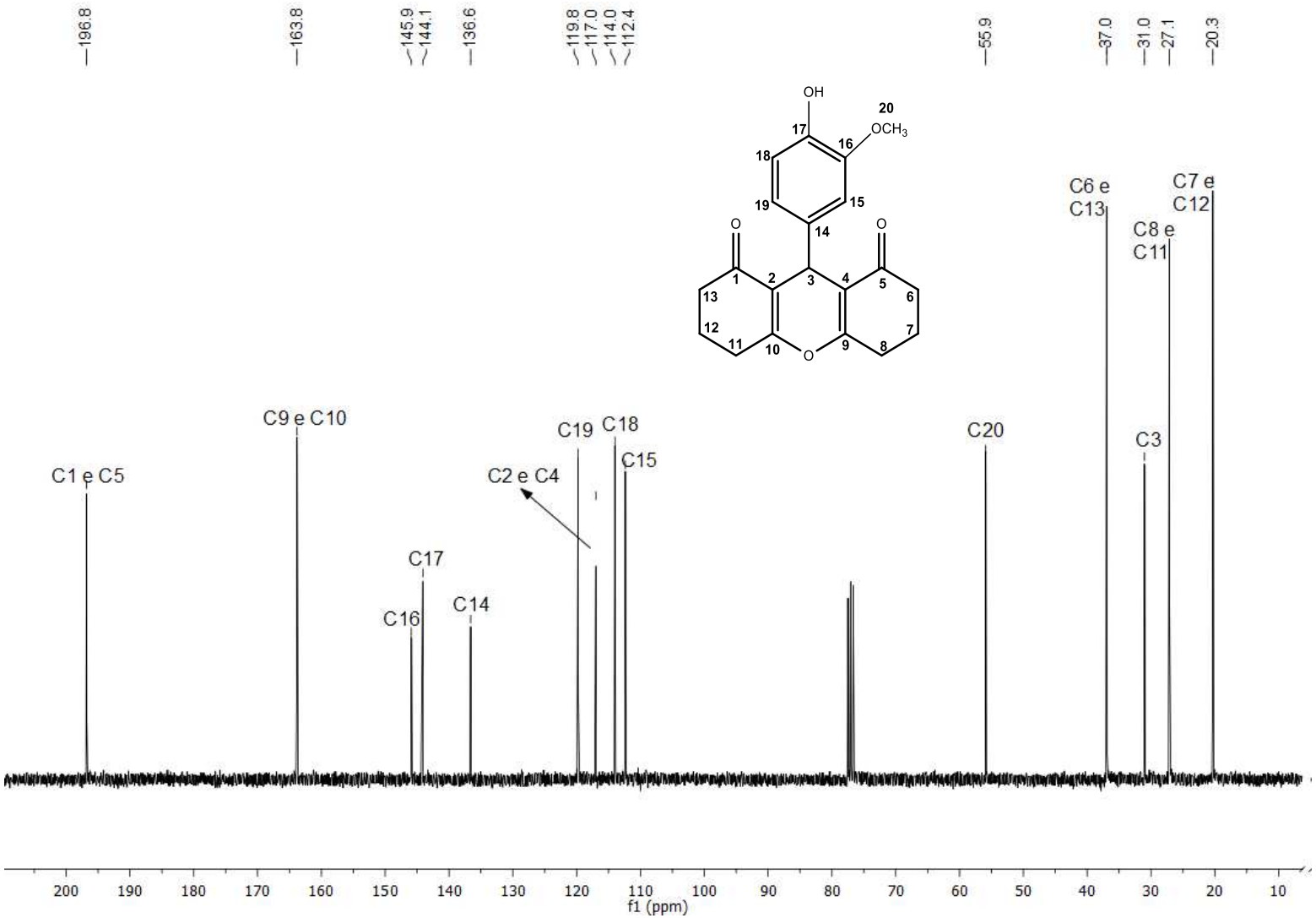

Figura 52. Espectro de RMN de ^{13}C (75 MHz, $CDCl_3$) do composto **13**.

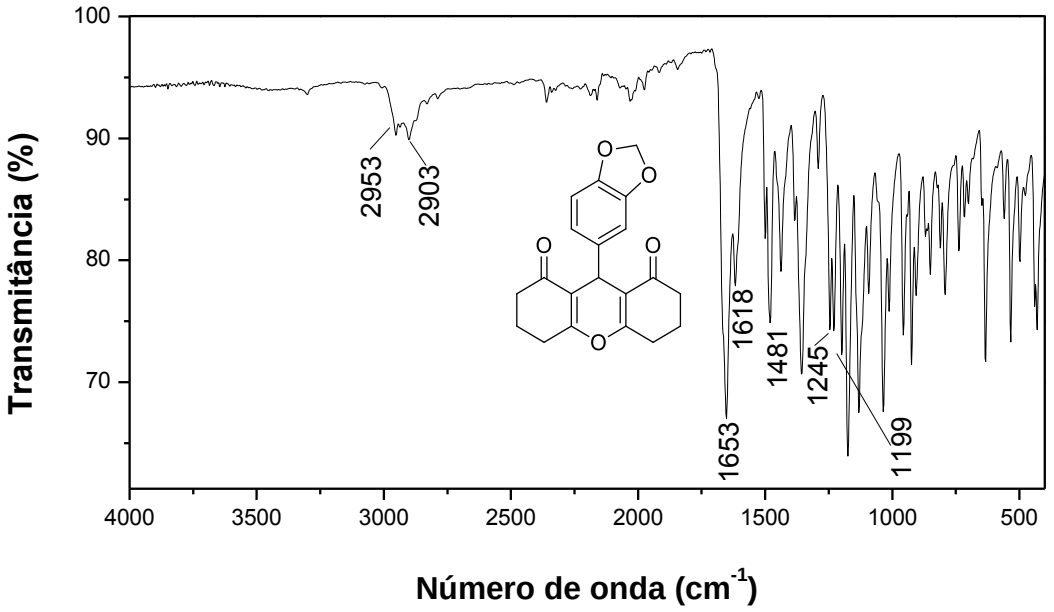

Figura 53. Espectro no infravermelho (ATR) do composto **14**.

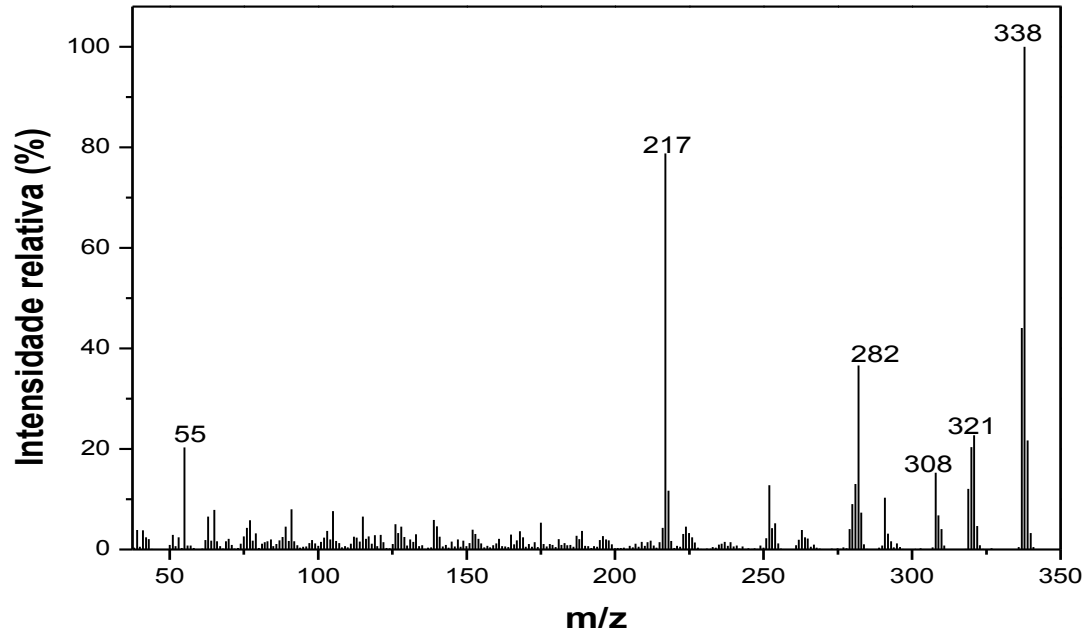

Figura 54. Espectro de massas do composto **14**.

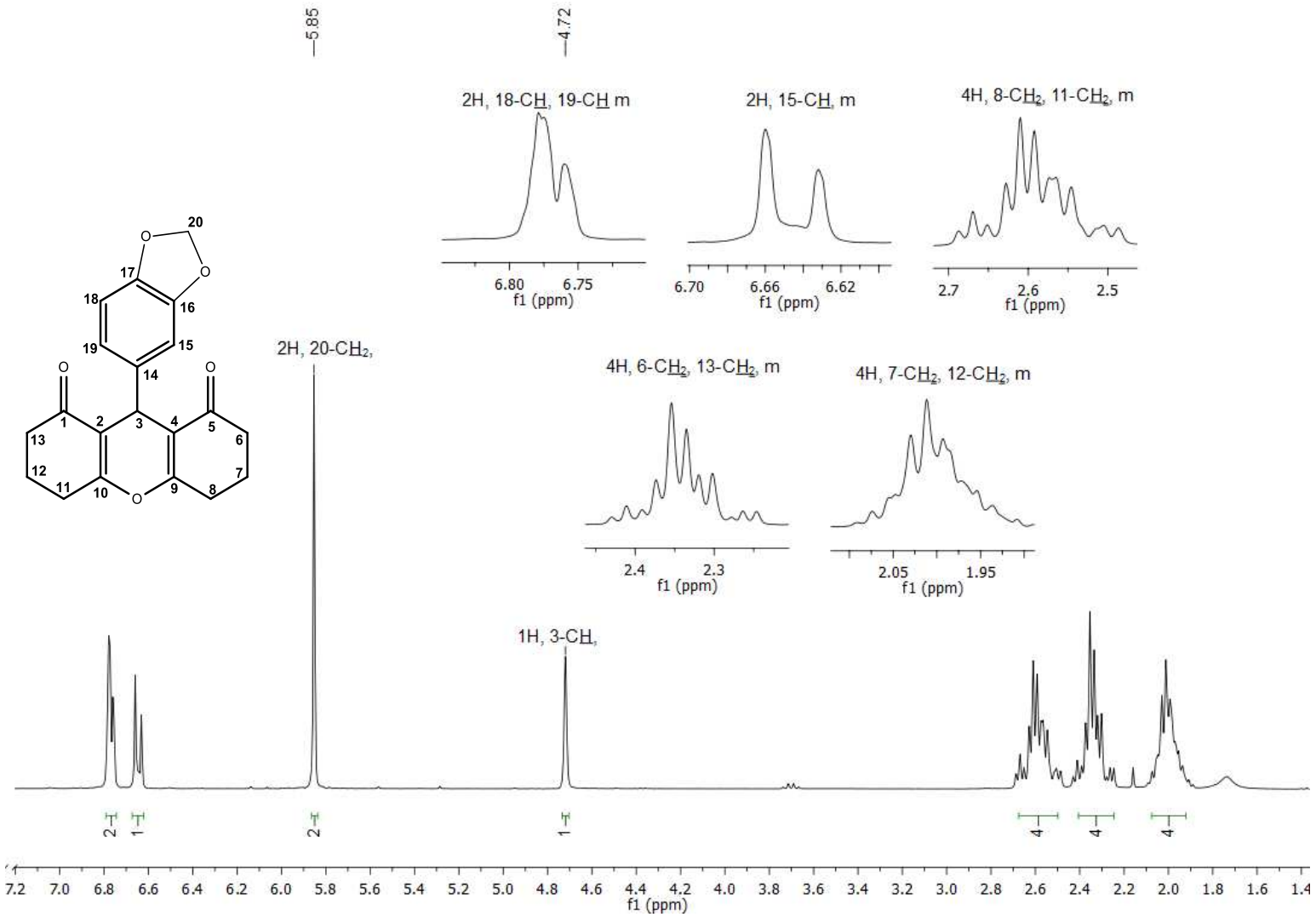

Figura 55. Espectro de RMN de ^{1}H (300 MHz, $CDCl_3$) do composto **14**.

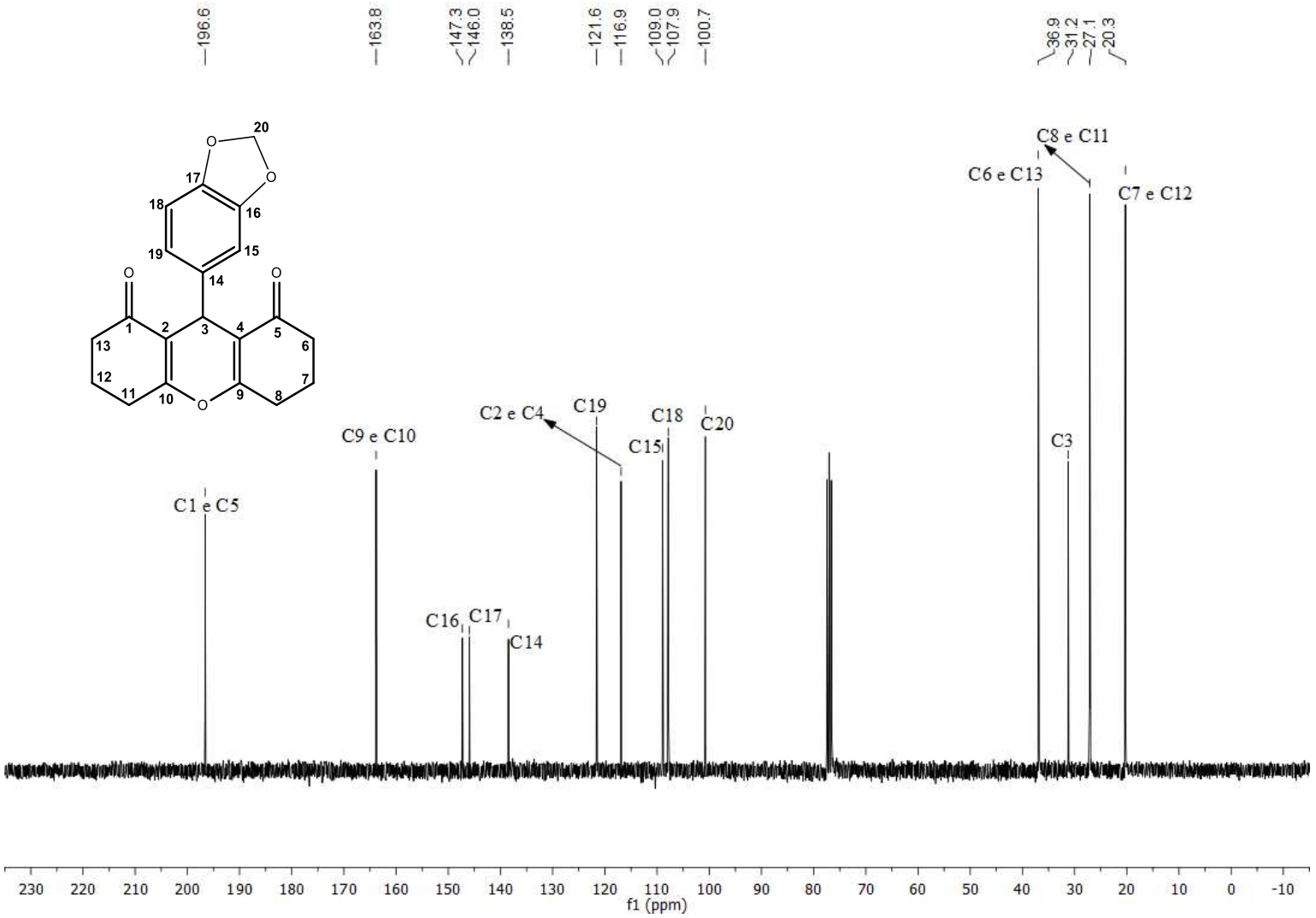

Figura 56. Espectro de RMN de ^{13}C (75 MHz, $CDCl_3$) do composto **14**.

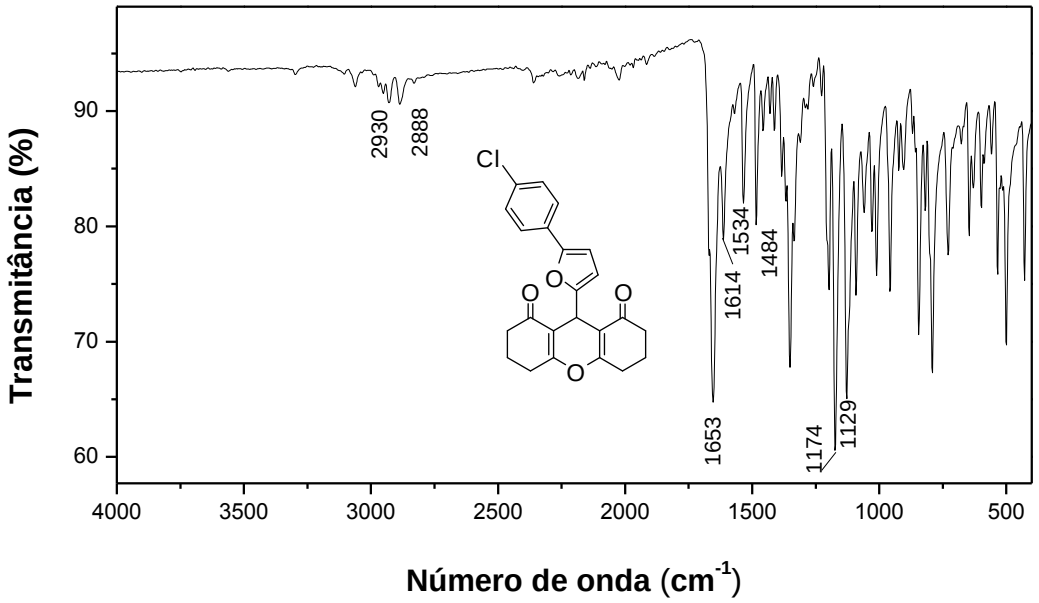

Figura 57. Espectro no infravermelho (ATR) do composto **15**.

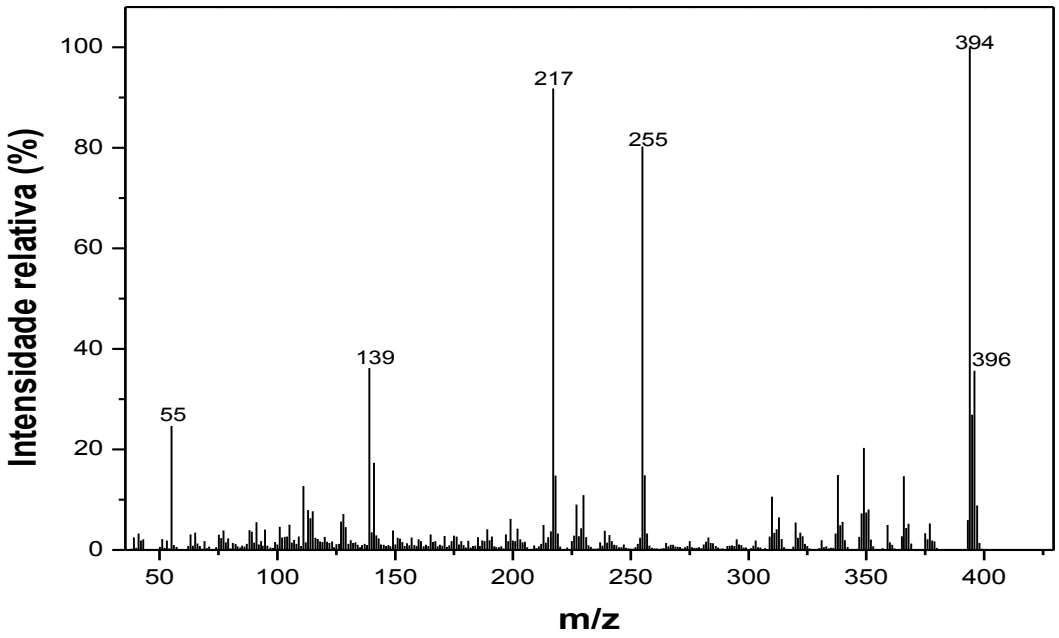

Figura 58. Espectro de massas do composto **15**.

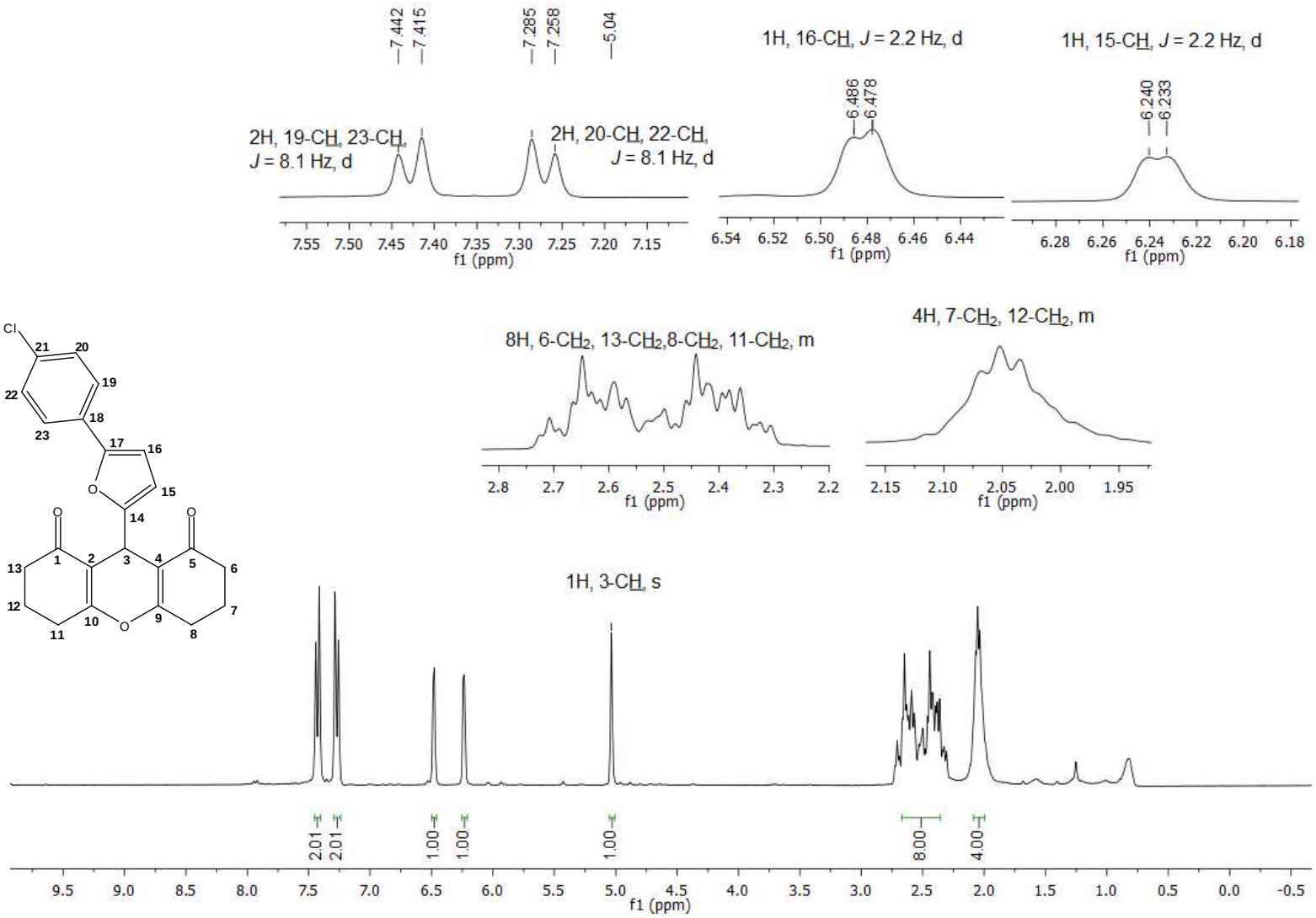

Figura 59. Espectro de RMN de ^{1}H (300 MHz, $CDCl_3$) do composto **15**.

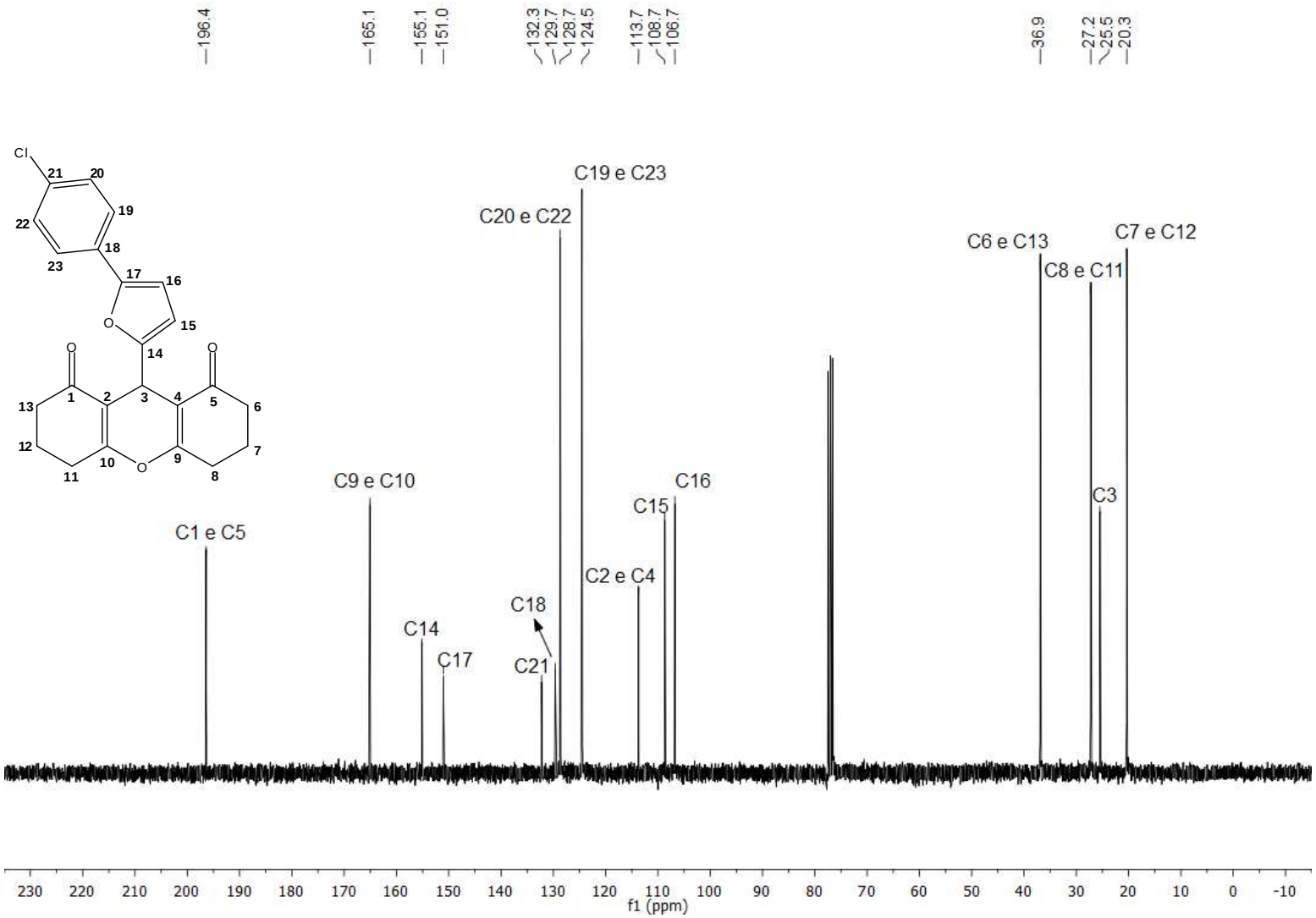

Figura 60. Espectro de RMN de ^{13}C (75 MHz, $CDCl_3$) do composto **15**.

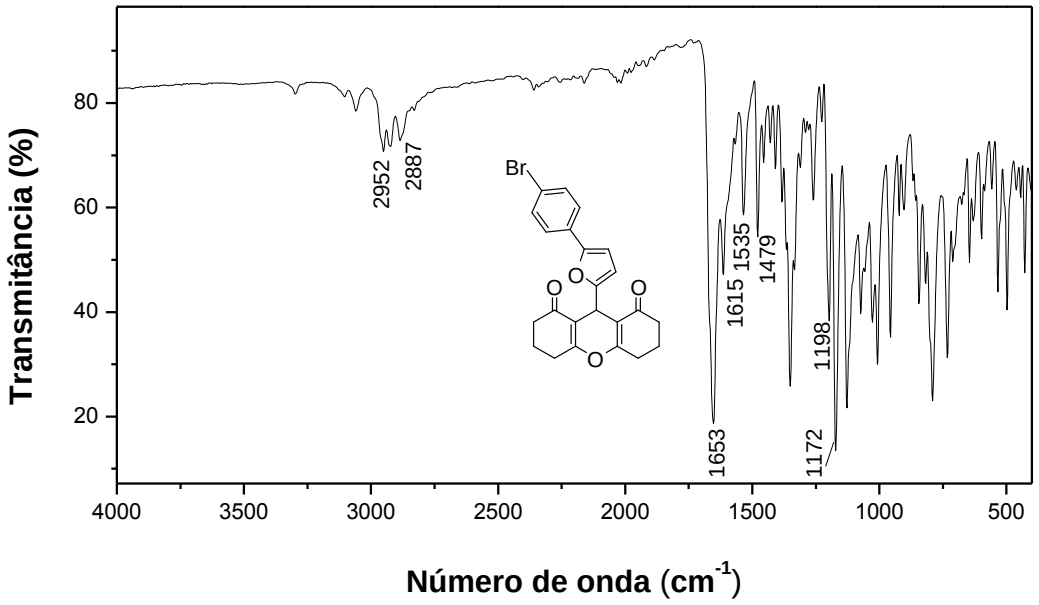

Figura 61. Espectro no infravermelho (ATR) do composto **16**.

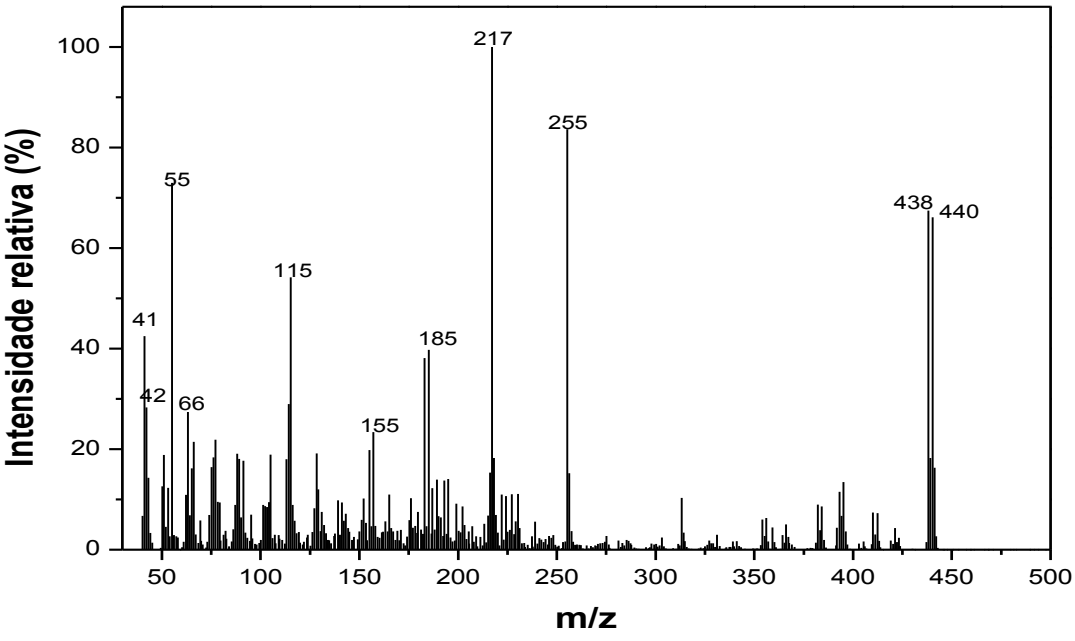

Figura 62. Espectro de massas do composto **16**.

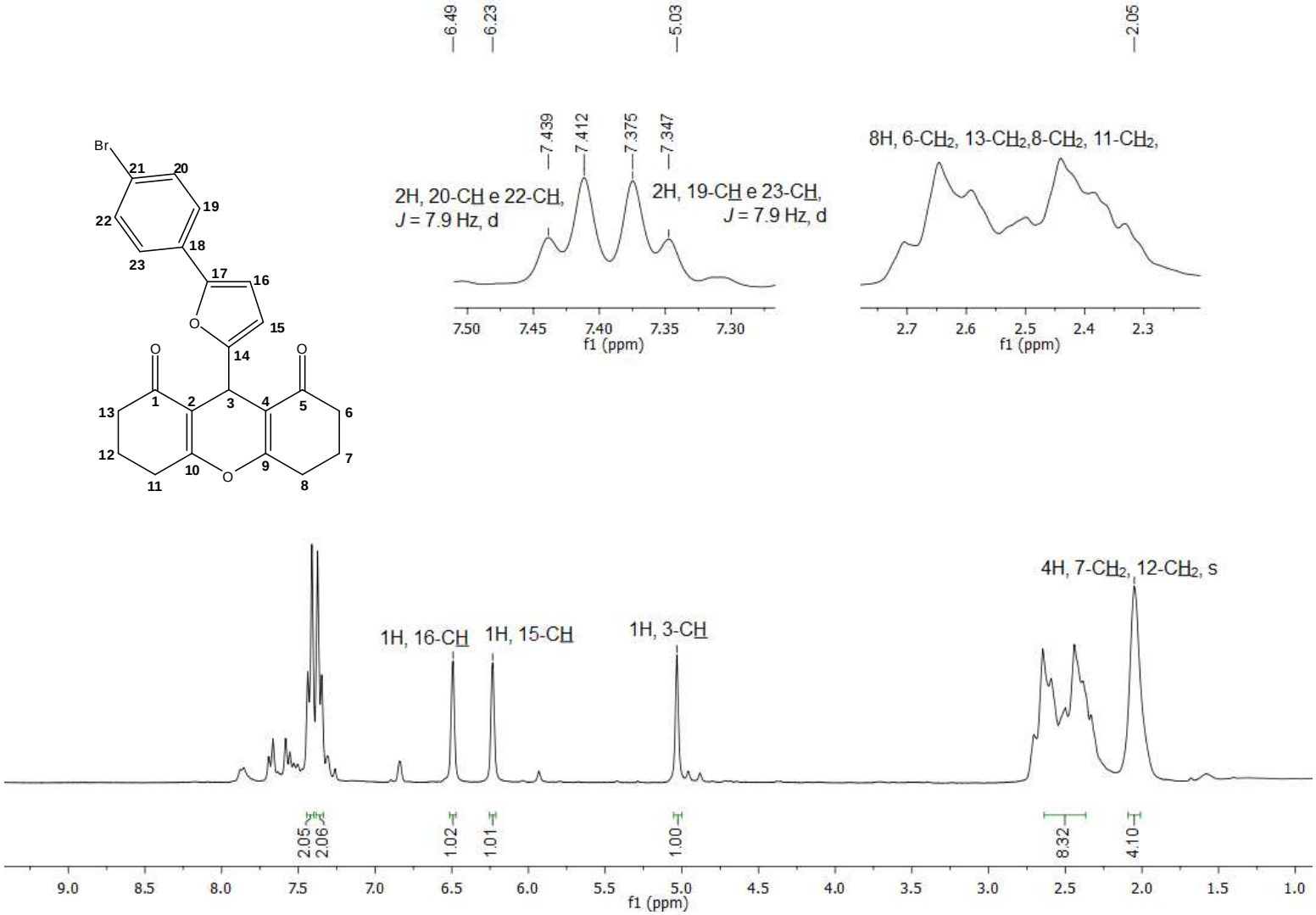

Figura 63. Espectro de RMN de ^{1}H (300 MHz, $CDCl_3$) do composto **16**.

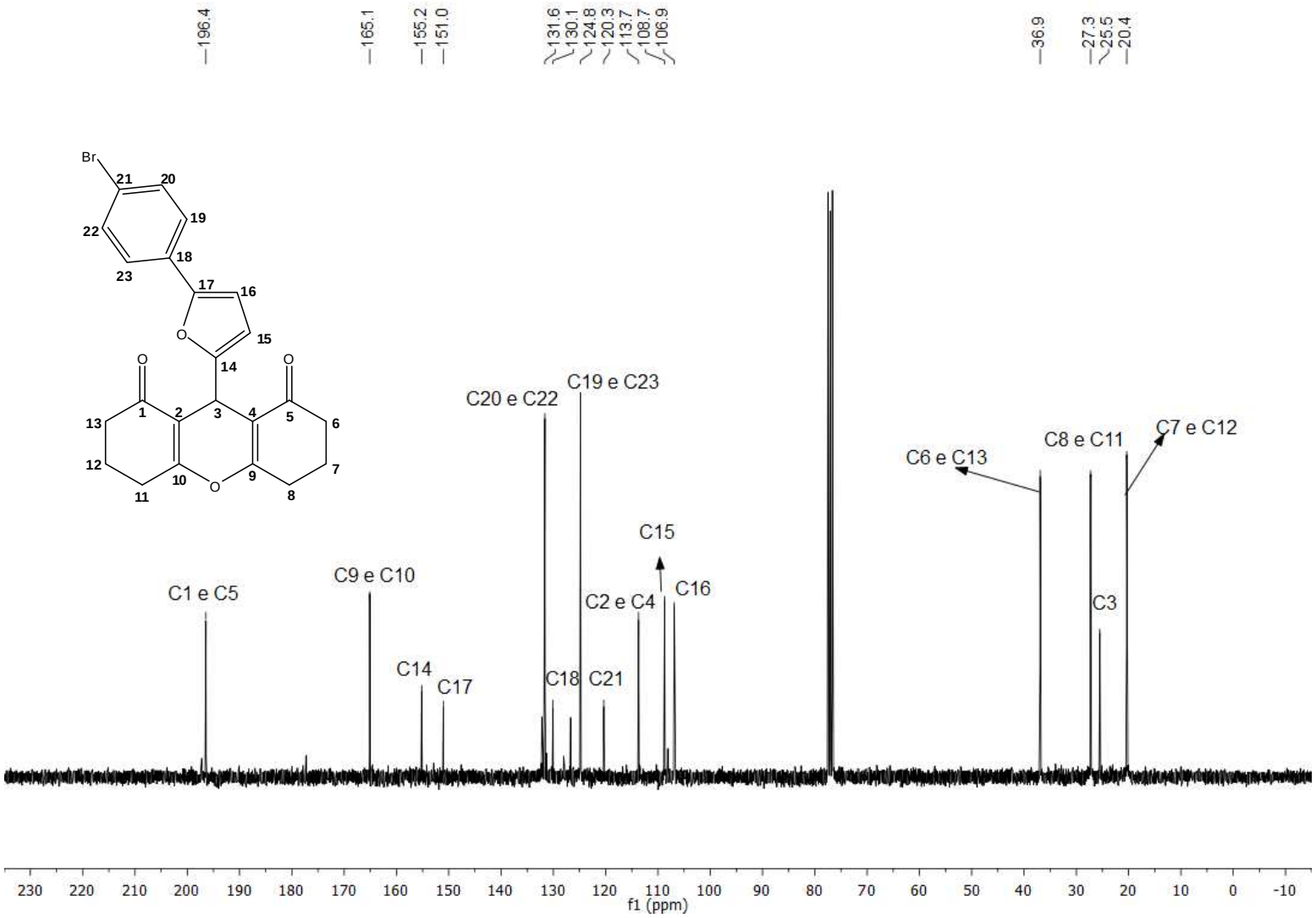

Figura 64. Espectro de RMN de ^{13}C (75 MHz, $CDCl_3$) do composto **16**.

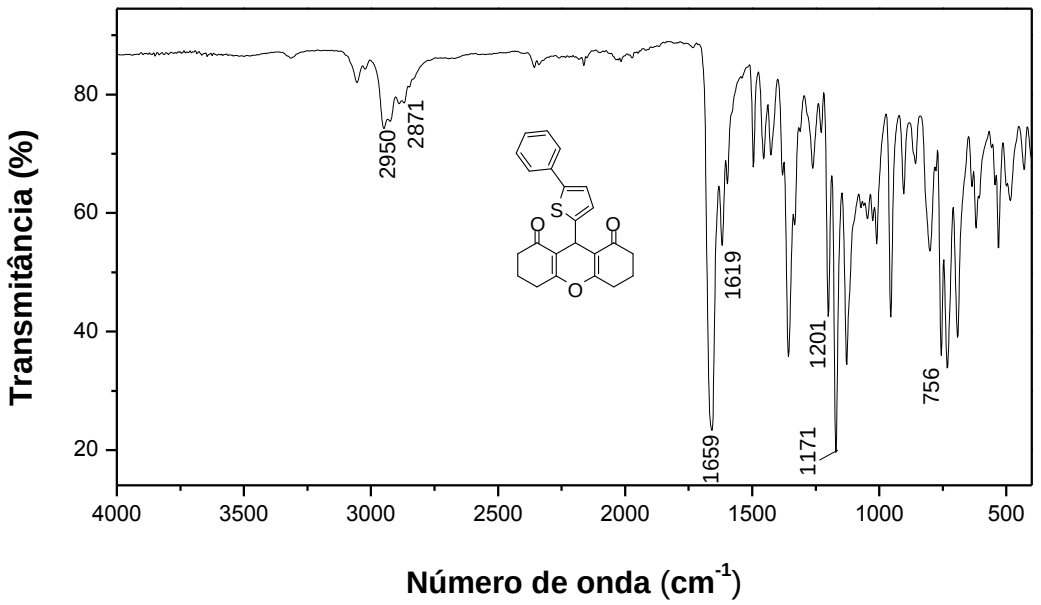

Figura 65. Espectro no infravermelho (ATR) do composto **17**.

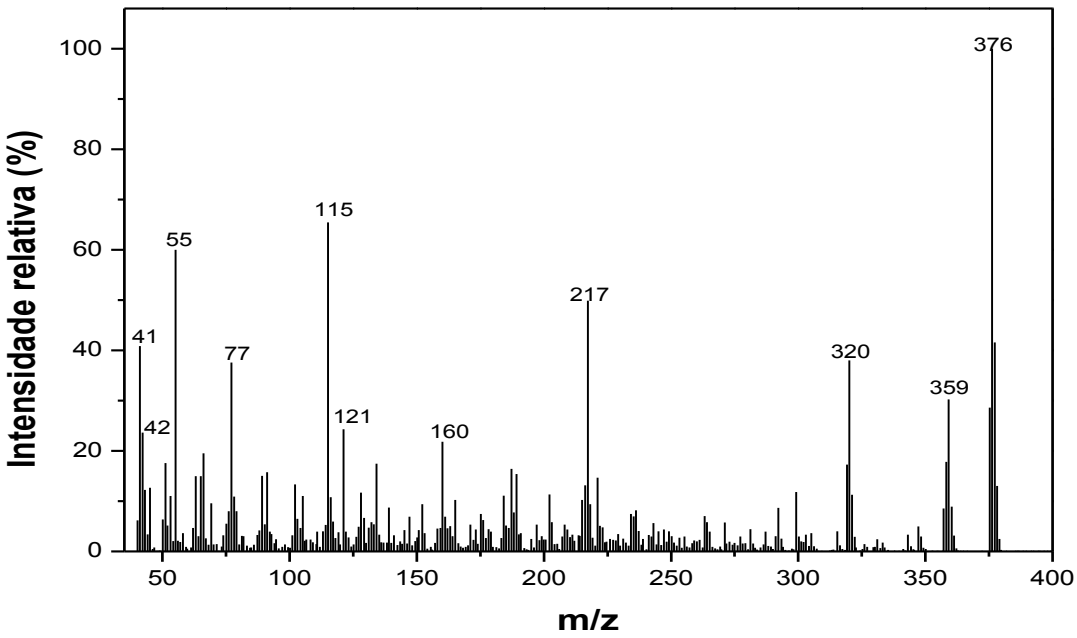

Figura 66. Espectro de massas do composto **17**.

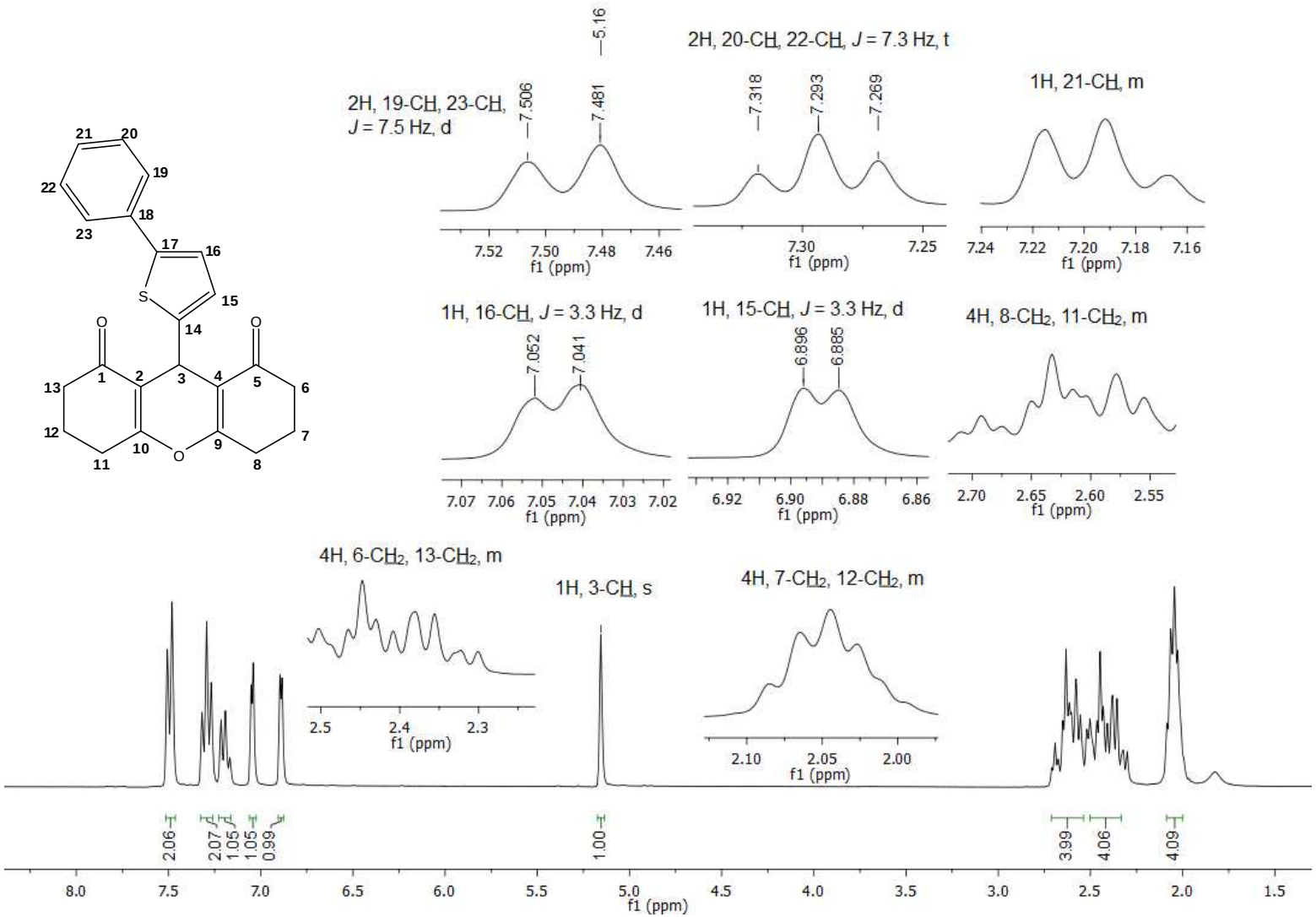

Figura 67. Espectro de RMN de ^{1}H (300 MHz, $CDCl_3$) do composto **17**.

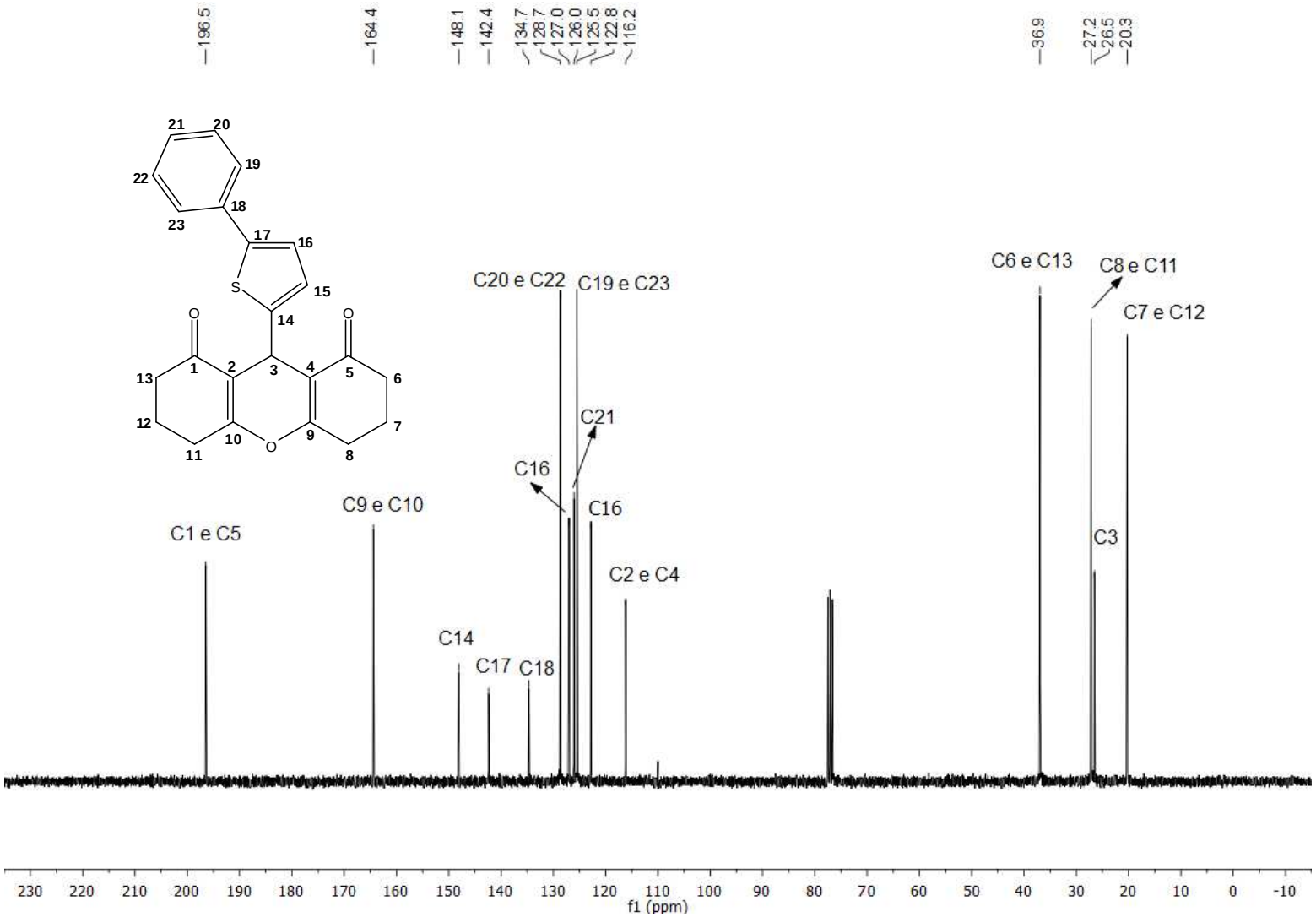

Figura 68. Espectro de RMN de ^{13}C (75 MHz, $CDCl_3$) do composto **17**.

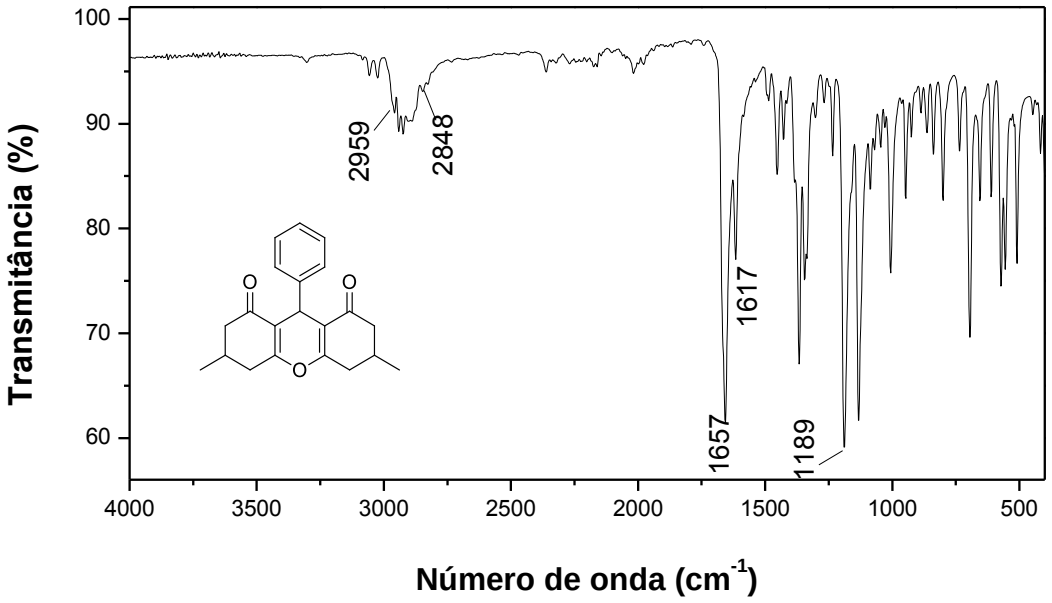

Figura 69. Espectro no infravermelho (ATR) do composto **18**.

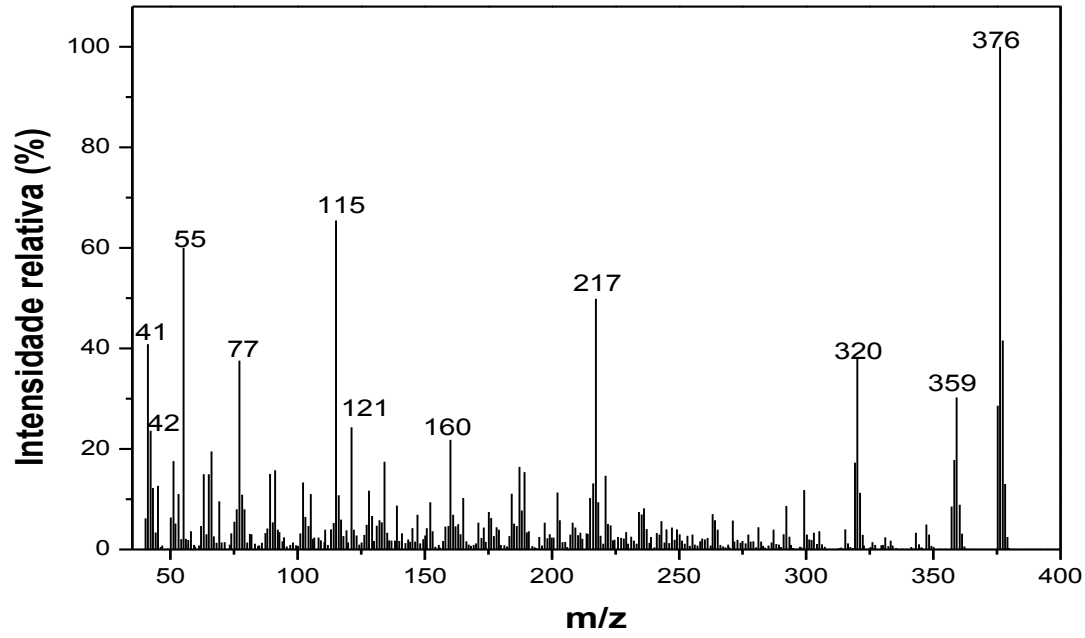

Figura 70. Espectro de massas do composto **18**.

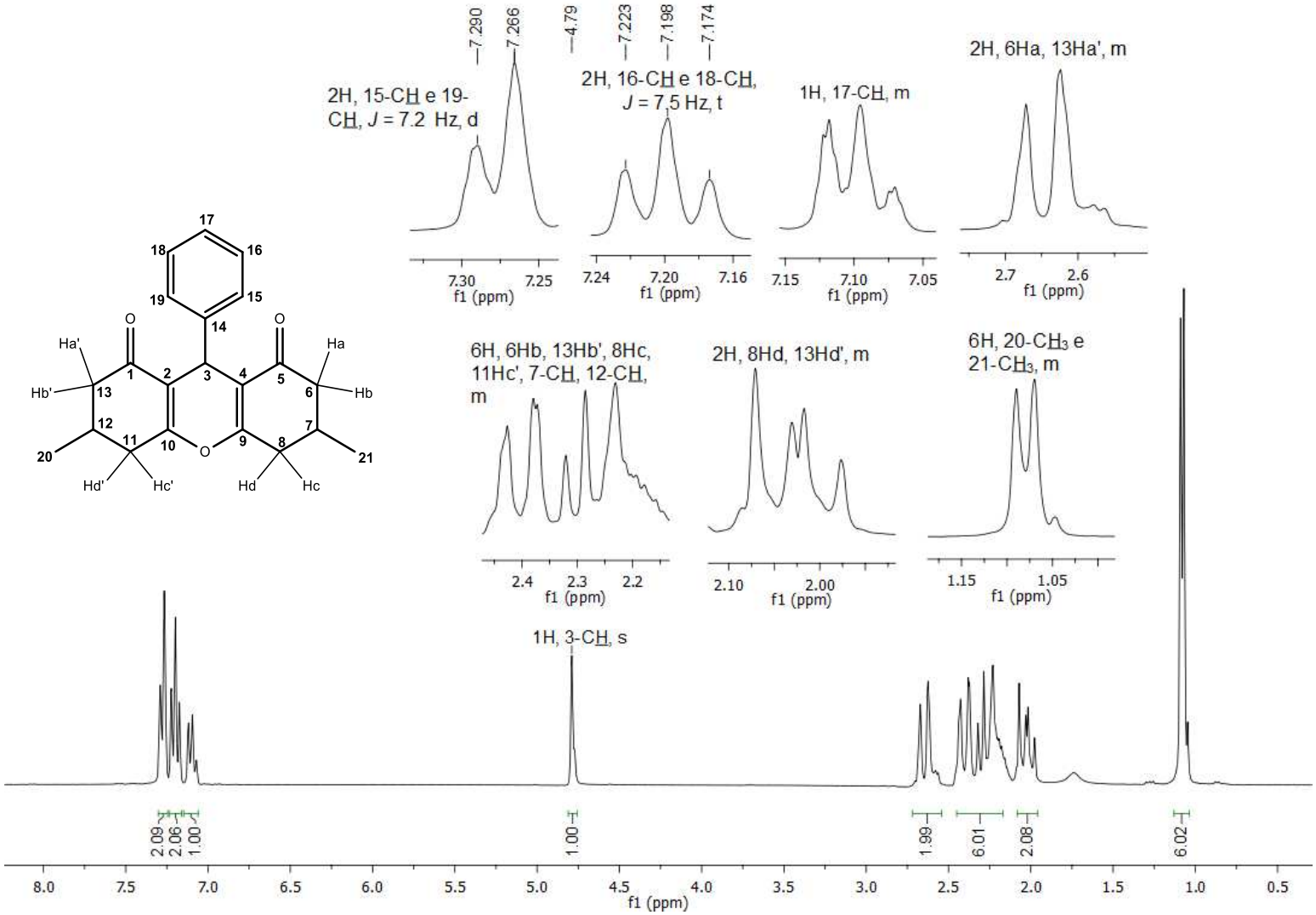

Figura 71. Espectro de RMN de ^{1}H (300 MHz, $CDCl_3$) do composto **18**.

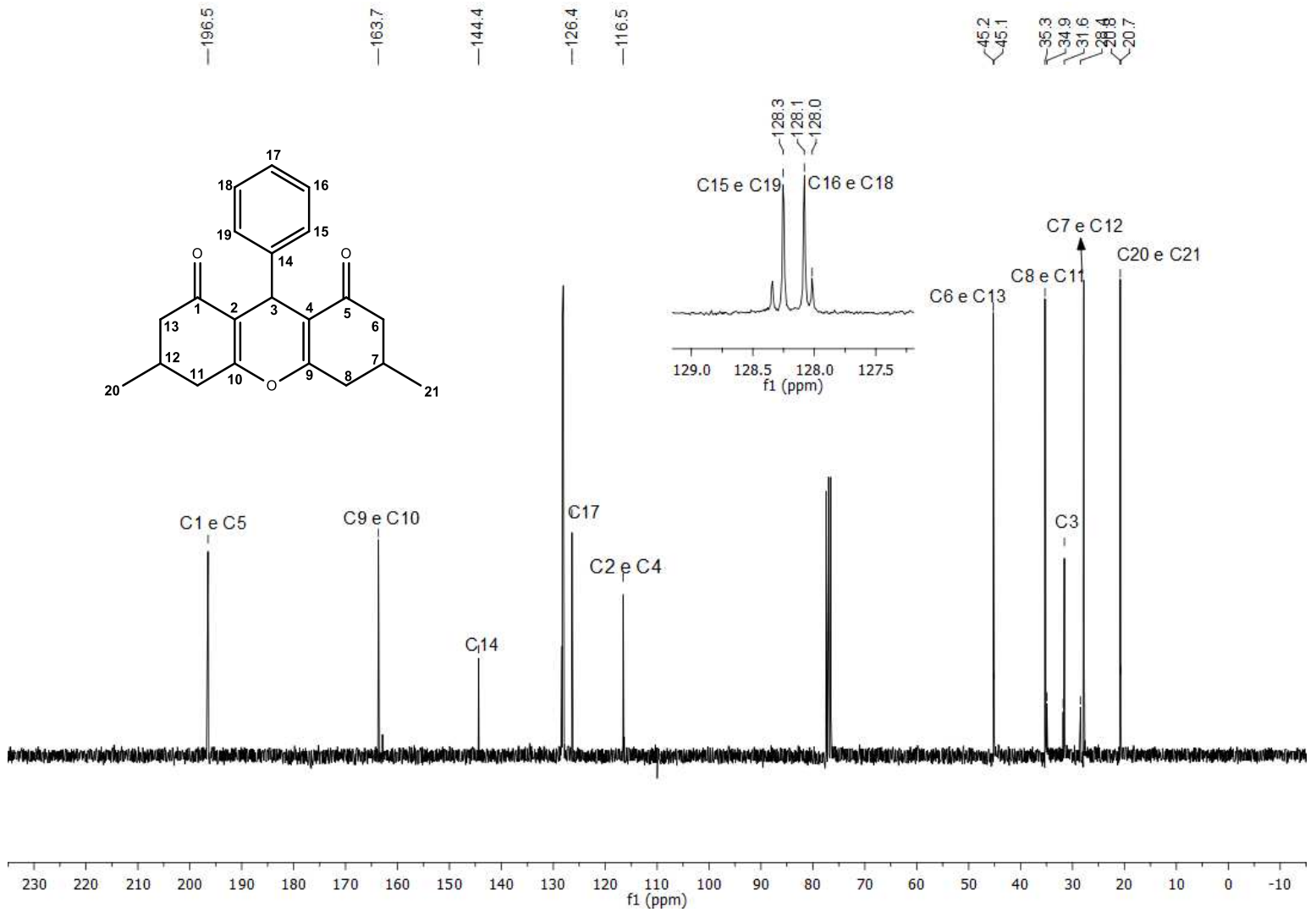

Figura 72. Espectro de RMN de ^{13}C (75 MHz, $CDCl_3$) do composto **18**.

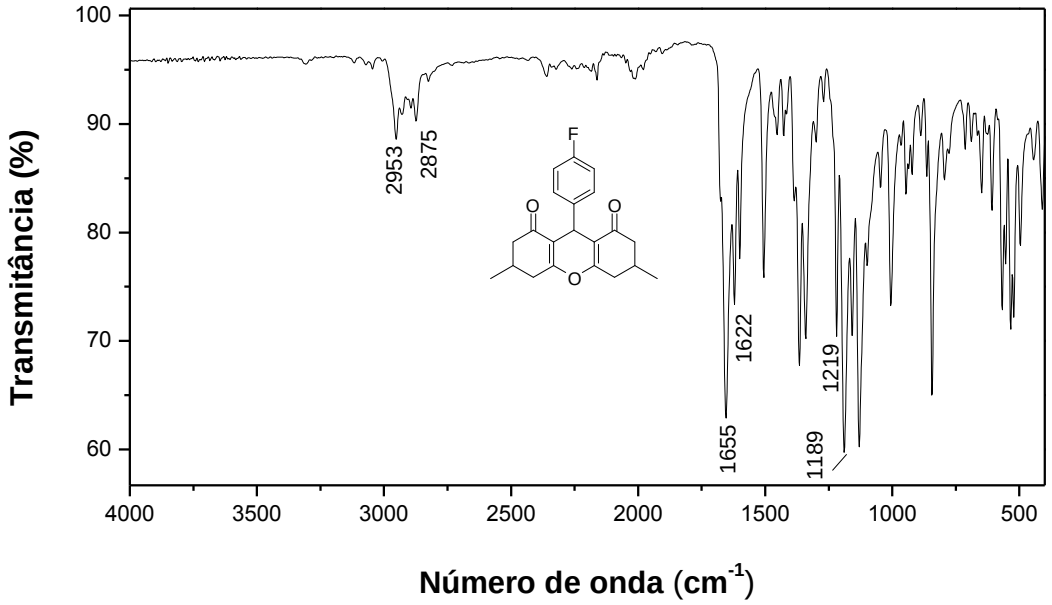

Figura 73. Espectro no infravermelho (ATR) do composto **19**.

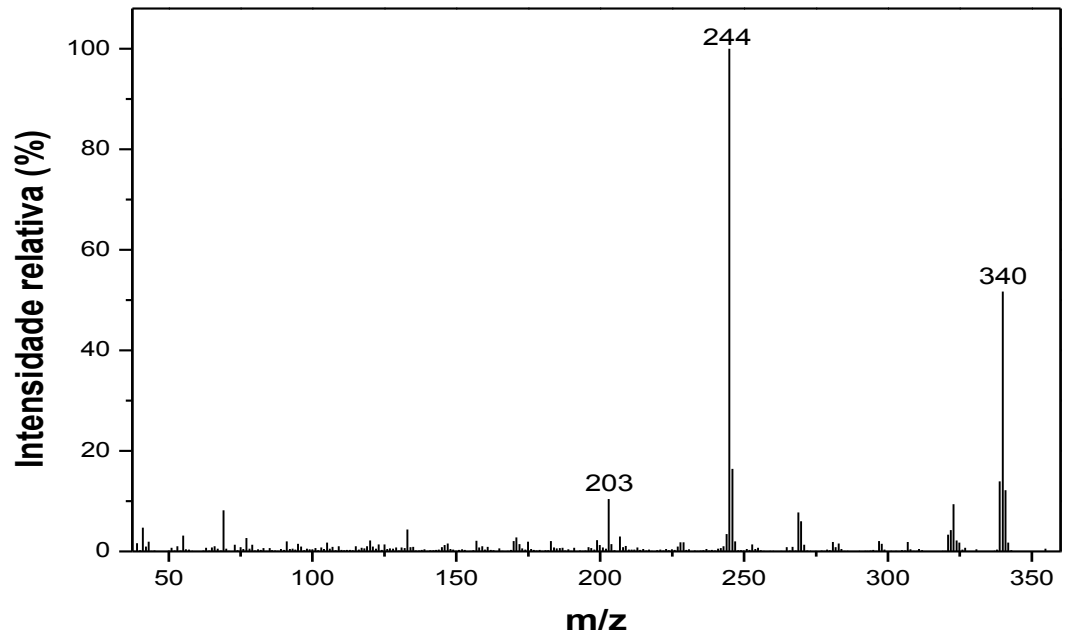

Figura 74. Espectro de massas do composto **19**.

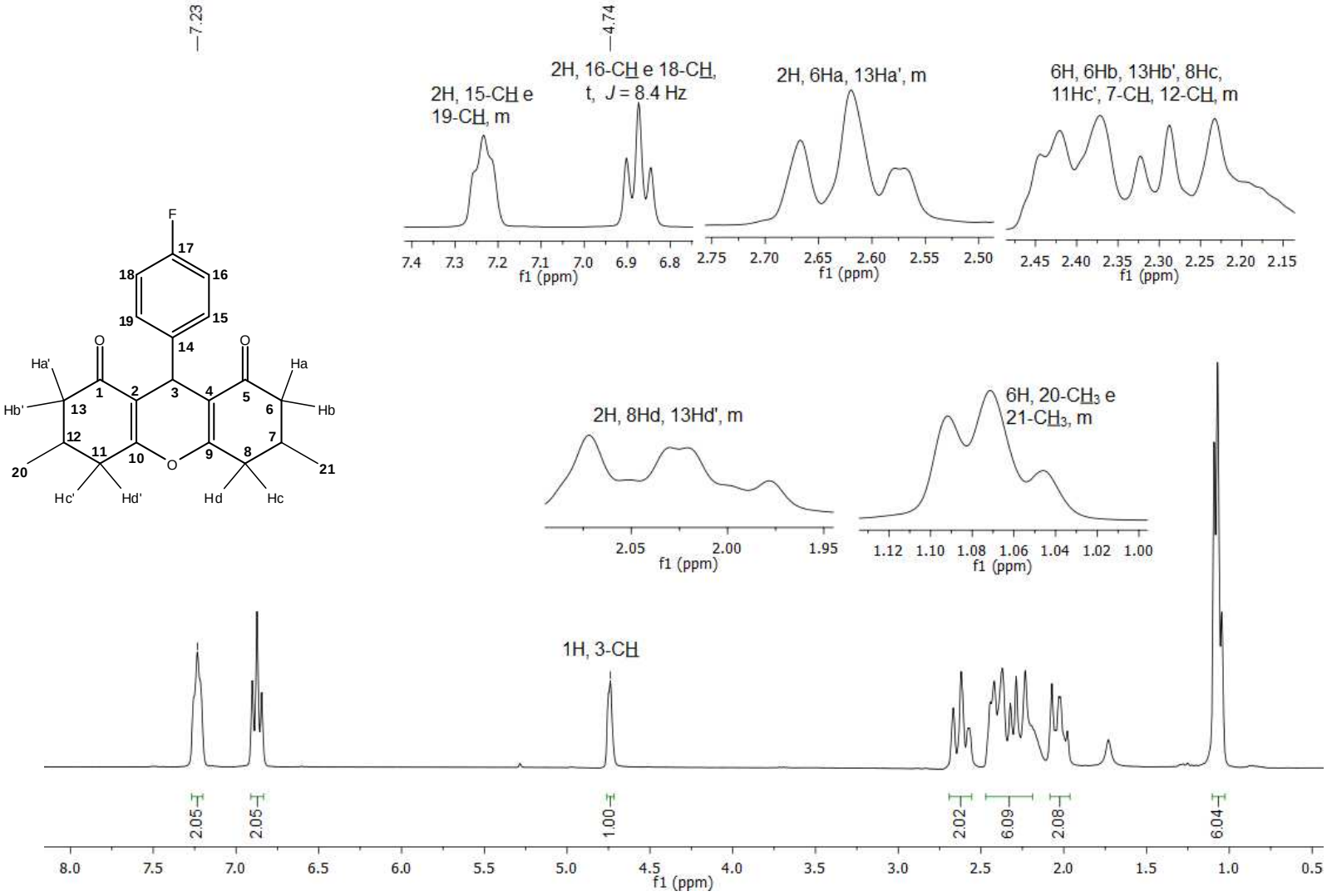

Figura 75. Espectro de RMN de ^{1}H (300 MHz, $CDCl_3$) do composto **19**.

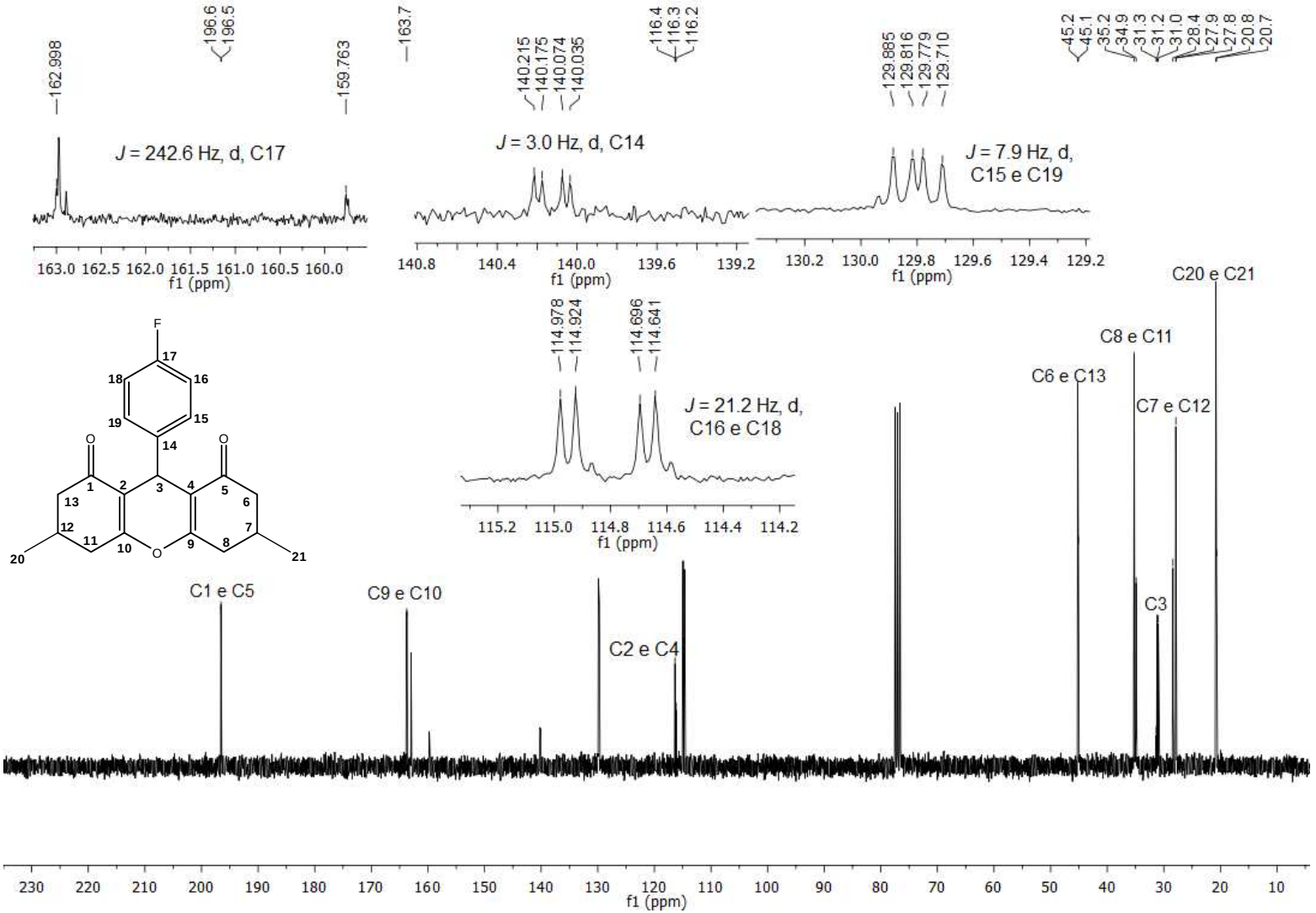

Figura 76. Espectro de RMN de ^{13}C (75 MHz, $CDCl_3$) do composto **19**.

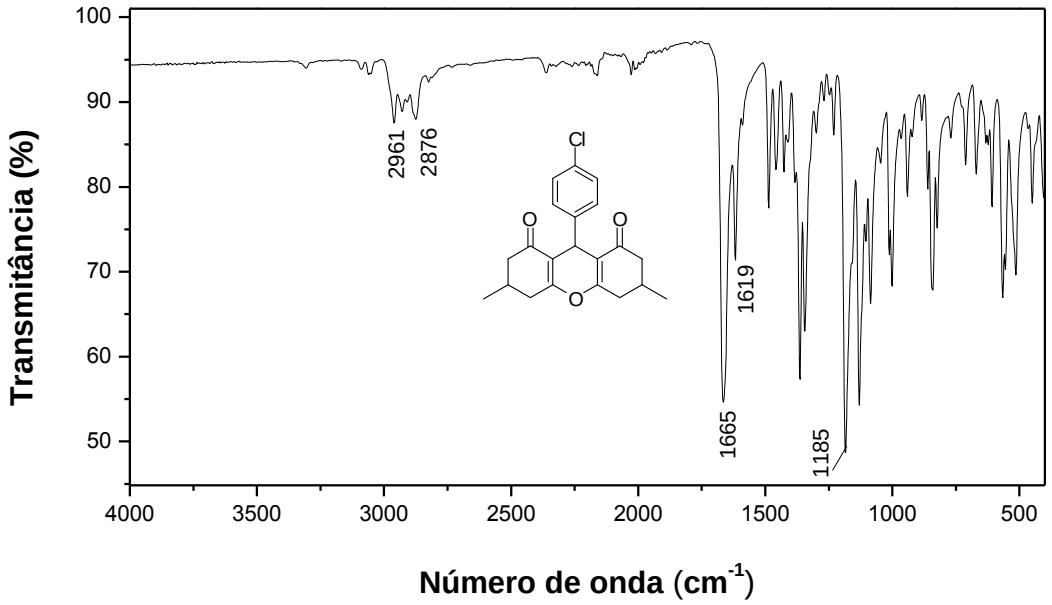

Figura 77. Espectro no infravermelho (ATR) do composto **20**.

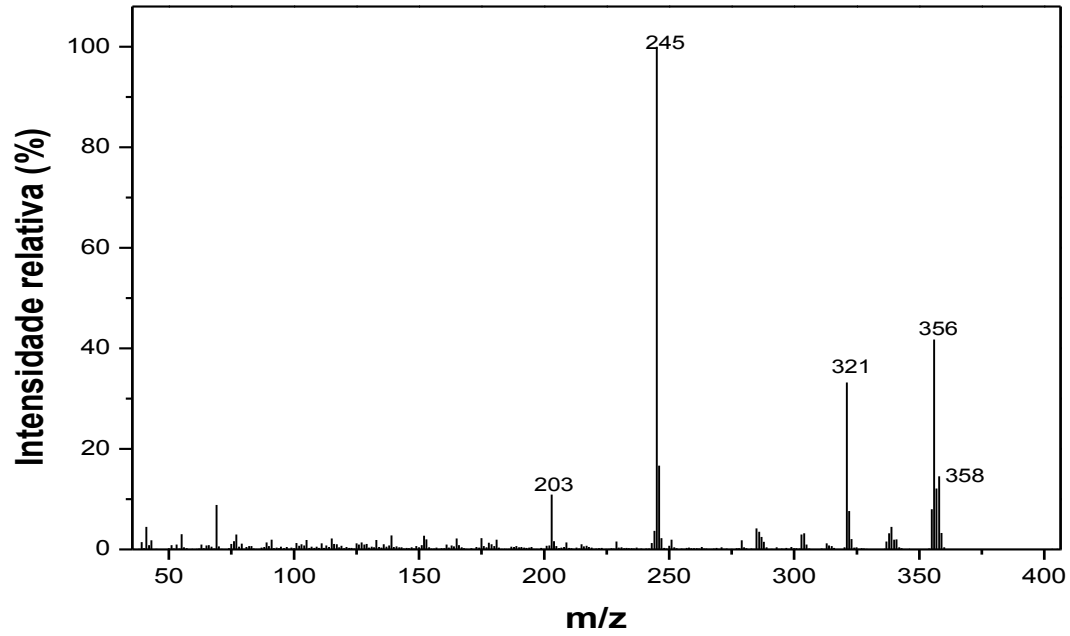

Figura 78. Espectro de massas do composto **20**.

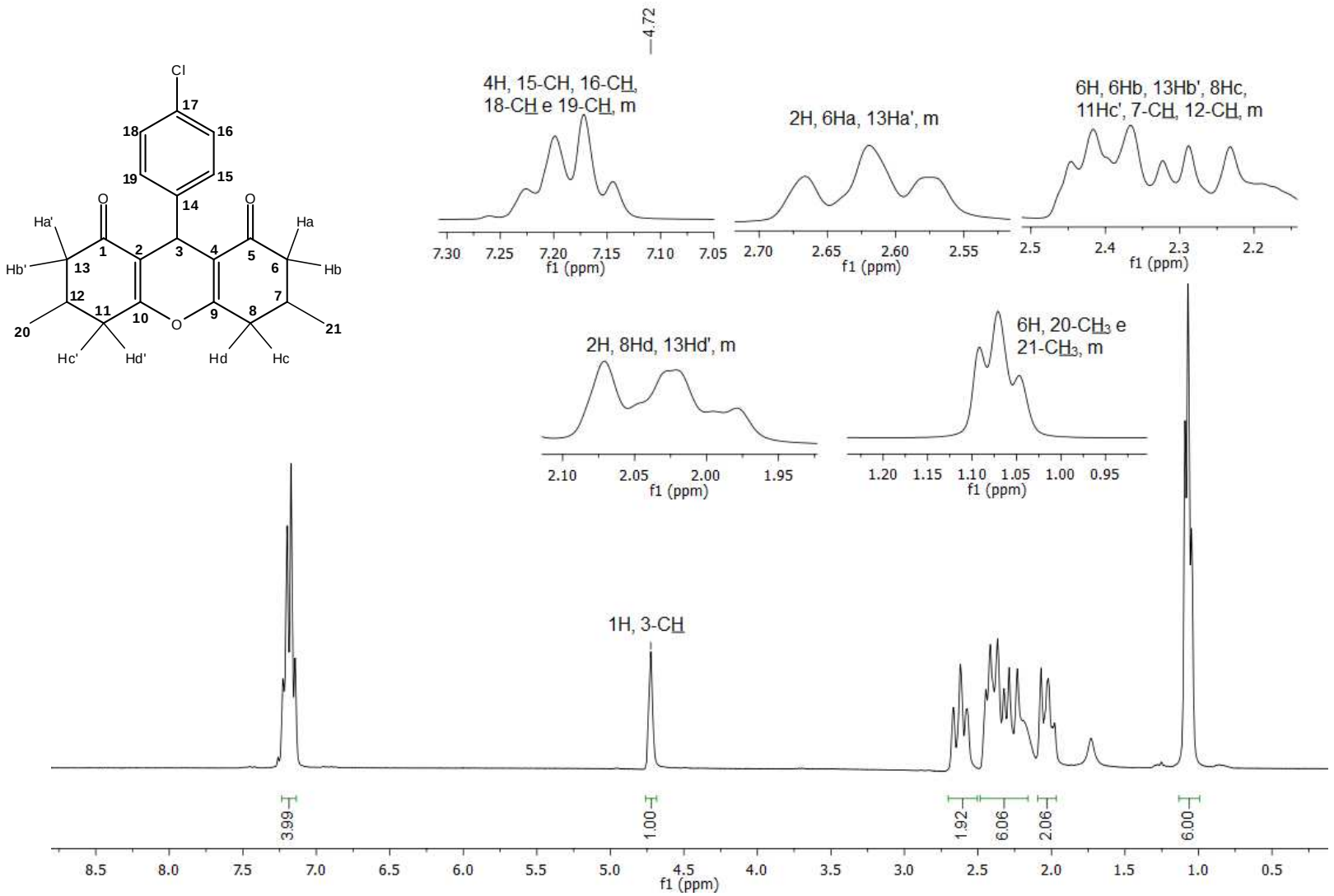

Figura 79. Espectro de RMN de ^{1}H (300 MHz, $CDCl_3$) do composto **20**.

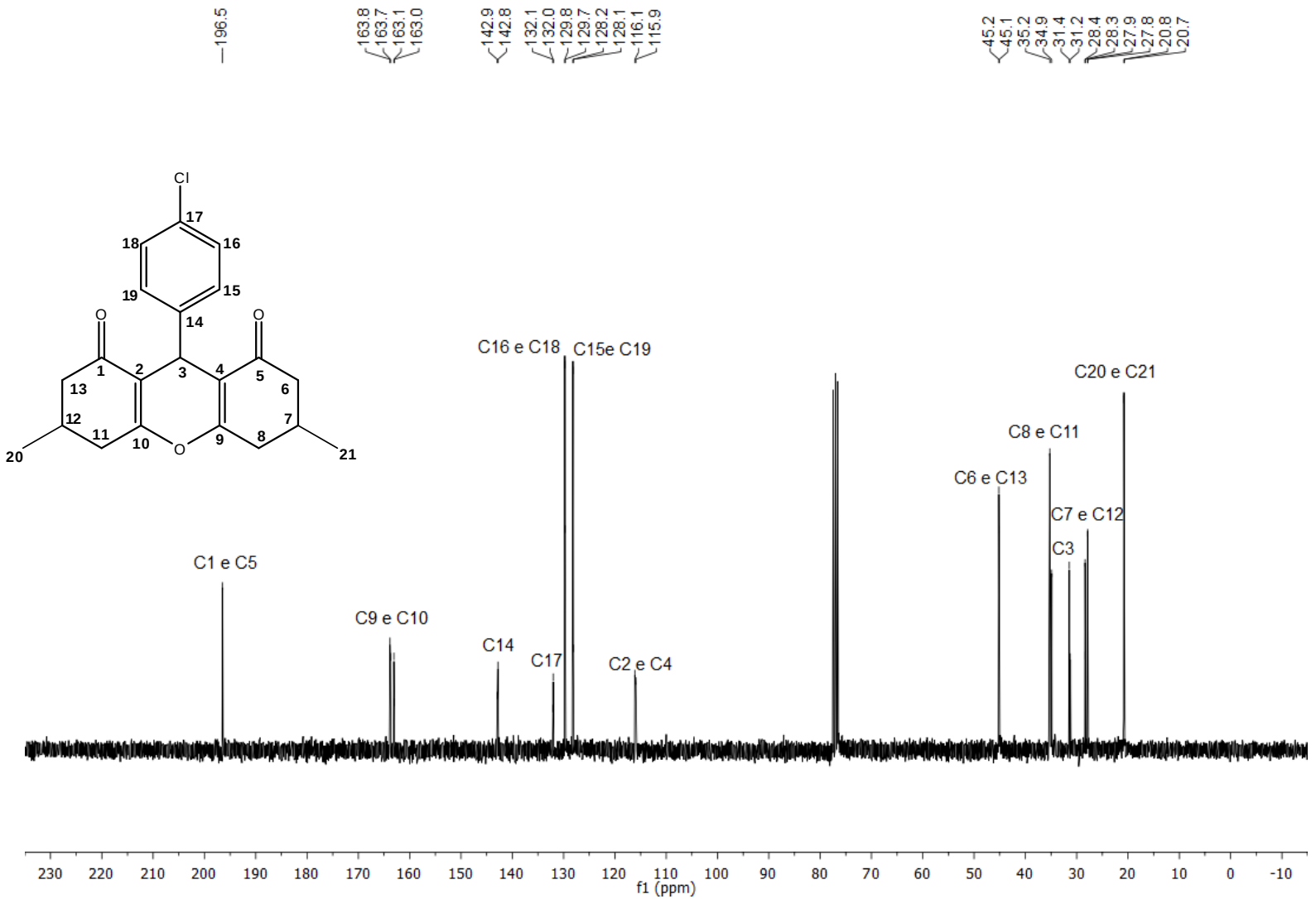

Figura 80. Espectro de RMN de ^{13}C (75 MHz, $CDCl_3$) do composto **20**.

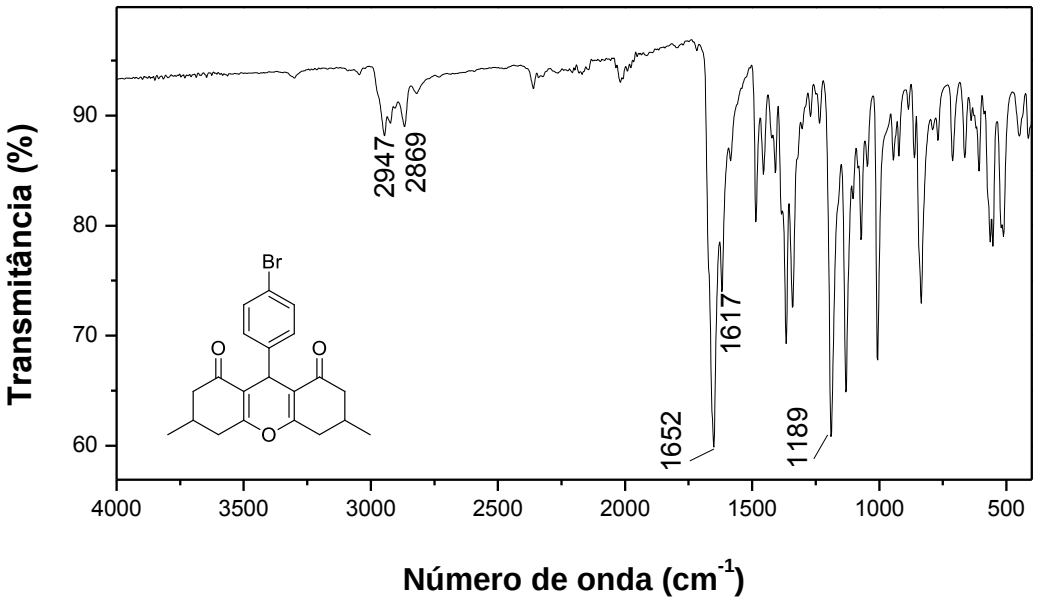

Figura 81. Espectro no infravermelho (ATR) do composto **21**.

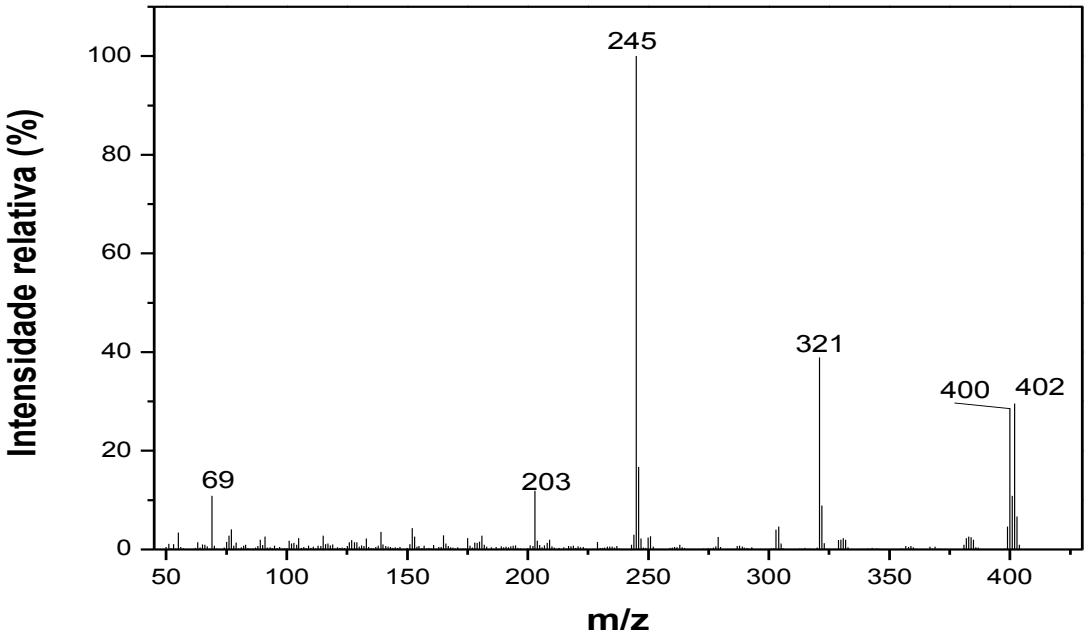

Figura 82. Espectro de massas do composto 21.

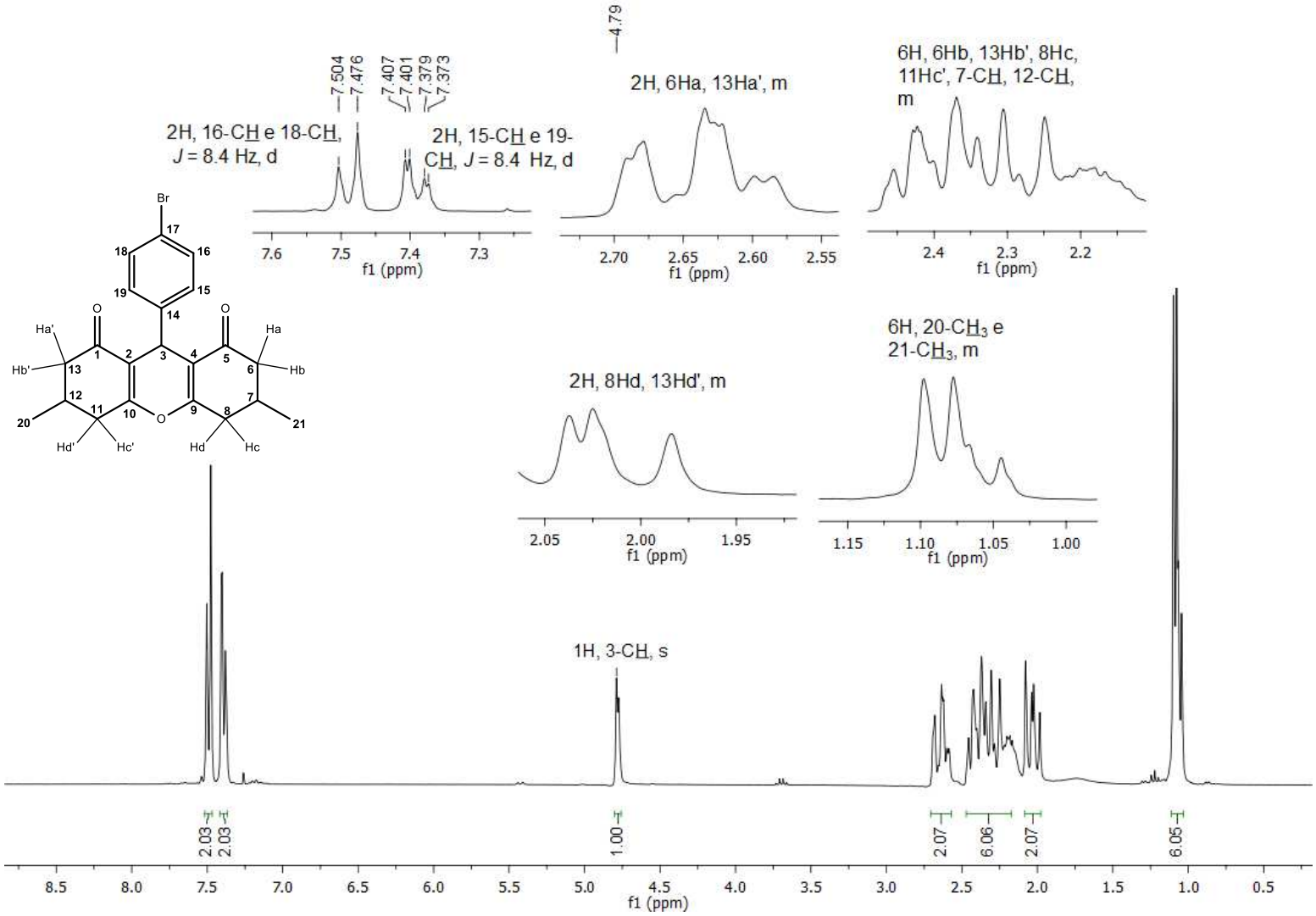

Figura 83. Espectro de RMN de ^{1}H (300 MHz, $CDCl_3$) do composto **21**.

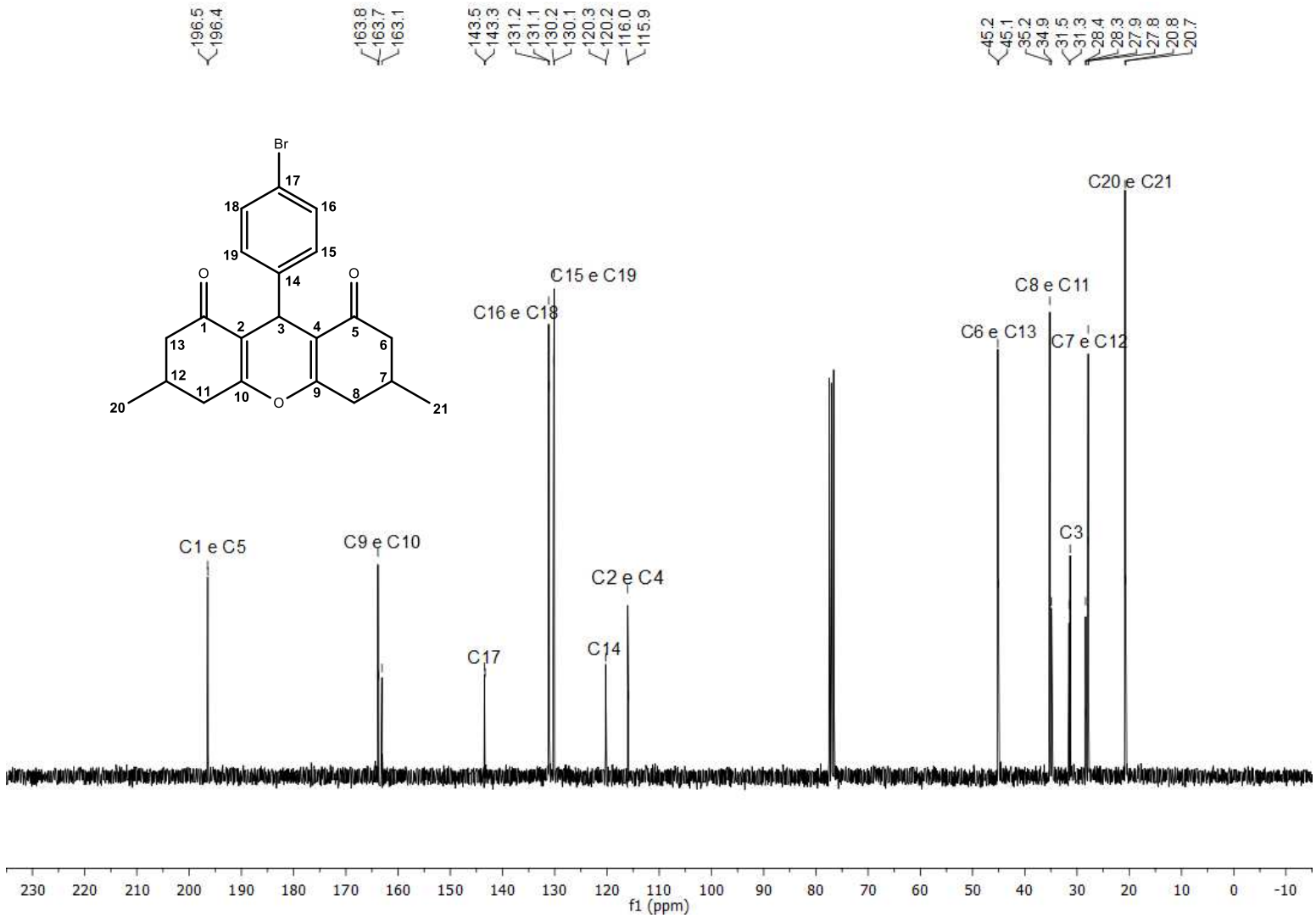

Figura 84. Espectro de RMN de ^{13}C (75 MHz, $CDCl_3$) do composto **21**.

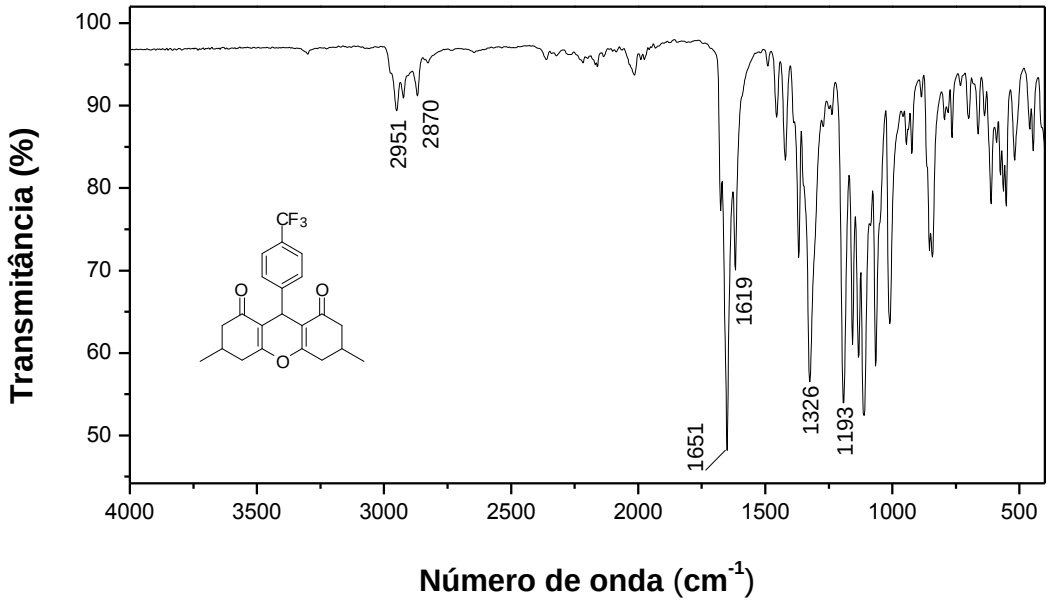

Figura 85. Espectro no infravermelho (ATR) do composto **22**.

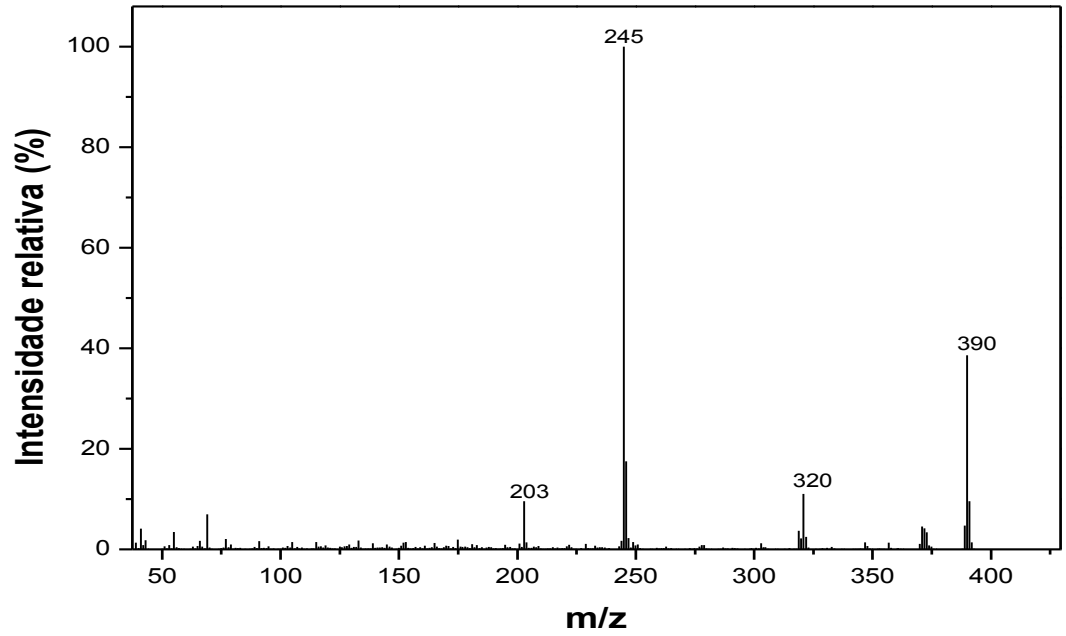

Figura 86. Espectro de massas do composto **22**.

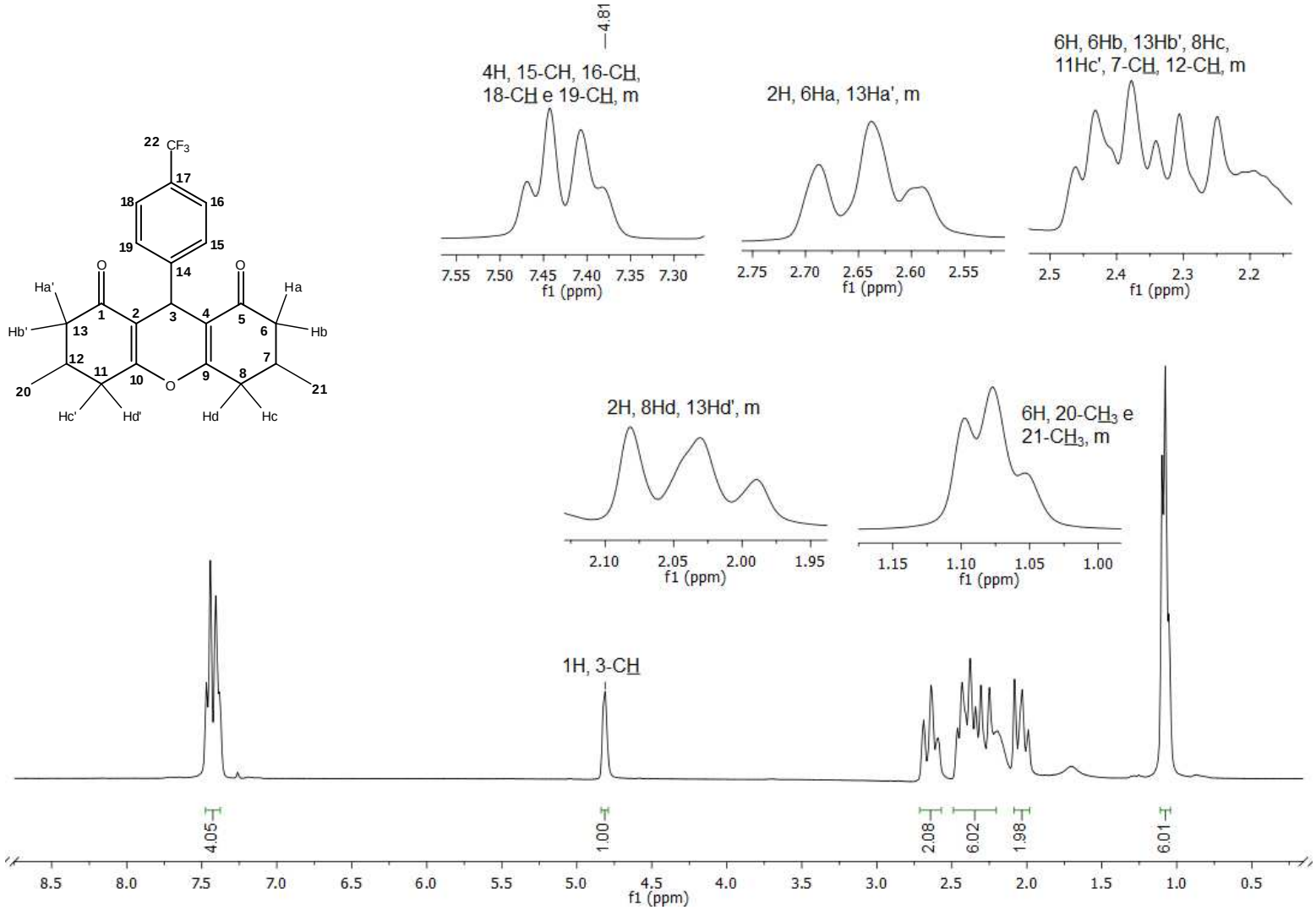

Figura 87. Espectro de RMN de ^{1}H (300 MHz, $CDCl_3$) do composto **22**.

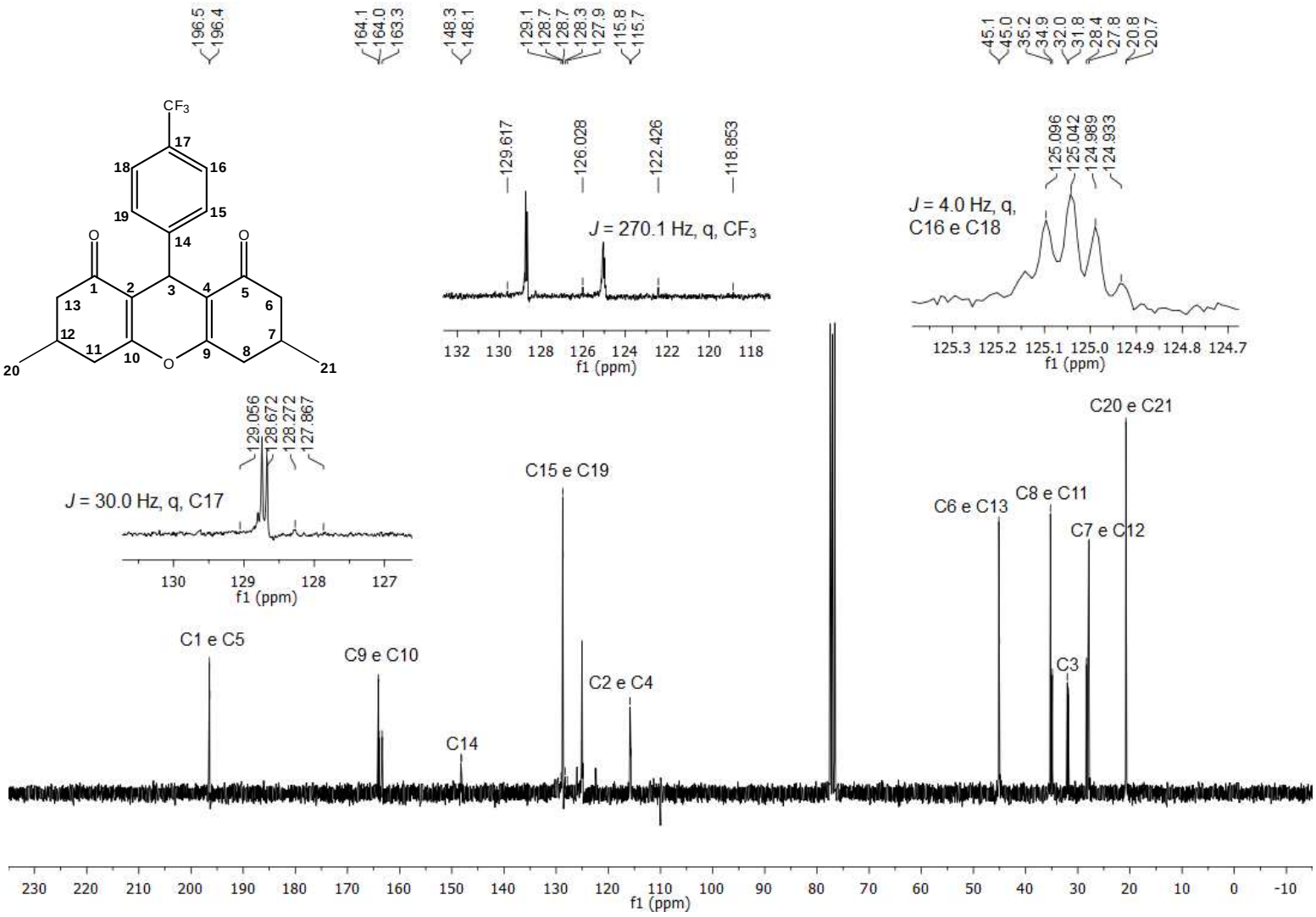

Figura 88. Espectro de RMN de ^{13}C (75 MHz, $CDCl_3$) do composto **22**.

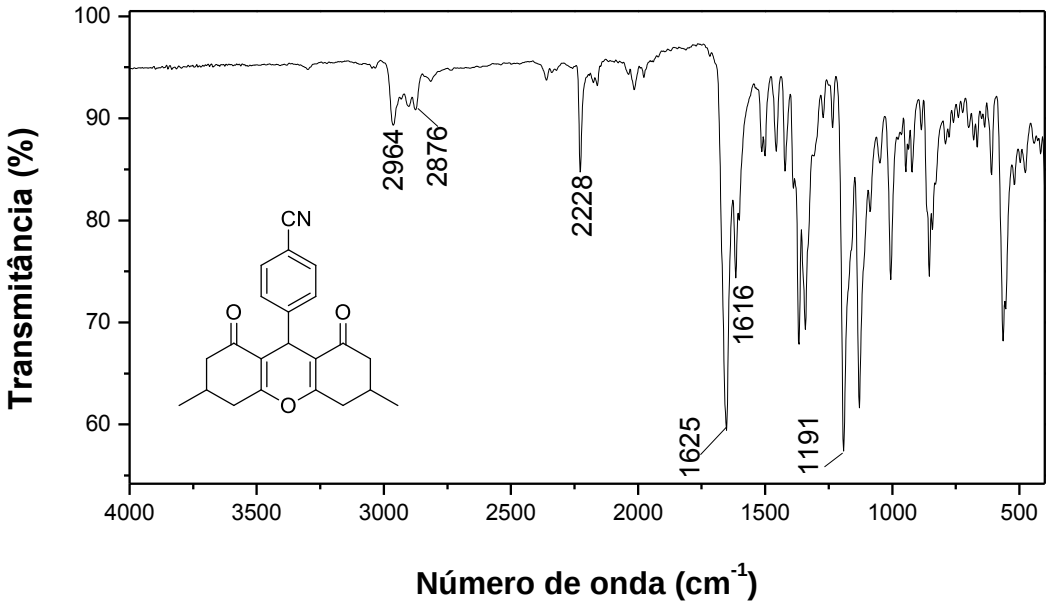

Figura 89. Espectro no infravermelho (ATR) do composto **23**.

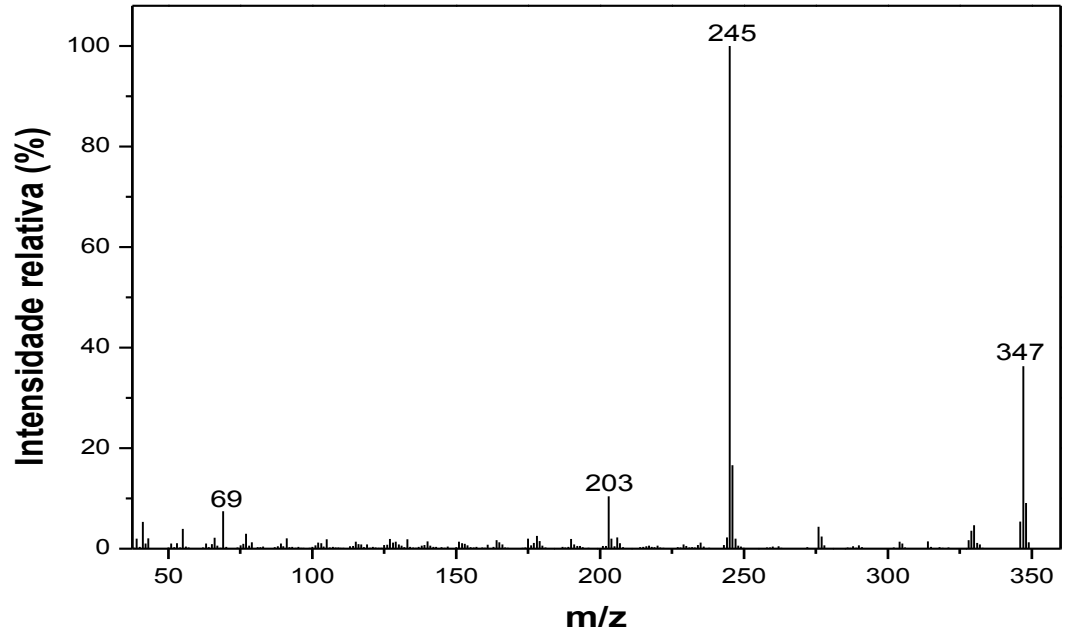

Figura 90. Espectro de massas do composto 23.

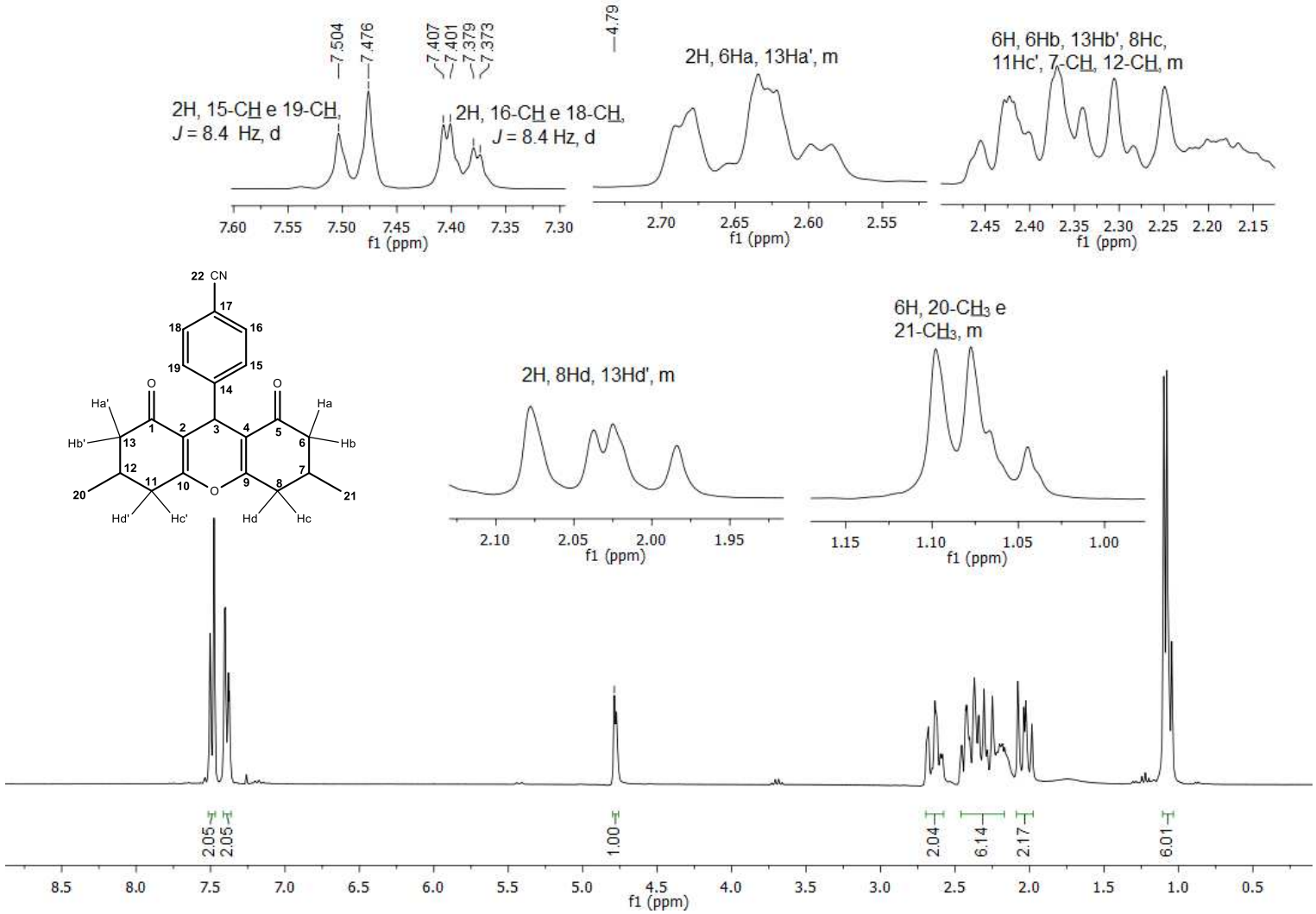

Figura 91. Espectro de RMN de ^{1}H (300 MHz, $CDCl_3$) do composto **23**.

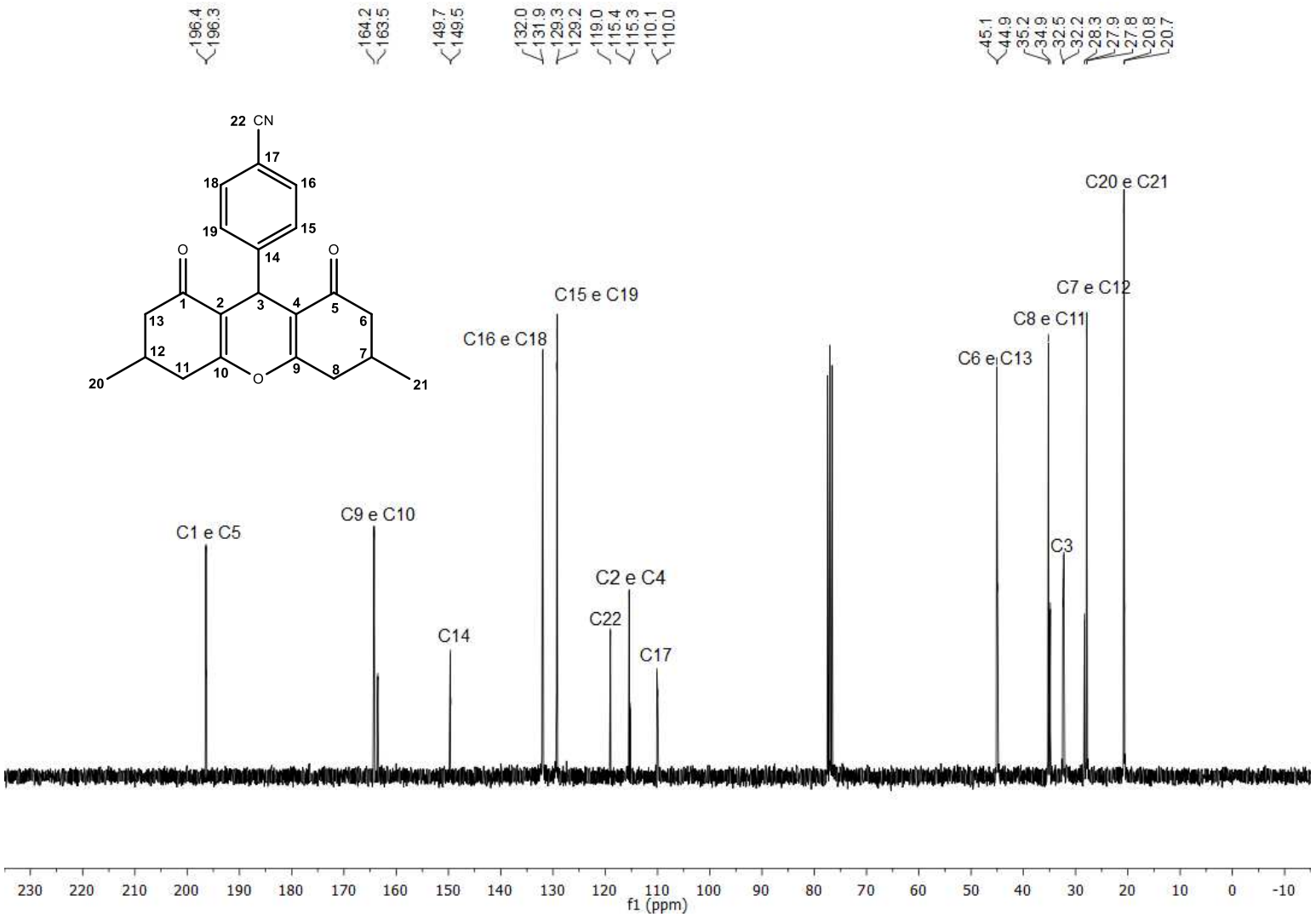

Figura 92. Espectro de RMN de ^{13}C (75 MHz, $CDCl_3$) do composto **23**.

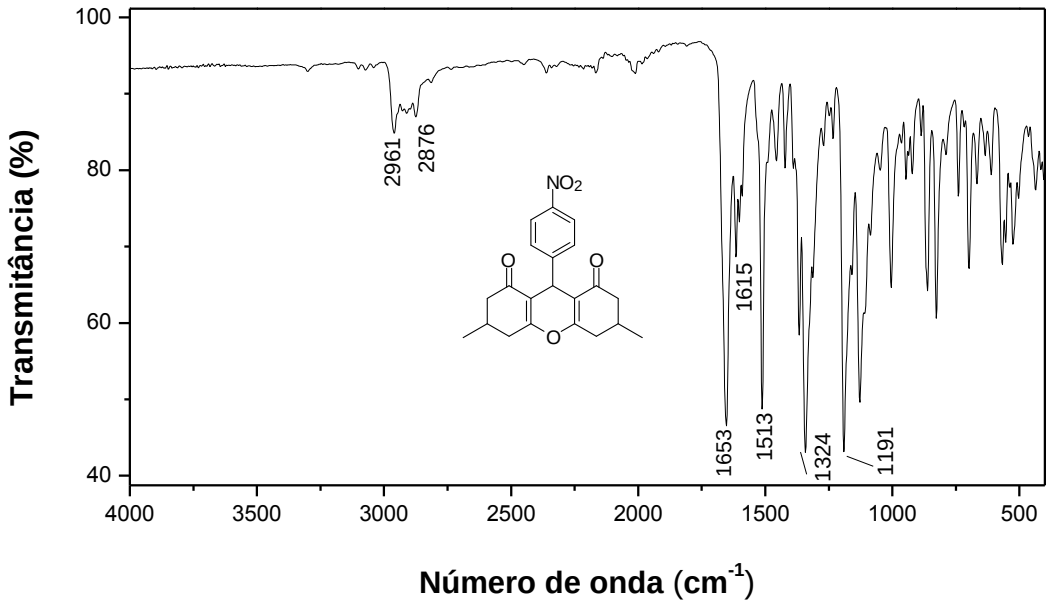

Figura 93. Espectro no infravermelho (ATR) do composto **24**.

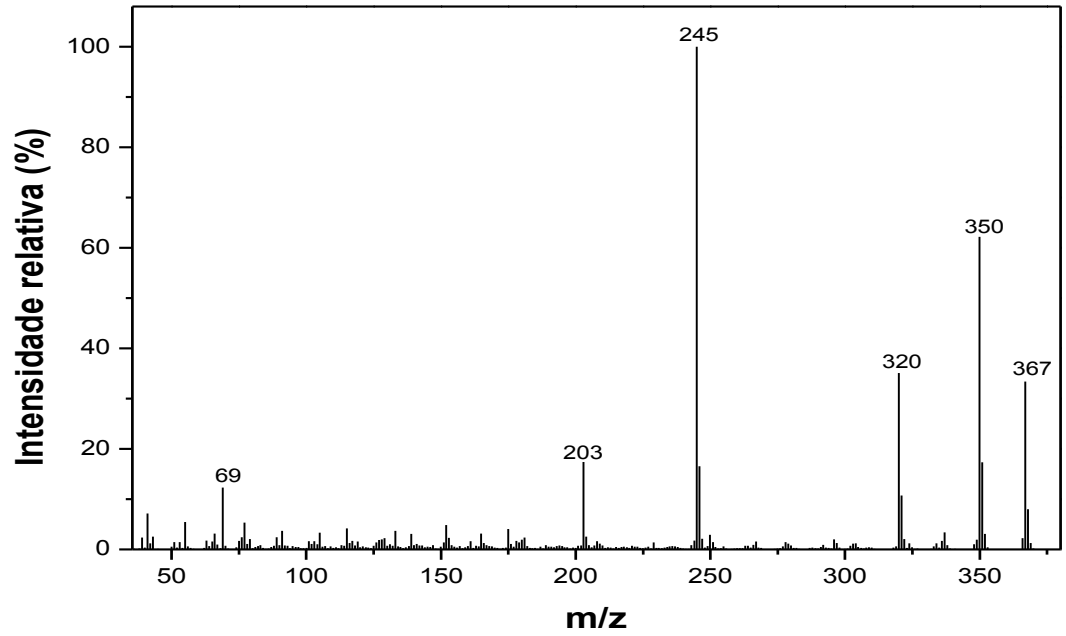

Figura 94. Espectro de massas do composto **24**.

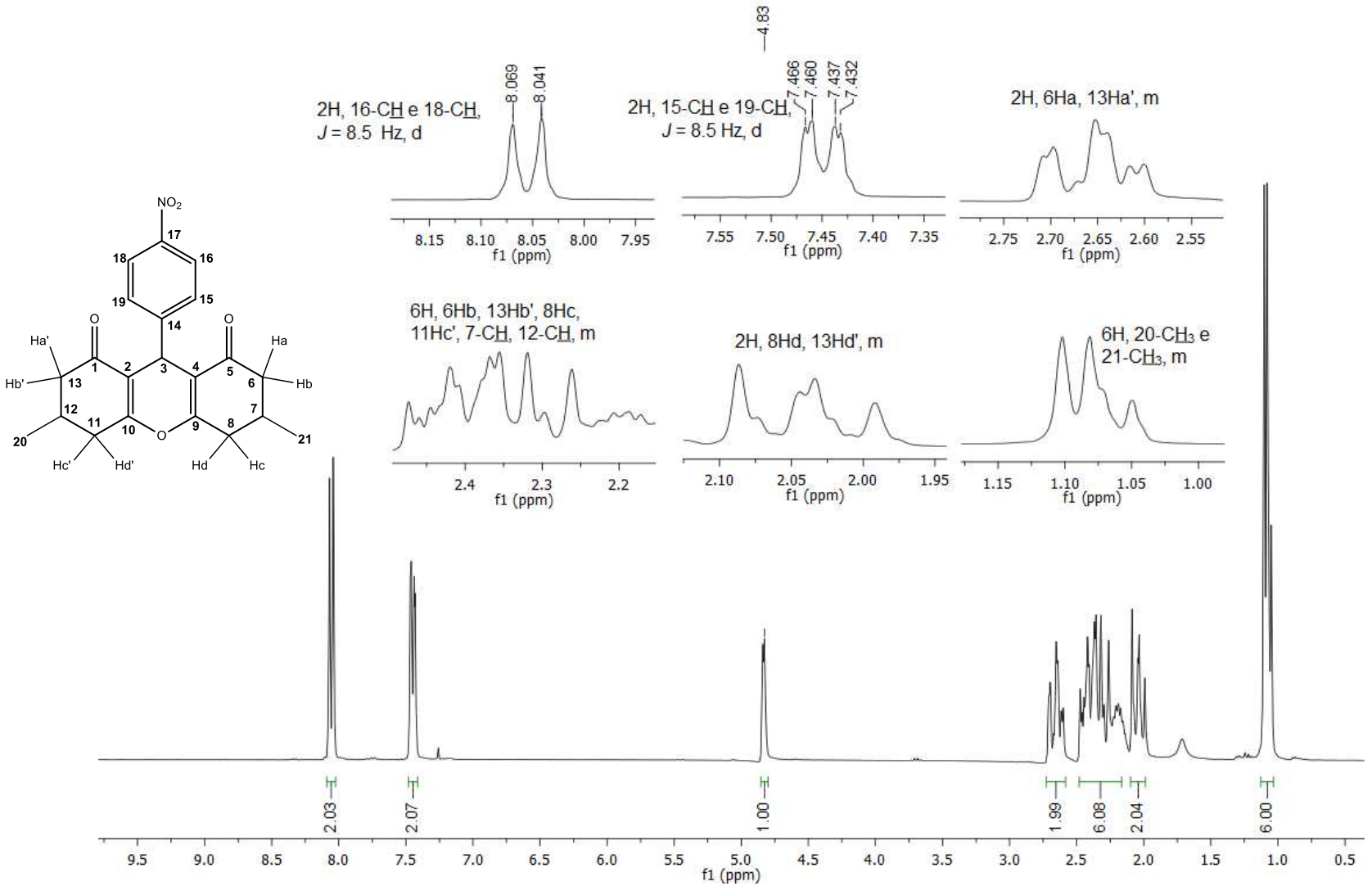

Figura 95. Espectro de RMN de ^{1}H (300 MHz, $CDCl_3$) do composto **24**.

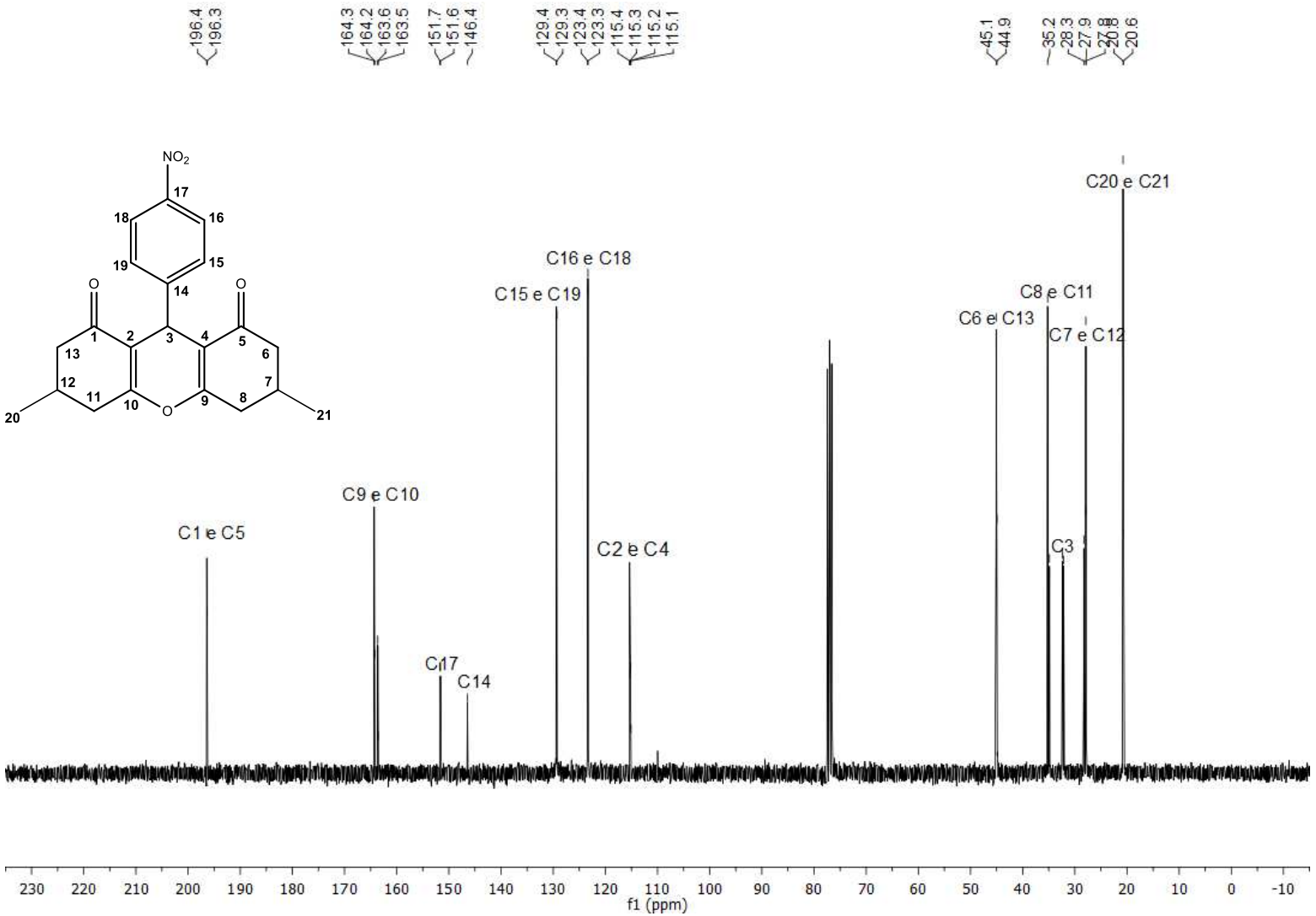

Figura 96. Espectro de RMN de ^{13}C (75 MHz, $CDCl_3$) do composto **24**.

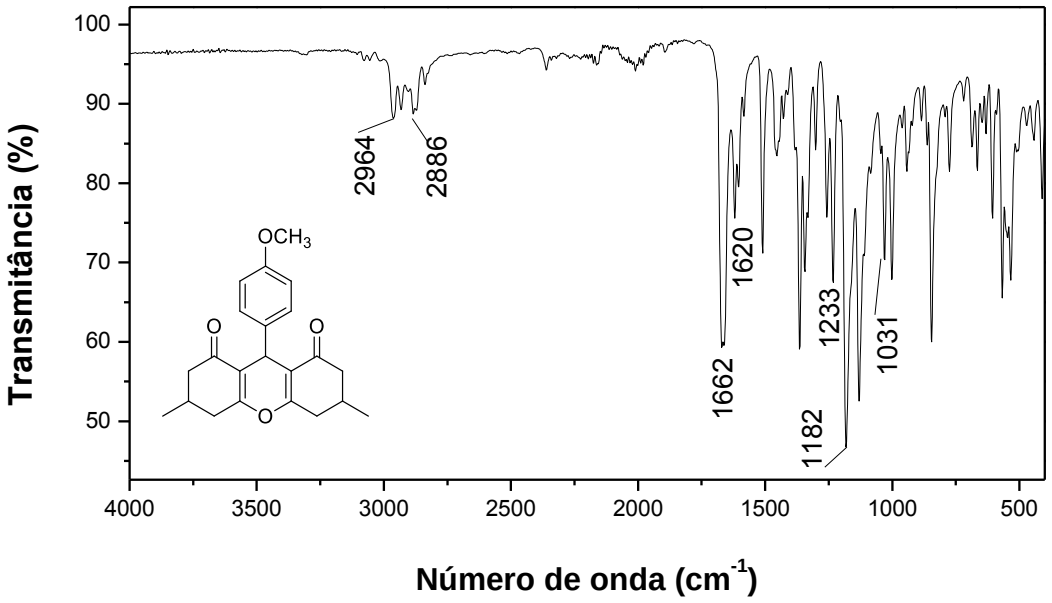

Figura 97. Espectro no infravermelho (ATR) do composto **25**.

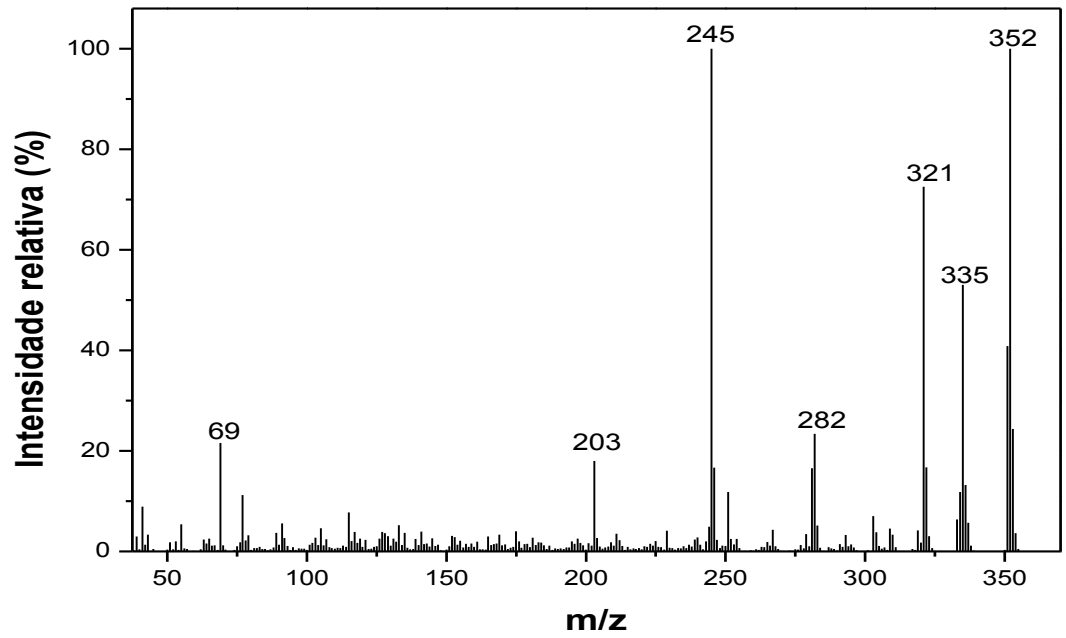

Figura 98. Espectro de massas do composto **25**.

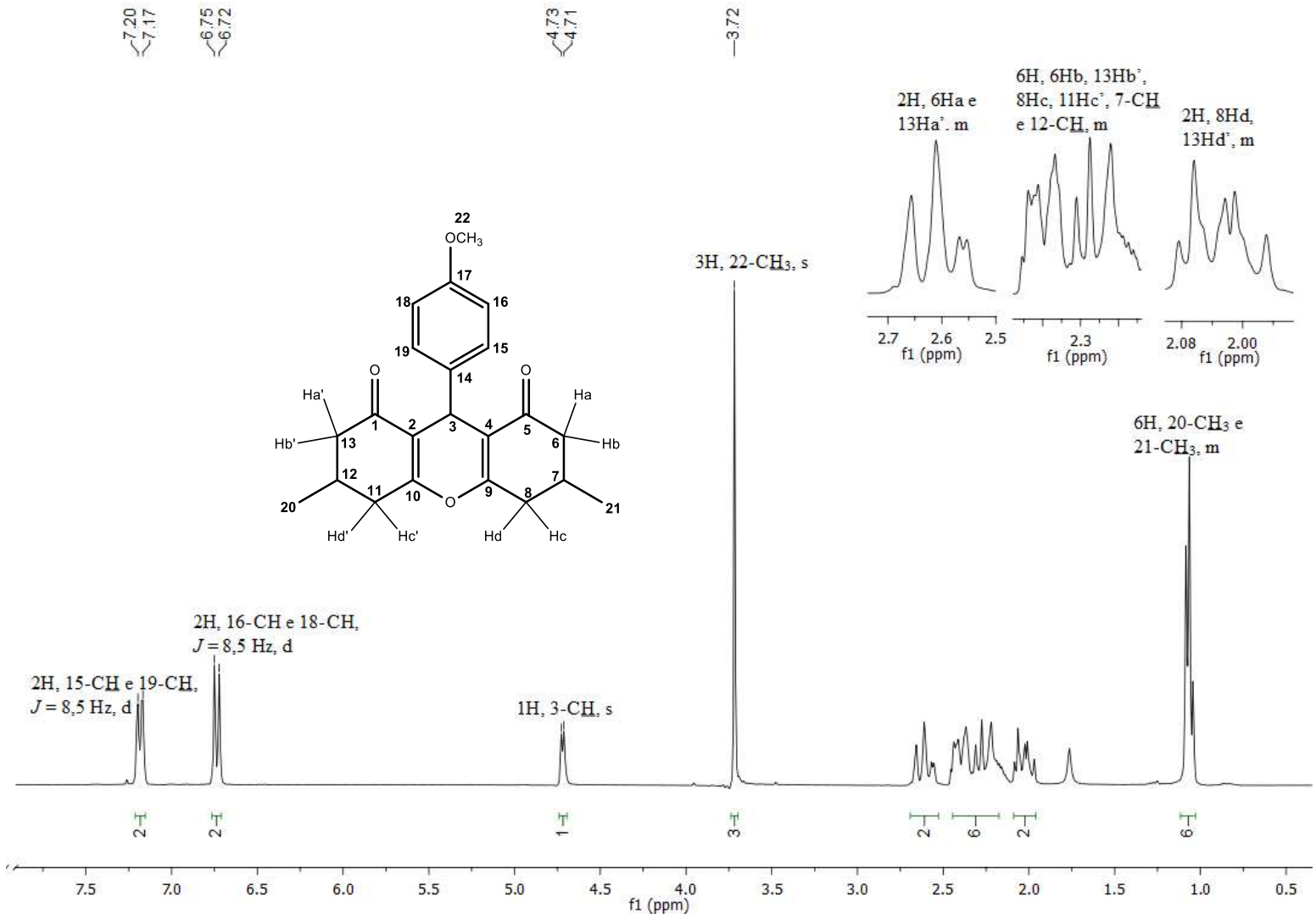

Figura 99. Espectro de RMN de ^{1}H (300 MHz, $CDCl_3$) do composto **25**.

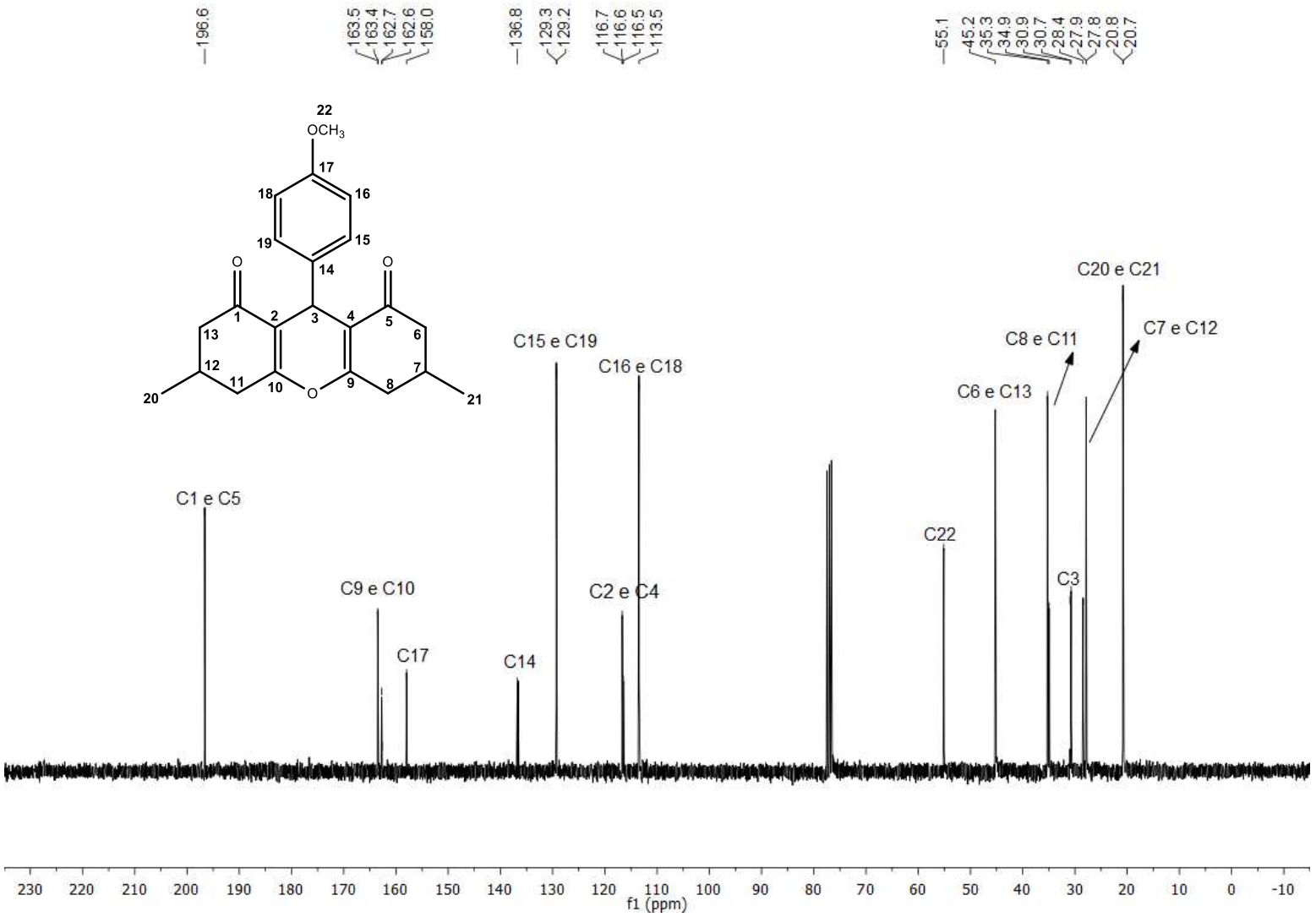

Figura 100. Espectro de RMN de ^{13}C (75 MHz, $CDCl_3$) do composto **25**.

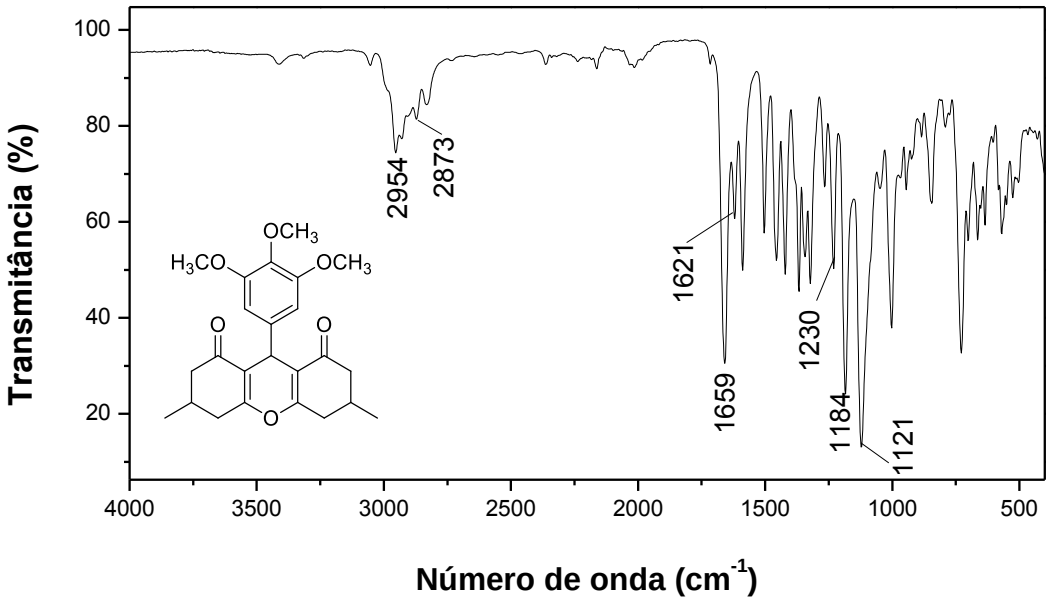

Figura 101. Espectro no infravermelho (ATR) do composto **26**.

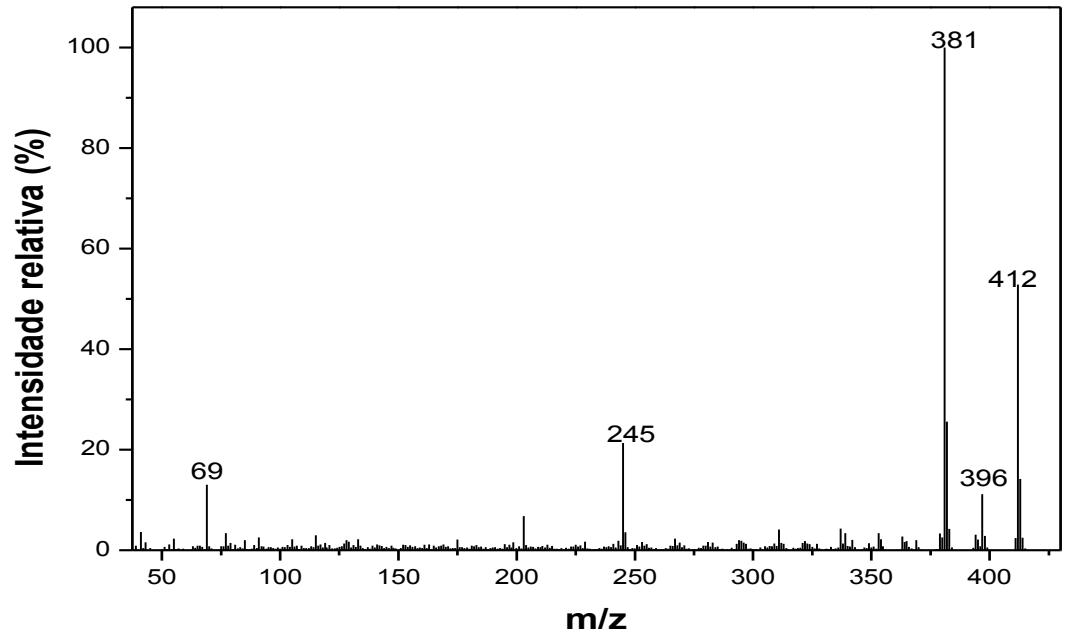

Figura 102. Espectro de massas do composto **26**.

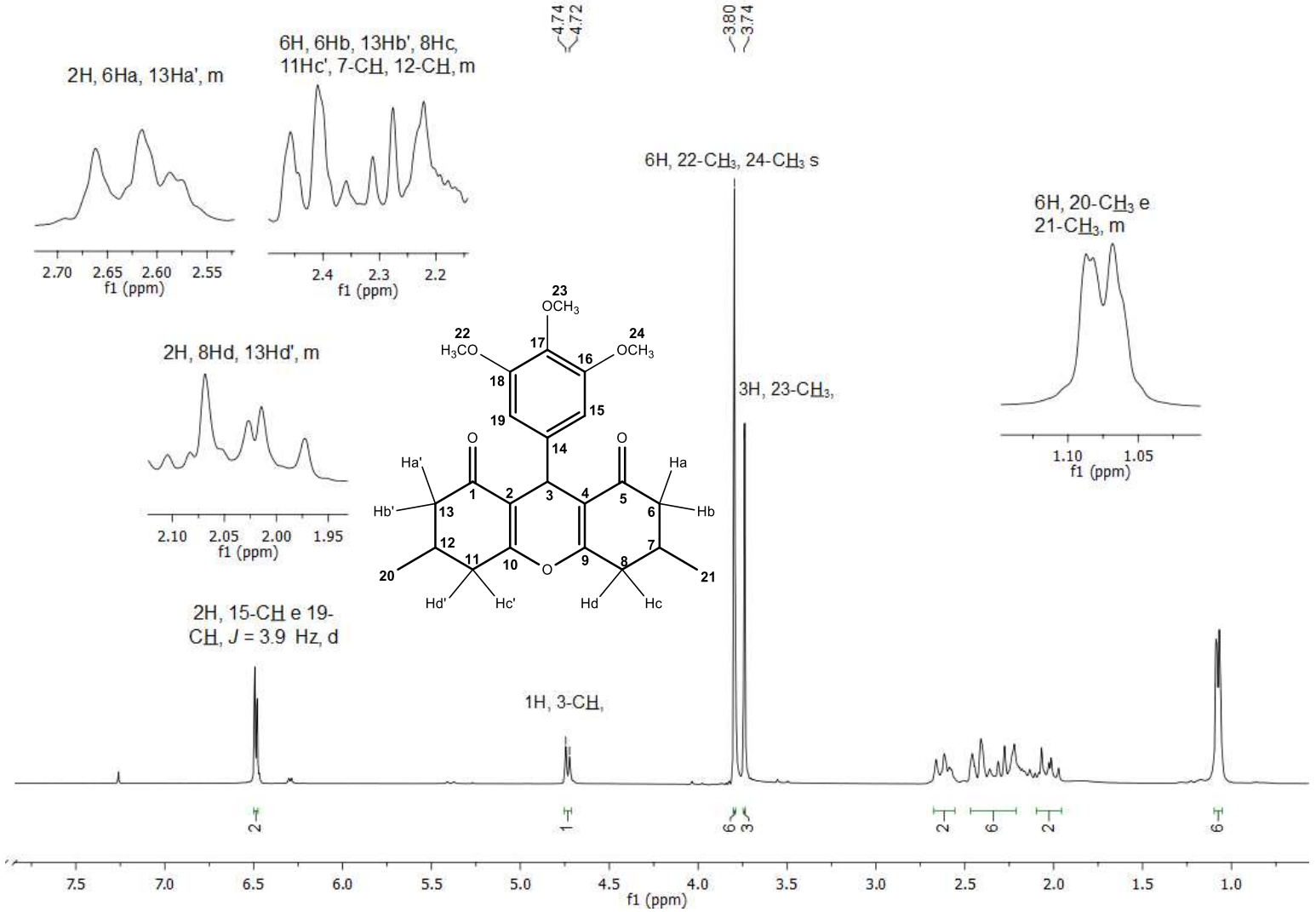

Figura 103. Espectro de RMN de ^{1}H (300 MHz, $CDCl_3$) do composto **26**.

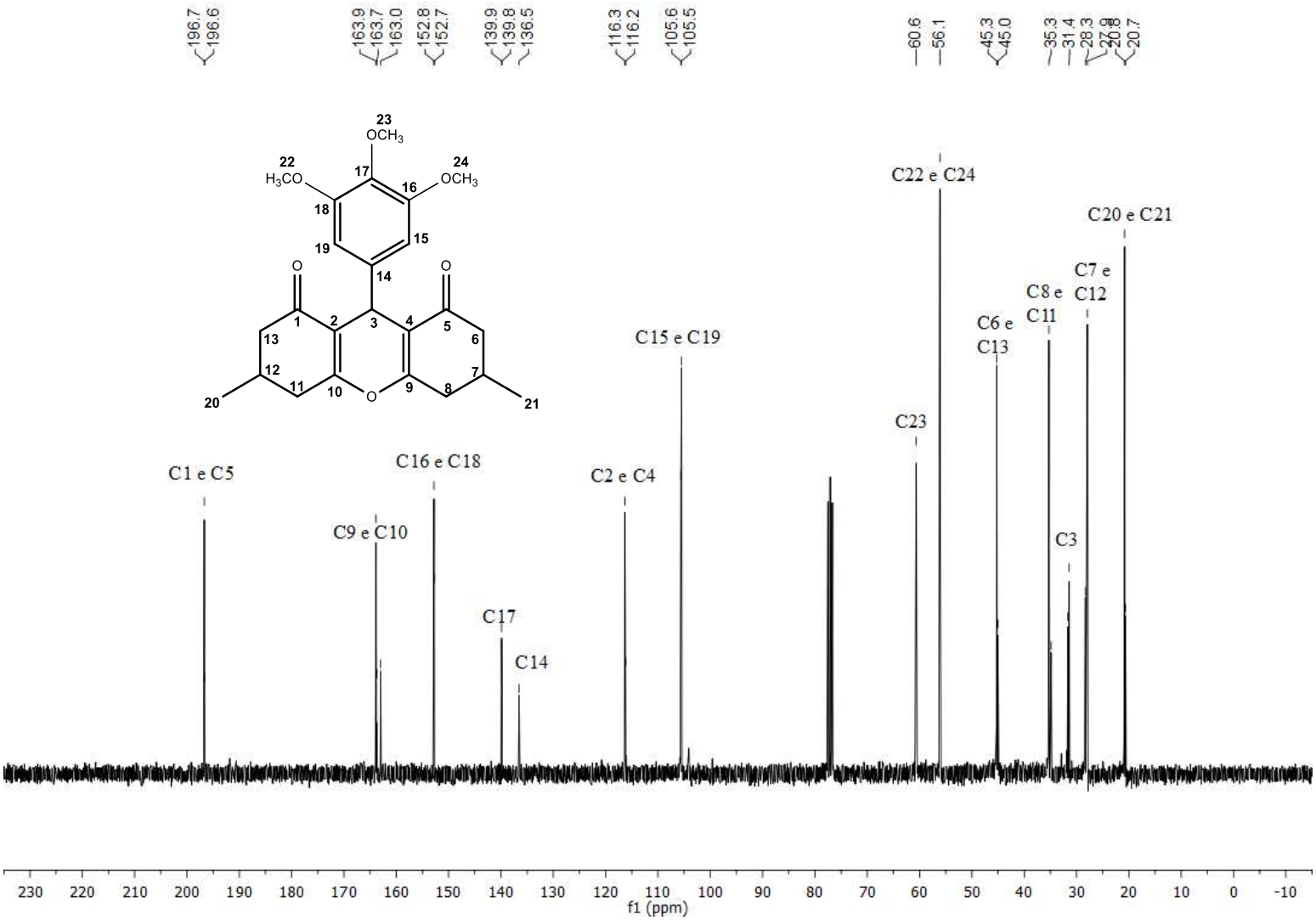

Figura 104. Espectro de RMN de ^{13}C (75 MHz, $CDCl_3$) do composto **26**.

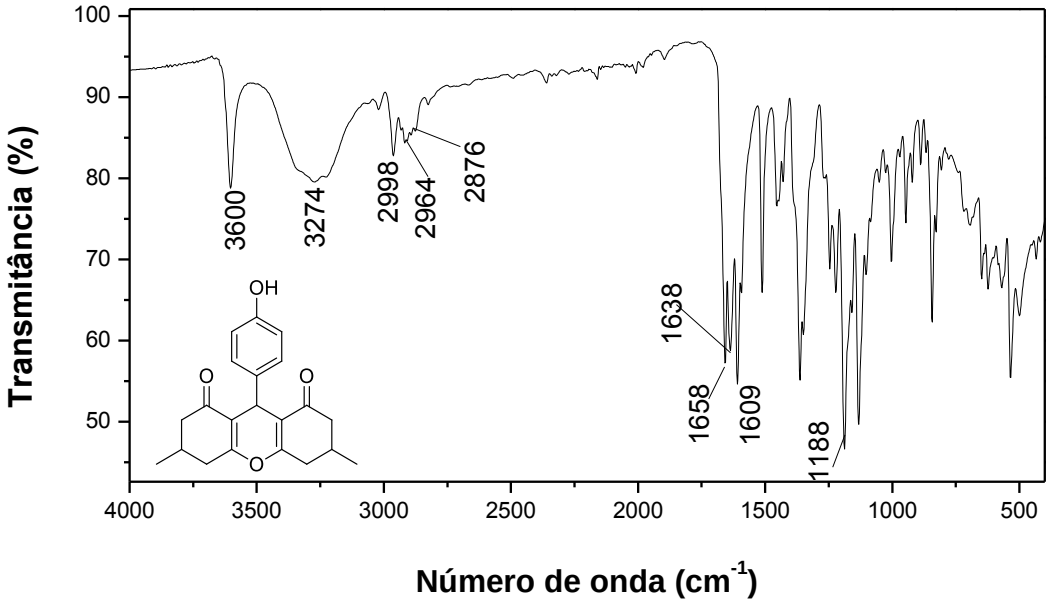

Figura 105. Espectro no infravermelho (ATR) do composto **27**.

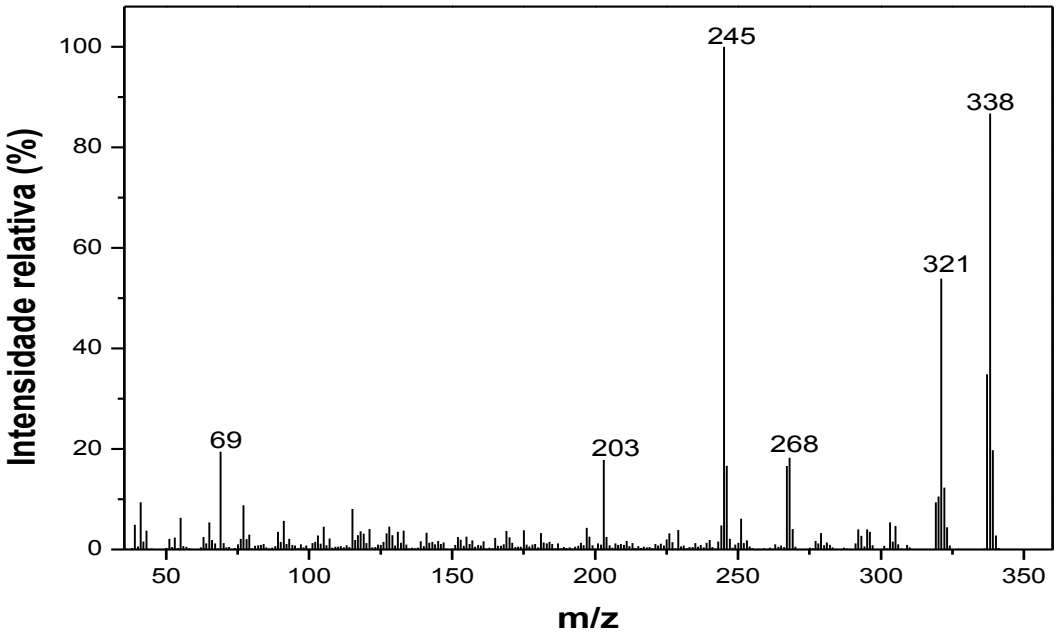

Figura 106. Espectro de massas do composto **27**.

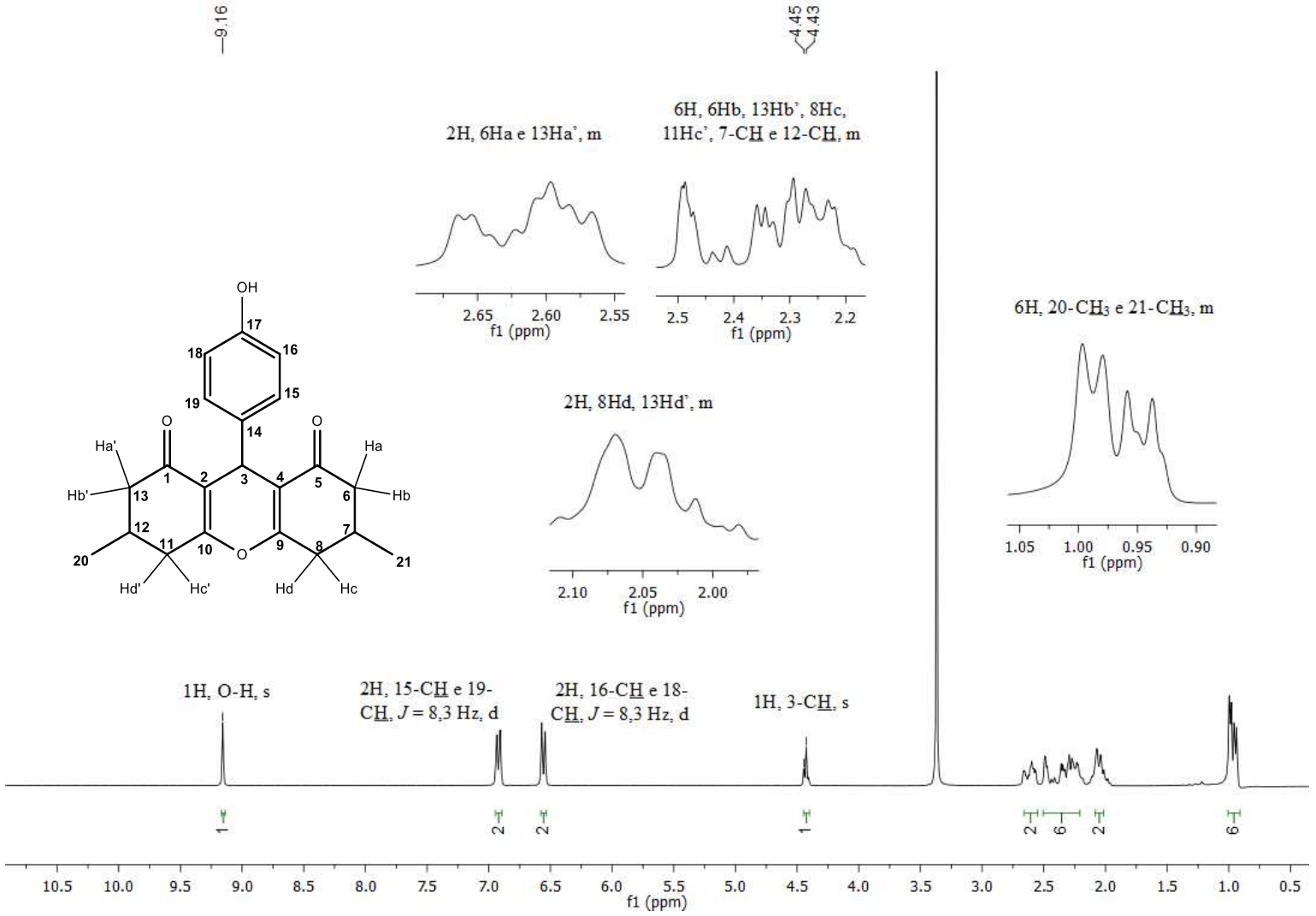

Figura 107. Espectro de RMN de ^{1}H (300 MHz, DMSO-d6) do composto **27**.

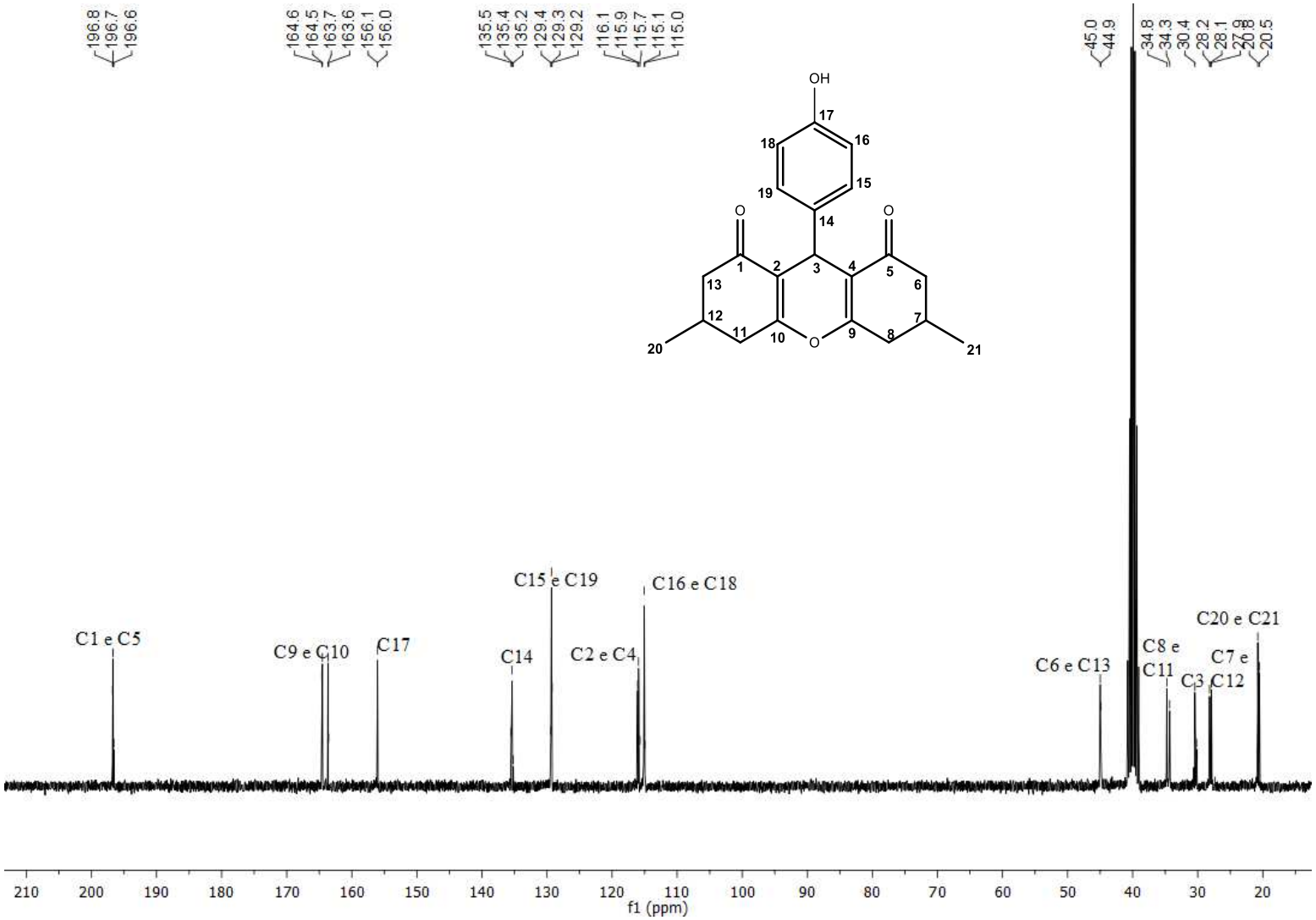

Figura 108. Espectro de RMN de ^{13}C (75 MHz, DMSO-d6) do composto **27**.

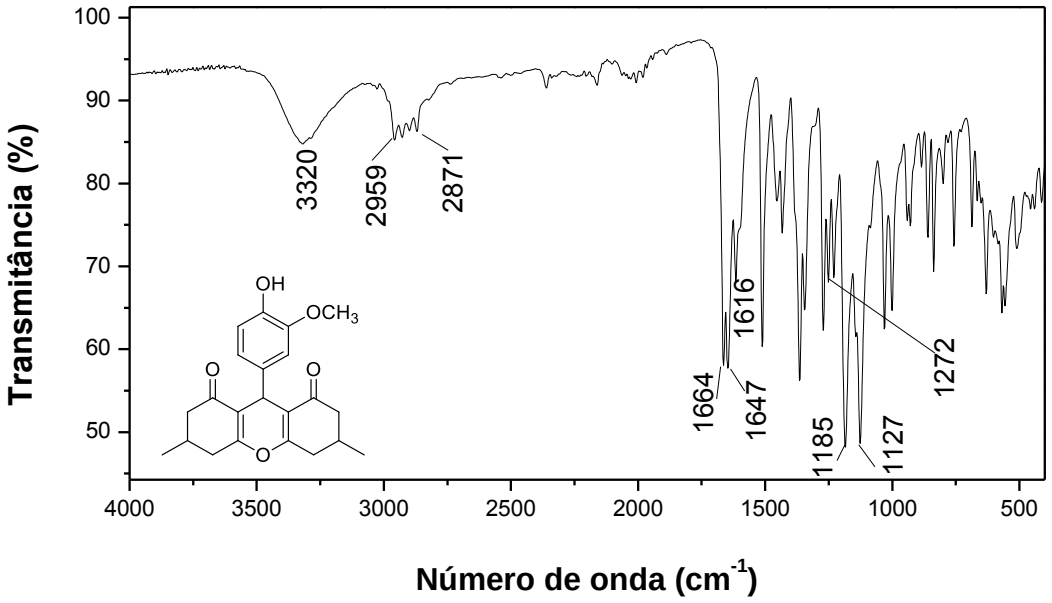

Figura 109. Espectro no infravermelho (ATR) do composto **28**.

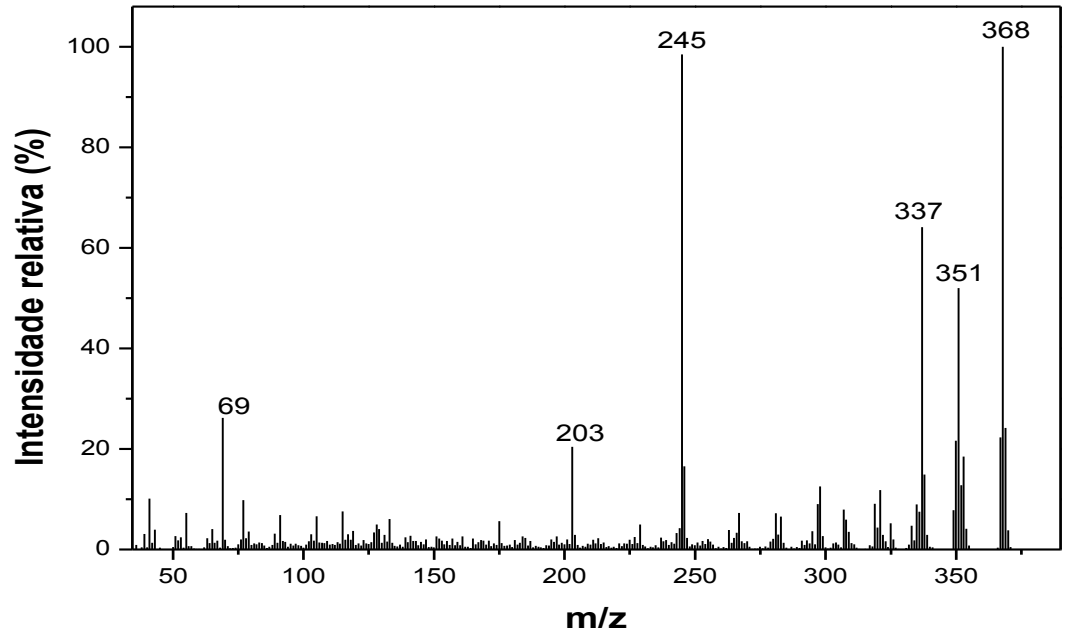

Figura 110. Espectro de massas do composto **28**.

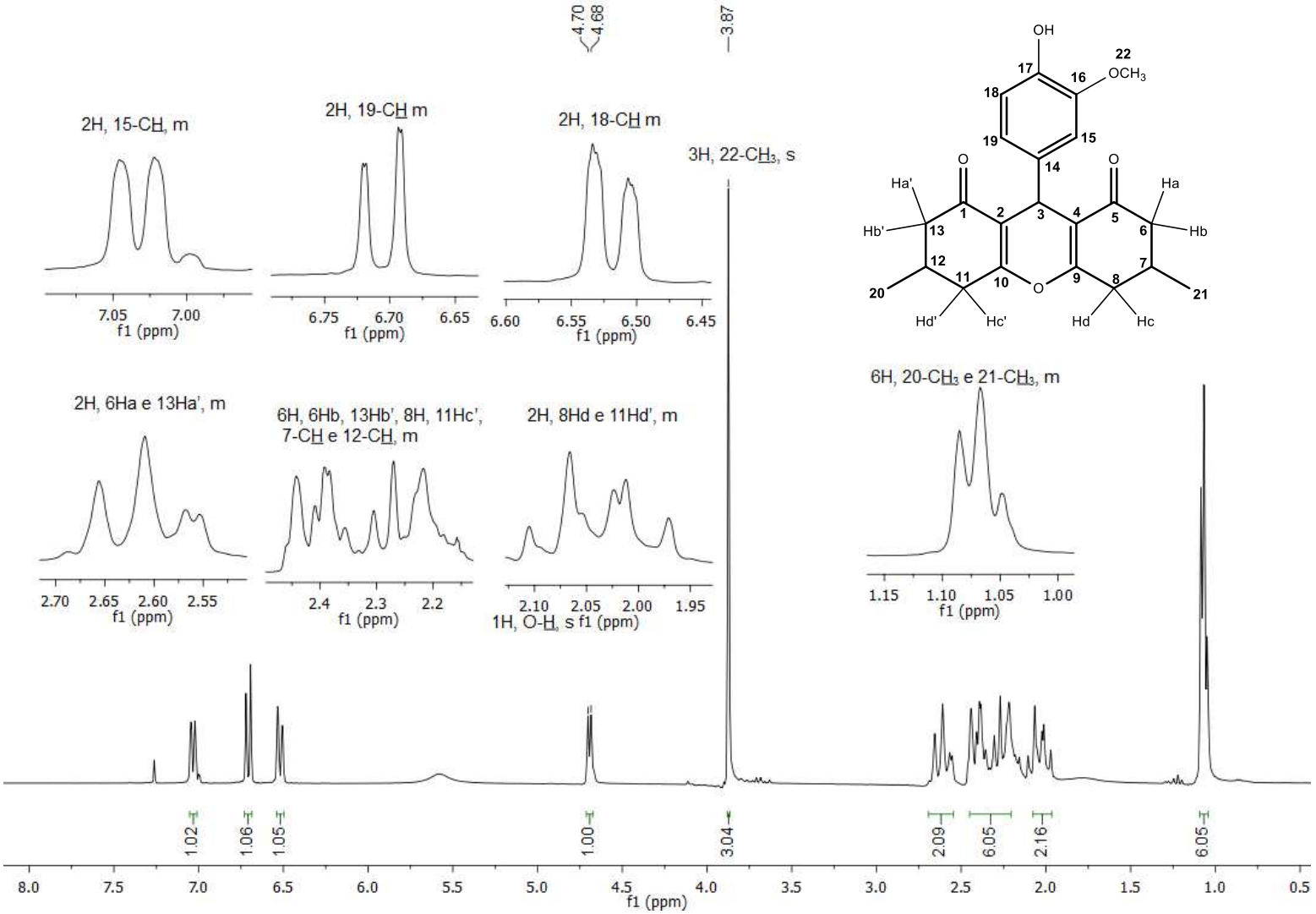

Figura 111. Espectro de RMN de ^{1}H (300 MHz, $CDCl_3$) do composto **28**.

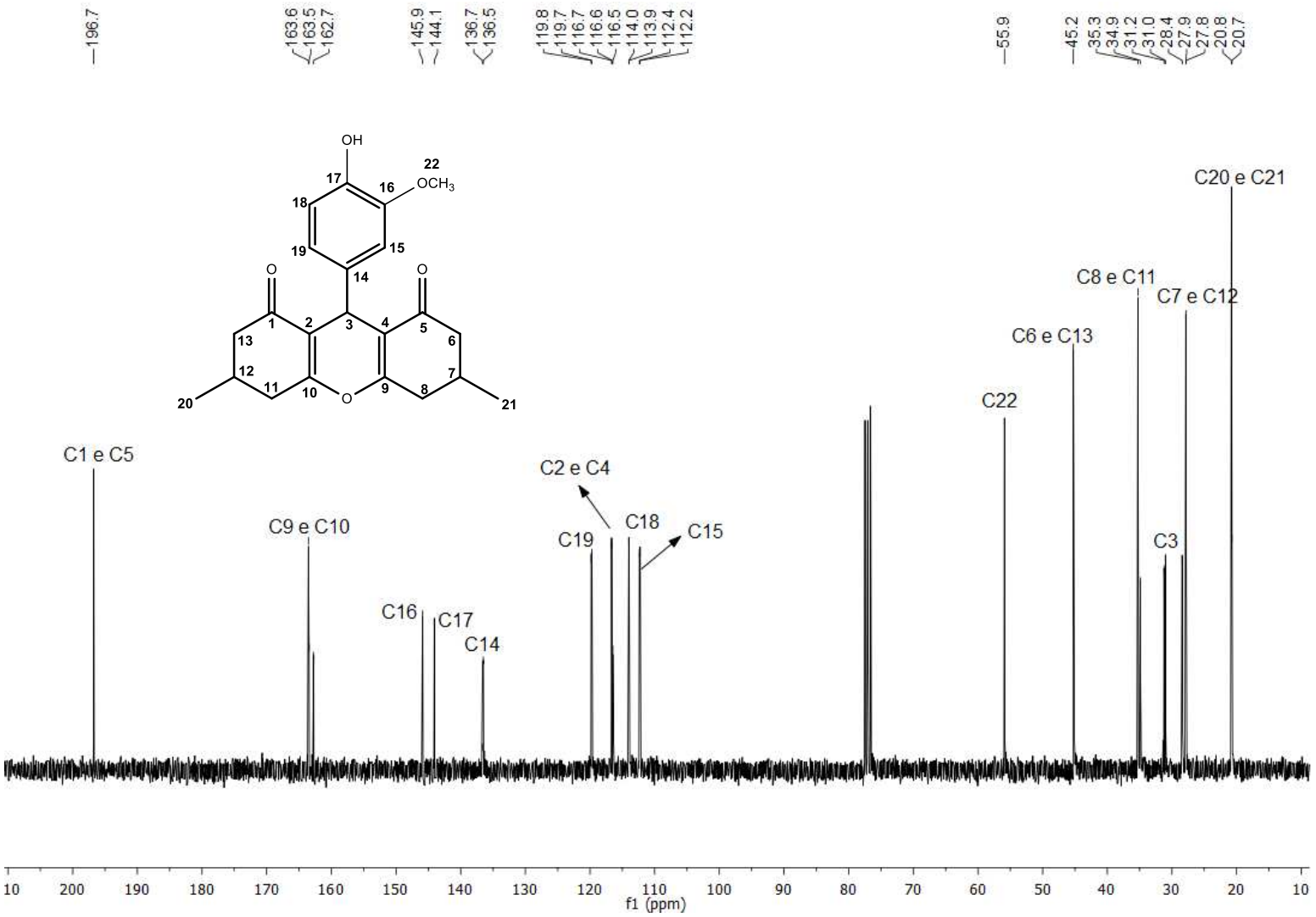

Figura 112. Espectro de RMN de ^{13}C (75 MHz, $CDCl_3$) do composto **28**.

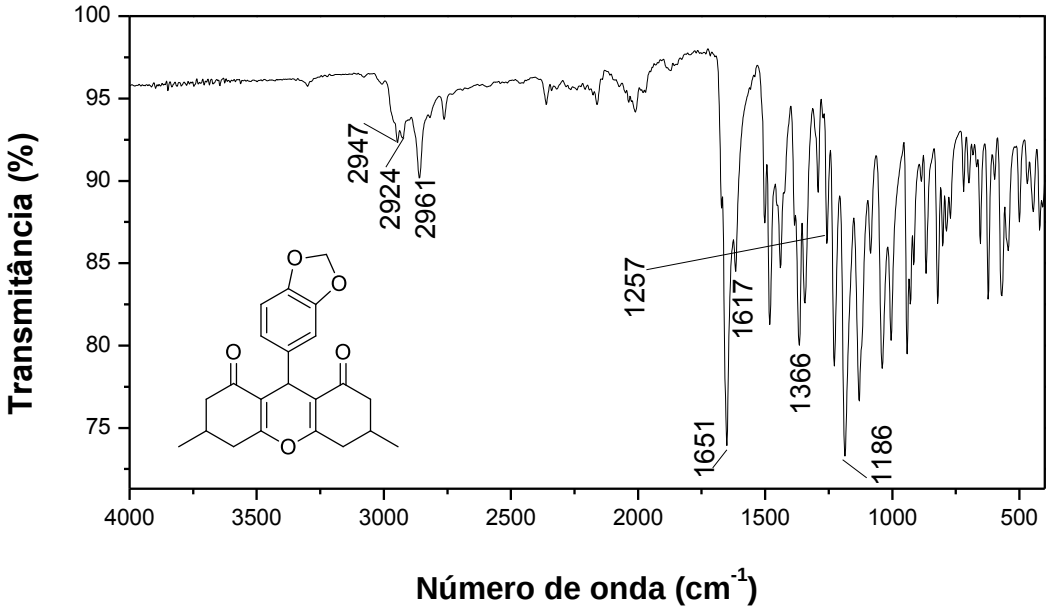

Figura 113. Espectro no infravermelho (ATR) do composto **29**.

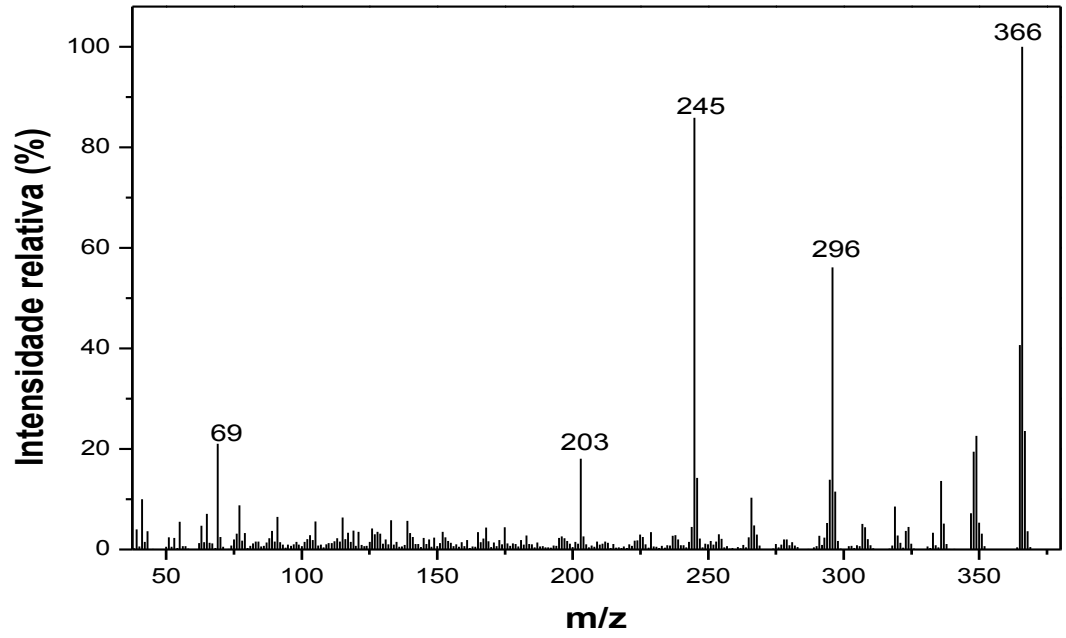

Figura 114. Espectro de massas do composto **29**.

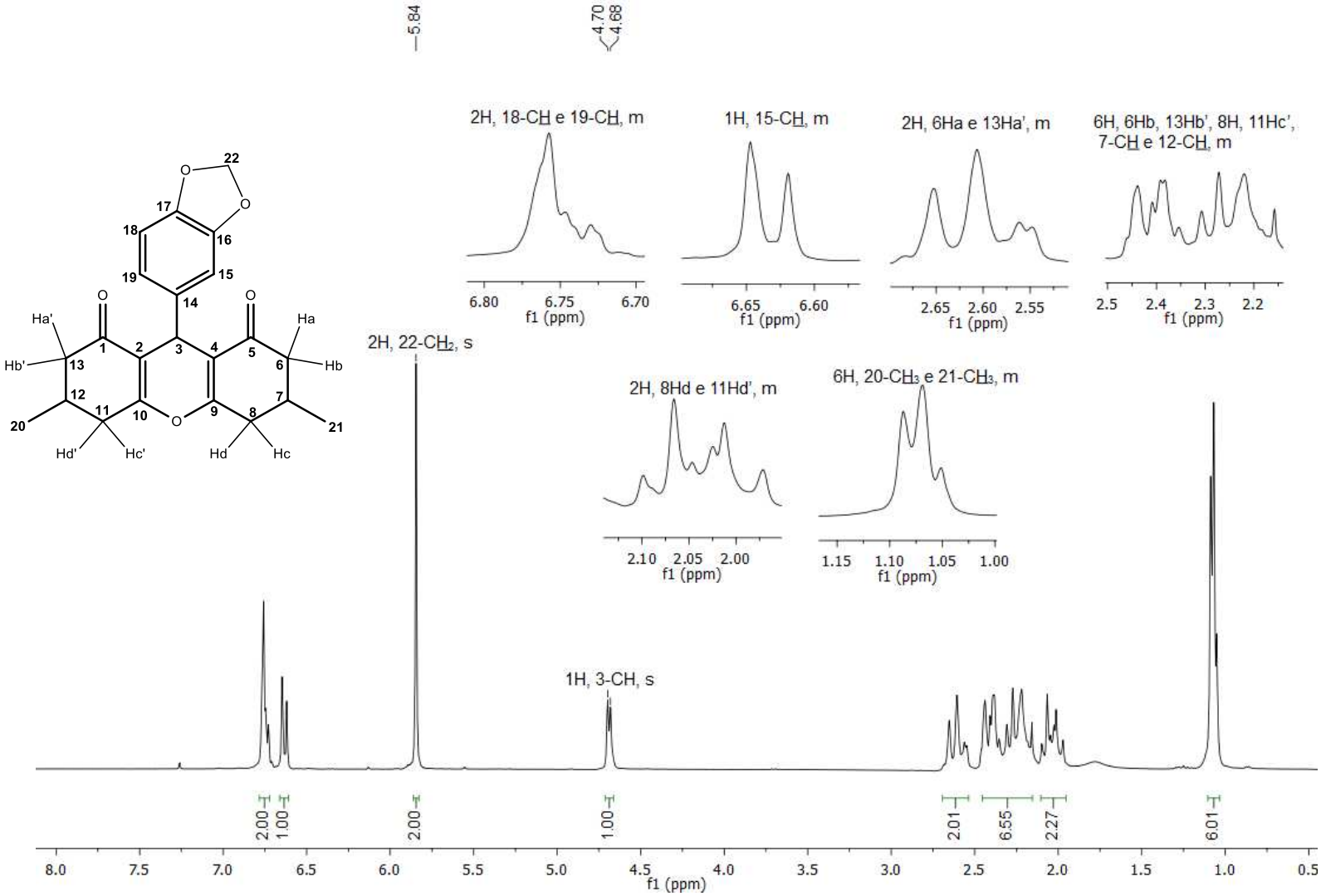

Figura 115. Espectro de RMN de ^{1}H (300 MHz, $CDCl_3$) do composto **29**.

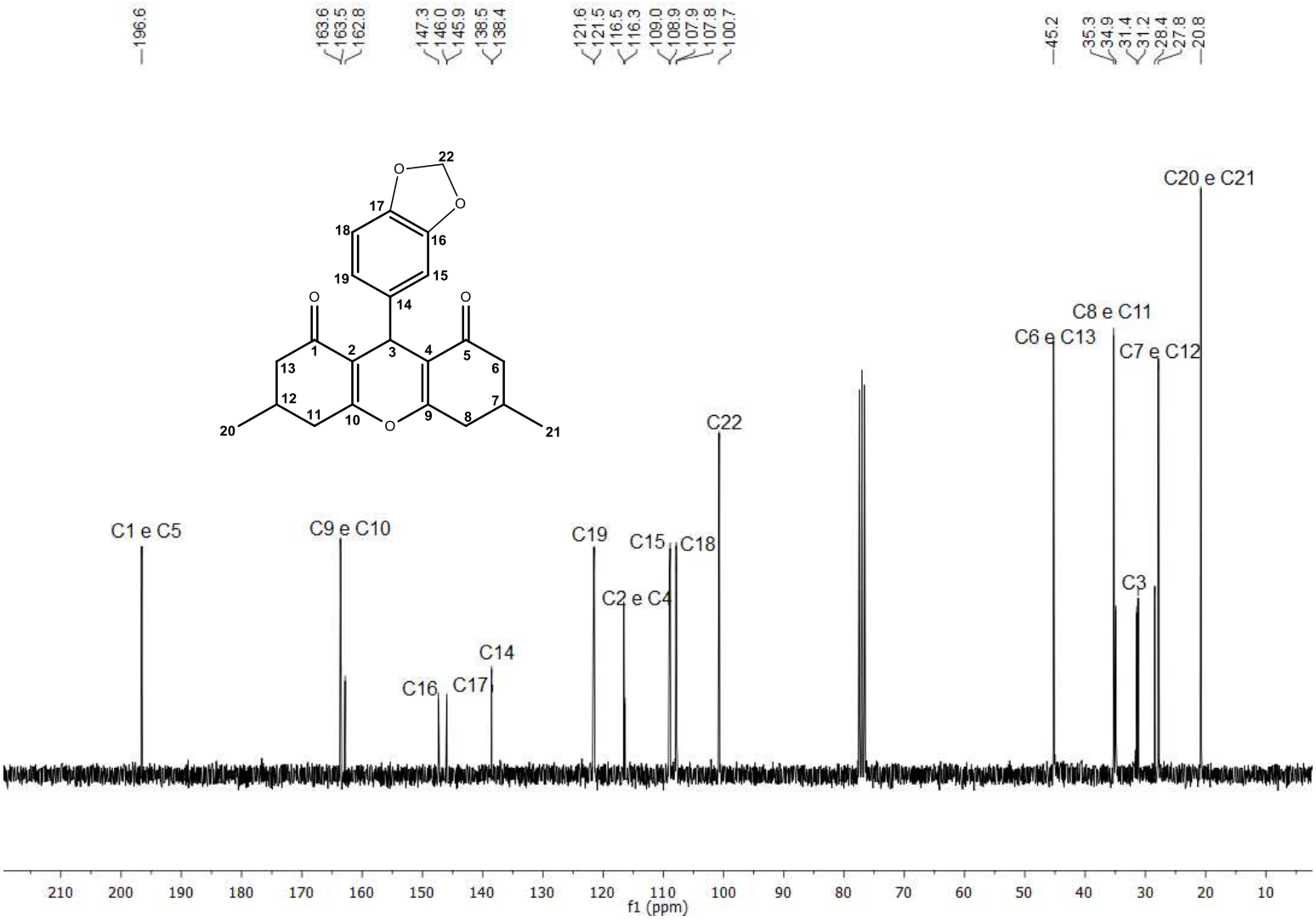

Figura 116. Espectro de RMN de ^{13}C (75 MHz, $CDCl_3$) do composto **29**.

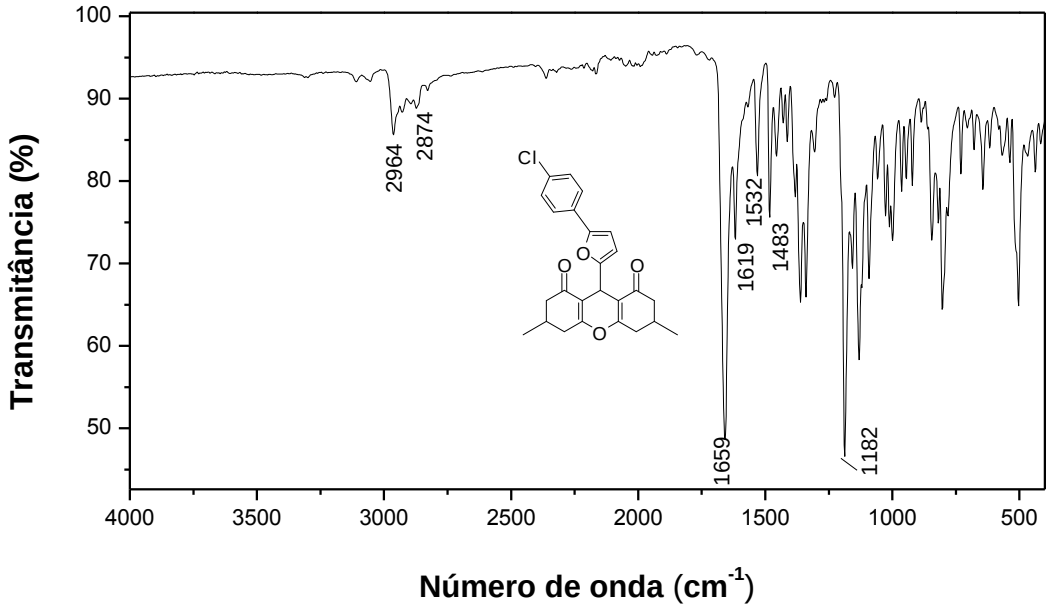

Figura 117. Espectro no infravermelho (ATR) do composto **30**.

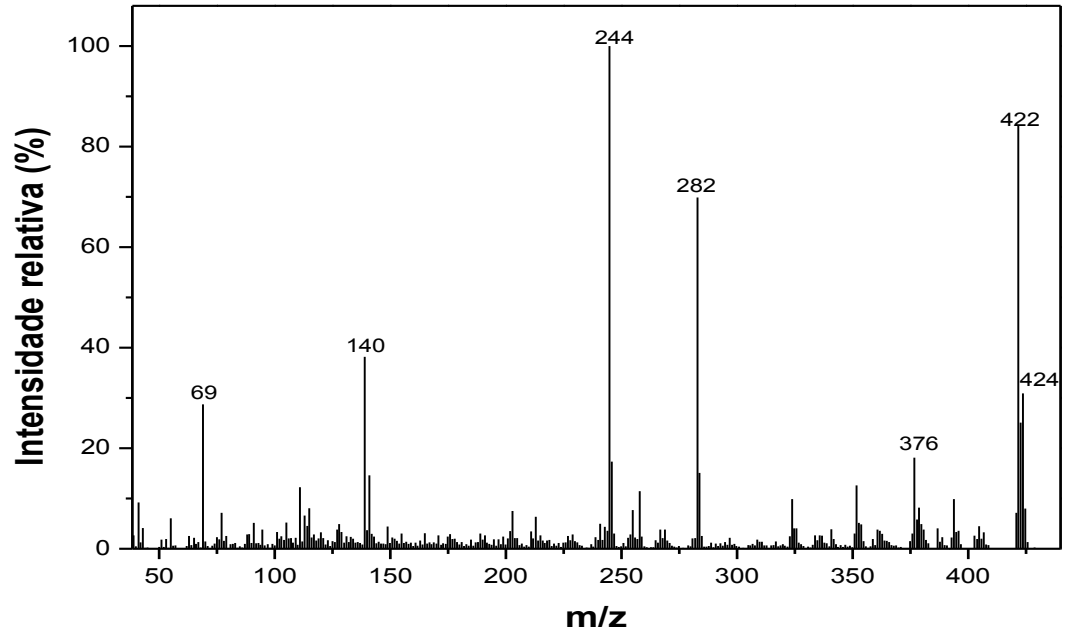

Figura 118. Espectro de massas do composto **30**.

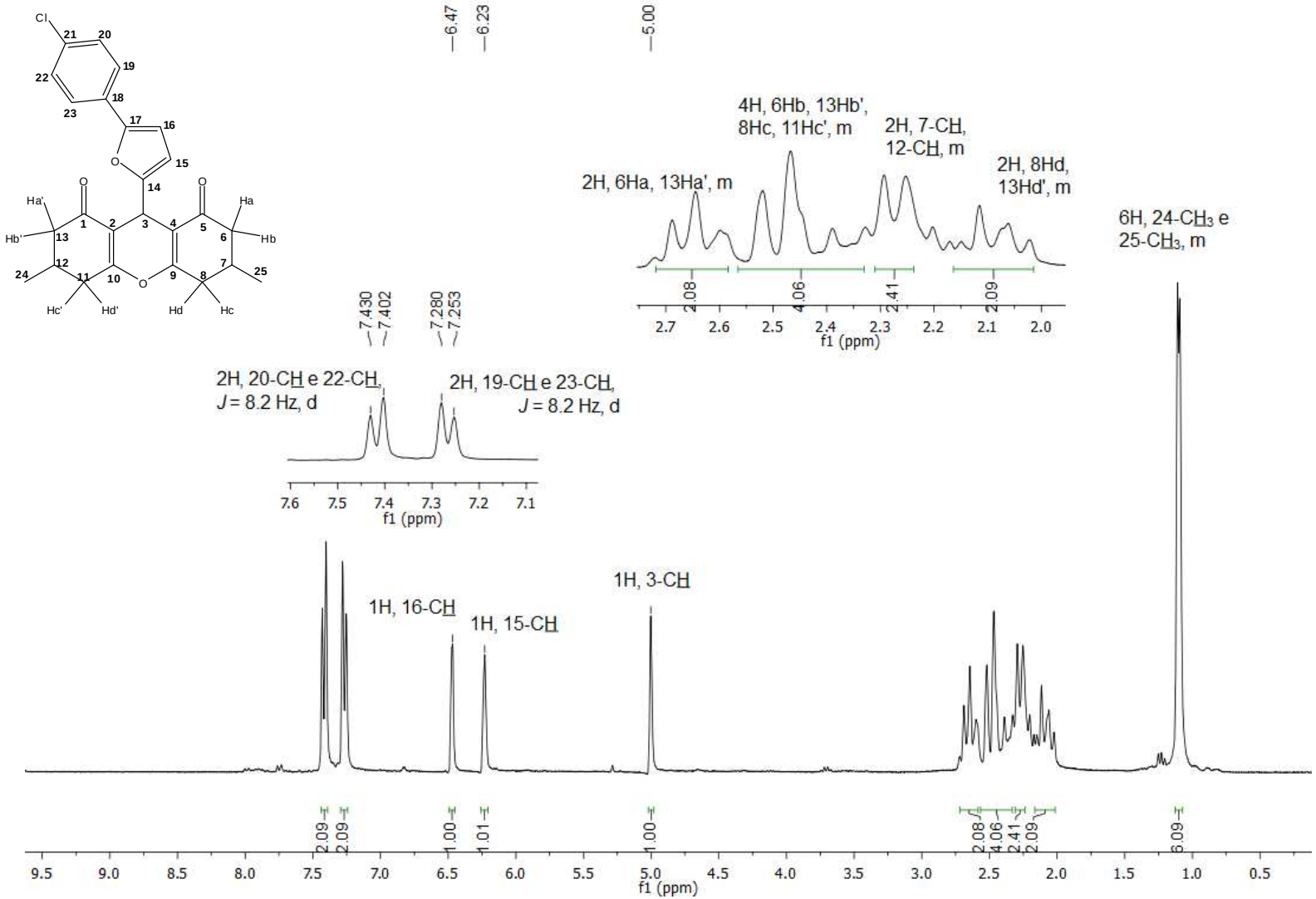

Figura 119. Espectro de RMN de ^{1}H (300 MHz, $CDCl_3$) do composto **30**.

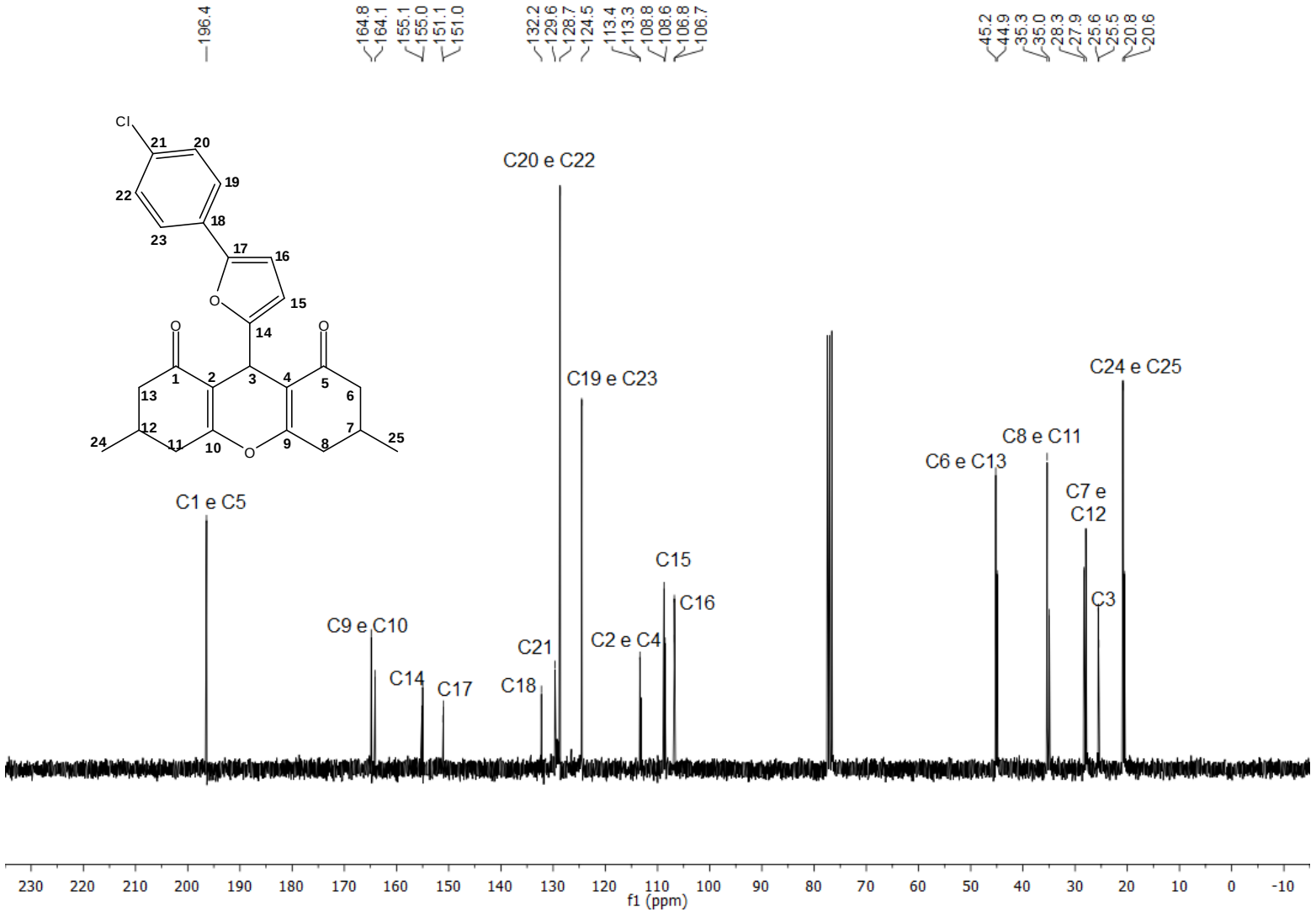

Figura 120. Espectro de RMN de ^{13}C (75 MHz, $CDCl_3$) do composto **30**.

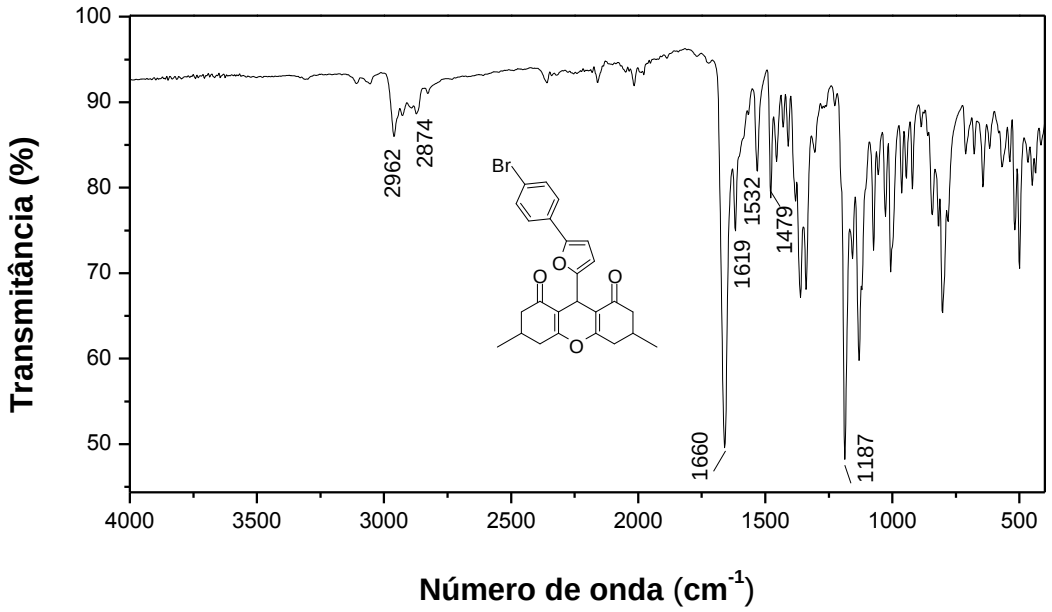

Figura 121. Espectro no infravermelho (ATR) do composto 3**1**.

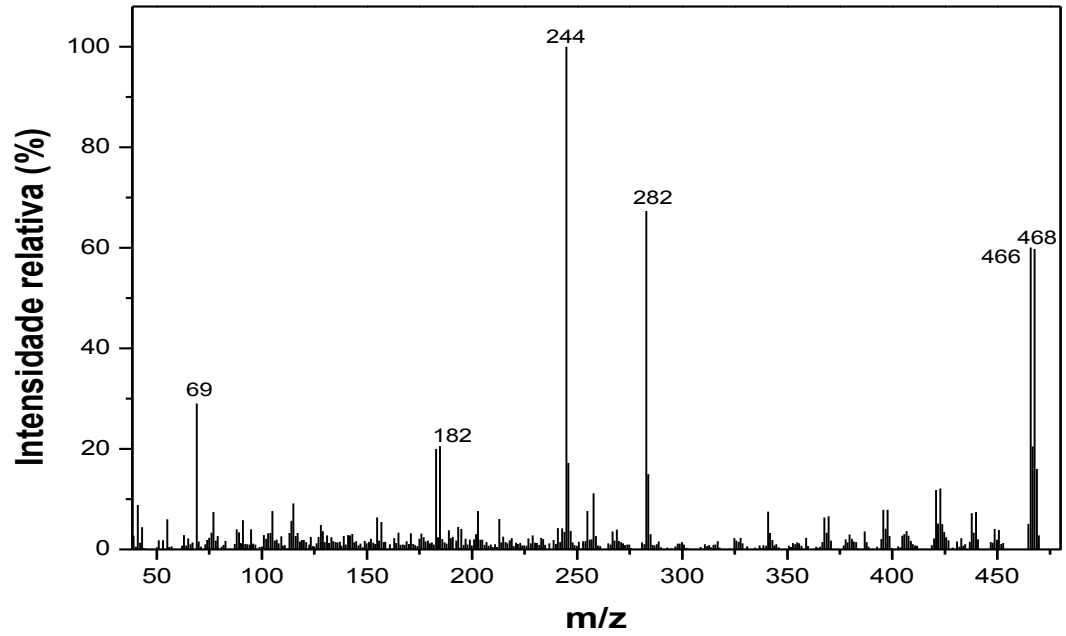

Figura 122. Espectro de massas do composto 3**1**.

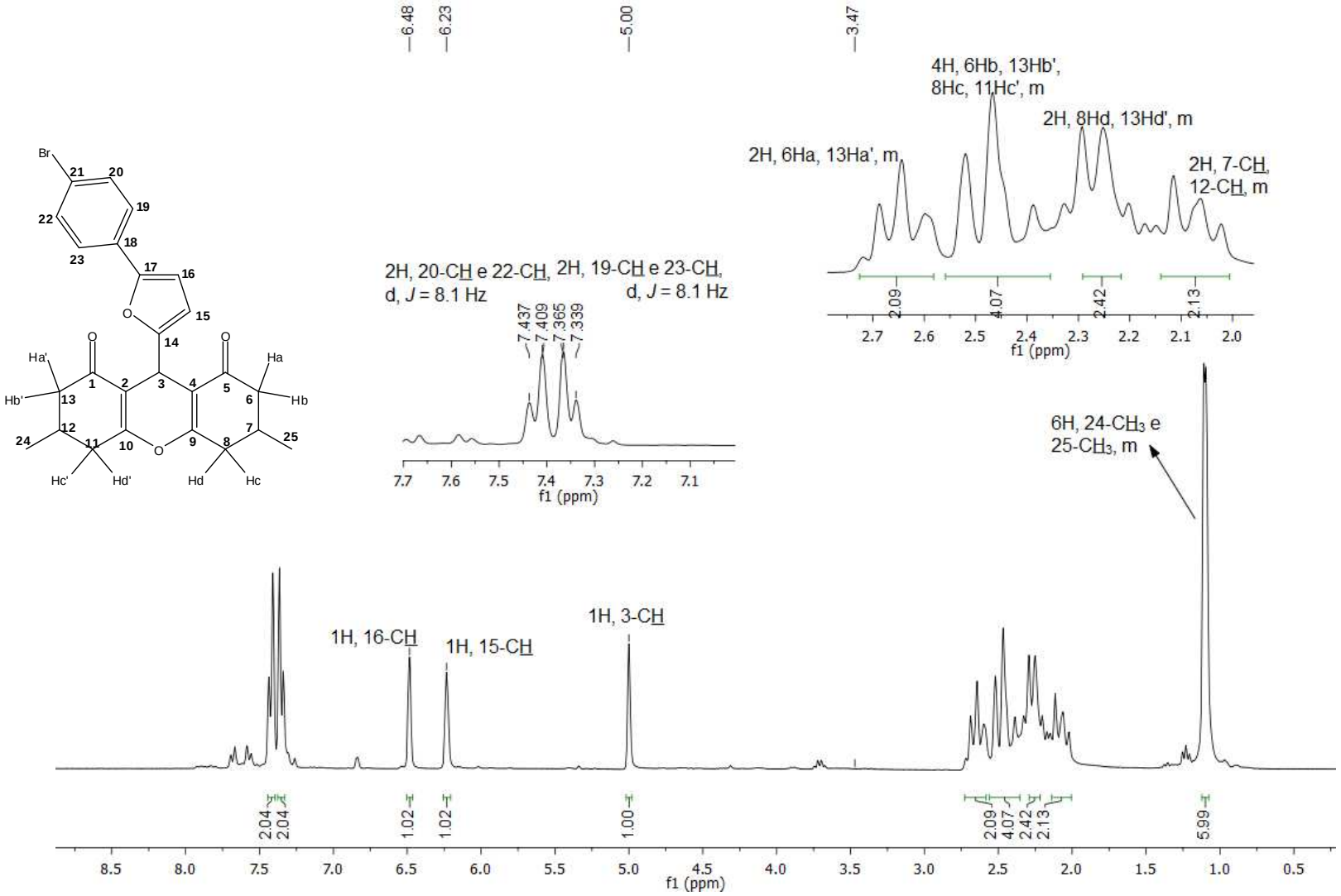

Figura 123. Espectro de RMN de ^{1}H (300 MHz, $CDCl_3$) do composto **31**.

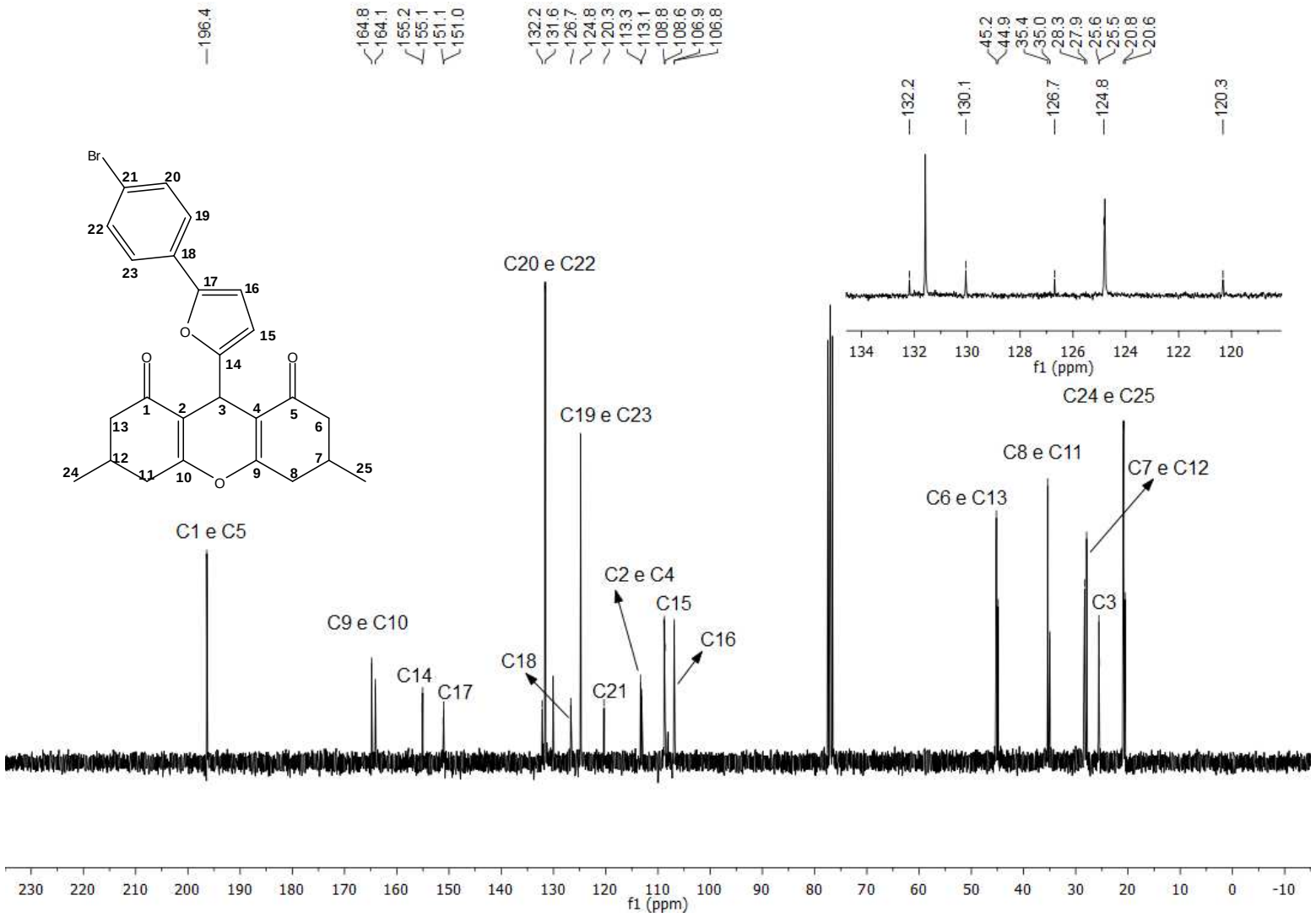

Figura 124. Espectro de RMN de ^{13}C (75 MHz, $CDCl_3$) do composto **31**.

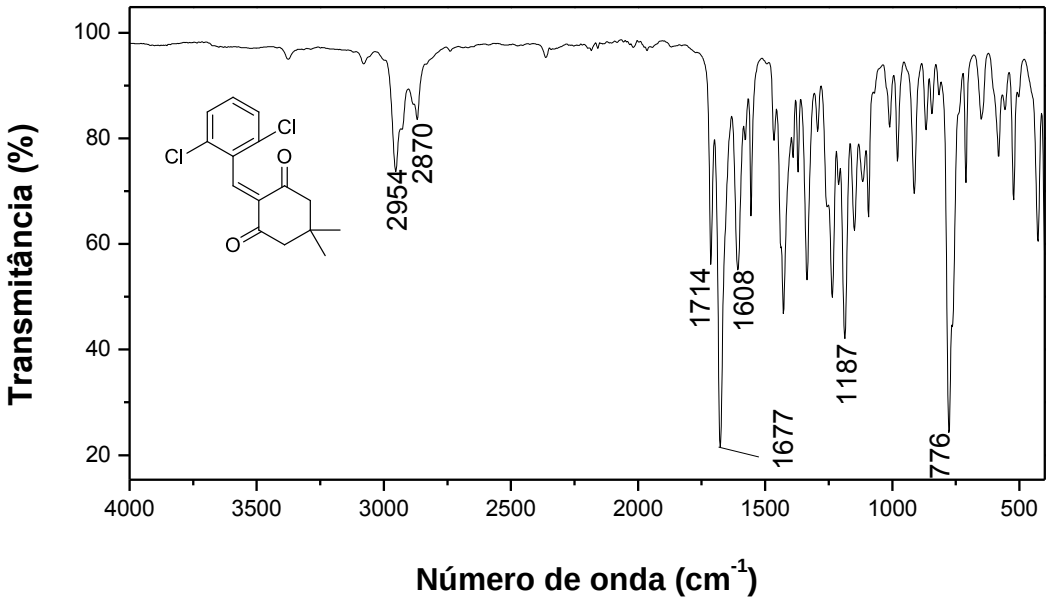

Figura 125. Espectro no infravermelho (ATR) do composto **32**.

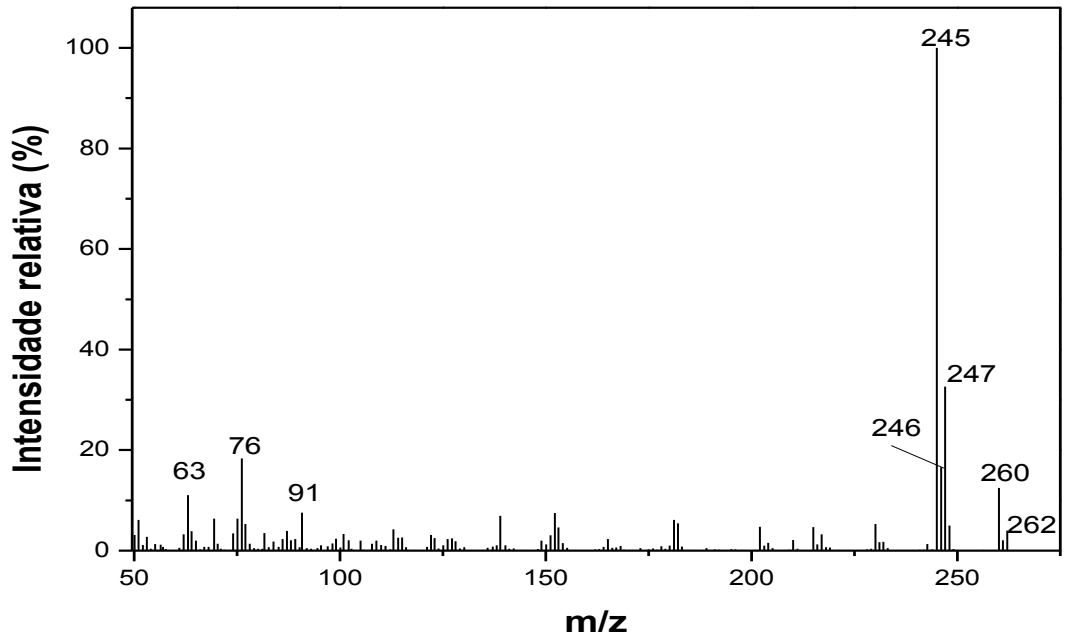

Figura 126. Espectro de massas do composto **32**.

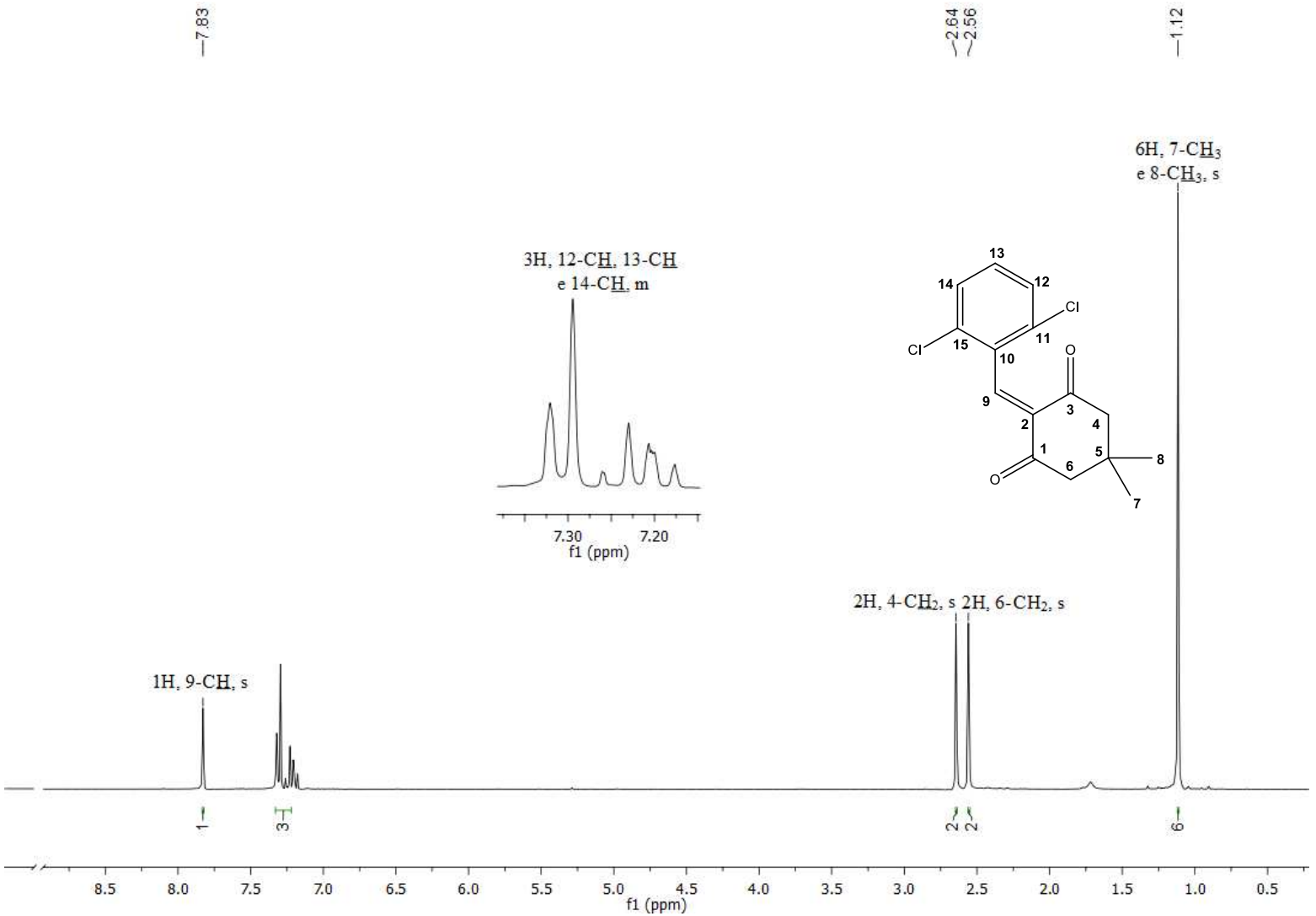

Figura 127. Espectro de RMN de ^{1}H (300 MHz, $CDCl_3$) do composto **32**.

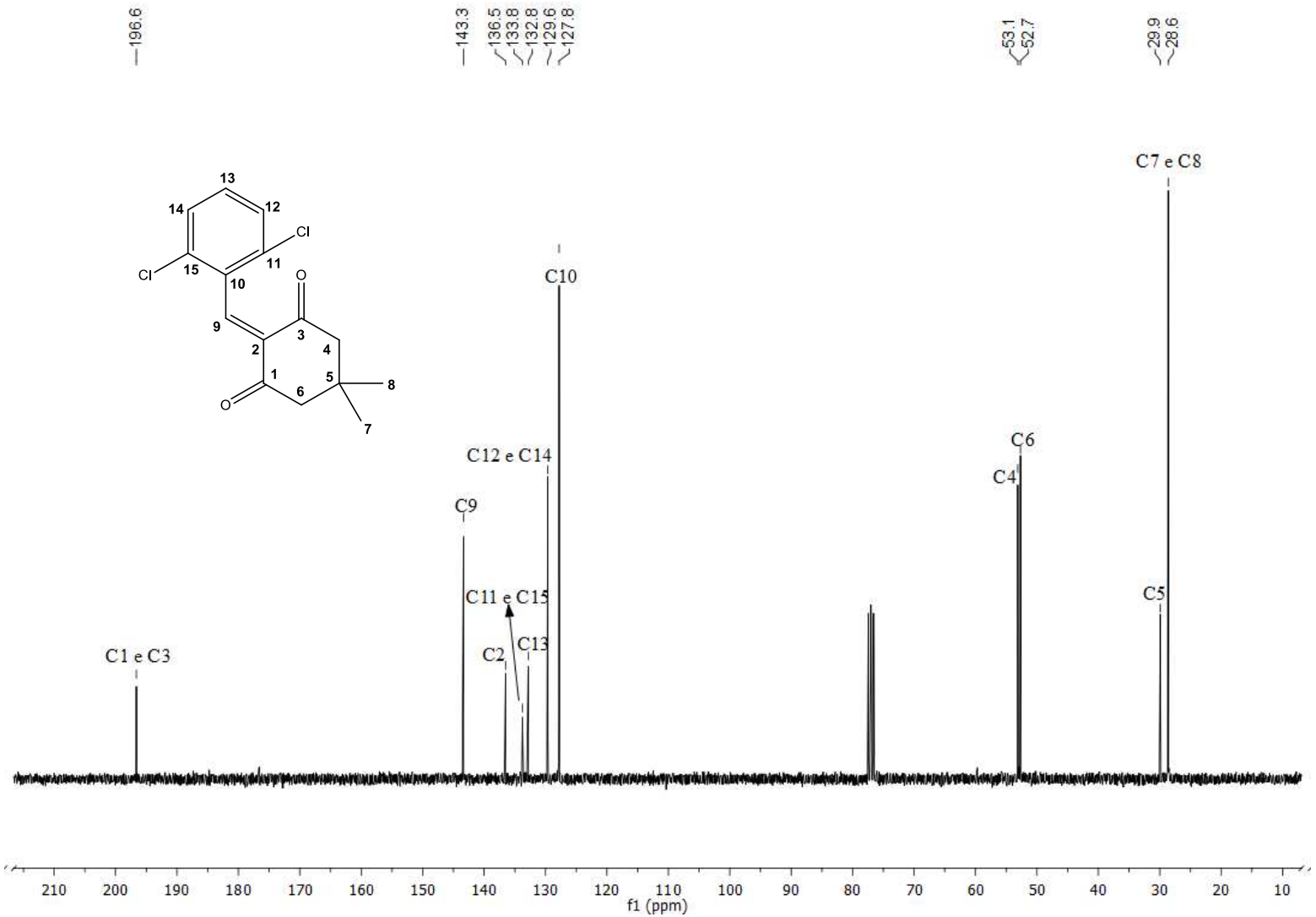

Figura 128. Espectro de RMN de ^{13}C (75 MHz, $CDCl_3$) do composto **32**.

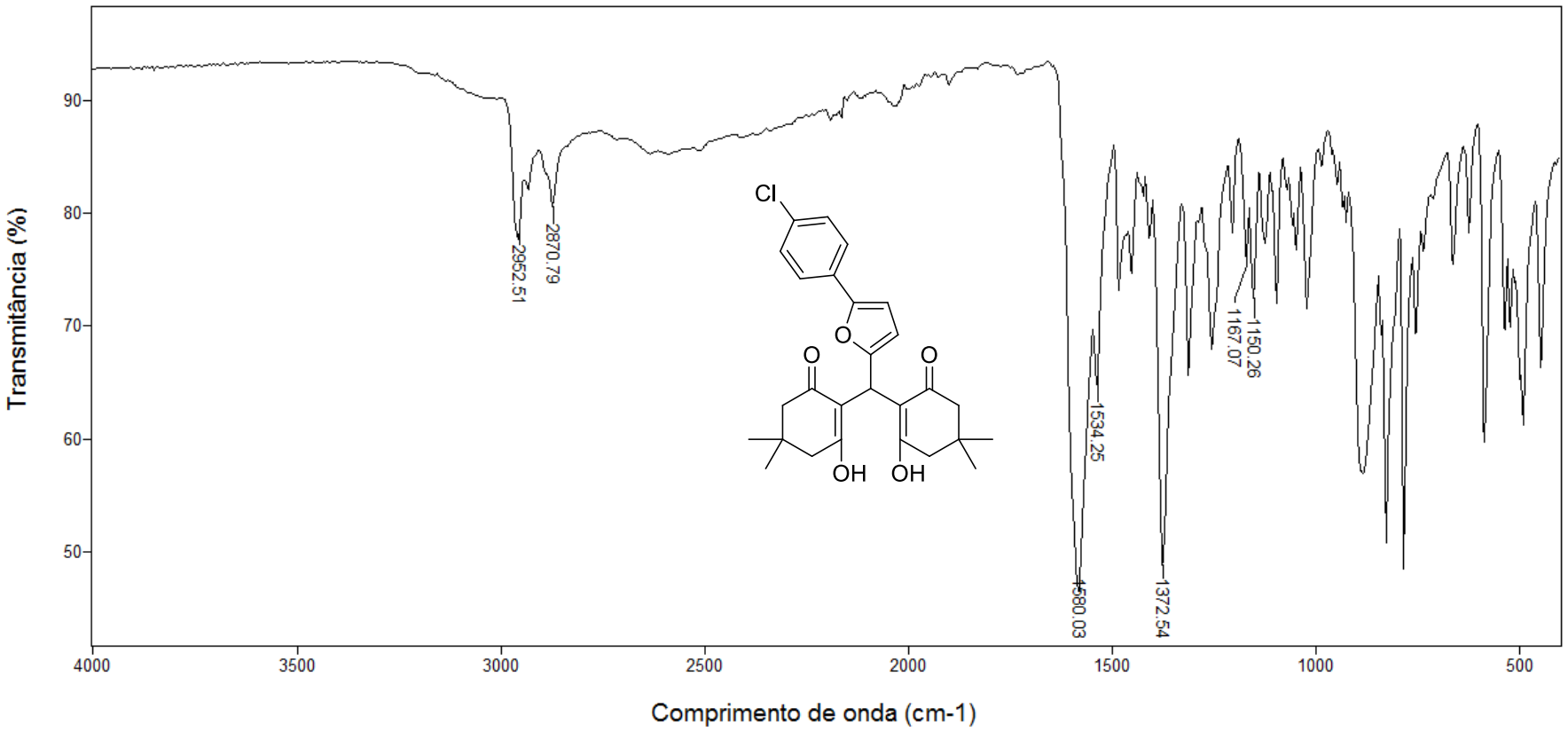

Figura 129. Espectro no infravermelho (ATR) do composto **33**.

.

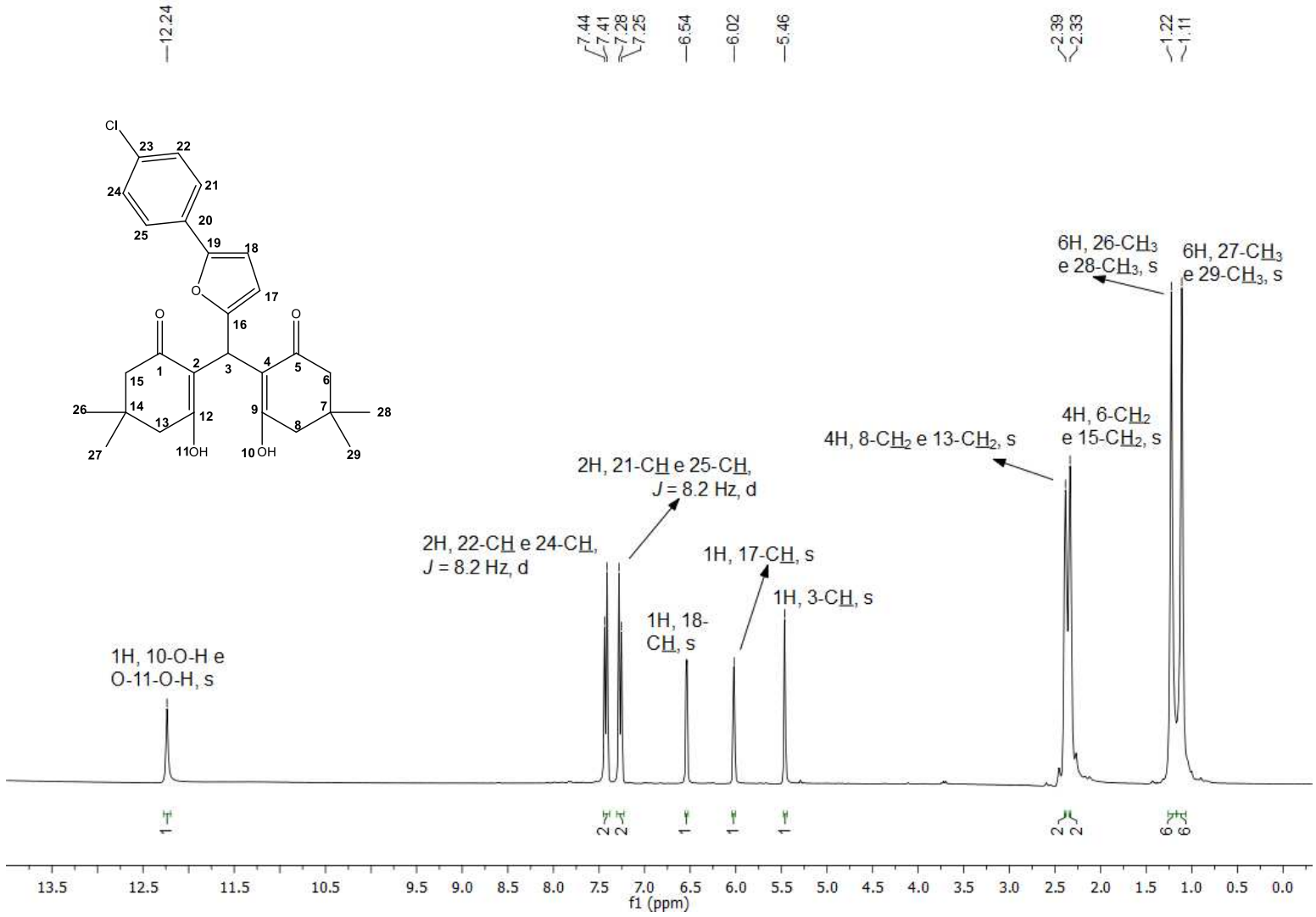

Figura 130. Espectro de RMN de ^{1}H (300 MHz, $CDCl_3$) do composto **33**.

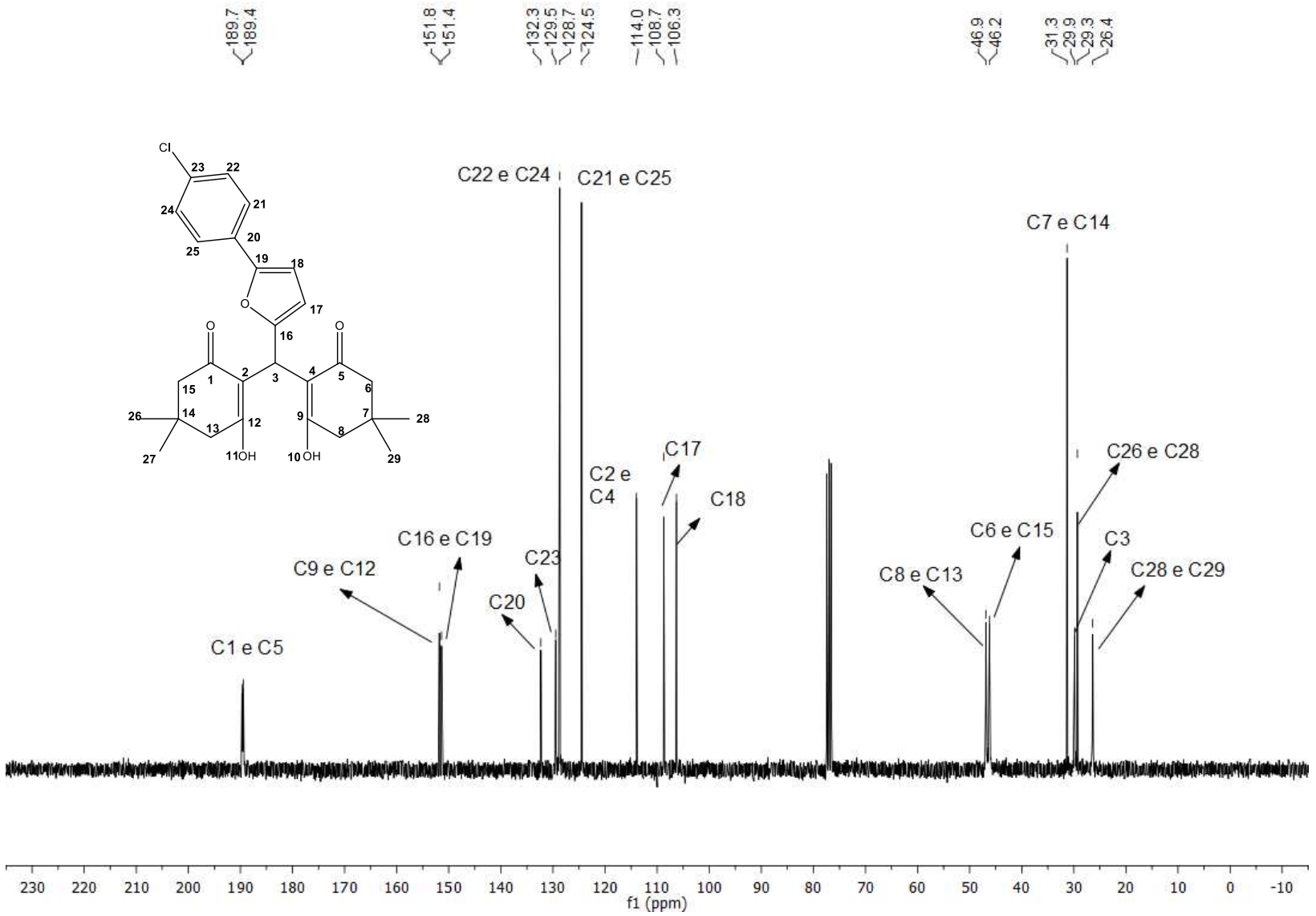
189.7
189.4
151.8
151.4
132.3
129.5
128.7
124.5
114.0
108.7
106.3
46.9
46.2
31.3
29.9
29.3
26.4
Cl
O
O
O
OH
OH
C22 e C24
C21 e C25
C7 e C14
C17
C2 e C4
C18
C26 e C28
C16 e C19
C23
C6 e C15
C3
C9 e C12
C8 e C13
C28 e C29
C20
C1 e C5
230 220 210 200 190 180 170 160 150 140 130 120 110 100 90 80 70 60 50 40 30 20 10 0 -10
f1 (ppm)

Figura 131. Espectro de RMN de ^{13}C (75 MHz, $CDCl_3$) do composto **33**.

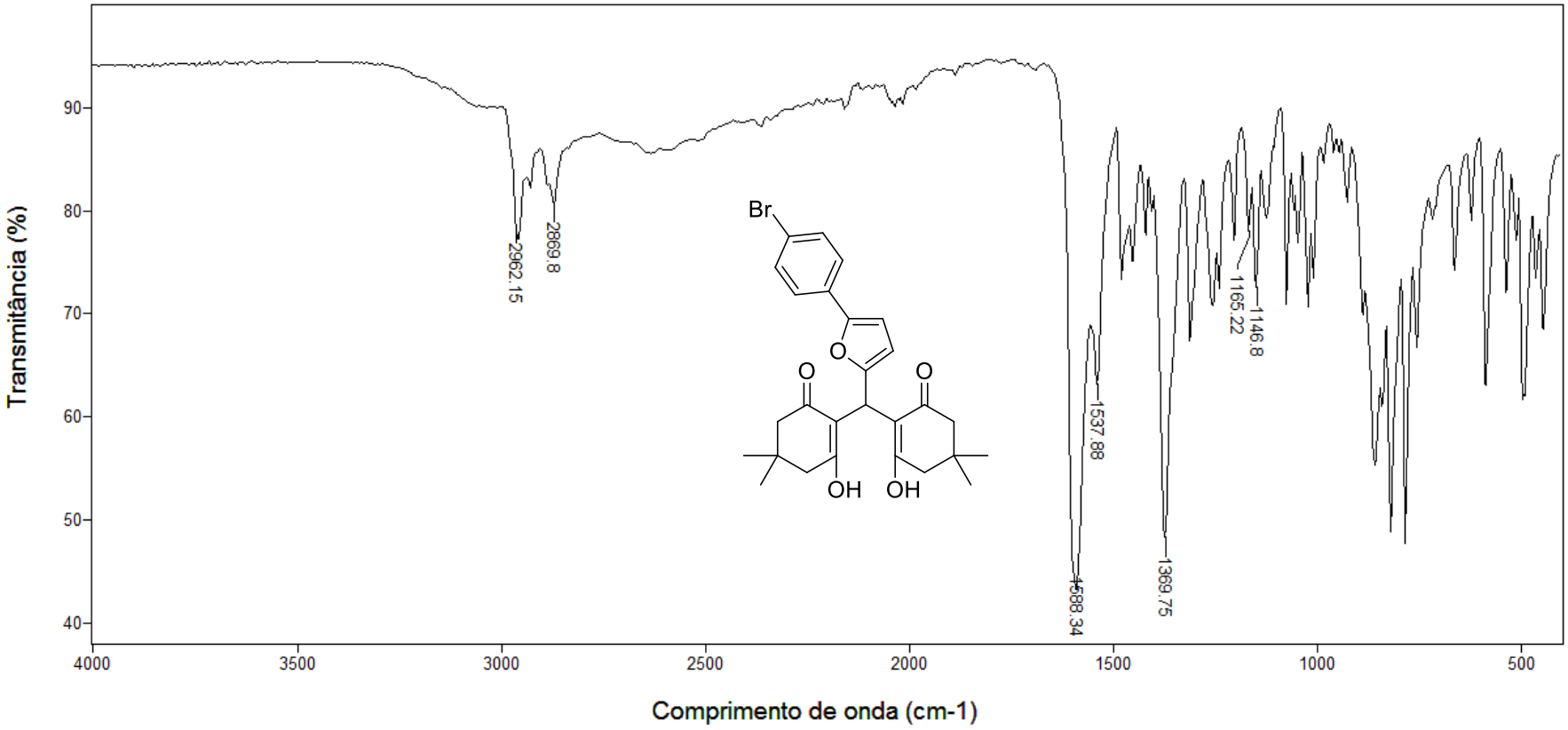

Figura 132. Espectro no infravermelho (ATR) do composto **34**.

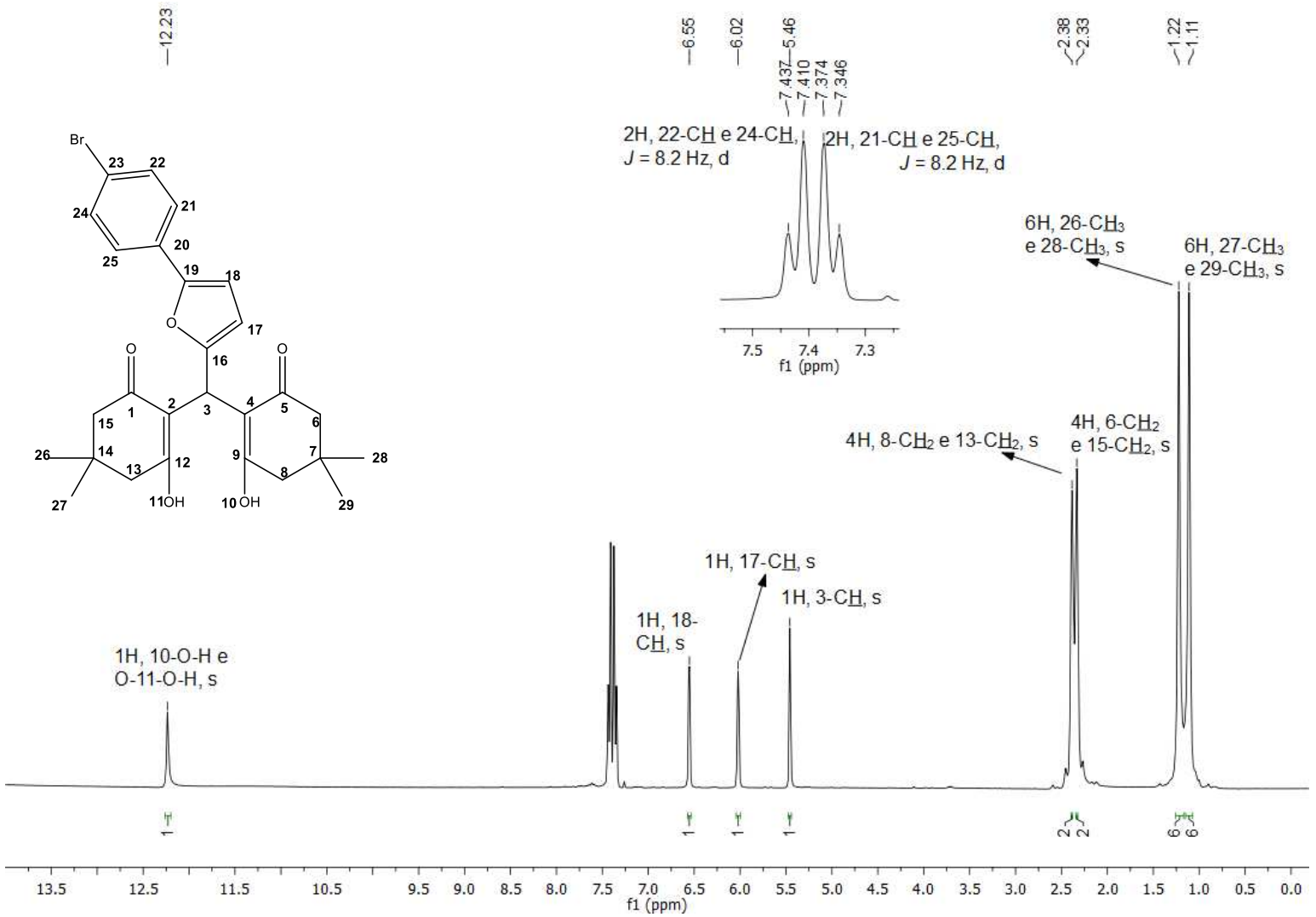

Figura 133. Espectro de RMN de ^{1}H (300 MHz, $CDCl_3$) do composto **34**.

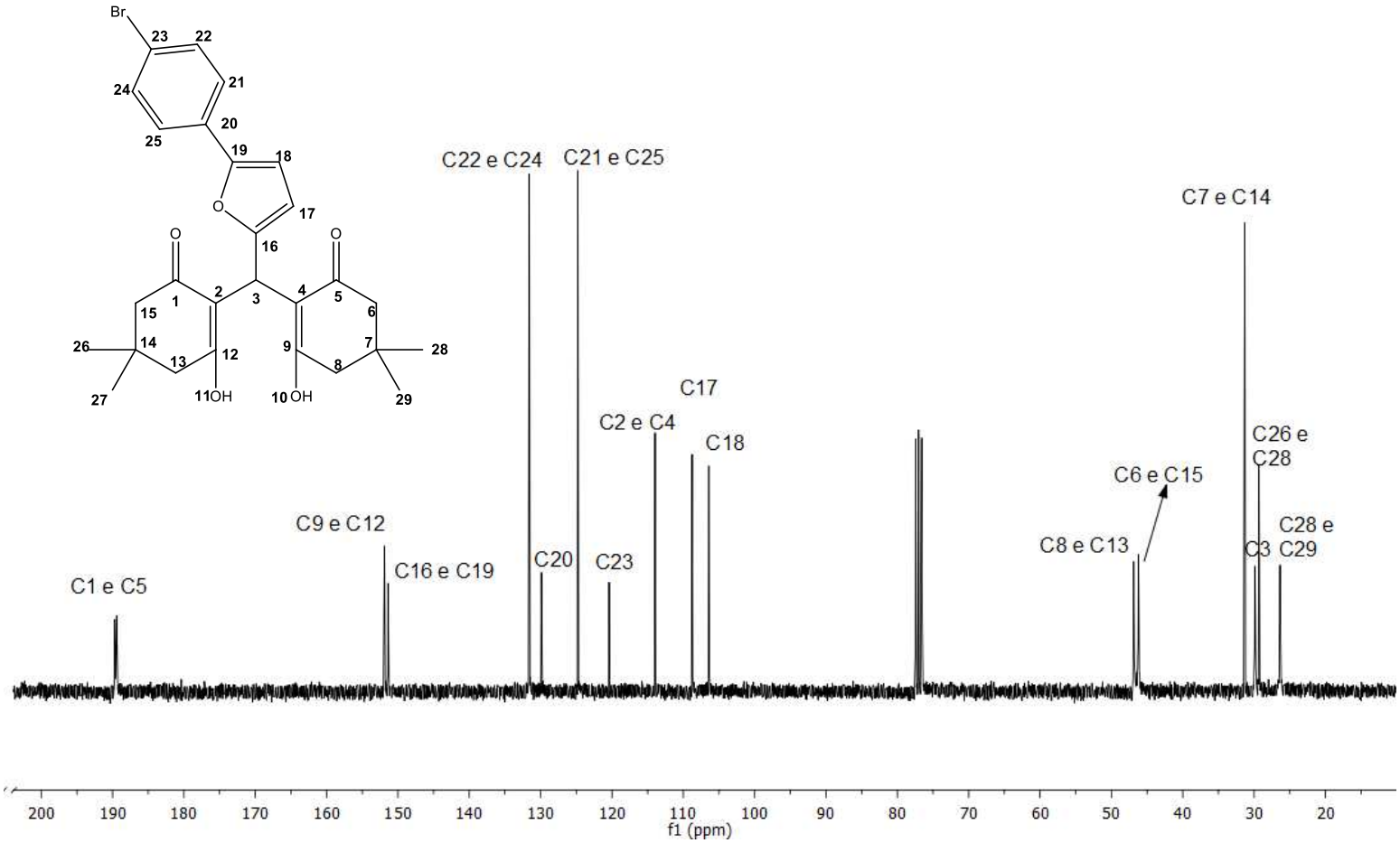

Figura 134. Espectro de RMN de ^{13}C (75 MHz, $CDCl_3$) do composto **34**.

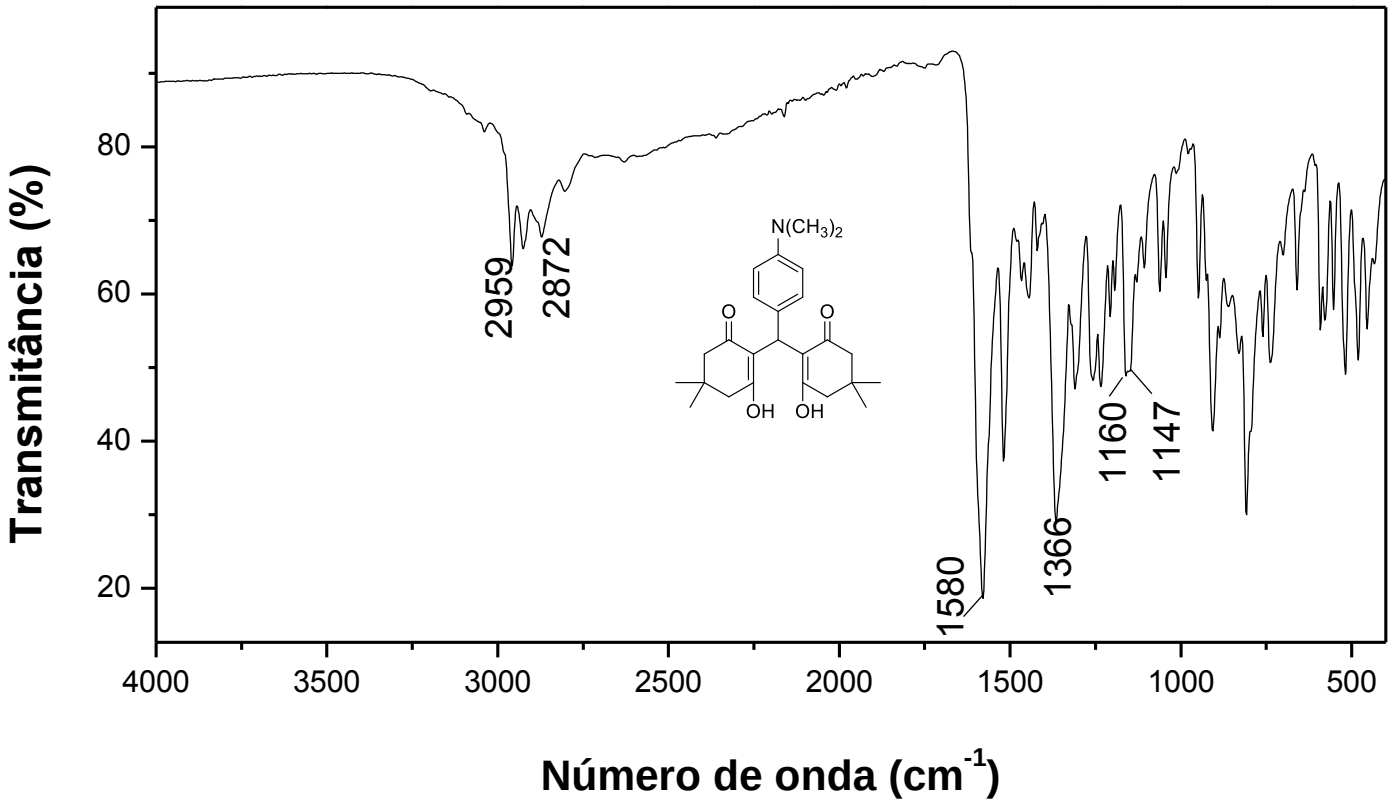

Figura 135. Espectro no Infravermelho (ATR) do composto **35**.

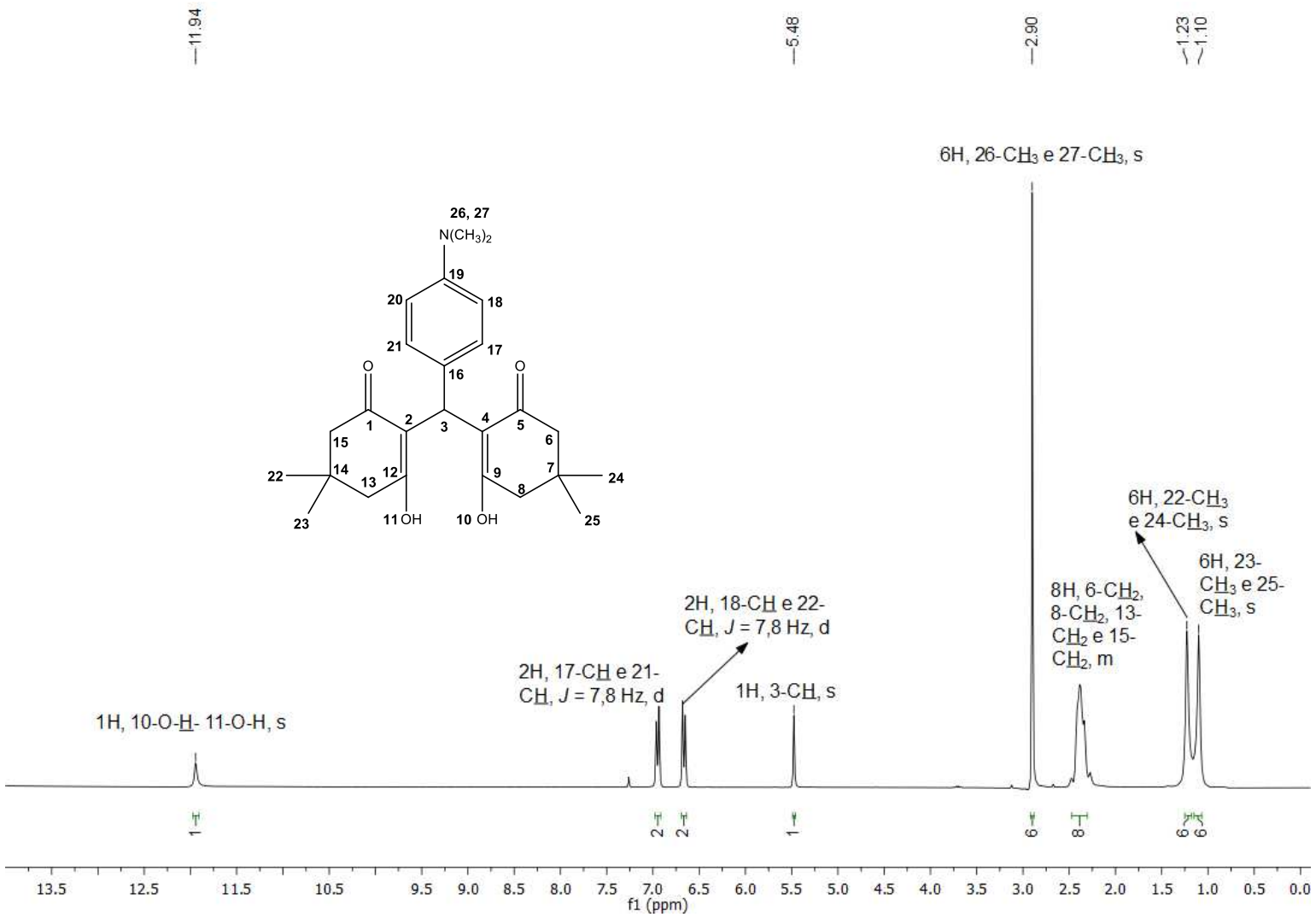

Figura 136. Espectro de RMN de ^{1}H (300 MHz, $CDCl_3$) do composto **35**.

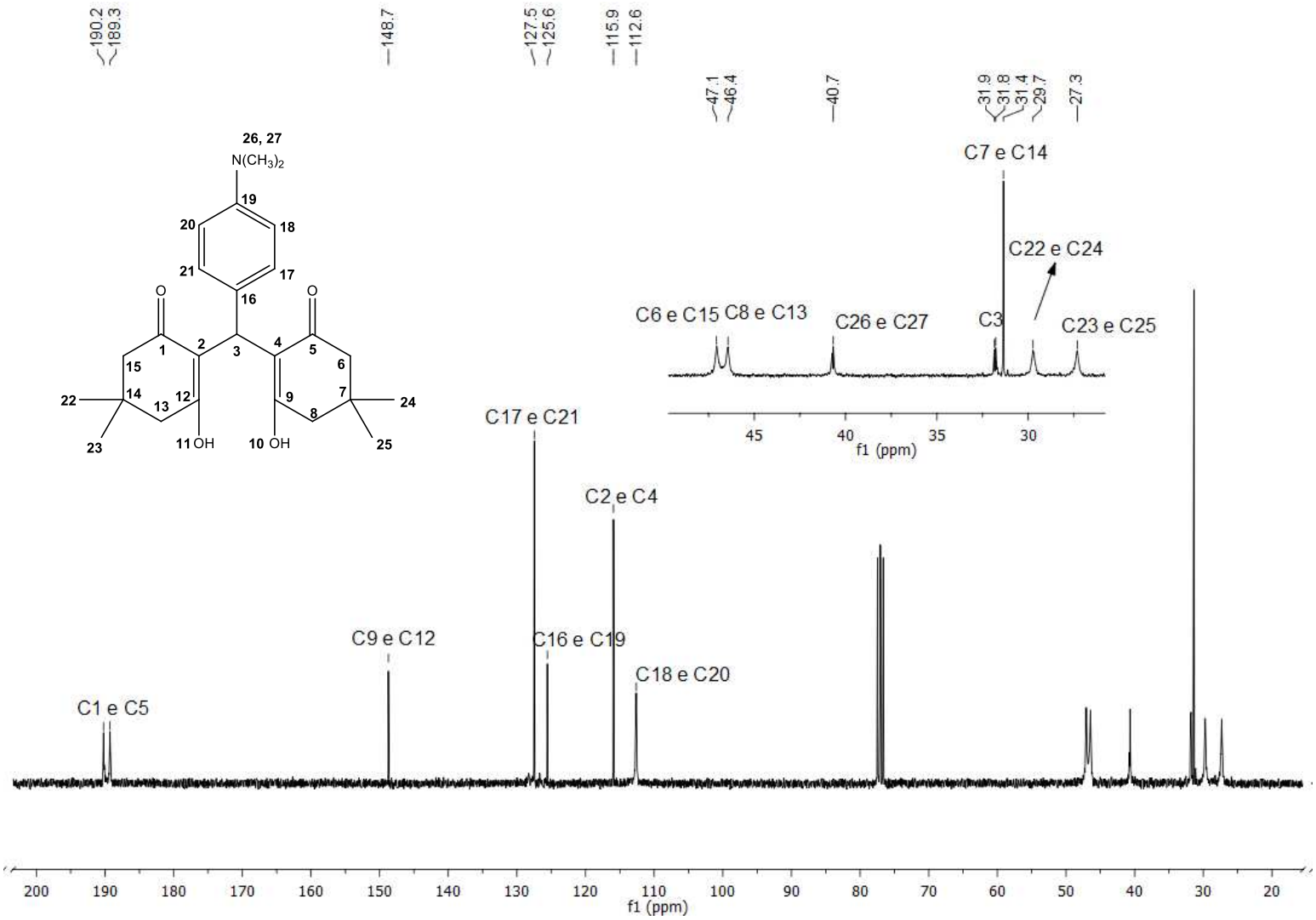

Figura 137. Espectro de RMN de ^{13}C (75 MHz, $CDCl_3$) do composto **35**.

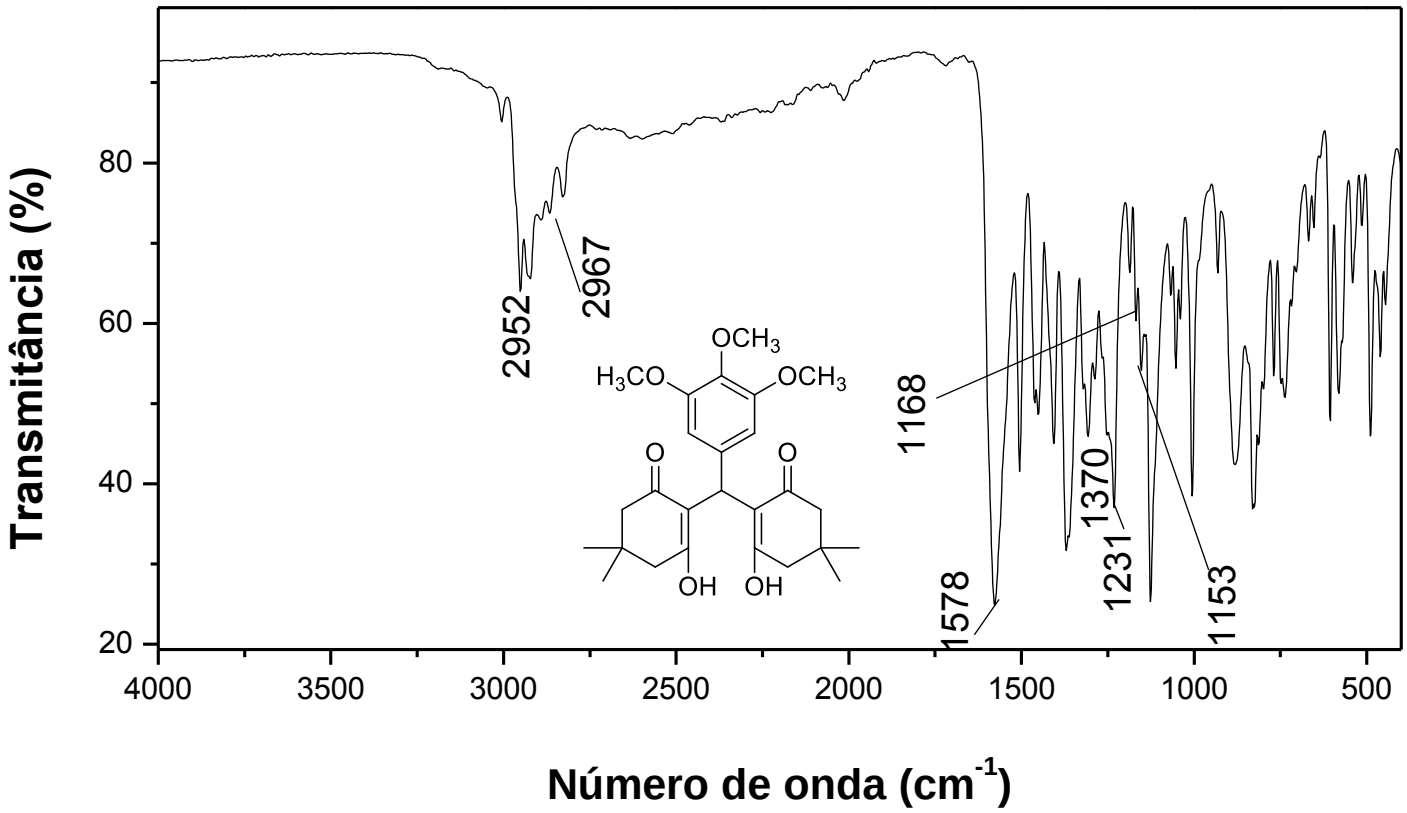

Figura 138. Espectro no Infravermelho (ATR) do composto **36**.

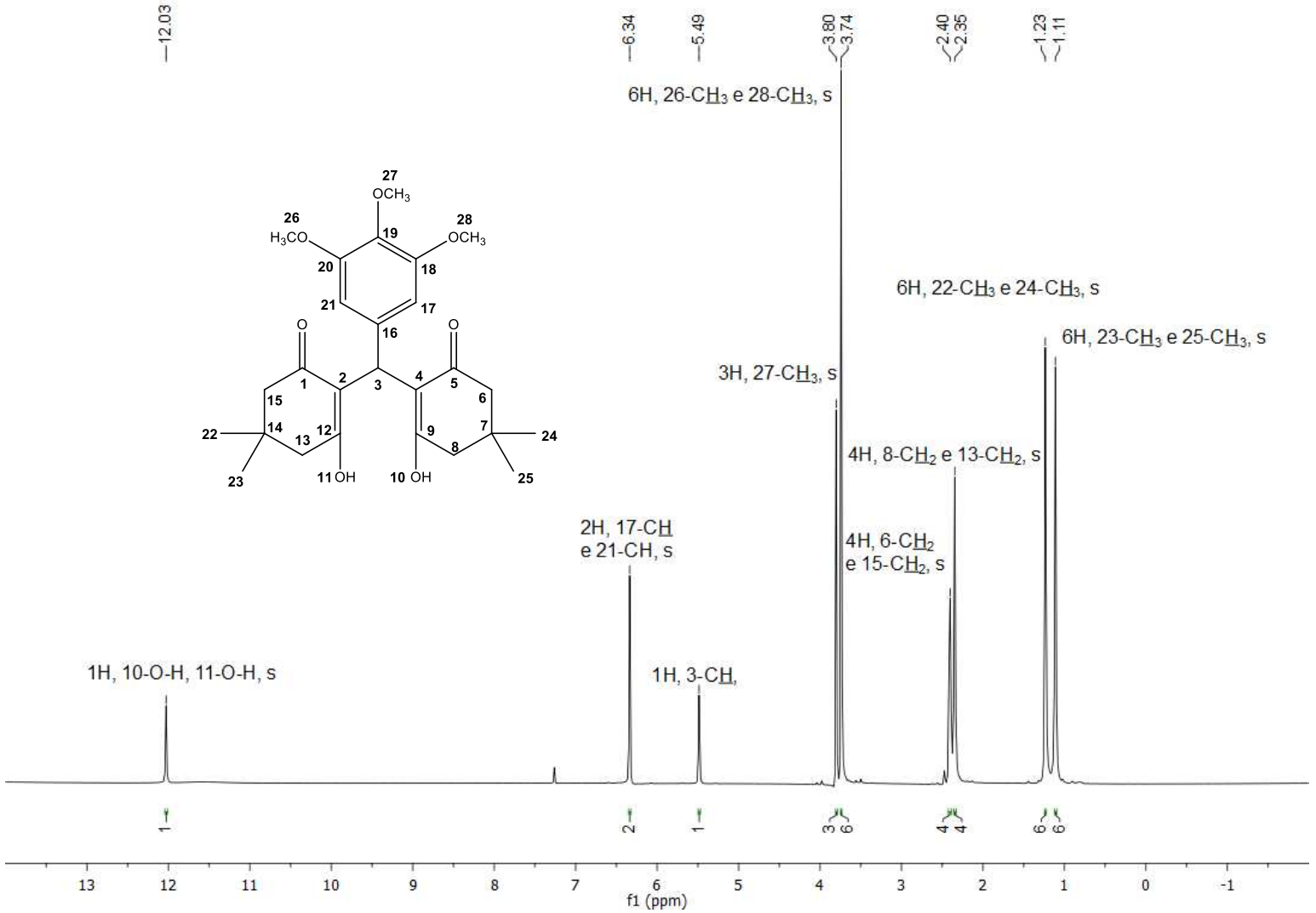

Figura 139. Espectro de RMN de ^{1}H (300 MHz, $CDCl_3$) do composto **36**.

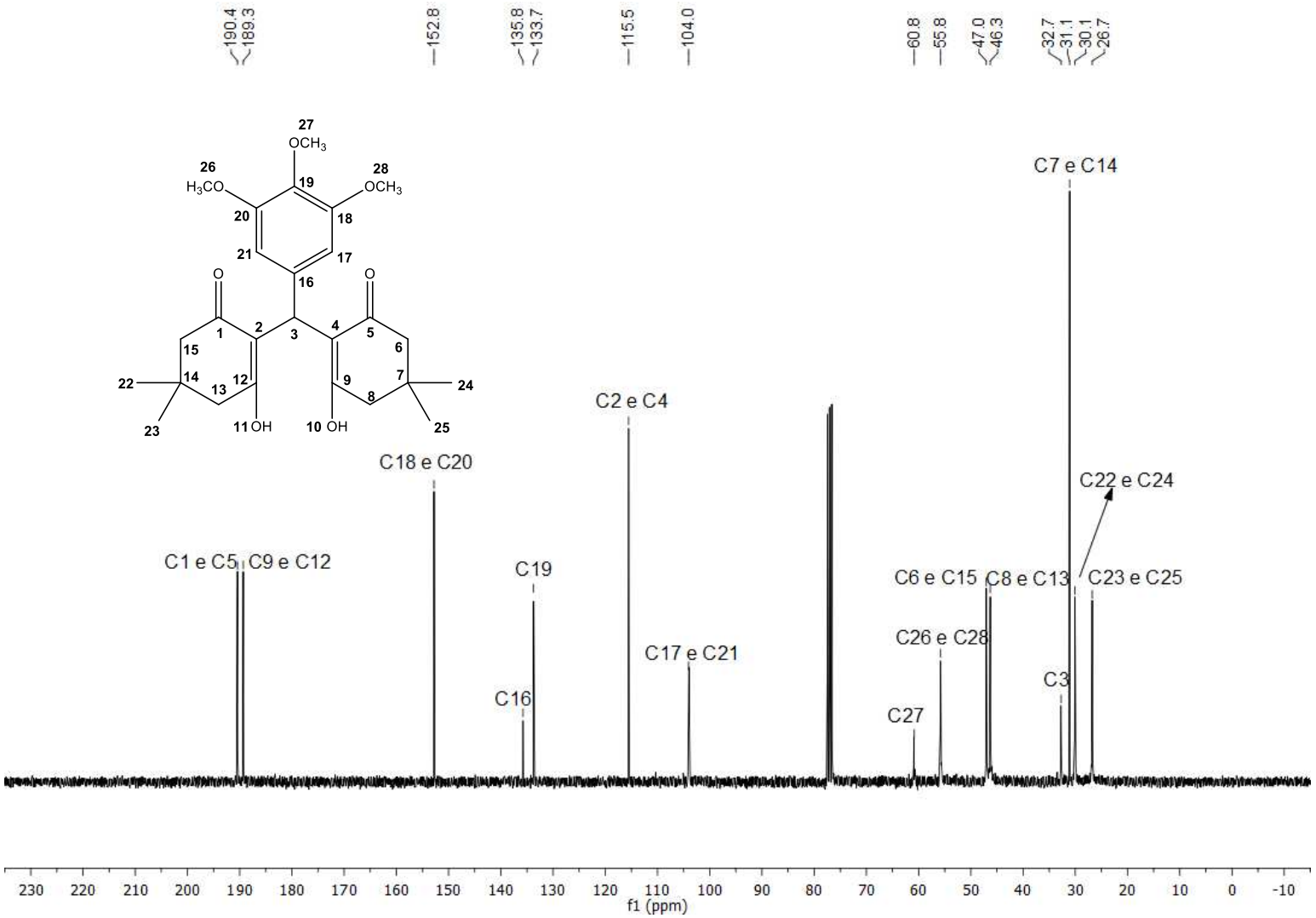

Figura 140. Espectro de RMN de ^{13}C (75 MHz, $CDCl_3$) do composto **36**.

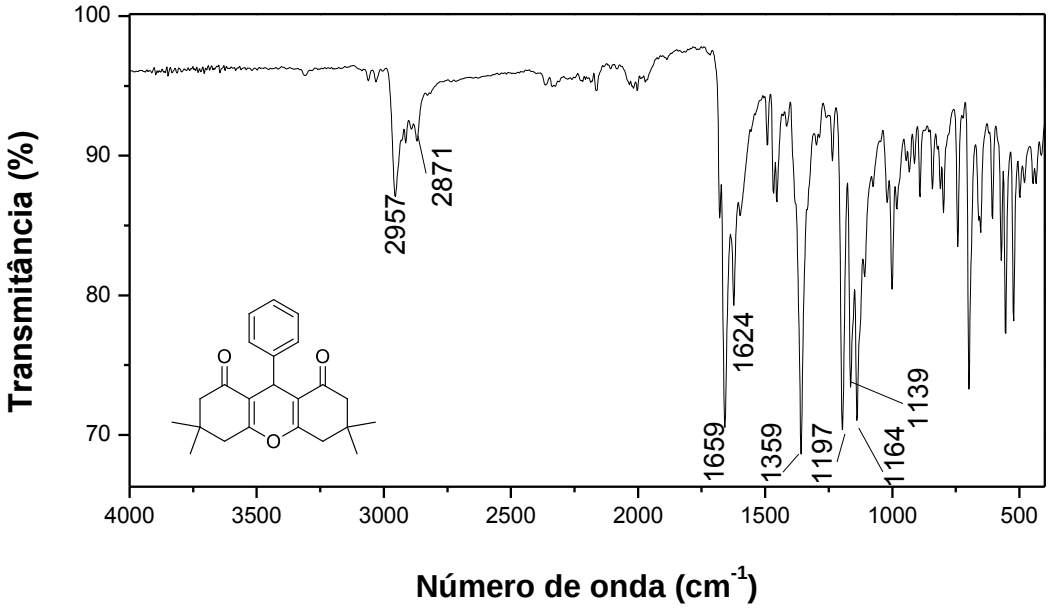

Figura 141. Espectro no Infravermelho (ATR) do composto **37**.

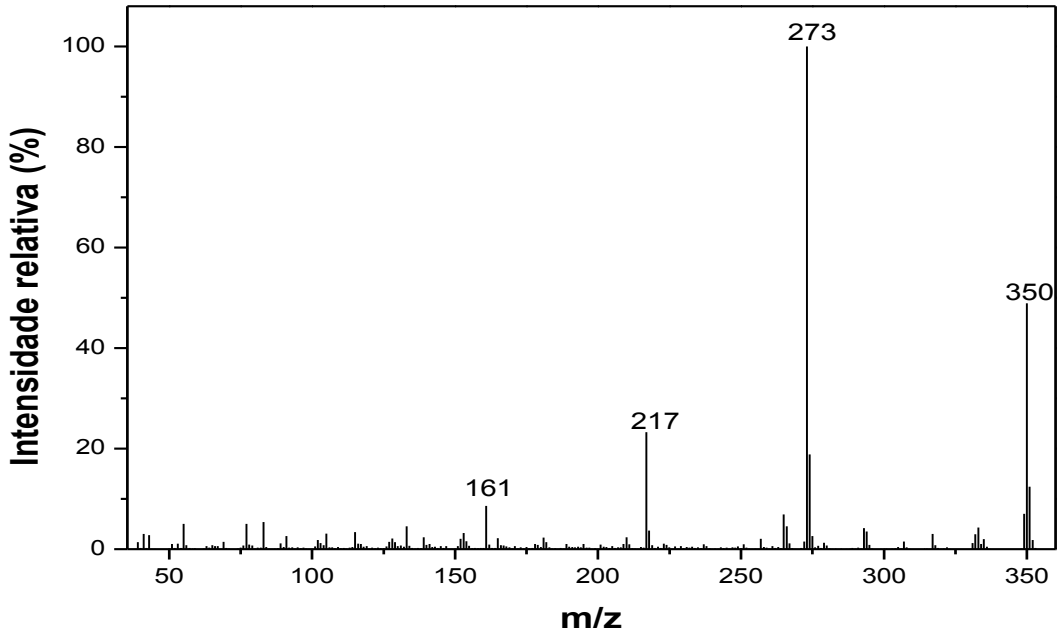

Figura 142. Espectro de massas do composto **37**.

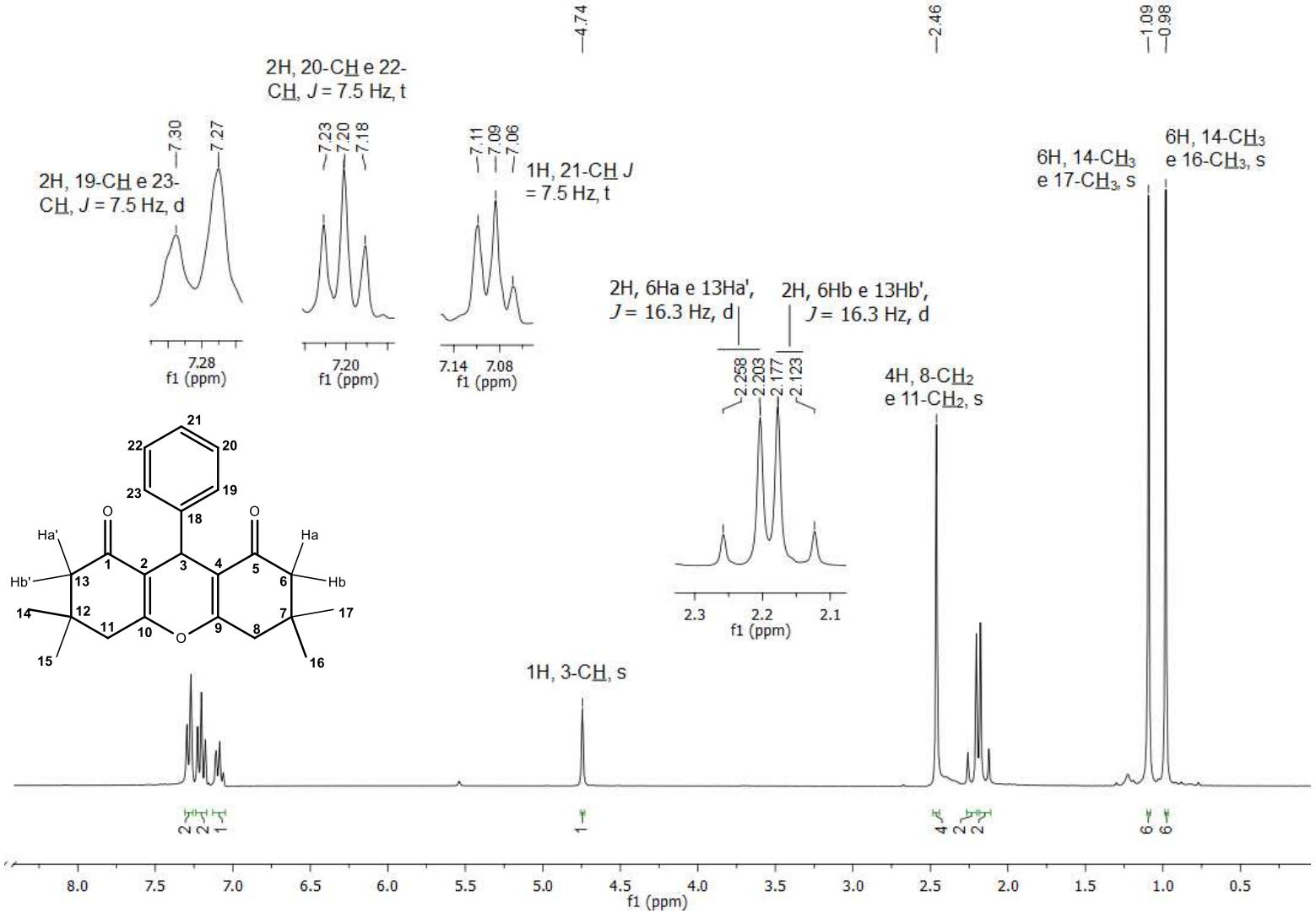

Figura 143. Espectro de RMN de ^{1}H (300 MHz, $CDCl_3$) do composto **37**.

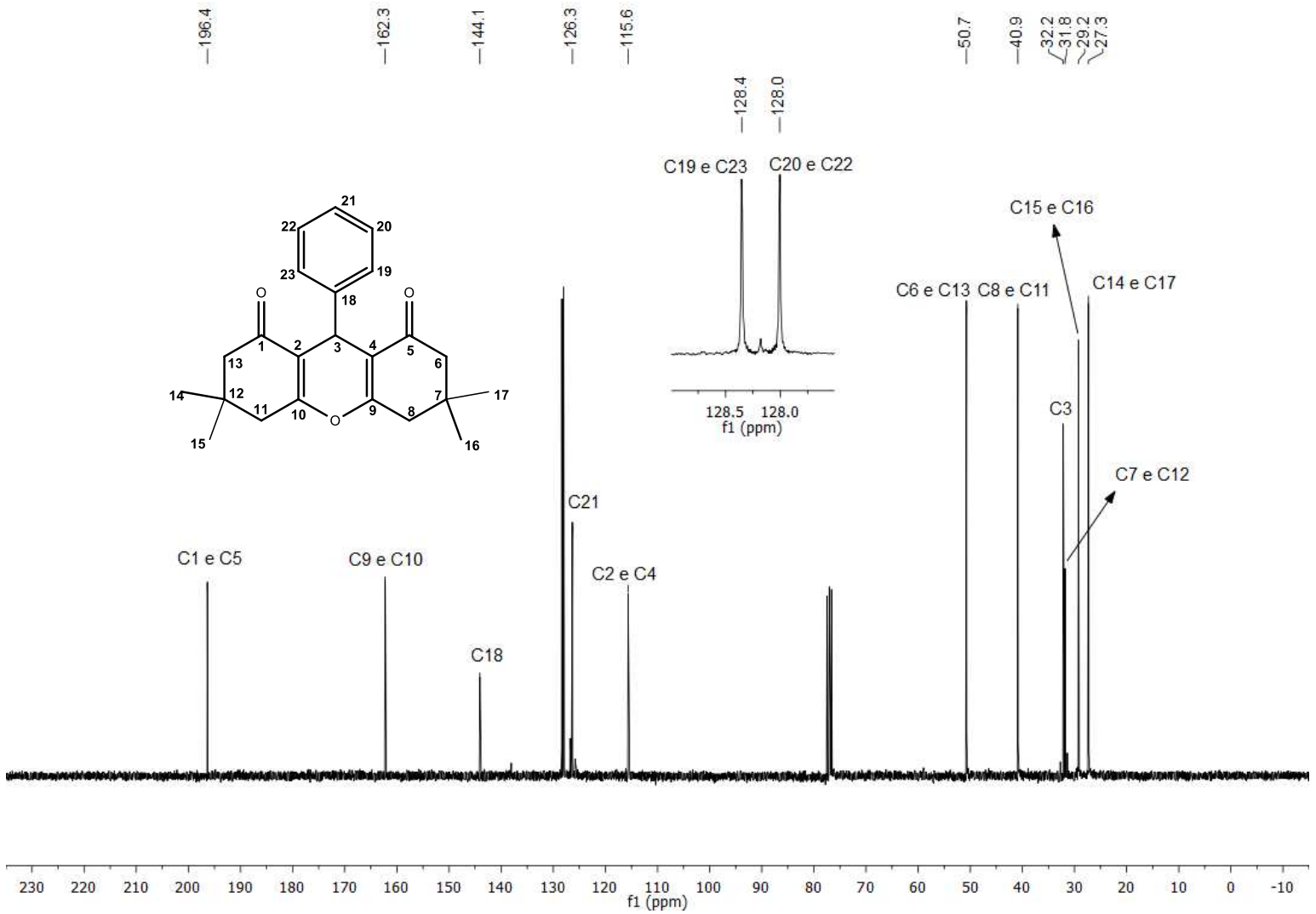

Figura 144. Espectro de RMN de ^{13}C (75 MHz, $CDCl_3$) do composto **37**.

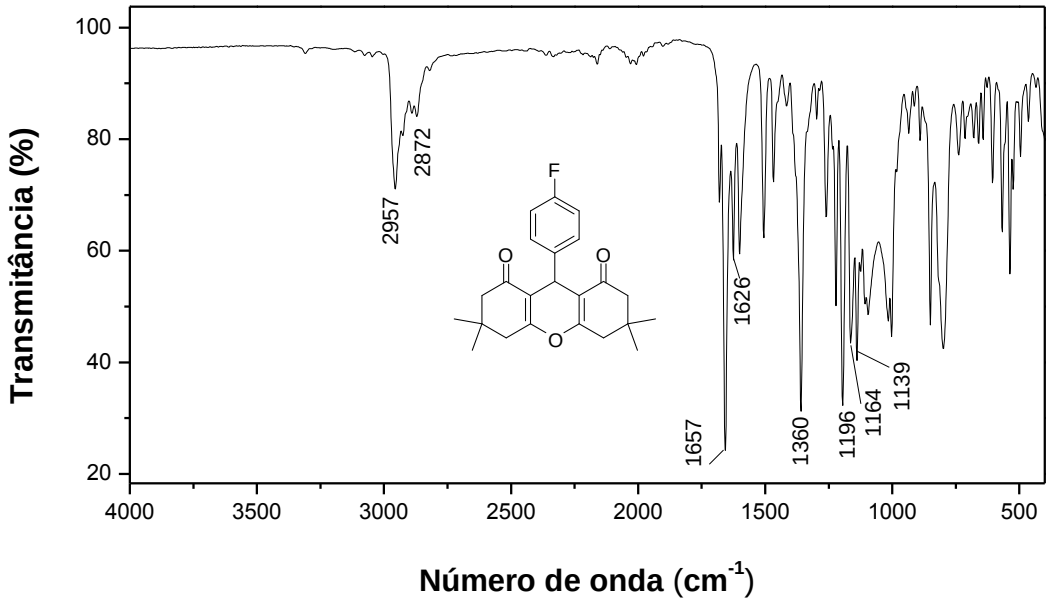

Figura 145. Espectro no infravermelho (ATR) do composto **38**.

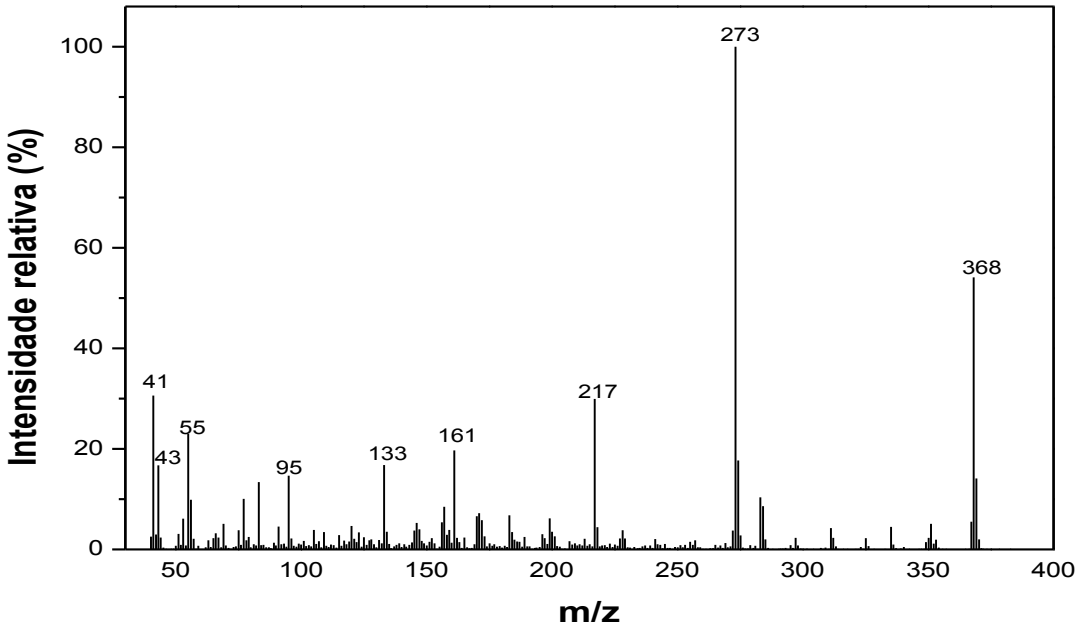

Figura 146. Espectro de massas do composto **38**.

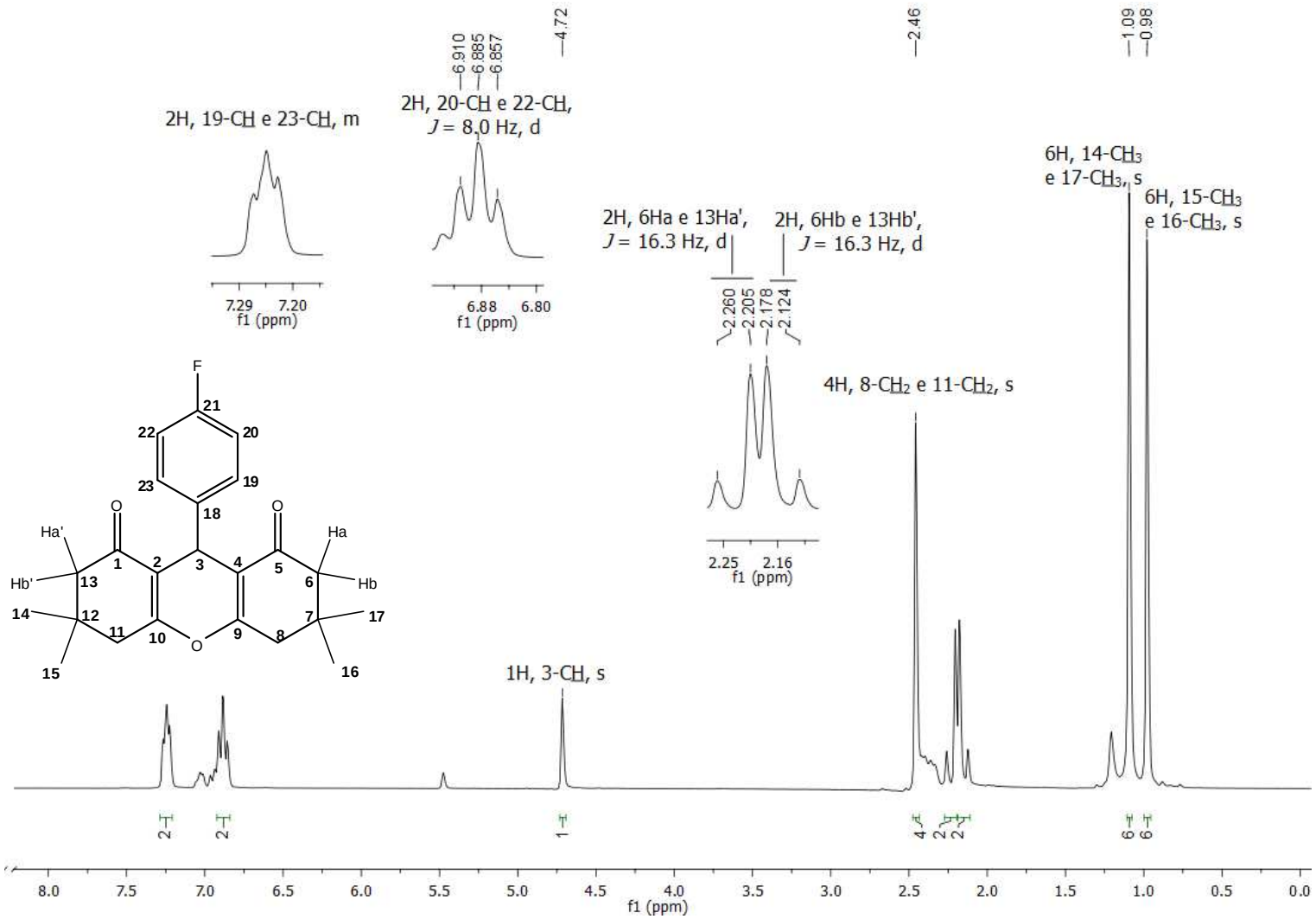

Figura 147. Espectro de RMN de ^{1}H (300 MHz, $CDCl_3$) do composto **38**.

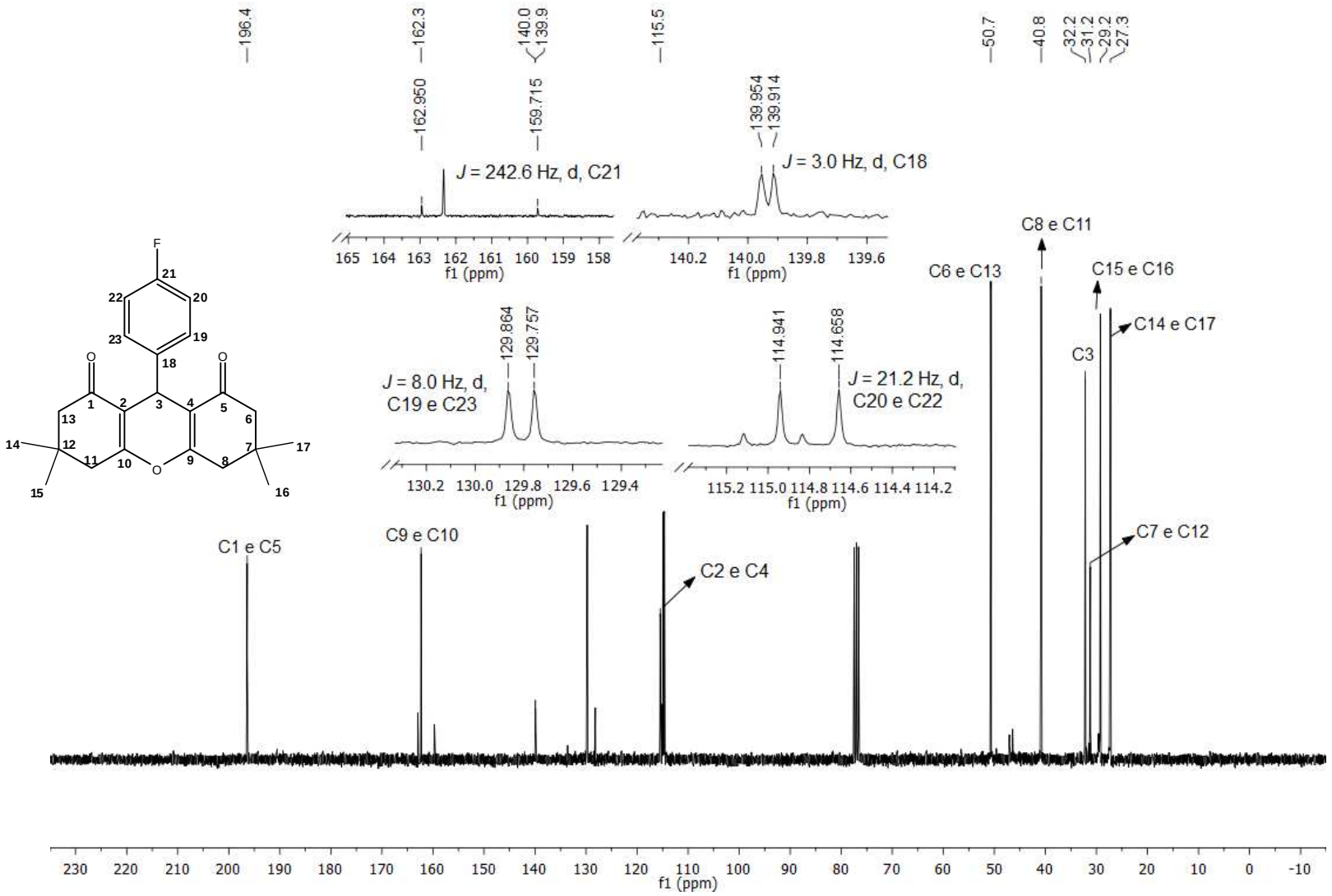

Figura 148. Espectro de RMN de ^{13}C (75 MHz, $CDCl_3$) do composto **38**.

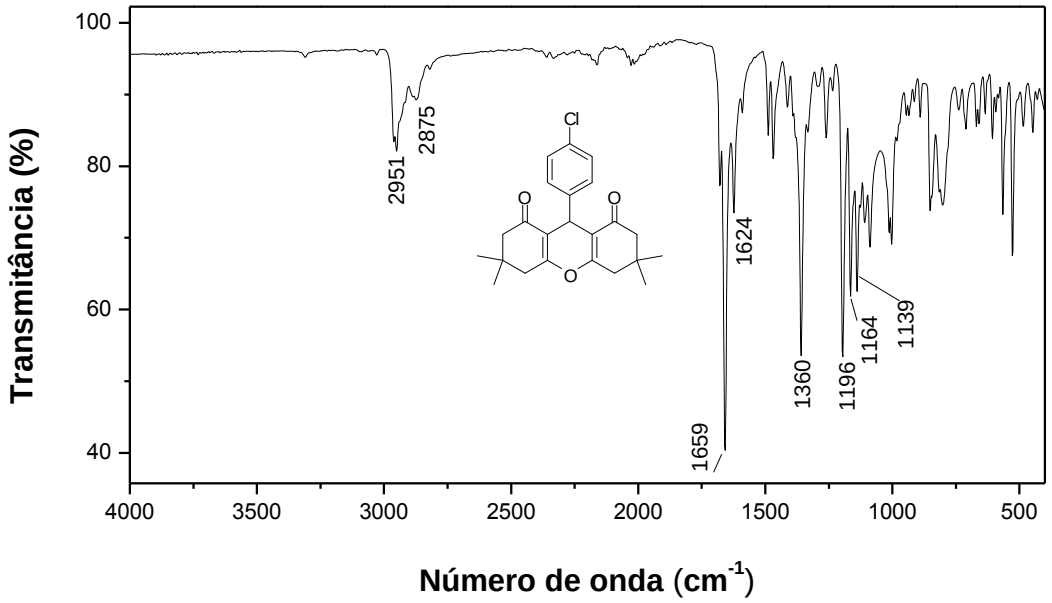

Figura 149. Espectro no infravermelho (ATR) do composto **39**.

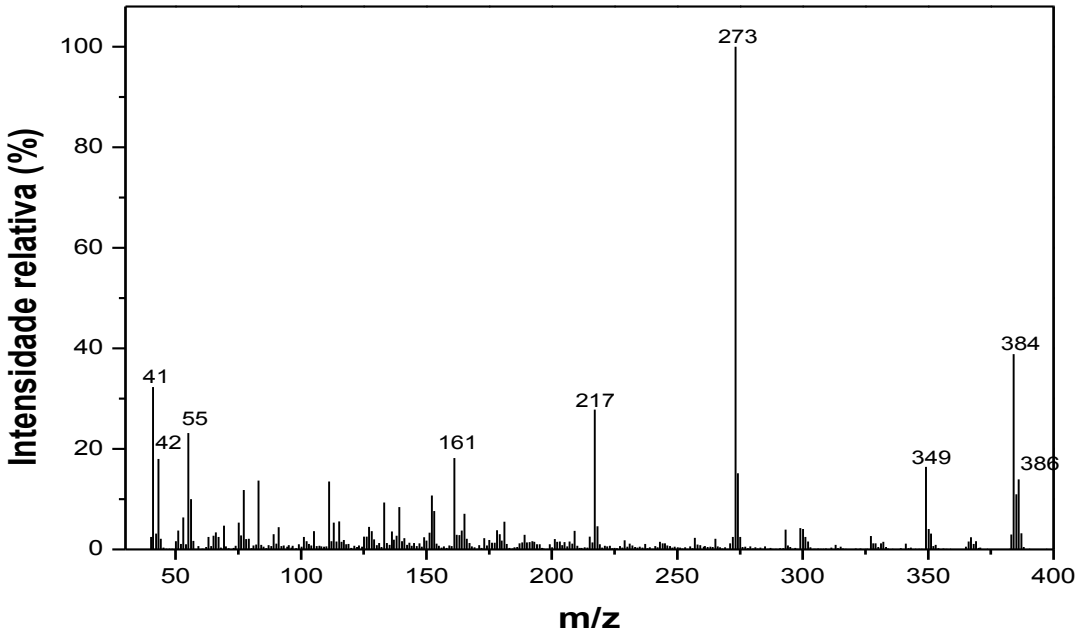

Figura 150. Espectro de massas do composto **39**.

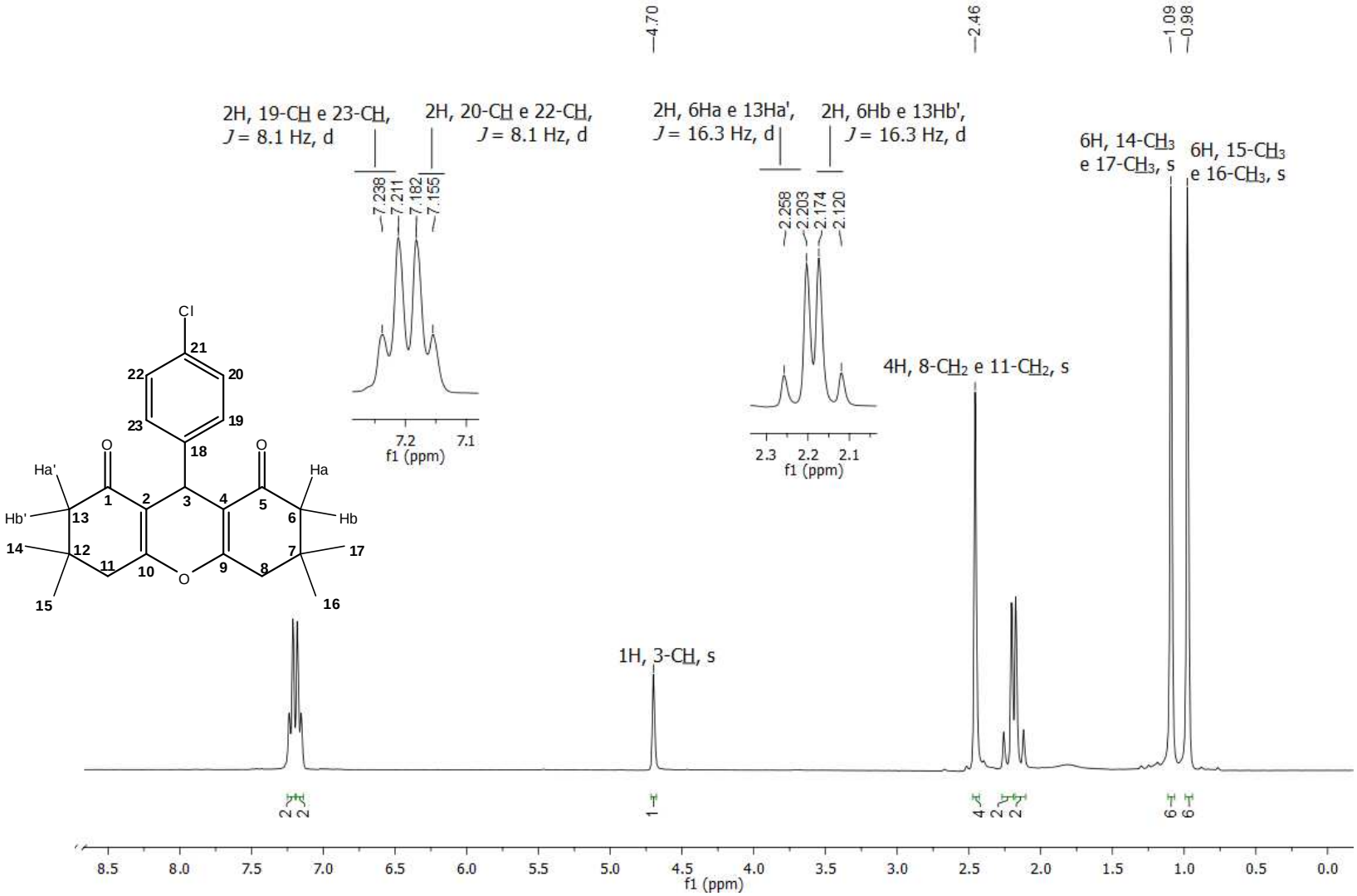

Figura 151. Espectro de RMN de ^{1}H (300 MHz, $CDCl_3$) do composto **39**.

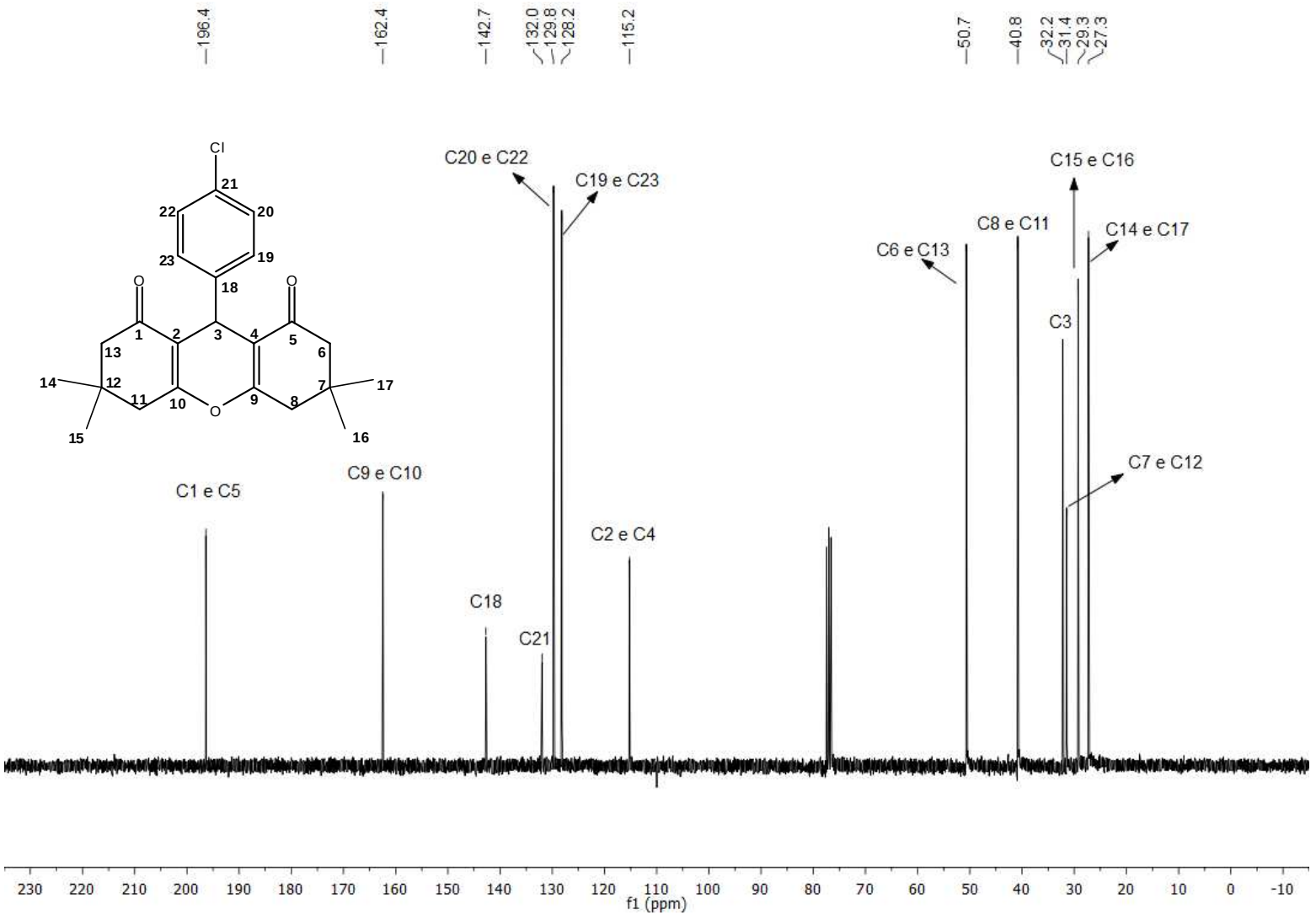

Figura 152. Espectro de RMN de ^{13}C (75 MHz, $CDCl_3$) do composto **39**.

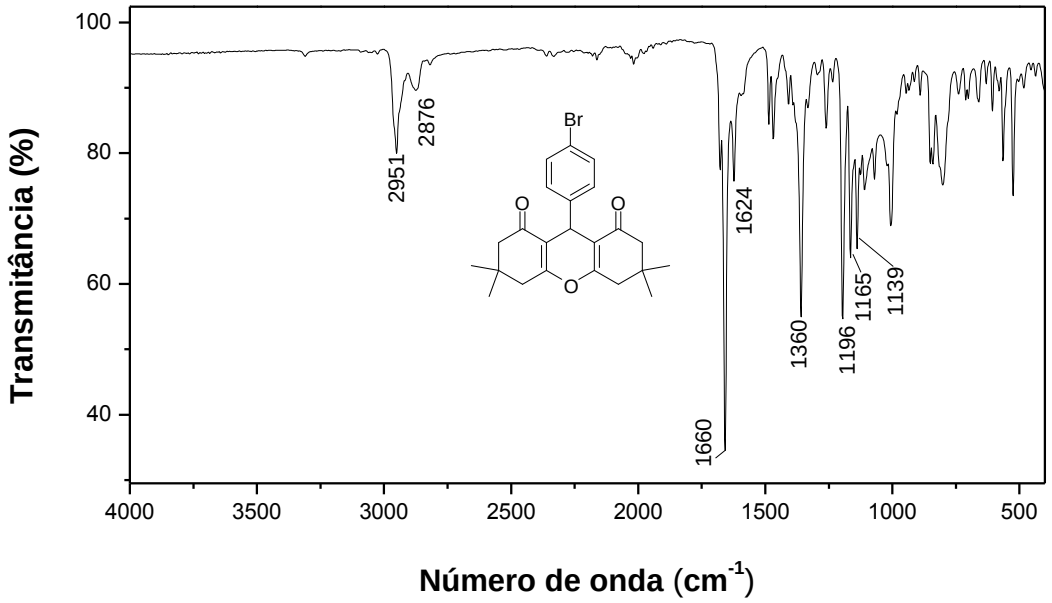

Figura 153. Espectro no infravermelho (ATR) do composto **40**.

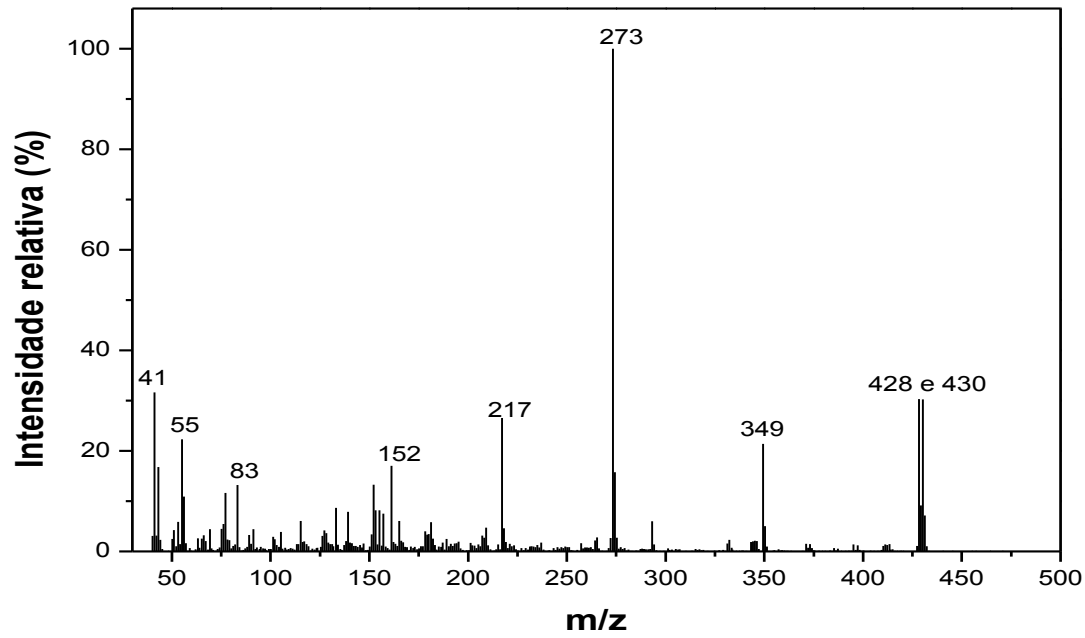

Figura 154. Espectro de massas do composto **40**.

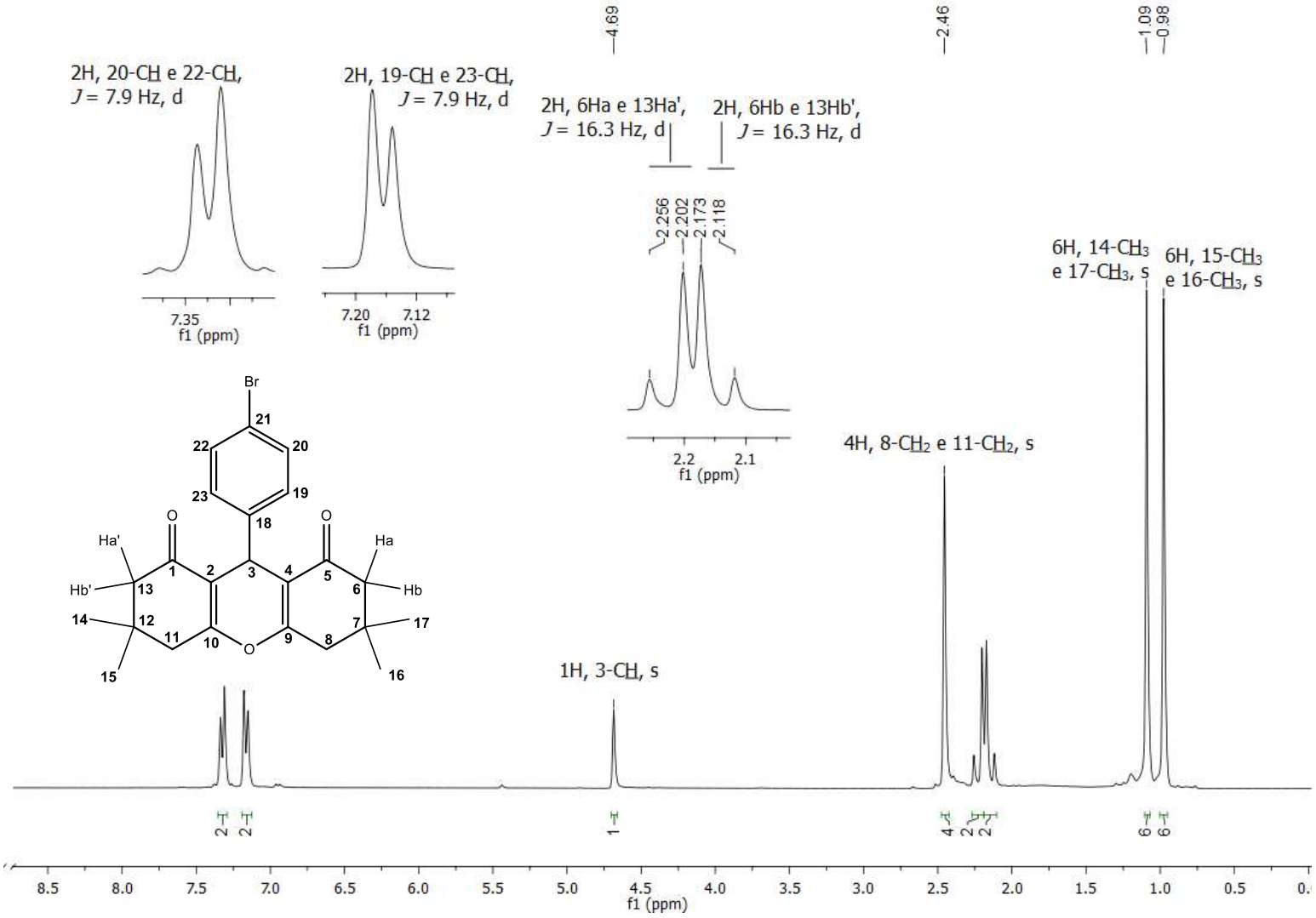

Figura 155. Espectro de RMN de ^{1}H (300 MHz, $CDCl_3$) do composto **40**.

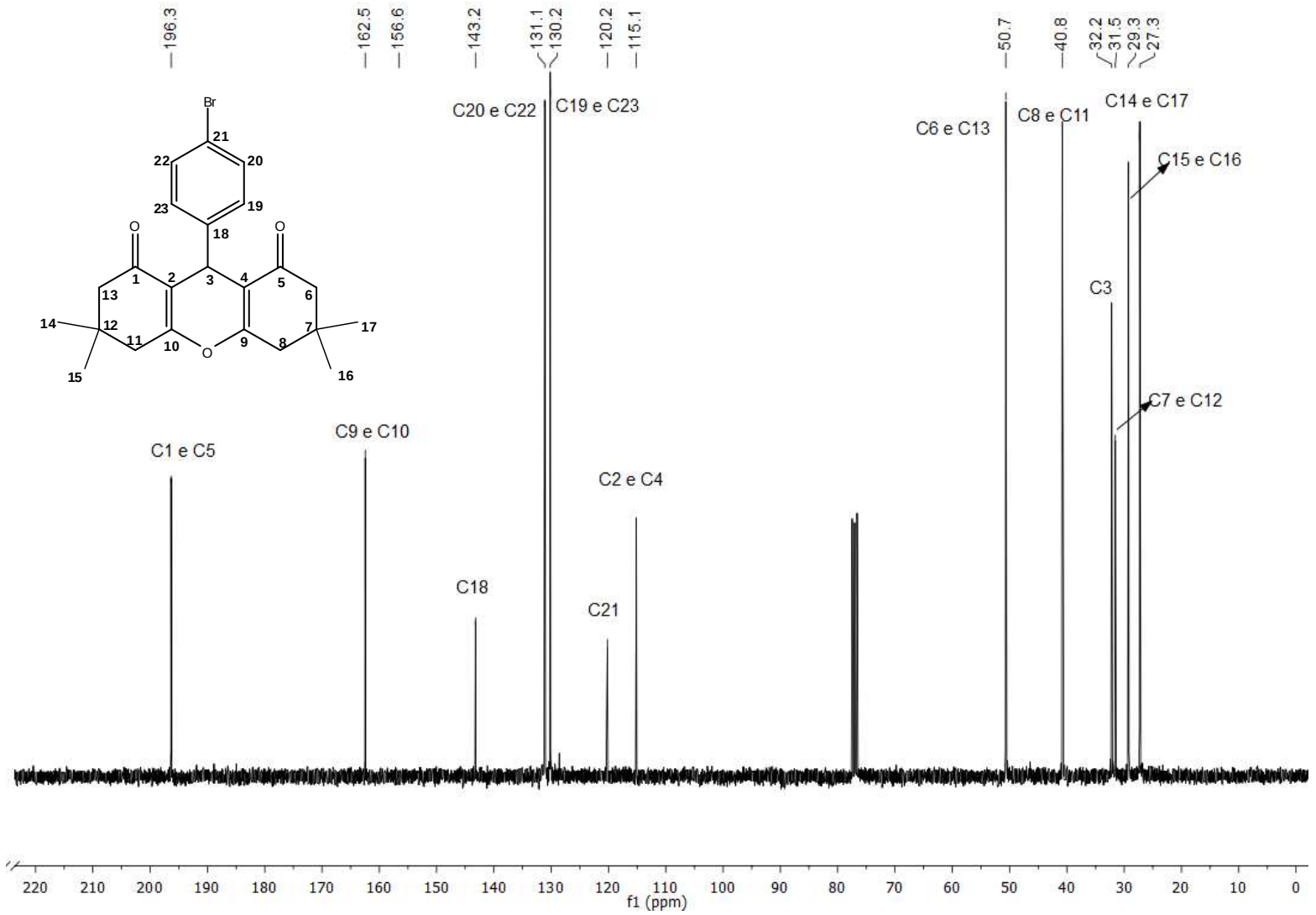

Figura 156. Espectro de RMN de ^{13}C (75 MHz, $CDCl_3$) do composto **40**.

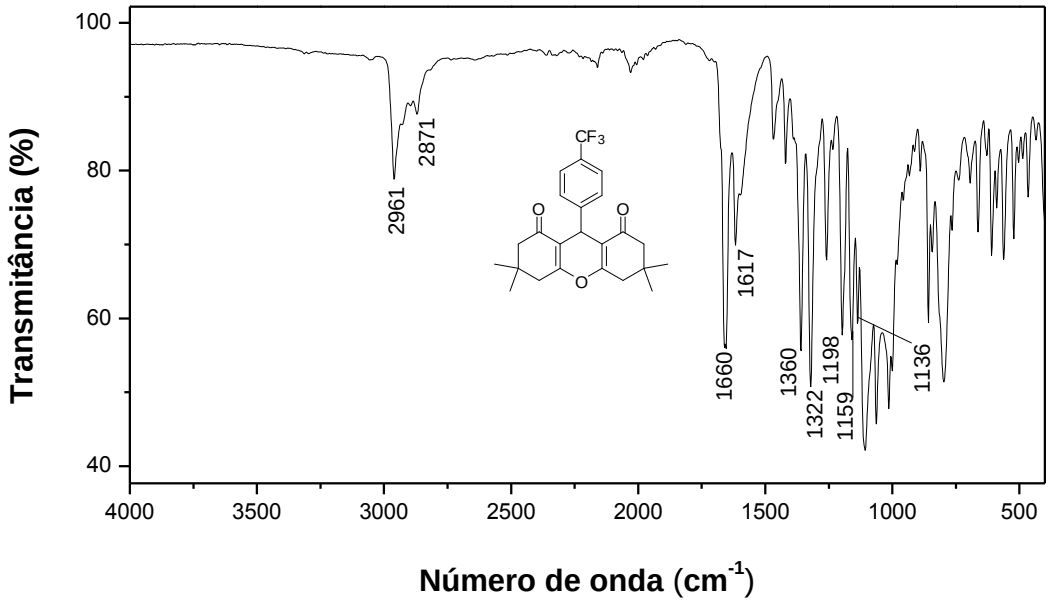

Figura 157. Espectro no infravermelho (ATR) do composto **41**.

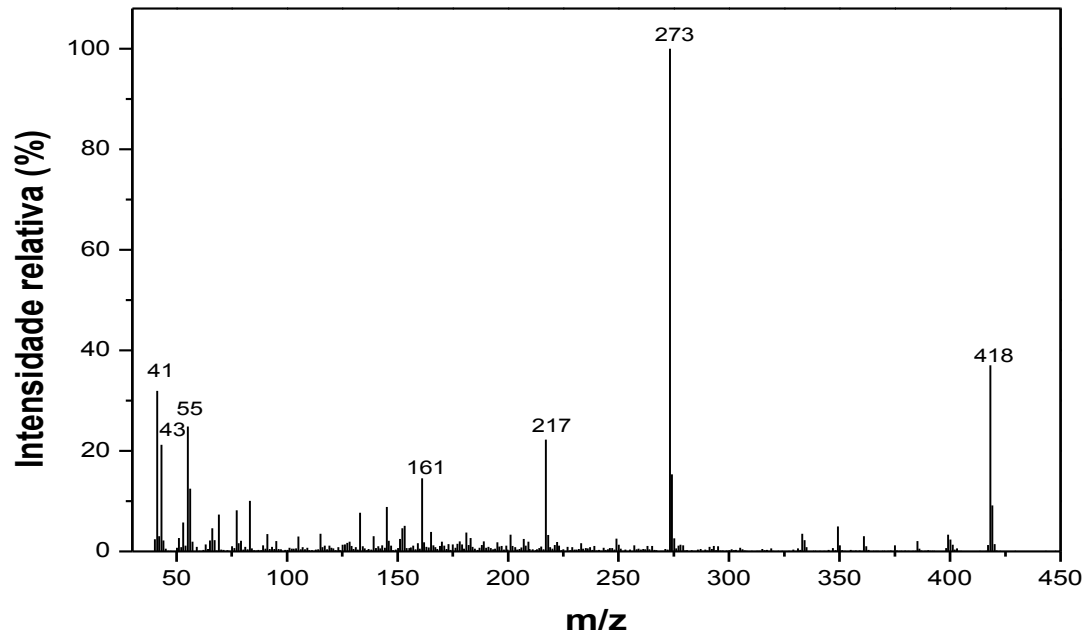

Figura 158. Espectro de massas do composto **41**.

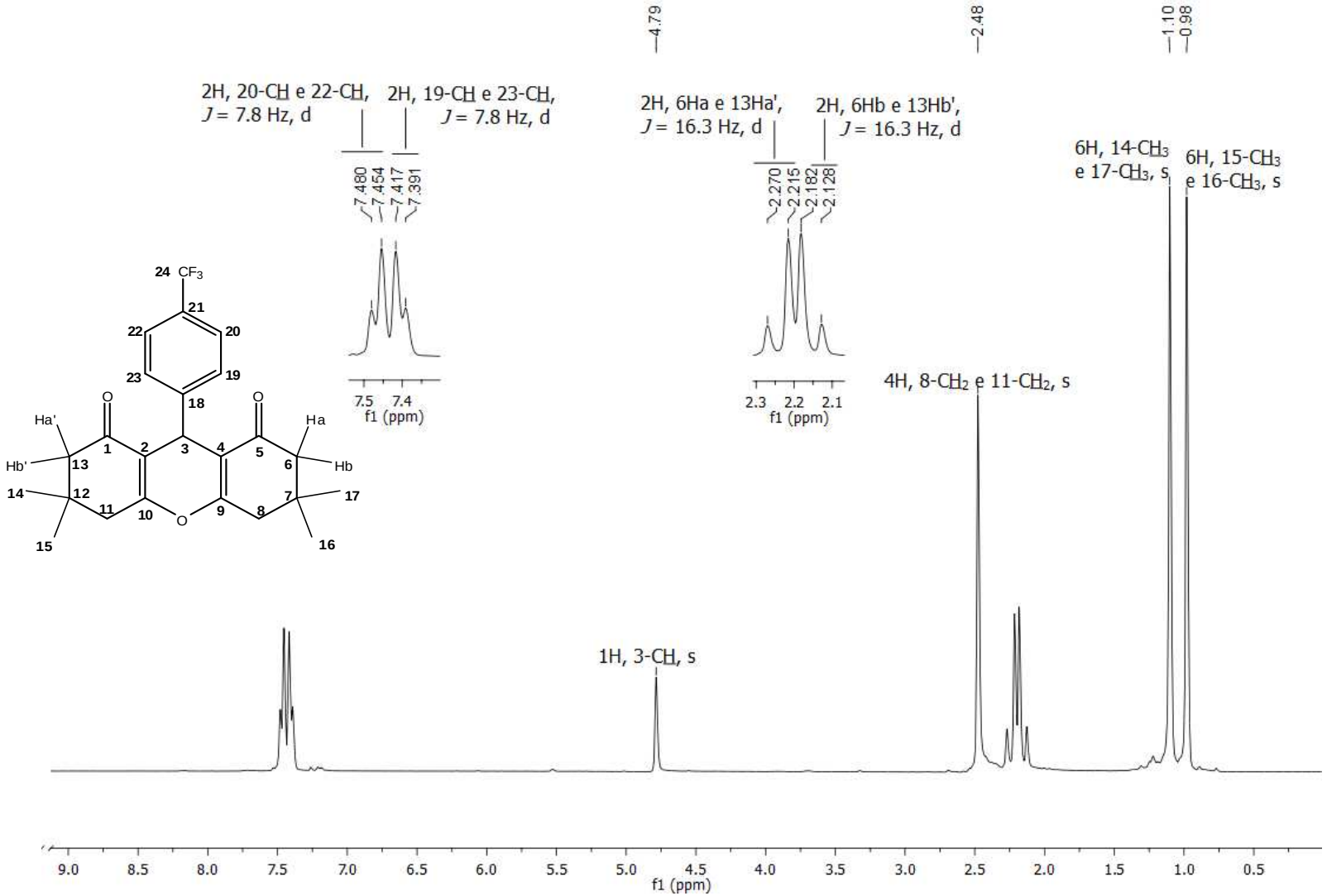

Figura 159. Espectro de RMN de ^{1}H (300 MHz, $CDCl_3$) do composto **41**.

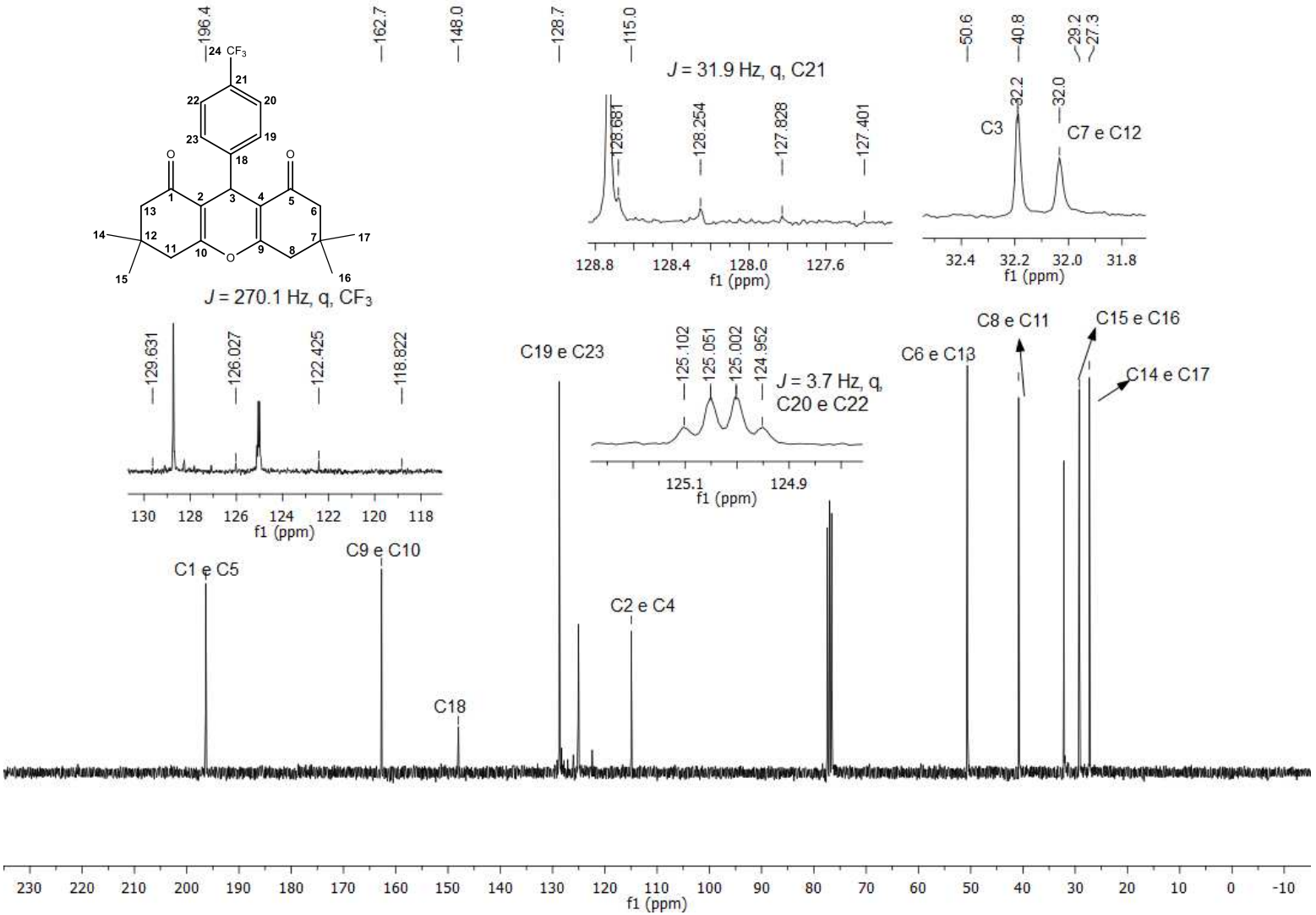

Figura 160. Espectro de RMN de ^{13}C (75 MHz, $CDCl_3$) do composto **41**.

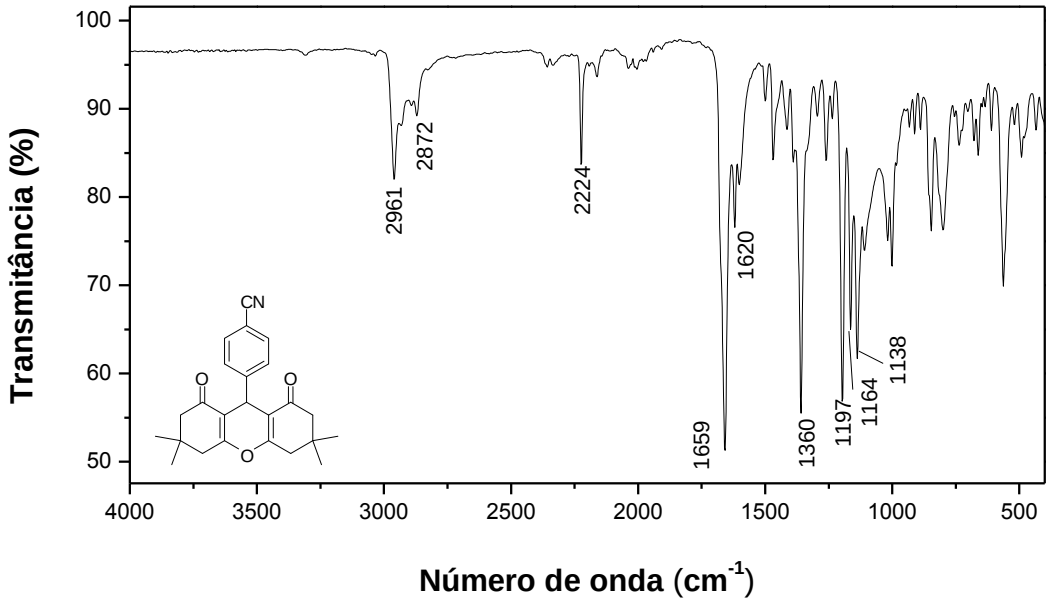

Figura 161. Espectro no infravermelho (ATR) do composto **42**.

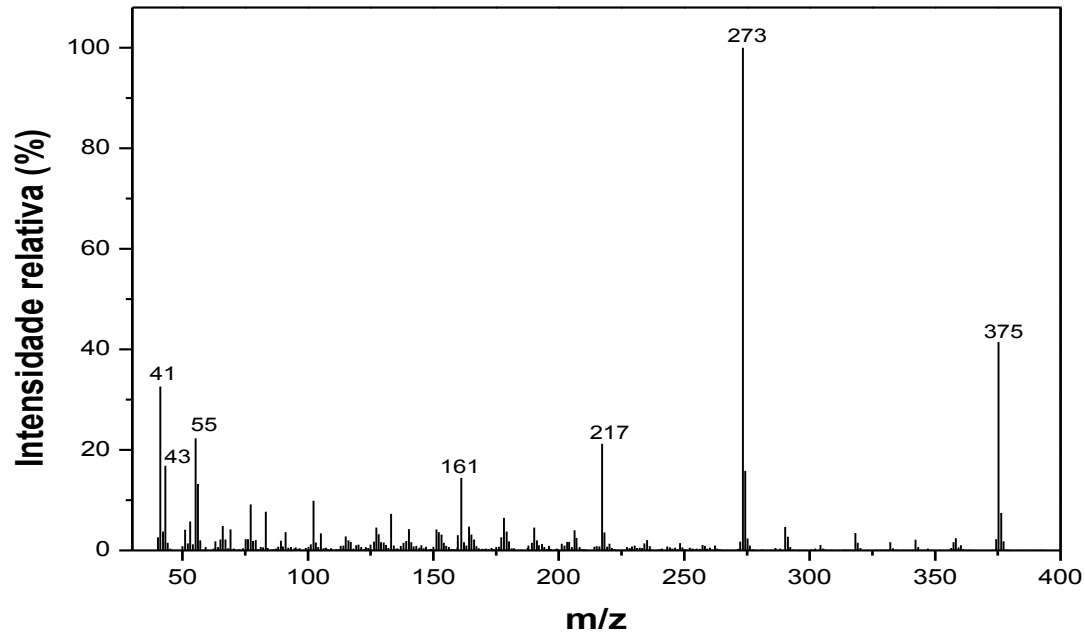

Figura 162. Espectro de massas do composto **42**.

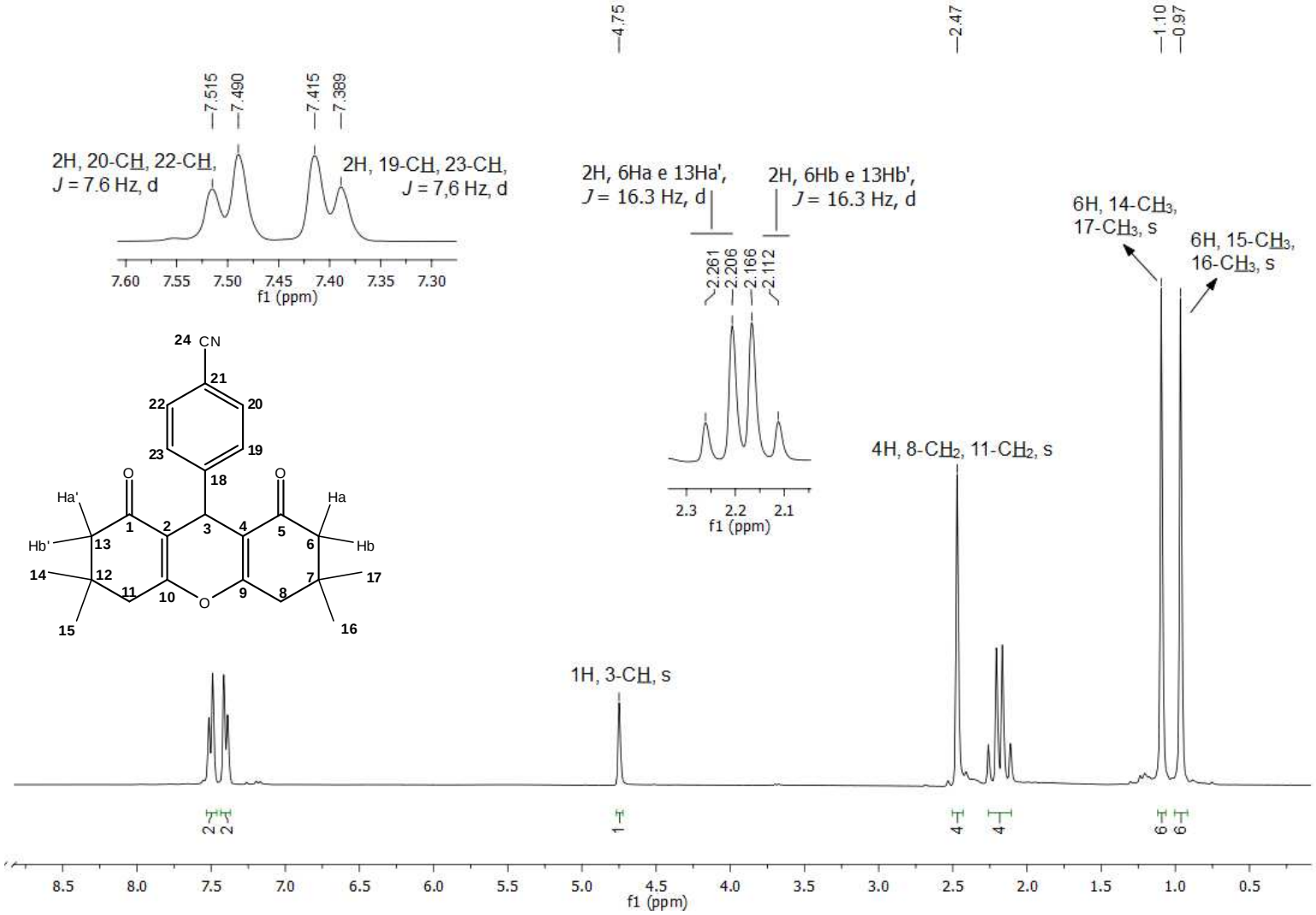

Figura 163. Espectro de RMN de ^{1}H (300 MHz, $CDCl_3$) do composto **42**.

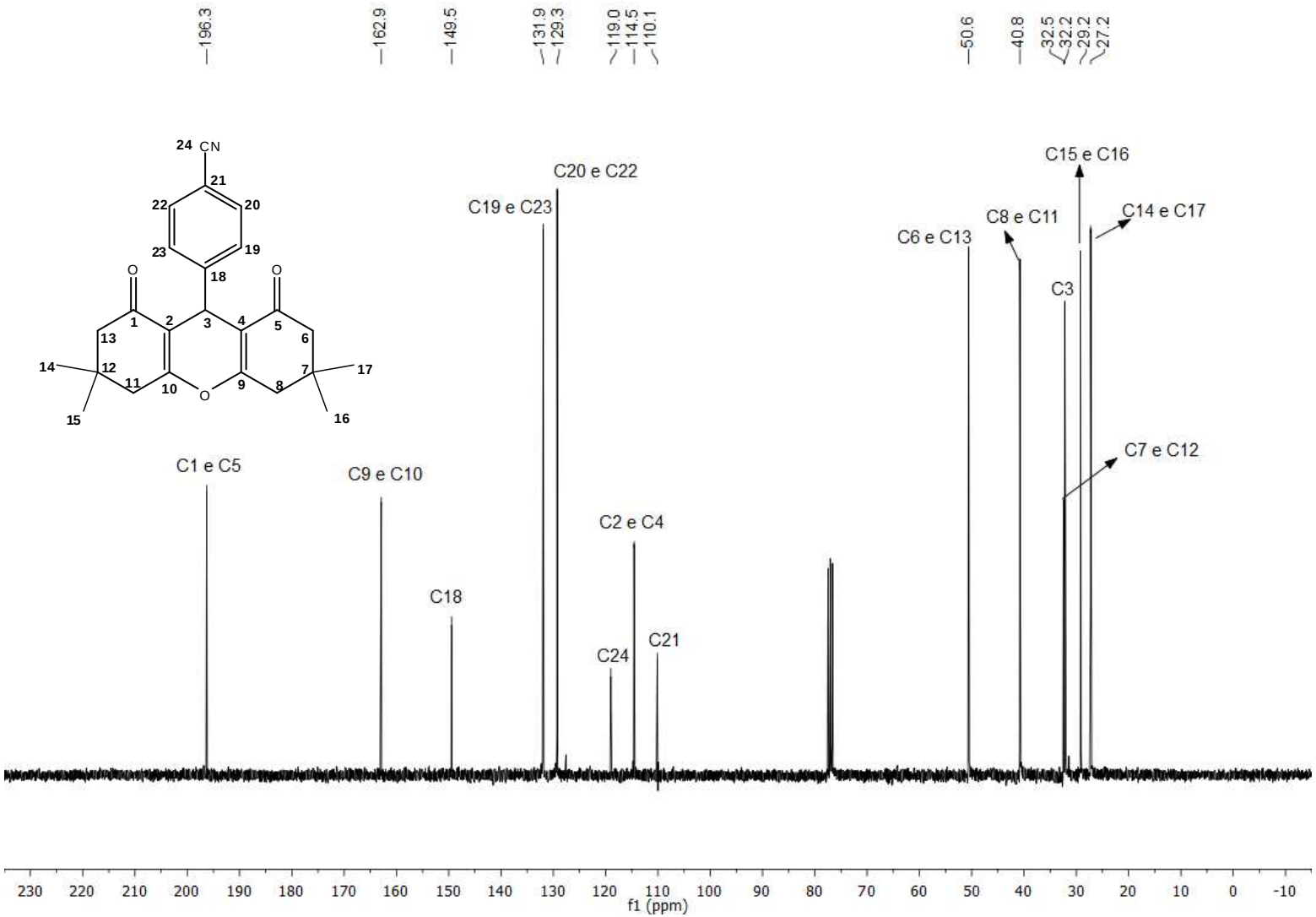

Figura 164. Espectro de RMN de ^{13}C (75 MHz, $CDCl_3$) do composto **42**.

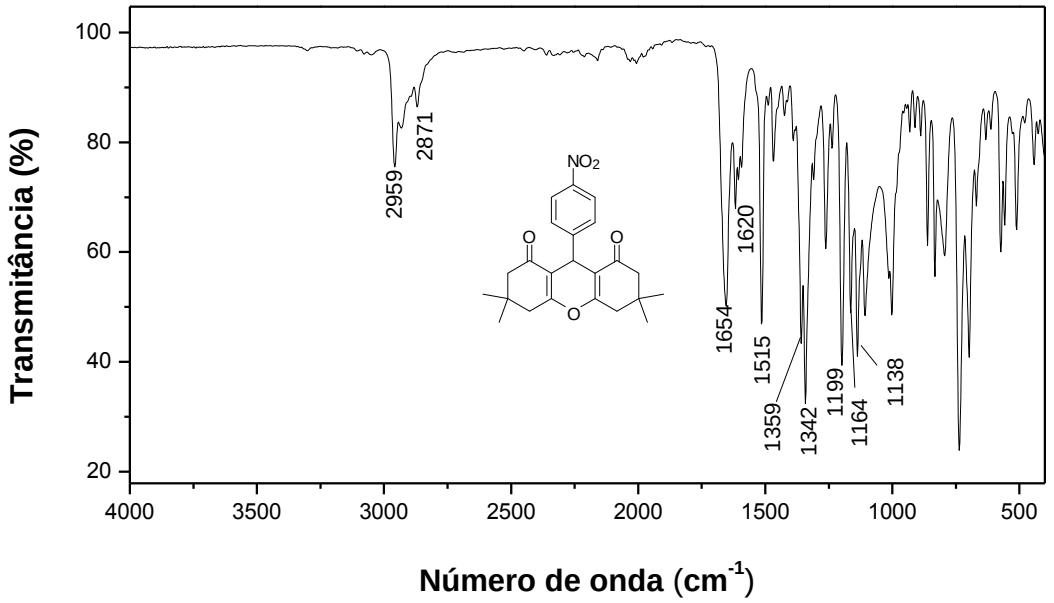

Figura 165. Espectro no infravermelho (ATR) do composto **43**.

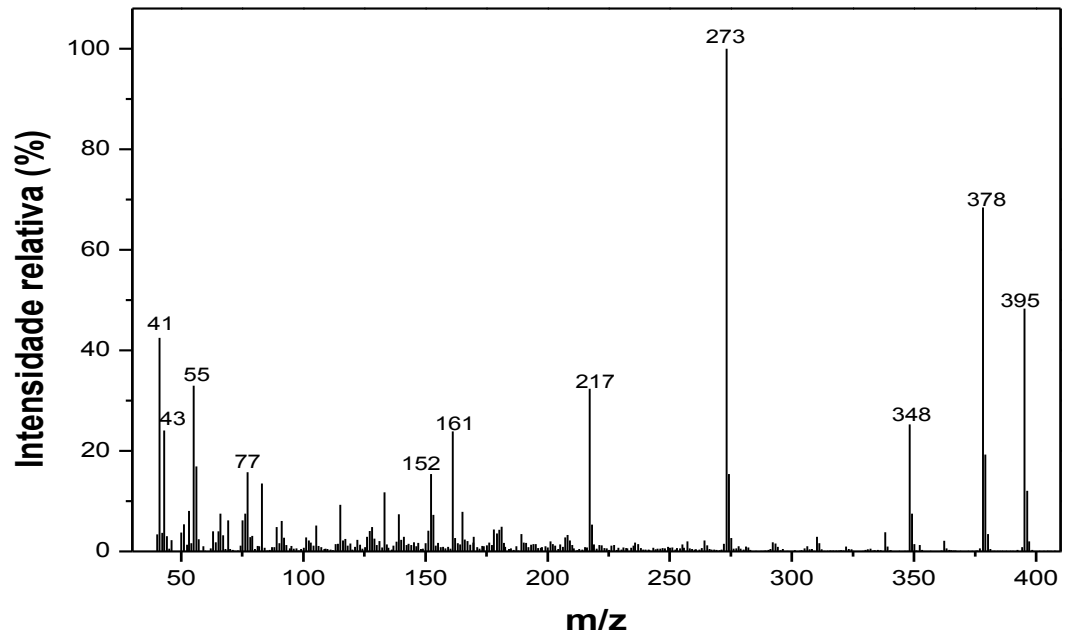

Figura 166. Espectro de massas do composto **43**.

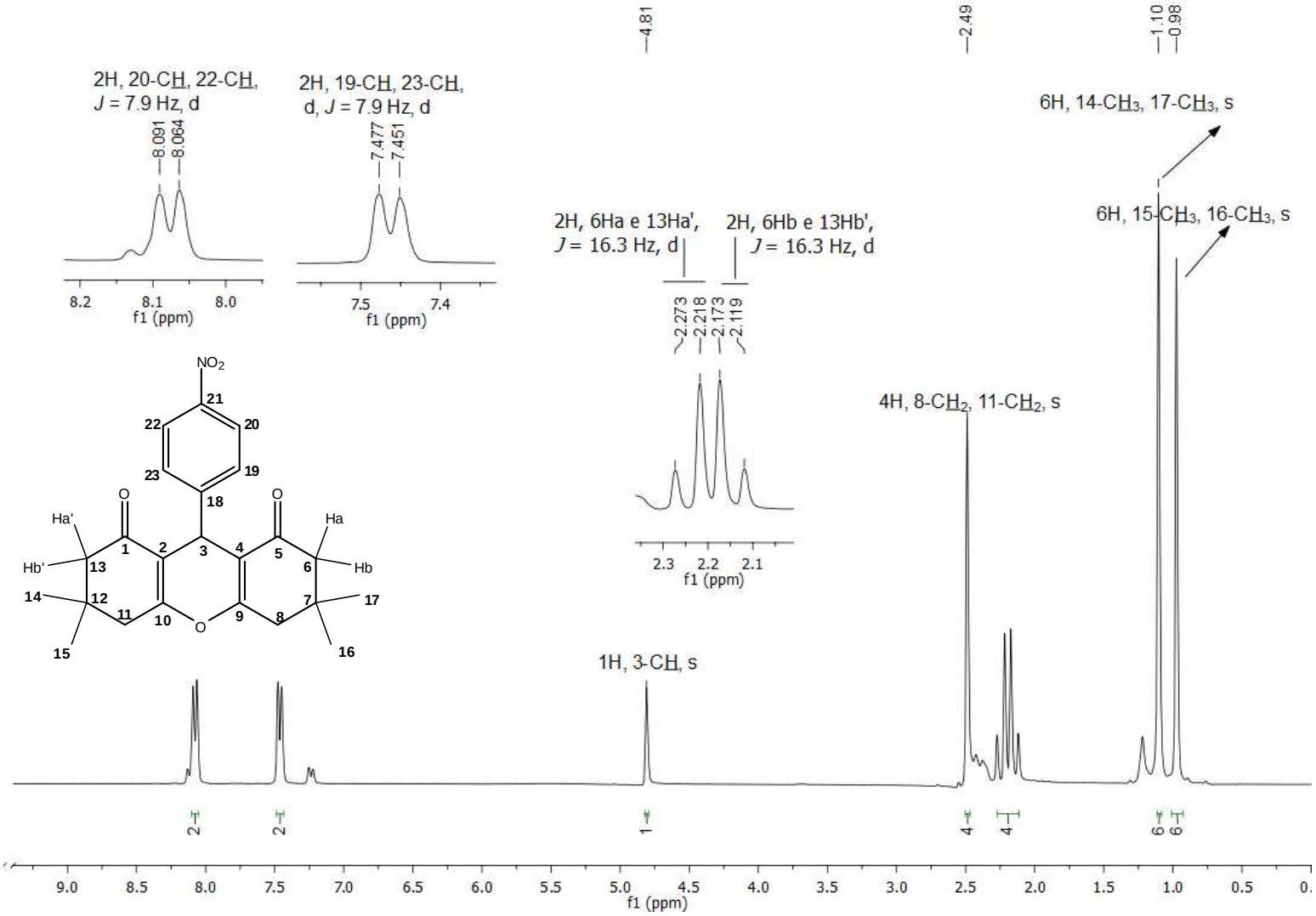

Figura 167. Espectro de RMN de ^{1}H (300 MHz, $CDCl_3$) do composto **43**.

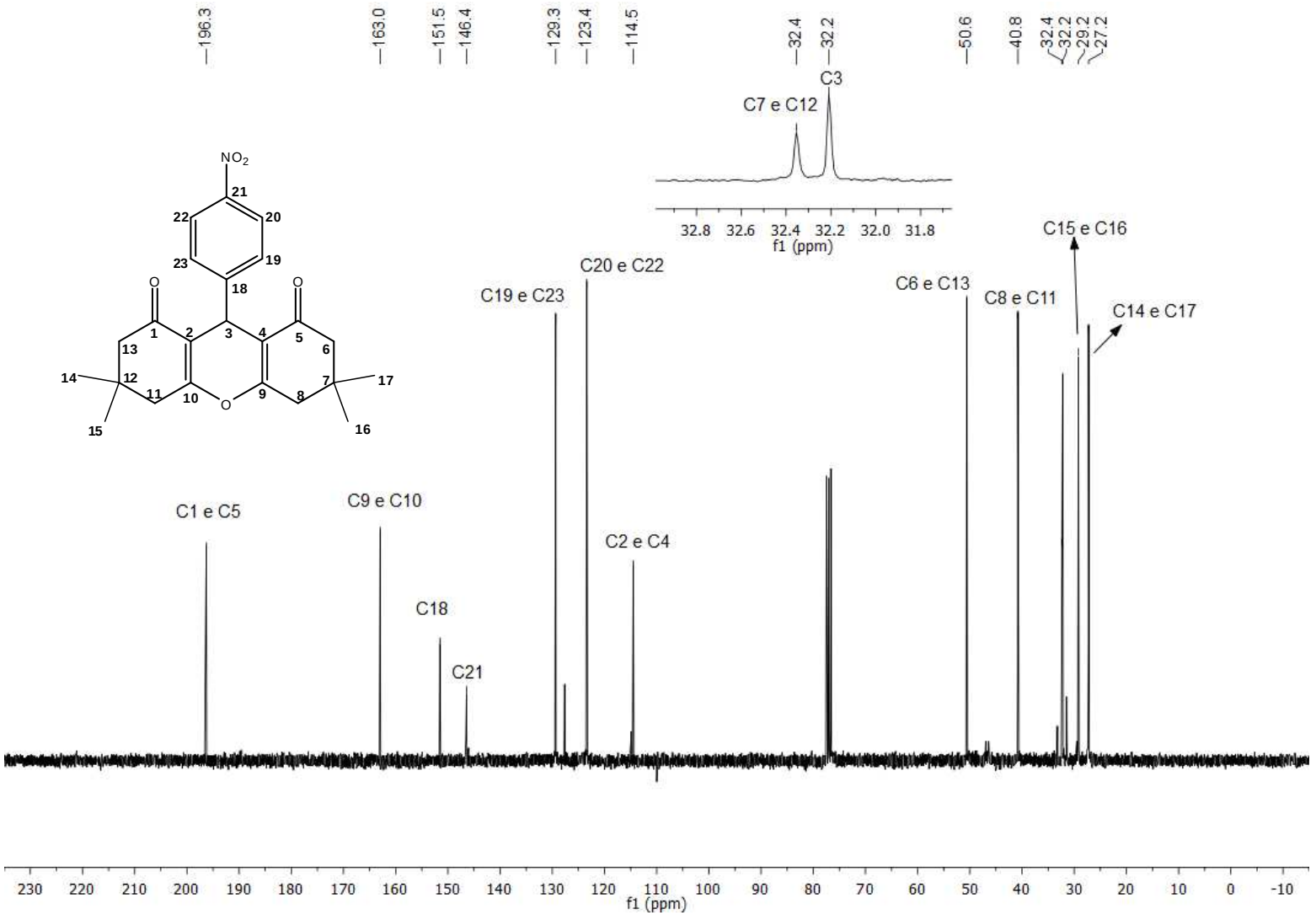

Figura 168. Espectro de RMN de ^{13}C (75 MHz, $CDCl_3$) do composto **43**.

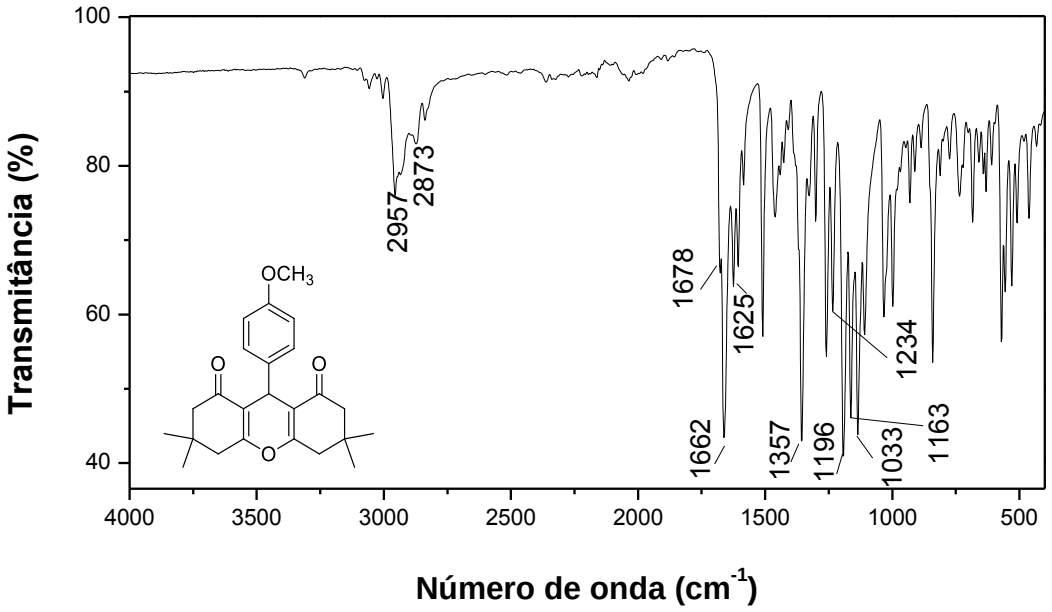

Figura 169. Espectro no Infravermelho (ATR) do composto **44**.

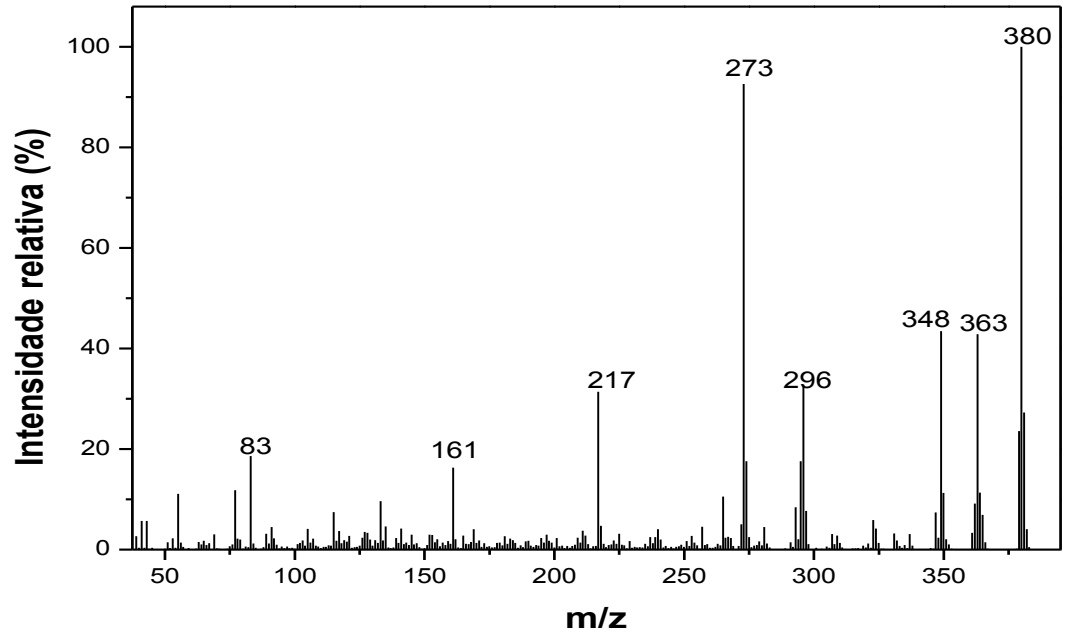

Figura 170. Espectro de massas do composto **44**.

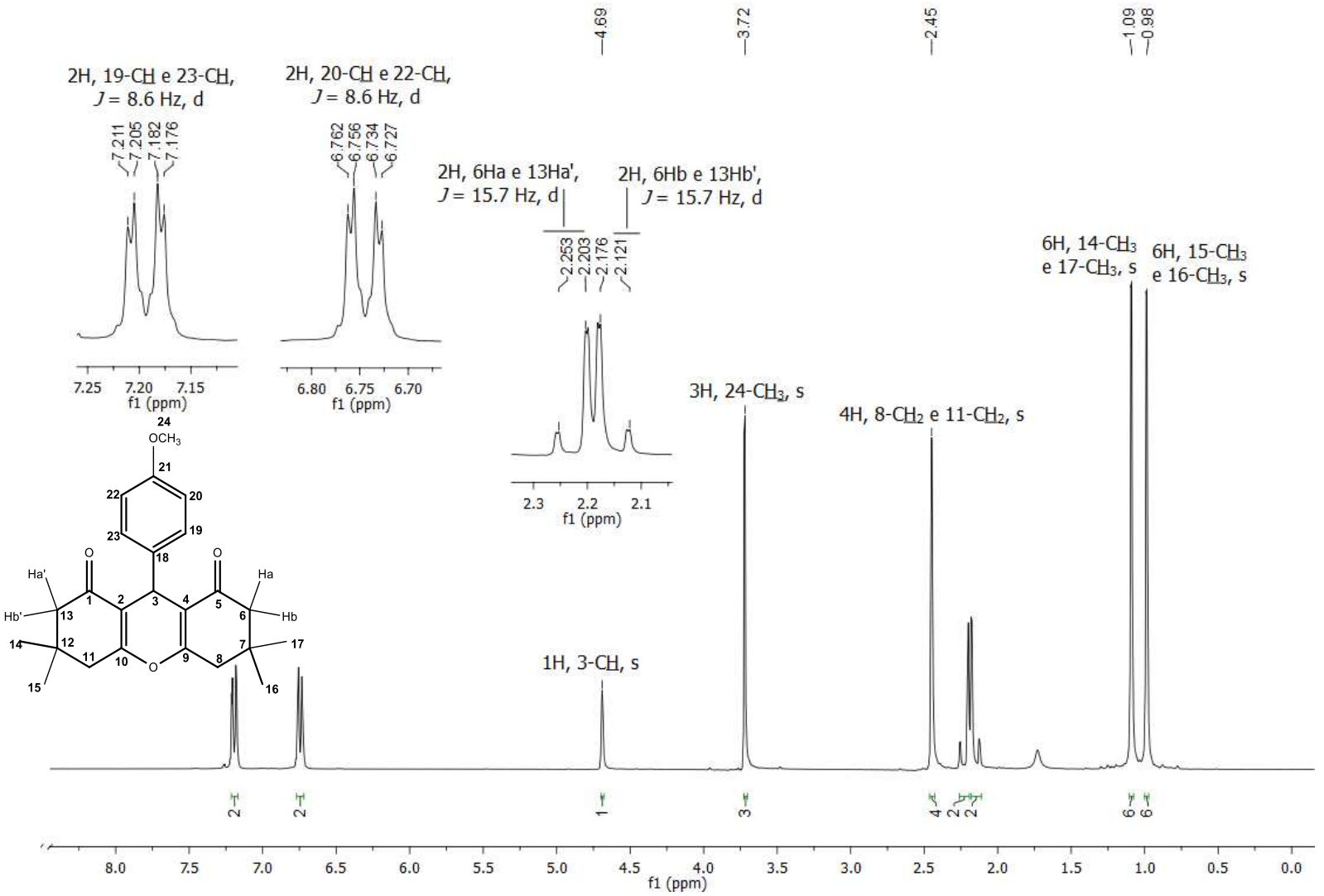

Figura 171. Espectro de RMN de ^{1}H (300 MHz, $CDCl_3$) do composto **44**.

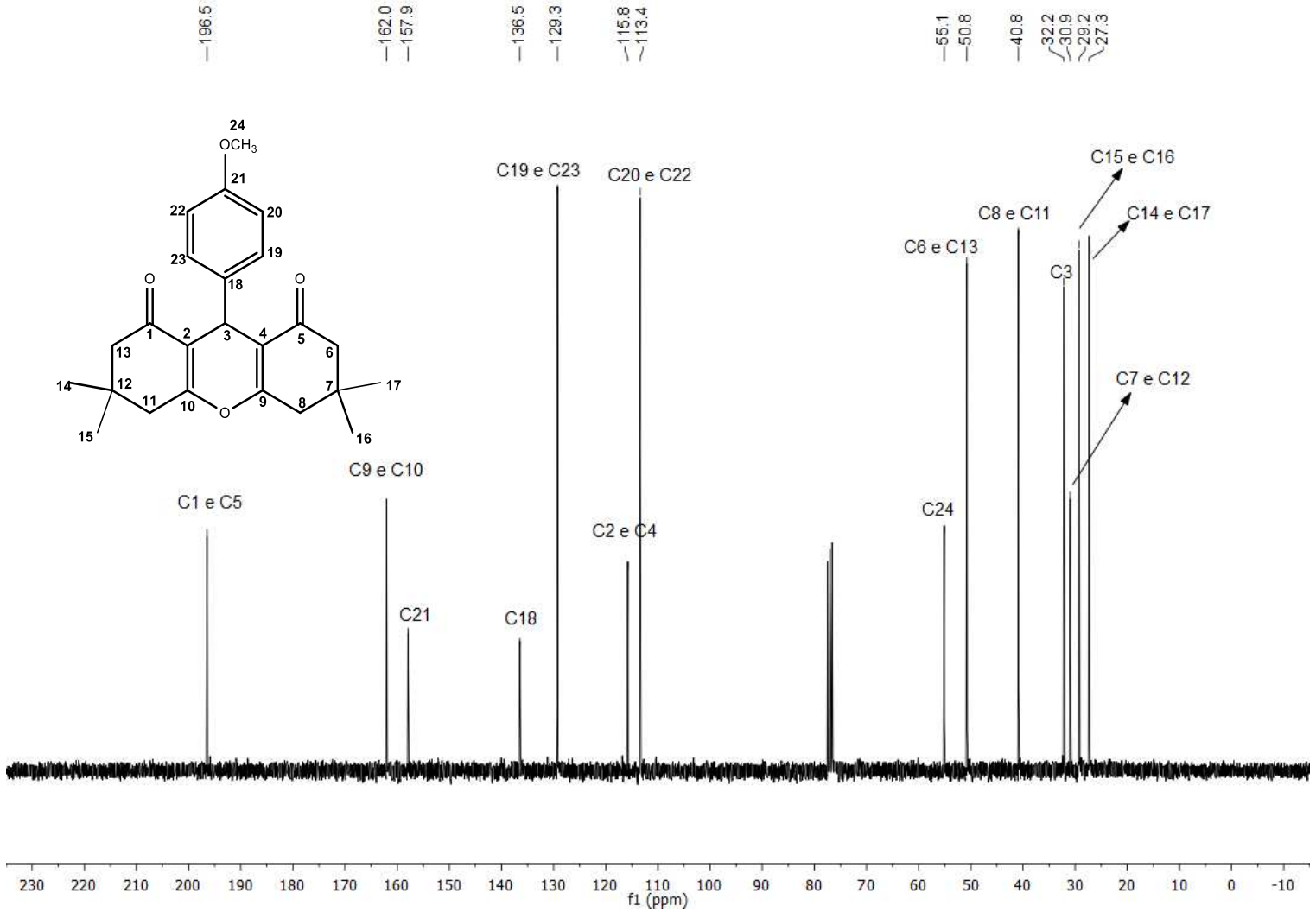

Figura 172. Espectro de RMN de ^{13}C (75 MHz, $CDCl_3$) do composto **44**.

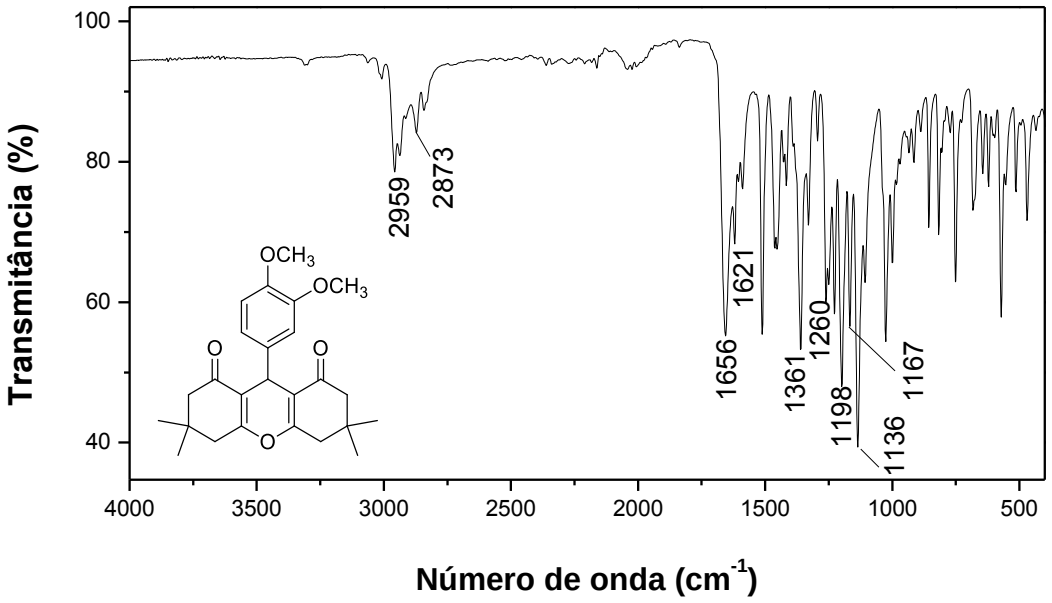

Figura 173. Espectro no Infravermelho (ATR) do composto **45**.

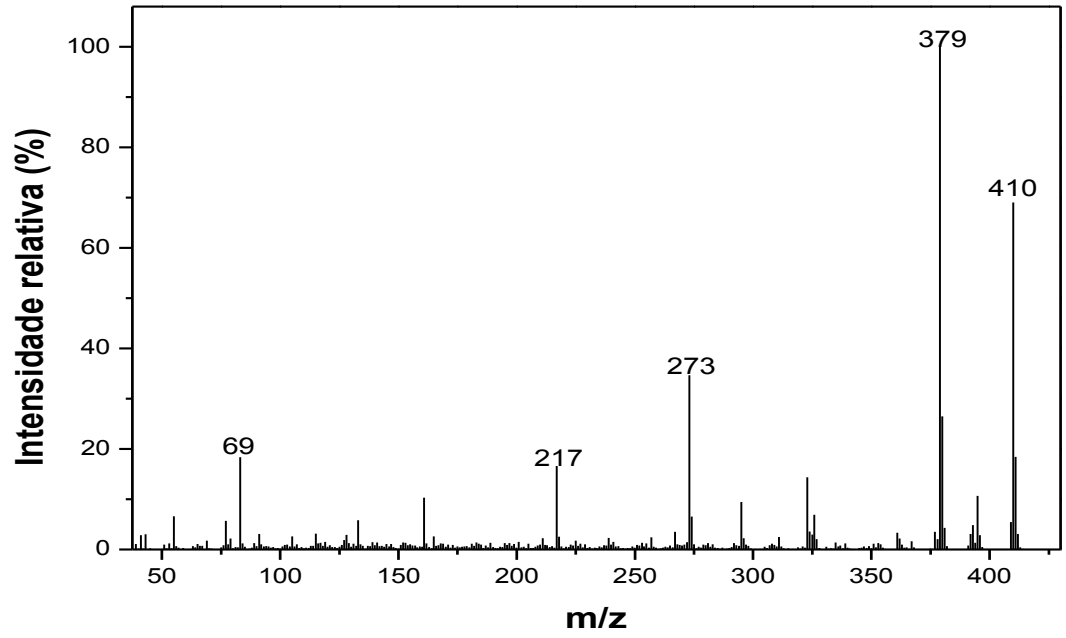

Figura 174. Espectro de massas do composto **45**.

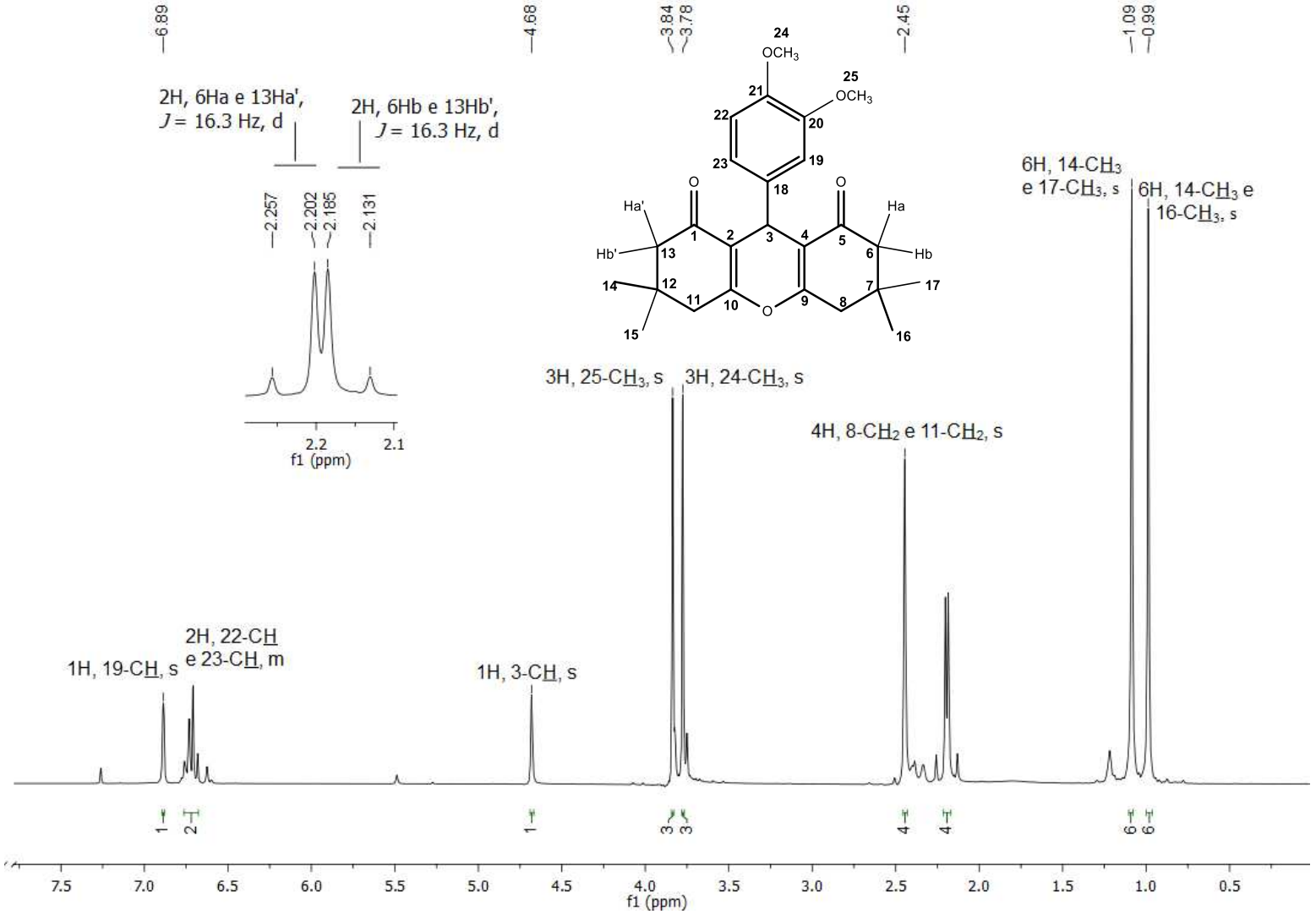

Figura 175. Espectro de RMN de ^{1}H (300 MHz, $CDCl_3$) do composto **45**.

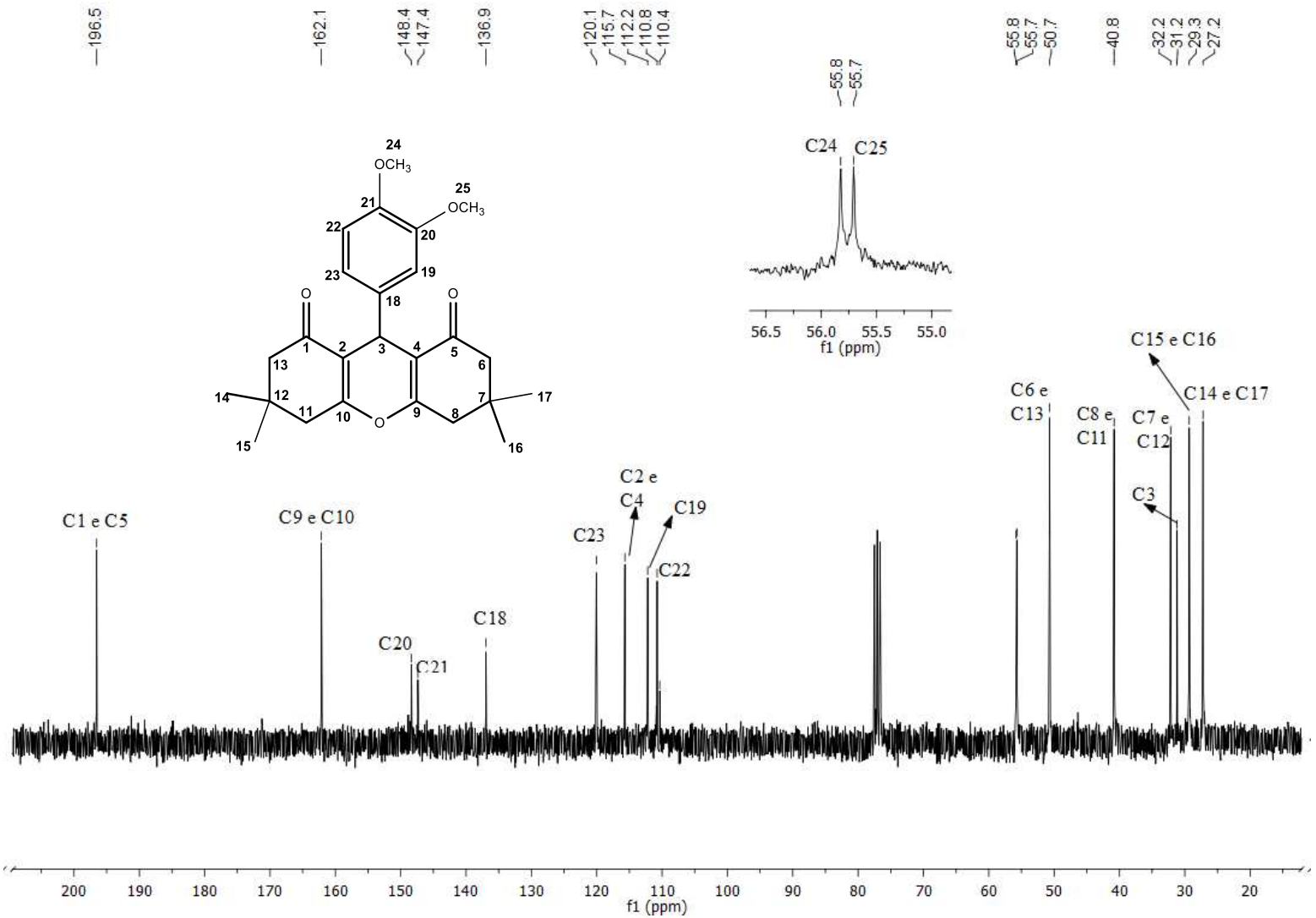

Figura 176. Espectro de RMN de ^{13}C (75 MHz, $CDCl_3$) do composto **45**.

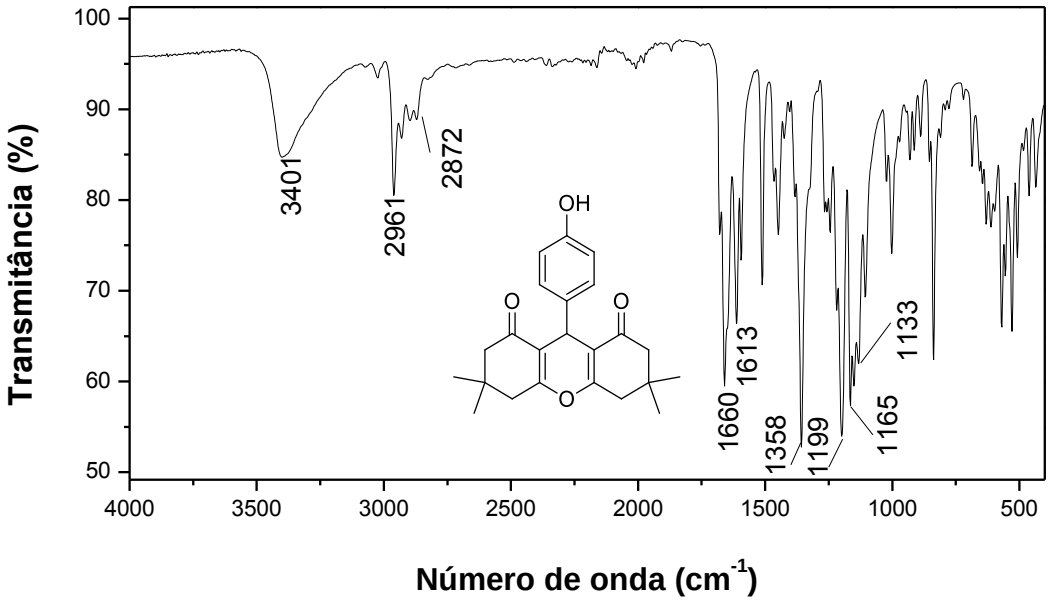

Figura 177. Espectro no Infravermelho (ATR) do composto **46**.

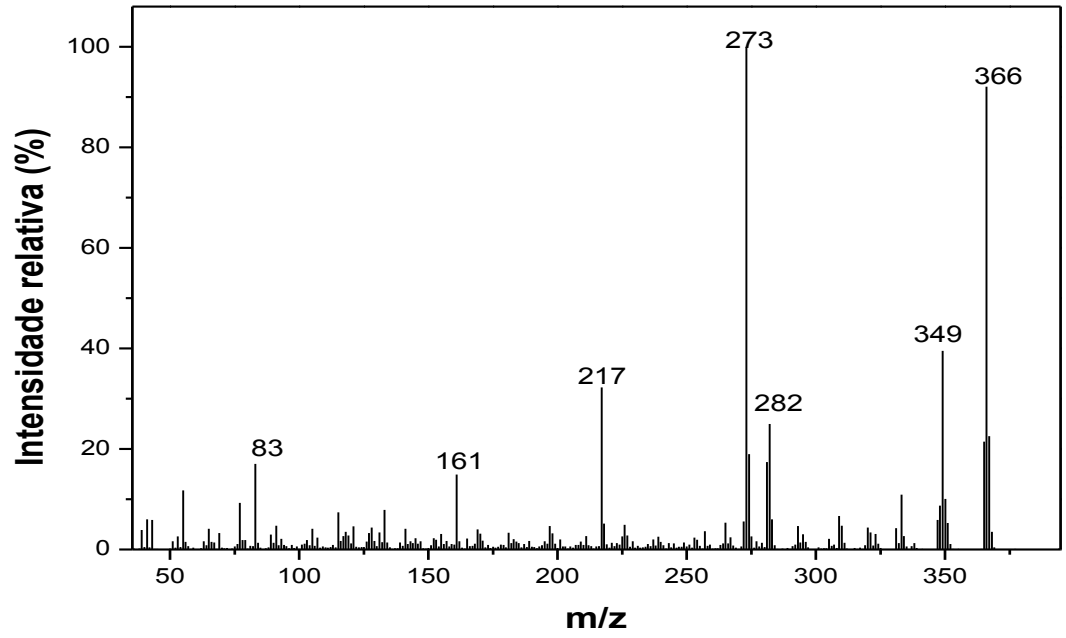

Figura 178. Espectro de massas do composto **46**.

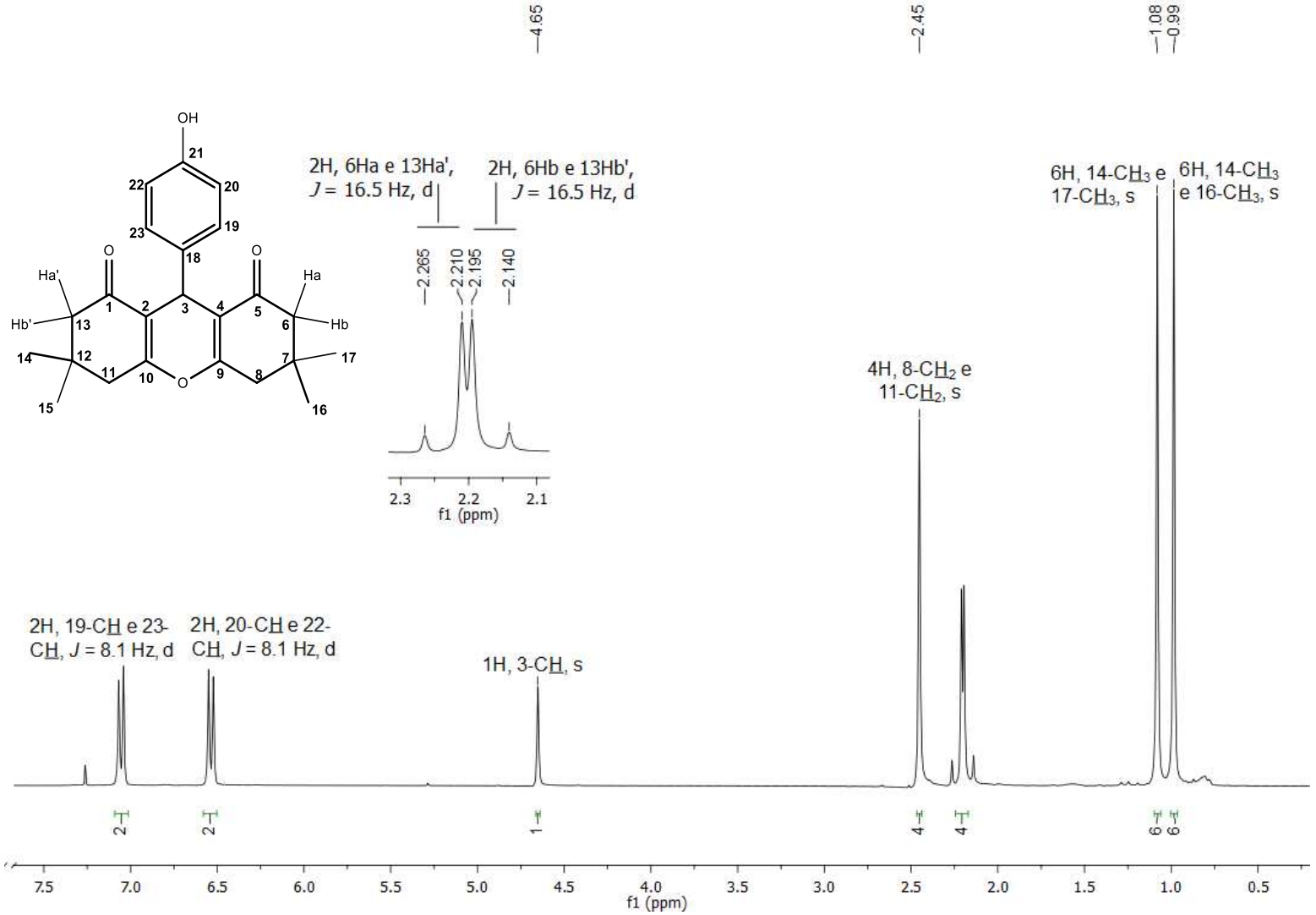

Figura 179. Espectro de RMN de ^{1}H (300 MHz, $CDCl_3$) do composto **46**.

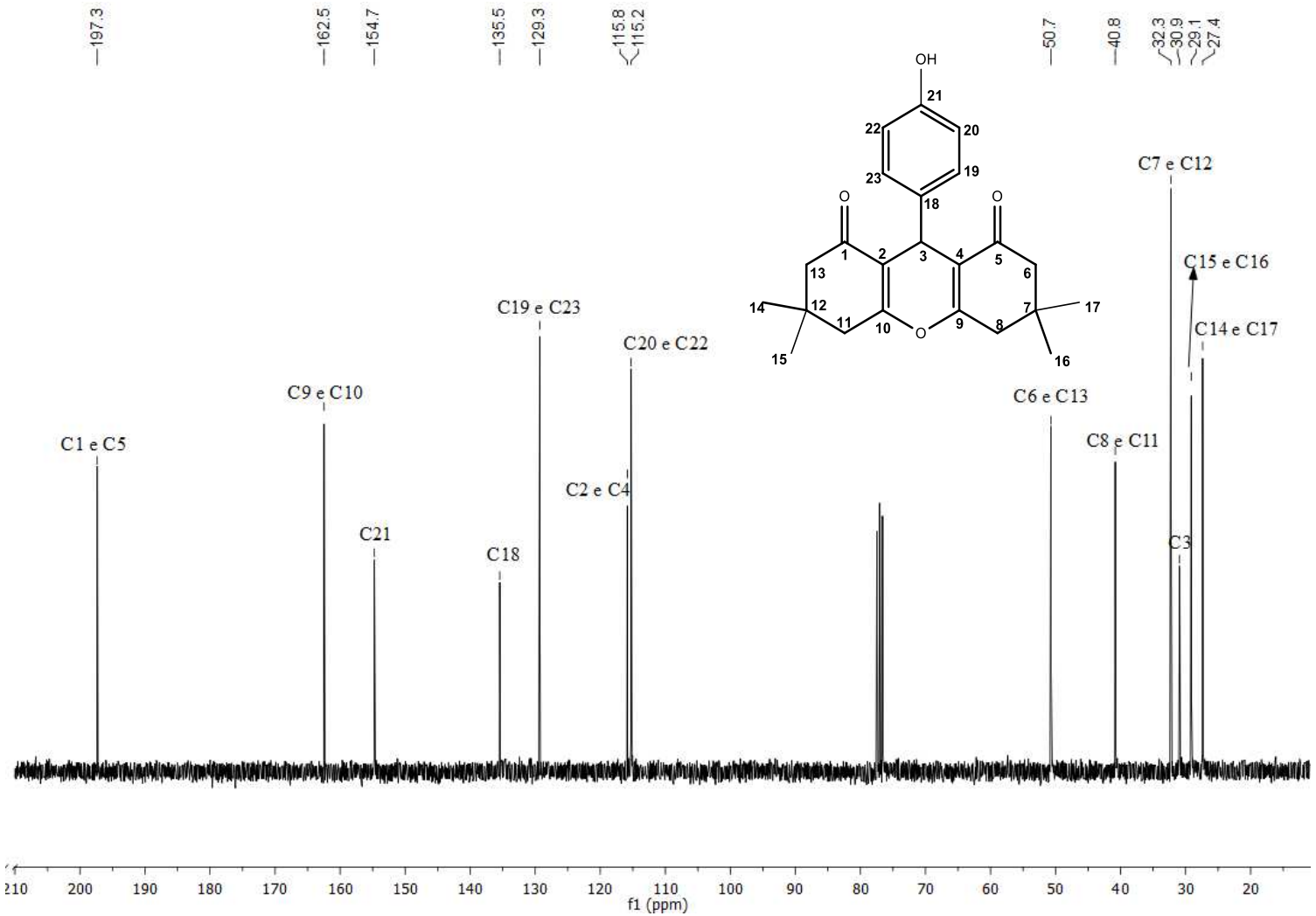

Figura 180. Espectro de RMN de ^{13}C (75 MHz, $CDCl_3$) do composto **46**.

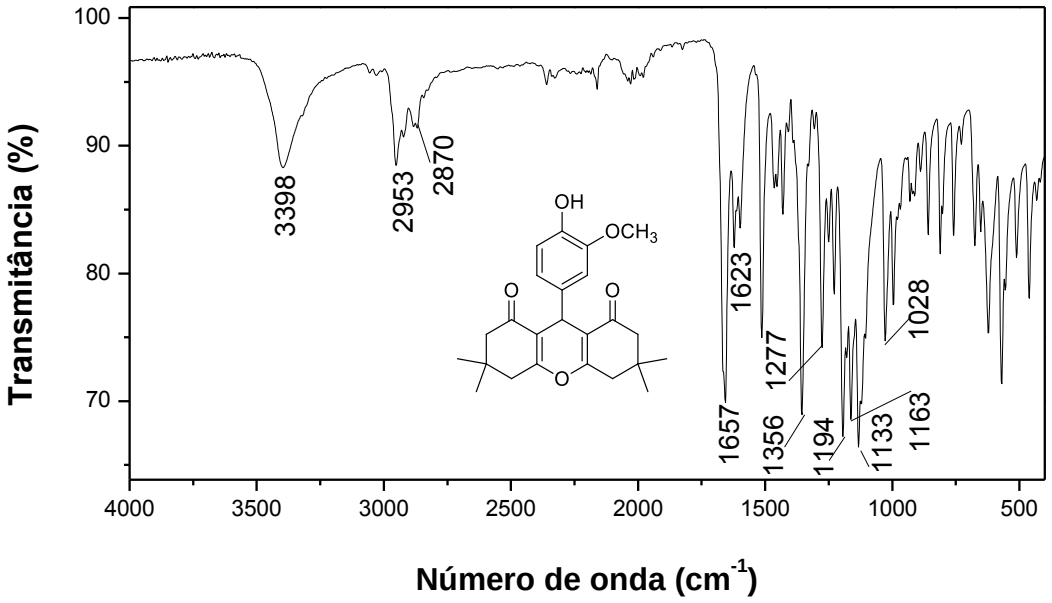

Figura 181. Espectro no Infravermelho (ATR) do composto **47**.

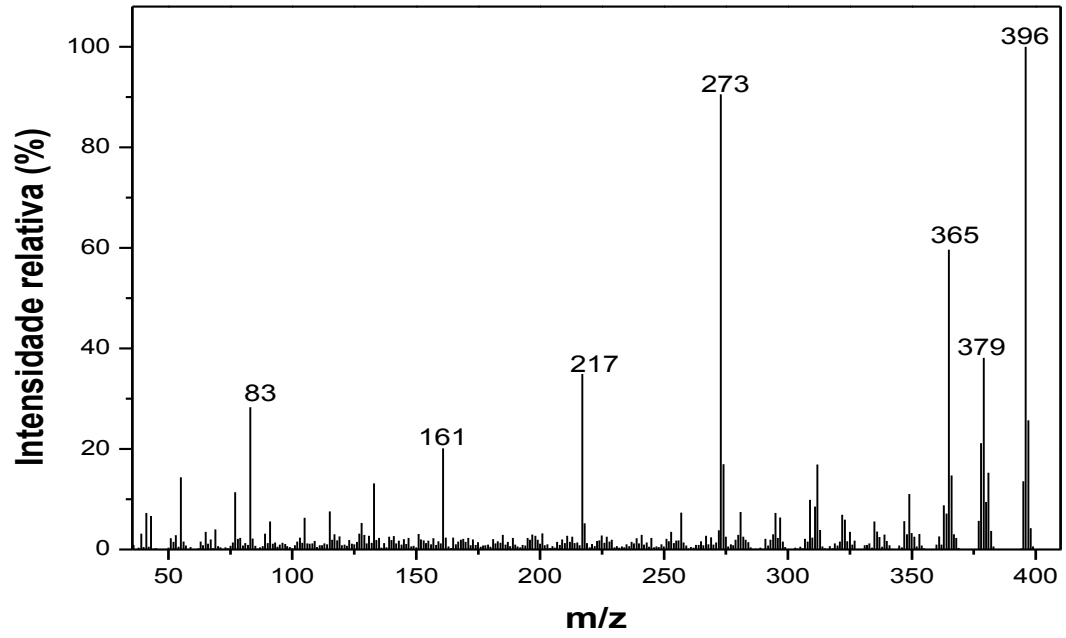

Figura 182. Espectro de massas do composto **47**.

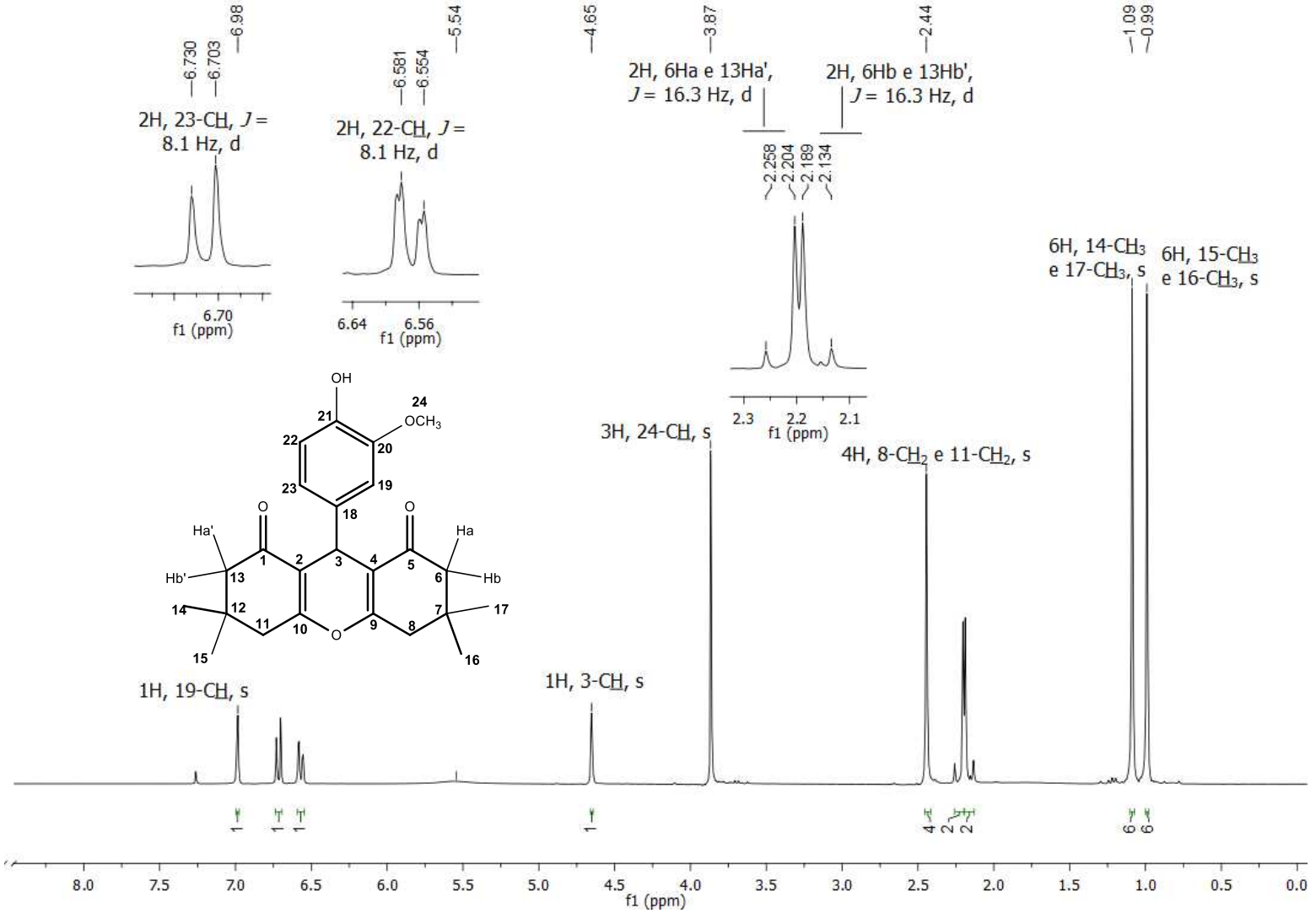

Figura 183. Espectro de RMN de ^{1}H (300 MHz, $CDCl_3$) do composto **47**.

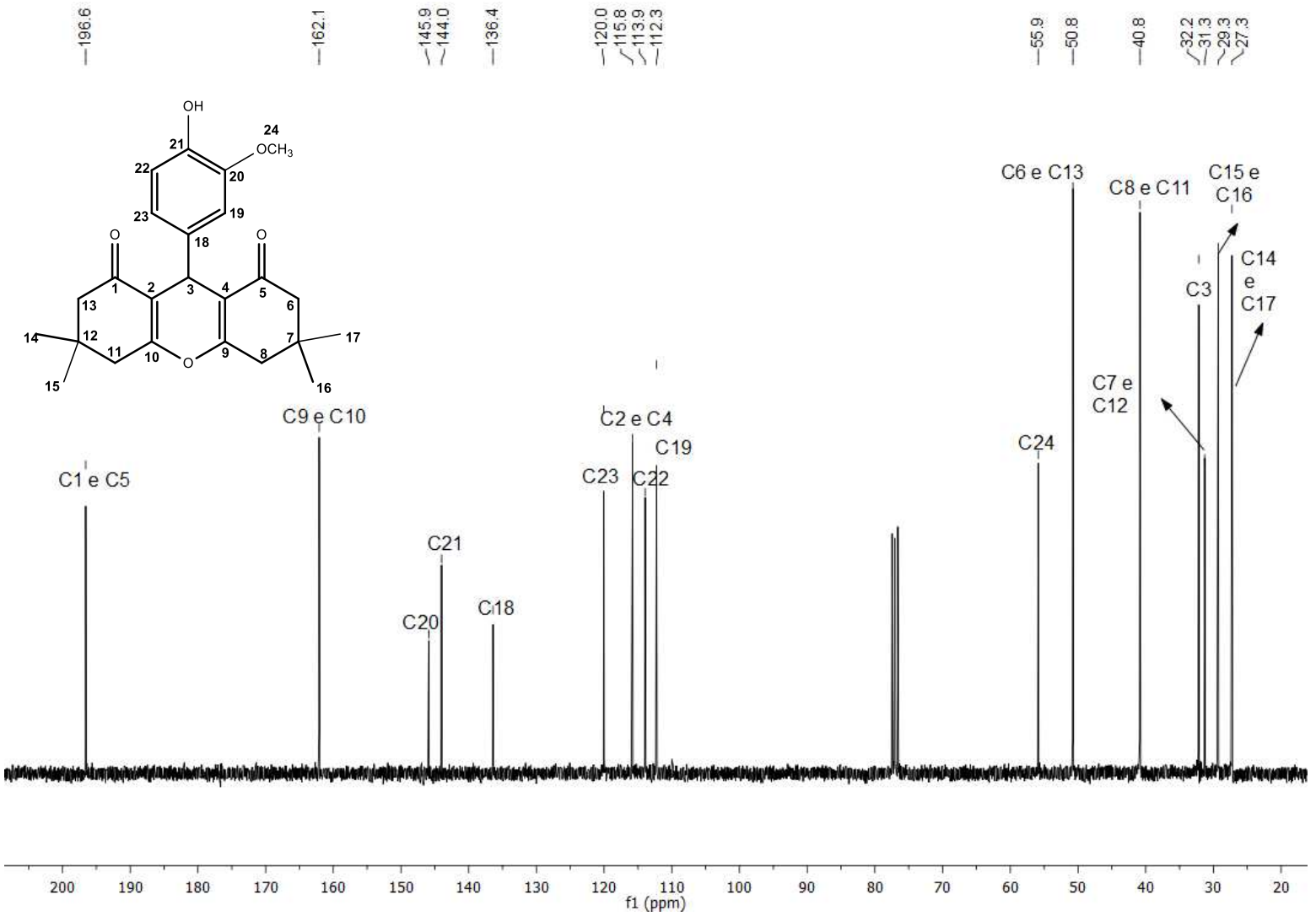

Figura 184. Espectro de RMN de ^{13}C (75 MHz, $CDCl_3$) do composto **47**.

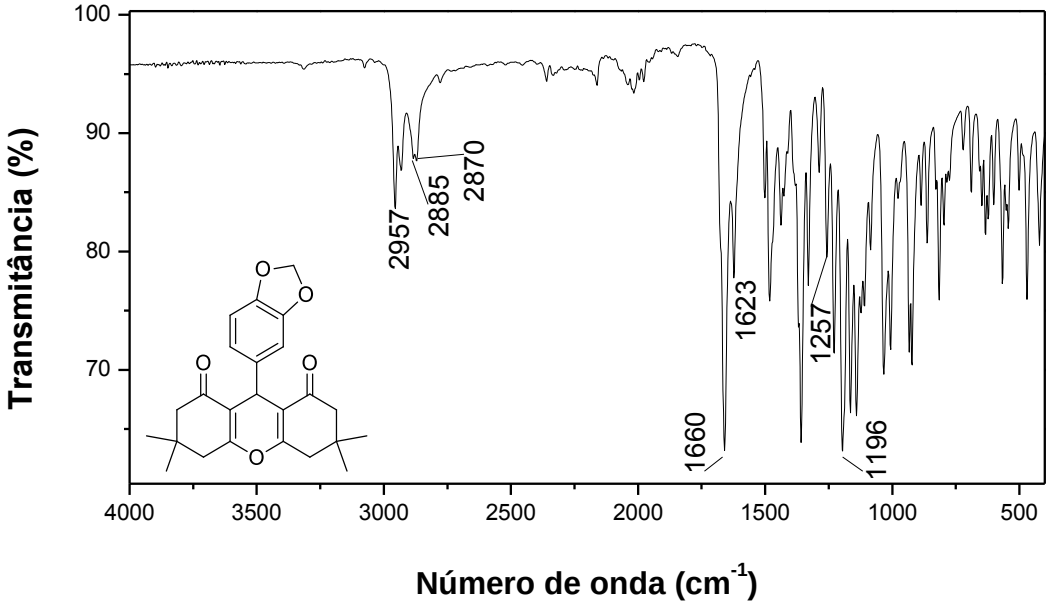

Figura 185. Espectro no Infravermelho (ATR) do composto **48**.

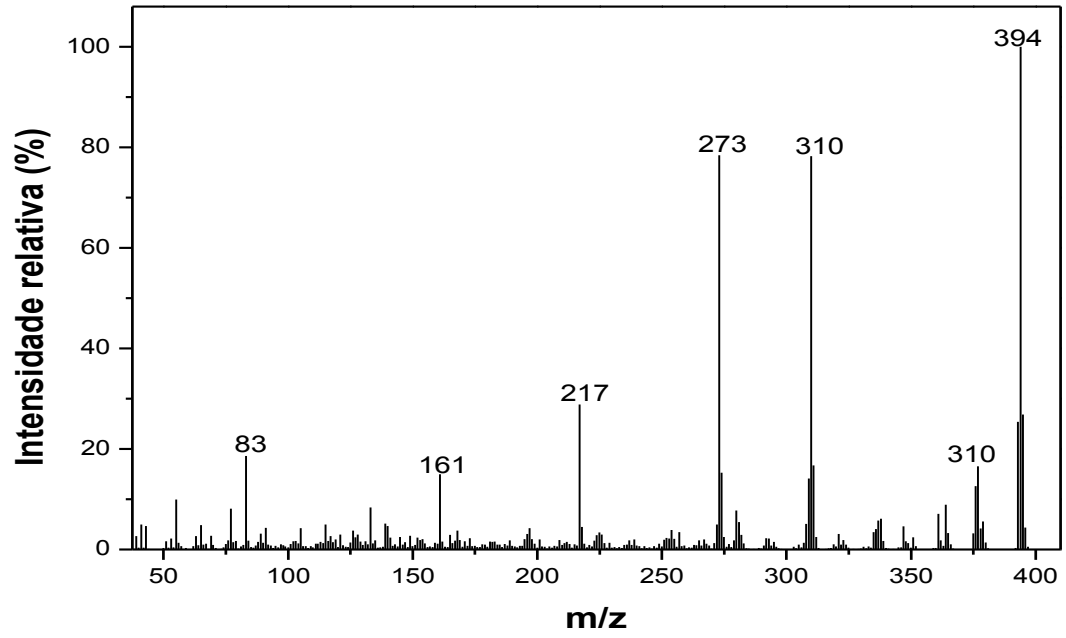

Figura 186. Espectro de massas do composto **48**.

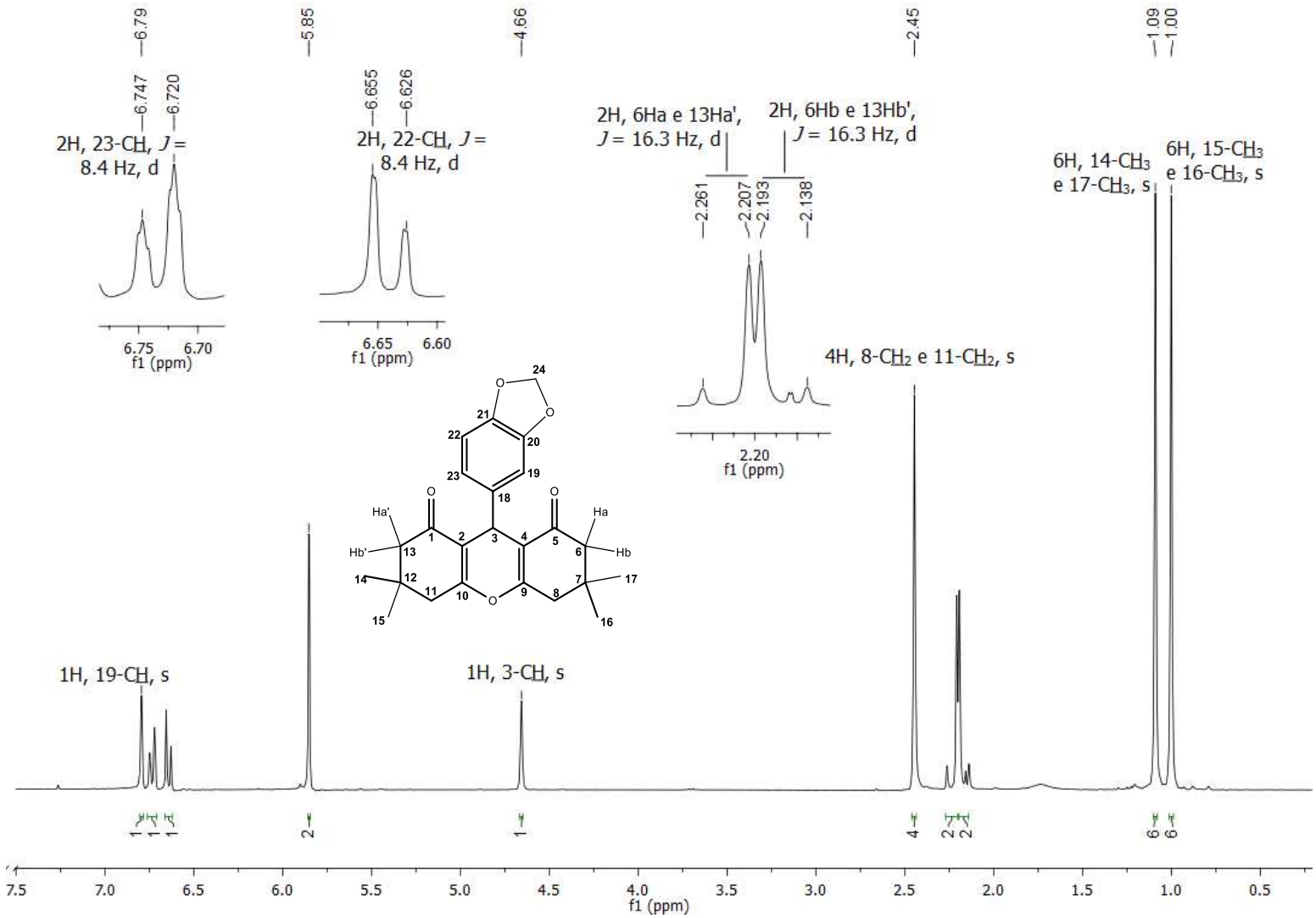

Figura 187. Espectro de RMN de ^{1}H (300 MHz, $CDCl_3$) do composto **48**.

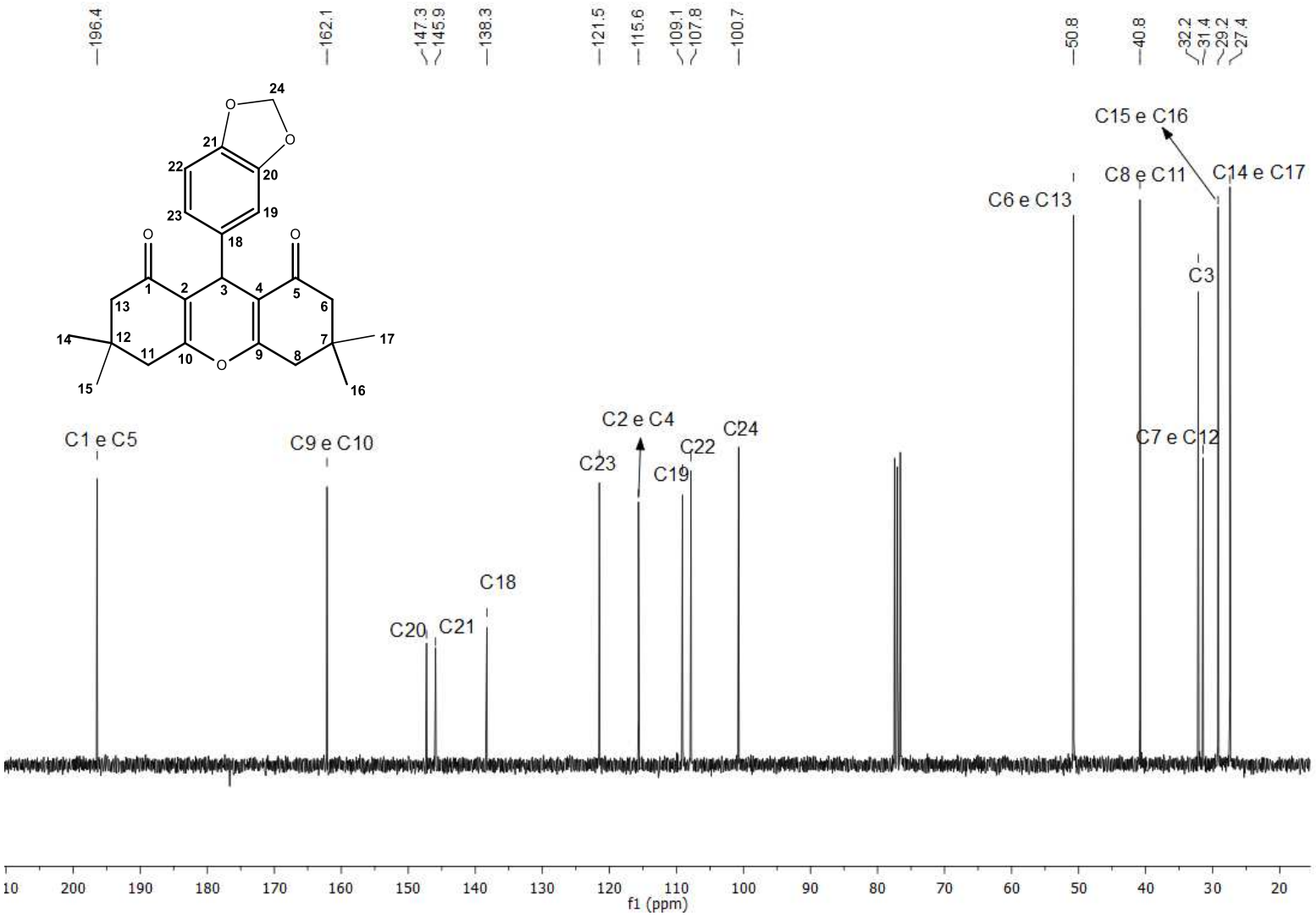

Figura 188. Espectro de RMN de ^{13}C (75 MHz, $CDCl_3$) do composto **48**.

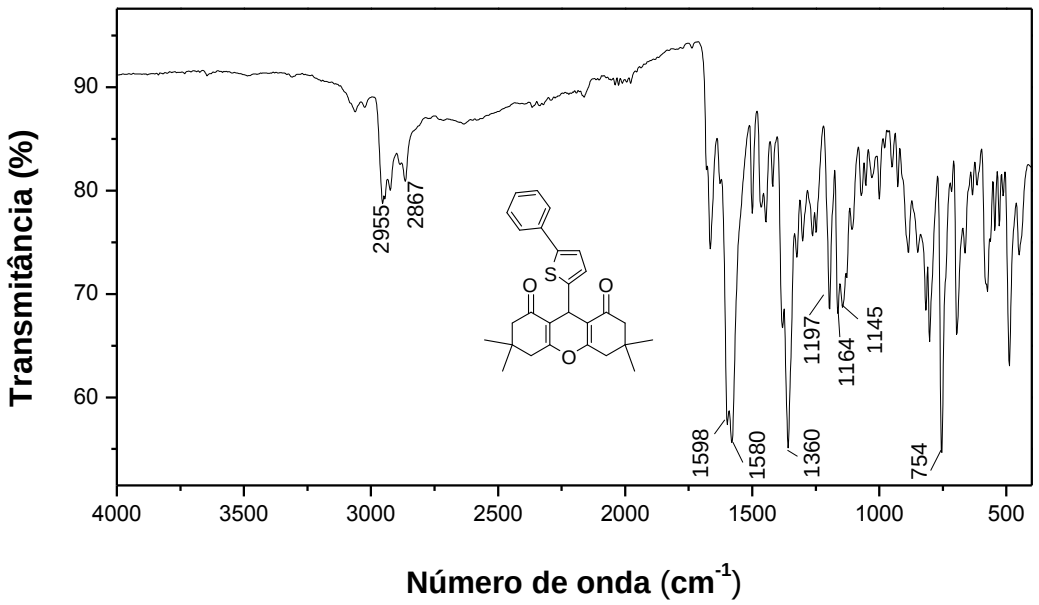

Figura 189. Espectro no infravermelho (ATR) do composto **49**.

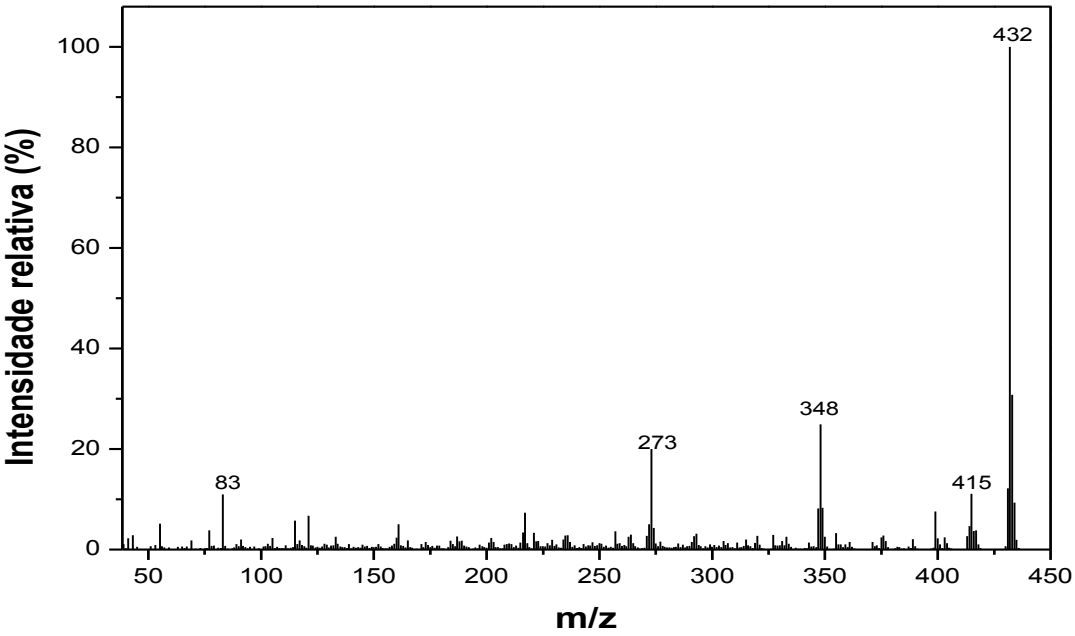

Figura 190. Espectro de massas do composto **49**.

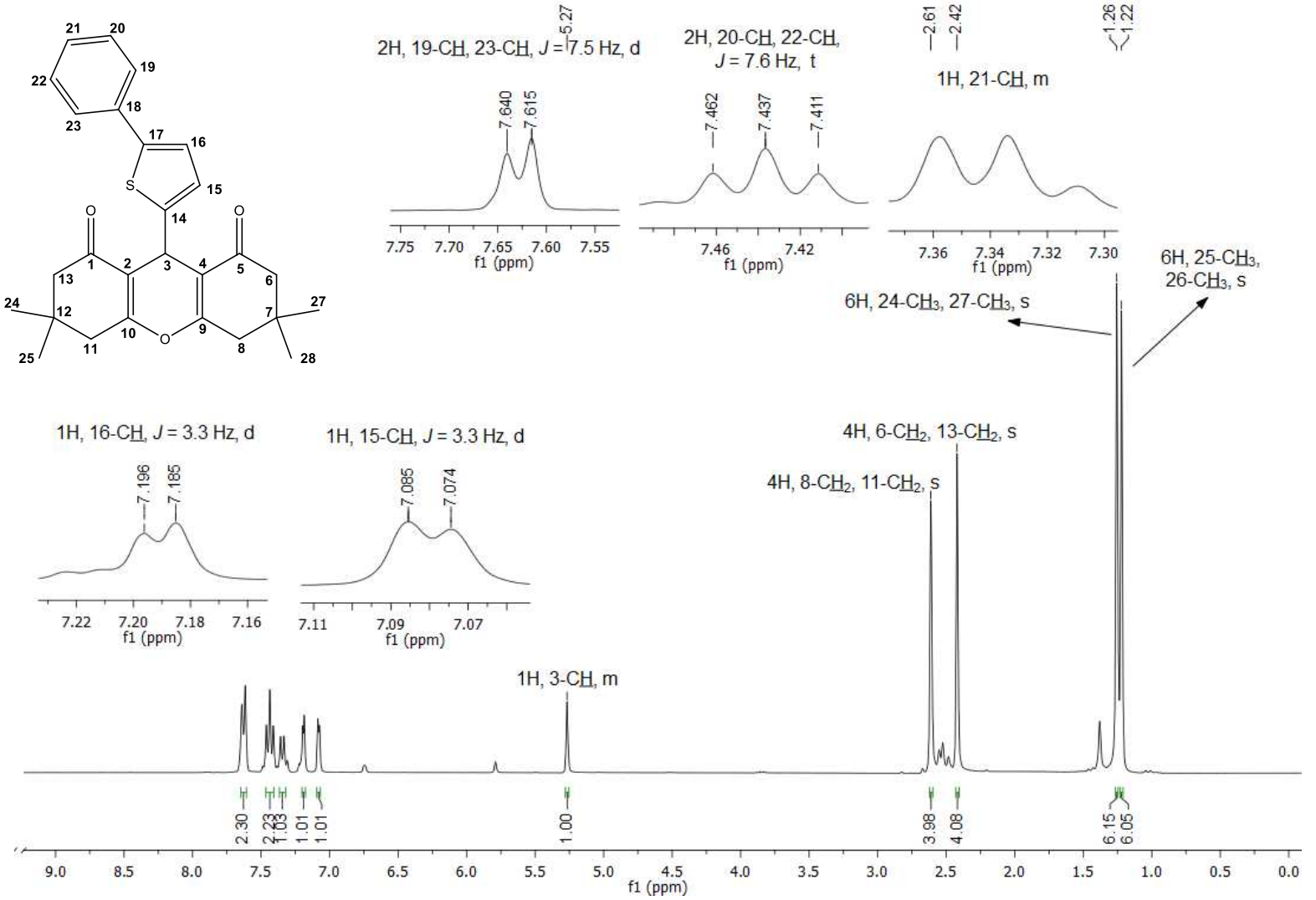

Figura 191. Espectro de RMN de ^{1}H (300 MHz, $CDCl_3$) do composto **49**.

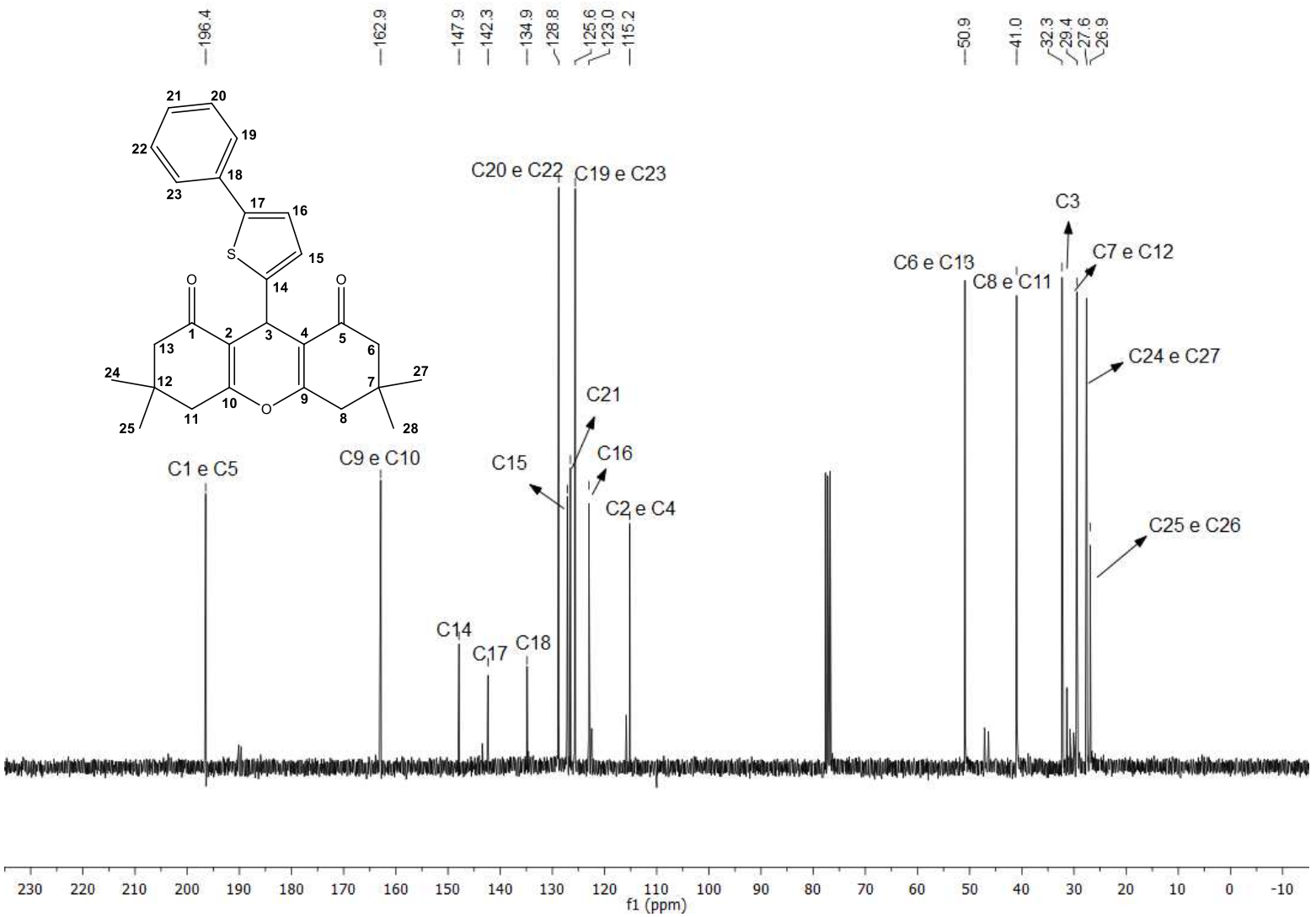

Figura 192. Espectro de RMN de ^{13}C (75 MHz, $CDCl_3$) do composto **49**.

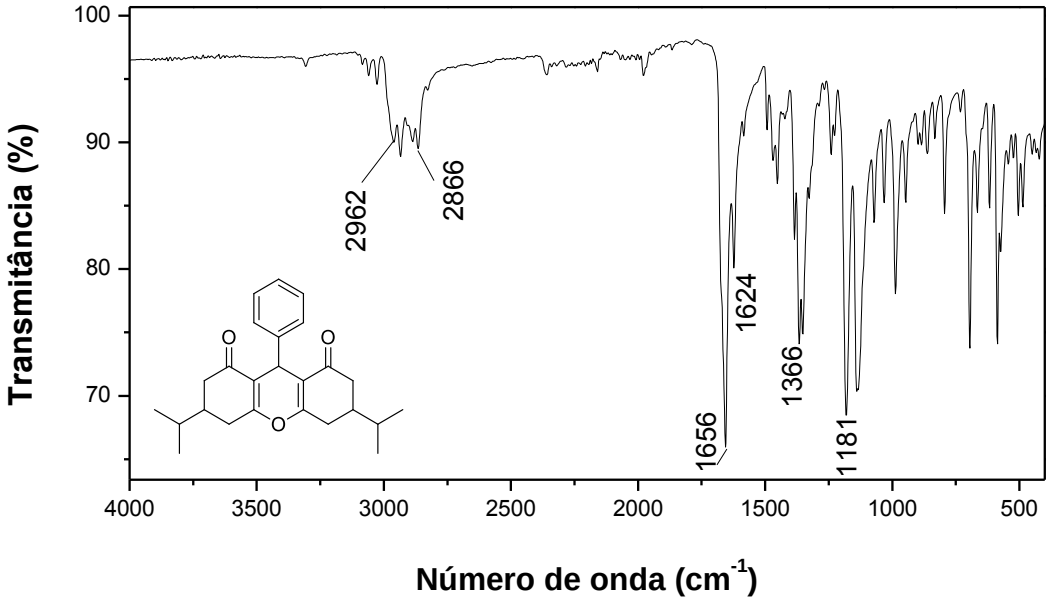

Figura 193. Espectro no Infravermelho (ATR) do composto **50**.

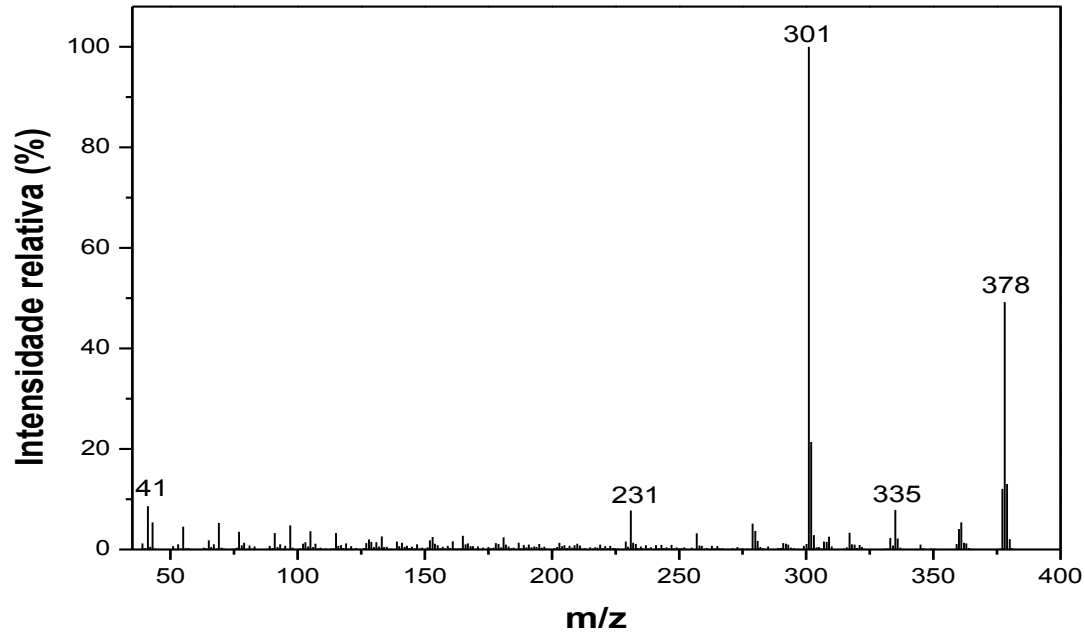

Figura 194. Espectro de massas do composto **50**.

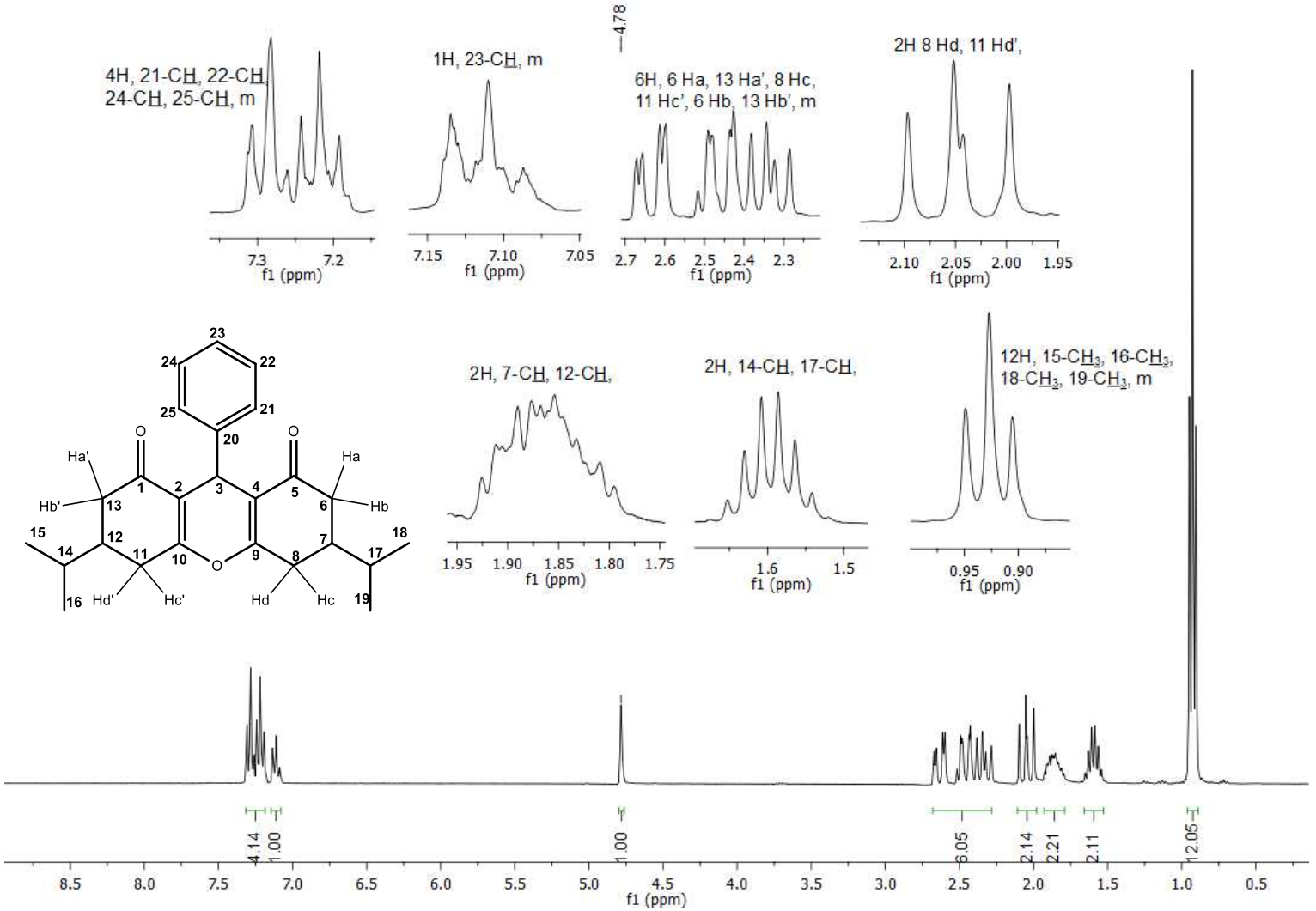

Figura 195. Espectro de RMN de ^{1}H (300 MHz, $CDCl_3$) do composto **50**.

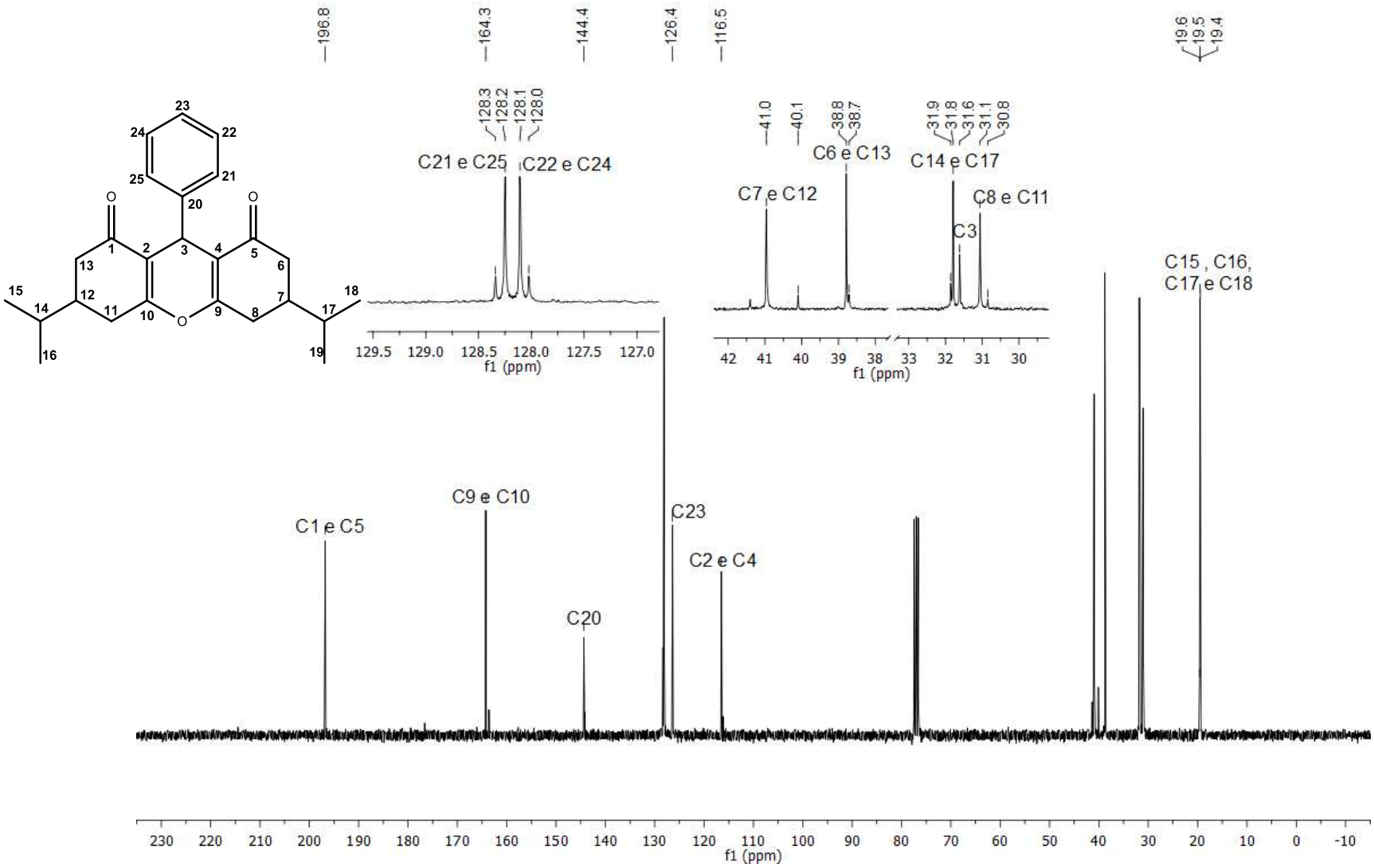

Figura 196. Espectro de RMN de ^{13}C (75 MHz, $CDCl_3$) do composto **50**.

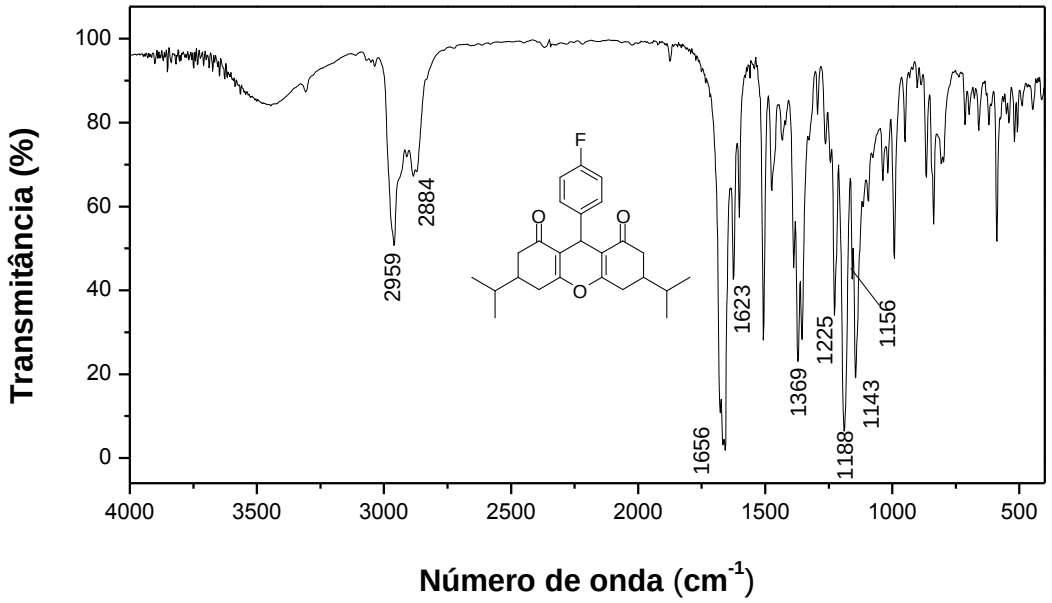

Figura 197. Espectro no infravermelho (KBr) do composto **51**.

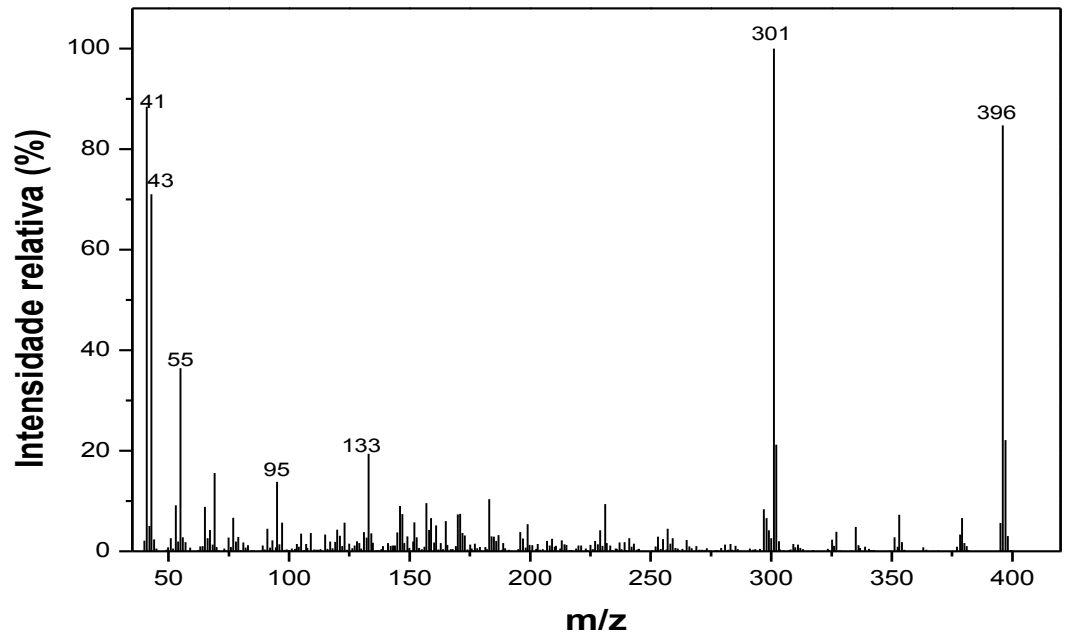

Figura 198. Espectro de massas do composto **51**.

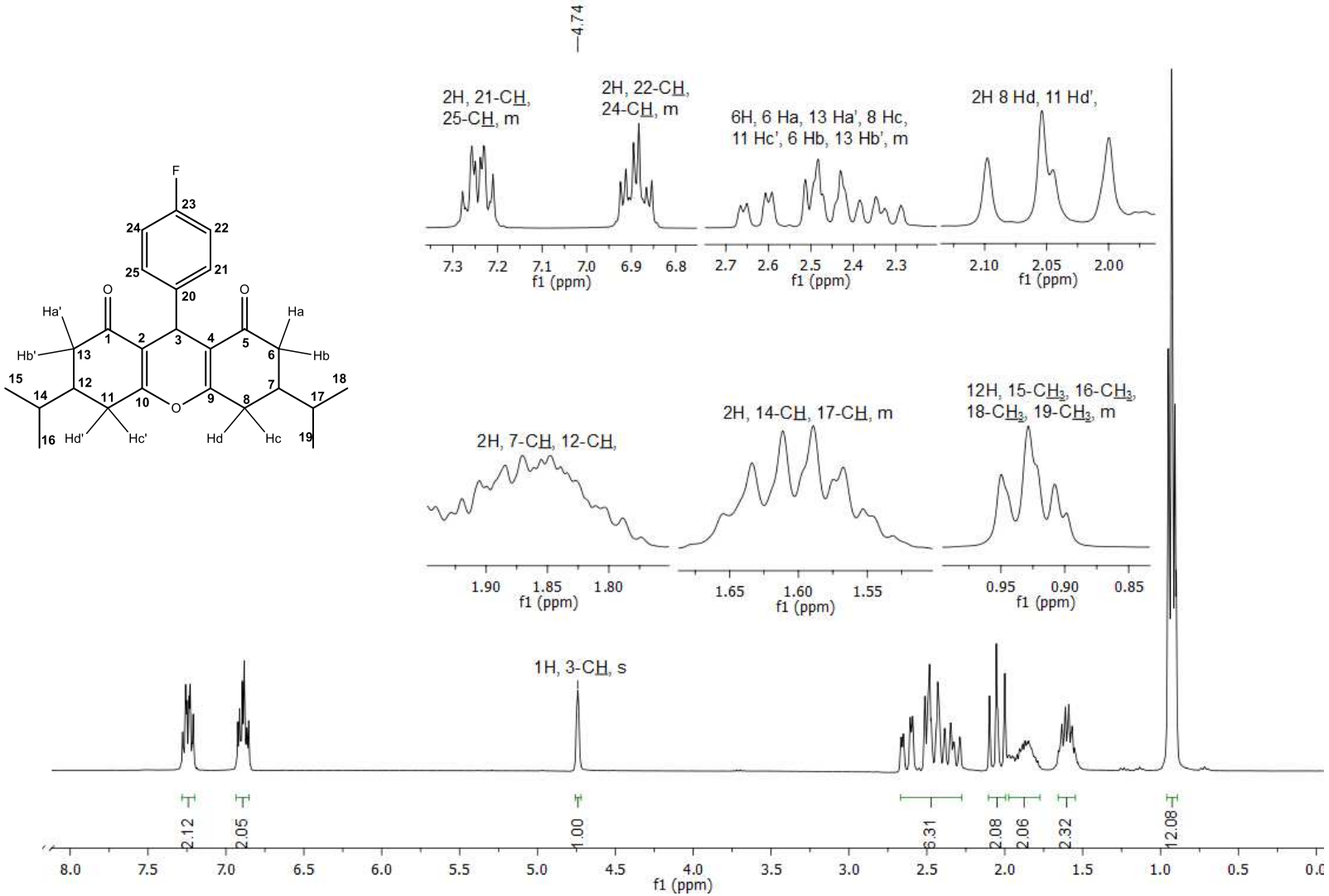

Figura 199. Espectro de RMN de ^{1}H (300 MHz, $CDCl_3$) do composto **51**.

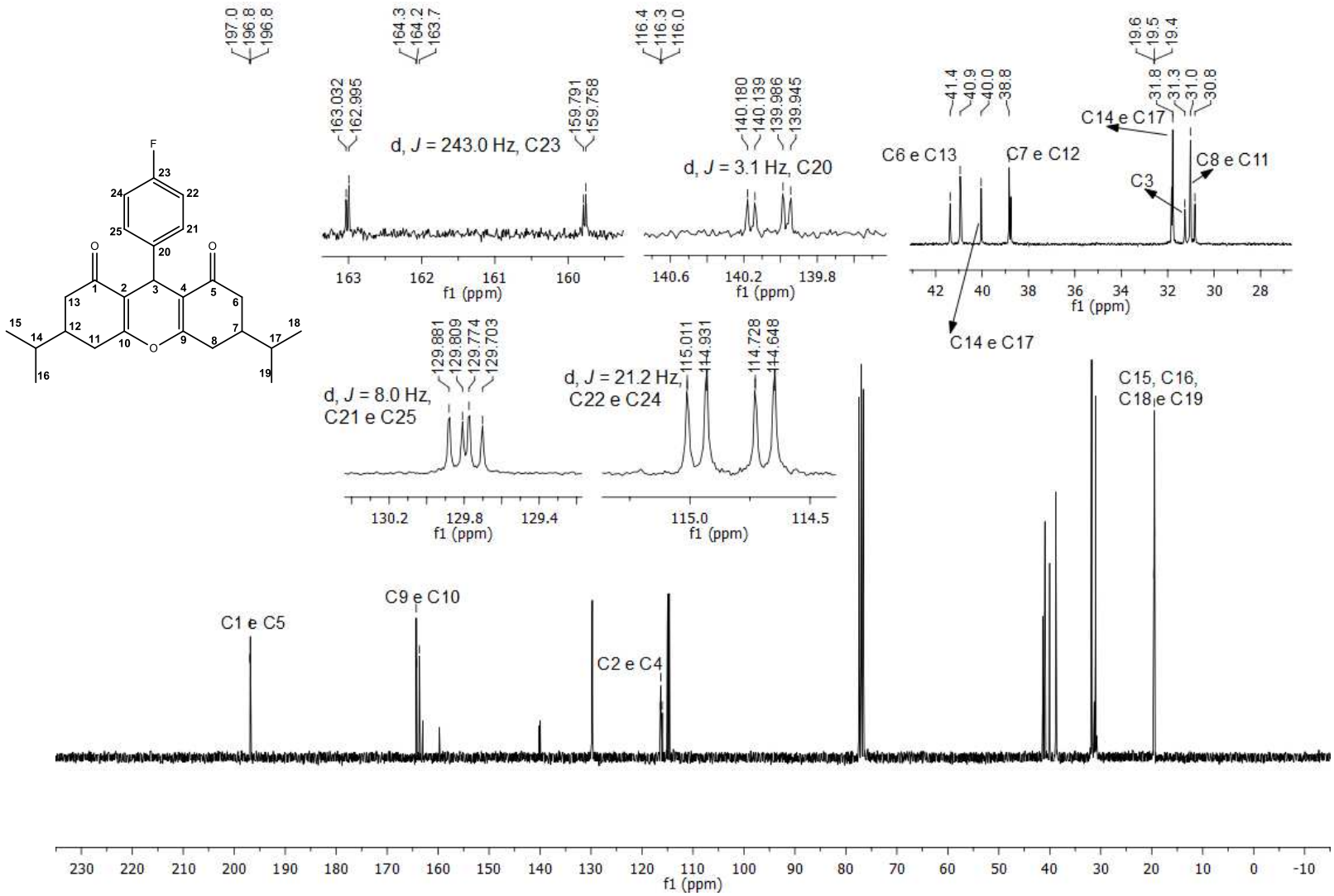

Figura 200. Espectro de RMN de ^{13}C (75 MHz, $CDCl_3$) do composto **51**.

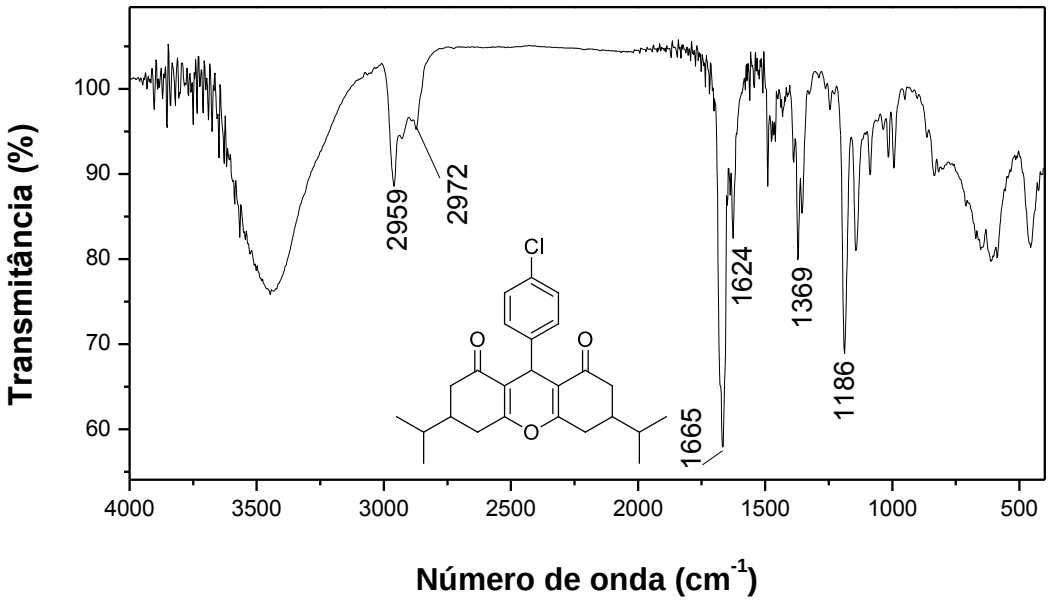

Figura 201. Espectro no Infravermelho (KBr) do composto **52**.

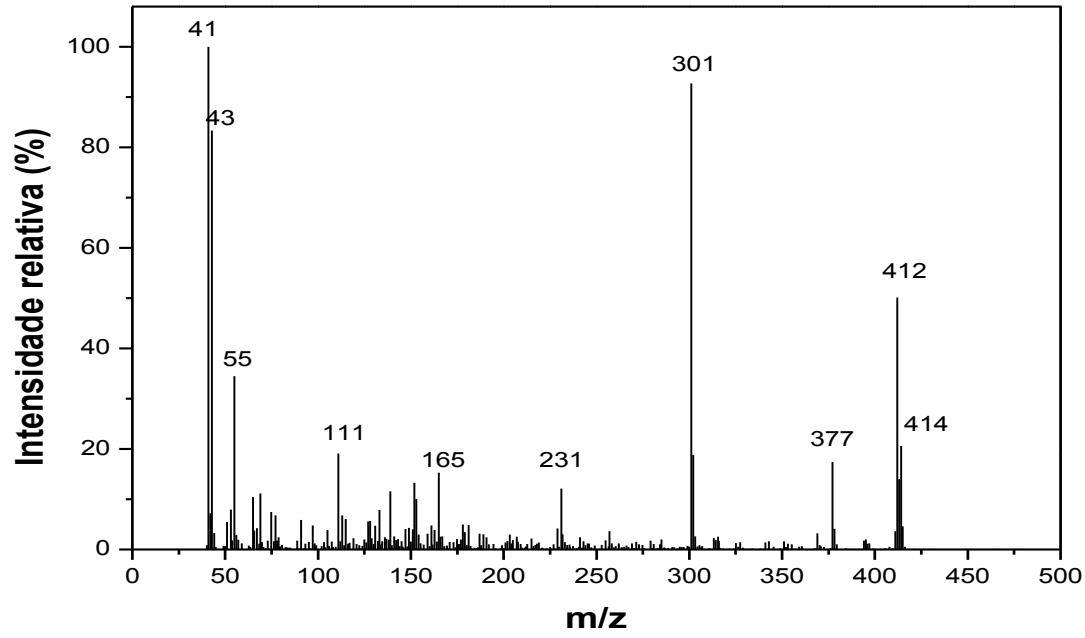

Figura 202. Espectro de massas do composto **52**.

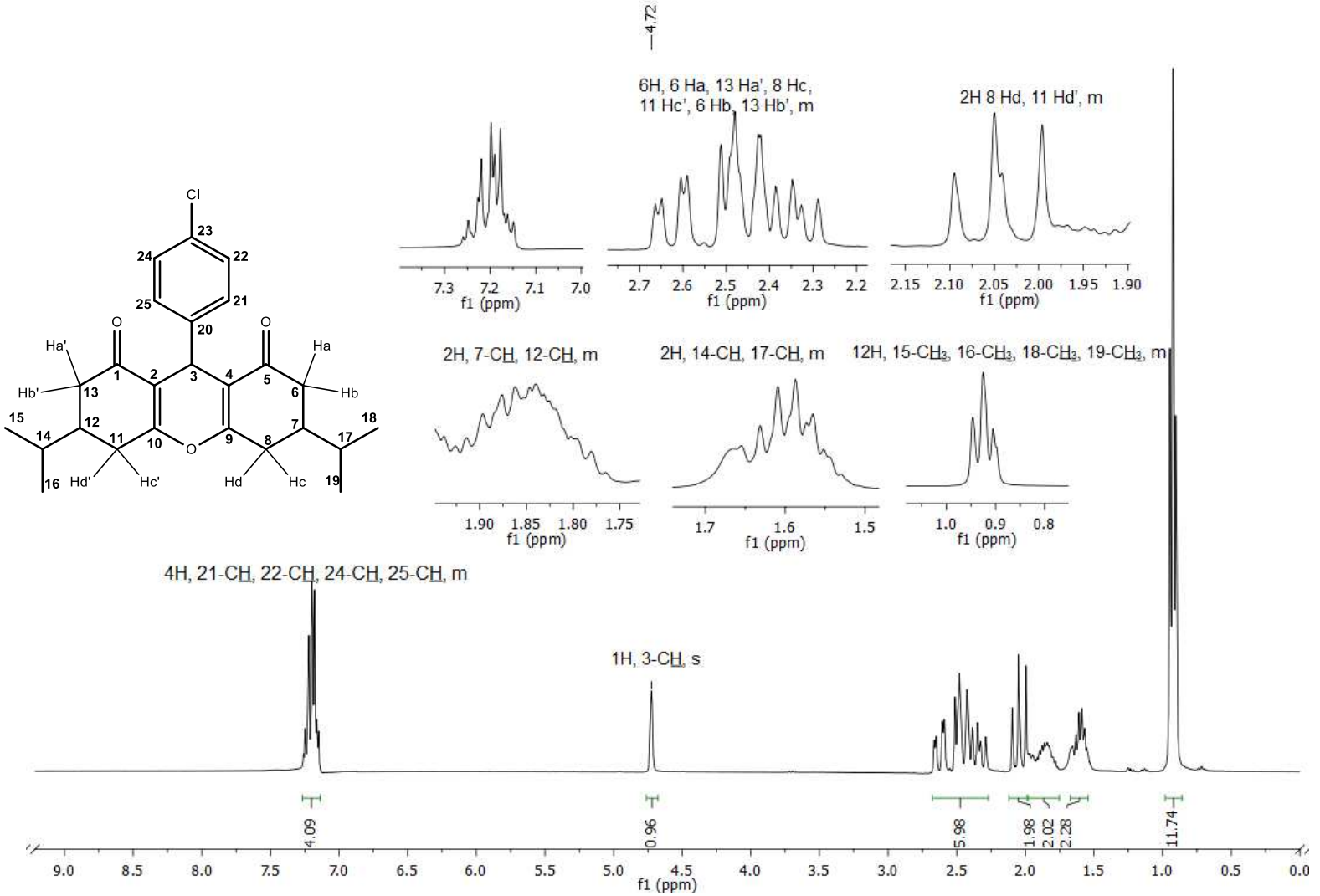

Figura 203. Espectro de RMN de ^{1}H (300 MHz, $CDCl_3$) do composto **52**.

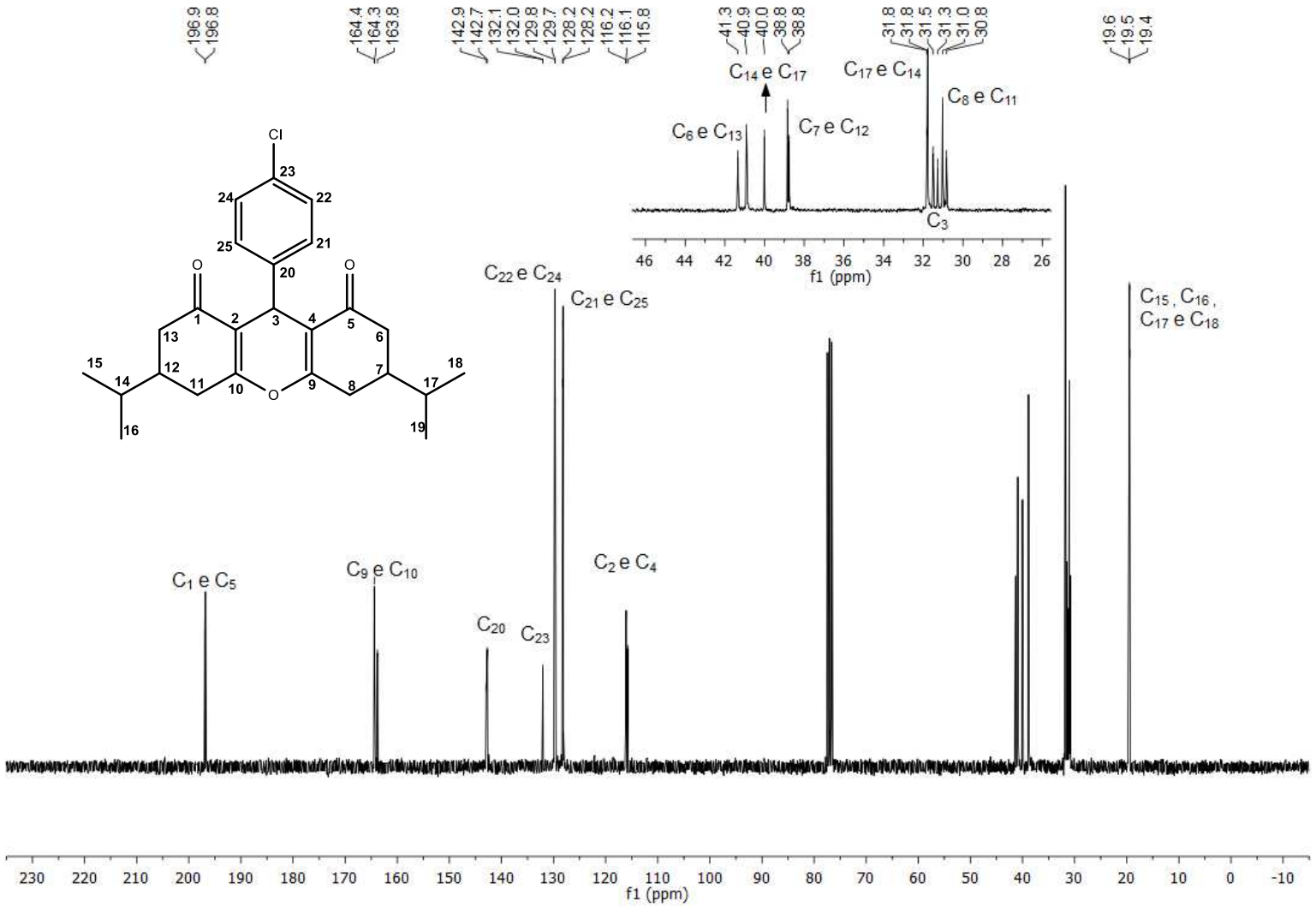

Figura 204. Espectro de RMN de ^{13}C (75 MHz, $CDCl_3$) do composto **52**.

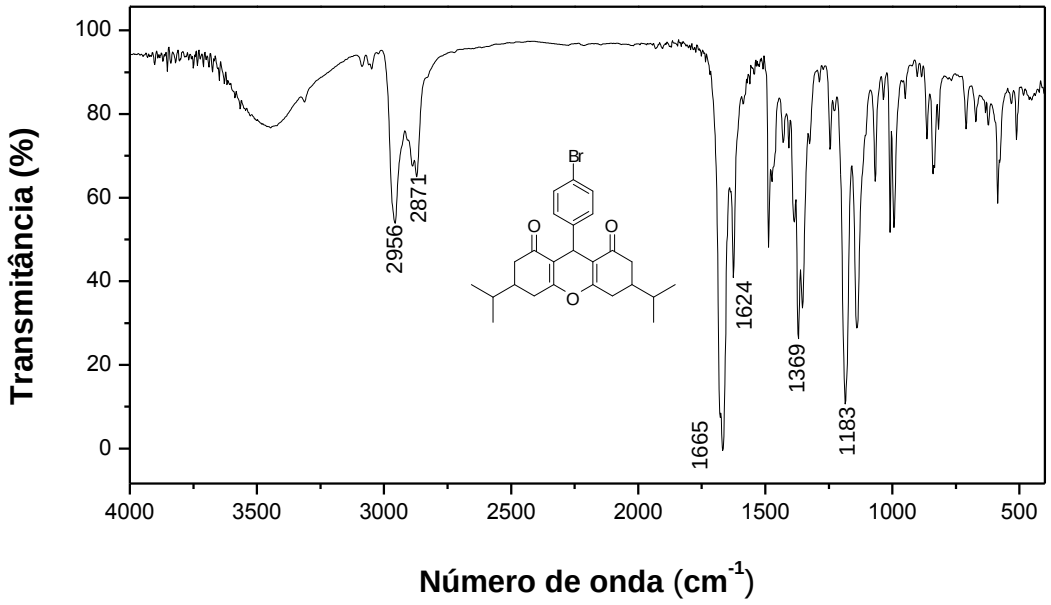

Figura 205. Espectro no infravermelho (KBr) do composto **53**.

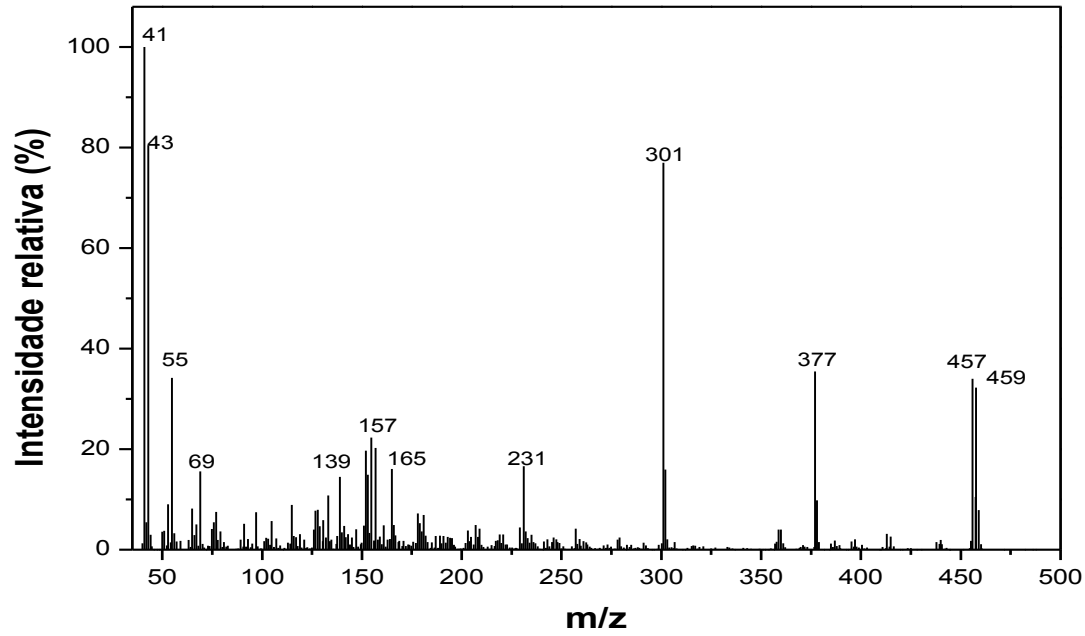

Figura 206. Espectro de massas do composto **53**.

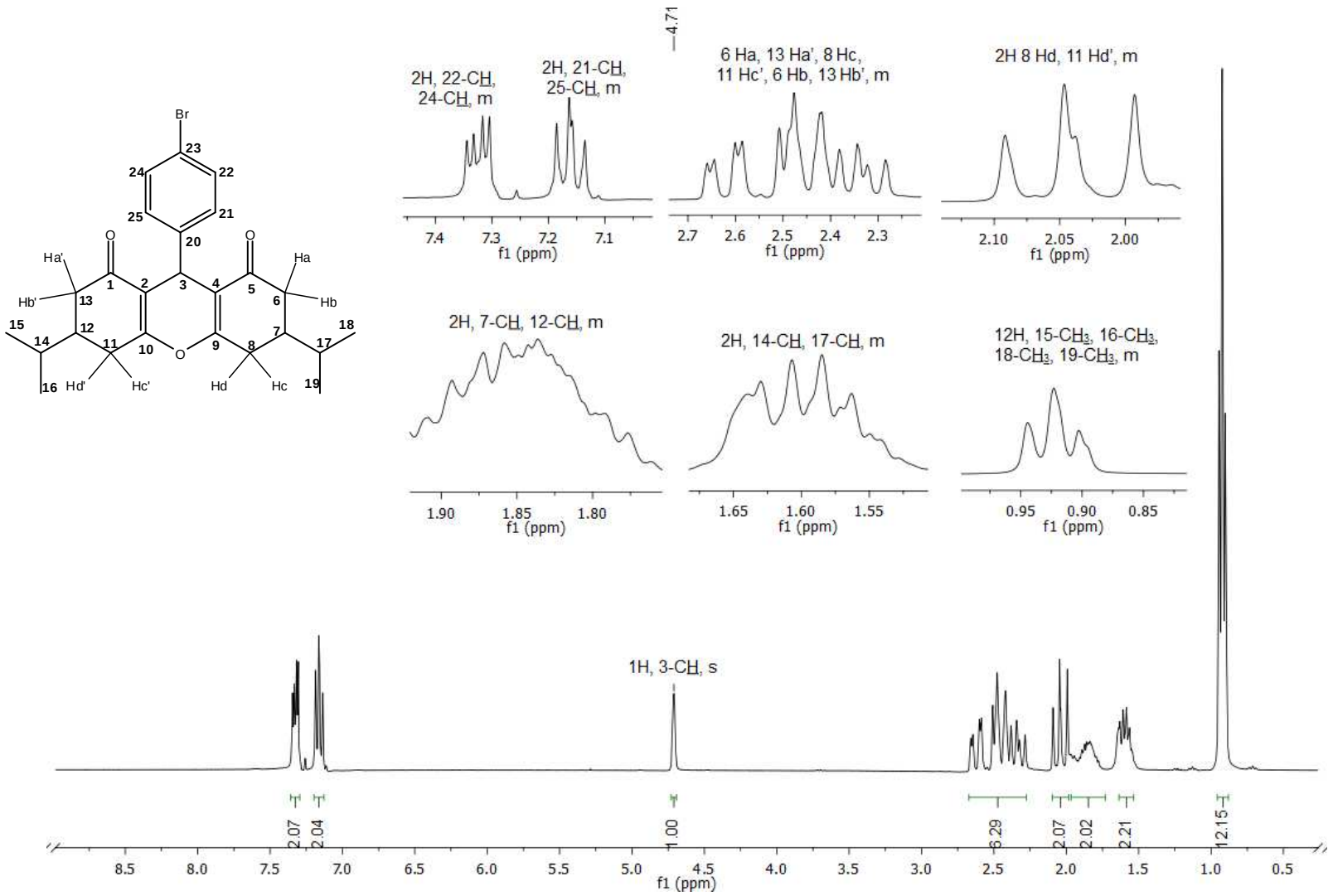

Figura 207. Espectro de RMN de ^{1}H (300 MHz, $CDCl_3$) do composto **53**.

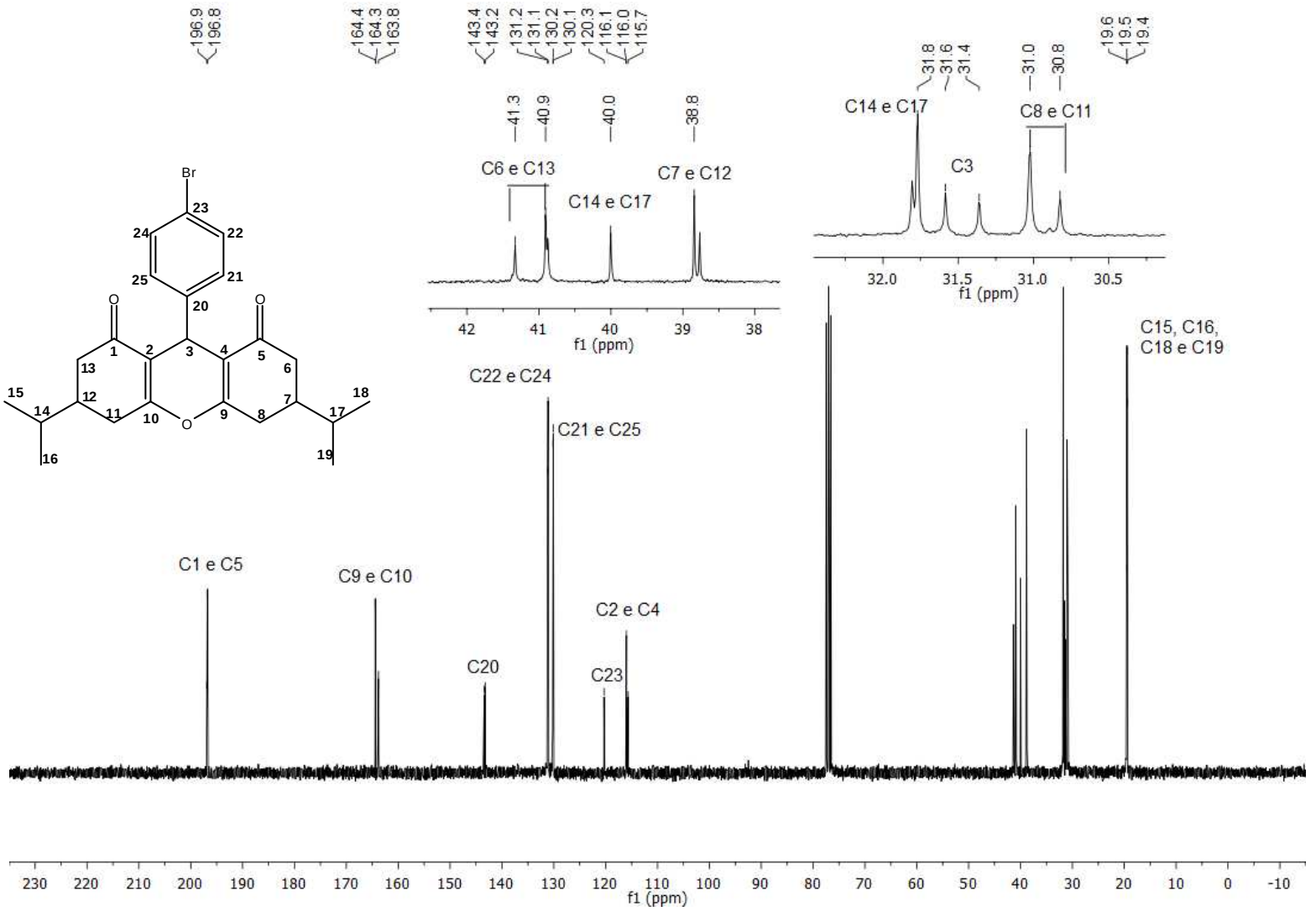

Figura 208. Espectro de RMN de ^{13}C (75 MHz, $CDCl_3$) do composto **53**.

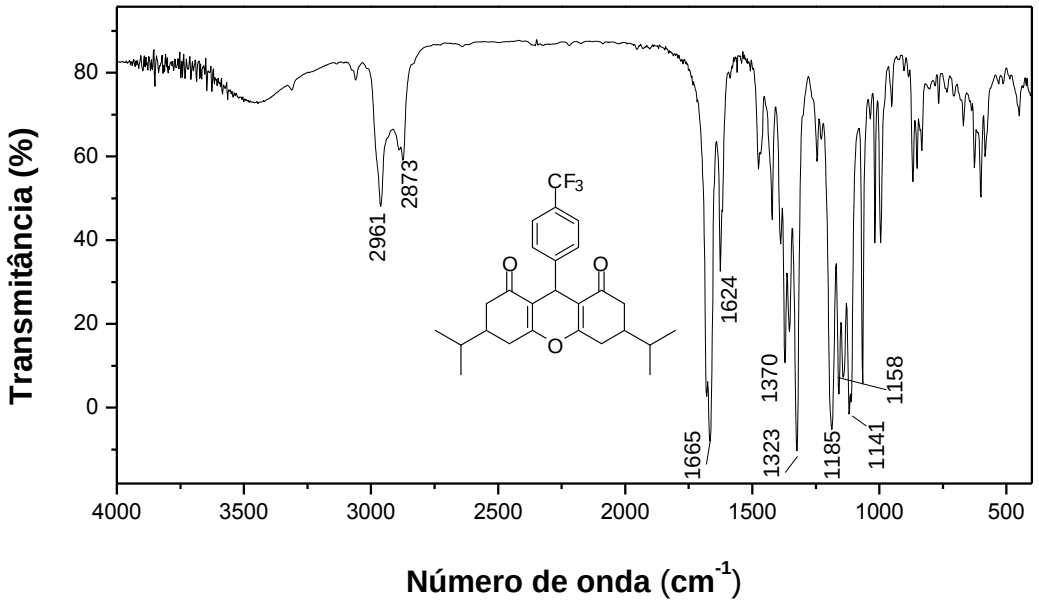

Figura 209. Espectro no infravermelho (KBr) do composto **54**.

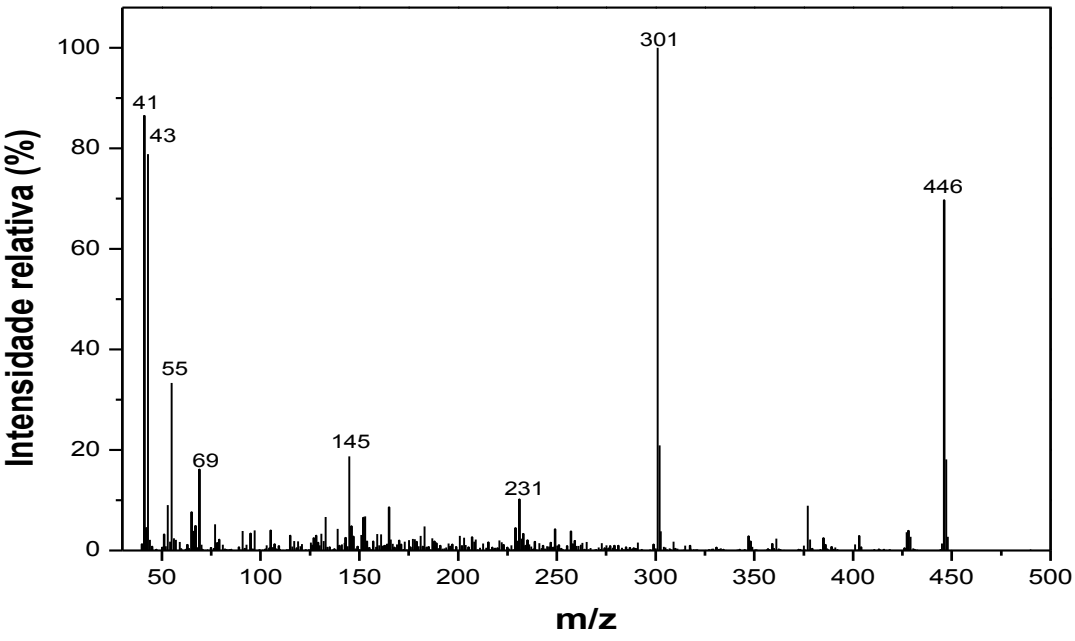

Figura 210. Espectro de massas do composto **54**.

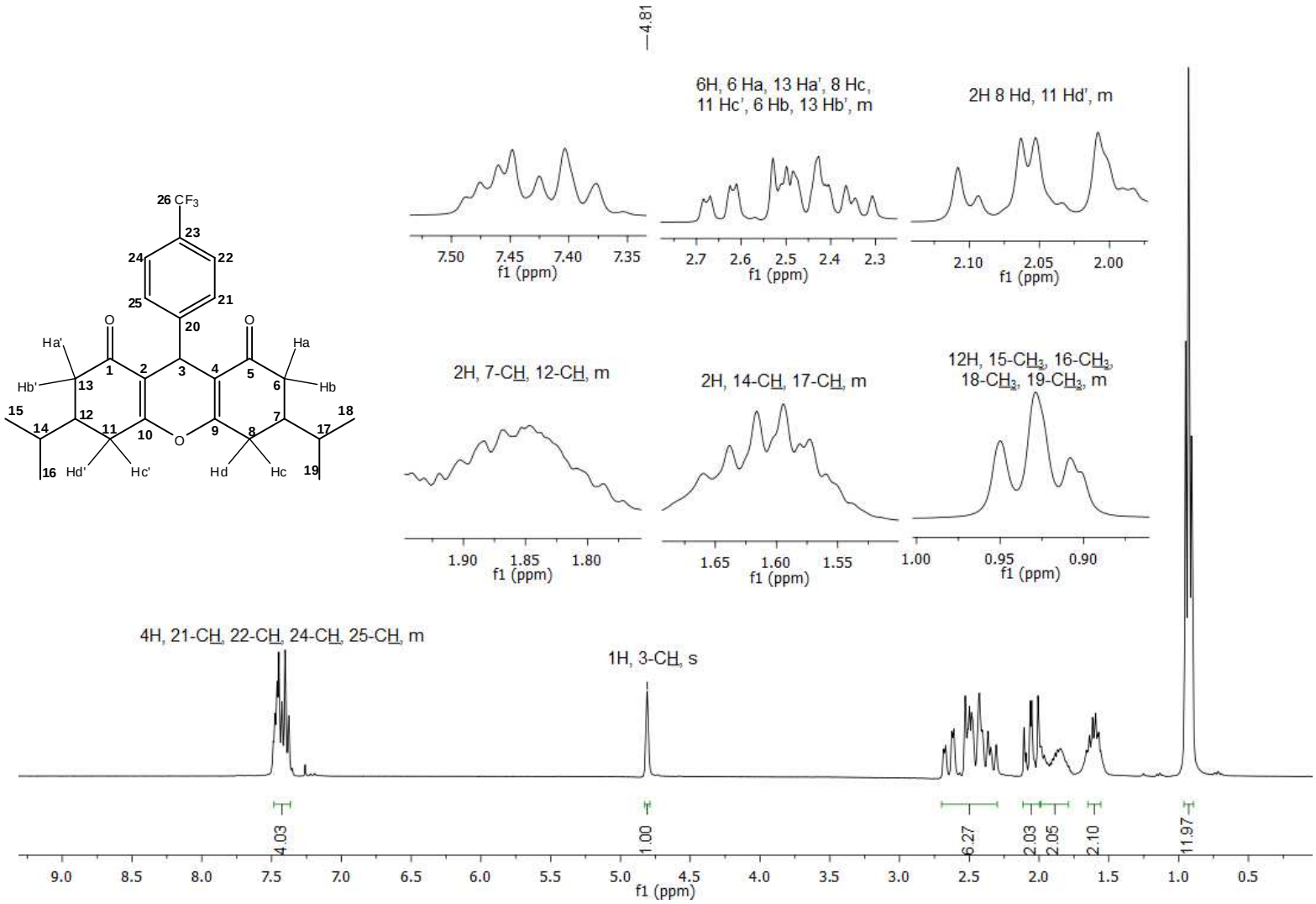

Figura 211. Espectro de RMN de ^{1}H (300 MHz, $CDCl_3$) do composto **54**.

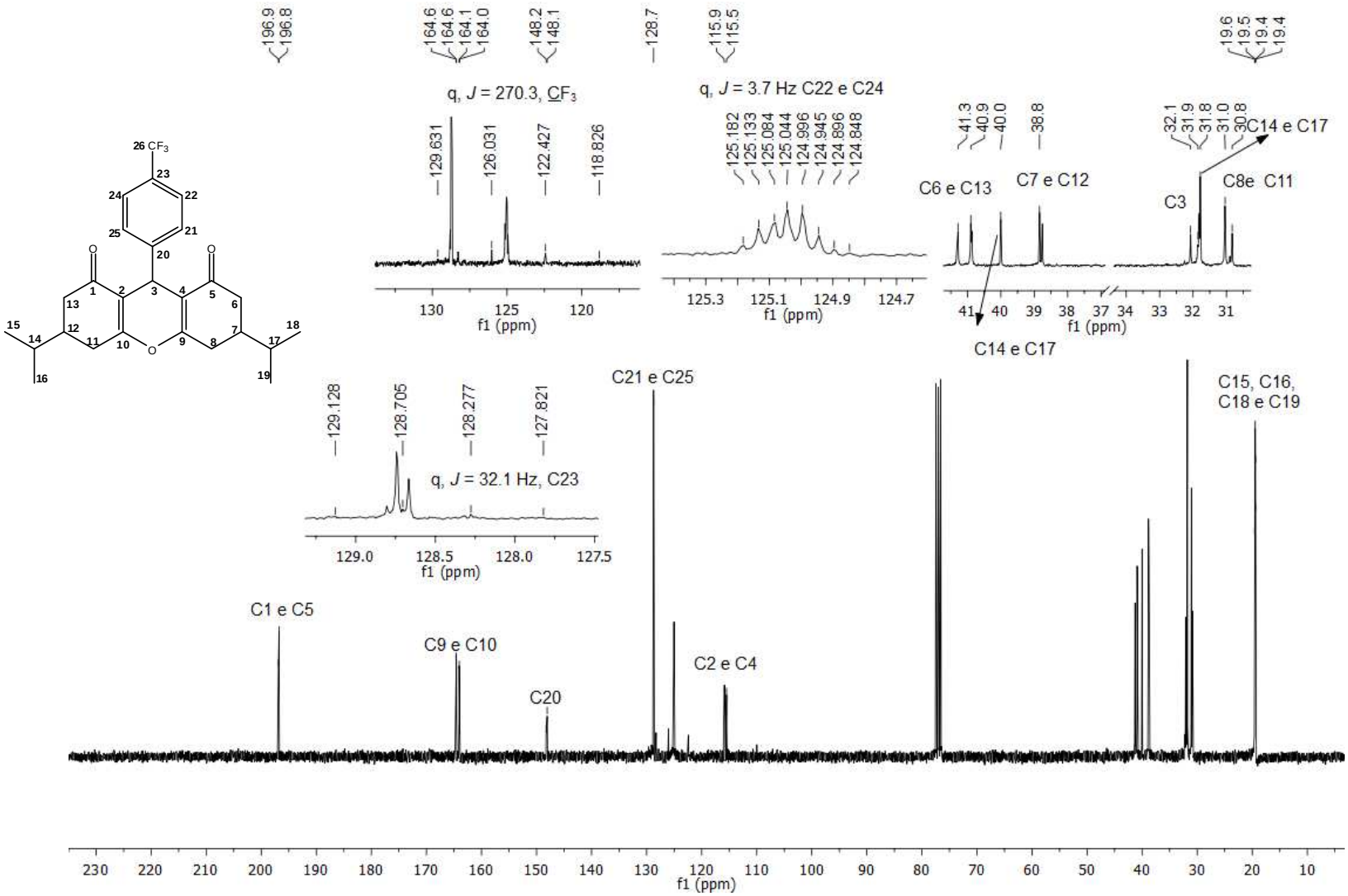

Figura 212. Espectro de RMN de ^{13}C (75 MHz, $CDCl_3$) do composto **54**.

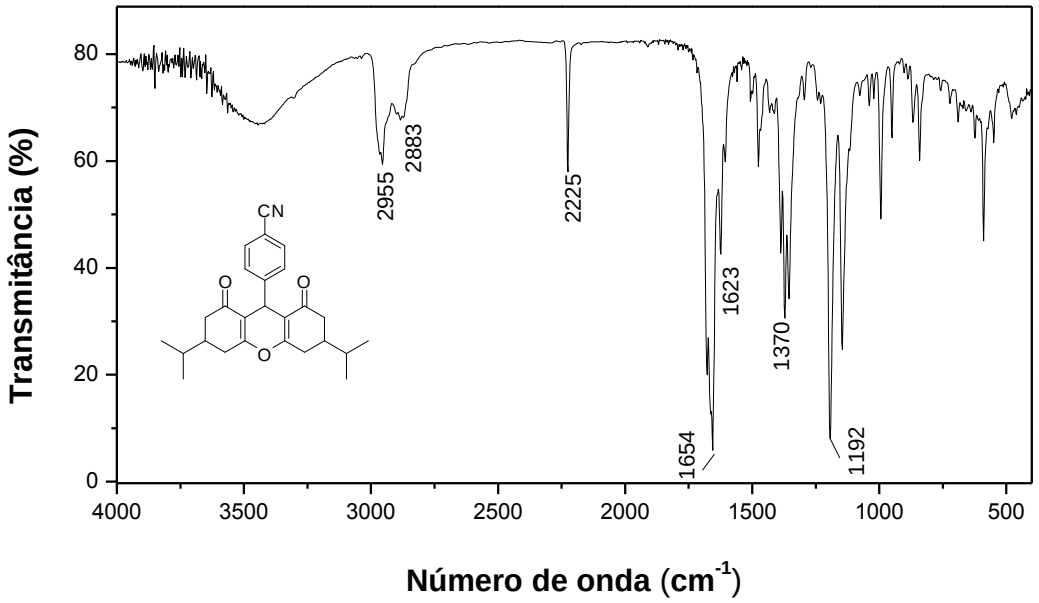

Figura 213. Espectro no infravermelho (KBr) do composto **55**.

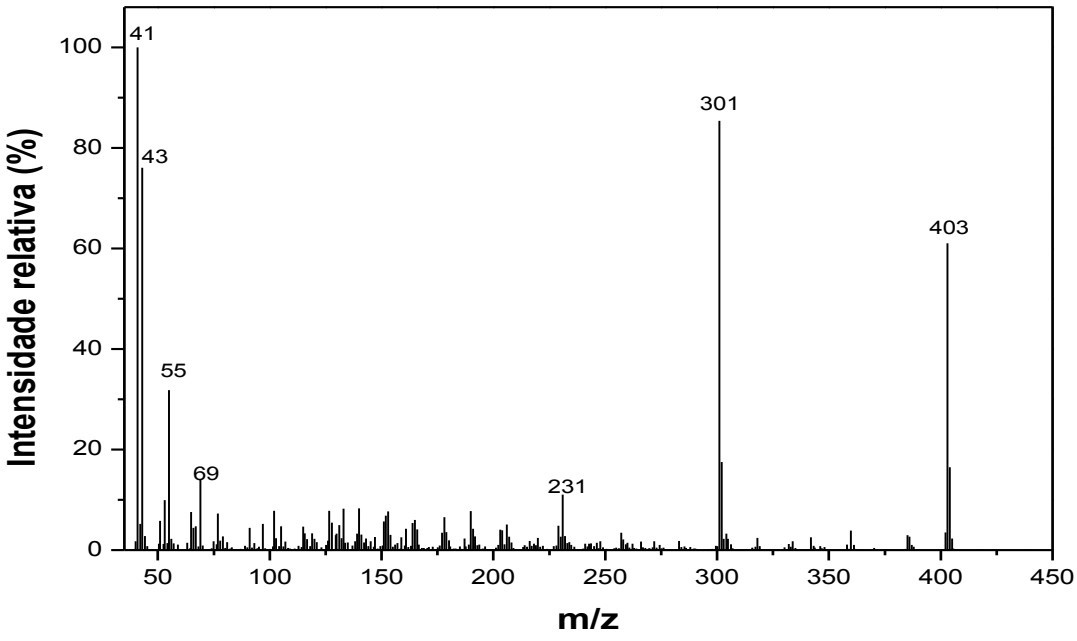

Figura 214. Espectro de massas do composto **55**.

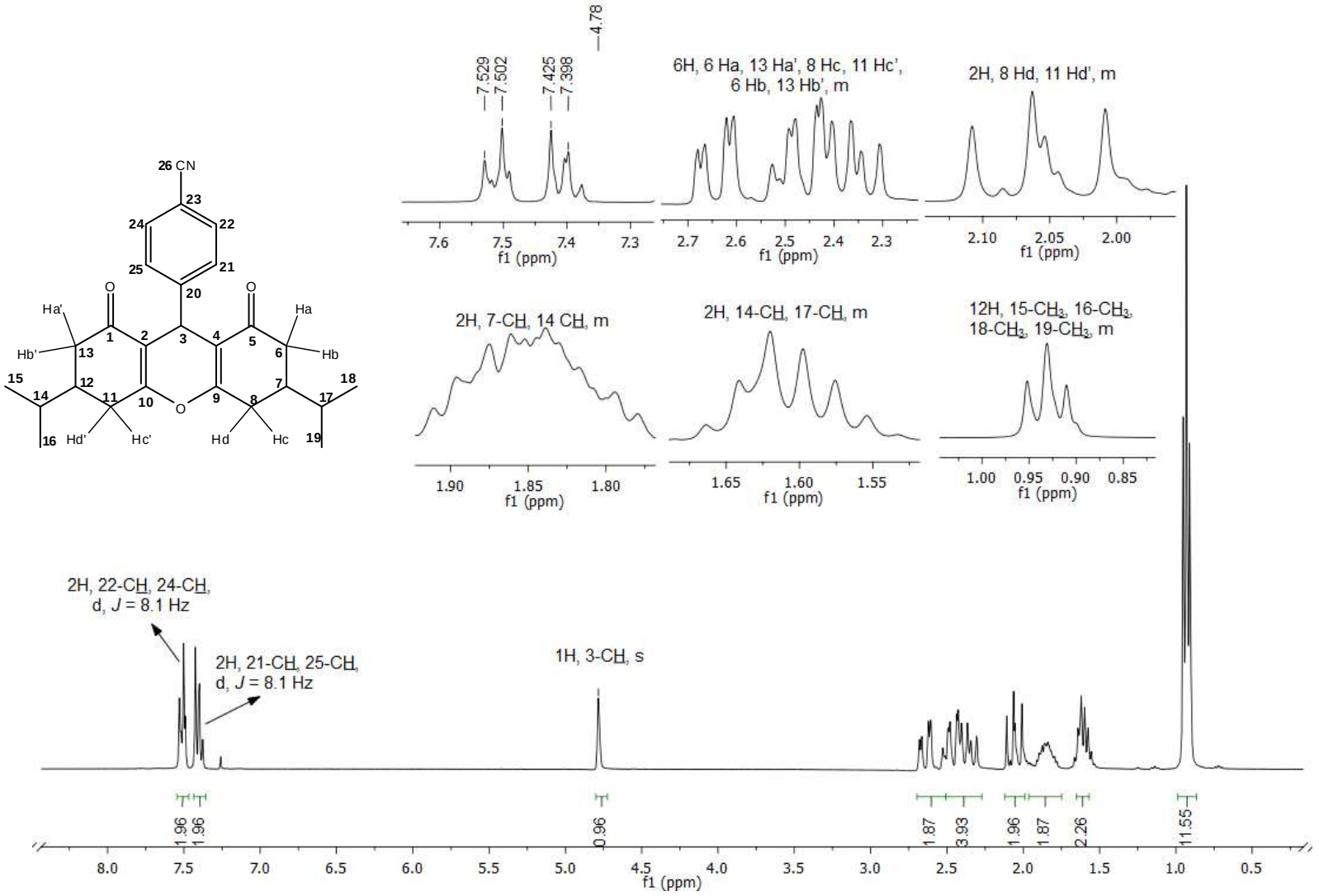

Figura 215. Espectro de RMN de ^{1}H (300 MHz, $CDCl_3$) do composto **55**.

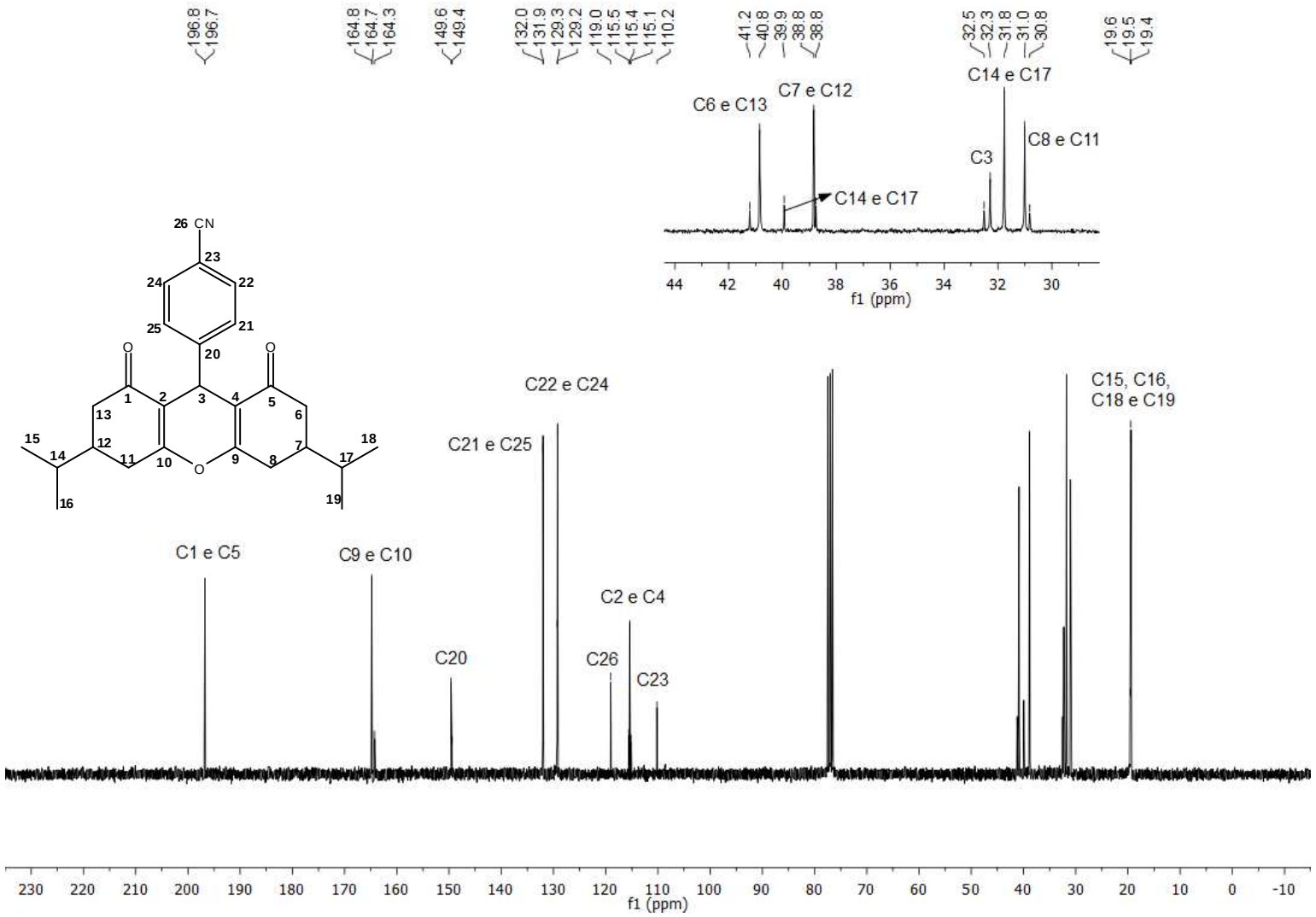

Figura 216. Espectro de RMN de ^{13}C (75 MHz, $CDCl_3$) do composto **55**.

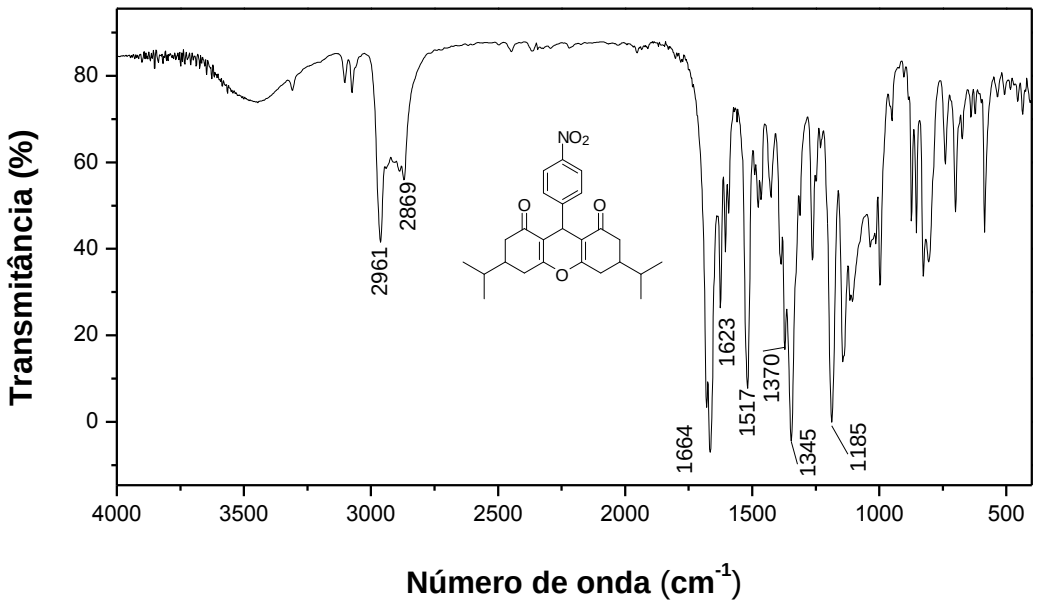

Figura 217. Espectro no infravermelho (KBr) do composto **56**.

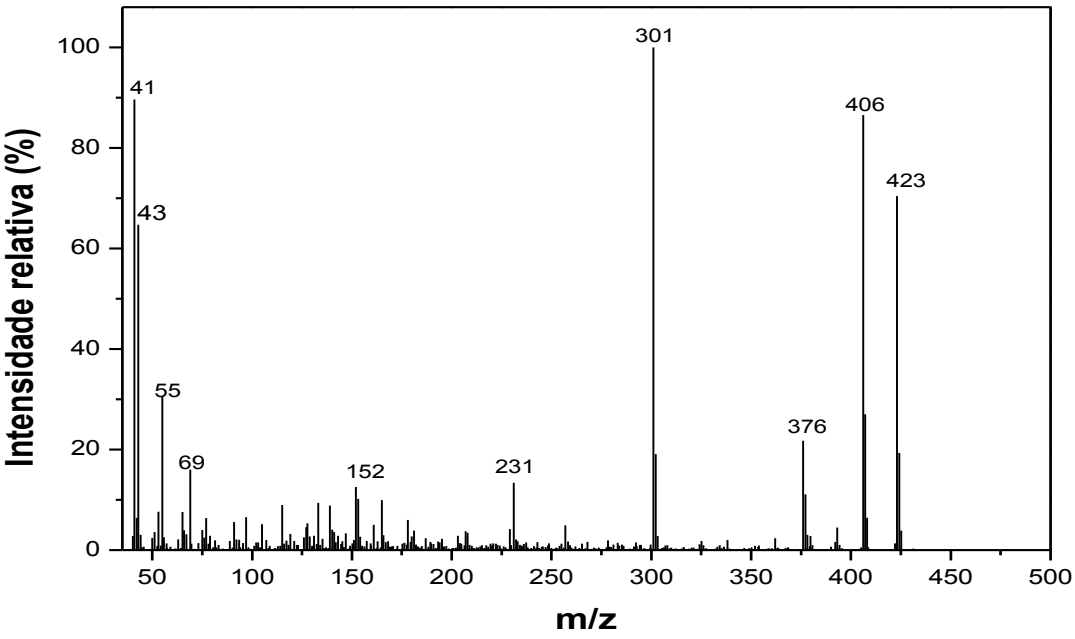

Figura 218. Espectro de massas do composto **56**.

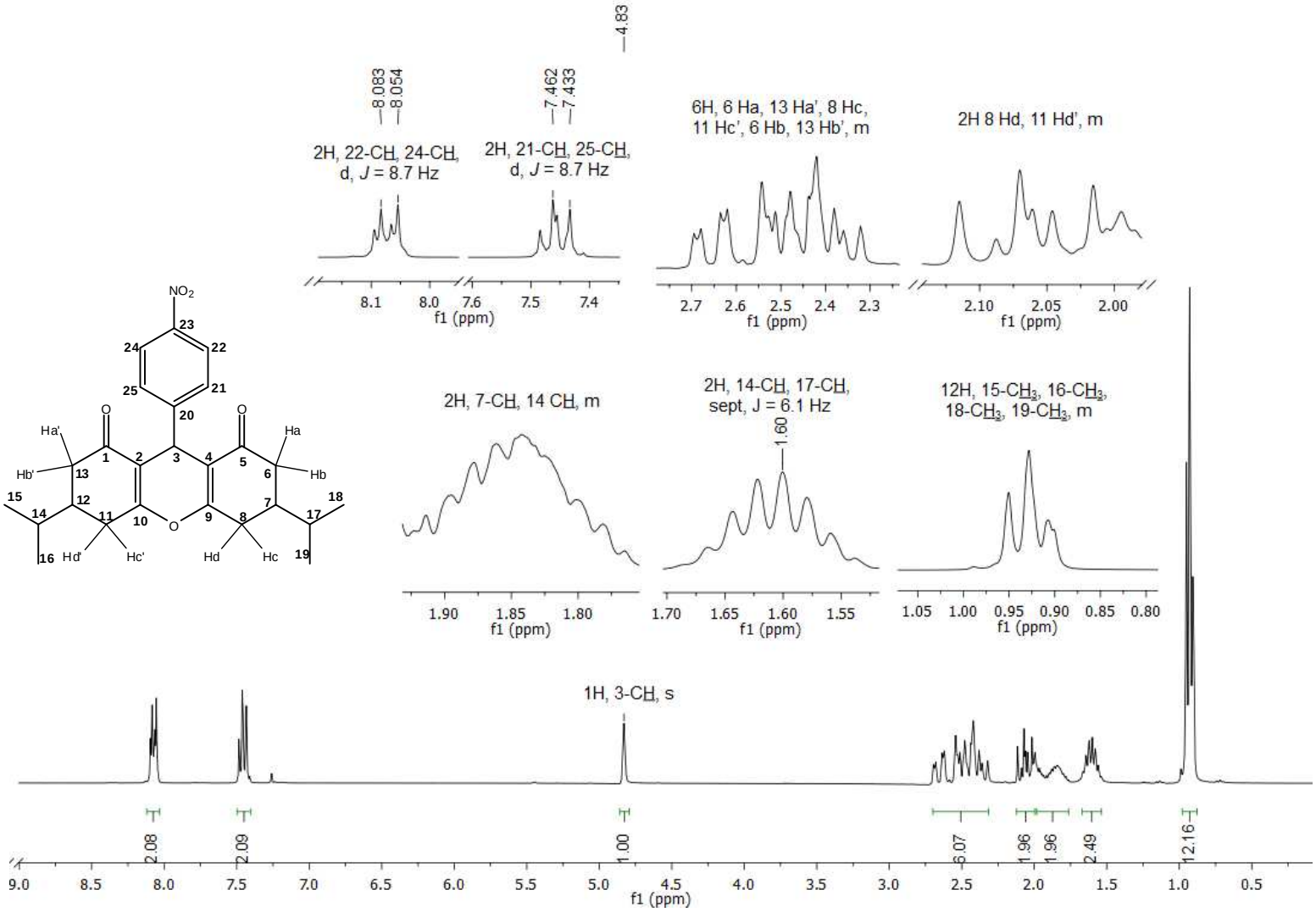

Figura 219. Espectro de RMN de ^{1}H (300 MHz, $CDCl_3$) do composto **56**.

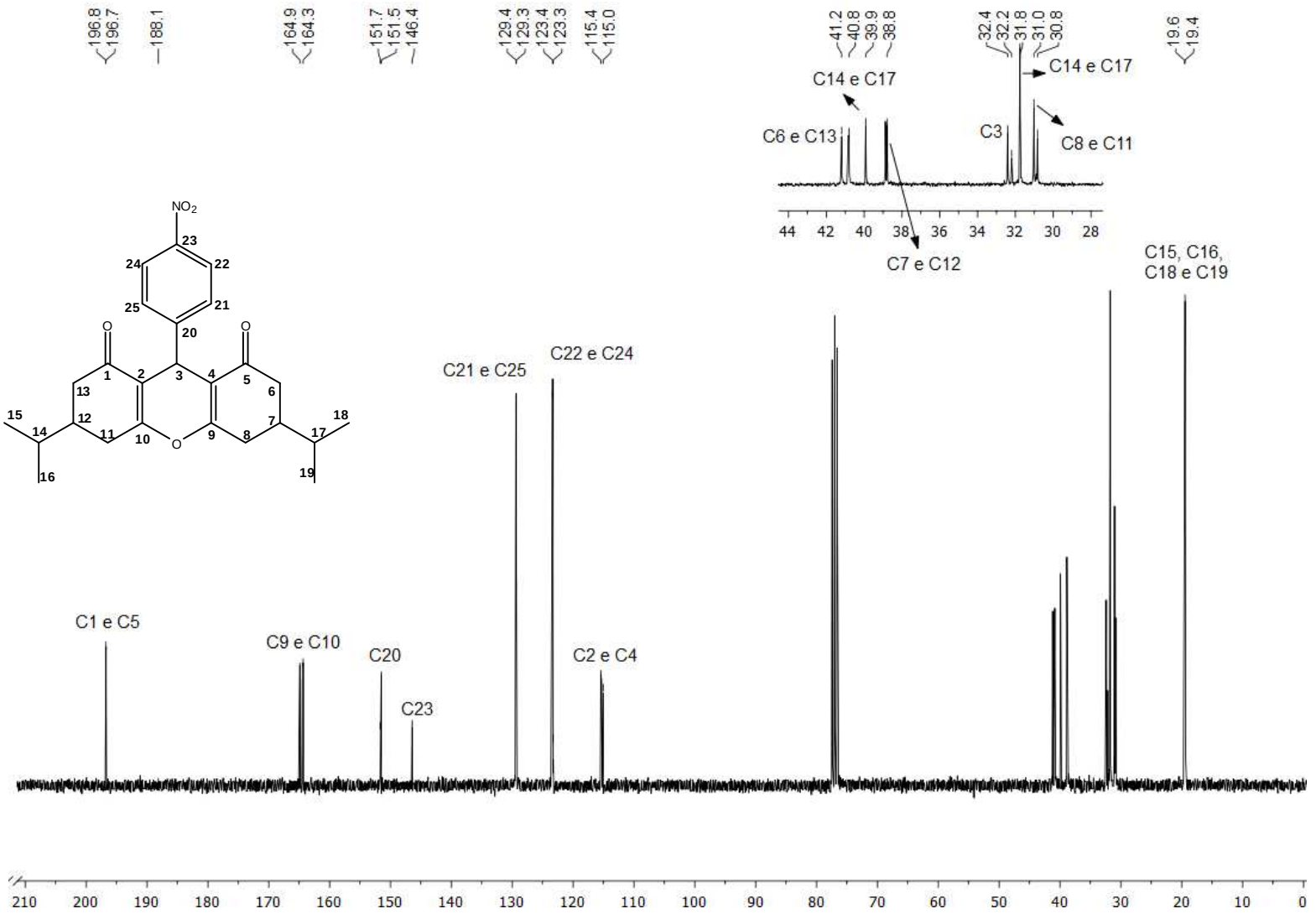

Figura 220. Espectro de RMN de ^{13}C (75 MHz, $CDCl_3$) do composto **56**.

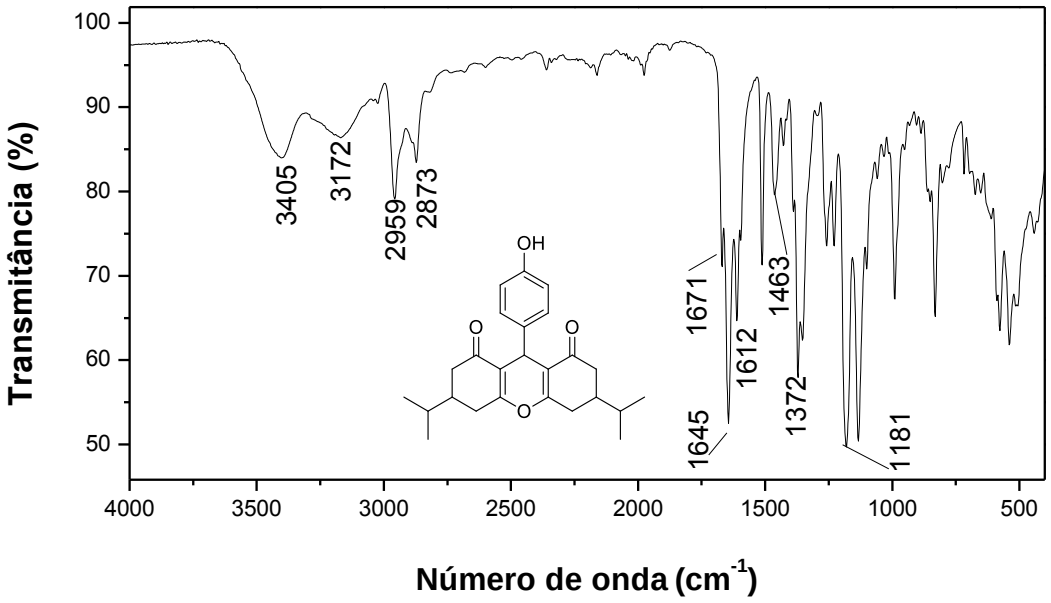

Figura 221. Espectro no infravermelho (ATR) do composto **57**.

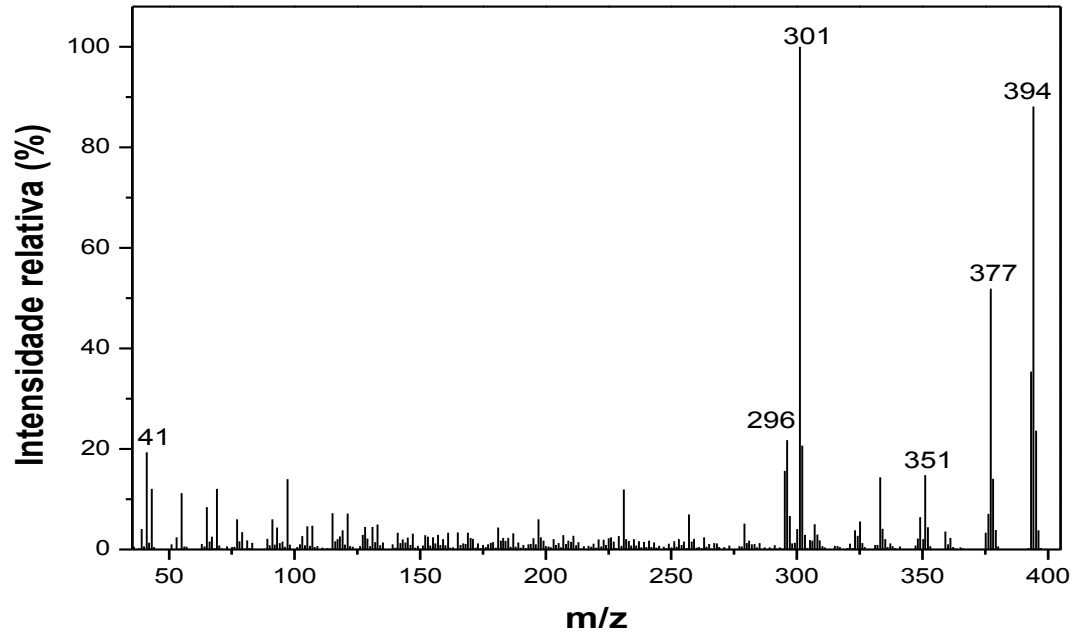

Figura 222. Espectro de massas do composto **57.**

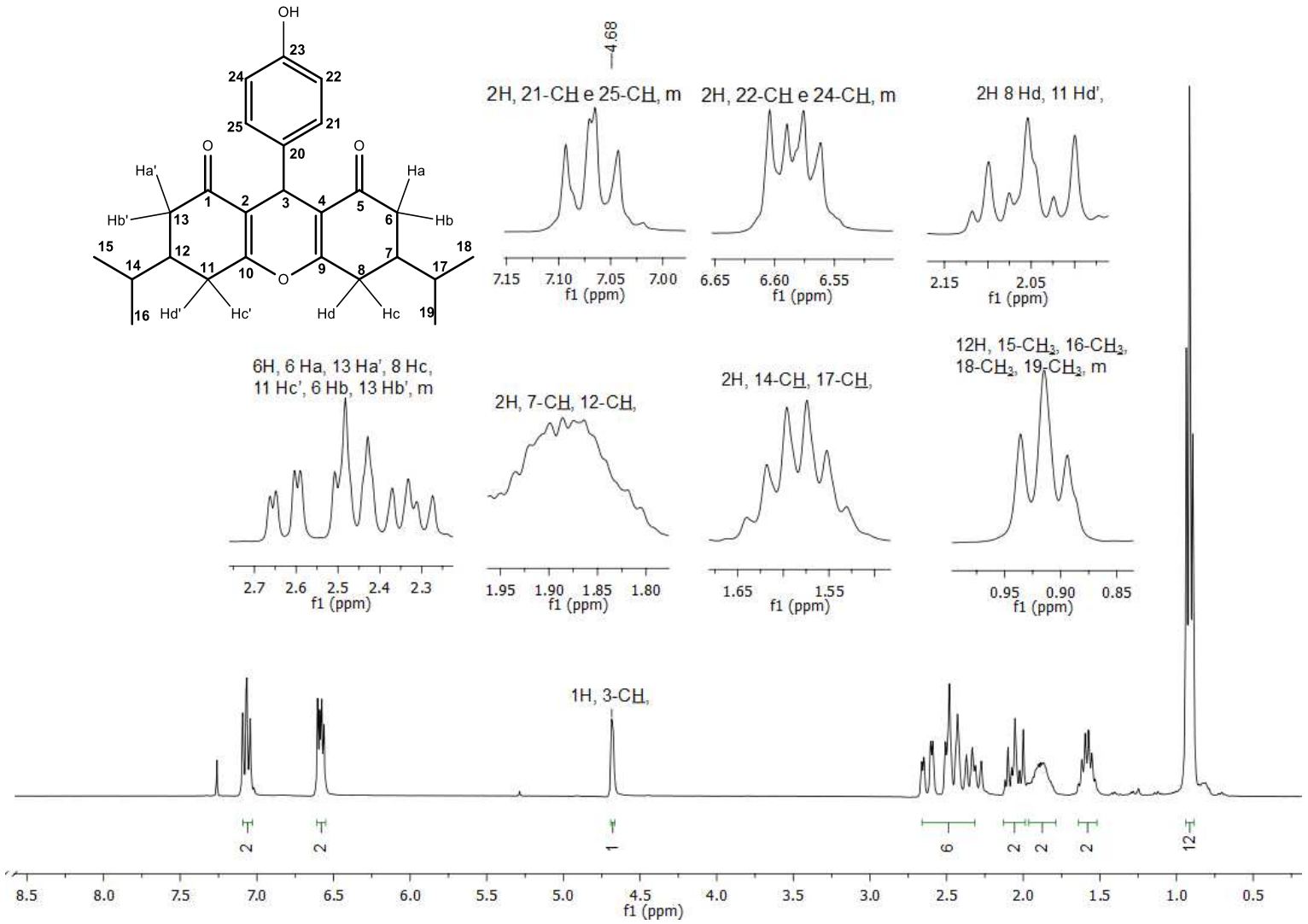

Figura 223. Espectro de RMN de ^{1}H (300 MHz, DMSO-d6) do composto **57**.

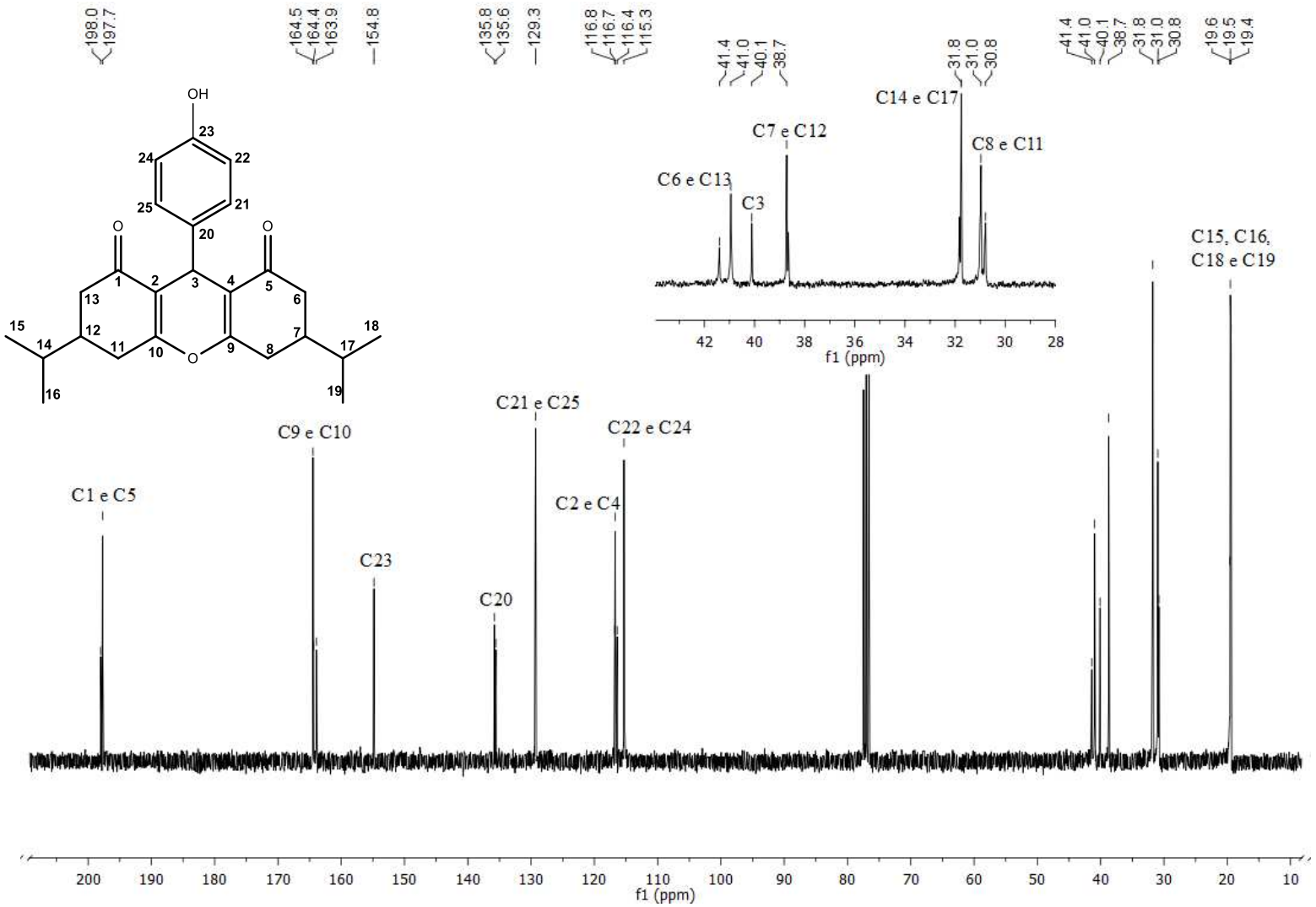

Figura 224. Espectro de RMN de ^{13}C (75 MHz, DMSO-d6) do composto **57.**

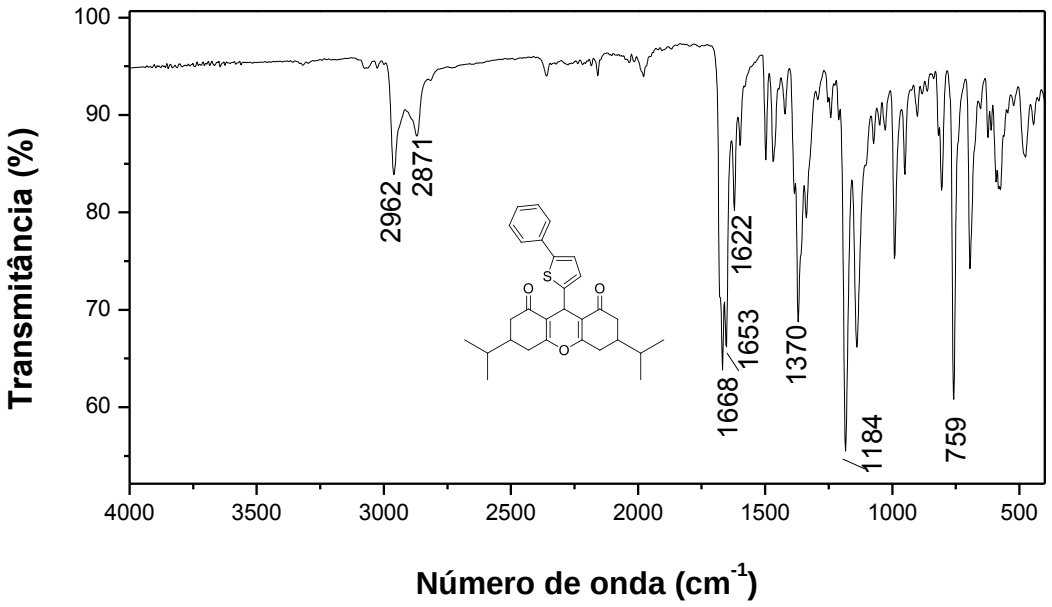

Figura 225. Espectro no infravermelho (ATR) do composto **58**.

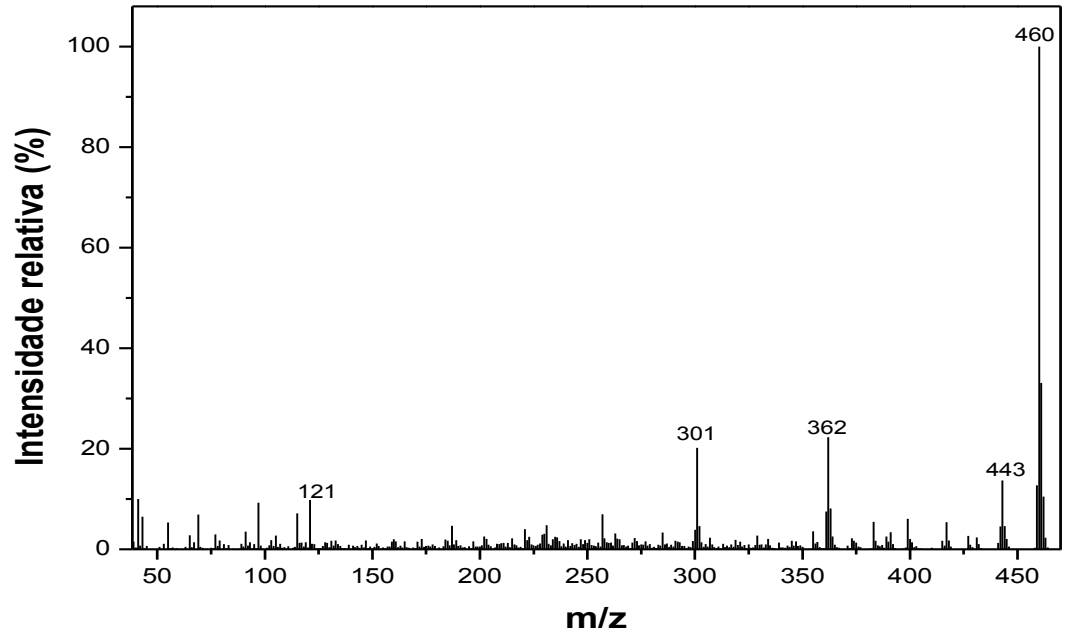

Figura 226. Espectro de massas do composto **58**.

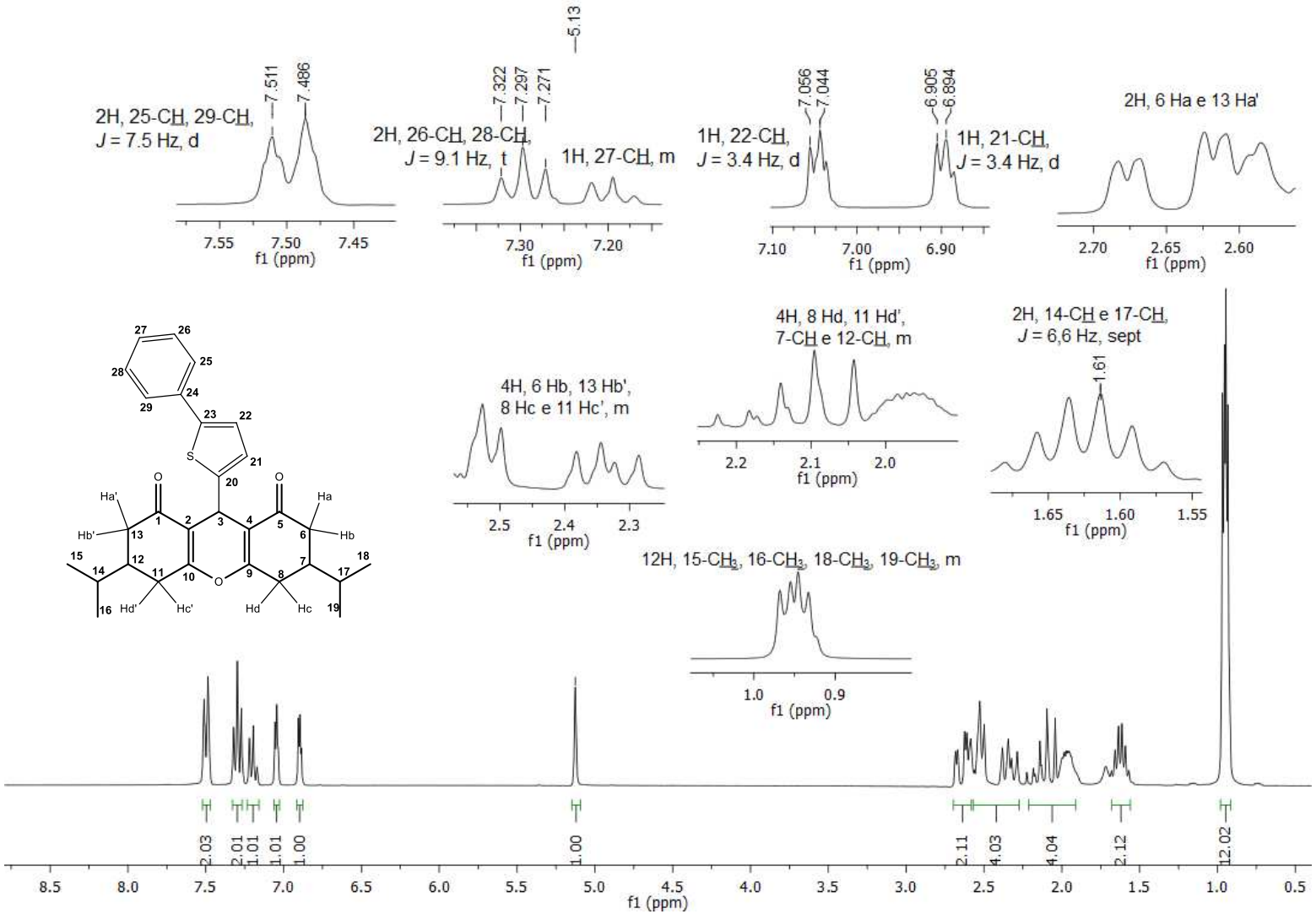

Figura 227. Espectro de RMN de ^{1}H (300 MHz, $CDCl_3$) do composto **58**.

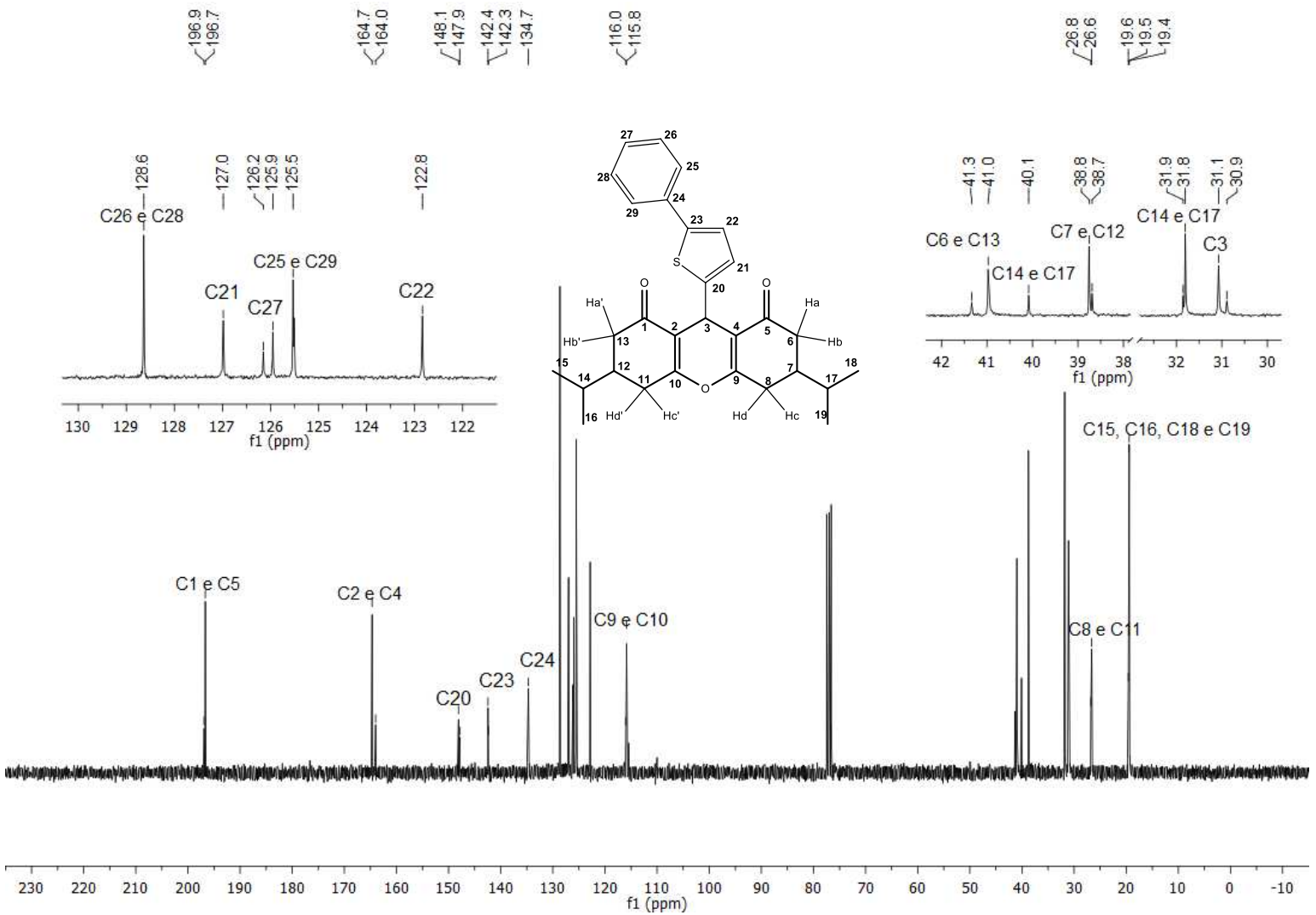

Figura 228. Espectro de RMN de ^{13}C (75 MHz, $CDCl_3$) do composto **58**.